Flinders University

EVolving the Liquid Biopsy: Extracellular Vesicles for Assessing Liver Function and Disease

By

Lauren Newman

Bachelor of Medical Science (Honours)

Thesis
Submitted to Flinders University
for the degree of

Doctor of Philosophy

College of Medicine and Public Health
3 July 2024

TABLE OF CONTENTS

ABSTRACT

Liver cells release extracellular vesicles (EVs) carrying diverse molecular information involved in homeostatic processes and the pathogenesis of metabolic associated fatty liver disease (MAFLD). Applying a liver-specific immunocapture method, this thesis explores the utility of circulating liver derived EV biomarkers to convey the impact of MAFLD on hepatic function and makes vital contributions to this approach for clinical sample analysis. Whereas solid tissue biopsy is preclusively invasive, EVs are an appealing tool to assess organ function and inform disease diagnosis, prognosis and predicted response to interventions via a minimally-invasive liquid biopsy; however, several challenges in EV isolation and analysis currently limits clinical translation.

EVs in biofluids, including blood, exist among a complex milieu of non-vesicular material that impacts the specific recovery and detection of target molecules. Enrichment of EV marker proteins and depletion of co-isolated matrix contaminants reflect the yield and purity of EV isolates to provide critical assessments of sample quality. Here, development and validation of a novel targeted proteomic assay is described that achieves sensitive, multiplexed, high-throughput and absolute quantification of EV markers and contaminants. Importantly for clinical studies, these improvements compared to standard protein detection methods, accommodates quality control on an individual sample level in limited sample volumes. The impact of donor characteristics and physiological variability, including diurnal, prandial and sex differences, on circulating EV abundance and cargo is investigated to establish basal ranges in global and liver-specific EVs. Increased abundance of circulating liver-specific EVs during the day highlights an important consideration for study protocols sampling liver-derived EV biomarkers.

EVs released by the liver constitute a minor fraction of the heterogenous population in the systemic circulation and methods for EV isolation poorly distinguish subpopulations containing markers of interest. Thus, advanced isolation methods targeted towards the tissue of origin are expected to improve the sensitivity and specificity of low abundance disease-associated biomarkers, including microRNA. Expression of liver-enriched miRNA with reported dysregulation in NAFLD (miR -122, -192, -128-3p) were compared in total plasma, global EVs and liver-specific EVs in mild and

severe disease and healthy controls. Increased expression of each miRNA is associated with disease in liver-specific EVs but not the other less specific sources. Although liver-derived EVs carry a minor proportion of total plasma miRNA, this proportion increases significantly in disease. The results suggest changes are specifically occurring in the EV export of miRNA from hepatic cells and highlight the importance of removing background (non-EV and non-liver) signal for improved diagnostic performance.

Patients with MAFLD exhibit variability in exposure and response to medications resulting from differences in abundance of hepatic drug metabolising enzymes (DMEs) and drug target proteins. Key DMEs and MAFLD drug targets were readily detected and quantified in EVs isolated from liver tissue, supporting potential for *in vivo* monitoring of interactions of drugs with the liver. Moderate-strong correlation ($r>0.6$) of 13 from 14 DMEs between EVs and paired tissue supports utility for reporting on between-subject variability. The work described in this thesis advances the analytical framework for applications of liver-specific EV liquid biopsy in clinical samples and contributes to best practice in characterisation and reporting aligned with international standards in the field. These contributions lay the foundation for future development of EV-based precision medicine strategies for MAFLD and beyond.

DECLARATION

I certify that this thesis:

1. does not incorporate without acknowledgment any material previously submitted for a degree or diploma in any university

2. and the research within will not be submitted for any other future degree or diploma without the permission of Flinders University; and

3. to the best of my knowledge and belief, does not contain any material previously published or written by another person except where due reference is made in the text.

Signed.....L Newman.....

Date..23/02/2024.....

ACKNOWLEDGEMENTS

To Professor Andrew Rowland, from my beginning as an undergraduate research student in your lab over five years ago, I have had the absolute privilege of working with and for a brilliant mind in clinical pharmacology, receiving your attentive support and encouragement as a supervisor and mentor and gaining opportunities to further myself both personally and professionally. You have shown dedication to shaping me as a scientist over these many years, modelled how to advocate for my ideas and demonstrated belief in me even when I lacked it in myself. I thank you for teaching me not to pin all my hopes, self-worth and outlook on life on the outcome of a single experiment. Thank you for fostering my autonomy, giving me the space to generate my own ideas and work at my pace and rhythm. You have maintained trust in me as an individual and a scientist while never being too far to reach out to when I needed guidance. I am grateful for every impromptu mentoring session, your patience and willingness to accommodate whenever I would randomly pop into your office for anything from how to interpret a weird bit of data, to general life and career advice. You genuinely always have your door open and could never miss a teachable moment, pen and paper at the ready to explain a concept – which as a visual learner was incredibly effective for me. You have unlocked a breadth of opportunities and pushed me to pursue them and I know I will always look back on this time with fondness and deep gratitude for the formative role they have played in my early career.

To my colleague, co-author, confidant, work bestie, Dr Zivile Useckaite, I could not have achieved half of this without you. Your technical expertise has been paramount to the successful completion and publication of my work and I thank you for your contributions to generating data and providing valuable input to the planning and execution of experiments. The time we spent critically evaluating our work and discussing the next steps are some of the most energised and enthused I have felt in my time as a student. I could always depend on you to listen to my concerns and guide the way forward as someone who has been there before.

The other members, past and present, of the Flinders University Precision Medicine Group and Department of Clinical Pharmacology who offered support and advice, senior academics who willingly fielded my questions and shared their wisdom, co-authors on my publications who added to

the methodological robustness, data analysis and helped to improve my writing, all the past students whom I had the pleasure of growing alongside and were always up for a chat and to add a fun social element to a hard day – I thank you all.

Also to my HDR assessors Dr Jess Logan and Professor Simon Conn, I appreciate the time you have given to attend my seminars, review my progress and provide valuable feedback over the course of my candidature. Similarly, I thank my HDR mentor, Dr Dusan Matusica, for so generously sharing his time and empowering me to go after what I want and need.

To my industry mentor, Dr Tony Simula, and the team behind the Industry Mentoring Network in STEM (IMNIS) program, I extend my deepest gratitude for getting the mentor match up so right. I was very lucky to be connected with someone who truly understands me as a person and how those personality traits meld with my professional endeavours. Tony, I am so grateful for your wisdom and advice, for every Friday morning coffee and the meetings that ran well over an hour as we lost track of time chatting. Thank you for your unwavering patience for my ramblings on the trials and tribulations of my PhD journey, for openly sharing your own challenges and keys to success, and for showing up with genuine interest and compassion.

I acknowledge our collaborators in the Department of Hepatology and Flinders Medical Centre for their efforts to recruit and screen patients and collect blood samples for my research. A huge thank you to all the individuals, both patients and healthy volunteers, who kindly gave their time and donated samples. Your participation is a crucial contribution to the generation of new knowledge and I am honoured to be trusted with it.

I was fortunate to be involved in the collaborations between our group and prominent international pharmaceutical companies and had the opportunity to visit one of these in the United States to share my work and consult on the methodology I had played a role in developing. These experiences have given me vital exposure to the interactions of industry and academic research, helped me to forge my international career goals and aspirations and demonstrated the incredibly rewarding possibilities for the direct translation of my work to important clinical and commercial applications.

I would further like to acknowledge the Australia and New Zealand Society for Extracellular Vesicles (ANZSEV), including the committees and fellow members, for creating such a welcoming and inspiring community of EV researchers, bolstering ECRs and providing numerous opportunities to engage in the functions of the society. I have had the privilege of serving on the ECR subcommittee, which has allowed me to develop connections with other ECRs all around the country and in NZ, to gain valuable experience in hosting events and workshops that aim to benefit fellow ECRs, and to assist with the planning and delivery of the annual meeting in my home state. I am grateful that these activities have ultimately helped to build my leadership qualities and confidence among the broader scientific community beyond my lab.

It would not be possible to engage so committedly in my professional development without the funding support from both the Australian Government Research and Training Program Scholarship providing a stipend and offset of fees, and additional Scholarship Top-up from Flinders University, so I sincerely thank each of these sources.

Last but not least, to my loved ones, you all share in this achievement as I would be nowhere if it were not for you. I am indebted to your everlasting support, encouragement, comfort and unconditional love, to your shared value of learning and discovery and to your tolerance for the periods in which I was incapable of thinking or talking about anything other than my work. My parents and grandparents, I thank you for all you have done to minimise the pressure on me with simple acts of generosity and kindness, and to my partner and close friends for creating richness in my life outside of study to retreat into and re-equilibrate. To my twin sister Elise, bouncing ideas off one another has always been my favourite part of studying. Thank you for giving me the space and time to think out loud and discuss my work in more detail than you could ever genuinely care about, just because you know how useful it is for me to talk it out with you. Infallibly, you have inspired me to be the best version of myself and to cultivate resilience over many years. In the absence of judgement, with deep empathy and immunity to vaingloriousness, no one can compare to the way you have helped me to embrace my achievements, learn from my mistakes and step into my confidence.

LIST OF PUBLICATIONS AND PRESENTATIONS

Peer-reviewed publications resulting from the thesis

Newman LA, Useckaite Z, Wu T, Sorich MJ, Rowland A. 2023. Analysis of Extracellular Vesicle and Contaminant Markers in Blood Derivatives Using Multiple Reaction Monitoring. In: Greening DW, Simpson RJ, editors. *Serum/Plasma Proteomics: Methods and Protocols*. New York, NY: Springer US; p. 301-20.

Newman, L. A., Useckaite, Z. & Rowland, A. 2022c. Addressing MISEV guidance using targeted LC-MS/MS: A method for the detection and quantification of extracellular vesicle-enriched and contaminant protein markers from blood. *Journal of Extracellular Biology*, 1, e56.

Newman, L. A., Useckaite, Z., Johnson, J., Sorich, M. J., Hopkins, A. M. & Rowland, A. 2022. Selective Isolation of Liver-Derived Extracellular Vesicles Redefines Performance of miRNA Biomarkers for Non-Alcoholic Fatty Liver Disease. *Biomedicines*, 10, 195.

Newman, L. A., Muller, K. & Rowland, A. 2022. Circulating cell-specific extracellular vesicles as biomarkers for the diagnosis and monitoring of chronic liver diseases. *Cellular and Molecular Life Sciences*, 79, 232.

Newman, L. A., Fahmy, A., Sorich, M. J., Best, O. G., Rowland, A. & Useckaite, Z. 2021. Importance of between and within Subject Variability in Extracellular Vesicle Abundance and Cargo when Performing Biomarker Analyses. *Cells,* 10**,** 485.

Additional peer-reviewed publications during the candidature

Welsh, J. A., Goeberdhan, D. C. I., O'Driscoll, L., Buzas, . I., Blenkiron, C., Bussolati, B., Cai, H., Di Vizio, D., Driedonks T. A. P., Erdbrügger, U., Falcon-Perez, J. M., Fu, Q.-L., Hill, A. F., Lenassi, M., Lim, S. K., Mahoney, M. G., Mohanty, S., Möller, A., Nieuwland, R., … **Newman, L. A.**, … Witwer,

K. W. 2024. Minimal information for studies of extracellular vesicles (MISEV2023): from basic to advanced approaches. *Journal of Extracellular Vesicles*, e12404. https://doi.org/10.1002/jev2.12404

Qiu, R., Fonseca, K., Bergman, A., Lin, J., Tess, D., **Newman, L.,** Fahmy, A., Useckaite, Z., Rowland, A., Vourvahis, M. & Rodrigues, D. 2024. Study of the Ketohexokinase Inhibitor PF-06835919 as a Clinical Cytochrome P450 3A Inducer: Integrated Use of Oral Midazolam and Liquid Biopsy. *Clinical and Translational Science*, 17, e13644.

Useckaite, Z., **Newman, L. A.**, Hopkins, A. M., Klebe, S., Colella, A. D., Chegeni, N., Williams, R., Sorich, M. J., Rodrigues, A. D., Chataway, T. K. & Rowland, A. 2023. Proteomic Profiling of Paired Human Liver Homogenate and Tissue Derived Extracellular Vesicles. Proteomics, e2300025.

Rodrigues AD, van Dyk M, Sorich MJ, Fahmy A, Useckaite Z, **Newman LA**, et al. 2021. Exploring the Use of Serum-Derived Small Extracellular Vesicles as Liquid Biopsy to Study the Induction of Hepatic Cytochromes P450 and Organic Anion Transporting Polypeptides. *Clin Pharmacol Ther*.

Useckaite Z, Rodrigues AD, Hopkins AM, **Newman LA**, Johnson JG, Sorich MJ, et al. 2021. Role of extracellular vesicle derived biomarkers in drug metabolism and disposition. *Drug Metabolism and Disposition.* 49(11):961.

Presentations given during the candidature

Australia and New Zealand Society for Extracellular Vesicles (ANZSEV) Conference

Barossa Valley, South Australia, Australia, 2023.

Oral presentation: *Application of liver specific extracellular vesicles as liquid biopsy for metabolic associated fatty liver disease.*

Australia and New Zealand Society for Extracellular Vesicles (ANZSEV) Education Day

Adelaide, South Australia, Australia, 2023.

Oral presentation: *EV Biogenesis and Isolation Strategies.*

Invited Seminar, Pfizer Groton

Groton, Connecticut, USA, 2023

Oral presentation: *Applications of extracellular vesicles in tracking liver function and impact of disease.*

International Society for Extracellular Vesicles (ISEV) Annual Meeting

Seattle, Washington, USA, 2023.

Poster presentation: *Application of liver-specific extracellular vesicles to track changes in drug clearance in patients with metabolic associated fatty liver disease.*

Agilent LCMS User Group Meeting

Adelaide, South Australia, 2023

Oral presentation: *Targeted proteomics of extracellular vesicles using Agilent QQQ LCMS.*

Australia and New Zealand Society for Extracellular Vesicles (ANZSEV) Conference

Gold Coast, Queensland, Australia, 2022.

Poster presentation: *Addressing MISEV guidance using targeted LC-MS/MS: A method for the detection and quantification of extracellular vesicle-enriched and contaminant protein markers from blood.*

International Society for Extracellular Vesicles (ISEV) Annual Meeting

Held virtually, 2021.

Poster presentation: *Comparative analysis of miRNA biomarkers in total circulating RNA and vesicular RNA from global and liver-derived extracellular vesicles in non-alcoholic fatty liver disease.*

LIST OF FIGURES

LIST OF TABLES

LIST OF ABBREVIATIONS

Abbreviation	Definition
AASLD	American Association for the Study of Liver Diseases
ACACA	Acetyl-CoA carboxylase 1
ACACB	Acetyl-CoA carboxylase 2
ADME	Absorption, distribution, metabolism and excretion
AFP	Alpha-fetoprotein
AH	Alcoholic hepatitis
aHSC	Activated hepatic stellate cell
ALB	Albumin
ALD	Alcoholic liver disease
ALIX	ALG-2 interacting protein
ALT	Alanine transaminase
ANOVA	Analysis of Variance
AOC3	Membrane primary amine oxidase
ARF6	ADP-ribosylation factor 6
ASGR1	Asialoglycoprotein receptor 1
ASGR2	Asialoglycoprotein receptor 2
AST	Aspartate aminotransferase
AU	Arbitrary units
AUC	Area under the curve
AUROC	Area under the receiver operator characteristic curve
BCA	Bicinchoninic acid
BLOQ	Below limit of quantification
BMI	Body mass index
BSA	Bovine serum albumin
CANX	Calnexin
CCR5	C-C motif chemokine receptor 5
CD	Cluster of differentiation protein
CES1	Carboxylesterase 1
CES2	Carboxylesterase 2
CI	Confidence interval
CTRL	Control
CV	Coefficient of variance
CYP	Cytochrome P450
DDIs	Drug-drug interactions
DGAT2	Diacylglycerol O-acyltransferase 2

DILI	Drug induced liver injury
DME	Drug metabolising enzyme
DMET	Drug metabolising enzymes and transporters
DNA	Deoxyribonucleic acid
DTT	Dithiothreitol
ECM	Extracellular matrix
EDTA	Ethylenediaminetetraacetic acid
ELF	Enhanced liver fibrosis
EMV	Electron multiplier voltage
ER	Endoplasmic reticulum
ESCRT	Endosomal sorting complex required for transport
ESI	Electrospray ionisation
EV	Extracellular vesicle
EV-TRACK	Extracellular Vesicle - Transparent Reporting and Centralising Knowledge
FASN	Fatty acid synthase
FIB-4	Fibrosis 4 index
GCP	Good clinical practice
GGT	Gamma-glutamyl transpeptidase
GLP1R	Glucagon-like peptide 1 receptor
HbA1c	Glycated haemoglobin
HBV	Hepatitis B
HCl	Hydrochloric acid
HCV	Hepatitis C
HDL	High-density lipoproteins
HLM	Human liver microsomes
HR	Hazard ratio
HSD17B13	Hydroxysteroid dehydrogenase 17 beta 13
IAA	Iodoacetamide
IAC	Immunoaffinity capture
IDL	Intermediate density lipoprotein
ILV	Intraluminal vesicle
IP	Immunoprecipitation
IR	Insulin resistance
ISEV	International Society for Extracellular Vesicles
KCl	Potassium chloride
KDa	Kilodalton
KHK	Ketohexokinase
L-HMG	Liver tissue homogenate

LC-MS	Liquid chromatography - mass spectrometry
LDL	Low density lipoproteins
LGALS3	Galectin 3
LLOQ	Lower limit of quantification
LOD	Limit of detection
LOXL2	Lysyl oxidase like 2
LSEC	Liver sinusoidal endothelial cells
LT-EV	Liver tissue extracellular vesicles
MAFLD	Metabolic associated fatty liver disease
MAP3K5	Mitogen activated protein kinase kinase kinase 5
MDF	Maddrey discriminant function
MELD	Model for end-stage liver disease
MFI	Mean fluorescence intensity
MIFlowCyt-EV	Minimal information about a flow cytometry experiment on EVs
miRNA	Micro ribonucleic acid
MISEV	Minimal Information for the Study of Extracellular Vesicles
MRM	Multiple reaction monitoring
mRNA	Messenger ribonucleic acid
MS	Mass spectrometry
MS/MS	Tandem mass spectrometry
MV	Microvesicle
MVB	Multivesicular bodies
MW	Molecular weight
NAFL	Non-alcoholic fatty liver
NAFLD	Non-alcoholic fatty liver disease
NASH	Non-alcoholic steatohepatitis
nFC	Nano flow cytometry
NFS	NAFLD fibrosis score
NK	Natural killer
nPES	Nano-plasmonic enhanced scattering assay
NTA	Nanoparticle tracking analysis
OATP	Organic anion transporting polypeptides
OR	Odds ratio
PBS	Phosphate buffered saline
PCR	Polymerase chain reaction
PD	Pharmacodynamic
PK	Pharmacokinetic
PM	Plasma membrane

POCT	Point of care testing
PPARA	Peroxisome proliferator activated receptor alpha
PPARG	Peroxisome proliferator activated receptor gamma
PVDF	Polyvinylidene difluoride
QC	Quality control
qHSC	Quiescent hepatic stellate cell
qPCR	Quantitative polymerase chain reaction
QQQ	Triple quadrupole
RIPA	Radioimmunoprecipitation assay buffer
RNA	Ribonucleic acid
RPMI	Roswell park memorial institute
RQ	Relative quantities
RSD	Relative standard deviation
RT	Room temperature
RT	Retention time
RT-qPCR	Reverse transcription- quantitative polymerase chain reaction
SAHREC	Southern Adelaide Human Research Ethics Committee
SD	Standard deviation
SEC	Size exclusion chromatography
sEV	Small extracellular vesicle
SIL	Stable isotope labelled
TEM	Transmission electron microscopy
Tris-HCl	Tris buffered hydrochloric acid
TSG101	Tumour susceptibility gene 101
UC	Ultracentrifugation
UGTs	Uridine 5'-diphospho-glucuronosyltransferase
VLDLs	Very low density lipoproteins

CHAPTER 1

INTRODUCTION: CIRCULATING CELL-SPECIFIC EXTRACELLULAR VESICLES AS BIOMARKERS FOR THE DIAGNOSIS AND MONITORING OF CHRONIC LIVER DISEASES

Author Contributions

This chapter is published in *Cellular and Molecular Life Sciences* (Appendix 1). The manuscript appears in this thesis unchanged from the peer-reviewed version. I was the first and sole primary contributing author and contributed to conceptualisation, preparation of the first draft, reviewing and editing, culminating in approximately 90% of the work. The additional two co-authors reviewed the paper and contributed to conceptualisation and editing of the paper.

Overview

Chronic liver diseases represent a significant global health burden that is set to grow in the coming decades (Chen et al., 2018b, Moon et al., 2020). Alcohol-related liver disease and non-alcoholic fatty liver disease (NAFLD) are two of the most common aetiologies and are precipitated, respectively, by excessive alcohol consumption and the combination of high calorie diet and sedentary lifestyle (Povero et al., 2020, Hernández et al., 2020). The growing prevalence of NAFLD, in particular, parallels that of obesity, type 2 diabetes and other features of metabolic syndrome (Newman et al., 2020). The pathology of each of these disorders, as well as chronic infection with hepatitis B (HBV) or hepatitis C (HCV) viruses, manifest inflammatory and pro-fibrogenic processes in the liver that may progress to cirrhosis and hepatocellular carcinoma (HCC). Accordingly, chronic liver disease is a leading cause of mortality in many parts of the world (Wong et al., 2019, Li et al., 2020).

By way of example, independent of other factors, the average all-cause mortality among NAFLD patients is 11.7% higher compared to individuals without the disease (hazard ratio (HR) 1.93

[1.86-2.00]). The impact of NAFLD on mortality increases with increasing disease severity and ranges from 8.3% (HR 1.71 [1.64-1.79]) for simple steatosis up to 18.4% (HR 2.44 [2.22 – 2.69]) for non-alcoholic steatohepatitis (NASH) with fibrosis (Simon et al., 2020). Adding to the challenge, the capacity to treat NAFLD diminishes with increasing disease severity. Targeted weight loss slows progression in mild disease, but is less effective in moderate to severe disease (Ando and Jou, 2021). Importantly, while there have been considerable breakthroughs in the prevention and treatment of viral hepatitis in recent years (Almeida et al., 2021), no medicine is currently approved for NAFLD and progress has been slow with costly failures in late phase trials due to an inability to easily monitor treatment response.

Despite significant shortcomings in accuracy and practicality, liver biopsy remains the gold standard diagnostic tool to assess the presence and stage of various liver diseases. This technique is currently the most reliable way to determine the pattern and severity of inflammation and fibrosis (Mann et al., 2018). For patients with NAFLD, a diagnosis of the more severe form steatohepatitis (NASH) can only be made by histological identification of cardinal features, such as hepatocellular ballooning and lobular inflammation (Newman et al., 2020). Since liver biopsy is a highly invasive technique, it comes with the risk of severe complications and cannot be regularly repeated to track changes in the liver over time (Povero et al., 2020). Moreover, the technique is associated with considerable interobserver and sampling variability, produces only a limited representation of total liver tissue and, consequently, often underestimates disease severity (Sumida et al., 2014). These issues limit its widespread and repeated use and give rise to the urgent need for non-invasive biomarkers, to aid diagnosis and monitoring of patients with chronic liver disease. Currently, various scoring systems may be applied to non-invasively stratify patient risk, such as FIB-4 index, Maddrey Discriminant Function (MDF) and Model for End-stage Liver Disease (MELD), which rely on blood biochemistry. Non-invasive diagnoses may employ imaging studies (e.g. magnetic resonance imaging and ultrasound) (Sehrawat et al., 2021, Wong et al., 2018) and liver stiffness may be assessed via transient elastography (e.g. FibroScan) to estimate the degree of fibrosis (Petta et al., 2015).

In 2019 the American Association for the Study of Liver Diseases identified the insufficient performance of these current non-invasive tools to diagnose early disease and track progression as the critical barrier to treating chronic liver diseases (Younossi et al., 2019). The limitation being these approaches lack specificity and sensitivity, particularly for mild and early disease. To meet this demand, considerable research effort has focussed on the development of blood-based biomarkers that can reflect early pathological processes, disease progression and response to treatment (Mann et al., 2018). In recent times, circulating extracellular vesicles (EVs) have emerged as a potential source of such biomarkers. These nanosized particles contain a distinct molecular signature of protein, RNA and lipid moieties, that is both indicative of their cell type of origin, and also the homeostatic or pathological stimuli that induced their release (Eguchi et al., 2017). EVs are shown to play a role in immune modulation and autoimmune disease, tissue repair, neurodegenerative disease, cardiovascular disease and the development and proliferation of tumours (Koeck et al., 2014). A breadth of work now evidences the crucial biological activities of EVs in multiple facets of chronic liver pathophysiology, including the cell injury, inflammation and fibrosis shared across diverse aetiologies (Newman et al., 2020). Technological developments in high-throughput multi-omics approaches promise to unveil the intricacies of EV molecular cargo and streamline the clinical application of highly sensitive, disease-specific biomarkers (Gho and Lee, 2017).

The purpose of this review is to summarise the key works that establish how EVs contribute to normal liver physiology and processes central to the development and progression of chronic liver diseases. The current state and future direction of circulating EV biomarker analyses will also be explored, with a particular focus on techniques to selectively isolate and analyse cell- or tissue-specific EVs for the detection and tracking of chronic liver diseases.

Extracellular Vesicles

EVs are a heterogenous population of small, non-replicating, membrane-encapsulated particles, released by virtually all cell types. Alongside soluble factors and signalling molecules, they have emerged as a fundamental constituent of the cellular secretome (Sung et al., 2018). Regular

release under basal conditions contributes to the maintenance of homeostasis, while changes to the magnitude and composition of EVs communicate responses to stressful or pathological stimuli between neighbouring and distant cells. Signalling is mediated by receptor-ligand interactions on the EV and cell surfaces, which may directly trigger intracellular pathways or result in the fusion or internalisation of vesicles and their associated cargo (Chen et al., 2014). The importance of the role of EVs in intercellular communication is underscored by its evolutionary conservation (Mann et al., 2018). Signalling or regulatory molecules transferred in this way are stable and protected from degradation, may be transported through the systemic circulation to distant organs and can easily be taken up by target cells. Notably, the expression of specific surface proteins, such as integrins, promote homing of EVs to target recipient cells (Malhi, 2019).

EV Subtypes

As the field of EV research has matured, so too has the complexity of defining distinct EV subpopulations. Vesicles secreted not only by different cell types, but also from the same cell, possess inherent heterogeneity in physical and biochemical properties (Gho and Lee, 2017). Conventionally, EV subtypes are characterised based on their mode of biogenesis. Exosomes, typically 50-150 nm in diameter, are produced via the endosomal pathway. Inward protrusions of the early endosomal membrane create intraluminal vesicles (ILVs) which leads to the formation of multivesicular bodies (MVB). MVB trafficking and fusion to the plasma membrane results in the extracellular release of ILVs, thereby giving rise to exosomes. The production of exosomes may be dependent or independent of the endosomal sorting complex required for transport (ESCRT) machinery. ESCRT -0, -I, -II, and -III protein complexes associate sequentially to facilitate membrane fission and loading of EV cargo (Malhi, 2019). ESCRT-independent exosome release occurs via the production of ceramide and sphingolipid membrane rafts and the activity of neutral sphingomyelinase 2 (Mathieu et al., 2019). Alternatively, microvesicles (MVs), 100-1000 nm in size, are shed directly from the plasma membrane. Specific membrane domains are enriched with proteins that permit curvature and budding via higher order oligomerisation and rearrangement of actin-cytoskeletal networks. ESCRT proteins and ceramides are also implicated in MV formation, in addition to ADP-ribosylation factor 6 (ARF6) which participates in cargo selection (Malhi, 2019). MV formation is

highly dependent on calcium influx and amenable to activation by cell stress (Greening and Simpson, 2018, Tetta et al., 2011).

Given the challenge of identifying the exact intracellular origin of EVs isolated from the extracellular milieu, other characteristics such as size, density and expression of specific surface markers are employed to distinguish EV subpopulations. Though, a recent report of comprehensive EV proteomic characterisation revealed significant heterogeneity in marker expression within subtypes, particularly amongst small EVs with or without endosomal origin (Kowal et al., 2016). Importantly, most of the commonly used isolation techniques produce a mixture of vesicle populations of varying purity and enrichment. Accordingly, current guidance imparted by the Minimal Information for the Study of Extracellular Vesicles (MISEV) (Théry et al., 2018), states that isolates should be described generically as “extracellular vesicles”, but may be classified as small EVs (<200 nm) or medium/large EVs (>200 nm), by specific molecular components (e.g. ASGR1+ EV) or by cell of origin (hepatocyte-derived EV). It should be noted that for the purpose of biomarker discovery, rigorous separation of EV subtypes may only be necessary to the degree to which sufficient sensitivity and specificity can be achieved.

EV Composition and Cargo

EVs contain biologically functional cargo, comprised of proteins (including metabolically active enzymes), lipids, metabolites and nucleic acids, such as messenger RNA, microRNA, long non-coding RNA and DNA (Jeppesen et al., 2019) (Figure 1.1). EV-enriched proteins are largely derived from their pathways of biogenesis. Tetraspanins (CD63, CD81 and CD9) and human leukocyte antigen class 1 (HLA-I) are transmembrane proteins commonly found in EV membranes, while tumour susceptibility gene 101 (TSG101), ALG-2 interacting protein (ALIX) and syntenin are cytosolic proteins involved in EV formation that are ultimately exported in vesicles (Théry et al., 2018). In addition to general markers of EVs, cell type-specific proteins expressed on cell membranes may be integrated into the membrane of secreted EVs (Larssen et al., 2017). The identification of cell-type specific surface proteins on EVs has been exploited for immunoaffinity-based isolation of cell- or tissue- specific EVs from the global circulating pool. This has vast potential

to improve the sensitivity and specificity of low abundance and ubiquitously expressed disease biomarkers against the background noise resulting from constitutive systemic EV release.

Current evidence for the selective packaging of EV molecular cargo is supported by high variability and discordance in protein and RNA levels between EVs and their parental cell (Li et al., 2020, Malhi, 2019). While the exact mechanisms for regulated sorting of cargo remain unclear, the roles of various RNA-binding proteins, Rab GTPases, and post-translational modifications, such as ubiquitination and phosphorylation, have been reported (Kostallari et al., 2018, Greening and Simpson, 2018). The abundance and composition of EVs may be altered in response to ER stress (Dasgupta et al., 2020) or phenotypic activation. Li et al. (2020) demonstrated that, compared to quiescent hepatic stellate cells, EV were released at 4.5-fold greater rate upon transdifferentiation to a myofibroblastic phenotype, and contained more abundant proteomic information associated with extracellular matrix production and metabolic activity.

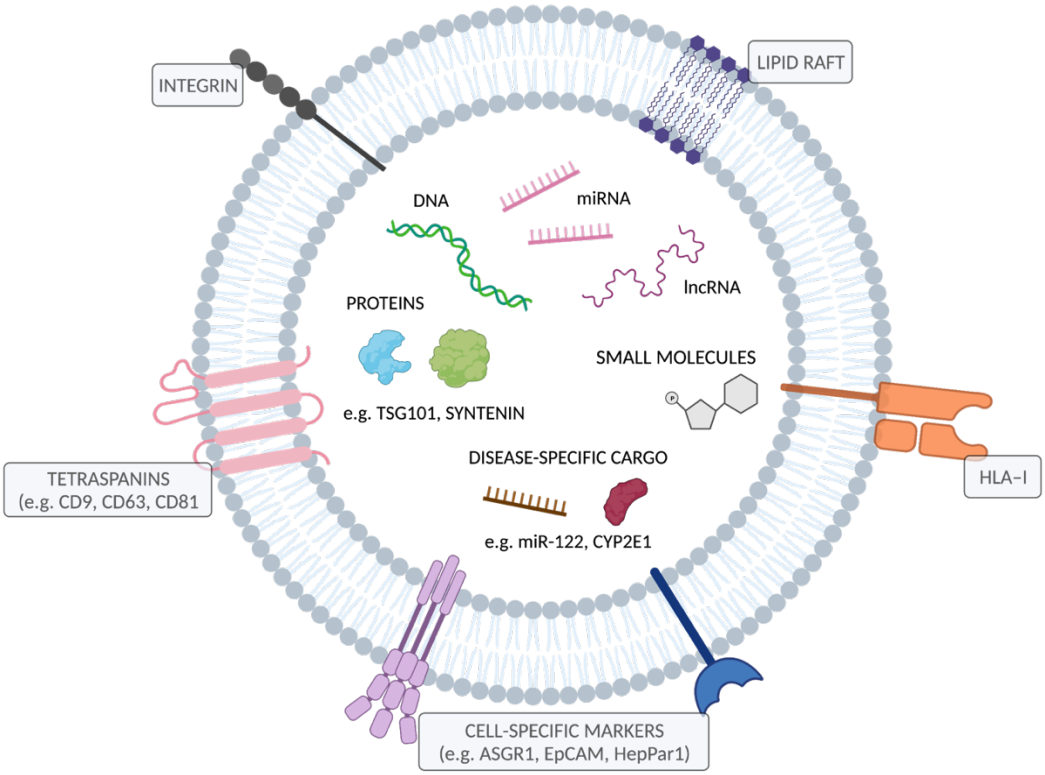

Figure 1.1 Structure and cargo of an extracellular vesicle.
Figure was created using BioRender.com.

EVs as Minimally Invasive Biomarkers

EVs are considered attractive biomarkers for a host of reasons. Vesicles are abundant and highly stable in biofluids, exhibiting longer half-lives than other circulating components, such as free proteins or RNA complexes (Sung et al., 2018). Durable lipid bilayer membranes protect molecular cargo from degradation, thereby providing a sort of “biomarker reservoir” (Sun et al., 2020). Since this diverse cargo is dynamic in nature, directly related to the phenotype of parent cells, it may be used to understand function at the organ, tissue or cellular level and track changes in real time. In line with this application, and in contrast to traditional tissue biopsy, sampling of EVs is easily performed through access to peripheral blood and is repeatable with minimal patient risk. As will be explored throughout this review, the pertinence of EVs as a biomarker source is underpinned by the biological activity of these entities across elements of chronic liver disease. These mechanistic links may be the key to establishing a disease-specific molecular signature from affected tissues. Notably, changes in EVs have been demonstrated at earlier stages than overt tissue damage or other clinical and histological signs (Li et al., 2019). However, as total blood EV is comprised of vesicles released from multiple tissues into the circulation, the development of biomarker strategies is increasingly geared towards selective analysis based on tissue-specific markers (Shah et al., 2018).

EV-based Therapeutics

In addition to their role as a key diagnostic and monitoring tool for the treatment of liver diseases, the application of EVs as a therapeutic intervention for multiple forms of liver disease has emerged. The properties of EV membranes make them ideal vehicles for therapeutic cargo, including miRNA, small interfering RNA (siRNA), chemotherapy agents or other drugs, which may act to promote tissue regeneration, reduce or reverse inflammation and fibrosis, or target cancer cells in the liver. Promising results have been demonstrated regarding the use of mesenchymal stem cell-derived EVs in various pre-clinical models. However, the requirements to initiate human trials are very different between a biomarker and an intervention. EV-based therapeutics face several challenges related to the cost and scale of manufacturing pure EVs that adhere to regulatory and quality control standards for use in humans. Meanwhile, much of the recent research regarding the role of EVs as biomarkers has come from human data. Beyond pre-clinical studies identifying EV cargo that reflect molecular changes in liver diseases, a key focus of the present review is the

detection of circulating EVs in human patients. Thus, the application of EVs as therapeutics will not be extensively reviewed here but may be found in references (Bruno et al., 2020, Malhi, 2019, Szabo and Momen-Heravi, 2017).

EVs in Normal Liver Physiology

The liver is the largest internal organ in the body, functionally and anatomically complex and responsible for a diverse set of metabolic, synthetic, digestive, detoxifying, storage and regulatory roles. Approximately 80% of total liver volume is comprised of hepatocytes, which are responsible for the central physiological processes, while a further 6.5% accounts for non-parenchymal cells that function in support of hepatocytes and maintenance of the hepatic microenvironment (Sung et al., 2018, Azparren-Angulo et al., 2021). These cells include liver sinusoidal endothelial cells (LSECs), hepatic stellate cells (HSCs), cholangiocytes and the population of liver-resident macrophages, known as Kupffer cells. The organised lobular architecture of the liver facilitates cooperation and inter-regulatory functions of diverse cell types through anatomical proximity (Giugliano et al., 2015). Effective cell-to-cell communication is also achieved by the network of EV interactions, as each cell is both a donor and recipient of EVs from the same and other hepatic cell types (Figure 1.2). The bi-directional transfer of molecular information is imperative to homeostatic control in the liver as well as the broader inter-organ communicative landscape.

Hepatic cell-derived EVs

The function of EVs derived from different hepatic cell types is summarised in Table 1.1. Multiple enzymes involved in the metabolism of carbohydrates, lipids, endogenous compounds and xenobiotics are among key molecular cargo identified in hepatocyte-derived EVs (Conde-Vancells et al., 2008). Hepatic metabolic activity may be transferred to or induced in extra-hepatic niches. For example, hepatocyte-derived EVs carrying arginase-1 were found to regulate endothelial cell function and alter serum metabolites associated with oxidative stress in the systemic vasculature (Royo et al., 2017). In the liver, hepatocyte-EVs have also been shown to promote the proliferation of cholangiocytes and other hepatocytes in paracrine and autocrine fashions, respectively

(Azparren-Angulo et al., 2021, Cai et al., 2017). Hepatocyte-derived EVs have demonstrated the remarkable capacity to mediate regeneration of functional liver mass. Nojima et al. (2016) EV-mediated transfer of sphingosine-1-phosphate (S1P), sphingosine kinase 2 (SK2) and ceramidase between hepatocytes promoted liver regeneration in mice following 70% hepatectomy. HSC are the key fibrogenic cells in the liver, and exchange of EVs between them is crucial in balancing extracellular matrix (ECM) production and degradation. LSEC-derived EVs contribute to modulation of this balance. The EVs normally maintain HSC quiescence, but when stimulated, EVs containing upregulated sphingosine kinase 1 (SK1) are released in order to activate HSC (Wang et al., 2015). Quiescent HSC (qHSC) release EVs containing miRNAs (miR-214 and -199-5p) and the transcription factor, Twist-1 (Chen et al., 2016, Chen et al., 2015). This cargo suppresses connective tissue growth factor (CTGF) to maintain quiescence in other qHSC or downregulate pro-fibrotic genes, including α-smooth muscle actin (αSMA) and collagen, in activated HSC (aHSC) (Li et al., 2020, Chen et al., 2014). Conversely, aHSC-derived EVs promote ECM production by transferring CTGF (Charrier et al., 2014). Lastly, EVs from cholangiocytes participate in bile acid homeostasis through the transfer of long non-coding RNA H19 to hepatocytes (Li et al., 2018), and in wound-healing responses by delivering hedgehog ligands to promote angiogenesis, growth and differentiation in recipient LSECs (Witek et al., 2009).

Table 1.1 Hepatic cell EVs function and cargo.

Originating cell	Example cargo	Recipient cells	Functions	Reference
Hepatocytes	DMET proteins and mRNA	Hepatocytes, extrahepatic cells	Transfer metabolic activity	Conde-Vancells et al. (2008) Kumar et al. (2017) Rowland et al. (2019) Rodrigues et al. (2021)
	Arginase-1	Endothelial cells	Regulate endothelial cells in systemic vasculature	Royo et al. (2017)
	S1P, SK2, ceramidase	Hepatocytes	Promote proliferation and liver regeneration	Nojima et al. (2016)
Liver Sinusoidal Endothelial Cells	SK1	HSC	Modulate quiescent/active phenotype	Wang et al. (2015)
Hepatic Stellate Cells	miR-214, miR-199-5p, Twist-1, CTGF	HSC	Modulate quiescent/active phenotype	Charrier et al. (2014) Chen et al. (2014) Chen et al. (2015) Chen et al. (2016) Li et al. (2020)
Cholangiocytes	lncRNA H19	Hepatocytes	Regulate bile acid homeostasis	Li et al. (2018)
	Hedgehog ligands	LSEC	Promote wound healing response	Witek et al. (2009)

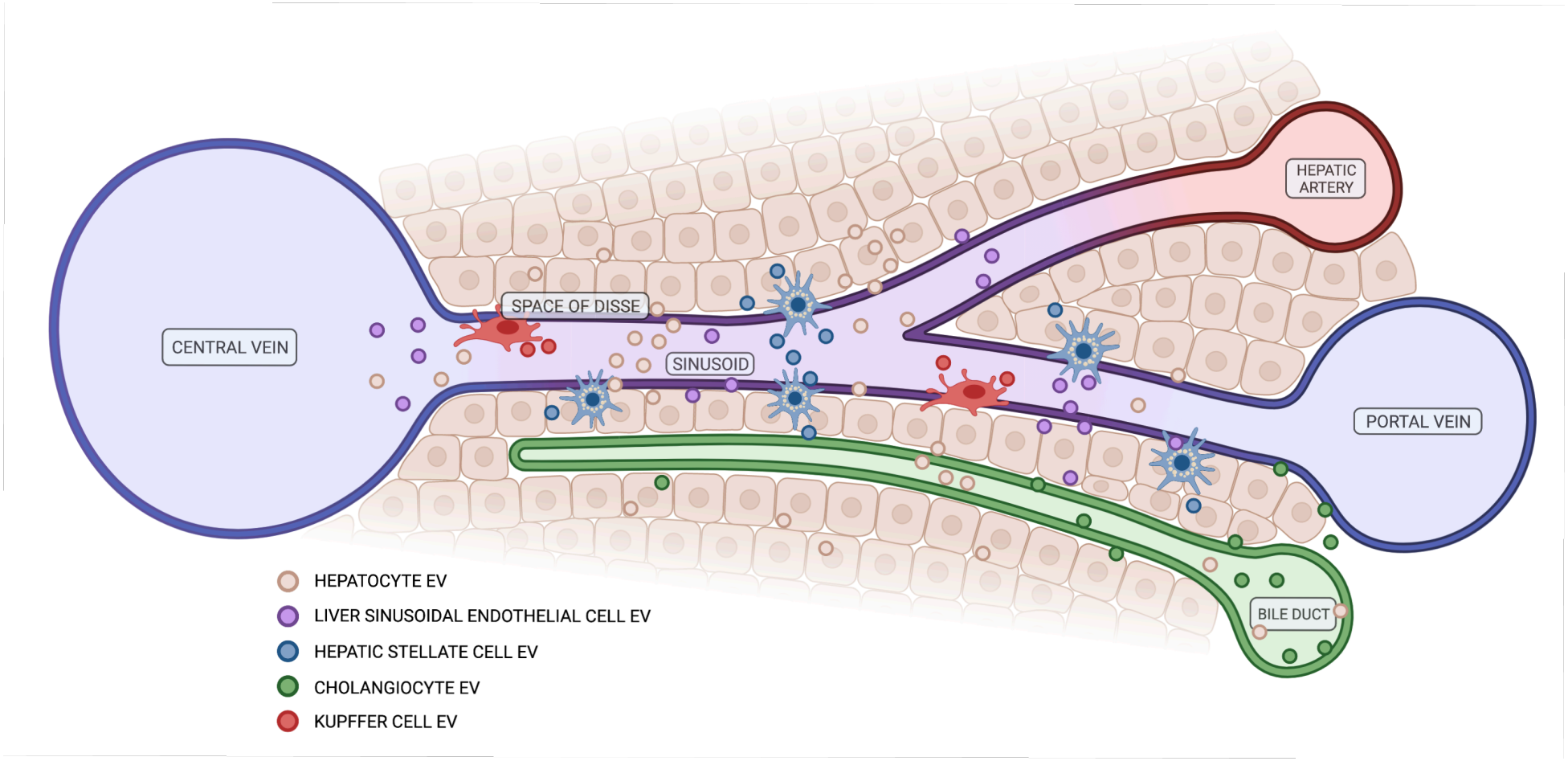

Figure 1.2 Extracellular vesicles released by various hepatic cells in normal liver function.

Figure was created using BioRender.com.

Metabolism

Hepatic metabolism plays a critical role in regulating the abundance of endogenous chemicals, such as bile acids, fatty acids, steroid hormones and bilirubin. Similarly, it serves as a major clearance mechanism for xenobiotics including drugs, dietary chemicals and environmental toxins. Specifically, metabolic clearance is the major route of elimination for more than 80% of pharmaceutical drugs (Achour et al., 2021, Rodrigues and Rowland, 2019). Notably, the mRNA transcripts and active proteins of drug metabolising enzymes and transporters (DMET), cytochrome P450 (CYPs), UDP-glucuronosyltransferase (UGTs), glutathione S-transferase and organic anion transporting polypeptides (OATPs) have been detected in EVs derived from hepatocytes and in the blood. CYP protein and mRNA is enriched in circulating EVs relative to total plasma, which suggests selective packaging (Kumar et al., 2017, Rowland et al., 2019, Rodrigues et al., 2021). The transfer of DMET in circulating EVs has physiological significance with respect to protection of extra-hepatic cells from systemic toxicants or increasing metabolic activity in tissues with lower basal DMET expression, such as the lungs or brain (Gerth et al., 2019). Clinically, this notion has potential applications as liquid biopsy to indicate chronic alcohol, nicotine or illicit drug use, liver disease, or to assess metabolic drug-drug interactions (DDIs) and inter-individual variability in drug exposure. For example, CYP2E1 is induced by chronic use of alcohol or paracetamol overdose. This is reflected in greater release of hepatocyte EVs that transfer the capacity for CYP2E1-mediated metabolism, resulting in oxidative stress and acute injury in hepatic and non-hepatic cells (Kumar et al., 2017). A recent review described how disease-associated alterations in CYP protein expression and activity may impact drug exposure in patients with NAFLD (Jamwal and Barlock, 2020). The capacity to monitor changing pharmacokinetic profile is paramount for the development of novel therapeutics for NAFLD and in optimal dosing of existing treatments for common comorbidities.

Assessing variability in metabolic clearance within or between individuals, resulting from variable hepatic DMET expression or activity, DDIs, presence of liver disease or other factors, is an appealing avenue for EV-based DMET profiling. Work by our group showed that EV-derived CYP3A4 was highly concordant with apparent oral clearance of its probe substrate midazolam in healthy subjects pre- and post- dosing of the inducer, rifampicin (Rowland et al., 2019). Since then, Achour

et al. (2021) evaluated hepatic elimination based on circulating EV mRNA of clinically important DMET, reporting sound correlations with protein expression in liver tissue. Interestingly, this study normalised the data to a panel of 13 liver-specific RNA markers (e.g. apolipoprotein A2 and fibrinogen-beta) as part of a novel shedding factor to account for variability in liver EV release into the bloodstream. Instead, we recently applied our novel two-step anti-ASGR1 immunocapture technique to selectively isolate hepatocyte-derived EVs from global EVs and successfully tracked the induction of CYPs 3A4, 3A5 and 2D6 and OATPs 1B1 and 1B3 during pregnancy and following rifampicin administration (Rodrigues et al., 2021). Together these reports position EV liquid biopsy as a viable strategy for individual DMET phenotyping to aid precision dosing or classification of clinical trial participants at enrolment.

EVs in Liver Pathobiology

Chronic liver diseases result from prolonged injurious stimuli that exceed the regenerative capacity of the liver. Over time, unresolved inflammatory and fibrogenic activation from disorders such as ALD, NAFLD, HBV and HCV infection can ultimately lead to fibrosis, cirrhosis and HCC (Sung et al., 2018). EVs have emerged as potent pathogenic drivers in several of these processes and a breadth of pre-clinical data establishes the key molecular information carried in EVs that mediate liver cell cross-talk in different chronic liver diseases. In several instances, these EV cargoes have been analysed in the circulation of animal models or human patients and demonstrate the capacity for circulating EVs derived from specific cellular sources to reflect pathological events in affected organs. For each chronic liver disease, Table 1.2 lists the cell-specific EVs and their cargoes, with recipient cells and resulting function (if defined), divided into studies that examined EVs in circulation (green) and *in vitro* studies of EV cargo yet to be translated to circulating EVs (grey).

Table 1.2 EV cargo from specific cellular origins, effect on recipient cells and detection in circulation in chronic liver diseases.

Condition	Originating cell / source	Cargo	Recipient cells	Function	Additional information	Reference
NAFLD	***Cargo detected in circulating EVs***					
	Hepatocytes	miR -122, -192, -128-3p	N/A	N/A	Increased in plasma of NAFLD patients	Newman et al. (2022b)
	Hepatocytes	mtDNA	N/A	TLR9 activation -> inflammation	Increased in plasma of NASH patients and mouse model	Garcia-Martinez et al. (2016)
	Hepatocytes	ASGR1, CYP2E1	N/A	N/A	Increased in plasma of mice over-expressing IRE1α	Dasgupta et al. (2020)
	Adipocytes	miR-99b	Hepatocytes	Suppress FGF-21 -> promotes steatosis	Demonstrated transfer of cargo via circulation in mice with genetically altered miRNA processing in adipocytes	Thomou et al. (2017)
	Hepatocytes Macrophages Neutrophils Platelets	ASGR1, CYP2E1 Galectin 3 Ly-6G/6C CD61	N/A	N/A	Increased in NAFLD mouse model	Li et al. (2019)
	Hepatocytes	ASGR1, SLC27A5	N/A	N/A	Increased in NASH patient serum	Povero et al. (2020)
	NK T-cells Macrophages	Valpha24/Vbeta11 CD14	N/A	Inflammation	Increased in NAFLD patient serum	Kornek et al. (2012)
	Hepatocytes	ASGR2, CYP2E1	N/A	N/A	Decreased in patients with NAFLD resolution	Nakao et al. (2021)
	Hepatocytes	ASGR1, HepPar1	N/A	N/A	Decreased in patients with bariatric surgery	Rega-Kaun et al. (2019)
	Cargo not yet analysed in circulating EVs					
	Lipotoxic hepatocytes	TRAIL	Hepatocytes, macrophages	Hepatocyte death, macrophage activation & pro-inflammatory cytokine (IL-1β, IL-6)	Upregulated, *in vitro*	Hirsova et al. (2016a)
	Lipotoxic hepatocytes	CXCL10	Macrophages	Macrophage chemotaxis	Upregulated, *in vitro*	Ibrahim et al. (2014) Ibrahim et al. (2016)
	Lipotoxic hepatocytes	C16:0 ceramide, SK1	Macrophages	Macrophage chemotaxis	Upregulated, *in vitro*	Kakazu et al. (2016) Dasgupta et al. (2020)
	Lipotoxic hepatocytes	miR-128-3p	HSC	Suppress PPARγ -> profibrotic gene expression	Upregulated, *in vitro*	Povero et al. (2015)
	Lipotoxic hepatocytes	VNN1	LSEC	Promote pathologic angiogenesis	Upregulated, *in vitro*	Povero et al. (2013)
	Adipocytes	MCP-1, IL-6, MIF	Hepatocytes	Promote insulin resistance	Adipose tissue explant EVs applied to hepatocytes *in vitro*	Kranendonk et al. (2014)

	Adipocytes	miRNA profile	Hepatocytes, HSC	Target TGF-β pathway -> inhibits fibrolytic enzymes e.g. MMP-7	Adipose tissue EVs applied to hepatocytes *in vitro*	Koeck et al. (2014)
ALD	***Cargo detected in circulating EVs***					
	Hepatocytes	mtDNA	Macrophages	TLR9 activation -> pro-inflammatory cytokine release (IL-1β, IL-17)	Increased in murine AH model	Eguchi et al. (2020)
	Hepatocytes	mtDNA	Neutrophils	Neutrophilia, macrophage recruitment to liver	Increased in murine chronic-plus-binge ethanol feeding model	Ma et al. (2020)
	Hepatocytes	CD40 ligand	Macrophages	Phenotypic activation -> Upregulated pro-inflammatory cytokine (IL-1β, IL-6, TNF-α)	Increased in human AH patients	Verma et al. (2016)
	Hepatocytes	miR-122	Monocytes	Suppress haem oxygenase 1 -> sensitise to pro-inflammatory stimuli	Increased in human acute alcohol use and mice binge and chronic alcohol consumption	Momen-Heravi et al. (2015)
	Serum EV	miR -122, -155	N/A	N/A	Increased in EV-fraction of circulation in mice	Bala et al. (2012)
	Serum & plasma EV	let-7f, miR -29a, -340	N/A	Target genes involved in inflammation and cancer development	Increased in mice with AH	Eguchi et al. (2017)
	Hepatocytes	ASGR2, CYP2E1 Sphingolipids	N/A	Promote inflammation and cell death in AH	Increased in AH patient serum	Sehrawat et al. (2021)
Viral Hepatitis	***Cargo detected in circulating EVs***					
	HCV-infected hepatocytes	Replication competent HCV-RNA	Hepatocytes	Viral transmission	Identified in human HCV patients	Bukong et al. (2014)
	HCV-infected hepatocytes	miR-19a	HSC	TGF-β pathway activation -> profibrotic gene expression	Upregulated in human HCV patients	Devhare et al. (2017)
	CD8+ and CD4+ T-cell	CD147	HSC	Induce MMP enzymes -> promote ECM degradation in HCV-related fibrosis	Increased in active HCV patients	Kornek et al. (2011)
	Cargo not yet analysed in circulating EVs					
	HBV-infected hepatocytes	HBV RNA and protein	Peripheral blood monocytes	Induce PDL-1 expression	Identified *in vitro*	Kakizaki et al. (2019)
	HCV-infected hepatocytes	HCV protein E2	N/A	Mimic viral particles -> hinders neutralising antibody response	Identified *in vitro*	Deng et al. (2019)
	LSEC	IFN-stimulated genes	Hepatocytes, LSEC	Promote antiviral response	Identified *in vitro*	Giugliano et al. (2015)
HCC	***Cargo detected in circulating EVs***					
	Malignant hepatocytes	miR-93 miR-224 miR-665	Hepatocytes	Promote HCC proliferation	Each upregulated in human HCC patients	Xue et al. (2018) Cui et al. (2019) Qu et al. (2017)
	Malignant hepatocytes	miR-9-3p miR-638	Hepatocytes	Inhibit HCC proliferation	Each downregulated in HCC patients	Tang et al. (2018) Shi et al. (2018)

		miR-718 miR-744				Sugimachi et al. (2015) Wang et al. (2019)
	Malignant hepatocytes	miR-1247-3p	Fibroblasts	Phenotypic switch to cancer-associated fibroblasts in lung metastasis, increased pro-inflammatory cytokine (IL-6 and IL-8) secretion	Increased in HCC patients with lung metastasis	Fang et al. (2018)
	Tumour (HCC/ICC/PSC) EV in serum	Proteomic signature	N/A	N/A	Differential expression between pathologies and healthy controls	Arbelaiz et al. (2017)
	Tumour (HCC) EV in serum	Annexin V, EpCAM, ASGR1, CD133	N/A	N/A	Panel of markers distinguishes HCC from cholangiocarcinoma	Julich-Haertel et al. (2017)
	Tumour (HCC) EV in plasma	HepPar1	N/A	N/A	Increased with HCC recurrence	Abbate et al. (2017)
	Tumour (HCC) EV in plasma	ASGR1, EpCAM, CD147, 10 mRNA transcripts	N/A	N/A	Differential expression between HCC, other primary malignancies and non-cancer	Sun et al. (2020)
	Cargo not yet analysed in circulating EVs					
	Malignant hepatocytes	miRNA profile	Hepatocytes	Modulate TAK1 pathway -> promote cancer growth	Identified *in vitro*	Kogure et al. (2011)
	Malignant hepatocytes	linc-ROR	Healthy hepatocytes	Inhibit apoptosis and enhance proliferation	Upregulated *in vitro*	He et al. (2019)
	Malignant hepatocytes	MET proto-oncogene, caveolins, S100 family members	Healthy hepatocytes	Mobilisation, tumour invasion	Identified *in vitro*	He et al. (2015)
Fibrosis	***Cargo detected in circulating EVs***					
	Activated HSC	PDGFRα	HSC	Promote migration	Upregulated in human liver fibrosis patients	Kostallari et al. (2018)
	LSEC	SK1, S1P mRNA and protein	HSC	Promote AKT phosphorylation and migration	Upregulated in human AH patients and mice with experimental liver fibrosis	Wang et al. (2015)
	Hepatocytes, activated HSC	Hedgehog ligands	HSC, endothelial progenitor cells	Promote proliferation and angiogenesis	Upregulated in rats undergoing bile duct ligation	Witek et al. (2009)
	Serum EV	miR -34c, -151-3p, -483-5p, -532-5p and -687	Hepatocytes, activated HSC	Decrease hepatocyte death, hepatic fibrosis and inflammation	Downregulated in human liver fibrosis patient and mice with experimental liver fibrosis	Chen et al. (2018b)
	Cargo not yet analysed in circulating EVs					
	Activated HSC	Proteomic profile associated with ECM production and metabolic activity	HSC	Activate HSC, promote fibrogenesis	Identified *in vitro*	Li et al. (2020)

Non-alcoholic Fatty Liver Disease

NAFLD is the most common chronic liver disease, currently estimated to affect more than 25% of the global population (Srinivas et al., 2020). The condition may be considered a hepatic manifestation of the metabolic syndrome as it is often implicated with other features, such as insulin resistance (IR), obesity and type 2 diabetes mellitus (Newman et al., 2020). In line with this, recent expert consensus supports the updated nomenclature of metabolic associated fatty liver disease (MAFLD), to reflect advancing knowledge of disease phenotype, heterogeneity in drivers and coexisting conditions and diagnostic criteria that is based on inclusion rather than exclusion (particularly around alcohol use) (Eslam et al., 2020b, Eslam et al., 2020a).

The condition presents as a spectrum of clinical disease with some patients exhibiting simple steatosis (NAFL) while a fraction (~30%) will develop non-alcoholic steatohepatitis (NASH) (Suzuki and Diehl, 2017). NAFLD is the product of multiple dysregulated signalling pathways in the liver that involves abnormal lipid metabolism leading to lipotoxicity and inflammation (Dasgupta et al., 2020). While several risk factors relating to diet and lifestyle are linked to the incidence of NAFLD, genetic predispositions have also been noted, as recently reviewed by Jonas and Schürmann (2020). Further, the contribution of gut dysbiosis, liver-adipose cross-talk and increased cardiovascular disease-related mortality, underscores the systemic nature of this condition (Zhang et al., 2018). Current diagnostic tools remain inadequate for the early detection, risk stratification and monitoring of NAFL and NASH, presenting a significant hinderance to the clinical management of patients and development of effective pharmaceutical interventions (Younossi et al., 2019).

Numerous reports to date demonstrate changes in EVs released by hepatocytes under lipotoxic stress and their contributions to cellular and inter-organ cross-talk to promote inflammation and fibrosis in the liver. These were described in detail in a previous review (Newman et al., 2020). Key molecular cargo of lipotoxic hepatocyte-derived EVs include the death receptor ligand, TRAIL, which triggers hepatocyte death and macrophage activation with increased pro-inflammatory cytokine expression (interleukin [IL]-1β and IL-6) (Hirsova et al., 2016a). The macrophage chemoattractant C-X-C motif ligand 10 (CXCL10) was also detected in EVs induced by steatosis-related JNK activation in the liver (Ibrahim et al., 2014, Ibrahim et al., 2016). Further, lipotoxic EV

release was found to be dependent on ceramide pathways, activated by the ER stress sensor inositol-requiring enzyme-1α (IRE1α). IRE1α-stimulated EVs contained C16:0 ceramide and SK1 which promoted macrophage chemotaxis *in vitro* (Kakazu et al., 2016) and macrophage recruitment and hepatic inflammation in mice (Dasgupta et al., 2020). The authors also showed that mice over-expressing IRE1α had significantly elevated circulating EVs and their hepatocellular origin was identified by electron microscopy (EM) with immunogold labelling of ASGR1 and CYP2E1. Lipotoxic hepatocyte-derived EVs also modulate HSC phenotype in NAFLD. Specifically, EVs containing miR-128-3p suppressed peroxisome proliferator-activated receptor-γ (PPARγ) in HSC, resulting in upregulated profibrotic gene expression (Povero et al., 2015). The effect was dependent on EV internalisation by HSC, mediated by Vanin-1 (VNN1) on the surface of vesicles. Increased VNN1 expression on lipotoxic EVs was previously implicated with EV internalisation by LSEC resulting in pathologic angiogenesis (Povero et al., 2013). Increased expression of miR -128-3p was also identified in our recent work, alongside miR -122 and -192, in NAFL and NASH patient plasma EVs. This was only observed in circulating EVs derived specifically from hepatocytes (expressing ASGR1) (Newman et al., 2022b). Mitochondrial dysfunction and oxidative stress are common pathogenic events in fatty liver diseases related to both aetiologies, non-alcoholic and alcoholic (discussed in the following section) (Prasun et al., 2021). Mitochondrial DNA (mtDNA) has been identified as important EV cargo that promotes inflammation via TLR9 activation, thereby contributing to the transition from simple steatosis to steatohepatitis. Garcia-Martinez et al. (2016) found greater levels of mtDNA in plasma microvesicles of mice and patients with NASH, with concomitant increase in hepatocyte-specific marker, Arg-1, and demonstrated the capacity for these particles to activate TLR9.

EVs from visceral adipose tissue actively contribute to NAFLD pathogenesis by exacerbating systemic IR, inflammation and hepatic fibrosis (Kranendonk et al., 2014). Differentially expressed miRNAs in adipocyte-EVs from lean and obese individuals target the TGF-β pathway in hepatocytes and HSC, resulting in the inhibition of fibrolytic enzymes such as matrix metalloproteinase (MMP)-7 (Koeck et al., 2014). Another study emphasised the important contribution of adipocyte-EV to circulating miRNA levels and their capacity to modulate gene expression in the liver (Thomou et al.,

2017). The authors showed that fibroblast growth factor (FGF)-21 is a liver protein target of adipocyte-EV derived miR-99b. FGF-21 is implicated in many metabolic pathways and its suppression contributes to hepatic steatosis (Keinicke et al., 2020). In all, the current evidence positions EVs as key players in the pathogenesis and progression of NAFLD and supports the investigation of biomarkers within EV derived from adipocytes and hepatic cell populations.

Alcoholic Liver Disease

Alcoholic liver disease (ALD) follows a similar clinical course to that of NAFLD. Hepatic steatosis and alcoholic hepatitis (AH) may resolve with alcohol abstinence, but progressive disease can lead to cirrhosis and liver failure (Sharma and Arora, 2020). Liver biopsy is not usually necessary for ALD diagnosis as a history of significant alcohol consumption along with clinical, radiologic and biochemical findings are often sufficient. However, diagnosis may be complicated in alcoholic patients with unreliable history or co-existing risk factors for other conditions such as NAFLD; in such cases the threshold for “significant” alcohol intake may be reduced. The lack of accurate non-invasive biomarkers limits the dynamic assessment of inflammatory activity and degree of fibrosis in ALD, as well as the risk of developing cirrhosis. Considering that ALD accounts for 50% of cirrhosis-related deaths (Sehrawat et al., 2021), biomarker discovery is an area of intense research focus to improve the management of ALD and development of pharmacological strategies to halt or reverse the disease.

EV-mediated macrophage activation is increasingly recognised as a key feature of the inflammatory process in AH and parallels hepatic injury and fibrosis. A mouse model of AH had significantly increased EV levels in circulation and vesicles isolated from primary hepatocytes were found to be enriched in mtDNA (Eguchi et al., 2020). These EV activated TLR9 resulting in upregulated pro-inflammatory cytokine, IL-1β and IL-17 production in liver macrophages and promoted fibrogenic activation of HSC. Another study similarly found that hepatocyte-derived mtDNA-enriched vesicles released in response to chronic and binge ethanol feeding in mice contributed to macrophage and neutrophil infiltration in the liver (Ma et al., 2020). Verma et al. (2016) treated hepatocytes with ethanol *in vitro*, and showed greater release of EVs expressing CD40-ligand. These stimulated macrophage-to-M1 phenotypic switching, characterised by upregulated

pro-inflammatory cytokine expression (TNFα, IL-1β and IL-6). Increased CD40L-expressing EVs were also detected in the serum of patients with AH. Similarly, Momen-Heravi et al. (2015) demonstrated that EV containing miR-122 is transferred from ethanol-treated hepatocytes to monocytes, resulting in suppression of haem oxygenase 1 (HO-1) and subsequent sensitisation to pro-inflammatory stimuli, such as lipopolysaccharide. In addition, mice and humans subjected to acute alcohol binge, and mice also to chronic consumption, had more EVs in circulation. The levels of miR -122 and -155 in the EVs changed over time post-binge, suggesting variable packaging in response to alcohol. This notion is supported by earlier data comparing specific miRNA expression in circulating vesicle or protein fractions across models of liver injury with different aetiologies (Bala et al., 2012). The authors showed that in models of inflammatory (i.e. NAFLD) or alcohol-induced disease, miR -122 and -155 was mostly EV-associated, while predominantly protein-associated in DILI. This distinctive distribution of miRNA in chronic liver disease in contrast to the acute condition, DILI, supports the investigation of biomarkers localised in EVs in the circulation to improve performance and disease-specificity. EV miRNA profile was also explored in mice with AH induced by continuous intragastric ethanol infusion. Three miRNAs in blood EVs, including let-7f-5p, miR-29a-3p and miR-340-5p, discriminated AH mice from controls, as well as from obese mice and those with NASH or cholestatic injury (Eguchi et al., 2017). Various sphingolipids have also been implicated with inflammation and cell death in AH. Serum EVs from AH patients were recently shown to be significantly enriched in six sphingolipid species compared to healthy controls, heavy drinkers, NASH patients and alcoholic cirrhosis patients. The cargo was positively correlated with disease severity and predicted 90-day survival (Sehrawat et al., 2021).

Viral Hepatitis

Viral infections represent a significant cause of chronic liver diseases and are the most common aetiology for HCC (Wong et al., 2019). In addition to certain viral factors, the carcinogenic nature of HBV and HCV are linked to chronic inflammation, fibrosis and changes in signalling pathways implicated in hepatocyte survival and tumour surveillance and suppression (Zamor et al., 2017). While viral infections can be diagnosed by serological techniques and monitored with respect to viral load and immune status (Mann et al., 2018), a better understanding of the role of EVs in

pathogenesis and disease progression may facilitate non-invasive assessment of liver damage and identify early markers of increased HCC risk.

EVs are potent modulators of immune function. Hepatocytes infected with replicating HBV release EVs that induce programmed death ligand-1 (PDL-1) in recipient monocytes, possibly suppressing host antiviral activity (Kakizaki et al., 2019). Another study showed that HCV-infected hepatocytes secrete EVs coated with the HCV protein E2. These EV mimic viral particles thereby hindering the neutralising antibody response (Deng et al., 2019). Conversely, LSEC-derived EVs stimulated by interferon (IFN) -I and -III, contribute to the antiviral response (Giugliano et al., 2015). Interestingly, EVs were found to participate in viral spread during HCV infection. Using a rigorous multi-step approach to remove free virus contamination, Bukong et al. (2014) isolated EVs from infected patient sera and Huh7.5 cell culture supernatant. The EVs contained replication competent HCV-RNA in complex with argonaute-2, heat shock protein 90 and miR-122, which mediated new infection in hepatocytes. Hepatocyte-derived EV also activate HSC to promote fibrosis in HCV. TGF-β pathway activation was found to be triggered by EV-derived miR-19a *in vitro* and increased levels of the miRNA were detected in serum EV from chronic HCV patients compared to healthy controls and patients with non-HCV-related liver disease of similar fibrosis grade (Devhare et al., 2017). A previous study, however, found elevated circulating CD8+ and CD4+ T cell-derived EVs in patients with active HCV, that promoted ECM degradation by induction of MMP enzymes in HSC (Kornek et al., 2011). In summation, these reports provide avenues for development of novel biomarkers or therapeutic tools for chronic viral hepatitis.

Hepatocellular Carcinoma

Hepatocellular carcinoma accounts for more than 80% of primary liver malignancies and a third of global cancer related deaths (Lee et al., 2021). Chronic liver diseases, especially with cirrhosis, are major risk factors for HCC. Prognosis is poor, exhibiting only 20% 5-year overall survival, often due to late stage diagnoses (Lee et al., 2021). Ultrasound has acceptable sensitivity and specificity for HCC screening, but its capacity to detect early lesions is limited (Sun et al., 2020). Serum alpha-fetoprotein (AFP) is a biomarker of widely variable performance that may be elevated in late stages, but only in a subset of patients (Mann et al., 2018). Accordingly, a combination of

ultrasound and AFP assessment is recommended for surveillance by the Australian practice guidelines (Lubel et al., 2021). The use of ultrasound is also endorsed by the American Association for the Study of Liver Diseases (AASLD), with or without AFP (Marrero et al., 2018). EVs are one of three liquid biopsy approaches in oncology, among circulating tumour DNA and tumour cells (Sun et al., 2020). Since EVs carrying tumour-derived information are present in circulation earlier and persist through to advanced disease, they present the opportunity to initiate curative interventions.

The dysregulation of multiple signalling pathways and complex network of interactions between malignant and non-malignant cells in the tumour microenvironment are critical to tumour progression. EVs are known to play a role in regulating cell proliferation, migration, angiogenesis, metastasis, epithelial-to-mesenchymal transition (EMT), and immune escape. Specific HCC-EV miRNA cargo, for example, has been linked to enhanced HCC proliferation (including miR -93, -224 and -665) (Xue et al., 2018, Cui et al., 2019, Qu et al., 2017), while other cargo was found to have an inhibitory effect (miR -9-3p, -638, -718 and -744) (Tang et al., 2018, Shi et al., 2018, Sugimachi et al., 2015, Wang et al., 2019). Kogure et al. (2011) reported that selectively packaged miRNA and protein in HCC-derived EVs modulate the TGF-β activated kinase 1 (TAK1) pathway in other hepatic cells to promote cancer growth. More recently, HCC-derived EVs were found to inhibit apoptosis and enhance proliferation of hepatocytes via transfer of long intergenic non-coding RNA regulator of reprogramming (linc-ROR) (He et al., 2019).

EVs also promote the invasion of HCC tumours through normal liver tissue, as metastatic HCC-derived EV mobilise healthy hepatocytes via transfer of oncogenic cargo, such as mesenchymal-epithelial transition (MET) proto-oncogene, caveolins and S100 family members (He et al., 2015). EV from metastatic HCC also contain miR-1247-3p which facilitates the conversion of normal fibroblasts to cancer-associated fibroblasts (CAFs) in lung metastases and increased pro-inflammatory cytokine (IL-6 and IL-8) secretion (Fang et al., 2018). In HCC patients, lung metastasis was positively correlated with serum levels of EV-derived miR-1247-3p. EV protein cargo in serum was also shown to aid differential diagnosis of intrahepatic cholangiocarcinoma, HCC and primary sclerosing cholangitis, which is challenging with current non-invasive tools (Arbelaiz et al., 2017). These studies support the role of tumour-derived EV cargo in encouraging a tumour-favourable

environment for progression and metastasis through communication with cancerous and non-cancerous cells, and advance the notion that promising biomarker candidates linked to oncogenic processes may be detected in circulating EVs.

Fibrosis

Liver fibrosis is a significant cause of morbidity and strong independent risk factor for mortality in chronic liver diseases, especially NAFLD (Unalp-Arida and Ruhl, 2017). While effective treatment of the precipitating condition may reverse fibrosis in some patients, specific antifibrotic treatment options are scarce (Chen et al., 2018b) and patients may advance to cirrhosis and liver failure, often necessitating liver transplantation (Wang et al., 2015). HSC activation is the principal event at the cellular level leading to ECM deposition and, under persistent profibrogenic conditions, can produce fibrous scar and severely compromise liver function (Li et al., 2020, Chen et al., 2018b). Fibrosis is a typical progression common among multiple chronic liver diseases and can be characterised by a number of molecular pathways not specifically altered by a particular condition. These may be monitored via EV-derived markers as described below; Thus, in conjunction with disease-specific markers that identify the precipitating condition, fibrosis markers may be helpful in tracking the severity of this complication.

EVs from HSCs of both quiescent and myofibroblast phenotypes form a complex interplay of pro- and anti-fibrotic EV signalling in the injured liver. One study determined that HSCs treated with PDGF-BB *in vitro* released EVs enriched with PDGF receptor-alpha (PDGFRα) via a mechanism of selective packaging (Kostallari et al., 2018). The EVs promoted migration in recipient HSC and liver fibrosis in healthy mice, while inhibiting EV export of PDGFRα ameliorated fibrosis in carbon tetrachloride (CCL_4)-treated mice. Patients with liver fibrosis also had increased levels of PDGFRα in serum EV. HSC phenotype is further modulated by LSEC-derived EV. Wang et al. (2015) showed that the EV specifically transfer SK1 and S1P cargo, which upregulate AKT phosphorylation and migration. Expression of each at RNA and protein level was detectable in EVs from mice with experimental liver fibrosis and human patients with alcoholic fibrosis.

The Hedgehog (Hh) pathway is critical to the wound-healing response and tissue remodelling in chronic liver injury. Hh ligands released in EVs from damaged hepatocytes and aHSC, promote proliferation and angiogenesis in recipient HSC and endothelial progenitor cells, respectively; and have been detected at increased levels in the plasma and bile of rats with fibrosis induced by bile duct ligation (Witek et al., 2009). Further, discordant miRNA and protein cargo in EVs from qHSC and aHSC, either stimulate or inhibit fibrosis depending on the phenotype of originating and recipient cells. Serum EVs from healthy individuals contain “anti-fibrotic” miRNA which decreased CTGF, αSMA and collagen gene expression when applied to aHSC *in vitro* and reduced hepatic fibrosis and inflammation in CCL_4-treated mice (Chen et al., 2018b). Meanwhile, a proteomic comparison of qHSC- and aHSC-derived EV revealed greater protein content in the latter, associated with profibrotic, inflammatory and chemotactic functions (Li et al., 2020). Accordingly, the presence of distinct pro- and anti-fibrotic EV populations in the liver present the intriguing possibility to track fibrogenic activity and develop novel antifibrotic therapies.

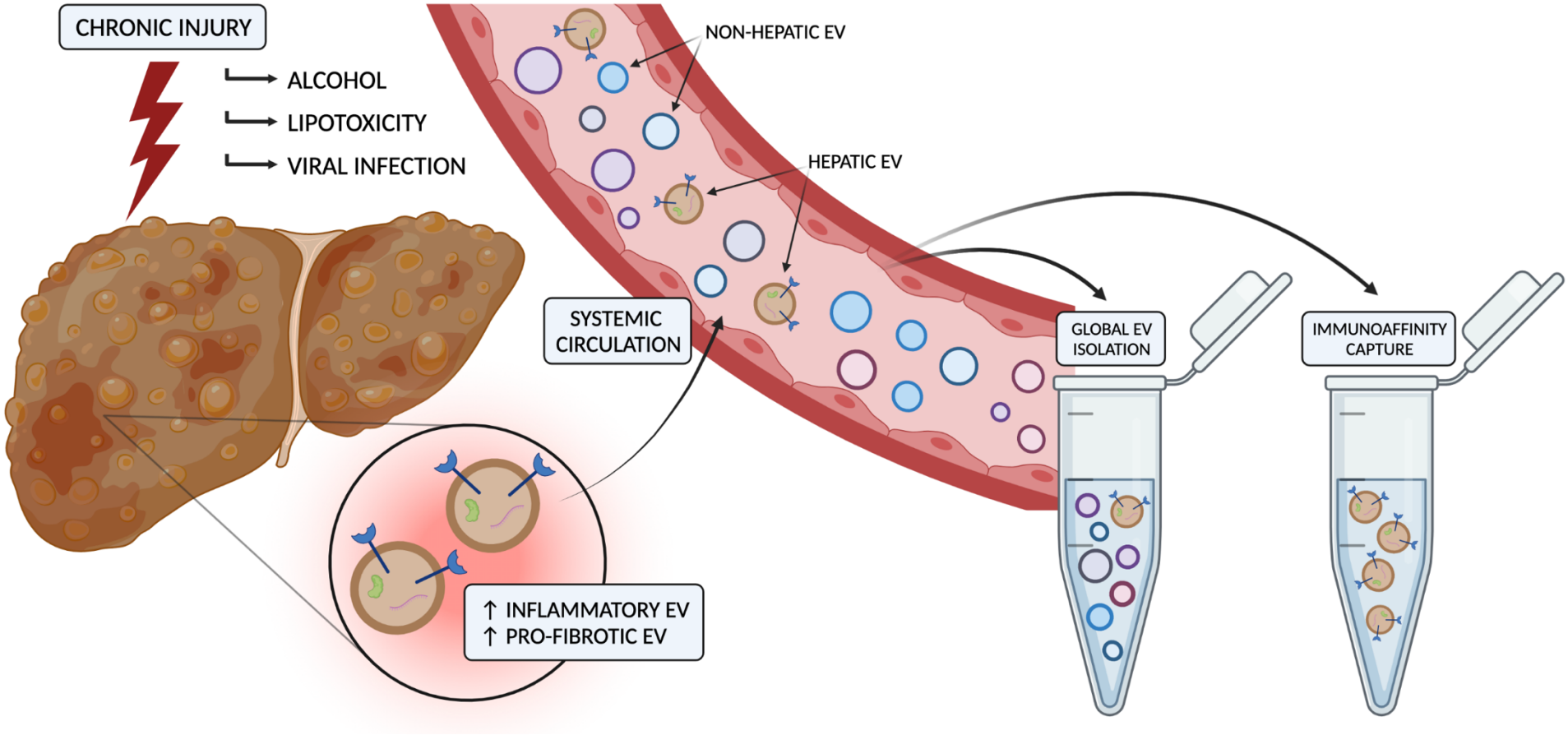

Figure 1.3 Extracellular vesicle liquid biopsy for chronic liver diseases.

Figure was created using BioRender.com.

Analysis of Circulating Tissue-Specific EV biomarkers

The studies described thus far indicate the potential for biomarkers with mechanistic links to chronic liver pathology to be released in EVs and detected in the circulation (Figure 1.3). However, the EVs harbouring these molecules of interest account for a relatively small proportion of the complex circulating mixture of vesicles, which are also derived from multiple other cells and organs. In plasma, platelets are a major source of EVs (originating up to 90%), followed by other haematopoietic or endothelial cell types (Konoshenko et al., 2018, Balaphas et al., 2019). While the reported proportion of hepatocyte-derived EVs in circulation varies widely (Povero et al., 2020, Li et al., 2019), this may be as small as a fraction of a percent. Since conventional methods separate vesicles from other blood components based on physical properties, producing bulk isolates of heterogenous composition, the background noise from non-hepatic EVs may preclude the sensitive detection of disease-related changes. This is likely to be particularly apparent in the diagnosis of early-stage patients (Rojalin et al., 2019). Evidently, the inability to efficiently isolate relevant subpopulations of EVs containing candidate biomarkers, represents a major barrier to their clinical translation. Immunoaffinity capture fits within a broader framework of EV sample collection and analysis for blood-based biomarker contexts. The methodology can be summarised in a generic workflow (Figure 1.4) that incorporates best practice (as reviewed by Useckaite et al. (2021)) and recommendations for characterisation and reporting (Théry et al., 2018, Newman et al., 2021). While the review of common isolation methods is beyond the present scope and described in detail elsewhere (Sidhom et al., 2020, Konoshenko et al., 2018), the following section will discuss the application of immunoaffinity-based capture methods to detect cell- or tissue-specific EVs and analyse their cargo in the context of chronic liver diseases. Supplemented by emerging technologies, we envision this to serve as a foundation for the implementation of informed and actionable biomarker strategies with broader relevance to any condition or application. Studies described in this section are also listed in Table 1.2 under *Cargo detected in circulating EVs* for the particular disease.

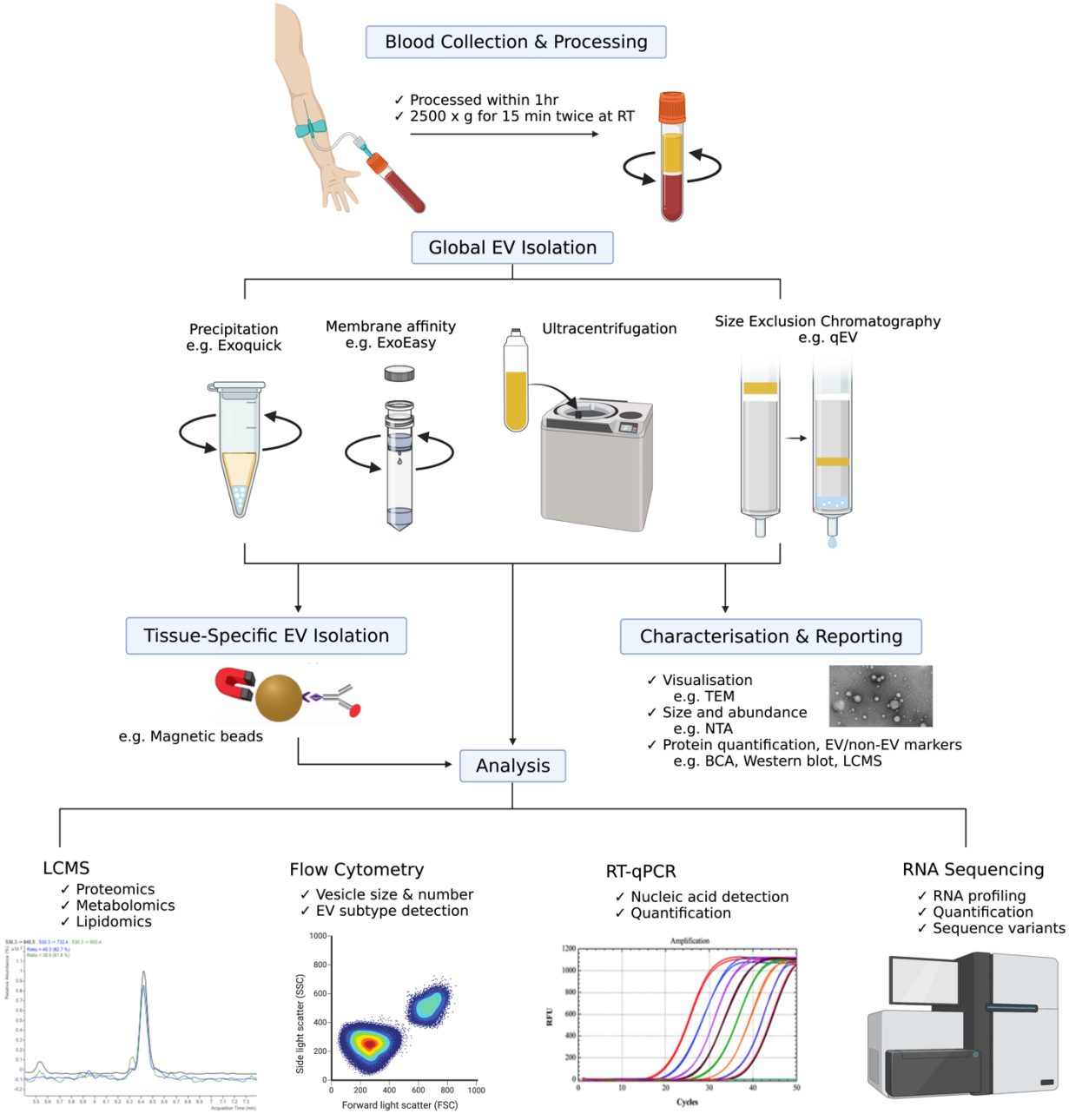

Figure 1.4 Generic workflow for the sample collection and analysis of EV-derived biomarkers.

Figure was created using BioRender.com.

Technologies to Assess Tissue-Specific EVs

Given the biogenesis pathway and cell of origin influence surface protein expression on EVs, the isolation of particular subpopulations can be achieved by immunoaffinity capture (IAC) (Mitchell et al., 2021). IAC is based on the interactions of EV surface molecules with antibodies, most commonly against tetraspanins, that are covalently linked to a fixed phase, such as magnetic or non-magnetic beads, plastic or silica plates, porous monolithic microtips or microfluidic devices (Konoshenko et al., 2018). Compared to conventional isolation methods, the use of antibodies permits the extraction of highly pure and specific EVs, lending itself to customisation against EV markers of interest (Sidhom et al., 2020, Mitchell et al., 2021). For instance, ASGR and CYP2E1 are known membrane-localised EV constituents with high specificity for EVs of hepatocyte origin, and have been applied for the selective analysis of hepatocyte-derived biomarkers for liver disease *in vivo* (Nakao et al., 2021). However, targeting specific EV populations inherently reduces yield. Efficient recovery by IAC depends on the availability of antibodies with sufficient specificity and stability. The high cost of antibodies also limits scaling of capture protocols to large sample volumes (Sidhom et al., 2020). Though some techniques can be performed directly from biofluids, IAC is usually preceded by global EV enrichment. Variability between different global isolation methods with respect to subtype enrichment and cargo (Mastoridis et al., 2018), underscores the importance of confirming compatibility of a chosen method with downstream analyses. Despite present limitations, emerging immunoaffinity-based technologies show promise to improve clinical biomarker analyses in a robust, timely and cost-effective manner.

Immunobead- or Plate-based Capture

The most common approach to selectively isolate EV subtypes involves incubation of EVs with antibodies conjugated to magnetic beads or on plates (Zarovni et al., 2015). EVs positive for cell- or disease-specific surface markers can then be selectively removed from the mixture by magnetic forces or immobilisation on the plate surface. This may also be used to improve the purity of samples, pre-enriched by precipitation or ultracentrifugation, by targeting tetraspanins (Sidhom et al., 2020). The method is compatible with downstream analyses, including polymerase chain reaction (PCR), for direct quantification of molecular cargo (Zarovni et al., 2015), however tight covalent bonds make the elution of bead- or plate-bound EVs challenging. Use of low pH buffers can release

intact EVs but may interfere with subsequent investigations of functional activity (Mitchell et al., 2021). Nonetheless, for diagnostic purposes, pull-down of specific EV samples presents the opportunity to comprehensively interrogate cargo across multi-omics platforms and identify disease-specific molecular signatures. Immunoprecipitation of cell-specific EVs from biofluids has been applied in biomarker discovery by a select number of groups, in the context of neuronal pathology (Mustapic et al., 2017, Shi et al., 2014, Fiandaca et al., 2015, Goetzl et al., 2016), cerebrovascular disease (Goetzl et al., 2017), transplant rejection (Vallabhajosyula et al., 2017), melanoma (Sharma et al., 2018) and prostate cancer (Mizutani et al., 2014). These reports consistently support the notion that EVs preferentially enriched for tissue origin are most informative of disease and thus enhance sensitivity and specificity of biomarker analyses. We recently isolated hepatocyte-derived EVs by anti-ASGR1 immunoprecipitation for the study of DMET induction by rifampicin and in pregnancy (Rodrigues et al., 2021) and to compare the performance of miRNA biomarkers for NAFLD in unfractionated plasma, global circulating EVs and liver-specific EVs (Newman et al., 2022b). Only in applying the selective isolation technique, was a strong significant trend observed in biomarker expression with disease severity in NAFLD patients; thereby providing the first evidence for the utility of tissue-specific EV isolation techniques to improve diagnostic performance in chronic liver disease.

Flow Cytometry

Flow cytometry is a powerful technique that can be applied to the enumeration and sizing of EVs from biofluids and phenotyping of specific subpopulations (Welsh et al., 2020). Particles in suspension are passed through a laser beam and measured based on light scatter and fluorescent emission. Conventional flow cytometers were designed for measuring single cells, thus the limit of detection is substantially larger than the typical EV size distribution (between 200 and 500 nm depending on the instrument) (Panagopoulou et al., 2020). Although modern developments in high-resolution flow cytometry have seen increased sensitivity towards lower limits (~100 nm), this still misses a significant portion of smaller EVs, as revealed by complementary techniques, such as nanoparticle tracking analysis (NTA) (Botha et al., 2021). Alternatively, larger complexes can be formed using immunobeads to detect the smaller range of EVs. This is useful for detecting EV subtypes based on surface composition but provides no direct insight into vesicle size (Panagopoulou et al., 2020). Multiplexed flow cytometry approaches allow the high-throughput

analysis of multiple markers of interest (Mastoridis et al., 2018, Koliha et al., 2016); however, like other immunolabelling approaches (e.g. Fluorescent NTA and immunogold-label EM), cargo detection is restricted to surface expression.

In chronic liver disease, such as NAFLD, flow cytometry approaches uphold the potential for cell-specific circulating EVs to diagnose and track progression. In a diet-induced mouse model of NASH, Li et al. (2019) followed changes in circulating EVs derived from hepatocytes (ASGR1+, CYP2E1+), macrophages (Galectin 3+), neutrophils (Ly-6G/6C+) and platelets (CD61+). Hepatocyte-specific EV levels were significantly elevated over the course of feeding, occurring prior to histological evidence of inflammation and correlated with NAFLD activity score and features of NASH, including lobular inflammation and ballooning. Similarly, macrophage- and neutrophil-derived EVs were increased and strongly associated with hepatic inflammation and fibrosis.

Povero et al. (2020) also investigated changes in circulating hepatocyte-derived EVs, bearing ASGR1 and bile acyl-coenzyme A synthetase (SLC27A5), in human NASH patients with and without cirrhosis. SLC27A5 is a key enzyme in fatty acid uptake and synthesis. While greater expression is observed in steatotic hepatocytes, down-regulation has been associated with progression to cirrhosis due to loss of fat and functional parenchyma. In serum, SLC27A5+ EVs increased up to 4-fold in NASH compared to healthy controls then decreased slightly in cirrhotic NASH. Meanwhile, ASGR1+ EV levels increased with disease severity, at almost 2-fold in pre-cirrhotic NASH and 3-fold in cirrhotic patients, compared to healthy controls. Liver-specific EV numbers exhibited strong correlations with features of NASH, including fibrosis stage, as well as various clinically relevant scores, such as FibroTest, Enhanced Liver Fibrosis (ELF) test and NAFLD Fibrosis Score (NFS). Additionally, hepatocyte-derived EVs could predict clinically significant portal hypertension (hepatic venous pressure gradient [HVPG] ≥ 10mmHg) in cirrhotic NASH patients with sensitivity of 92% and specificity of 75% (area under the receiver operating characteristic curve [AUROC] = 0.79), identifying the cut-off as ≥ 668 EVs/µl serum. Proteomic profiling also revealed several differentially expressed proteins that could distinguish advanced NASH from healthy controls (AUROC = 0.77) and pre-cirrhotic from cirrhotic NASH (AUROC = 0.80). Considering this analysis was performed on global circulating EVs and in late-stage NAFLD cohorts, the potential benefit of selectively analysing

hepatocyte-derived EV protein cargo may be explored in simple steatosis or early NASH development.

It is noted that the above studies employed nanoscale flow cytometry with detection thresholds set to count EVs in the range of 110-1000 nm (Li et al., 2019) and 200-1000 nm (Povero et al., 2020), respectively. Although limited to the larger EV range, earlier reports utilising conventional flow cytometers have also shown compelling results in support of tissue-specific EV biomarkers for chronic liver disease. Specifically, the profiling of immune cell-derived EVs discriminated patients with NAFL, NASH and HCV infection and healthy controls, and paralleled the extent of hepatic inflammation. Chronic HCV patients had greater circulating CD4+ and CD8+ T-cell-derived EVs, while NAFLD patients had more EVs from invariant natural killer T-cells and CD14+ macrophages. AUROC values ranged from 0.652–0.999 for various cohort pairs (Kornek et al., 2012). Later work demonstrated that the combination of surface markers, Annexin V, EpCAM, ASGR1 and CD133, could be used to identify tumour-associated EVs in circulation and distinguish between liver cancers (HCC and cholangiocarcinoma) and tumour-free cirrhosis (Julich-Haertel et al., 2017). Similarly, EVs expressing hepatocyte paraffin 1 (HepPar1) were found in great abundance in the circulation of patients with HCC, compared to virtually undetectable levels in tumour-free cirrhosis and healthy controls, and were proposed as an early marker of recurrence (Abbate et al., 2017).

Microfluidic Devices

Recent innovations in microfluidic hardware has driven the development of compact chip-like devices for the detection and isolation of EVs from biofluids. Microfluidic devices sort particles through a network of microchannels of varying diameter, ranging from tens to hundreds of microns (Panagopoulou et al., 2020, Konoshenko et al., 2018). Vesicle isolation is achieved either by actively applying electric, magnetic or acoustic forces, or in a passive manner, depending on immunoaffinity interactions and size exclusion (Chiriacò et al., 2018). In IA-based devices, antibody-functionalised surfaces immobilise target EVs flowing through the chip, to separate highly specific, pure vesicle subtypes. For example, the ExoChip device contains anti-CD63 to selectively capture exosomal small EV and has been applied for biomarker discovery in pancreatic cancer patients (Kanwar et al.,

2014). Progress in the design of these devices continue to improve sensitivity, reduce non-specific interactions and enhance capture efficiency by increasing surface area and mixing (Chiriacò et al., 2018).

Key advantages of IA microfluidic chips include rapid processing time and low sample volume, requiring as little as ten microliters of plasma but taking up to a few hundred microliters (Lee et al., 2021). It is noted that reducing sample input may be detrimental to downstream analyses, whereby biomarker yield in smaller volumes is insufficient for diagnostic purposes (Konoshenko et al., 2018). Despite their current complexity and cost, the development of integrated on-chip analysis of EV cargo positions microfluidic devices as promising novel tools for point of care testing (POCT) (Shao et al., 2018). Captured EVs may be lysed by chemical (e.g. Triton X-100) or physical (e.g. electrical) means, and intraluminal nucleic acid amplified and analysed on-chip by quantitative PCR. Protein cargo may be detected by ELISA or released for off-chip proteomics (Chiriacò et al., 2018, Panagopoulou et al., 2020).

Recently, Sun et al. (2020) designed an EV purification system, called EV Click Chips, to isolate HCC-derived EVs directly from 500µl of plasma, via surface expression of ASGR1, EpCAM and CD147. Expression of 10 HCC-specific mRNA transcripts, analysed by digital droplet PCR in the captured EVs, gave exceptional diagnostic performance across several cohorts. Specifically, HCC was distinguished from all non-cancer (AUROC = 0.87) and from other primary malignancies (AUROC = 0.95) and early HCC detection could be achieved amongst at-risk cirrhosis patients of viral hepatitis, ALD or NASH aetiology (AUROC = 0.93), outperforming serum AFP (AUROC = 0.69). While the application of microfluidic devices is mainly at the proof-of-concept stage (Zarovni et al., 2015), longitudinal follow-up and validation in larger cohorts may soon see this novel non-invasive tool implemented in clinical settings for early diagnosis and patient monitoring.

Nano-Plasmonic Enhanced Scattering Assay

Nano-plasmonic enhanced scattering assay (nPES) is a novel IAC technology that can isolate and quantify target EVs using capture and detection antibodies (Rojalin et al., 2019). The assay, initially developed for tumour-derived EV from pancreatic cancer patients (Liang et al., 2017), was shown to considerably reduce cost, sample volume and analysis time and improved sensitivity

compared to ELISA (Rojalin et al., 2019). Similar to microfluidic devices, nPES is attractive for POCT given the assay consumes as little as 1-5µl and can be performed directly from biofluids (Sehrawat et al., 2021).

One research group recently developed a novel nPES assay to quantify hepatocyte-specific EVs as biomarkers for AH diagnosis (Sehrawat et al., 2021) and for NAFLD resolution in obese patients undergoing weight loss surgery (Nakao et al., 2021). EV capture was achieved through ASGR2 or CYP2E1 and confirmed by CD63 positivity; and the capacity for circulating hepatocyte-specific EV levels to differentiate patients from controls was demonstrated in each cohort. Interestingly, hepatocyte-EVs correlated with steatosis and inflammation in NAFLD. The findings by Nakao and co-workers are in line with an earlier study that showed a 68% reduction in circulating hepatocyte-EVs (ASGR1+, HepPar1+) after bariatric surgery; however, the use of flow cytometry limited vesicle detection to those within 200-900 nm diameter (Rega-Kaun et al., 2019).

Finally, lipidomic analysis revealed differential sphingolipid cargo in global EVs that was integrated in multivariable logistic regression models with MELD score and log global EV count to predict 90-day mortality in AH (AUC = 0.91) (Sehrawat et al., 2021); and with body mass index and small EV (110,000 *x g* UC pellet) count to identify NAFLD (AUC = 0.80) (Nakao et al., 2021). Given the shortfalls of global EV analysis, further development and validation of nPES and other technologies to selectively analyse molecular signatures in cell-specific EVs, may advance clinical translation of predictive models such as these.

Concluding Remarks

EVs mediate a vast array of complex biological functions, related to the maintenance of liver homeostasis as well as the initiation and progression of liver diseases. A multiplicity of reports underpins the mechanistic link between EV-mediated cellular crosstalk and pathogenic processes that translate to differential expression in EV-based biomarkers across human patients and healthy subjects. The stability and accessibility of EV in peripheral blood are among attractive characteristics that compel their application as minimally invasive biomarkers. In the field of chronic liver disease, such tools for diagnosis and tracking of disease status and response to therapeutic intervention is in

critical demand. The advancement of platforms designed to specifically isolate and analyse EVs, derived from cells or tissues relevant to the condition of interest, may greatly enhance the sensitivity and reproducibility of circulating EV biomarker analyses. It is our overarching view that clinical use will be supported by the development of these technologies and a holistic approach to evaluating disease-specific EV signatures of composite molecular species.

Significance and Aims

EVs have emerged as a valuable source of molecular information that may be leveraged as minimally-invasive biomarkers to support diagnosis and patient monitoring and to guide treatment decisions. The capacity for circulating EVs to reflect molecular changes in specific organs in a liquid biopsy offers the opportunity to overcome several limitations associated with a solid organ biopsy, particularly with regard to invasiveness and possibility of serial testing. In the clinical management of NAFLD, histological evaluation by liver biopsy persists as the gold standard for the diagnosis of steatohepatitis and staging of fibrosis. Enrolment screening and primary endpoints based on histology also continue to be a mainstay of Phase 2/3 clinical trials. However, this fails to provide detailed molecular insights associated with treatment response or disease drivers that could identify subgroups of patients most likely to benefit from targeted medications. In recent years, there have been several costly failures in the development of drugs to treat NASH and, to date, no approved pharmacological intervention is available. Accordingly, there is a critical demand for minimally-invasive tools for the dynamic assessment of NAFLD patients both in clinical trial settings and more broadly for routine management. While molecular information contained in circulating EVs have demonstrated utility for characterising NAFLD patients, limitations of standard approaches for EV isolation and analysis hinders their clinical application.

The hypotheses underpinning this thesis are that (i) the selective isolation of circulating liver derived EVs by immunoprecipitation against hepatocyte surface marker ASGR1 allows the assessment of specific changes in the tissue of origin; and (ii) liver derived EVs are a source of RNA and protein biomarkers with diagnostic or predictive value. By developing and applying novel techniques, this thesis aimed to address several barriers to the translation of EV liquid biopsy to human clinical samples. In demonstrating the utility of liver derived EVs to reflect key hepatic functions and dysregulated molecular pathways associated with the pharmacological treatment of the disease, these advancements pave the way for precision medicine strategies in MAFLD. The aims as detailed below will be addressed in the following chapters.

Aim 1 – *Develop and validate a targeted liquid chromatography tandem mass spectrometry (LC-MS/MS) method for the quantification of markers associated with EVs and contaminant protein in human blood.*

The capacity to robustly characterise EV protein markers for assessment of yield and purity is typically done with crude semi-quantitative methods such as western blotting. Reporting of EV characterisation is often is limited to a subset of representative samples rather than each sample due to limitations in available sample volume and laboriousness of the procedure. However, clinical translation of EV biomarkers will require an approach to quality control of blood-derived EV isolates, on an individual sample level, in a highly sensitive, high-throughput and fully quantitative manner.

Aim 2 – *Define variability in circulating global and liver specific EV abundance and cargo resulting from physiological characteristics of the donors.*

Patterns of variability within (diurnal) and between individuals have the potential to confound biomarker analyses using circulating EVs. Addressing this aim serves to deepen understanding of basal variability under physiological conditions for improved interpretation of changes in disease and highlight considerations for standardised EV sampling protocols.

Aim 3 – *Compare the performance of miRNA biomarkers extracted from total plasma, global EVs and ASGR1+ EVs for predicting disease severity.*

Cell-free miRNA is stabilised in the circulation by a variety of carriers, including encapsulation in EVs. Under different conditions, the relative distribution of miRNA among these carriers may be altered. In NAFLD, reported changes to selective packaging and secretion of molecular cargo into EVs, including miRNA, suggests that RNA extracted from the EV fraction of plasma may be more diagnostically relevant. Standard methods for EV isolation cannot distinguish the tissue of origin in the complex mixture released into the systemic circulation. Consequently, EV biomarker analyses

that are not targeted toward the affected tissue achieve a trivial fraction of their potential utility when applied to blood samples. The use of immunoaffinity EV isolation against ASGR1 to selectively enrich liver derived EVs, thus presents the opportunity to improve detection of low abundance disease-specific biomarkers.

Aim 4 – *Quantify drug metabolising enzymes and MAFLD drug targets in EVs isolated from liver tissue and establish concordance with absolute abundance in paired tissue.*

Patients with MAFLD exhibit marked variability in exposure and response to medications resulting from differences in the abundance of hepatic drug metabolising enzymes (DMEs) and proteins in molecular pathways that constitute drug targets for pharmacotherapy. Differences in these hepatic functions are challenging to define on a molecular level *in vivo*. In addressing this aim, the work sought to detect and quantify a panel of key proteins related to the pharmacokinetic and pharmacodynamic interactions of drugs with the liver in EVs derived from liver tissue and provide evidence for the utility of liver derived EVs to define between subject differences in DME profile and within subject changes in MAFLD drug targets. Following on from this, exploratory analyses aimed to assess the feasibility of quantifying pharmacodynamic markers *in vivo* using a liver specific EV liquid biopsy.

Nomenclature

An emerging consensus among clinicians and scientists in the field of hepatology has led to the proposed renaming of non-alcoholic fatty liver disease (NAFLD) in order to support the diagnosis of the condition based on inclusion criteria (e.g. metabolic dysfunction) rather than exclusion criteria, particularly alcohol use. The updated nomenclature of metabolic associated fatty liver disease (MAFLD) is intended to reflect advancements in the understanding of pathogenic drivers, marked heterogeneity in the natural history of the disease and observed interplay of comorbidities and hepatic and non-hepatic risk factors, including alcohol use. For the purpose of this thesis, both NAFLD and MAFLD will appear in different chapters and may be interpreted as interchangeable terms.

CHAPTER 2

ADDRESSING MISEV GUIDANCE USING TARGETED LC-MS/MS: A METHOD FOR THE DETECTION AND QUANTIFICATION OF EXTRACELLULAR VESICLE-ENRICHED AND CONTAMINANT PROTEIN MARKERS FROM BLOOD

Author Contributions

This chapter is published in the *Journal of Extracellular Biology* (Appendix 2) and no changes have been made to the contents of the original peer-reviewed manuscript. The only alterations were formatting for consistency with the thesis. I was the first and sole primary contributing author, and was responsible for conceptualisation, developed the methodology, generated and analysed the majority of the data, wrote the first draft and reviewed and edited the paper, culminating in approximately 85% of the total contribution to the work. Author Z.U performed the TEM imaging and western blots. Author A.R contributed to conceptualisation and edited the paper.

Context in Thesis

With rapidly growing research interest in the EV field, the minimal information for the study of extracellular vesicles (MISEV) guidelines were established to promote standardisation, including robust characterisation of EV isolates. The analysis of proteins including positive EV markers and negative contaminant markers of commonly co-isolated components of the starting material is an important component for assessing yield and purity. Across studies that report adherence to the MISEV guidelines, western blotting is most frequently performed to analyse EV protein; however, this approach is limited in terms of quantitation and throughput and requires larger volumes than typically available for patient samples, including in the context of clinical trials. Accordingly, the successful application of EVs as a liquid biopsy in clinical contexts requires a high-throughput multiplexed approach to analyse protein markers from small volumes of starting material. To address

this issue, the following chapter documents the development and validation of a targeted liquid chromatography tandem mass spectrometry (LC-MS/MS) assay for the quantification of markers associated with EVs and non-EV contaminants from human blood samples. Considering the importance of standardising techniques for EV analysis and experimental reporting, the assay was specifically designed to address the MISEV guidelines. The assay was highly sensitive, requiring only a fraction of the sample consumed for immunoblots, fully quantitative and high throughput. Application of the assay to EVs isolated by commercially available isolation methods – size exclusion chromatography and precipitation – revealed differences in yield, purity and recovery of subpopulations. To account for potential differences in clinical study design and the effect of disease, the performance of the assay was also compared in healthy serum and plasma samples and in patients with NAFLD.

Introduction

In recent years, the field of extracellular vesicle (EV) research has exploded with publications documenting their biological properties, functionality, and potential diagnostic, prognostic and therapeutic applications in human disease (Shao et al., 2018, Van Deun et al., 2017, Théry et al., 2018). The term EV describes a heterogenous population of membrane-bound vesicles; including small EVs, such as exosomes (50-150nm), that arise from endosomal pathways within the cell, and EVs of various sizes up to 1000nm in diameter, shed directly from the plasma membrane (microvesicles) (Newman et al., 2020, Kowal et al., 2016). Whilst originally perceived simply as a pathway for cellular garbage disposal, EVs are increasingly recognised for their roles in local and systemic intercellular communication, diverse physiological processes and disease progression(Newman et al., 2020, Shao et al., 2018). These functions are facilitated via the transfer of biologically active cargo, including nucleic acids, proteins and lipids, into recipient cells resulting in phenotypic and functional changes (Newman et al., 2020, Greening et al., 2017).

The stability conferred through encapsulation within the vesicle membrane and accessibility in biological fluids such as blood and urine, makes EV cargo attractive as biomarkers and therapeutic

tools (Hirsova et al., 2016b). However, their clinical application is hindered by several challenges, particularly with respect to the competing imperatives of recovery and purity of isolated preparations (Webber and Clayton, 2013, Newman et al., 2020, Van Deun et al., 2017). To promote the standardisation of EV methodologies and reporting, the International Society for Extracellular Vesicles (ISEV) has provided guidelines that set out the minimal requirements for the study of extracellular vesicles (MISEV) (Théry et al., 2018). Researchers must provide robust evidence to claim the presence of EVs in isolates and assign physiological properties or functions to them. In addition, the EV-TRACK knowledgebase provides a platform for the detailed recording of experimental procedures through a checklist of 115 parameters, from which studies are assigned an EV-METRIC reflecting the capacity for the experiments to be properly interpreted and reproduced (Van Deun et al., 2017).

A key component of the EV-METRIC is analysing samples for the presence of accepted EV markers and absence or depletion of markers not associated with EVs (Van Deun et al., 2017) (+/- EV markers). EV enriched proteins are derived from the plasma membrane or cytosol and reflect the process of biogenesis and sorting of cargo(Shao et al., 2018). MISEV (2018) defines two categories of proteins to be analysed in all preparations, in order to robustly claim the presence of EVs. Markers frequently identified from Category 1 (transmembrane or GPI-anchored proteins) include tetraspanins (CD9, CD81, CD63) and major histocompatibility complex class 1 (MHC1) (Shao et al., 2018, Kowal et al., 2016, Théry et al., 2018). Category 2 comprises proteins that are incorporated from the cytosol into EVs, largely due to lipid- or membrane protein-binding capacity. Examples of these are tumour susceptibility gene 101 (TSG101), heat shock 70 kDa proteins and flotillins -1 & -2 (Théry et al., 2018). A third category of commonly co-isolated contaminants is also given for assessing purity. These are selected with respect to EV source; for example, apolipoproteins or albumin in blood-derived EV isolates (Théry et al., 2018). Further, proteins expressed in intracellular compartments other than plasma membrane or endosome, such as endoplasmic reticulum or nucleus, may be used as markers of large EVs, cellular components or apoptotic blebs (Shao et al., 2018). Common examples include calnexin, endoplasmin (GP96), or histones (Webber and Clayton,

2013, Kowal et al., 2016, Théry et al., 2018), and comprise Category 4, which must be addressed by researchers claiming the specific isolation of small EVs (Théry et al., 2018).

Currently, western blotting is the most common approach used to address reporting requirements relating to analysis of +/- EV markers (Théry et al., 2018). While western blotting is an established method for protein detection, the approach has many inherent limitations that impact applicability to certain sample types. By way of example, as an antibody-based (immunoblotting) method, western blotting is semi-quantitative and can reliably detect only one analyte per sample. This may not be an issue when working with EVs isolated from cell culture media as sample volumes are plentiful, allowing for multiple parallel analyses, and there is a greater ratio of vesicles to particulate contamination (Van Deun et al., 2017, Kreimer et al., 2015). This does, however, become a key limitation in the context of addressing reporting requirements when working with biospecimens from clinical trials or patient cohorts, as the resulting EV sample volume is often insufficient to accommodate multiple western blot analyses as control experiments. Additionally, the biospecimen sample matrix is typically more complex and variable between samples, which can impact the quality of western blot analysis. Importantly, western blots can also be limited by the performance of antibodies, as non-specific binding can increase background and reduce confidence in analyte detection (Liebler and Zimmerman, 2013). As EVs become an increasingly important 'liquid biopsy' platform and their application to clinical biospecimens gains increasing attention, there is a need for a robust, higher throughput, multiplexed approach to address +/- EV marker reporting requirements, ideally utilising the same platform that is applied to biomarkers of interest. Particularly when working with biospecimens, different EV isolation methods are known to enrich specific EV sub-populations and differ in terms of EV recovery and the extent and composition of vesicular and non-vesicular contamination. Accordingly, it is important to consider the compatibility of isolation strategy with the analytical platform.

In recent years liquid chromatography mass spectrometry (LC-MS/MS) analyses have facilitated expansive proteomic profiling of EVs (Rosa-Fernandes et al., 2017, Shao et al., 2018). LC-MS/MS has been applied in both untargeted and targeted workflows, to qualitatively screen for the presence of proteins and to quantify the abundance of specific proteins, respectively. Targeted

LC-MS/MS based protein quantification typically involves the enzymatic digestion of proteins into peptides, separation by reverse phase liquid chromatography, and quantification of specific fragmentation patterns associated with the peptide of interest using a triple quadrupole (QQQ) mass spectrometer (Kreimer et al., 2015, Rosa-Fernandes et al., 2017). This approach, referred to as multiple reaction monitoring (MRM), is highly sensitive, reproducible, and depending on instrument configuration can simultaneously analyse up to 20 proteins in a single sample. Additionally, targeted LC-MS/MS analysis enables absolute analyte quantification in a complex matrix when the magnitude of the response for the endogenous analyte is normalised using a stable isotope labelled (SIL) peptide and compared to an external calibrator spiked into a comparable matrix at a known concentration (Greening et al., 2017, Kreimer et al., 2015).

Few studies have previously employed targeted LC-MS/MS assays to assess purity of EVs from blood (Park et al., 2021, Wang et al., 2017), and have been useful in the development of novel isolation strategies (Nguyen et al., 2021) or to gain insight to membrane origin of circulating vesicles(Zhang et al., 2020b). Of these studies, only that by Park et al. (2021) was performed on clinically relevant volumes of sample (100µl plasma, while others used up to 200mL). However, the proteins included in this panel covered cytosolic EV-enriched proteins and non-EV contaminants while transmembrane (MISEV category 1) proteins were notably absent. Thus, the present manuscript describes the development and validation of a novel MRM-based panel specifically designed to address MISEV guidelines. This approach is sensitive, fully quantitative and high throughput. Establishing the presence of EV markers and depletion of contaminants is a critical component of sample characterisation, likely to be expanded upon in new iterations of MISEV (Witwer et al., 2021). Since the 2018 guidelines recognised the challenge of performing several characterisation experiments when sample volume is limited, we validate the application of this platform in small starting volumes. Hence, the method described here may be generalised to other EV-based research applications, of different cell-types or (patho)physiological condition, but we anticipate its particular value for the analysis of clinical biospecimens.

Methods

Blood Samples

Venous blood from healthy volunteers was collected into Z Serum Sep Clot Activator tubes or K_3EDTA plasma vacuettes (Greiner Bio-one, Frickenhausen, Germany) and centrifuged twice at 2500g for 15 minutes at 10°C. Serum or plasma was extracted and stored at -20°C until analysis. The study was approved by the Southern Adelaide Clinical Human Research Ethics Committee (SAHREC; number 261.18). Serum and plasma samples from patients with non-alcoholic fatty liver disease were purchased from Discovery Life Sciences (Hunstville, AL, USA).

Extracellular Vesicle Isolation

qEV Size Exclusion Chromatography

qEV Original (Legacy) 35nm and 70nm size exclusion chromatography (SEC) columns (iZon Science, Christchurch, NZ) were used to isolate EVs from serum or plasma. Prior to EV isolation, columns were equilibrated to room temperature and washed with 10mL of 0.2µm filtered phosphate-buffered saline (PBS). Serum (500µl) was loaded into the sample reservoir and allowed to completely pass into the column before PBS was added (no more than 2mL at any time) to begin elution. The first six fractions (3mL) eluted from the column was discarded and vesicles were collected as pooled fractions 7 to 11 (2.5mL) into 5mL Protein LoBind tubes (Eppendorf). Pooled vesicle fractions were mixed gently by inversion and concentrated to 100µL using Amicon Ultra-4 centrifuge filters (30kDa, Millipore-Sigma) pre-conditioned with PBS. Concentrated vesicle isolates were stored at -80°C until analysis.

ExoQuick Precipitation

Serum was centrifuged for 15 minutes at 3000 *x g* at 10°C to remove debris. Spun serum (50045) was combined with ExoQuick™ precipitation solution (126µL) and mixed 8 to 10 times by gentle inversion. Samples were incubated for 30 minutes on ice then centrifuged for 30 minutes at 1500g at 4°C to pellet EVs and again for 5 minutes in the same conditions, each time aspirating all supernatant. The pellets were resuspended in 100µL of filtered PBS/RIPA buffer and stored at -80°C until analysis.

Nanoparticle Tracking Analysis

Nanoparticle tracking analysis (NTA) was performed to quantify particle concentration and size distribution in EV samples using a NanoSight NS300 (Malvern Analytical, UK). Samples were diluted between 1:500 and 1:20000 in freshly 0.2μm filtered PBS. Five 60-second videos were captured at camera level 14 with a continuous sample flow (flow rate 100). Videos were analysed at detection threshold 5 using NTA 3.0 software.

Transmission Electron Microscopy

Samples were prepared based on a previously published protocol (Newman et al., 2021). Briefly, Ted-Pella B 300M carbon-coated grids (Ted-Pella, Redding, CA, USA) were cleaned and hydrophilized using plasma glow discharge for 15 seconds (Gatan SOLARUS Advanced Plasma Cleaning System, Gatan, Inc., Pleasanton, CA, USA) prior to use. Five microlitres of sample in 0.2μm-filtered PBS was placed on carbon-coated grids for 5 minutes. Carbon grids were washed once (15 seconds) at room temperature (RT) with 0.2μm filtered PBS and were contrasted with 2% uranyl acetate (3 minutes, RT), washed once, and examined by FEI TECNAI Spirit G2 TEM (Thermo Fisher Scientific, Waltham, MA, USA) operated at 100kV. TEM images were acquired at magnifications of 49,000× and 68,000× (Figure 2.1).

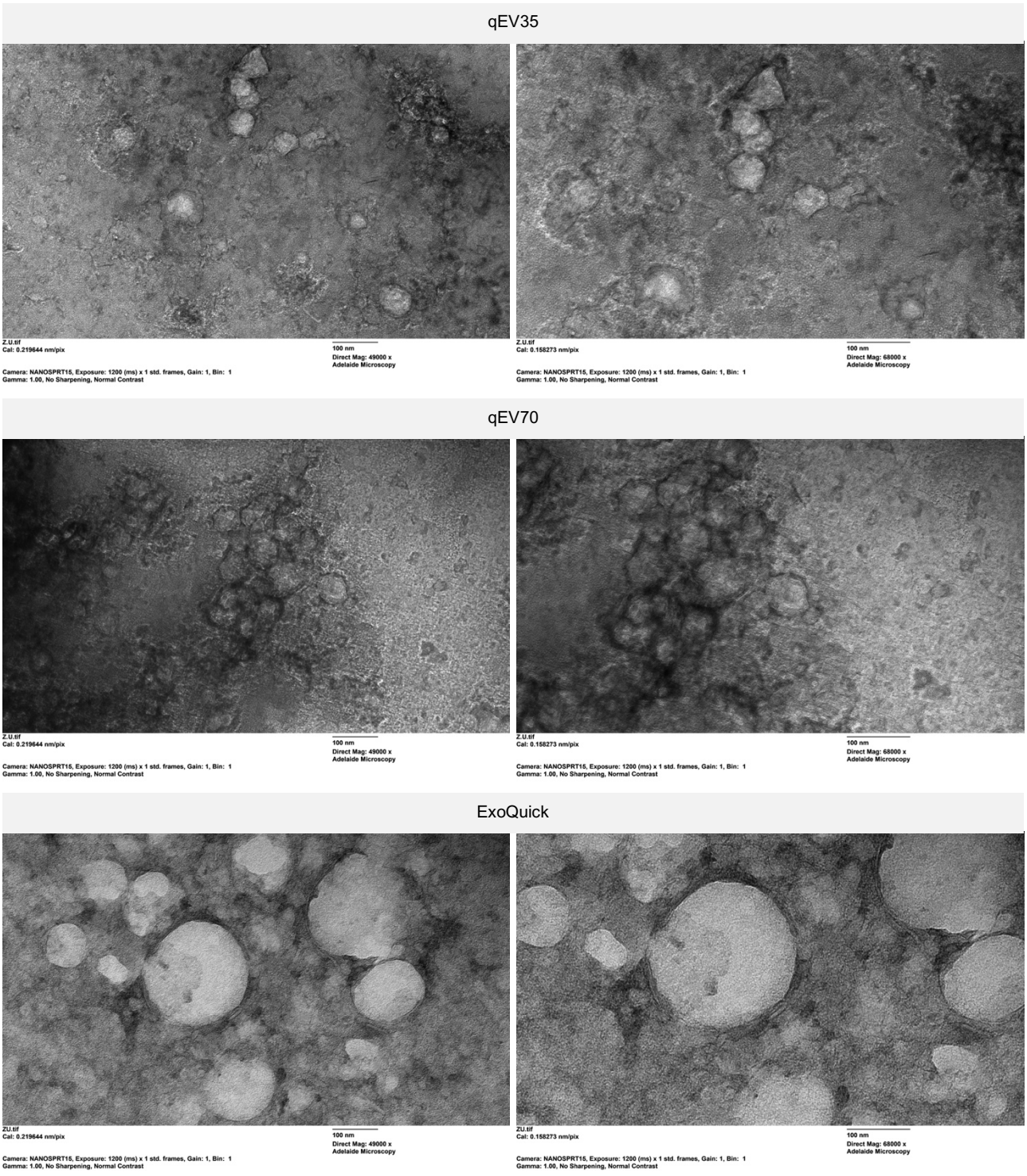

Figure 2.1 TEM images of EVs isolated by different methods.

Images taken at 49,000 x magnification (left panels) and 68,000 x magnification (right panels).

Human Liver Microsome Preparation

Pooled human liver microsomes (HLMs) were prepared by differential centrifugation as described by Bowalgaha et al. (2005). Briefly, liver portions (<1cm thickness) were suspended in phosphate buffer (0.1M, pH 7.4) containing potassium chloride (KCl; 1.15% w/v) and minced using scissors. The minced liver tissue was homogenized, initially with a Janke and Kunkle Ultra Turax at a speed of 24000rpm, and then with a Potter-Elvehem homogenizer (driven by a power drill) at a speed of 1480rpm. The homogenized tissue was centrifuged at 3000g for 10min at 4°C, and again at 10,000g for 10min at 4°C. The supernatant layer was collected and centrifuged at 105,000g for 1hr at 4°C. The resulting pellet was re-suspended in phosphate buffer (0.1M, pH 7.4) containing KCl (1.15% w/v) and then centrifuged at 105,000g for 1hr at 4°C. The final microsomal pellet was suspended in phosphate buffer (0.1M, pH 7.4) containing glycerol (20% v/v), aliquoted into 400µL samples, and stored at –80°C until use. Equal protein amounts of microsomes from five human livers (H7, female 44 years old (y/o); H10, female 67 y/o; H12, male 66y/o; H29, male 45y/o; and H40, female 54y/o) were used for the purpose of this study. Approval for the use of human liver tissue in xenobiotic metabolism studies was obtained from both the Clinical Investigation Committee of Flinders Medical Centre and from the donors' next of kin. All livers were obtained within 60 min of death and were immediately sliced and frozen in liquid nitrogen. Once frozen, livers were stored at -80°C until use.

Protein isolation from EVs for immunoblots

EVs isolated by qEV were lysed by mixing an equal volume (6µl) of EV sample in PBS with ice-cold RIPA (Radioimmunoprecipitation assay) lysis buffer (Thermo Fisher Scientific, IL, USA). ExoQuick isolated EVs (pellet) was lysed in 100µL of the above RIPA lysis buffer. All samples were incubated on ice for 25 minutes, centrifuged at 10,000g for 10 minutes at 4°C. Soluble protein was measured by micro BCA assay (Thermo Fisher Scientific, IL, USA), according to manufacturer's instructions. Briefly, working reagent (WR) was prepared using MA:MB:MC at 25:24:1 ratio. Lysed samples were diluted up to 300µl in 0.2 µm-filtered PBS. In a 96-well plate, equal volume of WR and either sample or bovine serum albumin (BSA) standard were mixed and assayed in duplicate. Absorbance of samples at 562 nm were compared to that of BSA standard curve (0-200 µg/mL) to determine protein concentration, using a SuperMax plate reader (Molecular Devices, CA, USA).

Protein isolation from human liver microsomes (HLM) and serum for immunoblots

HLM and serum protein was isolated by mixing equal volumes of HLM and ice-cold RIPA buffer, incubated on ice for 25 minutes, centrifuged at 10,000g for 10 minutes at 4°C. Soluble protein was measured, as above, by micro BCA assay (Thermo Fisher Scientific, IL, USA).

Immunoblotting

EV, HLM and serum protein (35 µg), isolated as described above, was used for immunoblotting as we previously described(Useckaite et al., 2020), except that 5% BSA/TBS containing 0.1% Tween 20 (TBST) was used. Protein lysates (EV, HLM and serum) were resolved on gradient SDS gels (Bio-Rad Laboratories, CA, USA) and the proteins where then transferred to Immun-Blot LF polyvinylidene difluoride (PVDF) membrane, 0.45 lm (Bio-Rad Laboratories, CA, USA), using a Turbo Blot transfer unit (Bio-Rad Laboratories, CA, USA). Stain-free imaging of the gel was performed using a ChemiDoc MP imager (Bio-Rad Laboratories, CA, USA) with a 1-min stain activation time as previously described(Colella et al., 2012). Total protein images were obtained at pre-blocking of PVDF (Figure 2.2). PVDF membranes were blocked with 5% (w/v) BSA in TBST and incubated overnight at 4°C with primary antibodies.

Primary antibodies (in 5%BSA/TBST) from Abcam (Abcam, Cambridge, MA, USA) were anti-human CD9 (Cat.#:ab92959; 1/1000); anti-human CD63 (Cat.#:ab68418; 1/1000); anti-human CD81 (Cat.#:ab109201; 1/1000); and anti-human Calnexin (Cat.#: ab2791; 1/1000). Primary antibody for anti-human TSG101 was from Invitrogen (Thermo Fishes Scientific, IL, USA; Cat.#:PA5-31260; 1/1000). Secondaries from Cell Signalling Cell Signalling Technology, MA, USA) were anti-mouse IgG, HRP-linked (Cat.#:7076; 1/1000) or anti-rabbit IgG, HRP-linked (Cat.#:7-74; 1/1000). Human liver microsome-lysate was included in all gels as a positive control. Serum lysate was added as a positive control for Albumin.

SuperSignal West Femto Chemiluminescent Substrate Kit (Thermo Fisher Scientific, IL, USA) was used for detection, imaging was performed using an automated ChemiDoc Touch Imaging System (Bio-Rad Laboratories, CA, USA) and densitometric analysis was performed using ImageJ tool (https://imagej.nih.gov/ij/index.html).

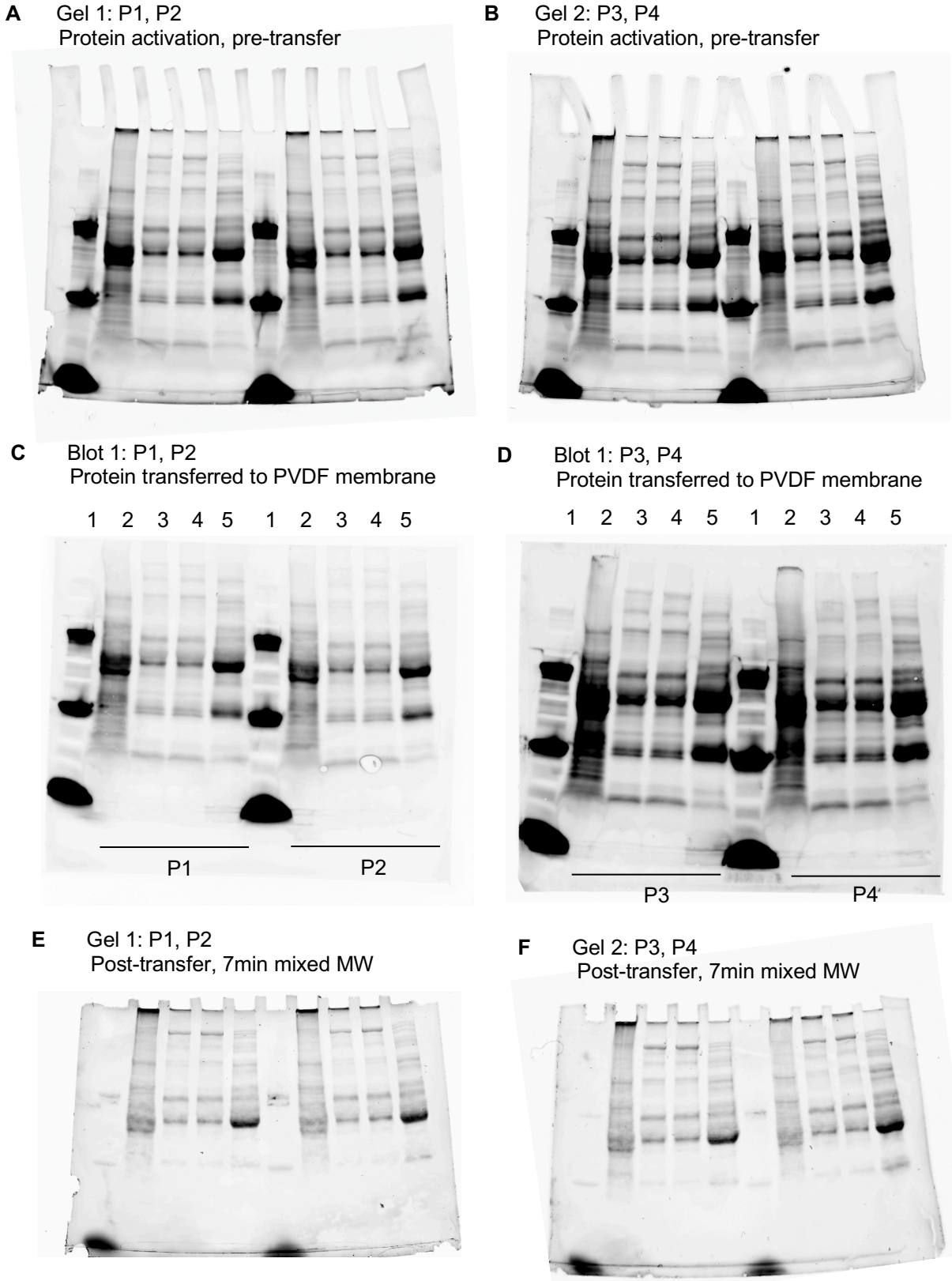

Figure 2.2 Full images of immunoblot gels.

A-B: total protein activation pre-transfer, C-D: PVDF membranes, E-F: post-transfer (C-D). No stain, 35µg of lysed HLM or EV protein loaded to each well. Lane 1= MW marker, Lane 2=HLM, Lane 3=qEV35, Lane 4=qEV70, Lane 5=ExoQuick.

Protein Digestion

EVs isolated by SEC columns and by ExoQuick precipitation, 50µl and 10µl respectively, were diluted up to 100µl in PBS; containing between 70-120 µg of SEC EV protein and 1132-1683 µg of ExoQuick EV protein. EVs were lysed by vortexing for 10 minutes using a MixMate sample mixer (Eppendorf) followed by three freeze-thaw cycles. Lysed samples were mixed with 50µL of ammonium bicarbonate (pH 7.8) and incubated with dithiothreitol (12.5 mM) for 90 minutes at 60°C. Samples were cooled to room temperature prior to addition of iodoacetamide (23.5 mM) and incubation for 60 minutes at 37°C. Trypsin Gold was then added to protein samples in a ratio of 1:40 and incubated for 17 hours at 37°C. Samples were mixed with 20µL of formic acid (10% v/v) in order to terminate digestions, then centrifuged at 16,000g for 10 minutes at 4°C. Resulting supernatant (100µL) was spiked with a SIL peptide cocktail (final [nM]: ALB: 10; CD81: 0.4; CD9: 0.1; CANX, TSG101: 0.2). SIL peptides were obtained from Vivitide (MA, USA), all of isotopic purity > 99%. Digested samples containing SIL peptides were run immediately and stored in the autosampler at 15°C over the course of the run. A 5µL aliquot of digested protein was injected for analysis by LC-MS/MS (Table 2.1). HLM and serum, diluted 1:100 in PBS, were digested in the same conditions and run as positive controls.

Table 2.1 Protein concentration of EVs and sample consumption for protein detection methods.
Total protein measured by micro BCA. Comparison of sample consumption for immunoblots and LC-MS/MS injections. Immunoblot protein loading = 35 µg. LC-MS/MS injection volume = 5µl.

			Immunoblots		**LC-MS/MS**	
Method	Donor	Protein Concentration (µg/µl)	Volume EVs Loaded (µl)	Equivalent Serum Volume (µl)	Protein per Injection (µg)	Equivalent Serum Volume (µl)
qEV35	1	1.71	20.4	102.1	4.28	12.5
	2	1.68	20.8	104.2	4.20	
	3	1.54	22.7	113.6	3.85	
	4	1.41	24.8	124.1	3.53	
qEV70	1	1.92	18.2	91.1	4.80	12.5
	2	1.67	20.9	104.7	4.18	
	3	2.40	14.6	72.8	6.00	
	4	1.85	18.9	94.6	4.63	
ExoQuick	1	139.27	0.25	1.26	69.64	2.5
	2	116.42	0.30	1.50	58.21	
	3	113.22	0.31	1.55	56.61	
	4	168.33	0.21	1.04	84.17	

Chromatography

Chromatographic separation of analytes was performed on an Agilent Advance Bio Peptide Map column (100mm x 2.1mm, 2.7µm) using an Agilent 1290 Infinity II liquid chromatography system. The temperature of the sample and column compartments was maintained at 15°C and 30°C, respectively. A panel of analytes comprising the EV makers CD81, CD9, and TSG101, and contaminants calnexin (CANX) and albumin (ALB), were separated by gradient elution with a flow rate of 0.2mL/min. The mobile phase consisted of 0.1% formic acid in water (mobile phase A) and 0.1% formic acid in acetonitrile (mobile phase B) held in a proportion of 97% A and 3% B for the first 3 minutes. The proportion of mobile phase B was then increased linearly to 30% over 30 minutes then increased to 50% in 5 minutes and held for 1 minute before returning to 3% over a further 5 minutes. Lastly, mobile phase B was held at 3% to re-equilibrate the column for 5 minutes.

Mass Spectrometry

Column eluant was monitored by mass spectrometry using an Agilent 6495B Triple Quadrupole mass spectrometer operating in positive electron spray (ESI+) mode. Target proteins were included in the panel in accordance with MISEV reporting guidelines. Proteotypic peptides for each protein marker were screened in EV samples and/or positive controls (HLM) and confirmed using Skyline software. Peptides contained between 7 and 22 amino acids for uniqueness and mass range of triple quadrupole instrument. Peptides had no methionine or cysteine residues. Sites of mutagenesis or post-translational modifications were avoided. For one peptide per protein, one quantifier and two qualifier ion transitions were included for optimisation of the multiple reaction monitoring (MRM) method based on signal intensity (Table 2.2). Three types of each analyte were detected; synthetic isotope labelled (SIL), endogenous and synthetic light peptide; as the latter was spiked into samples to supplement endogenous levels where required for assay validation. Skyline software was used to verify transitions and to select the optimal collision energy for each transition from seven predicted voltages. MassHunter Optimiser Software was used to optimise source parameters: capillary voltage, nebuliser pressure and nozzle voltage; and cell accelerator voltage was optimised manually between 3 and 8 V. Identities of endogenous peptides were confirmed by comparing retention time and quantifier/qualifier transition ratios to respective SIL peptide standards.

Table 2.2 Analyte sequences and transitions used for multiple reaction monitoring.
SIL (^): stable isotope labelled peptide; bold and underlined letter = heavy labelled amino acid. Bold values indicate product ions used as quantifier transitions.

Analyte	Type	Sequence	Retention Time (min)	Precursor Ion	Product Ions			Collision Energy (eV)
ALB	SIL	H2N-LVNEVTEFA**<u>K</u>^**-OH	20.7	579.3	603.3 (y5+)	702.4 (y6+)	**945.5 (y8+)**	18.8
	Light	H2N-LVNEVTEFAK-OH	20.7	575.3	595.3 (y5+)	694.4 (y6+)	**937.5 (y8+)**	18.8
CD81	SIL	H2N-QFYDQALQQAVVDDDANNA**<u>K</u>^**-OH	23.9	754.4	870.4 (y8+)	**969.4 (y9+)**	1068.5 (y10+)	17.3
	Light	H2N-QFYDQALQQAVVDDDANNAK-OH	23.9	751.7	862.4 (y8+)	**961.4 (y9+)**	1060.5 (y10+)	17.3
CD9	SIL	H2N-DVLETFTV**<u>K</u>^**-OH	24.3	530.3	603.4 (y5+)	732.4 (y6+)	**846.5 (y7+)**	22.3
	Light	H2N-DVLETFTVK-OH	24.3	526.3	595.4 (y5+)	724.4 (y6+)	**837.5 (y7+)**	22.3
CANX	SIL	H2N-IVDDWANDGWGL**<u>K</u>^**-OH	27.2	748.9	797.4 (y7+)	**868.4 (y8+)**	1054.5 (y9+)	24.1
	Light	H2N-IVDDWANDGWGLK-OH	27.2	744.9	789.4 (y7+)	**860.4 (y8+)**	1046.5 (y9+)	24.1
TSG101	SIL	H2N-GVIDLDVFL**<u>K</u>^**-OH	32.5	563.8	742.5 (y6+)	**857.5 (y7+)**	970.6 (y8+)	18.4
	Light	H2N-GVIDLDVFLK-OH	32.5	559.8	734.4 (y6+)	**849.5 (y7+)**	962.6 (y8+)	18.4

Assay Validation and Calibration

Calibration standards (n=8) were prepared to span the concentration ranges associated with qEV70 EV isolates, and to ensure a robust minimal concentration to exclude contamination (CANX and ALB) from human serum. In this range, assay linearity was determined for each analyte according to linear regression analysis. Assay sensitivity was determined for the panel. The limit of detection (LOD) was defined as a signal to noise ratio of 3:1 and the lower limit of quantification (LLOQ) as 5x the LOD.

Precision was assessed on the basis of intra- and inter-day variability in the slope produced by calibration curves run in triplicate on three separate days. Variability was recorded as percent relative standard deviation (% RSD) of triplicate injections (within run) and of average slope across different days (between runs). Repeatability was assessed by five consecutive injections of a mid QC sample and variability recorded as % RSD. Accuracy was determined based on the recovery of SIL peptide spiked into quality control (QC) samples at low (ALB: 6; CD81: 0.6; CD9: 0.06; CANX, TSG101: 0.12 [nM]), mid (ALB: 10; CD81: 1; CD9: 0.1; CANX, TSG101: 0.2 [nM]) and high (ALB: 18; CD81: 1.8; CD9: 0.18; CANX, TSG101: 0.36 [nM]) concentrations within the calibration curve. Carryover was assessed in two consecutive blank injections following the highest calibration standard.

The stability of analytes was evaluated in duplicate EV samples. Samples were kept at -20^{o}C, 4^{o}C, or 15^{o}C and analysed at baseline and after 6, 24 and 48 hours. Concentration was determined at each time point and changes from baseline of less than 20% were accepted as stable.

Matrix effects were assessed based on absolute and relative recovery of SIL peptides spiked in EV matrix or mobile phase. Calibrators 1 and 6 and a middle QC sample were prepared and analysed in each matrix and used to generate curves. Matrix effects were reported as % difference in slope and precision in each matrix was based on triplicate injections of each QC.

The reproducibility of the protocol was assessed based on the reproducibility of detecting analytes and of quantifying analytes. EVs were isolated in triplicate from the serum of three donors by each of the three isolation methods as described above, and peptide digests were performed in

duplicate, as also previously described. Reproducible detection across replicate isolations was defined by samples with average normalised response > LOD and reproducible detection in peptide digests was defined by equivalent response (both duplicates are < or > LOD) in each pair.

Additional analyses were performed to demonstrate the generalizability of the assay. Specifically, these analyses demonstrate the capacity to detect EV markers in plasma from healthy controls and serum and plasma from subjects with non-alcoholic fatty liver disease (NAFLD). These analyses were performed using EVs isolated by two distinct isolation approaches.

Statistical Analysis

Statistical analyses were performed using GraphPad Prism software version 9 (San Diego, CA, USA). Comparisons of group means were assessed by repeated measures one-way ANOVA with Tukey test for multiple comparisons. Linear regression analysis was performed using Microsoft Excel version 16.

EV-TRACK

We have submitted all relevant data of our experiments to the EV-TRACK knowledgebase (EV-TRACK ID: EV220163) (Van Deun et al., 2017).

Results

Characterisation of Extracellular Vesicles

Extracellular vesicles were isolated from human serum (n=3) by each of three commercially available methods; qEV70 and qEV35 SEC columns, and ExoQuick precipitation. TEM images revealed characteristic morphology and structurally intact vesicles isolated by each method, however, high background from non-vesicular contamination was prevalent in the ExoQuick image (Figure 2.3A). The mean particle concentration varied between methods, with significantly more particles isolated by ExoQuick compared to qEV70 (Figure 2.3B). Mean particle size measured by NTA was consistent across the three isolation methods (Figure 2.3C), although TEM images demonstrated the presence of a sub-population of larger vesicles in the ExoQuick isolate.

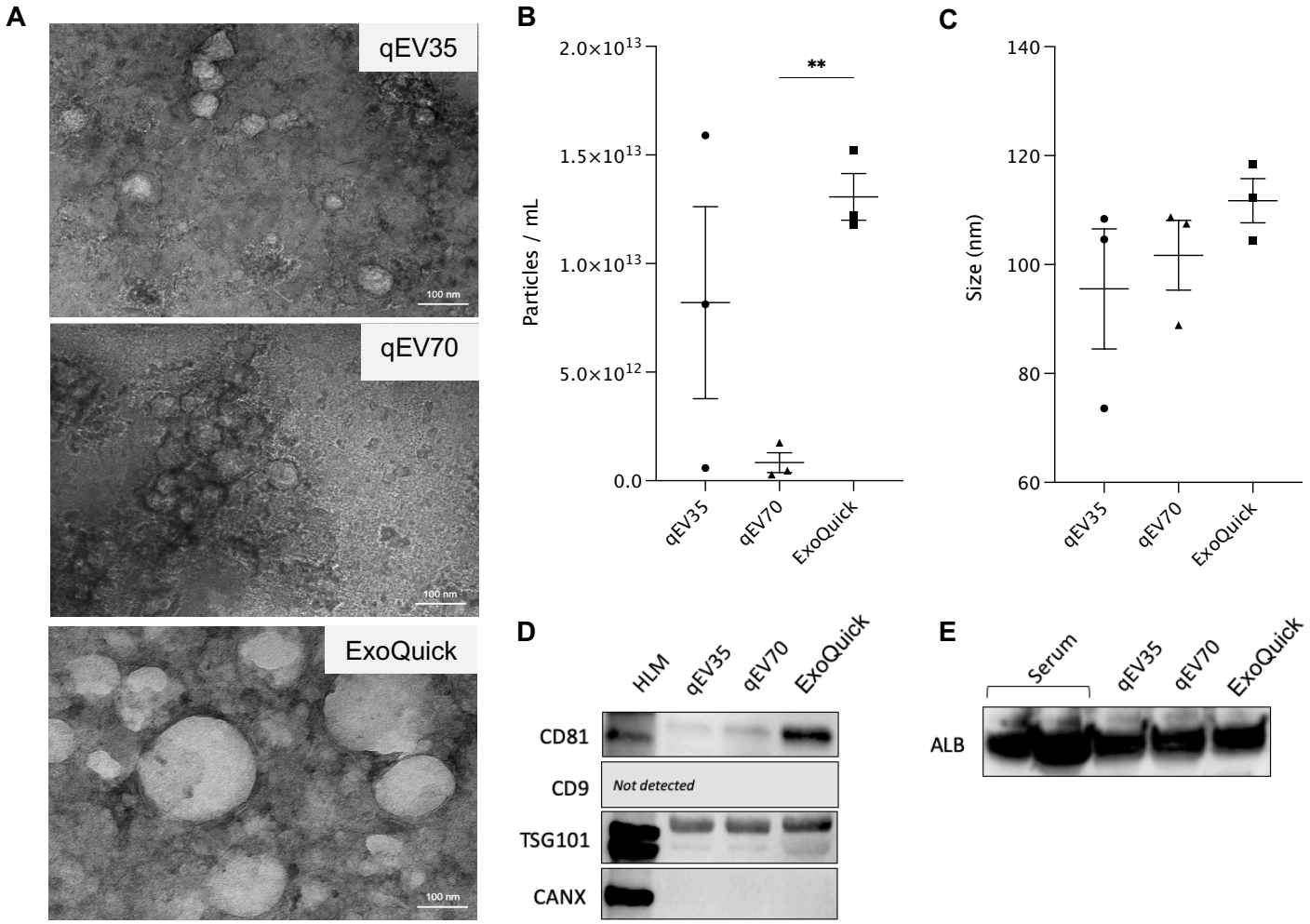

Figure 2.3 Characterisation of extracellular vesicles isolated by SEC and precipitation.

(A) Transmission electron microscopy images. Direct magnification x 30,000. Scale bar = 100nm. (B) Concentration and (C) Mean size of particles measured by nanoparticle tracking analysis. Data shown as mean ± standard deviation; ** $p < 0.01$; (n = 3), One-way ANOVA and Tukey test for multiple comparisons. (D) Representative images of key proteins considered to be markers of EVs (CD81, CD9 and TSG101), according to MISEV 2018 guidelines, in EVs isolated by qEV35, qEV70 and ExoQuick against HLM (non-EV control). Endoplasmic reticulum protein, CANX, was included as a marker of cellular structures considered to be enriched in cells relative to EVs (i.e. non-EV component, negative EV marker). (E) Representative image showing albumin contamination in EV samples isolated by qEV35, qEV70 and ExoQuick. Thirty-five micrograms of lysed EV or serum protein loaded per lane. Two lanes of albumin represent 35µg of protein that leaked to the neighbouring well due to pipetting error.

Irrespective of EV isolation method, common EV markers CD81 and TSG101 were detected by immunoblots in all EV samples (Figure 2.3D, Fig. 2.4), although differences in apparent abundance were observed (Figure 2.5). TSG101 abundance was comparable between EVs isolated by each of the SEC columns, while a greater amount was detected in ExoQuick samples. Similarly, samples isolated by SEC columns displayed low levels of CD81, with the highest signal detected in ExoQuick-isolated samples. Two bands were observed for TSG101 protein, in line with other publications using the same antibody (Schroeder et al., 2020, Hofmann et al., 2020). CD9 expression was not detected in any of the samples. The endoplasmic reticulum (ER) protein, CANX, was included in the analysis as a marker of cellular structures other than that of the endolysosomal pathway. CANX expression was below the limit of detection of the immunoblot method. While this method cannot provide a quantitative assessment, the lack of CANX detection may suggest either minimal cellular debris or large EVs.

Since EVs were isolated from human serum, an additional immunoblot was run to compare albumin contamination across EV samples resulting from different methods of EV isolation (Figure 2.3E, Fig. 2.6). Lysed serum protein was analysed as a positive control. Similar size bands were observed at approximately 70kDa across all EV samples, irrespective of isolation method. Importantly, blots were loaded with equivalent amount protein (35µg) for each sample type, so they do not reflect the analyte abundance in equal volumes of starting material. Specifically, the average volumes of serum corresponding to amount of loaded protein for EV samples isolated by qEV35, qEV70 and ExoQuick are 111µl, 91µl and 1.3µl, respectively (Table 2.1). This consideration of co-isolated contaminants per serum volume highlights the vastly greater levels of albumin recovered in ExoQuick isolates compared to SEC. Indeed, SEC has been reported to isolate a greater ratio of vesicle to serum proteins, compared to precipitation reagents or conventional techniques such as ultracentrifugation, and can reproducibly isolate vesicles containing characteristic EV markers(Vanderboom et al., 2021, Monguió-Tortajada et al., 2019). As qEV35 enriches for vesicles 35-350 nm in diameter while qEV70 enriches those 70-1000 nm, the former is prone to greater co-isolation of lipoproteins from the blood. For these reasons, development of the peptide assay was primarily performed using vesicles isolated by qEV70.

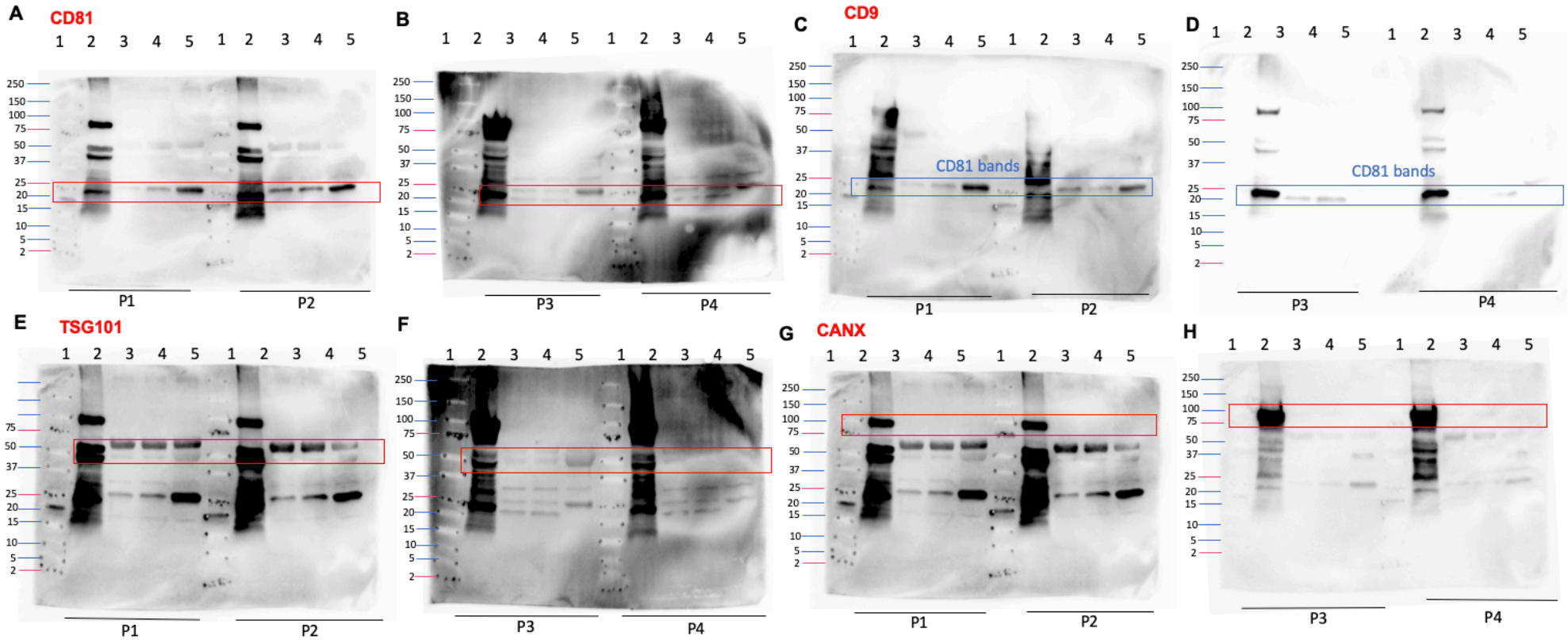

Figure 2.4 Full images of immunoblots with staining of EV markers.

(A-B) CD81, (C-D) CD9, (E-F) TSG101 and (G-H) CANX on PVDF. No CD9 band observed, unsuccessful stripping of CD81 antibody. Auto exposure, 35µg of lysed HLM or EV protein loaded to each well. Lane 1 = MW marker, Lane 2 = HLM, Lane 3 = qEV35, Lane 4 = qEV70, Lane 5 = ExoQuick. CD81 predicted band 25kDA, observed band 20kDa. CD9 predicted band 25kDa, reported 22kDa on manufacturers website. Not observed. TSG101 predicted band ~50kDa, observed double band at 48-55kDa. CANX predicted band at ~90kDa, observed at ~95kDa.

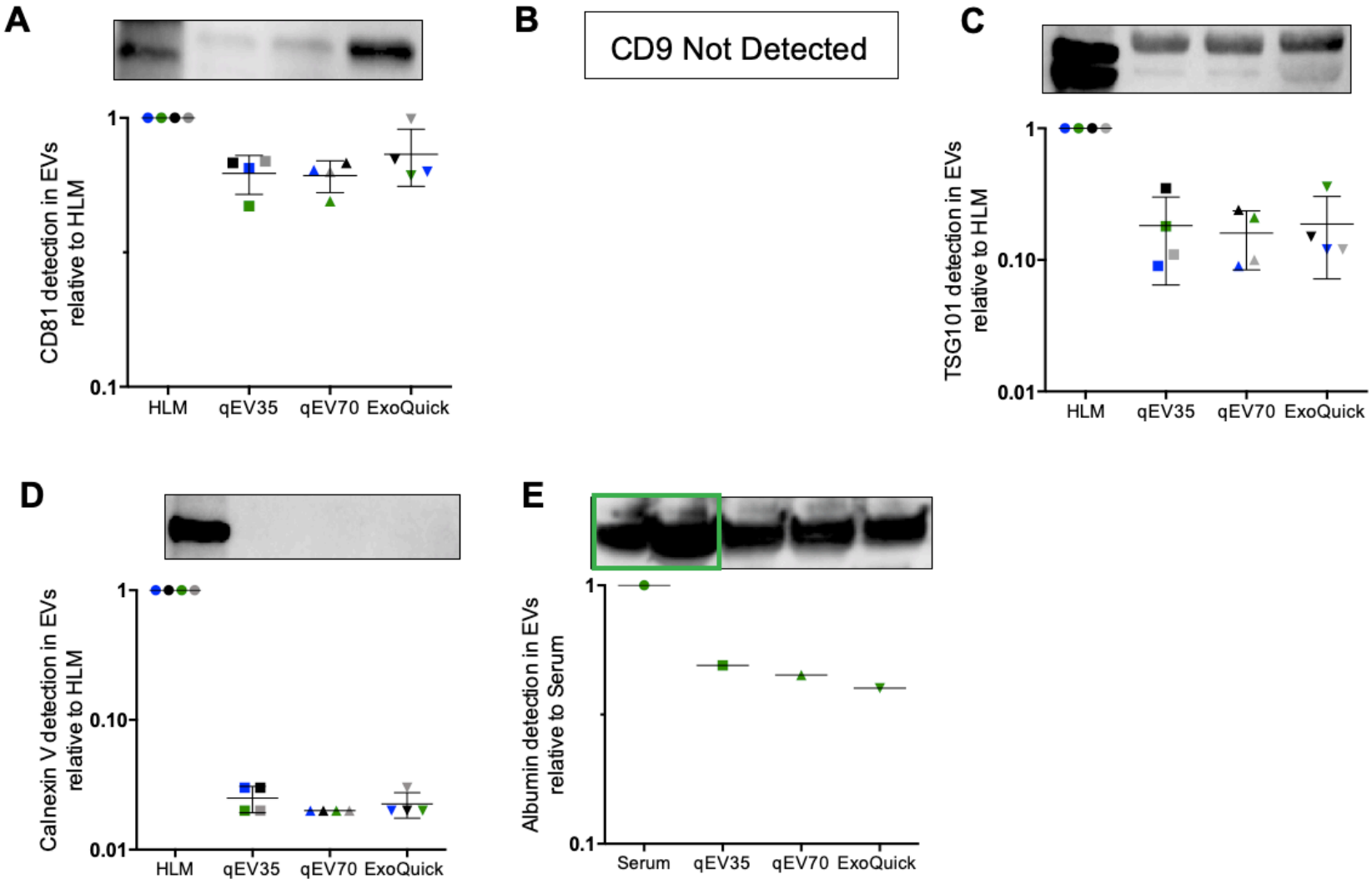

Figure 2.5 Relative protein quantification by ImageJ.

ImageJ obtained values for non-EV controls (A-D) and serum (E) were set to 1 and values obtained for corresponding EV lanes were expressed as fold change relative to non-EV control.

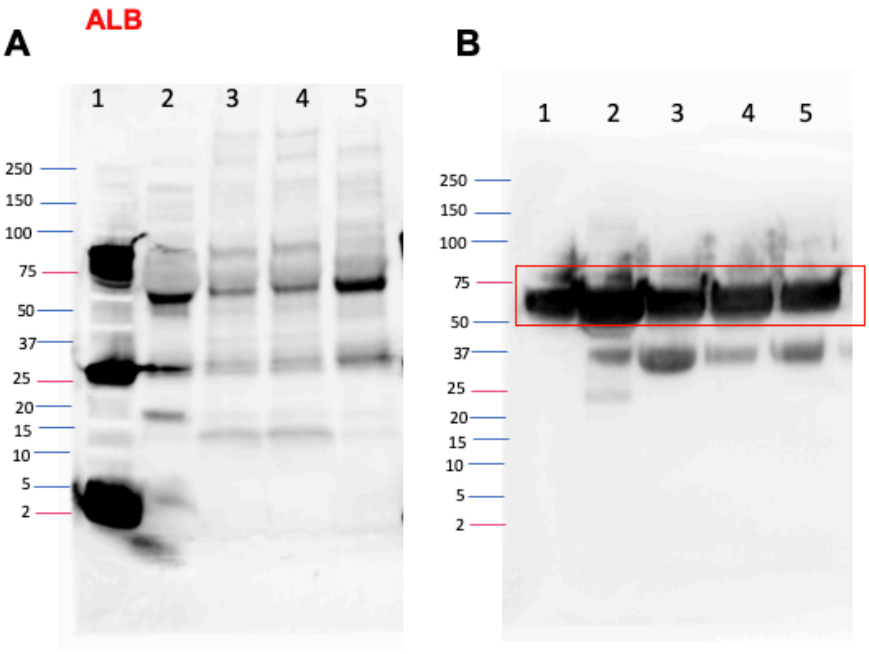

Figure 2.6 Full image of immunoblots showing staining of albumin.

(A) Full image of protein on PVDF/stain-free; (B) Full image of immunoblot showing albumin expression at ~ 70kDa. Lane 1= MW marker, Lane 2 = HLM, Lane 3 = qEV35, Lane 4 = qEV70, Lane 5 = ExoQuick.; Protein leaked from Lane 2 into Lane 1, therefore, Lane 1 and Lane 2 are considered to be one well in terms of albumin protein expression. EV protein and matched serum samples from P1 were used; 35µg of lysed serum or lysed EV protein loaded to each well.

MRM Method Development

Target proteins were selected to address the category reporting requirements outlined in the MISEV guidelines for EVs derived from blood products (serum or plasma)(Théry et al., 2018). The final protein panel comprised CD81 (Category 1[a]), CD9 (Category 1[b]) and TSG101 (Category 2a) as positive vesicle markers, albumin (ALB; Category 3) to represent matrix-associated contamination in EV isolates from the blood, and calnexin (CANX; Category 4) as a marker of cellular debris or large vesicles. Selected tryptic peptides corresponding to each target protein were detected in vesicles isolates and/or positive controls (HLM) and one precursor ion with three product ion transitions of greatest intensities were included for optimisation (Table 2.2). Instrument settings were optimised as described in materials and methods and values for optimised parameters are given in Table 2.3. Chromatograms of SIL peptides spiked into digested EVs (qEV70) is shown in Figure 2.7. Retention times were highly reproducible for each analyte measured in calibration standards with RSD between 0.04 and 0.07 %.

Table 2.3 Mass spectrometer instrument settings.

Parameter	Setting			
Time segment (min)	0-22	22-26	26-30	30-48
Delta EMV (V)	300	300	300	300
Capillary voltage (V)	3000	2500	3000	3000
Nebulizer pressure (psi)	30	25	30	30
Nozzle voltage (V)	1000	500	500	500
Cell accelerator voltage	5	3	5	4

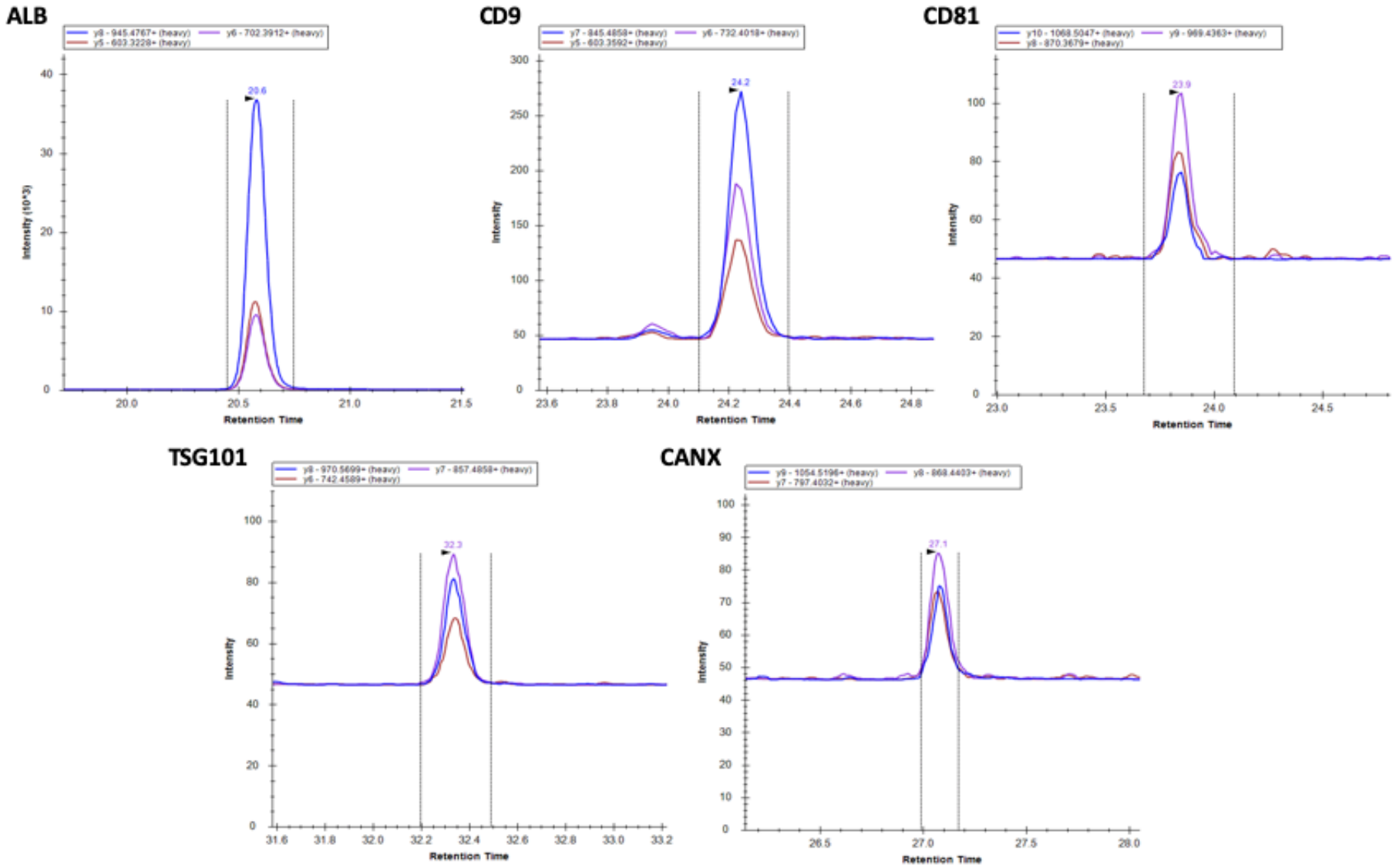

Figure 2.7 Representative chromatograms in Skyline.

Stable isotope labelled peptides [ALB: 80 pmol/mL, CD81: 8 pmol/mL, CD9: 0.8 pmol/mL, CANX: 1.6 pmol/mL, TSG101: 1.6 pmol/mL] spiked into EV digests (qEV70) from healthy human serum.

Assay Validation

Linearity and sensitivity

Calibration curves were generated for each analyte in the panel to encompass the concentration range typically observed for normal human serum (calibrators 1-6) and at points two and four times beyond that, as may be observed with increased levels of circulating EVs in various disease states (calibrators 7 and 8)(Nguyen et al., 2021, Povero et al., 2020, Malhi et al., 2021). The required range varied considerably between positive and negative EV markers: Albumin was validated between 2.0-80 pmol/mL while this range was 100-fold less for CD9 (Table 6). Linearity of response was assessed by linear regression analysis and produced coefficient of determination (r^2) values for each analyte ranging between 0.9966 and 0.9999 (Figure 2.4). The sensitivity of the assay was determined with respect to LOD and LLOQ, calculated as described in materials and methods. For most of the analytes, the validated calibration range extended towards the lower end of the assay's sensitivity. Details of these characteristics are summarised in Table 2.4.

Table 2.4 Details of calibration and quantification for analytes in the EV Marker Panel.

Analyte	Calibration Range (pmol/mL)	Calibration Curve Coefficient of Determination (r^2)	Limit of Detection (LOD) (pmol/mL)	Lower Limit of Quantification (LLOQ) (pmol/mL)
ALB	2.0 – 80	0.9999	0.004	0.020
CD81	0.2 – 8.0	0.9985	0.050	0.230
CD9	0.02 – 0.8	0.9982	0.005	0.025
CANX	0.04 – 1.6	0.9984	0.007	0.035
TSG101	0.04 – 1.6	0.9966	0.006	0.031

Assay precision, repeatability and accuracy

Assay precision was assessed based on intra- and inter-day variability in the slope of calibration curves run in triplicate on three separate days. The %RSD ranged from 0.4 to 13 % for within-run variability in analyte response, and between runs, variability ranged from 0.4 to 8 % (Table 2.5). Instrument repeatability was also determined in five consecutive injections of the same sample and gave RSD < 9 % for all analytes. Relative accuracy (within matrix) of the assay was determined by measurement of low, mid and high QC samples. These QC points were selected within the

concentration range typically observed for normal human serum (calibrators 1-6); nominal concentrations are given in table 8. For all analytes, accuracy ranged from 92-112 % at low, 97-116 % at mid, and 94-110 % at high QC concentration (Table 2.6).

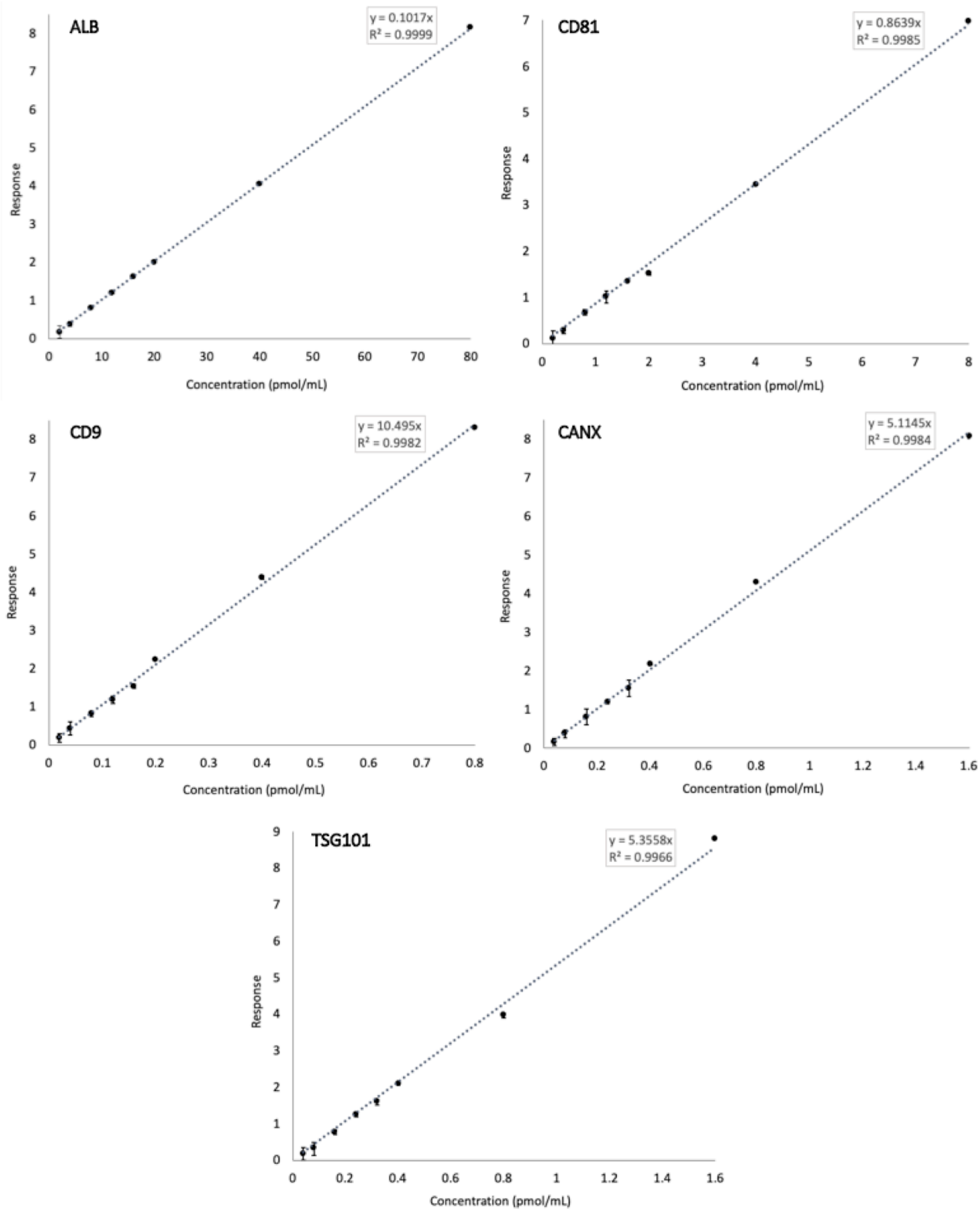

Figure 2.8 Calibration curves for analytes in the EV Marker Panel.

Error bars represent % relative standard deviation (% RSD) (n=3).

Table 2.5 Assay Precision.
Relative standard deviation (% RSD) of slopes of triplicate calibration curves run within day and on three different days.

Analyte	Variability (% RSD)	
	Intra-day	Inter-day
ALB	0.4	0.4
CD81	5.6	7.6
CD9	3.0	6.2
CANX	4.5	3.9
TSG101	13	4.6

Table 2.6 Assay Accuracy.

Analyte	QC Concentration (pmol/mL)								
	Low			Mid			High		
	Nominal	Measured	% True	Nominal	Measured	% True	Nominal	Measured	% True
ALB	6.0	6.75	112	10	10.9	107	18	20.2	110
CD81	0.6	0.550	92	1.0	0.972	97	1.8	1.72	96
CD9	0.06	0.063	105	0.1	0.094	94	0.18	0.187	104
CANX	0.12	0.112	93	0.2	0.232	116	0.36	0.340	94
TSG101	0.12	0.120	100	0.2	0.212	106	0.36	0.392	109

Carryover

Carryover was assessed in two consecutive 'blank' injections of mobile phase following injection of the highest calibration standard. Blank injections involved a full LC injection cycle. Albumin response was detectable in both injections (injection 1 = 4x LOD; injection 2 = LOD) but did not reach the LLOQ. For all other analytes, peak area response was less than LOD in both first and second injections.

Short-term stability

Analytes were tested for short term stability with storage at -20°C, 4°C, or 15°C. Concentration was determined at baseline and monitored in duplicate samples at 6, 24 and 48 hours. To calculate concentration, peak area response for endogenous analytes (or light peptide supplemented where required) was normalised to known concentrations of respective SIL peptide spiked in at baseline. Concentration of all analytes was generally stable across each time point

compared to baseline measures (Figure 2.9). ALB concentration varied less than 7% in all cases and variability between duplicates remained low over time (< 4% RSD). Indeed, there were no notable trends in %RSD as most measures varied no more than 19% between duplicates; except for CANX, for which variability increased up to the 24hr mark, especially in samples kept at -20°C (up to 34%). CANX concentration was otherwise stable over time, with most variability ± 17% from baseline. CD81 concentration was stable in samples stored at -20°C and 4°C with < 13% change from baseline. In 15°C samples, a slight decrease in SIL peptide response led to overestimated concentration by 26% at 24hr. Since SIL was spiked in at baseline and monitored concurrently with the light analyte, different rates of degradation will affect calculations of analyte concentration. When light and SIL peptide responses were assessed individually, there were also slight reductions in ALB and CD9 for samples kept at 15°C, but since signal was reduced in each light and SIL to a similar extent, no effect was observed in concentration. Lastly, TSG101 concentration was particularly stable over time in samples kept at -20°C and in 4°C and 15°C samples for 24 hours. In the latter two, however, levels had decreased by 20% and 29%, respectively by 48 hours. Overall, these data indicate that peptide concentration is stable during storage at -20°C and can also remain in the autosampler over the typical course of assay runs without significantly affecting results.

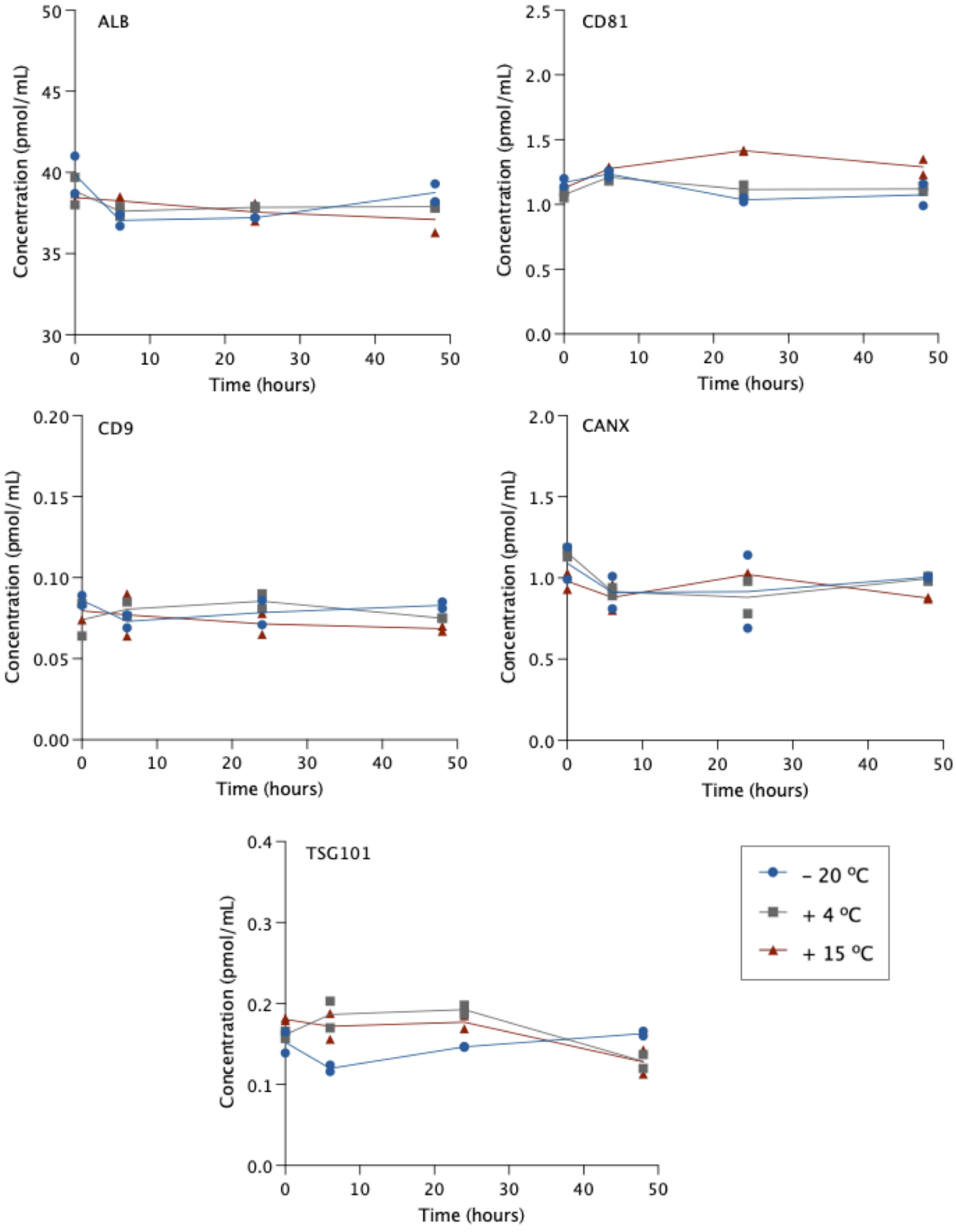

Figure 2.9 Short-term stability of peptide concentration at different storage temperatures.

Data reported from technical duplicates.

Matrix Effects

It is widely established that EV isolation methods are not equivalent in terms of both vesicle recovery and purity. The presence of non-vesicular contaminants can impact downstream analyses including detection and quantification of EV cargo by LC-MS/MS Thus, the effect of different EV matrices was assessed based on absolute and relative recovery of SIL peptides spiked into EV matrix or mobile phase. Relative recovery was determined in qEV35 and ExoQuick matrix using qEV70 as a comparator. Standard curves were generated using calibrators 1 and 6 and a middle QC. R^2 values exceeded 0.99 for all analytes; with the exception of CD81 in ExoQuick, which gave $r^2 = 0.977$ (Table 2.7). The ExoQuick CD81 curve was affected by imprecision at the lower calibration points. Precision is reported as %RSD of triplicate injections at each concentration level. The results were comparable with that observed in qEV70 matrix, though greater variability in CD81 quantification was observed in ExoQuick samples at the lower calibration point (27 %RSD). Only 22% of the CD81 response was recovered in ExoQuick matrix compared to qEV70, these data indicate that this analyte is impacted in ExoQuick matrix such that limits of detection and quantification occur at higher concentrations. Similarly, ALB response in ExoQuick was 40% of that in qEV70. The response for the remaining analytes were greater in alternate matrices compared to qEV70, most notably TSG101 was 164% and 171% in qEV35 and ExoQuick, respectively. Hence, this analyte, along with CD9 and CANX, may be detected and quantified at lower concentrations in qEV35 and ExoQuick EVs.

Table 2.7 Relative recovery of SIL peptides in EV matrices compared to qEV70.

Analyte	qEV35				
	Relative Recovery (%)		Precision (%RSD)		
	r2	% of Curve in qEV70	Lower	Mid	Upper
ALB	0.9999	107	16	6.9	10
CD81	0.9955	91	18	13	7.1
CD9	0.9994	147	18	3.6	9.1
CANX	0.9993	128	3.3	8.6	2.3
TSG101	0.9909	164	14	3.5	2.2
Analyte	**ExoQuick**				
	Relative Recovery (%)		Precision (%RSD)		
	r2	% of Curve in qEV70	Lower	Mid	Upper
ALB	0.9973	40	7.4	6.2	2.5
CD81	0.9770	22	27	15	14
CD9	0.9980	133	9.1	6.1	2.9
CANX	0.9998	127	2.3	4.3	0.9
TSG101	0.9974	171	10	3.6	1.7

To determine absolute recovery, the slope of the SIL peptide standard curves in each EV matrix were compared to that in mobile phase. Across each analyte, recovery in qEV70 matrix was observed at 38-69% of mobile phase, with TSG101 most impacted (Table 2.8). On average, qEV35 matrix exhibited the least impact on analytes (absolute recovery 52-88%). In ExoQuick matrix, albumin and CD81 peptide signals were significantly suppressed with recovery of just 22% and 13%, respectively.

Table 2.8 Absolute recovery of SIL peptides in EV matrices.

Analyte	Recovery (% of Curve in Mobile Phase)		
	qEV70	qEV35	ExoQuick
ALB	55	59	22
CD81	58	52	13
CD9	57	84	76
CANX	69	88	87
TSG101	38	54	57

The generalisability of the assay is demonstrated by analyses in serum and plasma from healthy donors and subjects with NAFLD. Analysis of markers in EVs isolated from plasma of NAFLD patients (n = 4) and healthy controls (n = 5) by qEV70 demonstrated a comparable capacity (relative to healthy serum) to detect positive EV markers and albumin. However, calnexin was only detected in 20% of healthy plasma EV samples. In EVs isolated by ExoQuick from NAFLD patient serum, markers were consistently detected across samples (Table 2.9).

Table 2.9 Detection of EV markers in serum and plasma EVs from healthy donors and patients with NAFLD using qEV70 and ExoQuick.

Analyte	qEV70 EVs > LOD (%)			ExoQuick EVs > LOD (%)	
	Healthy Serum (n=9)	Healthy Plasma (n=5)	NAFLD Plasma (n=4)	Healthy Serum (n=9)	NAFLD Serum (n=5)
ALB	100	100	100	100	100
CD81	78	80	100	100	100
CD9	100	100	100	100	100
CANX	100	20	80	78	100
TSG101	89	80	100	100	100

Reproducibility of Analyte Detection and Quantification

The reproducibility of the protocol was evaluated using the size exclusion chromatography and precipitation-based EV isolation methods. EVs were isolated from human serum (n=3) in triplicate using each of the three methods and duplicate peptide digests were analysed on the panel (i.e. 18 per isolation method). Concentration of analytes was determined based on normalised response (endogenous/SIL) in isolates from equivalent volumes of starting material using the three methods of isolation. Reproducibility was assessed based on analyte detection and analyte quantification, using LOD and LLOQ adjusted to reflect the observed effects of alternate EV matrices on relative recovery, as described above.

Given the primary function of the EV Marker Panel is to demonstrate the presence or absence of positive and negative markers in accordance with the MISEV guidelines, we first sought to determine the reproducibility of analyte detection in replicate samples. Reproducibility of isolation was based on average normalised response > LOD across triplicate isolations, and reproducibility

of peptide digests was defined by equivalent response (both duplicates are < or > LOD) in each pair (Table 2.10). Albumin and CD9 was detected in 100% of isolations and digests from all isolation methods. CD81 was also detectable in 100% of isolations and digests from qEV35 and ExoQuick EVs. However, from two of the donors, CD81 was not detected in qEV70 EVs in one isolation each, which reduced isolation reproducibility to 78% overall for this analyte. Further, some discrepancy between duplicate digests was observed, which may be attributed to the low abundance of CD81 in these samples. CANX and TSG101 were also detected reproducibly across isolations and digests in each isolation method.

Table 2.10 Reproducibility of analyte detection in EVs isolated by SEC or precipitation.

Analyte	Isolations > LOD (%) (n=9)			Equivalent Duplicate Digests (%) (n=9)		
	qEV70	qEV35	ExoQuick	qEV70	qEV35	ExoQuick
ALB	100	100	100	100	100	100
CD81	78	100	100	67	100	100
CD9	100	100	100	100	100	100
CANX	100	100	78	100	100	100
TSG101	89	100	100	89	89	100

To expand the applications of the assay beyond the binary determination of analyte detection, to those such as quantifying marker abundance for use as a normalisation strategy, the assay must demonstrate reproducibility of quantification. To this end, variability in concentration was determined in triplicate isolations and duplicate digests and presented as %RSD (Table 2.11). The variability of digests was less than 20% for all analytes above LLOQ in each isolation method. Cases in which replicate values were < LLOQ were considered reproducible, since the effect of noise precludes the calculation of accurate %RSD. TSG101, for example, could not be quantified in EVs from either SEC method. Meanwhile, this analyte was reproducibly quantifiable in ExoQuick isolates, exhibiting 14% and 6.9% RSD in isolations and digests, respectively. Similarly, CANX was < LLOQ in qEV70 but could be reproducibly quantified in qEV35 and ExoQuick EVs. Since CANX is relatively enriched in cells compared to EVs, human liver microsomes (HLM) were analysed as a positive control. Normalised to injected protein, CANX signal in EVs compared to HLM was 3.5% and 0.65% in qEV35 and ExoQuick, respectively. Positive EV marker CD9 could be reproducibly quantified across qEV70

and ExoQuick EVs (13% and 18% RSD, respectively). CD81 quantification was also reproducible in ExoQuick isolates but more variable in qEV35 at 37%, which was driven by the lack of quantifiable levels of the analyte in two of the triplicate isolations from one donor. Albumin concentration was 823-fold and 3.6-fold higher in ExoQuick and qEV35 isolates, respectively, compared to qEV70, and each exceeded the upper limit of quantification validated for the assay in qEV70 matrix. Relative to an equivalent volume of serum, the amount of albumin in samples isolated by each method was 0.7%, 0.003% and 0.001%, respectively. Despite significant depletion, albumin remains highly abundant in EV isolates compared to positive EV markers. Albumin quantification was reproducible across isolations in ExoQuick samples, while using SEC, variability was up to 36%. This suggests that while SEC columns, particularly qEV70, are more effective at removing albumin, the samples may be inconsistently affected by free protein contamination. Figure 2.10 shows the distribution of measured concentrations of analytes across all technical replicates with each isolation method with reference to limits of detection and quantification. Notably, ExoQuick samples are enriched for both CD81 and TSG101 in comparison to SEC samples, while the differences in CD9 are much less pronounced. While qEV70 samples have higher purity (less albumin), tetraspanins are more abundant in qEV35 EVs. Differences in marker abundance may be attributed to the columns enriching for vesicles of different size range. Further, recovery of vesicles (particularly CD81- and/or CD9- positive vesicles) is possibly compromised by decreasing contamination.

Table 2.11 Reproducibility of analyte quantification in EVs isolated by SEC or precipitation.

Analyte	Concentration (pmol/mL)			Isolation Variability (% RSD)			Digest Variability (% RSD)		
	qEV70	qEV35	ExoQuick	qEV70	qEV35	ExoQuick	qEV70	qEV35	ExoQuick
ALB	34	122	27984	36	30	6.5	2.5	8.1	3.4
CD81	0.25	0.38	8.54	19	37	20	3.8	6.4	20
CD9	0.04	0.16	0.24	18	22	13	20	9.2	6.9
CANX	< LLOQ	0.19	0.54	–	17	5.3	–	14	3.1
TSG101	< LLOQ	< LLOQ	1.55	–	–	14	–	–	6.9

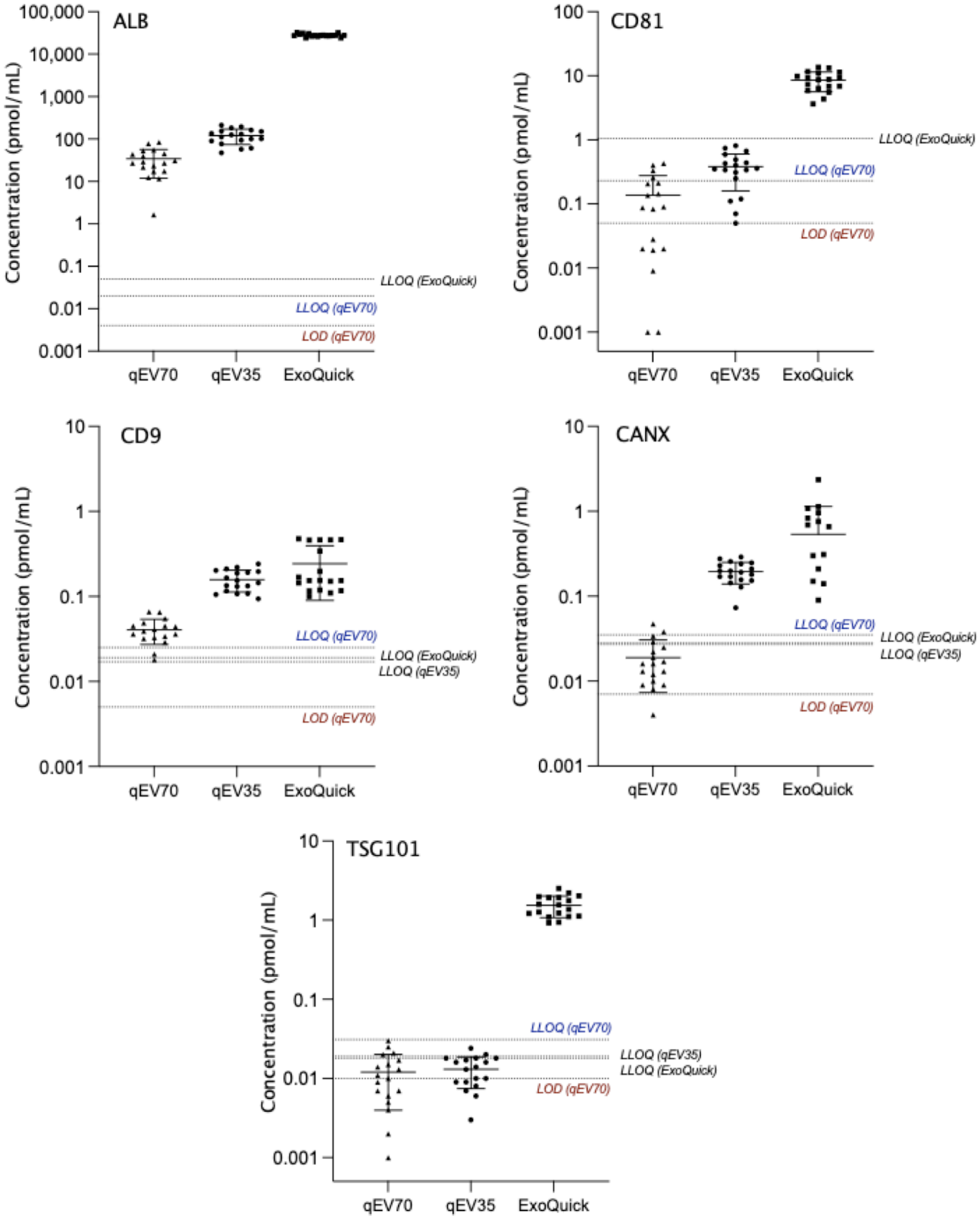

Figure 2.10 Concentration of EV marker analytes in EVs isolated by different methods.

Mean (±SD) concentration of analytes measured in duplicate peptide digests from triplicate EV isolations of n=3 biological replicates. Lower limit of quantification (LLOQ) and limit of detection (LOD) are indicated for qEV70 and LLOQ is given for analytes in alternate matrices where matrix effects (relative recovery differs > 20%) were observed.

Discussion

Here we describe the development and validation of a targeted LC/MS-MS peptide assay for the quantification of markers associated with extracellular vesicles and non-vesicle contaminants. A total of five EV +/- markers were included in the panel in accordance with the MISEV guidelines (Théry et al., 2018). As stated, samples should be characterised based on the presence of established transmembrane (CD9, CD81) or cytosolic (TSG101) proteins that incorporate in EVs due to roles in biogenesis and trafficking, and the absence or depletion of matrix-associated contaminants (e.g. serum protein, ALB) and non-endosomal intracellular compartment proteins (e.g. ER protein, CANX). The described workflow of in-solution peptide digest coupled with multiplexed panel format provides a high-throughput quantitative platform for the analysis of clinical samples, requiring only a fraction of that used for immunoblotting. In this regard, LC-MS/MS represents a valuable approach to streamline the acquisition of data for addressing reporting criteria, while reducing reagent costs, labour, and consumption of human biospecimens, which are often scarce in volume and irreplaceable.

Assay validation and calibration was primarily performed in EVs isolated by qEV70. Numerous studies (Veerman et al., 2021, Gámez-Valero et al., 2016, Brennan et al., 2020) compare the characteristics and molecular composition of EV isolates produced by various available methods, and increasingly, size exclusion chromatography is selected as the method of choice (Monguió-Tortajada et al., 2019, Sidhom et al., 2020, Liangsupree et al., 2021). Nonetheless, no single isolation method is considered suitable for all applications and downstream analyses. In the context of proteomic analyses, SEC has been favoured for the relative purity and detection of EV-associated proteins that can be achieved with marked reproducibility (Monguió-Tortajada et al., 2019, Veerman et al., 2021, Vanderboom et al., 2021). By comparison, methods that rely on precipitating agents, including ExoQuick, facilitate high recovery but may interfere with vesicle surface composition and co-isolate large amounts of soluble proteins that mask less abundant EV proteins (Gámez-Valero et al., 2016, Veerman et al., 2021). Similarly, conventional techniques such as ultracentrifugation suffer poor reproducibility and significant contamination with protein aggregates (Vanderboom et al., 2021).

The concentration range over which the assay was validated comprised eight calibrators to cover concentrations observed in healthy donor serum and beyond to increased levels that may be observed in various disease contexts (Povero et al., 2020, Nguyen et al., 2021, Malhi et al., 2021). For all analytes, calibration curves were linear (all $r^2 > 0.99$) and the assay exhibited good precision and accuracy. Notably, the concentration range validated for albumin was 100-fold greater than that for CD9. This aligns with previous findings that highly abundant serum proteins remain at concentrations in SEC isolates many orders of magnitude above that of EV markers (Nguyen et al., 2021, Vanderboom et al., 2021). Blood is a complex matrix from which to extract EVs, given their numbers are predominated by soluble proteins and various types of lipoproteins with similar physical properties. Irrespective, LC-MS/MS boasts exceptional sensitivity and the present assay exhibited detection limits in the picomolar range. The value of this sensitivity was realised in the context of sample consumption; where for SEC methods, the volume of serum used in immunoblotting was ~100µl on average, while only 12.5µl in equivalent serum volume was injected for LC-MS/MS analysis (Figure 2.11). Importantly, the latter approach permitted multiplexed analysis without compromising reliability of detection or requiring additional sample.

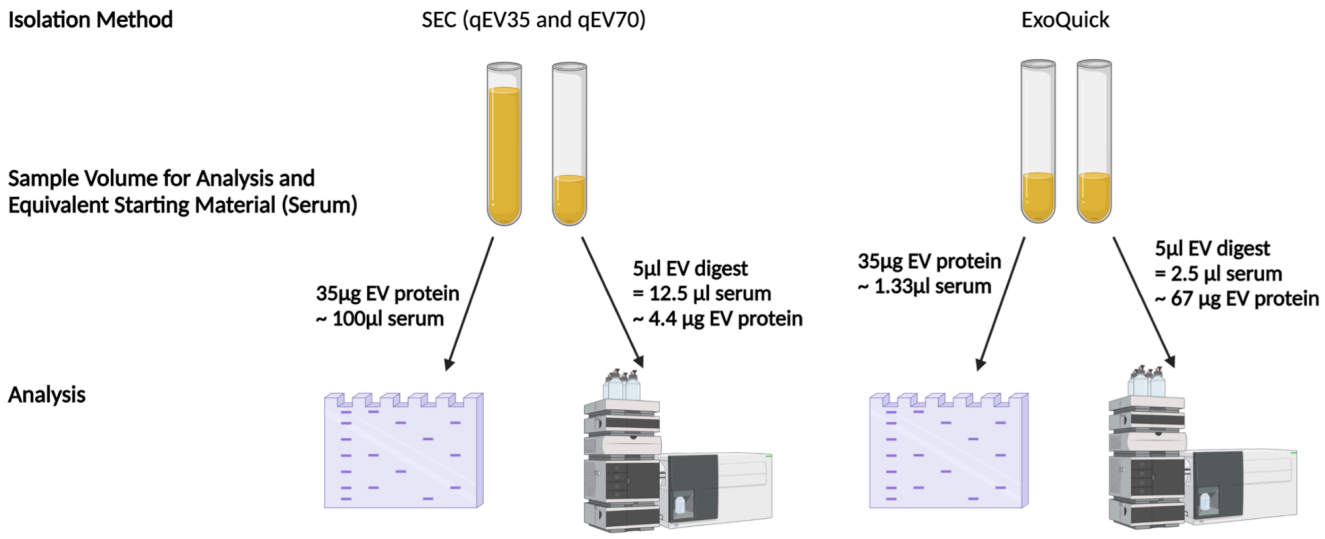

Figure 2.11 Comparison of sample consumption for immunoblots and LC-MS/MS injections in EV marker analytical workflow.

For immunoblotting, each biological repeat sample was run on a gel once, transferred onto PVDF membrane and re-probed for CD9, CD81, TSG101 and CANX. The ability to re-probe the

membrane following peroxidase deactivation has been previously demonstrated (Sennepin et al., 2009) and offers a time and sample-saving solution for multiple detections by western blot. However, in our case, this approach introduced several challenges. EV markers, CD9 and CD81 have a similar molecular weight (MW), with predicted bands at 25 kDa. As PVDF membranes were first probed and imaged for CD81, followed by the stripping, re-blocking and re-probing procedure for CD9, it was not possible to confidently assess both. In this case, stripping of the membrane was not successful and CD81 bands were still visible at MW of 25kDa. Under ideal conditions, enough sample is available to run a gel for one or two markers at different MW. When working with clinical samples of limited sample volume, there is often only enough sample for one immunoblot, presenting a challenge to the fulfilment of MISEV criteria (Théry et al., 2018). In this study, lysed EV samples were run only once using a set volume of starting material, thereby accentuating the limitations of immunoblotting that are overcome by our LC-MS/MS approach. With respect to quantitation, immunoblotting can successfully determine the presence and relative abundance of analytes between sample types or groups. Densitometric analysis was performed here but was affected by high background in some positive control (HLM) lanes (Figure 2.5 A & D), resulting in an overestimation of protein yield and skewed representation of the data from these lanes. In contrast, the LC-MS/MS assay could be validated for the absolute quantification of analytes using stable isotope-labelled peptides spiked into samples at known concentrations.

The degree and composition of contamination are key determinants of signal intensity and reproducibility in LC-MS/MS analysis. Peptides derived from non-vesicular material may co-elute with target EV markers and suppress ionisation; and those exhibiting similar mass to charge ratios may interfere with particular MRM transitions (Liebler and Zimmerman, 2013). The presence of different vesicle populations or contaminants, isolated by different methods, introduces different sources of interference (i.e. lipid or peptide composition) and therefore greater variability in marker detection and quantification. These matrix effects were evident in that the absolute recovery of several analytes was reduced in EV matrix irrespective of isolation method.

The reproducibility of the assay was considered within two distinct frameworks defined by the potential applications. Primarily, the EV Marker Panel can be used to demonstrate the presence

and absence of EV (+/-) markers in line with the characterisation and reporting criteria (Théry et al., 2018). Hence, reproducibility was assessed based on analyte response around the defined LOD. As the detection of analytes was highly reproducible across replicate isolations and digests using all methods, we demonstrate that the EV Marker Panel is fit-for-purpose. Importantly, this can be achieved using only a fraction of the sample that would otherwise be required for conventional methods, such as immunoassays.

In addition to addressing reporting requirements, quantification of EV markers may serve other functions, such as normalisation of EV-associated biomarker abundance, although such application would require assessment of quantitative reproducibility. While target analyte response is expected to be more variable in samples with greater levels of contamination, here, we found that in ExoQuick samples – which invariably contain large amounts of co-precipitated serum proteins – EV marker quantification was highly reproducible both in terms of replicate isolations and digests. Of the positive EV markers, CD9 quantification was most consistent across tested isolation methods and may be suitable for the purpose of normalising circulating biomarkers. The choice of isolation method is a key consideration for the analysis of both the biomarker and normaliser; but as seen in ExoQuick samples, certain levels of contamination may not be detrimental, providing acceptable reproducibility of isolation and quantification is achieved (Kreimer et al., 2015). The potential for human error is higher with SEC isolation due to greater hands-on time. A recent study also found more variability in proteomic profiles using methods that require more time and careful collection of EV-containing fractions (e.g. qEV70 and OptiPrep density gradient), in comparison to quicker and easier methods (including ExoQuick and ExoEasy) (Veerman et al., 2021). Even so, automation of SEC can mitigate user influence and improve reproducibility (Monguió-Tortajada et al., 2019). Given the major source of protein in most EV preparations are contaminants, and vesicle recovery and purity differ markedly across isolation strategies (Useckaite et al., 2021, Théry et al., 2018), the decision to normalise LC-MS/MS analyses to volume rather than total protein content is to avoid normalising to an artefact. For clinical samples, patient groups may have more vesicles and EV protein, so the analysis of less sample compared to controls could diminish the ability to detect important differences. When applied to EVs isolated by SEC or precipitation methods, the assay

demonstrated the differences in recovery and purity of EVs from equivalent starting material. As ExoQuick is a high recovery, low purity method, high abundance of EV-positive markers and albumin contamination were observed. Meanwhile, SEC methods show intermediate vesicle recovery and purity, with most substantial albumin depletion achieved by qEV70. Previous studies have also reported very low abundance or non-detection of TSG101 in SEC EVs from blood (Veerman et al., 2021, Brennan et al., 2020, Buschmann et al., 2018). The heterogenous presence and relative abundance of tetraspanins and other biogenesis pathway-related proteins in EVs is influenced by originating cell types (Kugeratski et al., 2021, Koliha et al., 2016). EVs isolated from the circulation generally comprise a large majority of haematopoietic cell-derived vesicles, especially platelet EVs (Palviainen et al., 2020, Matsumoto et al., 2020, Kugeratski et al., 2021, Koliha et al., 2016). Notably, platelet-derived EVs have been shown to be devoid of CD81 (Koliha et al., 2016), which may account for the levels of this marker observed in lower recovery isolation methods such as SEC.

Though endogenous CD81 was more abundant in ExoQuick, assay sensitivity was reduced in this matrix. The success of other EV applications such as untargeted profiling studies is dependent on pure sample preparations, since peptides derived from abundant serum proteins will be sampled more frequently than scarcer EV peptides in the MS (Liebler and Zimmerman, 2013). With minimal non-EV interference, profiling may reveal subtype-specific or tissue-specific vesicle markers (Karimi et al., 2018). Ultimately, these techniques performed in pure samples should continue to generate insights into EV biogenesis, functions, and diagnostic or prognostic value, and promote the development of novel affinity tools for the selective isolation of subpopulations to improve the utility of liquid biopsy (Newman et al., 2022b, Rodrigues et al., 2021).

To summarise, we have developed and validated a targeted LC-MS/MS method for the detection and quantification of a panel of positive and negative EV markers in EVs from blood. The described workflow may be applied for the fulfillment of standard characterisation and reporting criteria, described by the MISEV guidelines, or to quantify changes in EV proteins as a biomarker normalisation strategy. We illustrate how our approach overcomes several challenges faced with the use of immunoblotting when working with limited volume of clinical samples, particularly in regard to sensitivity, throughput and quantitation.

CHAPTER 3

IMPORTANCE OF BETWEEN AND WITHIN SUBJECT VARIABILITY IN EXTRACELLULAR VESICLE ABUNDANCE AND CARGO WHEN PERFORMING BIOMARKER ANALYSES

Author Contributions

This chapter is published in *Cells* (Appendix 3) and no changes have been made from the contents of the original peer-reviewed manuscript. The only alterations were to formatting for consistency with the thesis. I was the first and sole primary contributing author and was responsible for conceptualisation, developed the methodology, generated and analysed the majority of the data, wrote the first draft and reviewed and edited the paper, culminating in approximately 85% of the work. Author Z.U generated the TEM images and flow cytometry data and edited the paper. Author A.R contributed to conceptualisation and edited the paper.

Context in Thesis

Circulating EVs represent a promising source of biomarkers and a liquid biopsy tool to assess disease severity, monitor the effectiveness of interventions and to predict variability in drug exposure. Studies are focussed on characterising EVs and associated molecular cargo under various pathophysiological conditions in order to elucidate function and potential biomarker utility. Yet, little is known regarding the characteristics of circulating EVs in normal conditions, including the natural variability one might expect to observe in the abundance and expression of EV-enriched markers among healthy individuals. In the present chapter, the LCMS assay developed in the previous chapter is used to address this gap. In addition, another classical EV marker CD63 and liver marker ASGR1 are included to expand the scope of the analysis. The study described in this chapter sought to evaluate variability in abundance and cargo of global and liver-specific circulating EV, within (diurnal) and between individuals in a cohort of healthy subjects (n=10). Normal ranges are

presented for EV concentration and size and expression of generic EV protein markers and liver-specific ASGR1 in samples collected in the morning and afternoon. EV abundance and cargo was generally not affected by fasting, except CD9 which exhibited a statistically significant increase ($p=0.018$). Diurnal variability was observed in the expression of CD81 and ASGR1 which significantly decreased ($p=0.011$) and increased ($p=0.009$), respectively. These results have potential implications for study sampling protocols and normalisation of data when applying expression of EV cargo as a biomarker strategy, since an understanding of basal variability is a fundamental consideration in the interpretation of disease-associated changes. Specifically, the novel finding that liver-specific EVs exhibit diurnal variability in healthy subjects have broad potential implications in the study of drug metabolism and development of minimally-invasive biomarkers for liver disease.

Introduction

Extracellular vesicles (EVs) have emerged as a rich source of circulating biomarkers with potential applications in tracking variability in disease, intervention efficacy and drug exposure (Shah et al., 2018, Rowland et al., 2019, Rodrigues and Rowland, 2019). EVs are heterogeneous membrane encapsulated particles that are secreted into the blood and other biofluids by virtually all cell types (Newman et al., 2020). Several subtypes of EVs exist, comprising exosomes (classical and non-classical), arrestin-domain-containing protein 1-mediated microvesicles (ARMM), small apoptotic EV and small autophagic EV, and multiple larger EV classes also exist (Jeppesen et al., 2019). These vesicles contain a complement of nucleic acid (microRNA [miRNA], mRNA, and non-coding RNA), protein and small molecule cargo that are derived from their cell of origin (Mir and Goettsch, 2020). For the purpose of this study, we refer to this heterogenous population of isolated vesicles as EVs.

Some EV cargo is explicitly packaged through defined pathways that are specific to a particular EV type, while other cargo is indiscriminately incorporated as a by-product from the cellular milieu (Mir and Goettsch, 2020). Accordingly, the composition of EV cargo depends on EV type and the cell of origin. Differences in cargo between EV types is of continuing research interest and several

markers have been proposed to discriminate EV based on certain marker expression. EVs derived from the same cell have even been shown to vary in molecular composition (Kowal et al., 2016), yet the degree of normal variability in the abundance of circulating EV and their cargo remains poorly defined (Oggero et al., 2019). In order to robustly define thresholds of accuracy, precision and sensitivity for an EV-derived biomarker, it is essential to understand the normal degree of variability in circulating EV and to understand patterns (e.g. circadian) associated with EV abundance.

Of growing interest is the understanding of how EV derived from a specific cellular or subcellular location may be applied to gain even greater understanding of organ function. There are a number of studies that have defined protocols for the isolation of tissue- and organelle- specific EVs based on selective surface proteins (Goetzl et al., 2017, Gotanda et al., 2016, Goetzl et al., 2019, Mustapic et al., 2017). By way of example, liver-derived EVs can be selectively captured via the hepatocyte-specific surface protein asialoglycoprotein receptor 1 (ASGR1), and may be of great value to the study of drug metabolism (Rowland et al., 2019) or liver diseases (Newman et al., 2020). In order to robustly define abnormal expression, these applications require an understanding of the normal range of expression between individuals, typical variability in expression within an individual, and the contribution of different tissues to the global EV pool in circulation. This study sought to evaluate variability in circulating global and liver specific sEV abundance and cargo, and to define patterns of variability, within (diurnal) and between individuals, that have the potential to confound EV derived biomarker analyses. The experimental design for the study is summarised in Figure 3.1.

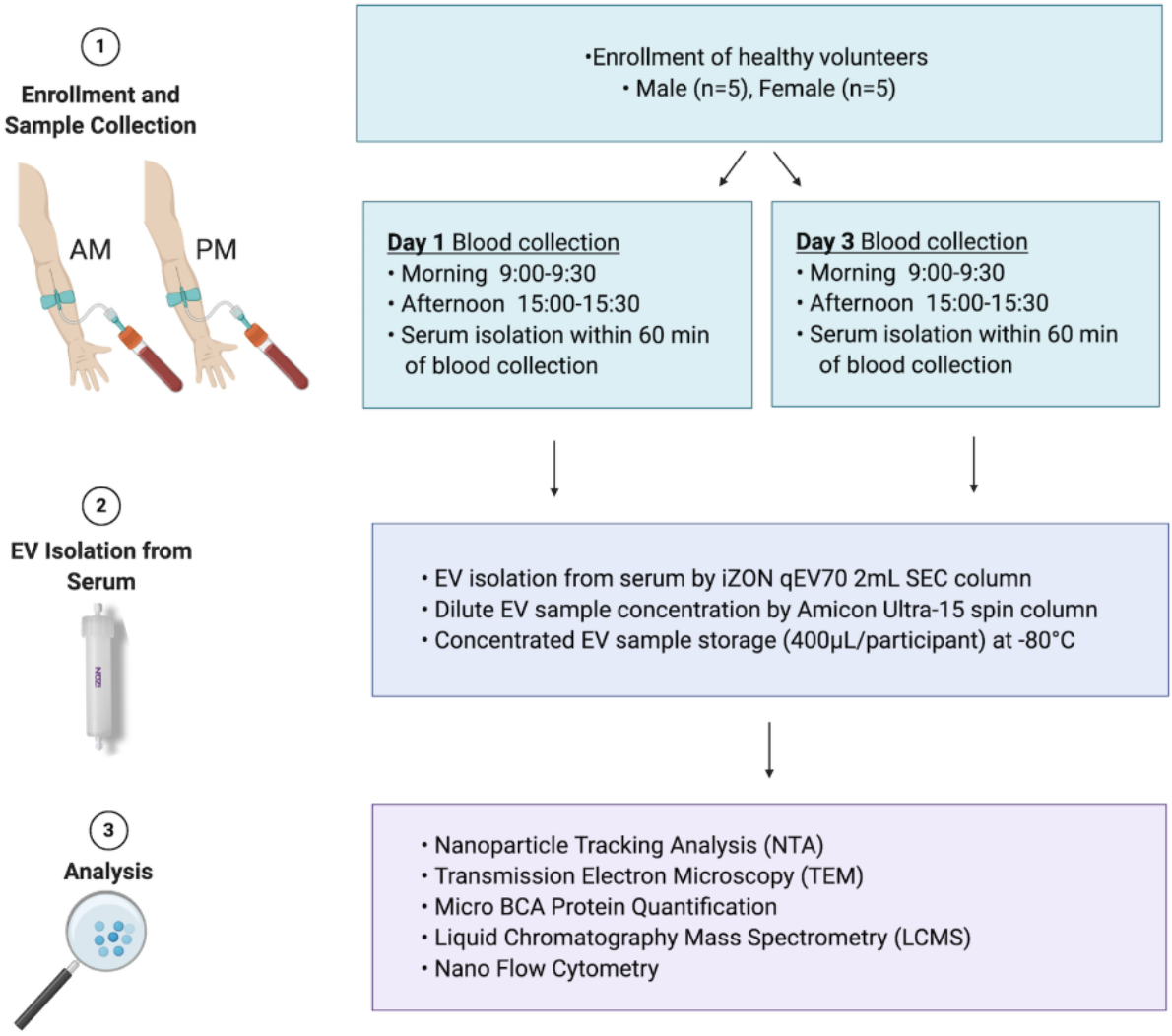

Figure 3.1 Study design.

A cohort of healthy males and females, aged 18 to 65 years old, were recruited (n=10) for extracellular vesicle variability (EVV) study. Blood was collected in the morning (AM) and the afternoon (PM) on day 1 and day 3 of the study. Participants were fed on day 1 and fasted on day 3 for morning blood collection. Serum was isolated from whole blood and used for EV isolation. EVs were isolated using qEV70 2mL SEC column, concentrated to 400 µl in PBS and used for downstream analyses. All experiments were reported in EV-TRACK (ID: EV210044).

Methods

Study Cohort

EVV is a single-centre, open-label, single-sequence biomarker study involving a cohort of healthy males and females aged 18 to 65 years old. Characteristics of the study cohort are detailed in Table 3.1. The study protocol was approved by the Southern Adelaide Clinical Human Research Ethics Committee (SAHREC 261.18), and written informed consent was obtained from each

participant prior to study enrolment. The study was conducted according to the principles stated in the Declaration of Helsinki and was compliant with CPMP/ICH/135/95 GCP standards.

Table 3.1 Characteristics of EVV study cohort.

Characteristic	Healthy Females (n=5)	Healthy Males (n=5)
Age (years)		
Mean (± SD)	28 (5.8)	30 (6.2)
Range	22-35	23-38
Height (cm)		
Mean (± SD)	166.8 (5.7)	184.2 (8.0)
Weight (kg)		
Mean (± SD)	55.4 (3.8)	86.4 (5.4)
BMI (kg/m^2)		
Mean (± SD)	20.0 (2.4)	25.5 (1.2)

Collection of Blood Serum

Morning samples were collected between 0900 and 0930 hrs, while afternoon samples were collected between 1500 and 1530 hrs. Participants presented fed for blood collection on day 1 and after an overnight fast on day 3. The participants were free to consume their regular meals of choice for the duration of the study when not required to be fasted. Eight millilitres of whole blood were collected into Z Serum Sep Clot Activator tubes (Greiner Bio-One) using a 21-gauge Vacuette Safety Blood Collection sealed vacuum device (Greiner Bio-One). To ensure sample quality the device was primed by collecting a 5 mL 'discard' tube immediately prior to sample collection. Serum was isolated from whole blood within 60 min of sample collection by two cycles of centrifugation at 2500 *x g* for 15 min at 4°C.

Extracellular Vesicle Isolation

Global EVs were isolated from serum by size exclusion chromatography (SEC) performed using 2 mL qEV70 columns (Izon Science, Christchurch, New Zealand). SEC methods have been shown to effectively separate EVs from lipoproteins and other contaminants in serum, and is attractive for clinical biomarker applications due to its scalability and efficiency (Monguió-Tortajada et al., 2019, Buschmann et al., 2018, Böing et al., 2014). The use of 2 mL columns ensured all

downstream analyses came from the same isolation. Prior to EV isolation, SEC columns were conditioned by washing with 10 mL of freshly 0.2 µm filtered phosphate-buffered saline (PBS). Thawed serum (2 mL) was added to the sample reservoir and EVs were eluted in PBS, which was added to the sample reservoir as the last of the serum entered the column. For the duration of the EV isolation, the volume of PBS in the reservoir was kept below 2 mL. The initial six fractions of flow-through were discarded, EVs were collected in the pooled fractions 7 to 11 using Protein LoBind tubes (Eppendorf, South Pacific, Australia). Resulting pooled EV fractions were mixed by gentle inversion 8 to 10 times and concentrated using pre-conditioned Amicon Ultra-4 centrifuge filters (30 KDa, Millipore-Sigma, Bedford, MA) to a final volume of 400 µL in PBS. EV samples were aliquoted to avoid freeze-thaw and stored at -80°C until analysed or processed further.

Human Liver Microsome Preparation

Pooled human liver microsomes (HLMs) were prepared by mixing equal protein amounts of microsomes from five human livers (H7, 44 year old woman; H10, 67 year old woman; H12, 66 year old man; H29, 45 year old man; and H40, 54 year old woman) obtained from the human liver "bank" of the Department of Clinical Pharmacology (Flinders University, Adelaide, SA, Australia). Approval for the use of human liver tissue in xenobiotic metabolism studies was obtained from both the Clinical Investigation Committee of Flinders Medical Centre and from the donors' next of kin. HLMs were prepared by differential centrifugation as described by Bowalgaha et al. (2005).

Nanoparticle Tracking Analysis

Nanoparticle tracking analysis (NTA) was performed to determine global particle abundance and size distribution using the NanoSight NS300. Samples were diluted between 1:1000 and 1:5000 using freshly 0.2 µm filtered PBS, five 60 second videos were captured and analysed under constant flow conditions (flow rate 50) using NTA 3.4 software.

Transmission Electron Microscopy (TEM)

Samples were prepared adapting a previously published protocol, with some modification (Useckaite et al., 2020). Briefly, carbon-coated grids (Ted-Pella B 300M, Mason Technology) were cleaned and hydrophilized using plasma glow discharge for 15s (Gatan SOLARUS Advanced Plasma Cleaning System) prior to use. 5µL of sample in 0.2 µm-filtered PBS was placed on carbon-

coated grids for 5 minutes. Carbon grids were washed once (15s) at room temperature (RT) with 0.2 μm filtered PBS and were contrasted with 2% uranyl acetate (3 min, RT), washed once, and examined by FEI TECNAI Spirit G2 TEM (Thermo Fisher) operated at 100 kV. TEM images were acquired at 30000 x and 68000 x (Figure 3.2)

Micro BCA Protein Quantification

A micro bicinchoninic acid (BCA) reagent kit (ThermoFisher Scientific), with a bovine serum albumin (BSA) standard curve (0–200 μg/mL), was used to determine total protein in samples, as per manufacturer's recommendations. EVs were lysed by addition of RIPA buffer 1:1 and incubation on ice for 25 minutes, followed by centrifugation at 10,000 x g for 10 minutes at 4^{o}C. Working reagent (WR) was prepared using MA:MB:MC at 25:24:1 ratio respectively. EV containing samples were diluted between 1:20-1:100 in 0.2μm-filtered PBS. 150μL of the WR was mixed with either 150μL of the BSA standard or 150μL of sample in duplicate using a 96-well plate. The plate was covered and incubated at 37°C for 2 hours. Absorbance was measured at 562nm using a plate reader (SpectraMax, Molecular Devices).

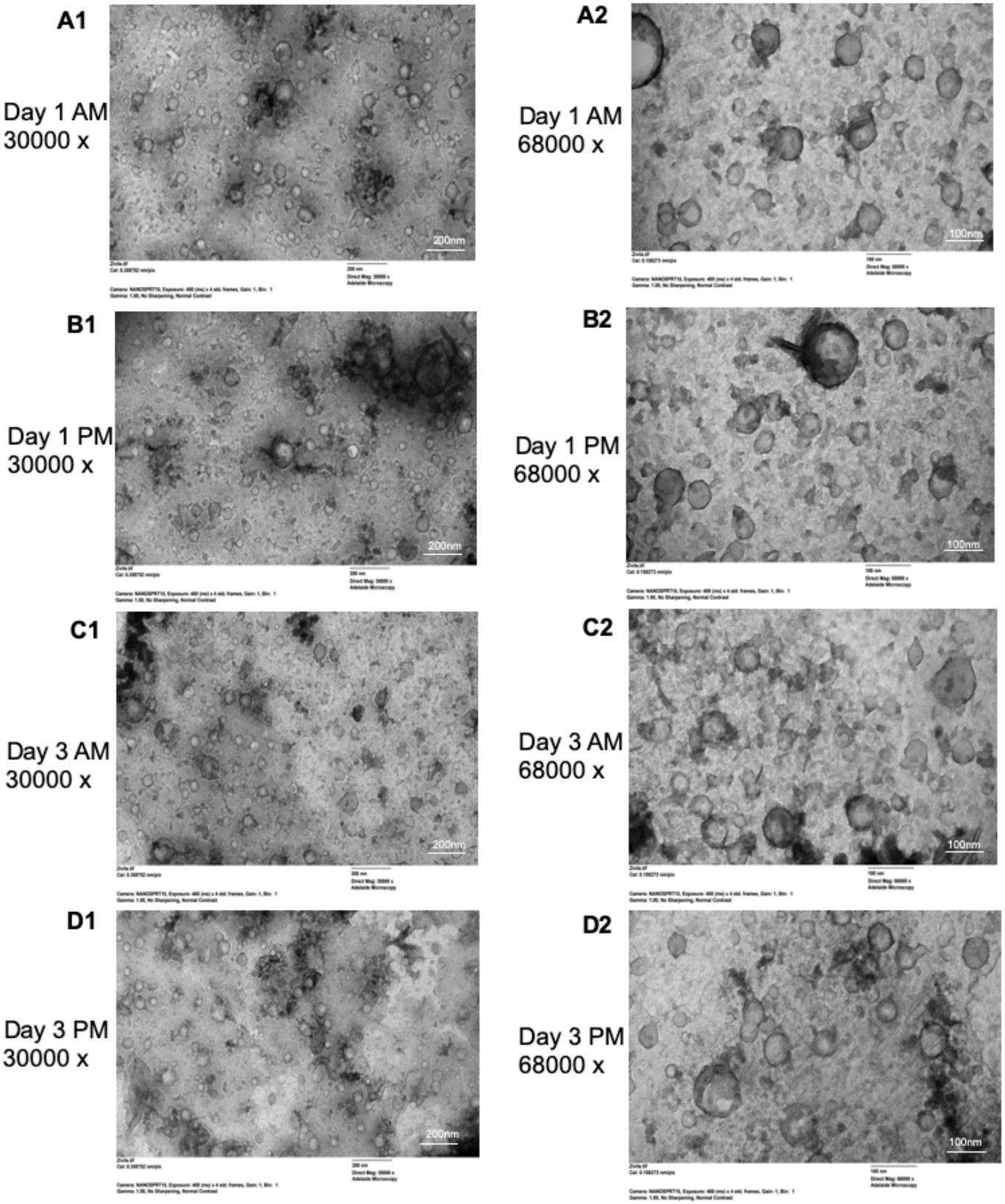

Figure 3.2 TEM images.

A-D (Panel 1) magnification of 30,000 x. A-D (Panel 2) magnification of 68,000 x.

Trypsin Digest

EV protein was prepared for LCMS analysis by trypsin digestion. EVs (50µl) diluted up to 100µl in PBS were vortexed for 10 minutes using a MixMate (Eppendorf) and subject to three freeze-thaw cycles to cause lysis. Dithiothreitol (12.5mM) and 50µl of ammonium bicarbonate (pH 7.8) were added to samples and incubated for 90 minutes at 60^{o}C. Samples were cooled to room temperature then incubated with iodoacetamide (23.5mM) for 60 minutes at 37^{o}C. The samples were then incubated for 18 hours at 37^{o}C with Trypsin Gold at a Trypsin to protein ratio of 1:40. Trypsin digestion was terminated by addition of 20µl formic acid and centrifuged at 16000 x g for 10 minutes at 4^{o}C. Supernatant (100µl) was extracted and stable isotope labelled (SIL) peptide standards were added at 2.5nM concentration. A 5µl aliquot was injected for analysis by LC-MS/MS. Serum (diluted 1:10000) and HLM were digested in the same conditions and run as positive controls.

Liquid Chromatography Mass Spectrometry (LCMS)

Chromatographic separation of analytes was performed on an Agilent Advance Bio Peptide Map column (100 x 2.1 mm, 2.7 µm) using an Agilent 1290 Infinity II liquid chromatography system. The temperature of the sample and column compartments was maintained at 4 and 30 °C, respectively. A panel of analytes comprising the EV makers CD9, CD63, CD81, and contaminants calnexin V and albumin, were separated by gradient elution with a flow rate of 0.2 mL/min. The mobile phase consisted of 0.1% formic acid in water (mobile phase A) and in acetonitrile (mobile phase B) held in a proportion of 90% A and 10% B for the first 2 minutes. The proportion of mobile phase B was then increased linearly to 60% over 13 minutes before returning to 10% over the next 4 minutes and held for a further minute to re-equilibrate. Total run time was 20 minutes. EV marker TSG101 was run independently using isocratic elution at flow rate 0.2mL/min. Mobile phase A was held at 80% and total run time was 6 minutes. The liver-specific EV protein marker ASGR1, also run independently, was separated by gradient elution at 0.2mL/min. Mobile phase B was increased linearly from 10% to 40% over 8 minutes then returned to 10% over 1.4 minutes. The column was re-equilibrated with a total run time of 10 minutes. Column eluant was monitored by mass spectrometry using an Agilent 6495B Triple Quadrupole mass spectrometer operating in positive electron spray (ESI+) mode. Multiple reaction monitoring (MRM) was performed with one quantifier and one qualifier ion transition for each peptide. Identities of endogenous peptides were confirmed

by comparing retention time and quantifier/qualifier transition ratios to respective SIL peptide standards. Peptide sequences are given Table 2.2. Additional markers, ASGR1 and CD63, have the respective peptide sequences SLESQLEK and NNHTASILDR. Marker expression is presented as relative response based on peak area of quantifier ion.

Nano Flow Cytometry (nFC)

Flow cytometry analysis was performed on the Beckman Coulter CytoFLEX S Flow Cytometer as previously described (Brennan et al., 2020). Briefly, for daily calibration of the flow cytometer, fluorescent beads (Megamix FSC & SSC Plus, BioCytex, Marseille, FRA) were used in sizes of 100, 160, 200, 240, 300, 500, and 900 nm. The gating strategy is depicted in Figure 3.3. The VSSC and SSC threshold was set as the trigger channel below the 0.1 µm bead population. A rectangular gate was set on the VSSC-H log x BSSC-H log cytogram containing the 100 nm and 240 nm bead populations and defined as '100 nm–240 nm Megamix gate' followed by a "stable time gate" set on the time histogram in order to identify the microparticle region. To avoid swarm effects each was serially diluted from 1:2 to 1:500 and measured with a flow rate of 10 µL/min prior to antibody labelling. EVs were labelled with 0.05µl anti-CD63-AlexaFluor488 (Invitrogen, Cat.MA5-18149) or anti-CD9-BV405, (R&D Systems, Cat.FAB1880V), anti-CD81-Alexa700 (Biolegend, Cat.349518), anti ASGR1-BV421 (BD Biosciences, Cat.74269) in 100µl PBS for 30 mins on ice in the dark. To avoid false positive event measurement, all antibodies used were run in PBS alone to ensure the absence of antibody aggregates and non-specific binding to the particles in PBS. To avoid carry-over effects between each sample measurement, a washing step was performed with filtered PBS for 1 min at an increased flow rate of 60 µL/min. EV lysis was performed by incubating PBS-diluted EVs in 0.05% Triton™ X-100 for 30 min at room temperature.

Based on recommendations in the MIFlowCyt-EV guidelines (Welsh et al., 2020), buffer only (PBS) control, buffer with antibodies, unstained controls (EVs in PBS) and stained EVs were run under the same settings (Figure 3.3).

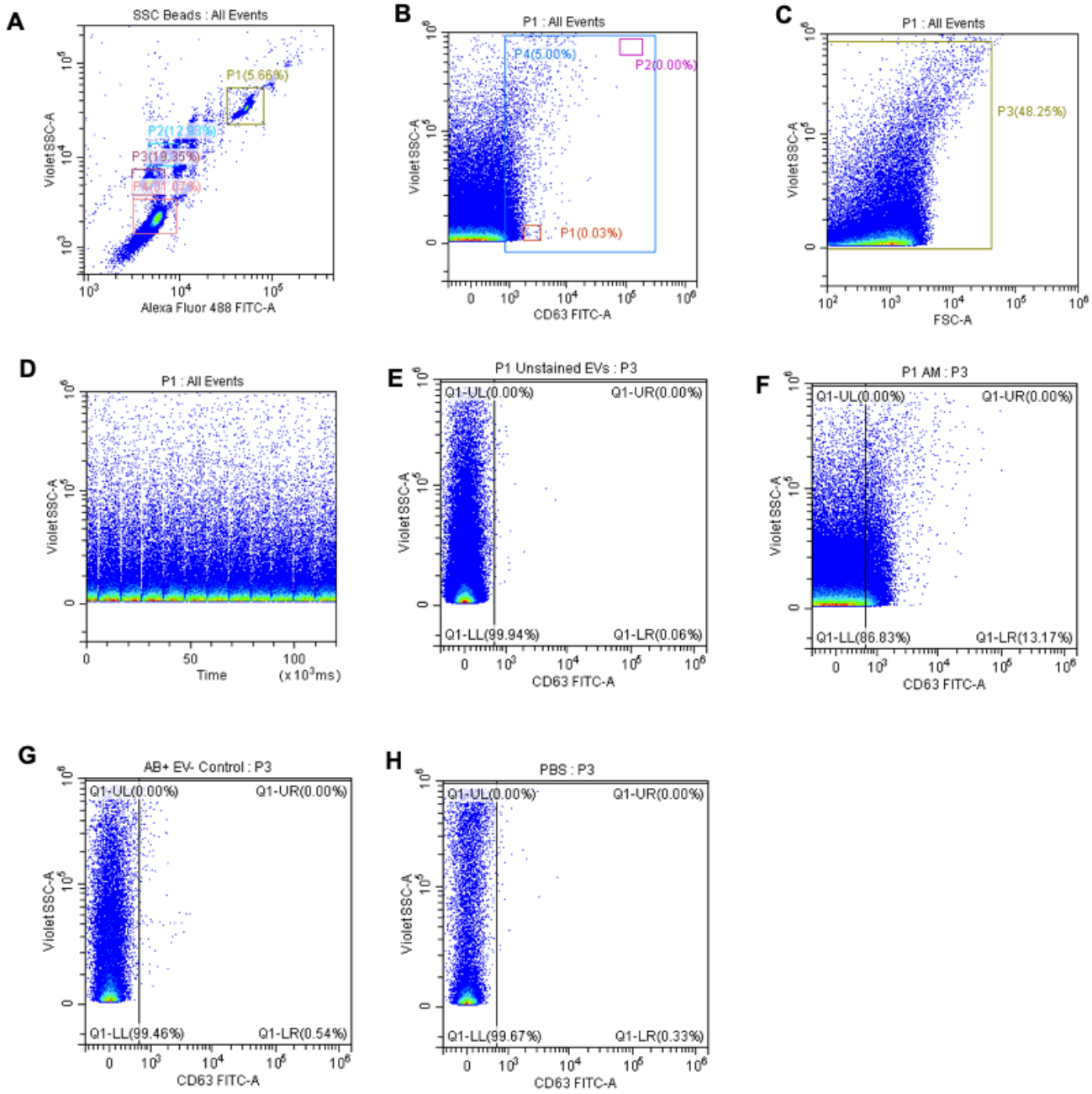

Figure 3.3 Gating strategy for EV analysis by flow cytometry.

(A) Megamix-Plus fluorescent beads in the range 100-900 nm were identified based on their fluorescent and light scatter properties. Regions were set as P1, P2, P3 and P4 according to the manufacturers recommendations (BioCytex). (B) EVs were gated based on Megamix-Plus beads in (A). (C) Data acquisition was performed using a constant flow rate and monitored using a VSSC vs time plot (D) Unstained EV fraction and (E) EV fraction stained for CD63. The percent positive cells and MFI values were calculated relative to unstained controls. (F) Antibody in PBS and (G) PBS alone controls.

Statistical Analysis

Statistical analysis was performed using GraphPad Prism software version 9.0 (San Diego, CA, USA). The D'Agostino-Pearson omnibus K2 test was used to assess normality and log transformation was applied to NTA and mass spectrometry data. All variables passed normality and lognormality tests, so parametric tests were applied, except in the case of total protein concentration, to which Wilcoxon test was used instead. Data was presented as mean ± 95% confidence interval and range. Statistical comparisons were performed between different time points (AM and PM, fed and fast) using paired t-tests and between independent groups (sex) using one-way ANOVA. Statistical significance was set at 0.05.

EV-TRACK

We have submitted all relevant data of our experiments to the EV-TRACK knowledgebase (EV-TRACK ID: EV210044) (Van Deun et al., 2017).

Results

Purity Assessment of EV Isolations from Serum

In order to assess the purity of EV isolations, a few samples were selected at random and imaged by TEM to evaluate the background, composition and EV structure. Representative images from TEM analysis (Figure 3.4) indicated that EV populations obtained by qEV70 SEC columns had limited non-vesicular contamination and the majority of EVs were 40–140 nm in size. EVs were round and appeared structurally intact.

Adhering to EV-TRACK transparent reporting platform recommendation, assessment of non-EV-enriched proteins was performed in all EV samples to evaluate EV sample purity and potential non-vesicular contamination. CANX and albumin levels were measured by LC-MS. Total protein matched serum and HLM samples were used as positive controls for albumin and CANX, respectively. The abundance of negative markers in EV samples is presented as a mean percentage of expression ± SD relative to HLM and serum for the respective markers. Compared to HLM,

minimal expression of CANX was detected in EV samples (0.52 ± 0.40 %). Similarly, albumin expression in EVs was minimal compared to the serum control (0.95 ± 0.32 %).

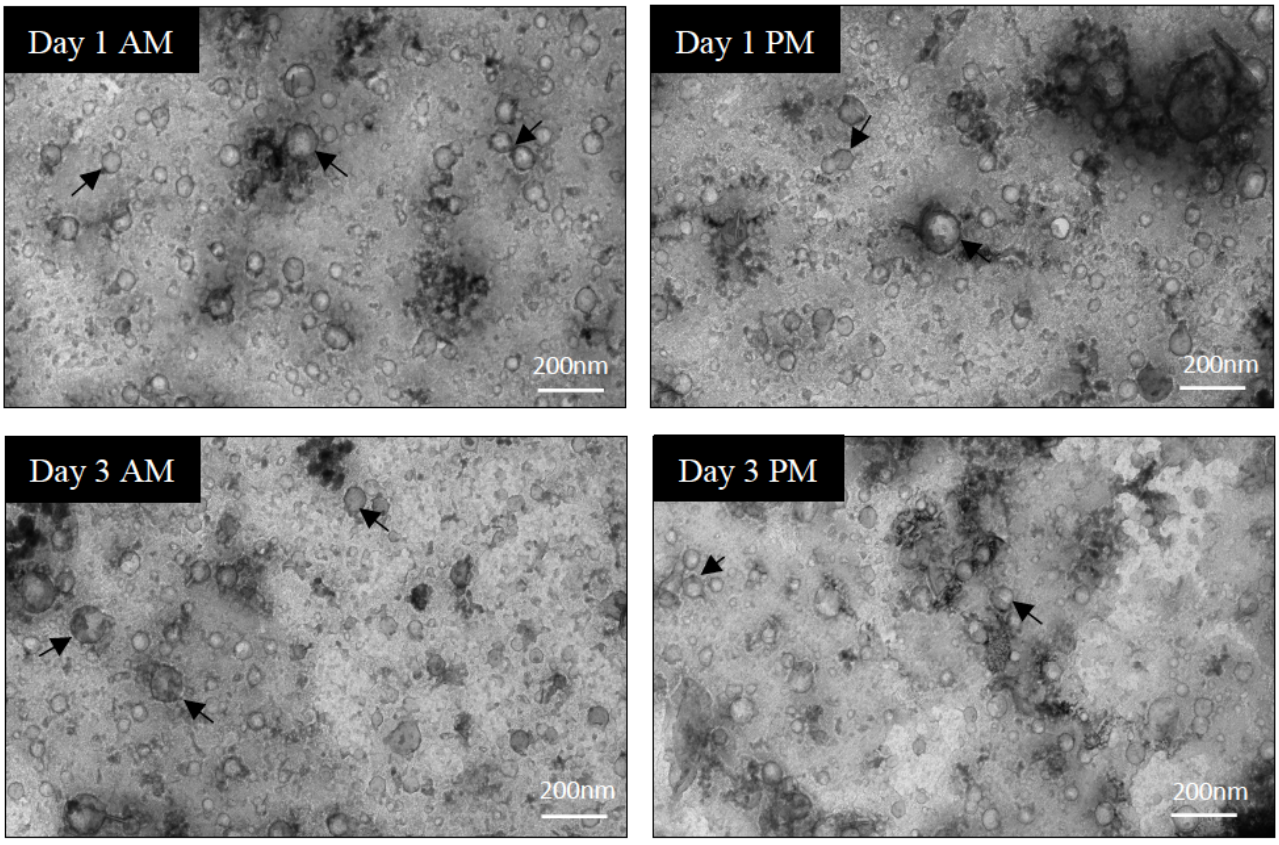

Figure 3.4 Sample quality assessment and characterisation of EVs by TEM.
Direct magnification: 30,000 x, no sharpening, normal contrast. Scale bar = 200 nm.

Normal Variability

Normal variability between individuals was assessed with respect to EV characteristics and the abundance of EV-associated protein markers on study day 1. Nanoparticle tracking analysis (NTA) was employed to determine size and concentration of particles in EV isolates (Figure 3.5A-B). The mean (± range) was 2.82 x 10^{11} (3.02 x 10^{10} – 1.26 x 10^{12}) and 2.40 x 10^{11} (4.37 x 10^{10} – 1.02 x 10^{12}) particles/mL for AM and PM samples, respectively (Table 3.2). Mode size of particles was 83.0 (64.9-99.3) nm in the morning and 84.7 (76.0-92.9) nm in the afternoon. Total protein in lysed EV samples was determined by microBCA assay and varied widely between participants in the morning and afternoon (Figure 3.5C). Mean (± range) concentration in respective AM and PM

samples was 2773 (26.4-2799.0) µg/mL and 1318 (27.9-1345.9) µg/mL (Table 3.2). Quantification of EV protein, particle concentration and size in the present study was consistent with previously reported ranges for EVs isolated by qEV from human serum (Buschmann et al., 2018).

Markers were selected based on the MISEV guidelines for confirming the presence of EV-enriched proteins and include those derived from the plasma membrane, endosomal pathway and cytosol (Théry et al., 2018). The panel was comprised of tetraspanins CD9, CD63 and CD81 and the cytosolic protein tumour susceptibility gene 101 (TSG101), as well as the hepatocyte-specific surface protein asialoglycoprotein receptor 1 (ASGR1), which is known to be expressed on EVs derived from this cell type (Newman et al., 2020, Povero et al., 2020). The expression of protein markers was determined by LCMS given as relative response (quantified peak areas) and assessed for variability between subjects in AM and PM EVs (Figure 3.5D-H). Generic EV markers (tetraspanins and TSG101) showed relatively low variation between subjects, except for CD63 which was significantly more variable in both the morning and afternoon. The liver-specific EV protein ASGR1 exhibited similarly high variability but only in the afternoon, as the range of values exceeded 16 times that of the morning EV samples. In the context of biomarker applications, understanding these differences in marker expression within and between individuals may aid the optimisation of sampling protocols.

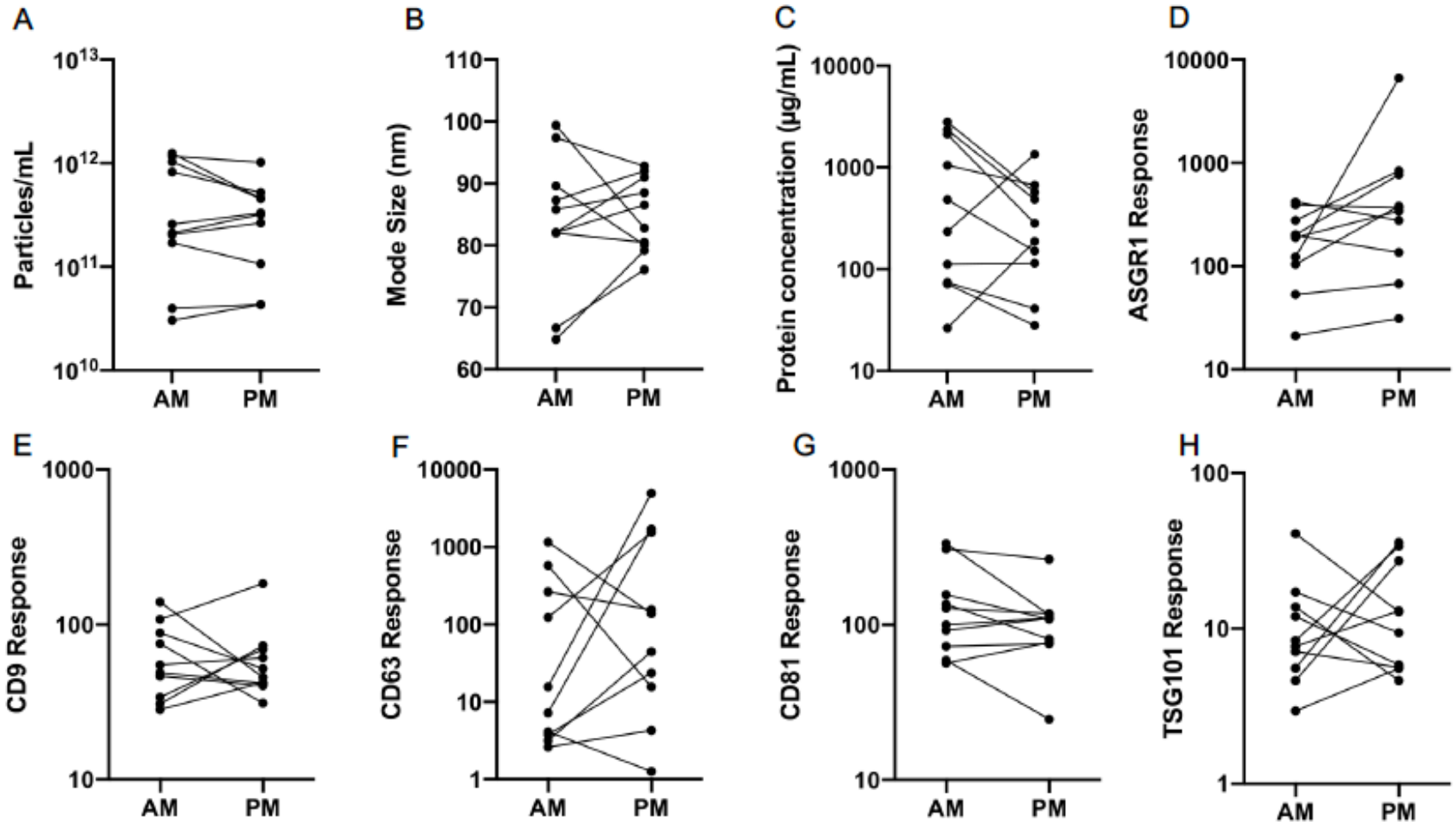

Figure 3.5 Normal Variability of EV abundance and cargo.

(A) Particle count / mL of EV isolate, (B) Mode size (C) Total protein concentration / mL EV isolate and (D-H) expression of EV-associated protein markers, in samples taken in the morning (AM) and afternoon (PM) of study day 1 from healthy volunteers (n=10). Marker expression presented as relative response (peak area units normalised to stable isotope labelled peptide).

Table 3.2 Normal variability in healthy donor EVs.
Geometric mean, 95% confidence interval (CI), minimum and maximum of particle count, mode size, total protein concentration, and EV-associated protein marker abundance quantified in EVs isolated in the morning and afternoon on study day 1 from serum of healthy volunteers (n=10).

	Particle Count (Particles/mL)		**Mode Size (nm)**	
	AM	PM	AM	PM
Mean	2.82E+11	2.40E+11	83.0	84.7
95% CI Lower	1.07E+11	1.12E+11	75.2	80.5
95% CI Upper	7.24E+11	5.13E+11	91.8	89.1
Minimum	3.02E+10	4.37E+10	64.9	76.0
Maximum	1.26E+12	1.02E+12	99.3	92.9
	Protein Concentration (µg/mL)		**ASGR1 Response**	
	AM	PM	AM	PM
Mean	347.5	219.8	147.9	331.9
95% CI Lower	104.2	90.8	76.6	115.9
95% CI Upper	1161.5	533.3	286.4	952.8
Minimum	26.4	27.9	21.2	31.2
Maximum	2799.0	1345.9	421.7	6622.2
	CD9 Response		**CD63 Response**	
	AM	PM	AM	PM
Mean	57.2	55.9	28.2	86.9
95% CI Lower	38.6	39.8	5.2	12.5
95% CI Upper	84.5	79.6	153.5	605.3
Minimum	28.2	31.0	2.6	1.3
Maximum	140.0	183.7	1158.8	4954.5
	CD81 Response		**TSG101 Response**	
	AM	PM	AM	PM
Mean	120.0	94.2	9.11	11.6
95% CI Lower	77.1	61.7	-0.73	6.6
95% CI Upper	187.1	143.9	15.5	20.4
Minimum	56.6	24.6	2.9	4.6
Maximum	334.2	264.9	40.9	35.8

Effect of Fasting

Quantification by NTA of serum EVs collected from participants in fed and fasted states, revealed respective mean (± 95% CI) particle concentrations of 2.82×10^{11} (1.07×10^{11} – 7.24×10^{11}) and 2.09×10^{11} (6.61×10^{10} – 6.46×10^{11}) particles/mL. No significant differences were detected by paired statistical tests (Table 3.3, Figure 3.6A-B). The mode particle size was slightly higher after fasting at 92.0 (80.4-105.4) nm compared to 83.0 (75.2-91.8) nm from fed individuals, but this difference did not reach statistical significance (p=0.093).

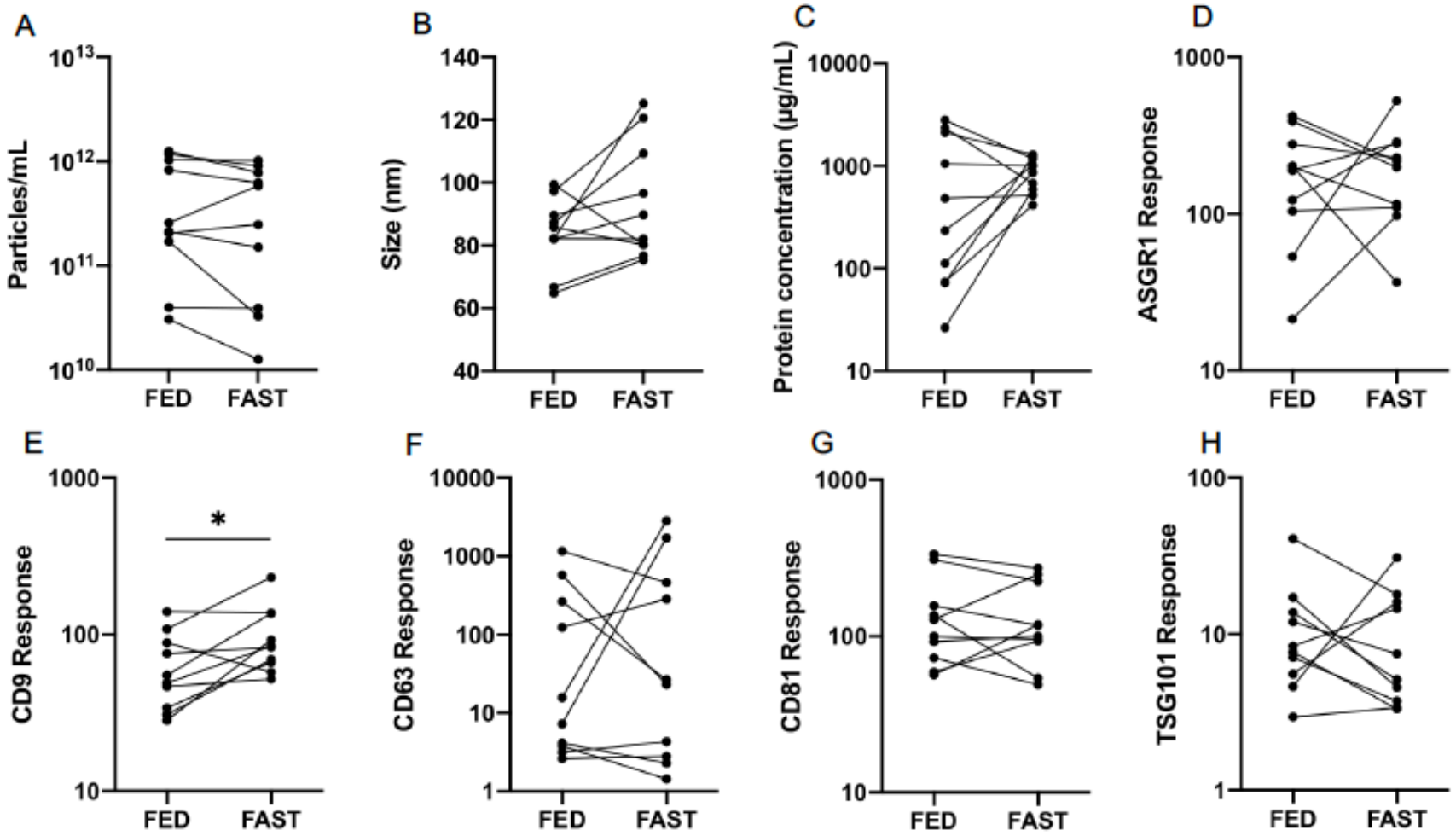

Figure 3.6 Effect of fed and fasted state.

(A) Particle count / mL of EV isolate, (B) Mode size (C) Total protein concentration / mL EV isolate and (D-H) expression of EV-associated protein markers, from healthy volunteers (n=10). Marker expression presented as relative response (peak area units normalised to stable isotope labelled peptide).

Table 3.3 Effect of fasting.
Geometric mean and 95% confidence interval (CI) of particle count, mode size, total protein con-centration, and EV-associated protein marker abundance serum EVs of healthy volunteers (n=10) in fed state and after an overnight fast.

	Particle Count (Particles/mL)				Mode Size (nm)			
	Fed	Fast	Difference	p	Fed	Fast	Difference	p
Mean	2.82E+11	2.09E+11			83.0	92.0		
95% CI Lower	1.07E+11	6.61E+10	ns	0.193	75.2	80.4	ns	0.093
95% CI Upper	7.24E+11	6.46E+11			91.8	105.4		
	Protein Concentration (µg/mL)				**ASGR1 Response**			
	Fed	Fast	Difference	p	Fed	Fast	Difference	p
Mean	347.5	822.2			147.9	168.7		
95% CI Lower	104.2	619.4	ns	0.1602	76.6	99.1	ns	0.732
95% CI Upper	1161.5	1094.0			286.4	287.7		
	CD9 Response				**CD63 Response**			
	Fed	Fast	Difference	p	Fed	Fast	Difference	p
Mean	57.2	90.6			28.2	41.5		
95% CI Lower	38.6	65.0	*	0.018	5.2	5.3	ns	0.680
95% CI Upper	84.5	126.2			153.5	322.9		
	CD81 Response				**TSG101 Response**			
	Fed	Fast	Difference	p	Fed	Fast	Difference	p
Mean	120.0	117.2			9.1	7.9		
95% CI Lower	77.1	76.6	ns	0.886	5.4	4.4	ns	0.668
95% CI Upper	187.1	179.5			15.5	14.1		

Total protein concentration and the abundance of EV protein markers in fed and fasted states were also compared (Table 3.3, Figure 3.6C-H). Mean protein concentration (± 95% CI) in respective fed and fasted states was 345.7 (104.2-1161.5) µg/mL and 822.2 (619.4-1094.0) µg/mL. While the difference between groups was not significant, the inter-individual variability was notably greater in fed samples (Figure 3.6C). Assuming constant stoichiometry, it follows that a lack of difference in particle concentration should be accompanied by no change in EV protein marker abundance. This was true of all markers except for CD9, which exhibited a statistically significant increase in fasted individuals (p=0.018). Similarly to observations of variability in CD63 abundance throughout the day (Figure 3.6F), a wide range was exhibited in fed and fasted states (Table 3.3, Figure 3.6F).

Diurnal Variability

In order to establish potential patterns of EV variability in healthy subjects, the analysis of EVs collected on study days 1 and 3 were pooled and compared between morning and afternoon. EV abundance and size as measured by NTA was consistent between the two time points (Figure 3.7A-B). Mean (± 95% CI) particle count in respective AM and PM samples was 2.29×10^{11} ($1.23 \times 10^{11} – 4.79 \times 10^{11}$) and 2.40×10^{11} ($1.41 \times 10^{11} – 3.89 \times 10^{11}$) particles/mL (Table 3.4). Mode size of particles was 87.1 (81.3-95.5) nm in AM and 83.2 (77.6-87.1) nm in PM samples.

Analysis of EV protein and abundance of generic markers revealed no difference in total protein concentration or response for CD9, CD63 and TSG101 at different times of the day. Interestingly however, CD81 was significantly lower in the afternoon compared to the morning ($p=0.011$) (Table 3.4, Figure 3.7H). With no concomitant change in particle number, this result may suggest a lower CD81 abundance per vesicle or a decrease in the proportion of CD81+ EVs. Additionally, a significant increase in ASGR1 response was observed from AM to PM samples ($p=0.009$), suggesting that the proportional contribution of the liver to the circulating global EV pool was greater in the afternoon (Figure 3.7D).

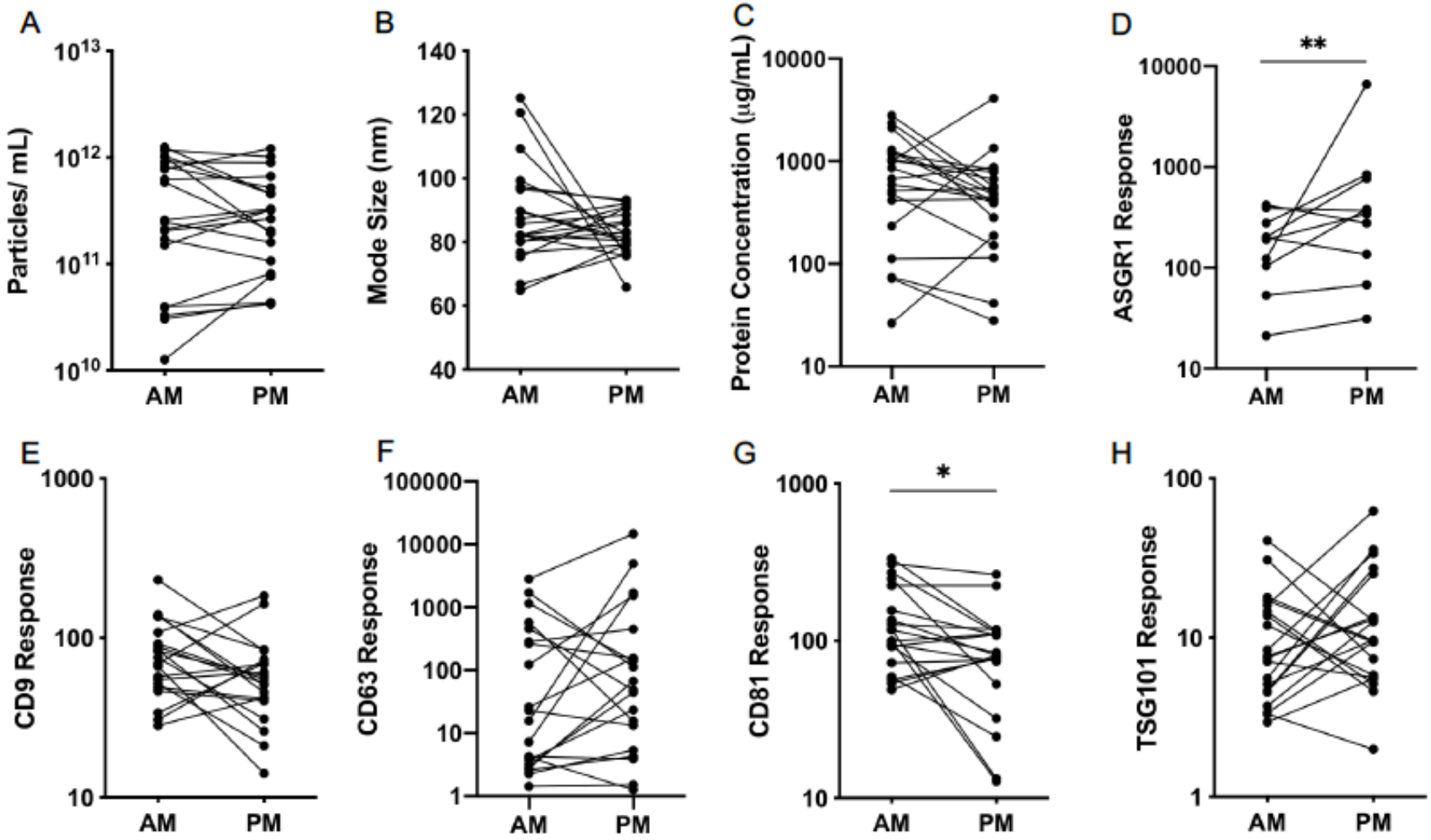

Figure 3.7 Diurnal variability.

(A) Particle count / mL of EV isolate, (B) Mode size (C) Total protein concentration / mL of EV isolate and (D-H) expression of EV-associated protein markers, on study days 1 and 3 in healthy volunteers (n=20). Marker expression presented as relative response (peak area units normalised to stable isotope labelled peptide). Statistical analysis performed using paired t-tests. * *p≤0.05,* ** *p≤0.01.*

Table 3.4 Diurnal variability.
Pooled analysis of serum EVs from healthy volunteers on study days 1 and 3 (n=20) comparing morning and afternoon. Data presented as geometric mean and 95% confidence interval (CI).

	Particle Count (Particles/mL)				Mode Size (nm)			
	AM	PM	Difference	p	AM	PM	Difference	p
Mean	2.29E+11	2.40E+11			87.1	83.2		
95% CI Lower	1.23E+11	1.41E+11	ns	0.863	81.3	77.6	ns	0.240
95% CI Upper	4.79E+11	3.89E+11			95.5	87.1		
	Protein Concentration (µg/mL)				**ASGR1 Response**			
	AM	PM	Difference	p	AM	PM	Difference	p
Mean	537.0	380.2			147.9	331.1		
95% CI Lower	295.1	223.9	ns	0.123	97.7	169.8	**	0.009
95% CI Upper	955	660.7			223.9	645.7		
	CD9 Response				**CD63 Response**			
	AM	PM	Difference	p	AM	PM	Difference	p
Mean	72.4	52.5			33.8	67.6		
95% CI Lower	56.2	38.9	ns	0.075	10.2	19.5	ns	0.239
95% CI Upper	93.3	70.8			114.8	234.4		
	CD81 Response				**TSG101 Response**			
	AM	PM	Difference	p	AM	PM	Difference	p
Mean	117.5	72.4			8.5	11.0		
95% CI Lower	49.0	12.9	*	0.011	5.9	7.6	ns	0.293
95% CI Upper	331.1	263.0			12.0	16.2		

Effect of Sex

The impact of sex was next explored as a potential source of variability in serum EV abundance and composition. Pooled analysis was performed for EVs collected on study days 1 and 3 in the morning and afternoon and compared between female (n=10) and male (n=10) healthy subjects. In this cohort, EV concentration in AM samples as determined by NTA was more than 10 times greater in males compared to females ($p<0.0001$) (Figure 3.8A). Mean (± 95% CI) particle count in female and male cohorts was 7.41×10^{10} ($3.47 \times 10^{10} – 1.58 \times 10^{11}$) and 7.76×10^{11} ($5.62 \times 10^{11} – 1.10 \times 10^{12}$) particles/mL (Table 3.5). This difference was less substantial in PM samples, at 1.10×10^{11} ($6.03 \times 10^{10} – 1.95 \times 10^{11}$) particles/mL in females and 1.95×10^{11} ($3.24 \times 10^{11} – 7.94 \times 10^{11}$) particles/mL in males, but retained statistical significance ($p=0.0002$). Meanwhile, mode size

of particles did not vary with sex in either the morning or afternoon (Table 3.5, Figure 3.8B). In AM EVs, mean (± 95% CI) protein concentration was 330.4 (154.5-706.3) µg/mL in females and 865.0 (335.0-2238.7) µg/mL in males. This significantly higher mean concentration in male subjects (p=0.037) did not persist into the afternoon (Table 3.5, Figure 3.8C).

The mean abundance of EV protein markers quantified by LC-MS showed no variations according to sex (Figure 3.8D-H, Table 3.5). Interestingly, the previously described diurnal pattern of ASGR1 response was exhibited in female and male subjects alike and no significant differences were observed between the two cohorts (Figure 3.8D). CD63 response also showed the same degree of variability between subjects as observed for the combined cohort, indicating that this finding was not independently influenced by either sex (Figure 3.8F).

Table 3.5 Effect of sex.
Pooled analysis of EVs collected from serum of healthy female (n=10) and male (n=10) volunteers on study days 1 and 3 in the morning and afternoon. Data presented as geometric mean and 95% confidence interval (CI).

	Particle Count (Particles/mL)							
	AM				PM			
	Female	Male	Difference	p	Female	Male	Difference	p
Mean	7.41E+10	7.76E+11			1.10E+11	1.95E+11		
95% CI Lower	3.47E+10	5.62E+11	****	<0.0001	6.03E+10	3.24E+11	***	0.0002
95% CI Upper	1.58E+11	1.10E+12			1.95E+11	7.94E+11		
	Mode Size (nm)							
	AM				PM			
	Female	Male	Difference	p	Female	Male	Difference	p
Mean	88.8	86.0			83.9	81.3		
95% CI Lower	77.8	76.5	ns	0.610	79.2	75.8	ns	0.622
95% CI Upper	101.4	96.8			88.8	87.2		
	Protein Concentration (µg/mL)							
	AM				PM			
	Female	Male	Difference	p	Female	Male	Difference	p
Mean	330.4	865.0			289.1	509.3		
95% CI Lower	154.5	335.0	*	0.037	97.5	358.1	ns	0.822
95% CI Upper	706.3	2238.7			855.1	722.8		
	ASGR1 Response							
	AM				PM			
	Female	Male	Difference	p	Female	Male	Difference	p
Mean	136.5	183.2			248.9	321.4		
95% CI Lower	70.2	110.4	ns	0.801	94.6	129.1	ns	0.844
95% CI Upper	265.5	304.1			654.6	799.8		

	CD9 Response							
	AM				PM			
	Female	Male	Difference	p	Female	Male	Difference	p
Mean	70.6	73.5	ns	0.987	56.8	49.3	ns	0.837
95% CI Lower	46.7	49.8			32.1	37.8		
95% CI Upper	106.9	108.4			100.7	64.4		
	CD63 Response							
	AM				PM			
	Female	Male	Difference	p	Female	Male	Difference	p
Mean	29.6	39.5	ns	0.964	57.9	78.9	ns	0.959
95% CI Lower	5.1	5.3			6.5	15.2		
95% CI Upper	171.0	293.1			515.2	408.3		
	CD81 Response							
	AM				PM			
	Female	Male	Difference	p	Female	Male	Difference	p
Mean	103.50	135.8	ns	0.641	73.0	71.9	ns	0.999
95% CI Lower	69.2	87.5			35.4	48.4		
95% CI Upper	155.2	210.9			150.3	107.2		
	TSG101 Response							
	AM				PM			
	Female	Male	Difference	p	Female	Male	Difference	p
Mean	8.0	9.0	ns	0.945	11.7	10.5	ns	0.944
95% CI Lower	5.3	4.6			5.7	6.6		
95% CI Upper	12.1	17.6			24.2	16.7		

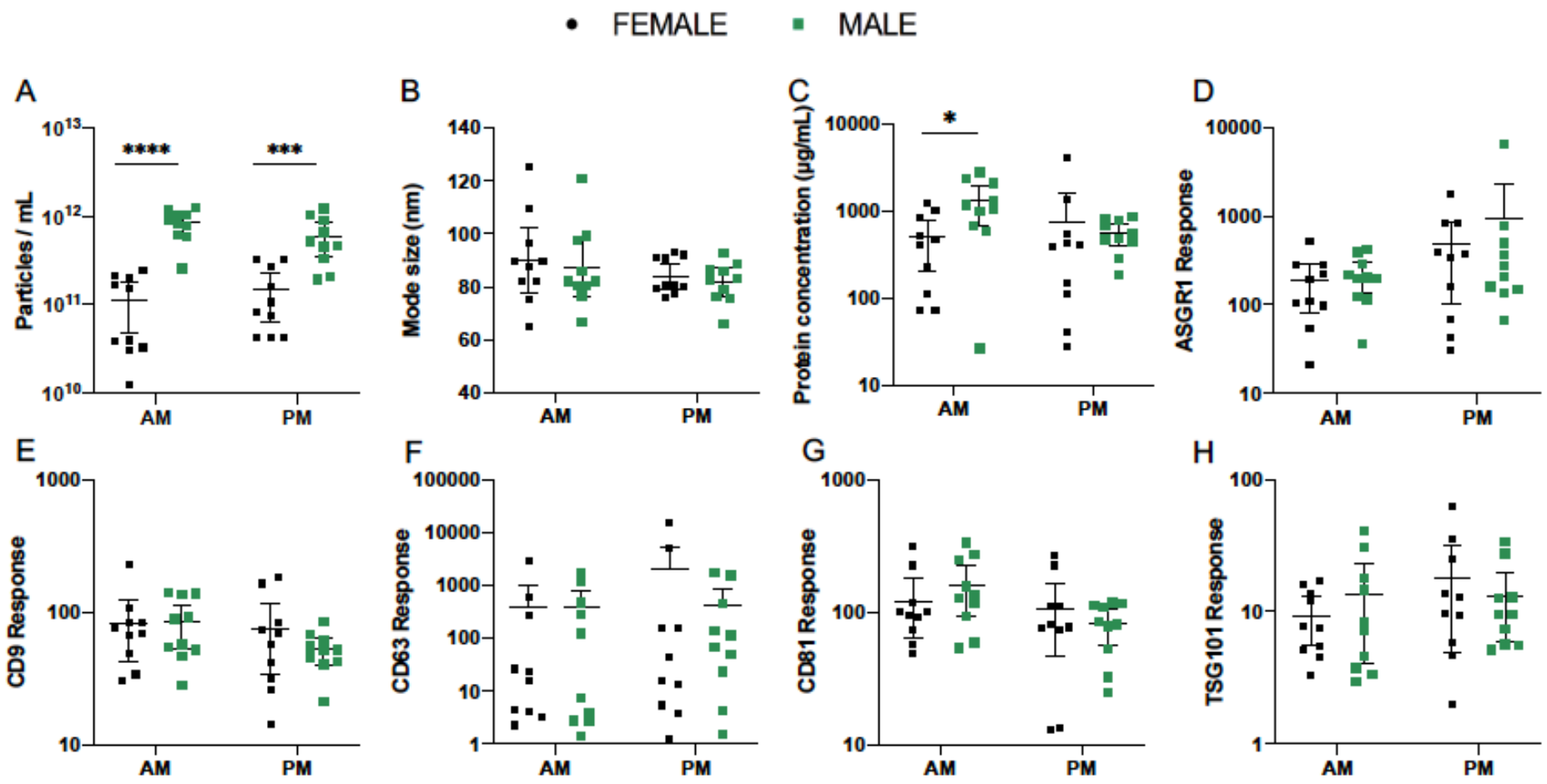

Figure 3.8 Effect of sex

(A) Particle count / mL EV isolate, (B) Mode size, (C) Total protein concentration / mL EV isolate and (D-H) Expression of EV-associated protein markers. Pooled analysis of EVs collected from serum of healthy female (n=10) and male (n=10) volunteers on study days 1 and 3. Statistical analysis performed using one-way ANOVA. * *p≤0.05, *** p≤0.001, **** p≤0.0001.*

Single EV Analysis by nano Flow Cytometry (nFC)

As LC-MS peptide analysis is a bulk analysis technique, it determines the marker abundance in the total sample following lysis of vesicles. To provide complementary insights and confirmation of marker detection, nFC was used to analyse surface EV markers on intact, individual EVs. The normal ranges, diurnal variability and effect of fasting and sex were also assessed across the time points from the healthy donors.

Normal ranges of EVs positive for CD9, CD63, CD81 and ASGR1 was determined on study day 1 based on quantification by mean fluorescence intensity (MFI) (Figure 3.9). No significant differences were observed for tetraspanin EV protein markers or for the liver-specific EV protein ASGR1. Notably, however, ASGR1 levels were the most variable of the markers between individuals in both the AM and the PM, being more pronounced in the PM samples (Figure 3.9A). MFI values ranged from 241.4 to 582.0 in AM samples and 235.1 to 884.0 in PM samples.

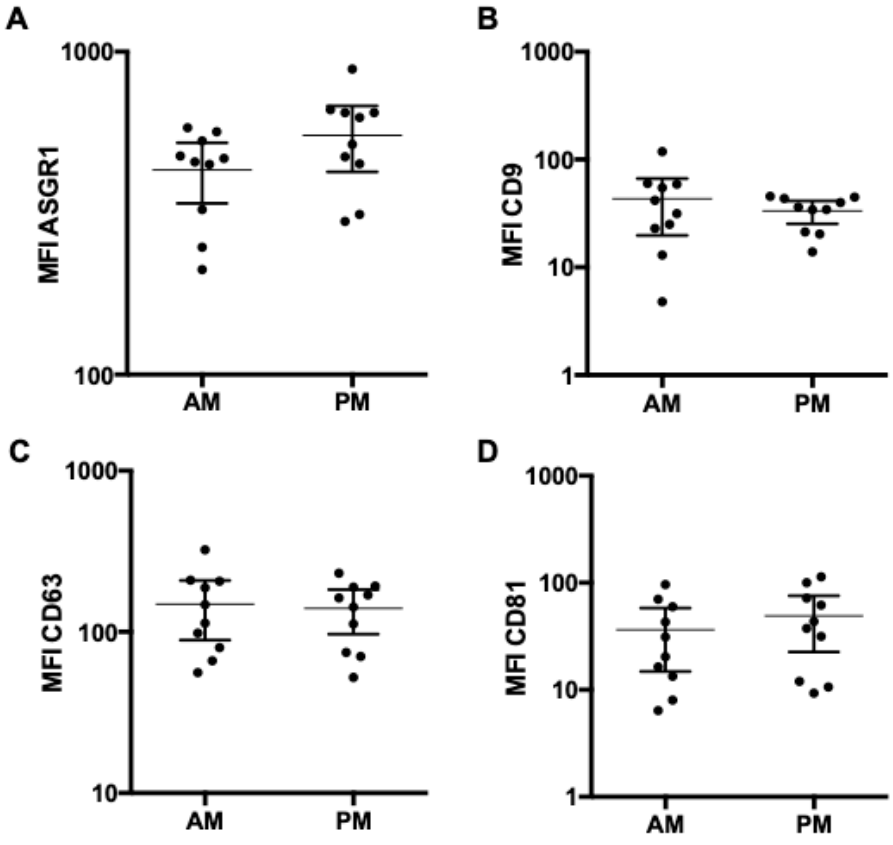

Figure 3.9 Single EV analysis showing normal variability in abundance of EV surface markers.

(A) ASGR1, (B) CD9, (C) CD63 and (D) CD81 presented as mean fluorescence intensity (MFI), in the morning (AM) and afternoon (PM) of study day 1 in healthy volunteers (n=10). Statistical analysis used paired t-test (differences not significant). Error bars represent mean with 95% CI.

Single EV analysis revealed effects of fasting on EV surface markers. A greater inter-individual variability in fed samples for ASGR1, CD63 and CD81 (Figure 3.10) and CD9 and CD81 levels were significantly different (p=0.049 and p=0.002 respectively) between fed and fasted samples. Interestingly, these data do not agree with bulk EV analysis by LCMS, which determined a significant increase in CD9 abundance and no change in CD81 (Figure 3.6 E & G).

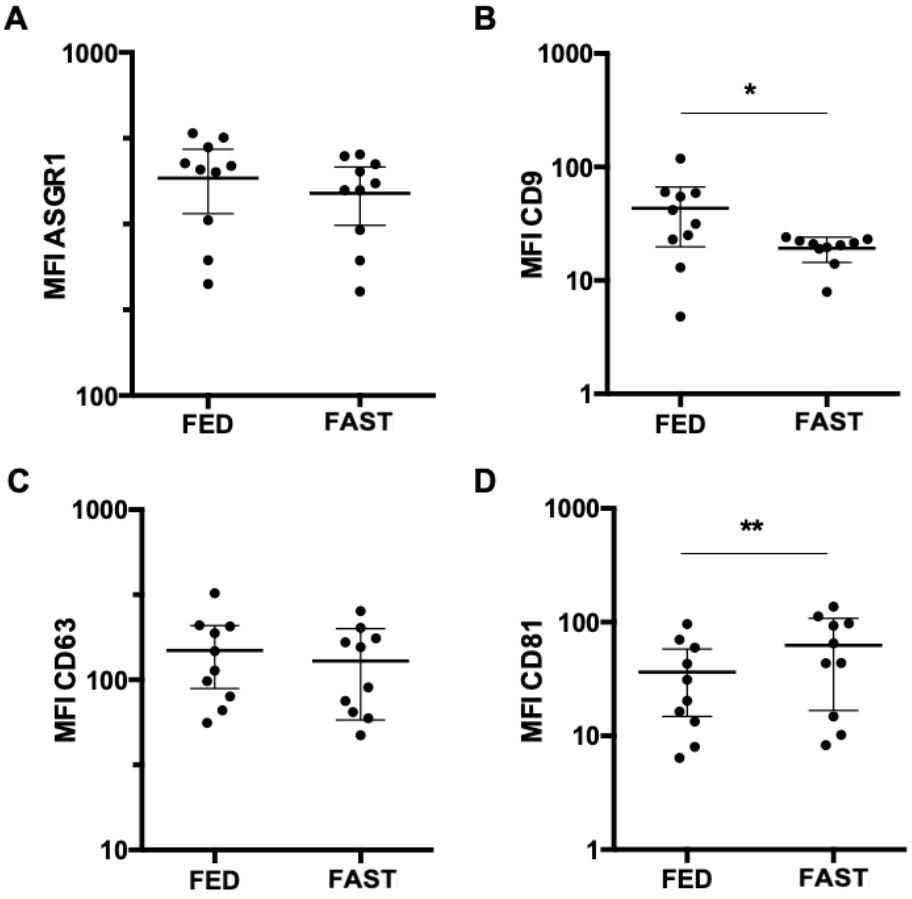

Figure 3.10 Single EV analysis showing effect of fed and fasted state on abundance of EV surface markers.

(A) ASGR1, (B) CD9, (C) CD63 and (D) CD81 presented as mean fluorescence intensity (MFI) and 95% CI. Statistical analysis using paired t-test; * *p≤0.05, ** p≤0.01.*

Diurnal variability in surface marker expression was assessed across AM and PM samples grouped from study days 1 and 3 (n=20). The single EV analysis revealed diurnal changes in abundance of ASGR1 and CD81 (Figure 3.11), as both markers exhibited statistically significant increases in MFI (p=0.002 and p=0.036, respectively). Greater inter-individual variability was also observed compared to the other markers. While this directional change in ASGR1 abundance was consistent with the bulk EV LCMS data, the result contrasted for CD81.

Single EV analysis revealed sex differences in abundance of CD81+ EV populations. MFI was significantly decreased in males compared to females in both AM (p=0.038) and PM (p=0.028) samples. No other markers differed with sex, in agreement with LCMS bulk EV analysis (Figure 3.12D).

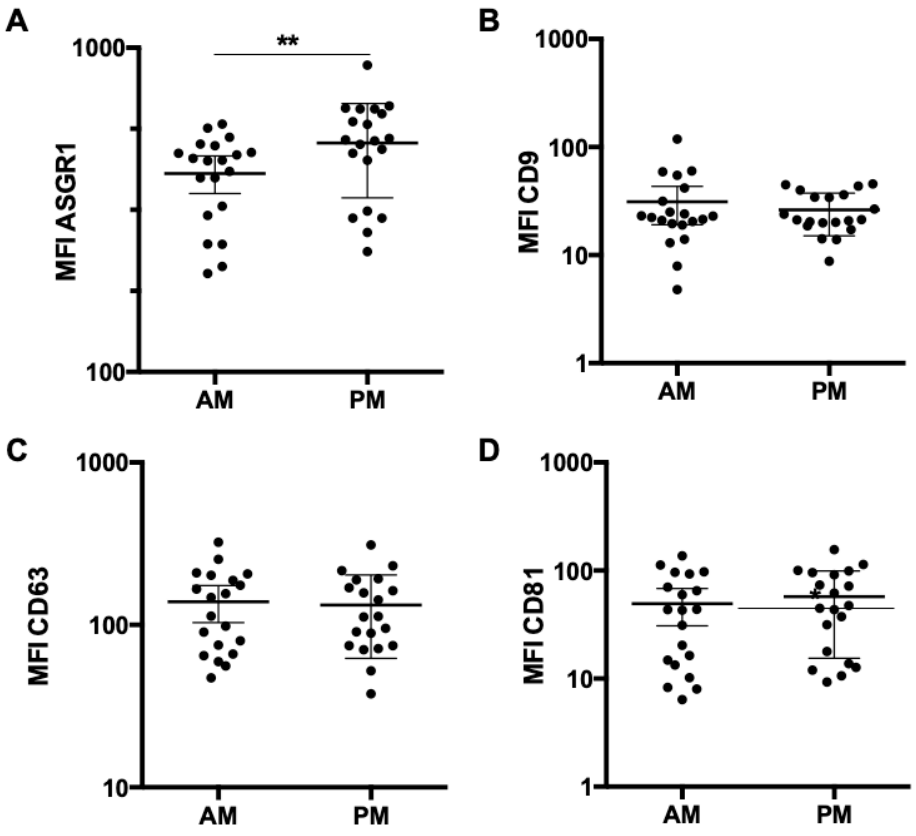

Figure 3.11 Single EV analysis showing diurnal variability in abundance of EV surface markers.

Pooled analysis of samples collected on study days 1 and 3 in the morning (AM) and afternoon (PM) (n=20). Abundance of (A) ASGR1, (B) CD9, (C) CD63 and (D) CD81 presented as mean fluorescence intensity (MFI) and 95% CI. Statistical analysis using paired t-tests; ** *p≤0.01.*

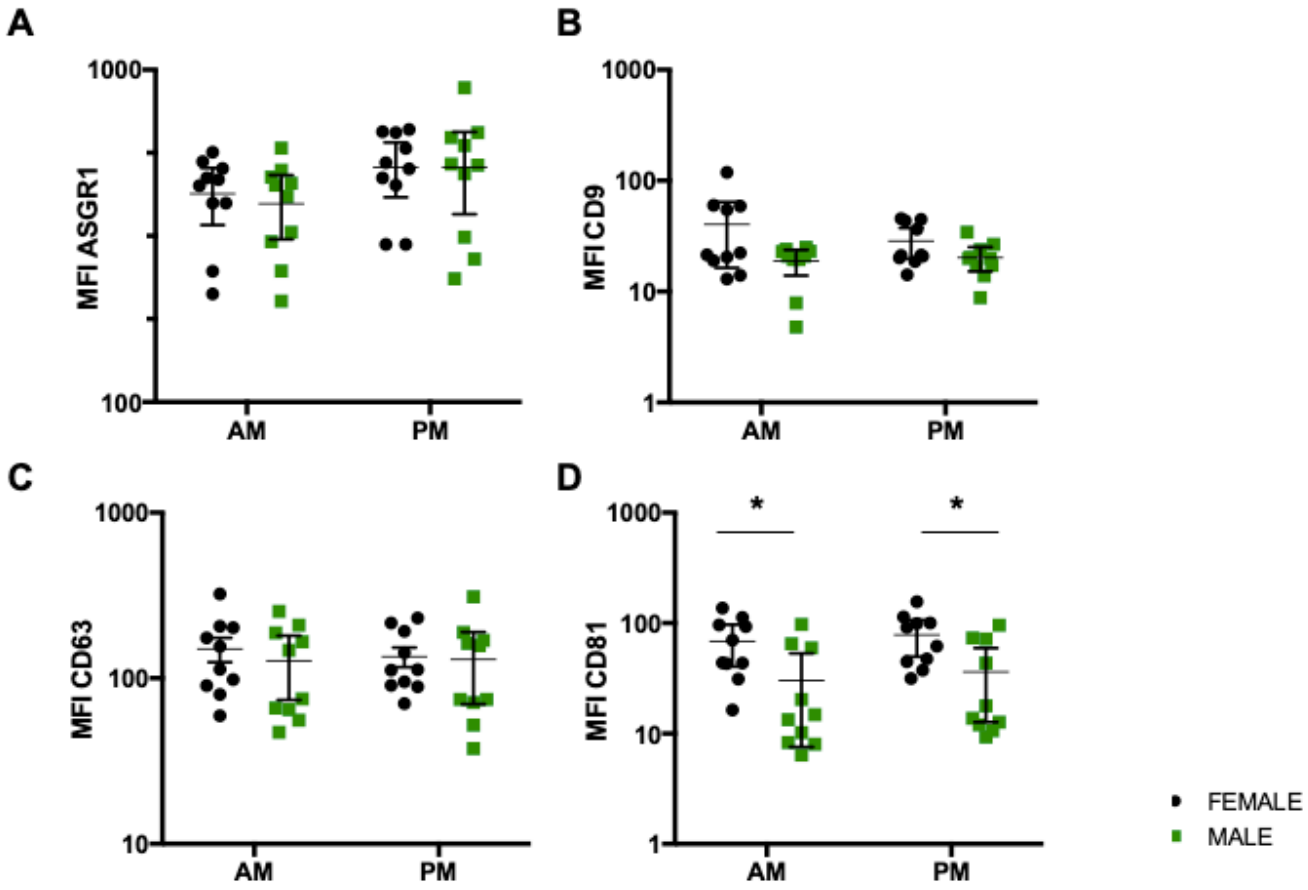

Figure 3.12 Single EV analysis showing effect of sex on abundance of EV surface markers.

(A) ASGR1, (B) CD9, (C) CD63 and (D) CD81 presented as mean fluorescence intensity (MFI) and 95% CI. Grouped samples collected on study days 1 and 3 in the morning (AM) and afternoon (PM) from healthy female (n=10) and male (n=10) donors. Statistical analysis using one-way ANOVA * *p≤0.05.*

Discussion

Here we report for the first time a diurnal pattern of expression for the liver-specific EV marker ASGR1 in healthy human serum. We observed greater abundance and wider variability between subjects in samples collected in the afternoon, indicating that the contribution of the liver to the global pool of circulating EVs changes throughout the day. Importantly, this pattern was consistent in males and females. Notably, in contrast to the observed diurnal variability in expression of ASGR1+ EVs, no difference in expression was observed between fed and fasted states. This observation indicates that the diurnal variability in expression of ASGR1+ EVs is not a post-prandial phenomenon. Data presented here indicate that accounting for diurnal variability in EV expression may be particularly important for the analysis of liver-specific biomarkers. Liver-specific EV markers are of relevance to the use of EVs in the study of drug metabolism (Rowland et al., 2019, Achour et al., 2021) and non-

alcoholic fatty liver disease (NAFLD) (Newman et al., 2020). While not addressed specifically in the current study, these data also raise the possibility that diurnal variability may cofound the analysis of EV markers originating from other tissues and have broader implications for the design of sampling protocols for other tissue-specific markers that may vary in a similar manner.

The potential for circulating EVs and their molecular cargo to be applied as minimally-invasive biomarkers is increasingly recognised for the diagnosis of a variety of conditions or tracking individual responses to pharmacological interventions (Greening and Simpson, 2018). However, a comprehensive understanding of how these circulating markers fluctuate in normal physiology is currently lacking. Thus, the present study involved the analysis of EVs isolated from the serum of healthy subjects collected at multiple time points. We reported ranges, reflective of the normal variability between individuals, for particle size and concentration of EV isolates, total EV protein concentration and the abundance of EV-associated protein markers. In establishing normal ranges for the characteristics and composition of EVs, investigators may better define the thresholds for disease-associated changes, thereby strengthening the foundations for diagnostic or prognostic applications.

As EVs and their molecular cargo are involved in numerous functions vital for homeostasis, their biogenesis and composition are readily altered by different cellular and extracellular stimuli, including changes in nutrient availability (de Jong et al., 2012). Circulating biomarkers may fluctuate in response to feeding or alternatively, their quantification may be confounded by natural variation in unrelated blood parameters, especially triglyceride and lipoprotein levels (Jamaly et al., 2018). To explore the effect of prandial state on the characteristics of EVs and abundance of associated protein markers in healthy individuals, serum EVs were compared with and without an overnight fast and it was found that particle number and size was not altered by fasting. These data contrast with prior reports of circulating EVs post-prandially. Mørk et al. (2016) found that food intake resulted in a 61% increase in particle count and a significantly greater median size. However, that study and later work by Jamaly et al. (2018), reported strong correlations between particle count and plasma triglyceride concentrations after feeding, suggesting the similarly sized lipoprotein particles interfered with measurements. Blood serum EVs are unavoidably co-isolated with a range of non-vesicular

materials such as protein aggregates and lipoproteins (Witwer et al., 2013, Tian et al., 2019). Neither of the aforementioned studies investigated EV purity. The latter of which isolated vesicles by ultracentrifugation, which is known to be more susceptible to lipoprotein contamination (Brennan et al., 2020), rather than size exclusion chromatography (qEV).

It is important to note that NTA lacks the capacity to distinguish vesicles from other particles of comparable size, such as contaminating protein aggregates or lipoproteins (Jamaly et al., 2018). Our assessments of EV purity by TEM and non-EV protein controls indicated highly pure vesicle preparations. Thus, effective removal of lipoproteins from both fed and fasted EV samples may account for differences seen in previous reports and mitigate the need for fasting in biomarker testing.

For the most part, the abundance of EV-associated protein markers, reported here, agrees with a recent study (Mørk et al., 2018) that employed a flow cytometry approach with specific detection of EV protein markers, including the tetraspanins (CD9, CD63 and CD81). While a significant increase in CD9 abundance was observed here, Mørk et al. (2018) found no changes between prandial states. It should be noted, however, that flow cytometry methods are limited to vesicles >100 nm in diameter, while LCMS permits analysis of all digested vesicular proteins in the samples (Danielson et al., 2016).

The effect of circadian rhythm is well appreciated across numerous physiological systems and presents in circulation as oscillations in haematological parameters, blood and immune cell activation and expression of surface markers (Witwer et al., 2013). This study sought to ascertain whether the characteristics of EVs and expression of associated markers exhibit diurnal variability. Particle size and concentration of EV isolates collected in the morning and afternoon did not vary, while the abundance of CD81 decreased and ASGR1 increased significantly.

While there is very limited commentary on the presence of diurnal variation in EV particle number and size over the course of a day, one study utilising nFC, reported an upward trend in EV size as well as a wider range in evening samples compared to the morning (Danielson et al., 2016). As previously mentioned, these disparate conclusions may be attributed to the capacity for NTA to

quantify particles in a size range below that of flow cytometry. Taken together, the results presented here do not support fluctuations in the number or size of EVs diurnally, but point to potential changes in their molecular composition. Accordingly, attention should be given to the time of day at which EVs are sampled to reduce the effects of intra- and inter-individual variability on the sensitivity of biomarker analyses.

Lastly, the participants' sex was explored as a potential covariate associated with variability in EVs from healthy subjects. NTA analysis revealed that EV samples taken in the morning from males had more than 10 times greater particle concentration than those from females. This difference persisted, albeit at to a lesser extent, in the afternoon. Notably, the stark difference in particle concentration between sexes was not accompanied by greater levels of generic EV markers in male subjects. Sex differences have been observed in prior studies using flow cytometry, whereby plasma-derived phosphatidylserine and other microvesicle markers (Gustafson et al., 2015), and urinary CD63+ EV levels were each higher in women (Jayachandran et al., 2015). Recently, however, an NTA analysis of plasma EVs isolated by precipitation found no difference in particle count between males and females (Noren Hooten et al., 2019). The pool of circulating EVs is contributed to by numerous cell types but is largely made up of those released by platelets (Oggero et al., 2019). Though currently unclear, particle number in male subjects in our study may have been influenced by undefined factors, such as diet, physical activity and immune activation, that prompted the release of particular EV subpopulations bearing cell-type specific markers (Denham and Spencer, 2020, Brahmer et al., 2019, Witwer et al., 2013). While interesting as an observation, in the absence of controlling for other sources of variability, data presented here demonstrating differences between sexes in particle abundance should be interpreted with caution as other factors such as exercise may have confounded the results in this small cohort.

Flow cytometry is an appealing tool that lends itself to the analysis of individual protein markers on the surface of intact EVs (Brennan et al., 2020). Based on our results, it is evident that data obtained by flow cytometry is not directly comparable to that from LCMS and has some limitations. A large proportion of EVs cannot be included in the quantification due to their size and the limit of detection of the flow cytometer. Conventional flow cytometers are capable of detecting

EVs of 100nm in diameter or greater, thus excluding all smaller EVs (Lucchetti et al., 2020). In this study, EVs between 100 and 900nm were analysed. While observed diurnal variations were not consistent between study participants, every participant showed some level of diurnal variation. This phenomenon was previously shown, however, studies involving a larger number of participants is required to fully appreciate diurnal changes (Danielson et al., 2016).

Moreover, further detailing the daily time course of changes in EVs and their cargo may facilitate the tracking of therapeutic interventions. Such objectives would be serviced by longitudinal studies, testing in more frequent intervals of the circadian clock and repeating measures across multiple days. Assessment of normal variability in healthy subjects might also be extended to include the effects of race and other demographic or clinical features.

In summary, circulating EVs have great potential to be utilised as biomarkers. The value of this diagnostic and prognostic tool with respect to sensitivity and specificity, however, requires a fundamental understanding of the differences that naturally exist in the healthy population. The findings of this study should, therefore, inform EV sampling and may be of particular importance in the context of liver-specific EV-derived biomarkers.

CHAPTER 4

SELECTIVE ISOLATION OF LIVER-DERIVED EXTRACELLULAR VESICLES REDEFINES PERFORMANCE OF MICRO-RNA BIOMARKERS FOR NON-ALCOHOLIC FATTY LIVER DISEASE

Author Contributions

This chapter is published in *Biomedicines* (Appendix 4). No changes have been made to the contents of the original peer-reviewed manuscript, with the exception of Figure 4.3 which includes additional unpublished data that was generated later and supplements the validation of the ASGR1 specific EV capture. Added in-text description relating to this figure has been highlighted. I was the first and sole primary contributing author and contributed to conceptualisation and research design, generated the data and performed the analysis, wrote the first draft and reviewed and edited the paper, culminating in 90% of the work. Author Z.U generated the TEM images, author A.M.H and A.R assisted with statistical analyses and author A.R contributed to conceptualisation and edited the paper.

Context in Thesis

Non-alcoholic fatty liver disease (NAFLD) is the most common chronic liver disease globally. Definitive diagnosis of the progressive form, non-alcoholic steatohepatitis (NASH), requires liver biopsy, but the invasiveness of this technique poses risks to patients and makes it unsuited to evaluating mild disease or for repeated measures for ongoing monitoring. The scarcity of minimally invasive tools for tracking changes in disease is a critical barrier to managing NAFLD burden. Altered circulating miRNA profile show potential in a liquid biopsy for this disease. In the blood, miRNA circulates in association with RNA-binding proteins, lipoproteins or encapsulated in extracellular vesicles. The profile found in EVs may provide a relatively more disease-specific source of biomarkers due to selective packaging of EV cargo reflecting parent cell pathophysiology. The

selective isolation of the circulating extracellular vesicle subset that originates from hepatocytes further presents an important opportunity to improve the performance of miRNA biomarkers of liver disease. This chapter describes a comparative analysis of the expression of liver-enriched miRNAs with reported roles in the disease (miR -122, -192, and -128-3p) across total cell-free RNA, global EVs, and liver-specific EVs from subjects with mild and severe NAFLD and healthy controls. In ASGR1+ EVs, each miR biomarker trended positively with disease severity and expression was significantly higher in NASH subjects compared with controls. The c-statistic defining the performance of each ASGR1+ EV derived miRNA was between 0.78 and 0.84. This trend was not observed in the alternative sources (global EV or total plasma). This study demonstrates the potential utility of liver-specific EV isolation to provide a more informative biomarker source and improve performance of miRNA diagnostics for NAFLD.

Introduction

Non-alcoholic fatty liver disease (NAFLD) is the most common chronic liver disease, affecting up to a third of the global population (Garcia-Martinez et al., 2020). The disease manifests on a spectrum of severity with most individuals presenting with benign hepatic fat accumulation (non-alcoholic fatty liver; NAFL) and approximately 30% exhibiting a more severe form known as non-alcoholic steatohepatitis (NASH) (Suzuki and Diehl, 2017). While insulin resistance, obesity and other features of the metabolic syndrome are commonly associated with NAFLD, aetiology of the disease remains largely unknown, particularly with respect to progression to NASH (Buzzetti et al., 2016, Ibrahim et al., 2018). Treatment guidelines consistently identify early detection and intervention as the key to improving clinical outcomes and reducing the burden of NAFLD (Ando and Jou, 2021, Younossi et al., 2019). NAFLD is an independent mortality risk factor, with all-cause mortality on average, 11.7% higher in individuals with NAFLD compared to those without. The impact on mortality among individuals with NAFLD is proportional to disease severity and ranges from 8.3% for NAFL up to 18.4% for NASH and fibrosis (Simon et al., 2020).

NAFLD is diagnosed in individuals that exhibit fatty changes in more than 5% of hepatocytes where other causes of steatosis have been excluded (Perumpail et al., 2017, Sumida et al., 2014). Liver biopsy is the gold standard for NAFLD staging and only approach to reliably define fibrosis (Hardy et al., 2016). The key limitation being that liver biopsy is an invasive procedure that carries a substantial risk of complication, including bleeding and infection. This precludes biopsy in low risk patients and limits utility in high risk patients, as the procedure can only be performed once every two years. Additionally, given the sporadic infiltration of NAFLD and the limited tissue sample achieved with a needle biopsy, there is a substantial risk of inaccurate diagnosis that underestimates disease stage (Sumida et al., 2014). Given these limitations, a range of minimally invasive approaches to diagnose and stage NAFLD have been proposed. These approaches are typically based on factors such as serum biomarkers, body composition, comorbid diseases and abdominal imaging (Perumpail et al., 2017, Hardy et al., 2016, Sumida et al., 2014). Different combinations of these factors produce the fatty liver index, hepatic steatosis index and liver fat scores, which are used as screening tools for NAFLD. While strong predictive performance has been reported for some indices, there is insufficient robustness to facilitate translation to routine clinical care, particularly for mild and early disease (Cusi et al., 2014). Indeed, in 2019 the American Association for the Study of Liver Diseases identified the inadequate performance of these tools as a critical barrier to the effective treatment of NAFLD patients (Younossi et al., 2019).

MicroRNAs (miRNA) are small non-coding RNA that have been shown to reflect disease-associated changes across numerous pathological conditions (Castoldi et al., 2016). Altered expression of miRNAs that mediate pathways involved in lipid metabolism, inflammatory activation and the development of fibrosis have been observed in tissue from individuals with NAFLD. The abundance of these miRNAs in blood has been postulated as potential biomarkers to diagnosis and track NAFLD (Newman et al., 2020, Dongiovanni et al., 2018). This approach potentially confers several advantages over liver biopsy. In addition to mitigating the risks of tissue biopsy, circulating miRNA analysis facilitates longitudinal evaluation of disease and potentially a more robust overview of disease stage. The stability of cell-free (cf) miRNA in blood is attributable to protection by RNA

binding proteins, such as argonaute 2 (Ago2), high-density lipoproteins (HDL) or encapsulation within extracellular vesicles (EV) (Endzeliņš et al., 2017).

EVs are small membrane-bound particles released by virtually all cell types into various biological fluids including blood, urine and cerebrospinal fluid (Carpintero-Fernández et al., 2017, Newman et al., 2021). EVs carry an array of nucleic acid (including miRNA), protein and lipid cargo derived from the parent cell (Newman et al., 2021, Rodrigues and Rowland, 2019). It has been proposed that isolating EVs from biological fluids may improve the fidelity of miRNA biomarker analyses as the EV fraction provides a source of miRNA that is selectively packaged in a more disease-specific manner (Nik Mohamed Kamal and Shahidan, 2020). Additionally, circulating EVs express cell surface markers from the originating tissue. Thus, in contrast to circulating miRNA bound to Ago2 and HDL, it is theoretically possible to selectively isolate EV miRNA that originates from a specific tissue. It has been proposed (Shah et al., 2018) that analysis of EVs selectively isolated from an afflicted organ will provide the most informative description of biomarker expression, as this fraction is less affected by ‘noise' associated with non-specific fluctuations in global EV and, in the case of miRNA, total circulating expression.

To date, studies of cell-free miRNA in NAFLD have focussed broadly on expression in whole plasma and serum. When simplified to a dichotomous analysis of healthy versus NAFLD, moderate diagnostic performance in terms of discriminating these two groups has been reported for a number of miRNAs both as individual markers and panels (Newman et al., 2020, Xin et al., 2020). Despite intriguing preliminary results, the consistency of results from miRNA profiling studies remains insufficient to be applied in practice (Endzeliņš et al., 2017). Further, this dichotomous grouping of healthy versus disease limits meaningful interpretation of an individual’s NAFLD risk, which differs substantially with disease severity. For the current study, three representative miRNAs were selected based on their reported liver specificity (miR-122), associations with steatosis and fibrosis (miR-122, 192 and 128-3p) and association with inflammation (miR-192). This study sought to identify trends in the expression of these three miRNAs and determine whether the sequential refinement of the source from which biomarkers are quantified, improves their predictive power with respect to differentiating NAFL, NASH and control subjects.

Methods

Study Population and Blood samples

Clinically annotated K_2EDTA plasma from NAFLD patients (NAFL n=8; biopsy-proven NASH n=6) and healthy donors (n=14) matched for age and sex were purchased from Discovery Life Sciences (Hunstville, AL, USA). Inclusion criteria included clinical diagnosis of NAFL or NASH by a physician and exclusion criterion was presence of viral disease. Samples were aliquoted for EV isolation and total RNA analysis according to the study workflow depicted in Figure 4.1 and stored at -80°C. All analyses were performed on all the patients, unless otherwise indicated. Demographic data describing each of the three study populations are presented in Table 4.1. All relevant data have been submitted to the EV-TRACK knowledgebase (ID EV210168) (Van Deun et al., 2017).

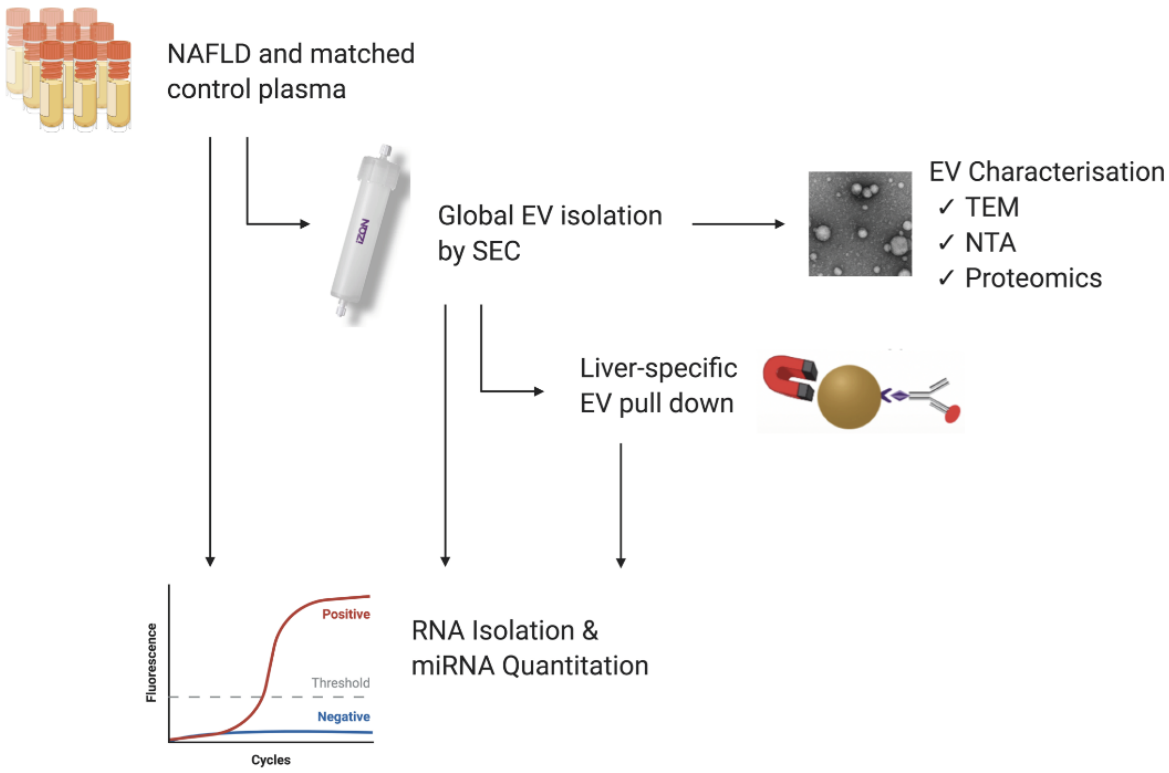

Figure 4.1 Study workflow.

Plasma samples from patients with non-alcoholic fatty liver disease and matched healthy controls were purchased from Discovery Life Sciences (DLS). Samples were aliquoted for miRNA quantitation directly from plasma and from EVs following their isolation by qEV size exclusion chromatography (SEC) and immunoprecipitation (IP). EVs isolated by qEV were characterised by transmission electron microscopy (TEM), nanoparticle tracking analysis (NTA) and protein expression. Figure was created using BioRender.com.

Table 4.1 Demographic information for controls, non-alcoholic fatty liver (NAFL) and non-alcoholic steatohepatitis (NASH) study populations.

Characteristic		Control (n=14)	NAFL (n=8)	NASH (n=6)
Age	Mean (±SD) years	46.5 (15.7)	48.7 (17.7)	53.2 (15.4)
Sex	Female (%)	42.9	57.1	50.0
Race	Caucasian (%)	78.6	57.1	83.3
	Other (%)	21.4	14.3	16.7
	Unknown (%)	0	28.6	0

Isolation of Extracellular Vesicles

Size Exclusion Chromatography

Global EVs were isolated using qEV2 70nm size exclusion chromatography (SEC) columns (iZon Science). Prior to performing isolations, columns were equilibrated to room temperature and washed with 10mL of 0.2µm filtered phosphate-buffered saline (PBS). Plasma (1700µl) was diluted up to 2mL with PBS, loaded into the sample reservoir and allowed to completely pass into the column, before eluting with PBS. The first six fractions eluted from the column were discarded and vesicles were collected as a pool of fractions 7 to 11 (10mL). Pooled vesicle fractions were concentrated to 400µl using Amicon Ultra-15 centrifuge 30kDa filters (Millipore-Sigma) pre-conditioned with PBS and stored at -80^{o}C until analysis.

Liver Specific EV Immunoprecipitation

EVs specifically derived from the liver were separated from global EV isolates following a previously published protocol(Rodrigues et al., 2021). Briefly, 1.5mg of Dynabeads M280 streptavidin magnetic beads (Thermo Fisher Scientific, Cat#11205D) were pre-washed with PBS and incubated with 15µg of biotinylated anti-asialoglycoprotein receptor 1 (ASGR1) polyclonal antibody (Sapphire Bioscience, Cat#LS-C685544, 0.5mg/mL) for 30 min at RT with gentle agitation. Antibody-conjugated beads were separated using a DynaMag-2 magnet (Thermo Fisher Scientific), washed with 0.1% bovine serum albumin in PBS and resuspended in PBS. Concentrated qEV70 vesicles (150µl) were added to antibody-coated beads and incubated for 24 hours at 4^{o}C on a rotating mixer. ASGR1+ EVs bound to the antibody-bead complexes were separated on the magnet, washed and resuspended in PBS. Captured EVs that were to be analysed by nanoparticle tracking analysis, were eluted from the beads using a low pH buffer. Bead-bound EVs were incubated with 1

volume of 0.2μm-filtered 0.1M glycine-HCl at pH 3 for 10 minutes with shaking. The beads were separated using the magnet and the supernatant neutralised with 0.1 volume of filtered 1M Tris-HCl.

Transmission Electron Microscopy

Samples were prepared based on a previously published protocol(Newman et al., 2021). Briefly, 5μL of EV sample in filtered PBS was placed on carbon-coated grids for 4 minutes (Ted-Pella B 300M, Mason Technology). Grids were washed for 15 seconds with 0.2μm filtered PBS at room temperature and were contrasted with 2% uranyl acetate (3 min at room temperature), washed once, and examined by FEI TECNAI Spirit G2 TEM (Thermo Fisher Scientific).

Nanoparticle Tracking Analysis

Nanoparticle tracking analysis (NTA) was performed to quantify particle concentration and size distribution in EV samples using a NanoSight NS300 (Malvern Analytical). Samples were diluted between 1:500 and 1:2000 in PBS. Ten 60-second videos were captured at camera level 14 with continuous sample flow (flow rate 100) and videos were analysed at detection threshold 5 using NTA 3.4 software.

Total Protein Concentration

EVs were lysed by addition of RIPA buffer at a ratio of 1:1, incubated on ice for 25 minutes and centrifuged at 10,000 x g for 10 minutes at 4^{o}C. Total protein concentration was determined using Pierce MicroBCA Protein Assay following manufacturer's instructions (Thermo Fisher Scientific).

Protein Digestion

EVs (50μl) were diluted up to 100μl in PBS, vortexed for 10 minutes using a MixMate sample mixer (Eppendorf), then lysed by freezing and thawing for three times. Lysed EVs were combined with 50μl of ammonium bicarbonate (pH 7.8) and incubated with dithiothreitol (DTT; 12.5mM) for 90 minutes at 60^{o}C. Samples were cooled to room temperature prior to addition of iodoacetamide (IAA; 23.5mM) and incubation for 60 minutes at 37^{o}C. Trypsin Gold was then added to EV protein samples in a ratio 1:40 and incubated for 18 hrs at 37^{o}C. Digests were terminated by the addition of 20μl of formic acid (10%v/v), then centrifuged at 16000 x g for 10 minutes at 4°C. A 100μl aliquot of the

resulting supernatant was combined with SIL peptide standards (25-2500 pM cocktail; Vivitide) and a 5µl aliquot was injected for analysis by LC-MS/MS.

LC-MS Peptide Analysis

Chromatographic separation of peptide analytes was performed on an Agilent Advance Bio Peptide Map column (100 x 2.1 mm, 2.7 µm) using an Agilent 1290 Infinity II liquid chromatography system. The temperature of the column and sample compartment was maintained at 30 and 4°C, respectively. Separation was achieved by gradient elution with a flow rate of 0.2 mL/min. The mobile phase consisted of 0.1% formic acid in water (mobile phase A) and 0.1% formic acid in acetonitrile (mobile phase B). The proportion of mobile phase B was held at 10% for 2 minutes then increased to 60% over 13 minutes, before returning to 10% for 1 minute. The column was re-equilibrated for 30 seconds and total run time was 16.5 minutes. Column eluant was monitored by mass spectrometry using an Agilent 6495B Triple Quadrupole mass spectrometer operating in positive electron spray (ESI+) mode. Multiple reaction monitoring (MRM) was performed with one quantifier and one qualifier ion transition for each peptide. Identities of endogenous peptides were confirmed by comparing retention time and quantifier/qualifier transition ratios to respective SIL peptide standards and relative abundance determined by quantifier ion peak area.

RNA Isolation

Total RNA was isolated from plasma and EV samples using TRIzol LS™ Reagent (Thermo Fisher Scientific) as per manufacturer's instructions with some modifications. Briefly, 750µl TRIzol LS was added to 200µl of plasma and 100µl of EVs (diluted up to 200µl in RNase-free water). Samples were spiked with 2.5 femtomoles of cel-miR-54 mirVana mimic [MC10279] (Thermo Fisher Scientific) to normalise for technical variability in RNA extraction and RT-qPCR efficiency. This exogenous control was employed in the absence of established endogenous genes for normalisation of plasma or EV-derived miRNA RT-qPCR data (Kroh et al., 2010, Poel et al., 2018). Isopropyl RNA precipitation was facilitated by addition of 40µg RNase-free glycogen (Thermo Fisher Scientific) and the RNA pellet was washed with ice cold 80% ethanol. RNA was resuspended in 30µl RNase-free water.

RT-qPCR

Equal volumes of RNA (5µl) were reverse transcribed using the TaqMan microRNA Reverse Transcription Kit (Thermo Fisher Scientific). Since the concentration of circulating cfRNA is usually below the limit of quantification for photometric or colorimetric techniques, equivalent mass could not be reliably determined. Thus, RNA input was based on a fixed volume rather than RNA mass (ng) as done previously(Mateescu et al., 2017, Marabita et al., 2016, Castoldi et al., 2016). Instead, alterations in miRNA levels in equivalent volumes of plasma or EV isolates were detected relative to the exogenous spike in. TaqMan Small RNA Assays (Thermo Fisher Scientific) were used to carry out qPCR assays with primers specific to the miRNA of interest (hsa-miR-122 [002245]; hsa-miR-192 [00491]; miR-128a [002216]; cel-miR-54 [001361]) in a Rotor-Gene 3000 (Corbett Research). Samples were assayed in duplicate and the same cycle threshold set across all runs.

Statistical Analysis

Cycle threshold (Ct) values derived from RT-PCR were used to calculate relative quantities (RQ) according to the formula: 2^–(mean biomarker Ct – mean spike-in Ct). Statistical analysis was performed using GraphPad Prism software version 9.0 (San Diego, CA, USA). Data is presented as mean ± SD unless specified. Statistical comparisons between NAFL, NASH and control groups were performed using Kruskal-Wallis test and Dunn's test for multiple comparisons. Statistical significance was set at 0.05. Receiver operating characteristic (ROC) analysis was used to assess diagnostic capacity of miRNA biomarkers between pairs of groups. Ordinal logistic regression was performed using R version 1.4 (Boston, MA, USA) to determine diagnostic value across the three groups.

Results

Isolation and characterisation of circulating EVs

The concentration and size of global EV particles isolated from NAFL, NASH and control subjects was determined by NTA. An apparent higher mean EV concentration (±SD) of 4.17×10^{11} ($\pm 1.76 \times 10^{11}$) particles/mL was observed in control subjects compared to NAFL (2.34×10^{11} ($\pm 9.03 \times 10^{10}$) particles/mL) and NASH (2.73×10^{11} ($\pm 1.01 \times 10^{11}$) particles/mL) subjects (Figure 4.2A, Table 4.2). However, given the marked within group heterogeneity, no statistically significant differences

in EV concentration were detected between groups. Mean particle size, given in Table 4.2, also did not vary between control, NAFL and NASH groups. Though it is noted that EV isolates can differ when starting with plasma or serum, the concentration and size of vesicles isolated from this cohort are consistent with the ranges reported in the previous chapter exploring normal variability.

Table 4.2 Particle analysis.
Mean concentration and size of particles in global EV isolates from control, NAFL and NASH subjects determined by nanoparticle tracking analysis.

Group (n=5)	Concentration (Particles/mL SEC eluate)	Mean Size (nm)
Control	$4.17 \times 10^{11} \pm 1.76e+11$	102.9 ± 2.7
NAFL	$2.34 \times 10^{11} \pm 9.03e+10$	113.3 ± 10.4
NASH	$2.73 \times 10^{11} \pm 1.01e+11$	110.1 ± 8.6

Global EVs were also analysed by TEM to assess sample composition and morphology. TEM images of EVs from NASH and control subjects isolated by SEC revealed characteristic EV morphology, size and limited non-vesicular contaminants (Figure 4.2B). While the EVs were predominantly of similar size between NASH and control subjects, the presence of a few larger EVs was noted in the control sample.

Established positive and negative EV protein markers were probed by targeted LC-MS peptide analysis (Newman et al., 2021). Positive markers, as described by the Minimal Information for Studies of Extracellular Vesicles (MISEV) (Théry et al., 2018) include tetraspanins, CD81 and CD9, and tumour susceptibility gene 101 (TSG101) and were detected in EV isolates from control, NAFL and NASH subjects (Figure 4.2C). Only CD81 was significantly different in NAFL compared to control samples, however, total protein concentration was similar between groups (Figure 4.2D). Samples were also analysed for negative markers of matrix contamination (albumin) and large vesicles/cellular debris (calnexin V). Soluble protein contamination represented by albumin, was depleted in EVs (0.21%) relative to the abundance in total plasma.

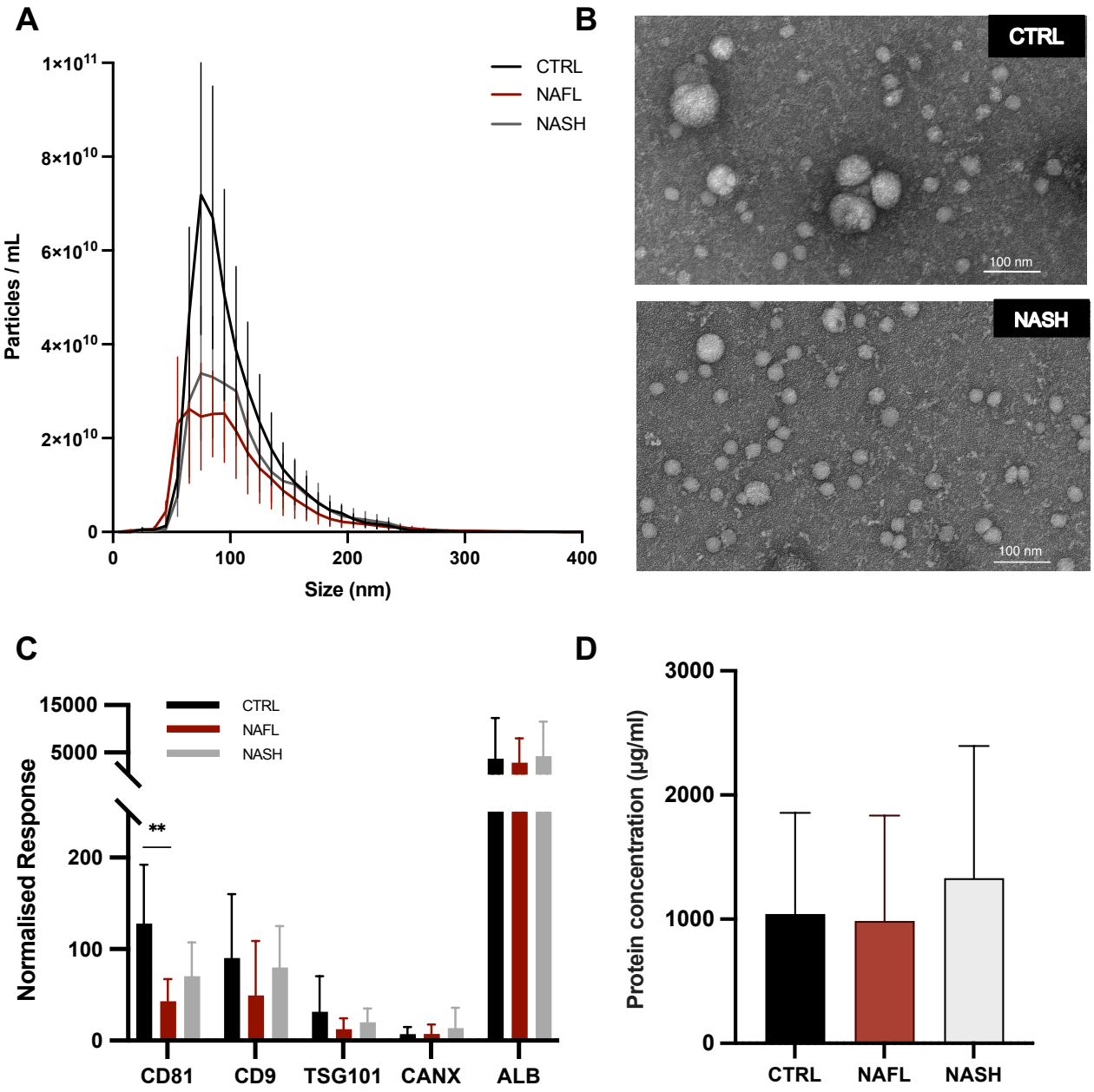

Figure 4.2 Characterisation of global circulating EVs from control, NAFL and NASH subjects.

(A) Particle concentration and size distribution by nanoparticle tracking analysis (NTA) (n=5). Error bars denote SEM (B) Representative TEM images of NASH patient and control global EVs. (C) Relative abundance of EV protein markers determined by mass spectrometry. (D) Total protein concentration in global EVs. Error bars denote SD. ** p≤0.01.

Characterisation of EVs isolated by anti-ASGR1 immunoprecipitation

The recovery of ASGR1+ vesicles from plasma was assessed in control plasma from five biological replicates. Global EVs were isolated and liver-specific EVs captured via anti-ASGR1 immunoprecipitation as described in Methods. Immunocaptured EVs were eluted from the beads using a low pH buffer for compatibility with NTA. Non-captured EVs were recovered following the 24hr incubation and separation of bead-bound EVs. Concentration of particles in global, captured and non-captured portions was determined by NTA and revealed that ASGR1+ EVs represented between 7.82 and 13.70 % of circulating EVs (Table 4.3). Total recovery (i.e. Captured + supernatant / global) was 82% on average. Losses of ASGR1- vesicles may be attributed to washing steps following collection of the non-captured portion. ASGR1 abundance was measured by targeted LCMS in global EVs, captured and non-captured samples. Relative to the global, ASGR1 signal was totally recovered in captured EVs (Figure 4.3A) indicating successful recovery of circulating EVs of liver origin.

Table 4.3 Recovery of liver derived EVs by immunoprecipitation.
Particle concentration in global EV isolates, ASGR1 immunocaptured samples and non-captured supernatant determined by nanoparticle tracking analysis, with percentage of ASGR1+ EV and total EVs recovered (captured + supernatant / global).

Sample	Concentration (Particles/mL)			Recovery (%)	
	Global	Captured	Supernatant	ASGR1+	Total
1	2.95E+10	3.91E+09	1.52E+10	13.25	64.78
2	1.11E+10	1.42E+09	8.33E+09	12.79	87.84
3	3.32E+10	4.55E+09	2.52E+10	13.70	89.61
4	2.11E+10	1.65E+09	1.56E+10	7.82	81.75
5	3.48E+10	2.95E+09	2.71E+10	8.48	86.35

While global EVs may originate from diverse tissues and organs, the predominant cell types contributing to the circulating population are those found in or contacting the blood, such as platelets, red blood cells, leukocytes and endothelial cells (Gustafson et al., 2015, Konoshenko et al., 2018). Other markers of hepatic origin and markers originating from tissues other than that of interest may be assessed to support the specific enrichment of the target population (Newman et al., 2023). As a

supplementary validation, targeted MS proteomics was thus used to measure the abundance of hepatic and non-hepatic proteins. The highly liver enriched drug metabolising enzyme cytochrome P450 3A4 (CYP3A4) was measured in ASGR1+ EVs according to the LCMS method described in Rodrigues et al. (2021). CYP3A4 enrichment in captured EVs support the hepatic origin of this vesicle population (Figure 4.3B). Marker proteins specific to red blood cell- and platelet- derived EVs were also measured according to the method in Newman et al. (2023) (Appendix 5). CD233 (erythrocyte specific) and CD41 (platelet specific) were largely recovered in the ASGR1- supernatant (Figure 4.3C-D), supporting the depletion of these EV populations. Taken together, these data support that the anti-ASGR1 immunoprecipitation method recovers circulating EVs of hepatocyte origin and depleted of common non-hepatic EV contamination.

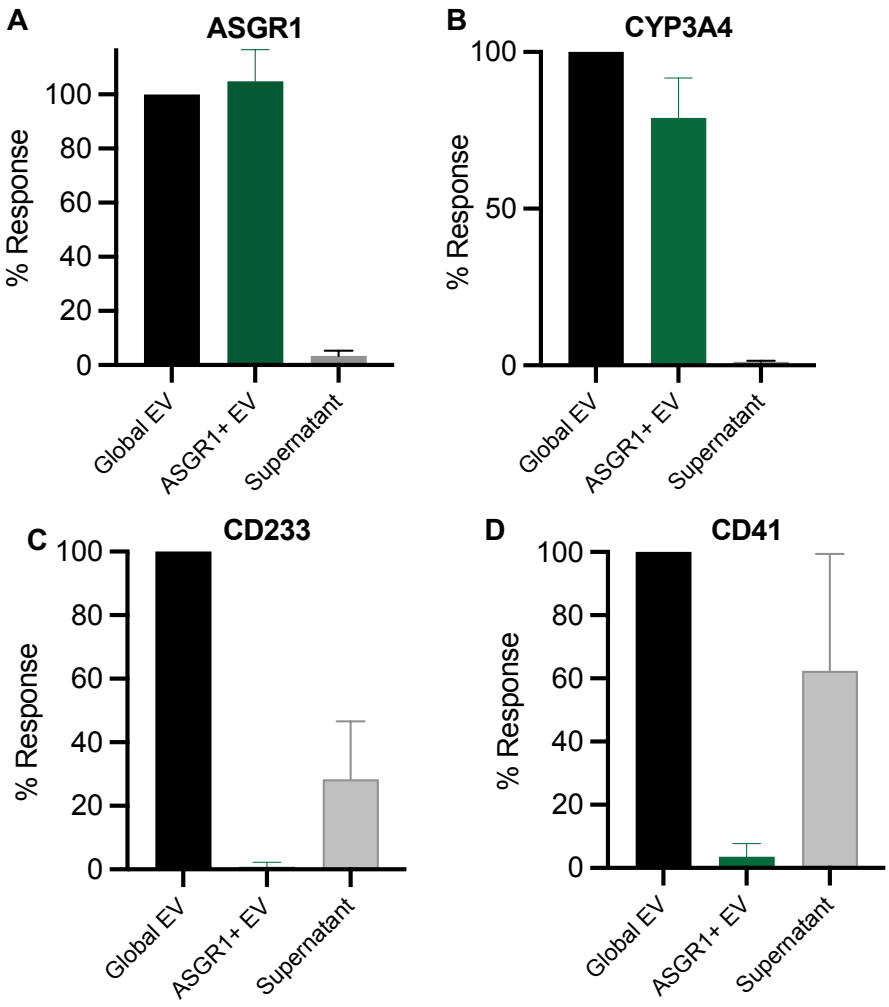

Figure 4.3 Abundance of hepatic and non-hepatic proteins in global EVs, ASGR1 immunocaptured and non-captured supernatant.

Data presented as mean % response of global EVs (± SD).
* Unpublished data in panels B-D were generated after publication of the rest of this chapter and are provided as additional validation of ASGR1 specificity for the purpose of this thesis.

Expression of total cell-free, global EV and liver-specific EV miRNA biomarkers

Expression of miRNA was quantified in total cfRNA, global EVs, and liver-specific EVs isolated by anti-asialoglycoprotein receptor 1 (ASGR1) immunoprecipitation. Relative quantities (RQ) for miR -122, -192 and -128-3p were calculated after normalising to an exogenous spike-in (cel-miR-54) and compared between control, NAFL and NASH subjects (Figure 4.4). Expression of all three miRNA biomarkers was significantly greater in ASGR1+ EVs from NASH subjects compared to controls ($p=0.012$ [miR-122], $p=0.013$ [miR-192], $p=0.032$ [miR-128-3p]. Interestingly, this trend was not observed when miRNA was analysed from total cell-free or global EV sources. In global EVs, only miR-128-3p exhibited altered expression with significantly lower RQ in NAFL ($p=0.009$) and NASH ($p=0.019$) subjects compared to controls. The apparent alterations in expression was consistent irrespective of using total cell-free or global EV as the source of RNA (Figure 4.4C), indicating that isolation of global EVs did not confer an appreciable benefit towards the capacity for miR-128-3p expression to distinguish the groups. Conversely, RQ for miR -122 and -192 did not vary between disease or control subjects in total cfRNA or global EV analysis. Overall, these data suggest that the selective analysis of miRNA biomarkers from liver-specific EVs has the potential to elucidate a useful trend in expression corresponding with disease stage for miRNA that are enriched in liver tissue.

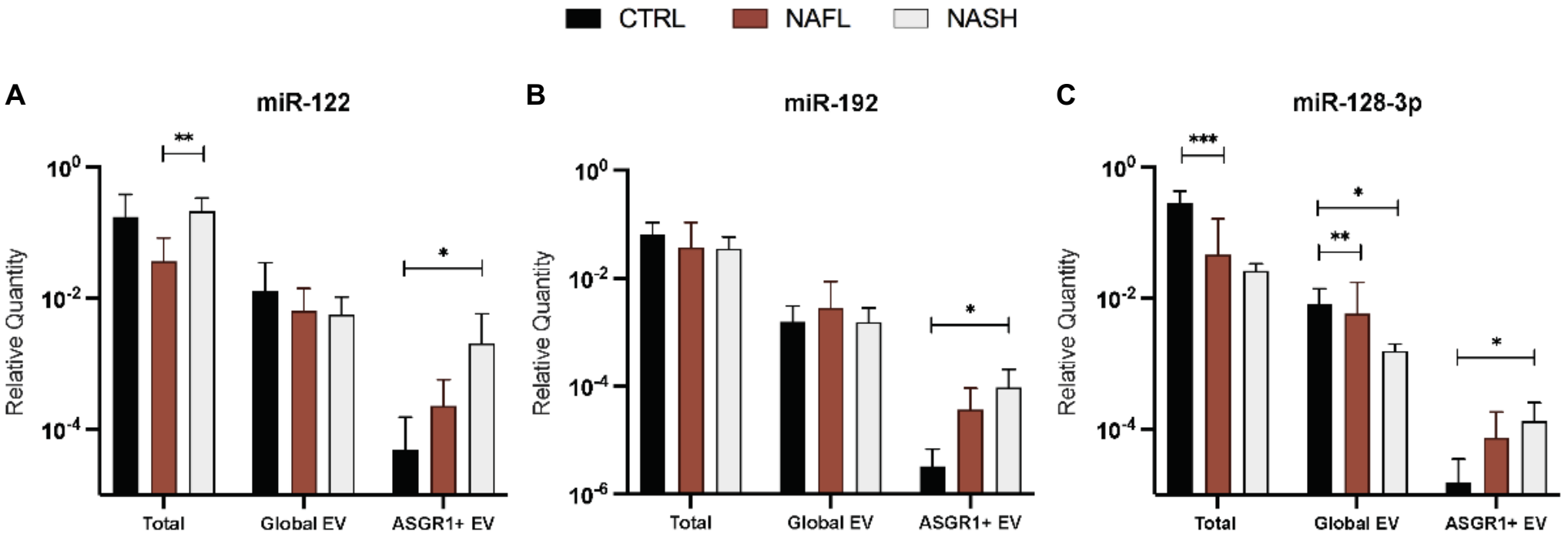

Figure 4.4 Differential expression of miRNA biomarkers in NAFLD.

Relative quantities of miR-122 (A), miR-192 (B) and miR-128-3p (C), normalised to cel-miR-54, in total circulating RNA, global EVs and asialoglycoprotein receptor 1 (ASGR1) positive EVs isolated from patients with NAFL and NASH and controls. Statistical analysis performed by Kruskal-Wallis test with Dunn's for multiple comparisons. * p≤0.05, ** p≤0.01, *** p≤0.001. Error bars represent standard deviation.

The proportion of circulating miRNA contained in EVs changes with NAFLD

To further explore the distribution of miRNA biomarkers amongst circulating fractions, RQs were used to calculate the expression of miRNA biomarkers in global EVs as a percentage of total cfRNA and in ASGR1+ EVs as a percentage of global EVs (Table 4.4). It has been observed that RNA isolation from unfractionated samples results in substantially higher yield compared to EVs due to the contribution of other circulating miRNA complexes. To ensure sufficient RNA recovery, the equivalent starting volume for EV RNA isolation was 2.5 x that for total cfRNA and reported proportions were normalised accordingly. The results demonstrated that in control samples, mean (± SD) percentage expression in global EVs/total RNA was no greater than 5.6 (± 10.0) %, suggesting that only a minor proportion of total cell-free RNA is found in EVs. Likewise, in control subjects, mean percentage expression in ASGR1+/global EVs was similarly low. Interestingly however, there was a positive trend in proportional expression of all miRNA biomarkers with NAFLD. In NASH, 27.1 % of vesicular miR-122 signal came from ASGR1+ EVs compared to just 2.4 % in control subjects (p=0.035) (Table 4.4, Figure 4.5A). Significantly greater ASGR1+/global EV expression was also observed for miR-128-3p between NASH and control subjects (p=0.022) (Figure 4.5C), while a similar trend in miR-192 did not reach significance (p=0.067). While only a small fraction of each miRNA is released in EVs expressing ASGR1, these data suggest that in NAFLD the contribution of the liver to circulating EV-derived miRNA increases.

Table 4.4 Relative miRNA expression in global and liver derived circulating EVs.
Data given as percentage expression in global EVs to total circulating RNA and in asialoglycoprotein receptor 1 positive (ASGR1+) EVs to global EVs from control, NAFL and NASH subjects.

Expression (%)		miR-122		miR-192		miR-128-3p	
		Mean	SD	Mean	SD	Mean	SD
Global EV / Total	Control	5.6	10.0	5.1	14.5	2.3	3.7
	NAFL	23.3	27.3	8.7	6.7	17.0	26.2
	NASH	5.1	10.6	3.0	3.4	2.6	1.0
ASGR1+ EV / Global EV	Control	2.4	6.6	0.5	0.8	0.6	1.4
	NAFL	9.9	20.7	10.4	17.0	13.3	20.2
	NASH	27.1	37.2	8.8	9.8	10.5	10.1

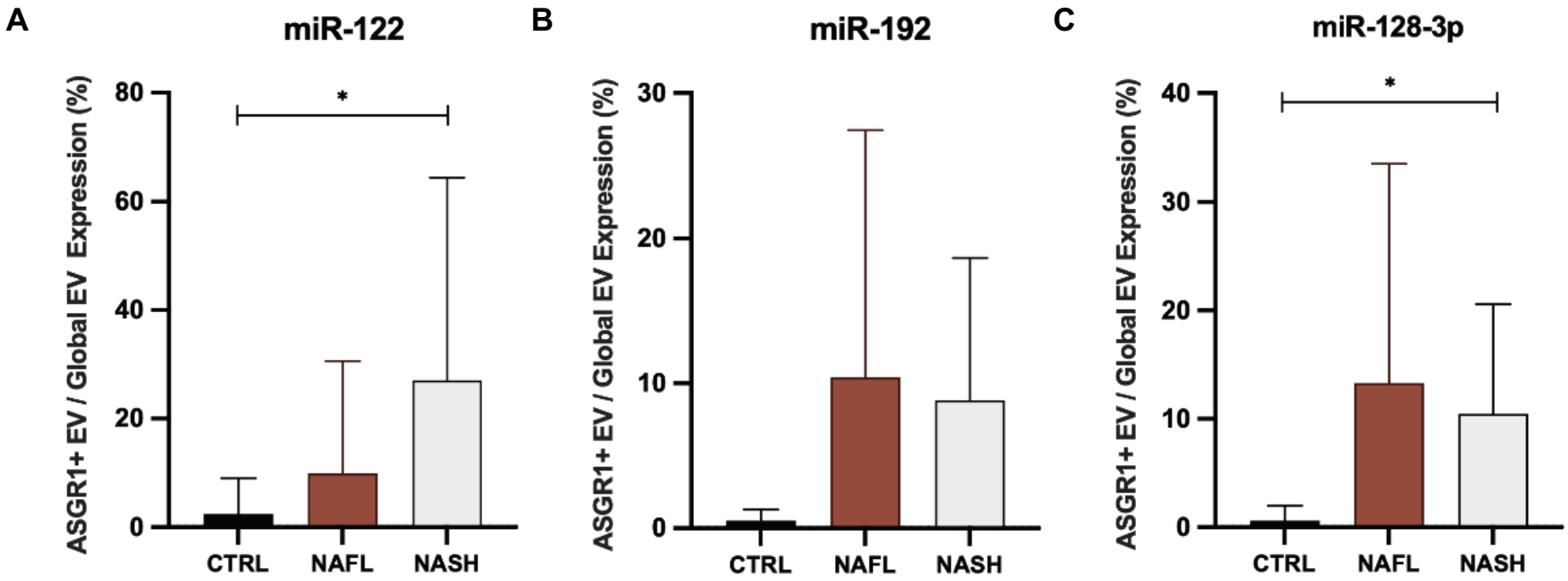

Figure 4.5 Relative expression of miRNA in liver-specific EVs.

Expression of miR-122 (A), miR-192 (B) and miR-128-3p (C) in asialoglycoprotein receptor 1 positive (ASGR1+) EVs as a percentage of global EVs in NAFL and NASH patients compared to controls. Statistical analysis performed by Kruskal-Wallis test with Dunn's for multiple comparisons. * $p \leq 0.05$. Error bars represent standard deviation.

Association between miRNA expression and disease severity

Ordinal logistic regression was performed to evaluate associations between miRNA abundance and the probability of a subject being healthy (control), NAFL or NASH. Significant associations between miRNA expression and group status were observed for all three miRNAs in liver-specific EVs (Figure 4.6). The C-statistic for miR-122 was 0.80 with an odds ratio (OR) of 0.60 (p=0.004), indicating that for every 1 unit decrease in ΔCt the subject was 40% more likely to be NASH than NAFL or NAFL than control. Similarly, the C-statistics for miR-192 and miR-128-3p were 0.84 and 0.78, with ORs of 0.51 (p=0.005) and 0.65 (p=0.016), respectively. Expression of miR-122 and miR-192 in total cfRNA and global EVs demonstrated no significant association with group status. Robust predictive performance was observed for total cfRNA and global EV derived miR-128-3p, with C-statistics of 0.78 (p=0.007) and 0.83 (p=0.009), respectively. Of the miRNA sources, only liver-specific EVs demonstrated a consistent trend amongst all miRNAs across increasing disease state.

Capacity to distinguish subjects with disease from control

Receiver operator characteristic (ROC) analysis was undertaken to establish the performance of each miRNA marker in the current analysis in a manner consistent with prior studies, as summarised in our recent review (Newman et al., 2020) (Table 4.5). The abundance of total plasma RNA derived miR-192 and miR-128-3p, but not miR-122, robustly distinguished individuals with NAFLD from controls (AUC ≥ 0.714). Comparatively poor performance was observed for global EV derived miRNAs, with only miR-128-3p (AUC = 0.888) distinguishing these groups. As per the ordinal logistic regression analysis, liver-specific EV-derived miRNAs demonstrated the strongest performance with respect to distinguishing individuals with NAFLD from controls. AUC values for liver-specific EV derived miRNAs were invariably >0.8.

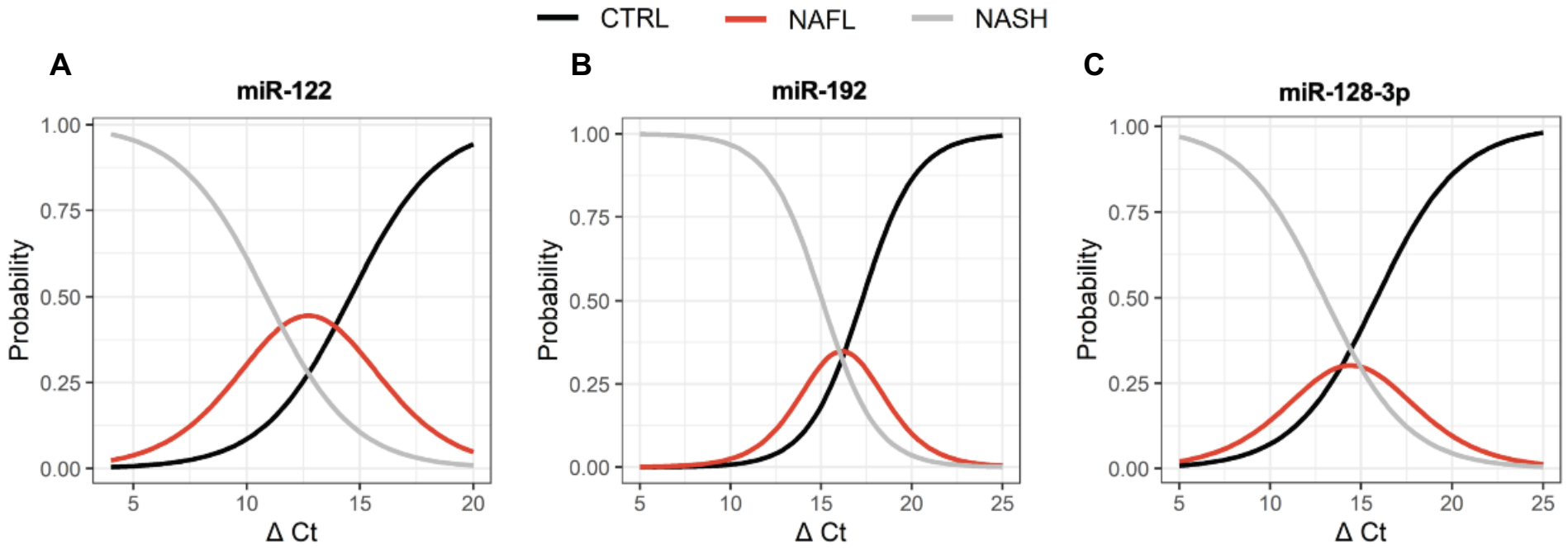

Figure 4.6 Ordinal logistic regression models.

Ordinal regression applied to distinguish control, NAFL and NASH subjects using ASGR1+ EV-derived miR-122 (A), miR-192 (B) and miR-128-3p (C).

Table 4.5 AUROC analysis for distinguishing all disease from controls.
Area Under the Receiver Operator Characteristic (AUC) Curve for miRNA biomarkers isolated from total cell-free RNA, global EVs and ASGR1+ EVs. Performance separating all disease subjects from controls. * denotes significant p values (≤0.05).

Source	All NAFLD – CTRL					
	miR-122		miR-192		miR-128-3p	
	AUC	p	AUC	p	AUC	p
Total RNA	0.607	0.335	0.714	0.054*	0.924	0.0001*
Global EV	0.505	0.963	0.582	0.462	0.888	0.001*
ASGR1+ EV	0.830	0.004*	0.895	0.003*	0.803	0.014*

The ROC analysis was also extended to distinguishing individual group pairings (i.e. control vs NAFL, control vs NASH and NAFL vs NASH) (Table 4.6, Figure 4.7), however, was limited in statistical power. While total plasma derived miRNAs performed well for several disease pairings, the direction of the change in expression was not consistent with prior reports (Newman et al., 2020). Interestingly, ASGR1+ EVs reflected increasing miRNA biomarker expression and strongly separated several of the NASH-CTRL (AUC=0.846-0.925) and NAFL-CTRL pairings (AUC=0.741-0.85) (Table 4.6).

Table 4.6 AUROC analysis for distinguishing disease severity.
Area Under the Receiver Operator (AUC) Characteristic Curve analysis for miRNA biomarkers isolated from total cell-free RNA, global EVs and ASGR1+ EVs in distinguishing NAFL, NASH and control groups. * denotes significant p values (≤0.05).

	miR-122					
	NAFL–CTRL		NASH–CTRL		NASH–NAFL	
	AUC	p	AUC	p	AUC	p
Total RNA	0.833	0.010*	0.678	0.213	0.938	0.007*
Global EV	0.533	0.796	0.544	0.756	0.500	0.999
ASGR1+ EV	0.741	0.065	0.881	0.008*	0.688	0.245
	miR-192					
	NAFL–CTRL		NASH–CTRL		NASH–NAFL	
	AUC	p	AUC	p	AUC	p
Total RNA	0.858	0.006*	0.844	0.016*	0.729	0.156
Global EV	0.650	0.245	0.511	0.938	0.625	0.439
ASGR1+ EV	0.850	0.048*	0.925	0.006*	0.625	0.522
	miR-128-3p					
	NAFL–CTRL		NASH–CTRL		NASH–NAFL	
	AUC	p	AUC	p	AUC	p
Total RNA	0.917	0.001*	0.933	0.002*	0.875	0.020*
Global EV	0.800	0.020*	0.989	0.001*	0.688	0.245
ASGR1+ EV	0.677	0.257	0.846	0.018*	0.667	0.361

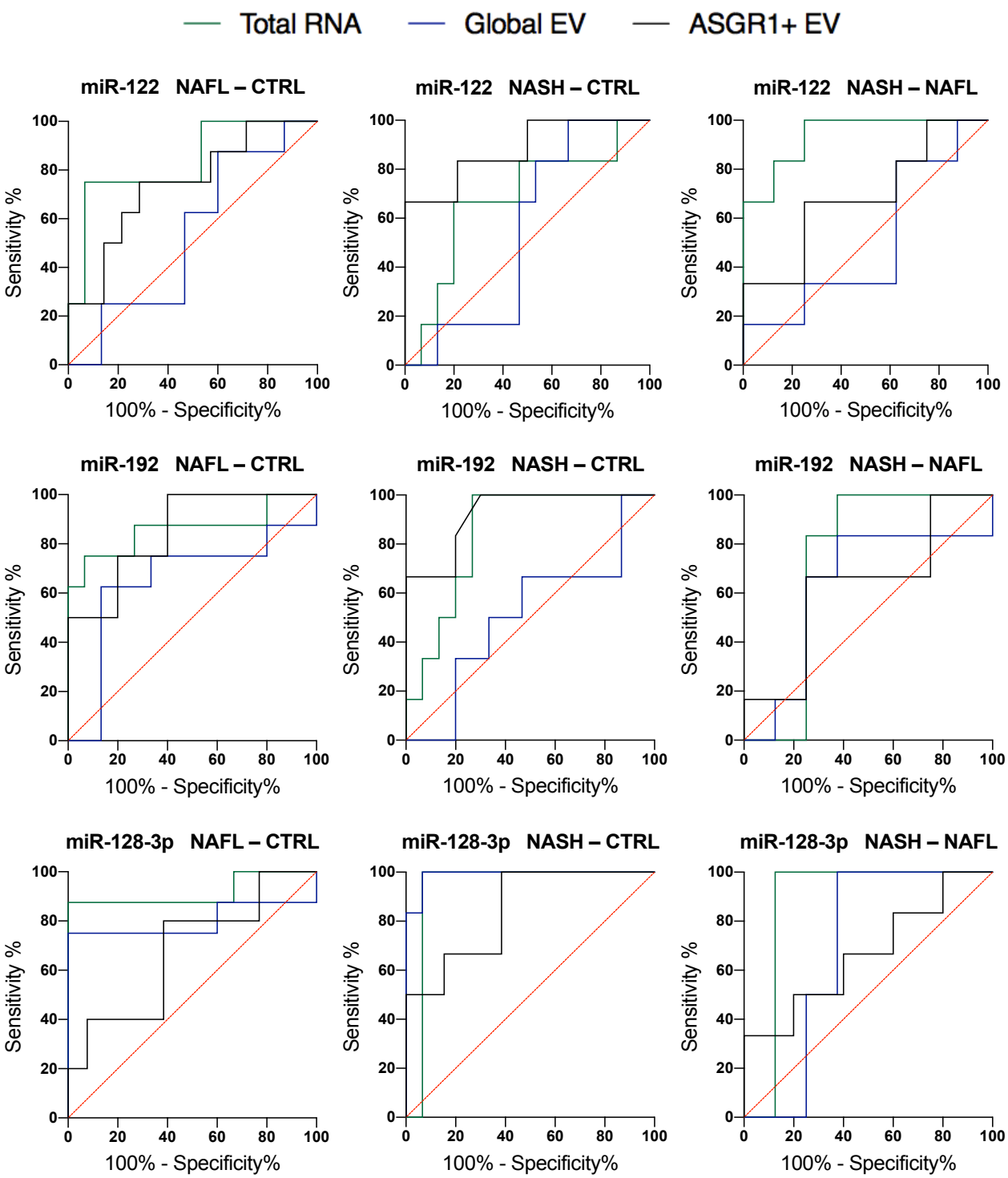

Figure 4.7 Receiver Operator Characteristic (ROC) curve analysis.

ROC analysis of miR-122, miR-192 and miR-128-3p in total cell-free, global EV and ASGR1+ EV RNA for distinguishing subjects in pairwise groupings (NAFL-CTRL, NASH-CTRL and NAFL-NASH).

Discussion

This study provides the first direct evidence supporting the transformative improvement in the predictive performance of existing NAFLD miRNA biomarkers achieved by isolating liver-specific EVs. Specifically, it is demonstrated that following anti-ASGR1 immunoprecipitation, the expression of liver-specific EV derived miR -122, -192 and -128-3p is significantly associated with disease severity. In all cases, there was a significant trend of greater miRNA expression in subjects with NASH compared to NAFL and NAFL compared to control subjects. Notably, this trend was not observed with either total cell-free or global EV derived RNA. Rather, analysis from these two sources of RNA revealed a significant decrease in miR-128-3p expression with disease, while miR -122 and -192 were not altered in comparison to controls. In all cases, liver specific (ASGR1+) EV-derived miRNA biomarkers demonstrated strong capacity to predict subject status as control, NAFL or NASH (Figure 33) with c-statistics 0.78-0.84. This performance was not observed with either total cfRNA or global EV derived miRNAs. While the improved predictive performance associated with liver-specific isolation provides additional support for these markers reflecting a hepatic manifestation, the possibility that these markers may also be associated with more systemic comorbidities cannot currently be excluded.

Indeed, each of the miRNAs investigated here are abundant in liver tissue; especially miR-122 which accounts for about 70% of all miRNA expression in the liver (Gjorgjieva et al., 2019). However, miR-122 is also found in cardiac and skeletal muscle, miR-192 is abundant in the kidneys, intestine and adipose tissue (Liu et al., 2020), and miR-128-3p is expressed in numerous tissues types, including in the CNS (Noetel et al., 2013) and adipose (Chen et al., 2018a). miR-128-3p also acts as a tumour suppressor miR and is reported to be dysregulated in several cancers, including lung (Pan et al., 2018), colorectal, and hepatocellular (Zhang et al., 2017, Huang et al., 2015). Fundamentally, circulating miRNAs lack tissue specificity, and their presence and stability in biological fluids results from release by multiple cell types and localisation within EV, lipoprotein and Ago protein complexes (Makarova et al., 2021). The mechanisms of miRNA export from cells is known to be differentially affected by disease states; accordingly, perturbation in the relative expression of circulating miRNAs in vesicular or non-vesicular compartments are anticipated

(Castoldi et al., 2016, Endzeliņš et al., 2017). Consistent with this phenomenon, it was observed that the fraction of total circulating miR-122 (which accounts for 70% of hepatic miRNA) contained within liver-specific EVs increased with disease stage. This observation further supports the hypothesis proposed by several recent studies that optimising the circulating miRNA source is a key step in translating miRNA biomarker analysis (Endzeliņš et al., 2017, Castoldi et al., 2016, Nik Mohamed Kamal and Shahidan, 2020, van Eijndhoven et al., 2016).

Jiang et al. (2021) recently reported that compared to total serum derived miRNA, differences in EV-derived miRNAs, including miR-122 (ROC = 0.79), more effectively discriminated subjects with NAFLD from healthy controls. In contrast to Jiang et al. (2021), in the current study isolation of global EVs did not improve the predictive performance of miRNA biomarkers with respect to identifying individuals with NAFLD. It is plausible that differences in performance gains achieved by global EV isolation relate to differences in the composition of the NAFLD cohort (i.e. the proportion of individuals with NAFL versus NASH, or the proportion of individuals with non-hepatic comorbidities). While this study did not reproduce the improvement in predictive performance achieved by isolating global EVs, we did demonstrate that further refinement of the miRNA source by tissue-specific EV isolation did markedly improve performance. This outcome is consistent with analyses demonstrating improved signal to noise for minimally-invasive protein biomarkers in plasma for neuronal pathology (Mustapic et al., 2017, Fiandaca et al., 2015, Shi et al., 2014, Goetzl et al., 2016) and cerebrovascular disease (Goetzl et al., 2017) with tissue specific isolation. Similar to the present study, selectively enriching the biomarker source was consistently found to increase sensitivity and specificity of analyses. One study further showed that expression of miR-382 in intestine-specific EVs, but not global EVs, could predict functional activity of human breast cancer resistance protein (Gotanda et al., 2016). Furthermore, we recently applied the liver-specific EV isolation method used here to describe the induction of hepatic drug metabolising enzymes and transporters resulting from metabolic drug interactions and pregnancy (Rodrigues et al., 2021). Collectively, these reports highlight the emerging potential to leverage tissue-specific EVs as minimally invasive liquid biopsy platform.

The use of anti-ASGR1 immunoprecipitation facilitated the analysis of EV encapsulated miRNA biomarkers released only by hepatocytes. Given the reported high abundance of miR-122 in hepatocytes, a high proportional expression of miR-122 in ASGR1+ EV relative to global EV derived miRNA was anticipated. However, in EVs isolated from control subjects the fraction of EV derived miR-122 recovered from ASGR1+ EVs was strikingly low (2.4% of global EV derived miR-122 and 0.13% of total circulating miR-122). This low expression of miRNA in ASGR1+ EVs likely reflects the low fraction of circulating EVs that are derived from hepatocytes. The substantial expression of miR-122 from non-hepatic sources emphasises the potential for trivial changes in non-hepatocyte derived miRNAs to markedly impact NAFLD biomarker analysis in the absence of liver-specific EV isolation. An additional explanation that cannot be excluded is the possibility that global EV preparations contained some non-EV RNA associated with contaminating proteins or lipoprotein complexes co-isolated from the plasma. Interestingly, the fraction of global EV and cfRNA derived miR-122, -192 and -128-3p recovered in ASGR1+ EVs was markedly higher in NAFL and NASH subjects compared to controls, despite the circulating EV count remaining unchanged. This marked increase in ASGR1+ EV derived miRNA expression is consistent with the reported roles of these miRNAs in the inflammatory processes and remodelling associated with NAFLD and supports the biological rationale for their use as biomarkers for this disease. It is worth noting that while expression of miR -122 and -128-3p was significantly increased in NAFL and NASH compared to control subjects, the proportion of these miRNAs in ASGR1+ EV still accounted for < 30% of global EV expression and < 2.5% of total cfRNA expression for each miRNA.

It is conceivable that a population of miRNA-containing hepatic EVs does not express the ASGR1 on their surface and hence are not captured by the immunoprecipitation method applied in the current analysis. Alternatively, various extra-hepatic tissues expressing these miRNAs may contribute more profoundly to their abundance in circulating global EVs. NAFLD is notably the hepatic manifestation of a broader multi-system disease associated with systemic inflammation and metabolic disturbances in several organs. It is likely that perturbations in other organs may contribute to the observed differences in global EV cargo derived from subjects with NAFL and NASH. This explanation further emphasises the potential benefits of selectively isolating liver-specific EVs for

biomarker analyses. Data presented in a recent study by Povero et al. (2020) indicated that EVs expressing ASGR1 comprise approximately 20% of the circulating global pool and that the number of hepatocyte-derived EVs increases with severity of NASH. However, in the limited sample size analysed here, no differences in global EV abundance were observed between groups. In this context, it is not clear if the increased proportional expression of miRNA with disease was due to greater number of ASGR1+ EVs or increased packaging and export of miRNA biomarkers into vesicles.

The observed increase in ASGR1+ EV miRNA expression is consistent with a large body of work describing the dysregulated miRNA profile in NAFLD liver and selective export into EVs. miRNAs have emerged as major players in the pathogenesis and progression of NAFLD, with altered hepatic expression of miR -122, -192 and -128-3p disrupting several facets of hepatic lipid metabolism, insulin sensitivity and cholesterol-lipoprotein trafficking (Gjorgjieva et al., 2019, Zhang et al., 2017, Wagschal et al., 2015). Prior studies have also emphasised the pathogenic consequences of vesicular miRNAs from hepatocytes in response to lipotoxic injury in NAFLD (Newman et al., 2020). EV-derived miR-192 was recently reported to induce pro-inflammatory polarisation of liver macrophages (Liu et al., 2020) and EV miR-128-3p internalised by hepatic stellate cells led to marked fibrogenic activation (Povero et al., 2015). Decreased cellular miR-122 abundance has been observed in conjunction with increased abundance in circulating EVs. This observation has been attributed to accelerated miR-122 export via the endosomal pathways resulting from metabolic and ER stress in hepatocytes (Mukherjee et al., 2016, Bhattacharyya et al., 2006). Indeed, multiple reports (Povero et al., 2014, Pirola et al., 2015, Bala et al., 2012) support the notion that miR-122 increases specifically in the circulating vesicle fraction in NAFLD, while other liver pathologies (e.g. drug-induced liver damage) are better characterised by changes in the protein-associated fraction (Bala et al., 2012, Castoldi et al., 2016). Further studies are required to elucidate the intracellular source of miRNAs that are packaged into EVs and the specific mechanisms of export during NAFLD and normal physiology. Nonetheless, the present findings are promising with respect to increasing specificity by targeting analyses to liver-derived miRNA expression.

It is acknowledged that additional clinical data regarding the patient cohort would have been useful and the inability to access these data is a limitation of the current study. Specifically, NAFLD and NASH are hepatic manifestations of metabolic syndrome and are closely associated with multiple comorbidities including type 2 diabetes and obesity, which if unaccounted for may confound biomarker screening. By way of example, while the miRNA markers evaluated here have previously been associated with NAFLD and NASH (Newman et al., 2020), the current study is unable to definitively exclude that these markers are specific to the hepatic manifestations of the syndrome, and not alternative comorbidities observed in this patient population. Additionally, it is acknowledged that while the purity of ASGR1+ EVs in control EV preparations was extensively characterised, limitations regarding sample volume precluded comparable analyses in the NAFLD samples. Future studies confirming the observations reported here will benefit from more extensive clinical data and the capacity to undertake additional characterisation of immunocaptured samples.

To date, studies of cell-free miRNA biomarkers have dichotomised subjects to discriminate controls from subjects with either NAFL, NASH or simply pooled as NAFLD. As summarised in our recent review (Newman et al., 2020), ROC analysis has identified strong predictive performance of several miRNA markers quantified from total cell-free RNA (Newman et al., 2020). Up to 7-fold increases in circulating miR -122 and -192 has been previously reported in NAFLD patients (Cermelli et al., 2011, Liu et al., 2016), however such significant dysregulation in total cfRNA was not observed in comparison to controls in this cohort. For a number of group pairings, however, ROC analysis produced similarly strong discrimination of cohorts as seen previously (Newman et al., 2020). However, in order to investigate the capacity for miRNA biomarkers from different sources (ASGR1+ EV, global EV, total cfRNA), to predict an individual's disease status across control, NAFL and NASH groups simultaneously, ordinal logistic regression was applied. With this more robust approach that incorporated the biological link of increased biomarker expression in a directional manner, ASGR1+ EVs consistently exhibited excellent diagnostic accuracy. For miR -122 and -192, statistically significant associations were achieved only by the analysis of liver-specific EV miRNA.

The findings presented here represent the first direct evidence supporting the hypothesis that tissue-specific isolation enhances predictive performance of EV derived miRNA biomarkers. This study further provides the necessary foundational evidence demonstrating that liver-derived EVs represent a promising solution to current shortcomings in regard to the clinical management of NAFLD. Specifically, this study determined that refining the source from which circulating miR biomarkers are analysed enhanced their capacity to distinguish NAFLD patients from controls. While total cfRNA has long dominated the focus of this field, the belief that markers obtained from a particular blood compartment may better represent disease-associated changes has emerged with the promise of improved biomarker specificity and reproducibility. Here we show that the selective isolation of liver-specific EVs by anti-ASGR1 IP has the potential to elucidate useful trends in miR expression, that may be applied to track NAFLD patients across the spectrum of clinical disease. This approach not only facilitates the use of biomarkers with ubiquitous expression in unrelated tissues, that may otherwise limit their utility, but also opens the possibility of discovering other highly disease-specific biomarkers, such as EV-derived proteins, from just the affected organ. Such tools can facilitate early diagnosis, identification of patients at greatest risk of progression, serial sampling and longitudinal monitoring. Thus, the development of liver EV biomarkers could improve patient management universally, with profound impacts on clinical practice, utilisation of healthcare resources and advancement of therapeutics.

CHAPTER 5

ESTABLISHING THE CAPACITY OF LIVER DERIVED EXTRACELLULAR VESICLE CARGO TO REFLECT VARIABILITY IN DRUG EXPOSURE AND RESPONSE

Author Contributions

A manuscript containing the contents of this chapter has been submitted to the *British Journal of Clinical Pharmacology* for peer-review and publication. I was the first and sole primary contributing author of the manuscript and was responsible for conceptualisation, generating the data and performing statistical analysis, wrote the first draft and reviewed and edited the paper, culminating in 85% of the work. Author Z.U generated the TEM images and NTA data and edited the paper. Author T.W assisted with the development of targeted proteomic assays. Author A.R contributed to conceptualisation and edited the paper.

Context in Thesis

Applying a method to isolate EVs directly from liver tissue yields an enriched population of liver derived EVs that are otherwise relatively rare in the total circulation. This offers an opportunity to investigate the fundamental assumption that the protein profile of EVs reflects that of their originating tissue. Given the impact of MAFLD on hepatic drug metabolism and the challenges associated with the clinical development of novel pharmacological therapeutics for this chronic liver disease, this work investigates the profile of key proteins related to the interaction of drugs with the liver. More specifically, these interactions relate to the pharmacokinetic (PK) and pharmacodynamic (PD) activities which in turn impact the exposure and response to a drug. Interindividual differences in the abundance of drug-metabolising enzymes (DMEs) and drug target proteins underpin PK and PD variability and impact treatment efficacy and tolerability.

As EVs carry protein cargo inherited from originating hepatic cells, they may be useful for defining differences in key proteins related to drug metabolism and the treatment of MAFLD.

Targeted LCMS proteomic assays were developed for a panel of DMEs and MAFLD drug target proteins with the aim of detection and quantification in liver tissue EVs (LT-EV) and to establish the profile relative to paired total liver tissue. The work described in this chapter provides evidence that key proteins related to PK and PD profiles can be measured in LT-EVs, and the abundance of liver-enriched DMEs is robustly correlated between paired tissue and EVs. This addresses the fundamental capacity for LT-EVs to define between-subject differences in DME profile and within-subject changes in MAFLD drug targets. These data support the potential to assess markers of drug exposure and response *in vivo* with a liver derived EV liquid biopsy.

Introduction

An individual's exposure and response to a drug is determined by the pharmacokinetic (PK) and pharmacodynamic (PD) profiles of the drug. The PK profile is influenced by the processes of absorption, distribution, metabolism and excretion (ADME), with clearance by metabolism being the primary determinant of PK for most drugs. Members of the cytochrome P450 (CYP) and UDP-glucuronosyltransferase (UGT) families of drug metabolising enzymes (DMEs) are responsible for the clearance of more than 80% of drugs (Rowland et al., 2013, Swen et al., 2023). The PD profile for a drug reflects interactions that alter the function of one or more molecular target in the body. More than 95% of molecular drug targets are proteins (receptors, enzymes, ion channels or transporters). Between subject differences in the abundance and activity (phenotype) of the proteins associated with a drug's PK and PD profiles underpin variability in treatment efficacy and tolerability (Rowland et al., 2018, Sorich et al., 2019). Differences in phenotype may result from normal physiological and genetic variability, environmental factors or perturbations caused by disease.

There are multiple prominent examples where assessment of genetic variants (genotype) explains a sufficient proportion of variability in observed DME phenotype to guide drug dosing (Swen et al., 2023). However, assessment of genotype is of limited value when differences in DME phenotype are predominantly driven by factors such as drug interactions and disease states (Rowland et al., 2019). In such cases direct quantification of protein abundance is substantially more useful in explaining variability in drug exposure. Measuring the tissue abundance of DMEs has

historically required collection of a liver tissue biopsy (Rodrigues and Rowland, 2019), which is preclusively invasive for seeking insights into PK variability or guiding drug dosing. In recent years, assessment of circulating extracellular vesicle (EV) cargo has been demonstrated as a promising alternate strategy to characterise changes in the abundance of hepatic CYP enzymes resulting from induction based drug interaction (Rowland et al., 2019, Rodrigues et al., 2021, Rodrigues et al., 2022). For example, the 3.7-fold increase in CYP3A4 protein abundance in circulating EVs following administration of rifampicin (600mg daily for 14 days) to healthy volunteers was consistent with strong induction reported with liver tissue biopsy and was predictive of observed changes in oral midazolam exposure (Rodrigues et al., 2021). Beyond induction of CYP3A4, it is plausible that assessment of EV protein cargo may similarly be used to understand between subject differences in DME phenotype. Indeed, liver derived EVs have been demonstrated to contain an array of DME messenger RNAs and protein cargo (Achour et al., 2021, Useckaite et al., 2023, Rodrigues et al., 2021, Rodrigues et al., 2022, Rowland et al., 2019). Establishing the utility of EVs with respect to accounting for between subject variability in phenotype requires evidence that the absolute DME protein abundance in EVs reflects the absolute protein abundance in the tissue.

Similarly, characterising changes in the phenotype of proteins that reflect the occupancy or modulation of a molecular drug target (proximal) or downstream biological effects (distal) during pre-clinical development provides insights to the likely PD profile for a drug. These proteins, referred to as markers of target engagement, may be used to enhance the understanding of a drug's clinical efficacy and tolerability by tracking their abundance before and after an intervention in clinical trials (Tan et al., 2009). Tracking changes in the abundance of target engagement markers conventionally requires collection of serial tissue biopsies from the target organ, which is preclusively invasive for most targets and solid organs. When considering the liver as an example of a target organ, there are an array of chronic liver diseases, including metabolic associated fatty liver disease (MAFLD), where pharmacological interventions may be useful (Newman et al., 2022a, Newman et al., 2020). Indeed, for MAFLD, drugs targeting multiple disease associated pathways, including hepatic lipogenesis, insulin resistance, mitochondrial dysfunction, inflammation and fibrogenesis have been proposed. However, clinical trials have encountered numerous challenges with many candidates

failing to meet efficacy endpoints (Ratziu and Friedman, 2020). These failures have been attributed to multiple potential factors including the inability to account for heterogeneity in disease, the inability to select appropriate intervention populations, or inefficacy of the drug to modulate the disease pathway in humans. In each case, more comprehensive and longitudinal understanding of the phenotype of target proteins and disease pathways presents the opportunity to focus development efforts on the most promising drug targets and treatment populations.

Recent untargeted proteomic profiling of paired human liver homogenate and tissue derived EVs demonstrated that approximately 60% of hepatic proteins were detected in EV (Useckaite et al., 2023). The incorporation of molecular drug targets and associated downstream proteins into EVs raises the intriguing potential of tracking markers of target engagement *in vivo* using a minimally invasive liquid biopsy. The use of EV cargo as markers of target engagement requires evidence that (i) the protein targets in EVs originate from the organ of interest, and (ii) changes in EV protein abundance are related (either directly or inversely) to changes in protein abundance in the tissue. The work of Useckaite *et al*. (2023) indicated that based on identification of unique proteins, approximately 50 % of EVs present in liver tissue are likely to be of extra-hepatic origin. This is an important consideration when evaluating the concordance between the absolute protein abundance in tissue homogenate and tissue derived EVs, particularly for proteins that exhibit substantial extra-hepatic expression.

This study sought to establish the fundamental capacity of liver derived EVs to (i) define between subject variability in DME protein abundance, and (ii) track within subject changes in the abundance of MAFLD drug targets. As such, the primary objective of the study was to demonstrate the capacity to robustly quantify the abundances of a panel of DME and MAFLD drug targets in EVs isolated from healthy liver tissue (LT-EV). The concordance between the absolute DME protein abundance in liver tissue homogenate (L-HMG) and LT-EVs was evaluated as a secondary outcome. Since approximately half of the EVs isolated from liver tissue are of non-hepatic origin (Useckaite et al., 2023), exploratory analyses were performed to evaluate the relationship between the correlation of protein abundances in liver tissue and LT-EV and the extent of extra-hepatic protein expression.

To ensure the robustness of data, LT-EVs were characterised in accordance with Minimal Information for Studies of Extracellular Vesicles (MISEV) (Welsh et al., 2024).

Methods

Tissue samples

Fresh frozen human liver tissue (n=11) was obtained from the liver "bank" of the Department of Clinical Pharmacology (Flinders University, Adelaide, SA, Australia). The use of tissue samples for research was approved by the donor's next of kin and the Clinical Investigation Committee of Flinders Medical Centre (SACHREC 059.056). Tissue was snap frozen using liquid nitrogen immediately upon collection and stored at -80°C until used. Tissue histopathology was confirmed by a pathologist on in-house haematoxylin & eosin (H&E) stained full-face tissue sections. The sample preparation workflow is described below.

Histopathology

Full-face histopathology slides were prepared from frozen liver tissue samples and stained with H&E stain. Histopathology slides were used to evaluate tissue morphology by pathologist examination and guide partitioning of the tissue samples into matched sections for homogenate preparation and EV isolation (Figure 5.1). To prepare full-face slides by cryo-sectioning, frozen tissue pieces (< 2 cm) were embedded into tissue moulds with two drops of Tissue-Tek optimal cutting temperature (OCT) medium (Sakura Finetek, USA). Sections of 10 µm thickness were cut in a cryostat at -20 °C. Tissue sections were transferred onto Superfrost Plus microscope slides (Fisher Scientific, USA) within 1 min of cutting then allowed to thaw on the slide and dried at room temperature prior to formalin fixing. Tissue samples were fixed onto the slides by placing in formalin for 10 min at room temperature. Slides were washed in deionised water for 2 min then stained with haematoxylin for 5 min. Slides were washed with tap water for 1 min and excess haematoxylin stain was removed by dipping the slides in acid alcohol and additional tap water wash. Slides were incubated in lithium carbonate for 4 min then briefly dipped in deionised water. Eosin counterstaining of slides was performed for 2 min then slides were washed in alcohol and dehydrated in xylene for 5 min. A drop of mounting medium was applied to the fixed tissue and a coverslip was slowly lowered

onto each slide. Slide were left in a horizontal position to dry overnight. Whole slide imaging of histopathology slides was performed using Olympus Brightfield BX53 Upright Microscope.

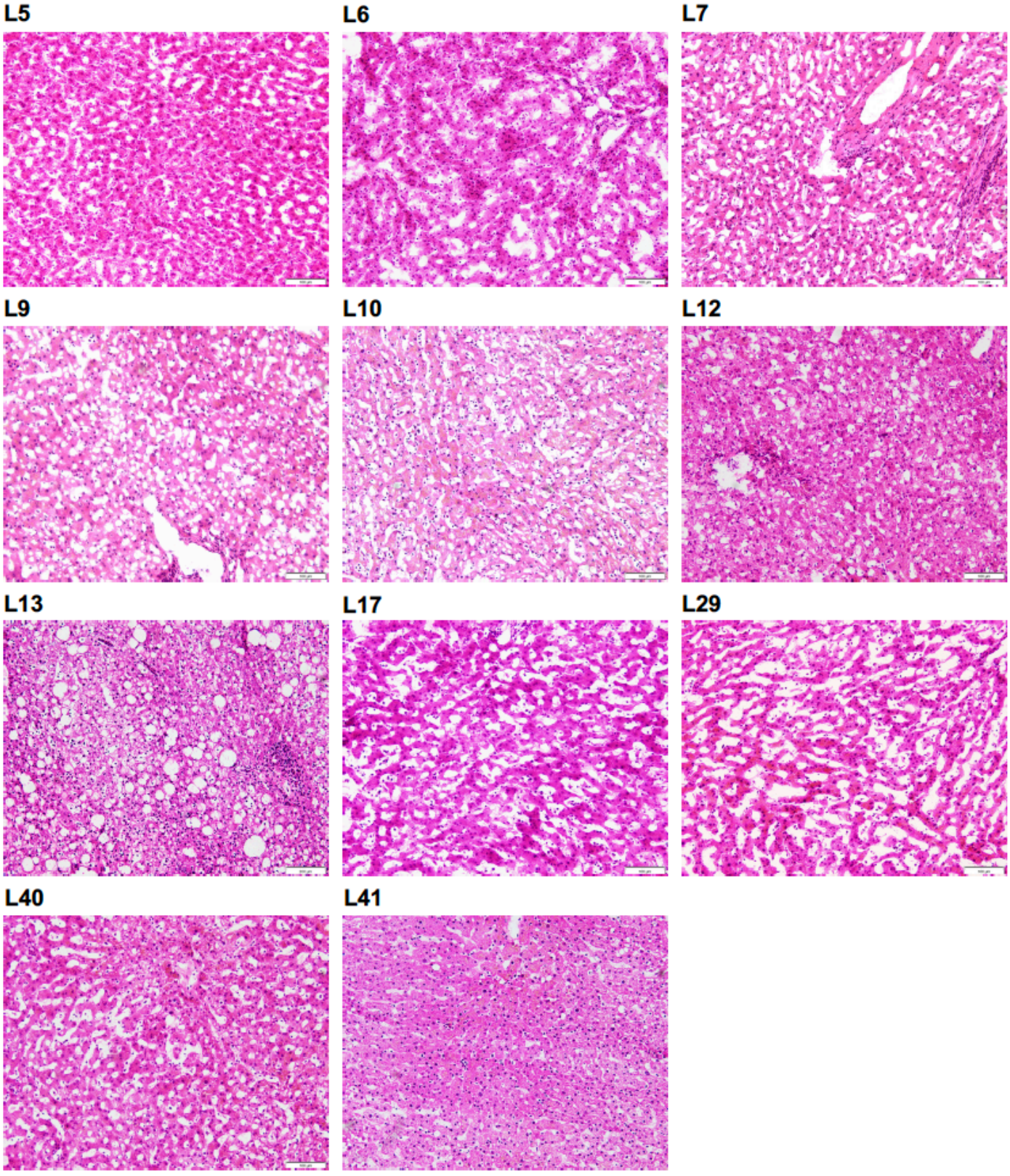

Figure 5.1 Histopathology slides of frozen liver tissue samples.
Liver tissue samples stained with haematoxylin and eosin. Images captured using Olympus Brightfield BX53 Upright Microscope at 200x magnification.

Transmission electron microscopy (TEM) imaging

Sections (1 mm^3) of liver tissue were immersed in primary fixative (2.5 % glutaraldehyde / 4 % paraformaldehyde in phosphate buffered saline (PBS) with 4% sucrose) for 48 hrs at 4 °C, then washed in PBS and 4 % sucrose. Tissue was then immersed in the secondary fixative (aqueous 2 % osmium tetroxide) for 1 hr, followed by dehydration through a graded series of ethanol solutions (50 to 100 %) and 100 % propylene oxide. Tissue was then infiltrated with 1:1 and 2:1 mixtures of epoxy resin/propylene oxide followed by three changes of 100 % epoxy resin. Tissue was embedded in fresh resin in BEEM capsules and polymerized in the oven at 60 °C for 48 hrs. Ultrathin sections (70 nm) were cut on a Leica EM UC7 ultramicrotome using a diamond knife, placed on grids and stained with heavy metals uranyl acetate and lead citrate for 8 mins each. Imaging was performed on an FEI Tecnai G2 Spirit TEM at 100kV at 1400x and 4800x magnification.

Human liver tissue homogenate preparation

Liver tissue samples (1 g) were placed in open top polycarbonate tubes containing 5 mL ice cold phosphate potassium chloride (KCl) buffer solution (10 mM phosphate buffer, pH 7.4 with 1.15 % KCl). Tissue samples were finely minced using surgical scissors then homogenised using an Ultra Turrax T25 at 20,500 rpm in two rounds of 30 sec. The ground samples in buffer were transferred to a 30 mL Potter-Elvehjem homogeniser and homogenised using an electric drill operating at full speed for eight full strokes. Resulting tissue homogenates were aliquoted in 2 mL Protein LoBind tubes (Eppendorf) and stored at -80 °C until analysis.

Isolation of extracellular vesicles

Enzymatic digestion of liver tissue

Liver tissue samples (0.2 g) were sliced using a disposable scalpel to form approximately 2 x 2 mm pieces. Release of EVs from the extracellular space of the tissue was achieved by gentle enzymatic dissociation as described previously (Useckaite et al., 2023). Tissue pieces were transferred into 2 mL Protein LoBind tubes (Eppendorf) containing 2 mL Roswell Park Memorial Institute (RPMI) 1640 with 2 mg/mL collagenase D and 40 U/mL DNase I. Samples were incubated for 45 min at 37 °C in a shaking water bath. Following incubation, the tissue-conditioned media was transferred to a 40 µM nylon cell strainer (BD Falcon) and allowed to pass through the filter by gravity.

Three hundred microlitres of 0.2 μm filtered PBS was passed through the filter into the sample collection tube. The tissue conditioned media was centrifuged at 300 g for 10 min at 4 °C and the supernatant was transferred to a new tube for additional centrifugation at 2000 g for 20 min at 4 °C. EVs were isolated from the clarified tissue-conditioned media (2 mL) using size exclusion chromatography (SEC) 2 mL columns (Stem Cell Technologies, USA).

Liver tissue EV isolation

Size exclusion columns were conditioned prior to EV isolation by washing with 20 mL of 0.2 μm filtered PBS. Clarified tissue-conditioned media (2 mL) was loaded in the sample reservoir and allowed to pass completely through the filter before elution buffer (filtered PBS) was added. The first 3 mL eluted from the column was discarded and subsequent 3 mL of EV-containing fractions were collected and pooled in 5 mL Protein LoBind Tubes (Eppendorf). For the duration of EV isolation, the total volume of elution buffer in the sample reservoir did not exceed 2 mL. Pooled EV-containing fractions were mixed by gentle inversion and concentrated using preconditioned Amicon Ultra 4 centrifuge filters (30 Kda, Millipore-Sigma, USA) to a final volume of 500 μL then aliquoted and stored at -80 °C until analysis.

Nanoparticle tracking analysis (NTA)

Nanoparticle tracking analysis was performed on a NanoSight NS300 (Malvern Panalytical, Malvern, UK; software v.3.4) to determine abundance and size distribution of particles in EV isolates. Samples were diluted by a factor between 4000x and 16000x with 0.2 μm filtered PBS and analysed in five 60 sec videos captured with constant flow (flow rate 100 AU).

Protein quantification

Total protein concentration in liver tissue homogenate and EV samples was measured using micro bicinchoninic acid (BCA) kit (Thermo Fisher Scientific, Aus) following manufacturer's instructions. Homogenates and EVs were diluted 1:1000 and 1:250, respectively, using 0.2 μm filtered PBS. Absorbance was measured at 562 nm using a plate reader (SpectraMax, Molecular Devices) and protein concentration was determined using a bovine serum albumin (BSA) standard curve (0 to 200 μg/mL).

Targeted proteomics

Protein selection

A representative panel of 30 proteins involved in the interaction of drugs with the liver were selected for this analysis. The panel comprised 15 DMEs with representation across the CYP, UGT and carboxylesterase (CES) enzyme families. These proteins are predominantly highly enriched in the liver compared to other organs and are involved in defining the PK profile for most drugs. The additional 15 proteins, which are expressed in the liver but typically also exhibit substantial extra-hepatic expression, are known molecular drug targets for chronic liver diseases (Dufour et al., 2022). The tissue expression profile and surrogate peptides for each protein are described in the supplementary material. Proteins were classified into three groups based on their reported specificity of liver expression determined by cross referencing UniProt accession numbers against the Human Protein Atlas (www.proteinatlas.org) (Uhlén et al., 2015) (Table 5.1)

Table 5.1 Selection and grouping of targets in representative protein panel.

Group	Protein	Uniprot accession	Tissue enrichment	Relative expression in liver	Relative expression in other tissues
Group 1 – Liver specific enrichment	Cytochrome P450 1A2 (CYP1A2)	P05177	Liver enriched	High	N/A
	Cytochrome P450 2B6 (CYP2B6)	P20813	Liver enriched	High	Medium in intestine
	Cytochrome P450 2C8 (CYP2C8)	P10632	Liver enriched	High	Low in intestine
	Cytochrome P450 2C9 (CYP2C9)	P11712	Liver enriched	High	Medium in intestine
	Cytochrome P450 2C19 (CYP2C19)	P33261	Liver enriched	High	Medium in intestine
	Cytochrome P450 2D6 (CYP2D6)	P10635	Liver enriched	High	Low in intestine
	Cytochrome P450 2E1 (CYP2E1)	P05181	Liver enriched	High	N/A
	Cytochrome P450 3A4 (CYP3A4)	P08684	Liver enriched	High	High in intestine
	Hydroxysteroid dehydrogenase 17 beta 13 (HSD17B13)	Q7Z5P4	Liver enriched	Medium	Low in many
	UDP-glucuronosyltransferase 1A1 (UGT1A1)	P22309	Liver enriched	High	Low in intestine
Group 2 – Enrichment in liver and 1-2 other tissues	Carboxylesterase 1 (CES1)	P23141	Liver, intestine, lung	High	High in lung, intestine
	Carboxylesterase 2 (CES2)	O00748	Liver, intestine	High	High in lung, intestine, kidney
	Diacylglycerol O-acyltransferase 2 (DGAT2)	Q96PD7	Liver, adipose	High	High in adipose
	Ketohexokinase (KHK)	P50053	Liver, intestine, kidney	High	High in intestine, kidney
	UDP-glucuronosyltransferase 1A6 (UGT1A6)	P19224	Liver, kidney	Medium	High in kidney, medium in intestine
	UDP-glucuronosyltransferase 2B4 (UGT2B4)	P06133	Liver, intestine, kidney	Medium	High in intestine, kidney
	UDP-glucuronosyltransferase 2B7 (UGT2B7)	P16662	Liver, kidney	High	High in kidney, medium in intestine
Group 3 – Extra-hepatic tissue enrichment or ubiquitous expression	Acetyl-CoA carboxylase 1 (ACACA)	Q13085	Non-specific	High	Ubiquitous
	Acetyl-CoA carboxylase 2 (ACACB)	O00763	Adipose, skeletal muscle	Medium	High in adipose
	Membrane primary amine oxidase (AOC3)	Q16853	Adipose	Low	High in lung, adipose, smooth muscle
	C-C motif chemokine receptor 5 (CCR5)	P51681	Lymphoid	Low	Ubiquitous
	Fatty acid synthase (FASN)	P49327	Adipose	High	High in intestine, kidney
	Glucagon-like peptide 1 receptor (GLP1R)	P43220	Pancreas	Low	High in pancreas
	Mitogen activated protein kinase kinase kinase 5 (MAP3K5)	Q99683	Non-specific	Medium	Ubiquitous
	Galectin 3 (LGALS)	P17931	Intestine	Low	Ubiquitous
	Lysyl oxidase like 2 (LOXL2)	Q9Y4K0	Smooth muscle	Medium	Ubiquitous
	Peroxisome proliferator-activated receptor alpha (PPARA)	Q07869	Tongue	Medium	Ubiquitous
	Peroxisome proliferator-activated receptor gamma (PPARG)	P37231	Adipose	Low	Ubiquitous

Sample preparation

Tissue homogenate and EV protein in a 50 µL volume of PBS were prepared for targeted peptide analysis as previously described with some modifications (Newman et al., 2022c). One hundred micrograms of total protein was digested per sample, corresponding to a mass of starting material between 8.99 and 19.35 mg for LT-EV and 0.55-1.05 mg for L-HMG (Table 5.2). Samples were lysed by three freeze-thaw cycles followed by vortex for 10 min at room temperature using a MixMate sample mixer (Eppendorf). Samples were combined with 25 µL of RapiGest surfactant (Waters, Aus) (0.3 % in 50 mM ammonium bicarbonate, pH 7.8) and incubated with dithiothreitol (12.5 mM) for 90 min at 60 °C. Samples were cooled to room temperature prior to addition of iodoacetamide (23.5 mM) and incubated in the dark for 60 min in a 37 °C shaking water bath. Trypsin Gold (Promega, NSW, Australia) was added to protein samples at a ratio of 1:50 (w/w) and incubated for 17 hours in a 37 °C shaking water bath. Digestion was terminated and Rapigest removed by addition of formic acid (10 µL, 10 % v/v) and further 30 min incubation at 37 °C followed by centrifugation at 16,000 g for 10 min at 4 °C. Clear supernatant was extracted and spiked with stable isotope labelled (SIL) peptides. Digested protein samples were analysed immediately and stored at 4 °C in the autosampler over the course of analysis.

Table 5.2 Protein concentration and equivalent sample consumption for liver tissue and EVs.
Total protein measured by micro BCA in biological replicates (n=11) of liver homogenate (L-HMG) and liver tissue EV (LT-EV), sample used for 100 µg protein digest and corresponding mass of starting tissue.

Sample ID		Protein concentration (µg/µL)	Sample (µL) used for digest	Tissue mass (mg) used for digest
L-HMG	L5	27.26	3.67	0.67
	L6	22.64	4.42	0.74
	L7	18.7	5.35	0.89
	L9	20.48	4.88	0.81
	L10	30.05	3.33	0.56
	L12	29.86	3.35	0.56
	L13	28.41	3.52	0.61
	L17	18.85	5.31	0.74
	L29	15.82	6.32	1.05
	L40	23.75	4.21	0.70
	L41	29.95	3.34	0.56
LT-EV	L5	2.07	48.37	19.35
	L6	2.19	45.71	18.29
	L7	3.8	26.33	10.53
	L9	3.71	26.93	10.77
	L10	3.94	25.37	10.15
	L12	2.19	45.71	18.29
	L13	2.9	34.52	13.81
	L17	4.45	22.49	8.99
	L29	3.32	30.14	12.06
	L40	4.22	23.7	9.48
	L41	3.15	31.76	12.7

Liquid chromatography mass spectrometry (LC-MS/MS)

Chromatographic separation of peptides was performed on an Agilent Advance Bio Peptide Map column (100 mm x 2.1 mm, 2.7 µm) using an Agilent 1290 Infinity II liquid chromatography system with a flow rate of 0.2 mL/min. Peptide targets were assessed across two analytical methods, including the EV marker panel described in Chapter 2 and a newly developed panel with chromatographic elution conditions and transitions as described in Table 5.3 and Table 5.4, respectively. Mobile phase consisted of 0.1% formic acid in water (mobile phase A) and 0.1% formic acid in acetonitrile (mobile phase B). Multiple reaction monitoring was performed on an Agilent 6495B Triple Quadrupole mass spectrometer operating in positive electron spray (ESI+) mode. Proteotypic tryptic peptides with at least one quantifier and 1 to 3 qualifier ion transitions per peptide were monitored (Table 5.4). Skyline software (v.22) was used to verify monitored transitions and the identity of detected peptides was confirmed by comparing retention time (RT) and ion transition ratios to spiked stable isotope labelled (SIL) or positive controls. Peak areas of endogenous analytes were

calculated using MassHunter Software (v.B.09.00) and endogenous analytes, for which SIL peptides were spiked into samples, were normalised to SIL peak area for relative quantification. Peak area data was normalised to represent equivalent tissue mass for comparisons between LT-EV and L-HMG. Absolute quantification of EV marker analytes was determined using standard curves of SIL spiked into liver tissue homogenate and EV matrices.

Table 5.3 Liquid chromatography elution conditions.

Time (min)	Mobile Phase A (%)	Mobile Phase B (%)	Column temp (°C)
0	98	2	37
32	70	30	
33	50	50	
34	50	50	
36	98	2	
37	98	2	

Table 5.4 Multiple reaction monitoring mass spectrometry acquisition.
Bold and underline indicates stable isotope labelled amino acid. SIL spiked at final concentration in protein digests of 5 nM.

Protein	Peptide	RT (min)	Precursor	Quantifier	Qualifier 1	Qualifier 2	Qualifier 3
ACACA	VNNADDFPNLFR	26.8	711.34	646.37	793.44	1023.49	–
	VNNADDFPNLF**R**	26.8	716.35	656.38	803.44	1033.50	–
ACACB	LGGIPVGVIAVETR	26.6	690.91	1040.61	520.81	844.49	–
ASGR1	SLESQLEK	14.1	467.25	733.37	604.33	–	–
	SLESQLE**K**	14.1	471.26	741.39	612.34	–	–
AOC3	YQLAVTQR	14.8	489.77	687.41	574.33	–	–
	YQLAVTQ**R**	14.8	494.78	697.42	584.34	–	–
CCR5	YLAVVHAVFALK	21.0	444.27	393.24	527.82	648.41	492.31
DGAT2	DTIDYLLSK	24.2	534.28	738.40	851.49	234.14	–
	DTIDYLLS**K**	24.2	538.29	746.42	859.50	242.16	–
FASN	GVDLVLNSLAEEK	26.3	693.88	903.48	790.39	–	–
	GVDLVLNSLAEE**K**	26.3	697.88	911.49	798.41	–	–
GLP1R	LEHLHIQR	11.2	523.30	402.24	553.32	–	–
	LEHLHIQ**R**	11.2	528.30	407.24	563.33	–	–
HSD17B13	GLTSELQALGK	23.4	558.82	204.13	629.40	845.47	–
	GLTSELQALG**K**	23.4	562.82	212.15	637.41	853.49	–
KHK	HLGFQSAEEALR	19.8	679.35	1107.54	1220.63	775.39	–
	HLGFQSAEEAL**R**	19.8	684.35	1117.55	1230.64	785.40	–
LOXL2	VEVLVER	15.0	422.25	615.38	516.31	403.23	–
	VEVLVE**R**	15.0	427.25	625.39	526.32	413.24	–
LGALS3	IQVLVEPDHFK	20.5	442.25	643.32	431.24	341.22	242.15
MAP3K5	ILTEDQDK	8.7	481.25	735.32	848.40	634.27	–
	ILTEDQD**K**	8.7	485.25	743.33	856.41	642.28	–
PPARA	LHLQSNHPDDIFLFPK	31.8	481.00	579.27	391.23	244.17	635.81
PPARG	LQEYQSAIK	13.5	540.29	709.39	418.27	554.34	–
	LQEYQSAI**K**	13.5	544.30	717.40	426.28	546.32	–
CYP1A2	YLPNPALQR	16.8	536.30	398.23	584.35	–	–
	YLPNPALQ**R**	16.8	541.31	403.23	594.36	–	–
CYP2B6	ETLDPSAPK	11.2	479.25	499.29	614.31	–	–
	ETLDPSAP**K**	11.2	483.26	507.30	622.33	–	–
CYP2C8	GLGIISSNGK	16.4	473.27	605.33	775.43	–	–
	GLGIISSNG**K**	16.4	477.28	613.34	783.45	–	–
CYP2C9	GIFPLAER	23.6	451.76	366.71	585.34	–	–
	GIFPLAE**R**	23.6	456.76	371.71	595.34	–	–
CYP2C19	GTTILTSLTSVLHDNK	30.4	567.31	664.36	771.43	–	–
	GTTILTSLTSVLHDN**K**	30.4	569.98	668.37	775.44	–	–
CYP2D6	DIEVQGFR	18.7	482.25	735.38	606.34	–	–
	DIEVQGF**R**	18.7	487.25	745.39	616.34	–	–
CYP2E1	FITLVPSNLPHEATR	24.2	565.65	561.29	717.89	–	–
	FITLVPSNLPHEAT**R**	24.2	568.98	566.29	722.89	–	–
CYP3A4	EVTNFLR	18.7	439.74	650.36	549.31	–	–
	EVTNFL**R**	18.7	444.74	660.37	559.32	–	–
CYP3A5	DTINFLSK	21.3	469.25	721.42	608.34	–	–
	DTINFLS**K**	21.3	473.26	729.44	616.35	–	–
UGT1A1	DGAFYTLK	19.5	457.73	671.38	524.31	–	–
	DGAFYTL**K**	19.5	461.74	679.39	532.32	–	–
UGT1A6	DIVEVLSDR	23.2	523.28	718.37	817.44	–	–
	DIVEVLSD**R**	23.2	528.28	728.38	827.45	–	–
UGT2B4	ANVIASALAK	19.3	479.29	673.42	560.34	–	–
	ANVIASALA**K**	19.3	483.30	681.44	568.35	–	–
UGT2B7	IEIYPTSLTK	21.7	582.83	646.38	922.52	–	–
	IEIYPTSLT**K**	21.7	586.84	654.39	930.54	–	–
CES1	AGQLLSELFTNR	29.4	674.86	866.44	979.52	–	–
	AGQLLSELFTN**R**	29.4	679.87	876.44	989.53	–	–
CES2	ADHGDELPFVFR	26.0	468.23	665.38	568.32	–	–
	ADHGDELPFVF**R**	26.0	471.57	675.39	578.33	–	–

Data analysis

Statistical analyses were performed using GraphPad Prism software v.10 (San Diego, USA). Parametric t-tests were used to compare groups with alpha value 0.05. Absolute quantification of protein targets was determined in LT-EV and paired tissue (L-HMG) for proteins with SIL peptide available to normalise for matrix effects between sample types. Proteins not detected in both sample types were excluded from the concordance analysis. The expression of protein targets in LT-EVs relative to L-HMG was normalised to equivalent starting material (tissue mass) and log-transformed. Pearson r values were generated to determine correlation in protein target abundance in total tissue and EV samples.

EV-Track

We have submitted all relevant data of our experiments to the EV-TRACK knowledgebase (EV-TRACK ID: EV231007) (Van Deun et al., 2017).

Results

Liver tissue characteristics

Demographic and molecular characteristics for tissue donors are described in Table 5.5. The proportion of female tissue donors was 45 %. The median age was 54 years (range of 18 to 67 years). Despite mild liver pathologies indicated by biopsy and clinical diagnoses in some cases, histopathology revealed morphologically normal tissue in study samples used for analysis, except for L12 and L13, which each exhibited focal lytic necrosis and mild steatosis.

Table 5.5 Characteristics of tissue donors and study samples.

Donor ID	Donor Age	Donor Sex	Smoking use	Alcohol use	Medications	Biopsy Findings	Clinical Characteristics	Study Sample Histopathology
L5	62	M	N/A	N/A	phenytoin, dexamethasone, gentamicin, ranitidine, cotrimoxazole	Normal lobular architecture. Fat droplets in very occasional hepatocytes. Very infrequent necrosis. Mild inflammatory cell infiltrate in portal tracts.	Mild fatty change, non-specific. Necrosis attributed to terminal ischaemia.	Normal
L6	18	M	N/A	social	penicillin, cotrimoxazole	Normal hepatic architecture. In several lobules small groups of liver cells contain fat droplets.	Normal	Normal
L7	44	F	none	social	dexamethasone	Mild fatty change, scattered lipogranulomas, fat laden macrophages in portal tracks and mild perivenular fibrosis. Potential alpha-one-antitrpysin inclusions in some liver cells.	Mild alcoholic liver injury. Possibly minor alpha1 antitrypsin deficiency.	Normal
L9	19	M	none	social	dopamine	Severe ischaemic damage. Coagulative necrosis in hepatocytes of perivenular region of liver acini.	No evidence of pre-existing liver disease	Normal
L10	67	F	none	social	dopamine, morphine, furosemide, midazolam	N/A	N/A	Normal
L12	66	M	none	moderate	insulin	N/A	Carcinoma of the colon (resected liver tissue adjacent to tumour); diabetes mellitus	Mild spotty necrosis
L13	61	F	none for 3yrs (1pk/day prior)	minimal	metoprolol, methyclothiazide, bethanecol	N/A	Metastatic leiomyosarcoma of the rectum (resected right lobe liver tissue adjacent to tumour); obesity	Mild microvesicular steatosis
L17	45	M	none	none	none	N/A	Liver transplant for solitary hepatoma in non-cirrhotic liver; sample is of normal left lobe	Normal
L29	45	M	heavy	4-5 drinks/day	none	N/A	N/A	Normal
L40	54	F	N/A	N/A	N/A	N/A	N/A	Normal
L41	66	F	N/A	N/A	N/A	Solitary tumour nodule, inflammatory cell infiltrate, pericellular fibrosis, sinusoidal dilatation and focal haemorrhage. Hepatic architecture elsewhere appears normal but mild steatosis concentrated in zone 1. Portal tracts are normal.	liver metastasis from colonic primary adenocarcinoma. mild fatty liver	Normal

Quantification of protein targets in EVs isolated from liver tissue

The primary outcome evaluated in the current study was the capacity to robustly detect and quantify proteins involved in the interaction of drugs with the liver in LT-EV. Of the 29 proteins evaluated, 27 (93 %) were detected in LT-EV. The absolute abundance of 15 DME proteins and 10 MAFLD drug targets were quantified in LT-EV, using SIL peptides spiked into protein digests (Figure 5.2). DMEs ranged in abundance from 0.15 to 220 pmol / 100 µg of EV protein and MAFLD drug targets ranged from 0.07 to 27 pmol / 100 µg of EV protein.

The sensitivity and specificity of DME protein detection in liver tissue using LT-EVs were described by confusion matrices (Figure 5.3). Except for CYP3A5, DMEs were all detected in both L-HMG and LT-EVs from all biological replicates (n=11), thereby giving 100% sensitivity. Only 2 of 11 subjects had detectable CYP3A5 protein in L-HMG and CYP3A5 was only detected in the paired LT-EVs for these two individuals, giving 100% sensitivity and specificity. For 10 out of 14 MAFLD drug targets (ACACA, ACACB, AOC3, CCR5, DGAT2, FASN, GLP1R, HSD17B13, KHK and MAP3K5) that were detected in all L-HMG samples, the respective proteins were also detected in all LT-EV samples. The only MAFLD drug target that was detected in all L-HMG samples but not all LT-EV samples was galectin 3 (LGALS3). This protein was detected in 9 of 11 LT-EV samples (82% sensitivity). Peroxisome proliferator-activated receptor alpha (PPARA) was not detected in any LT-EVs despite detection in 10 out of 11 L-HMG samples. Two MAFLD drug targets (LOXL2 and PPARG) were below the limit of detection for both L-HMG and LT-EV.

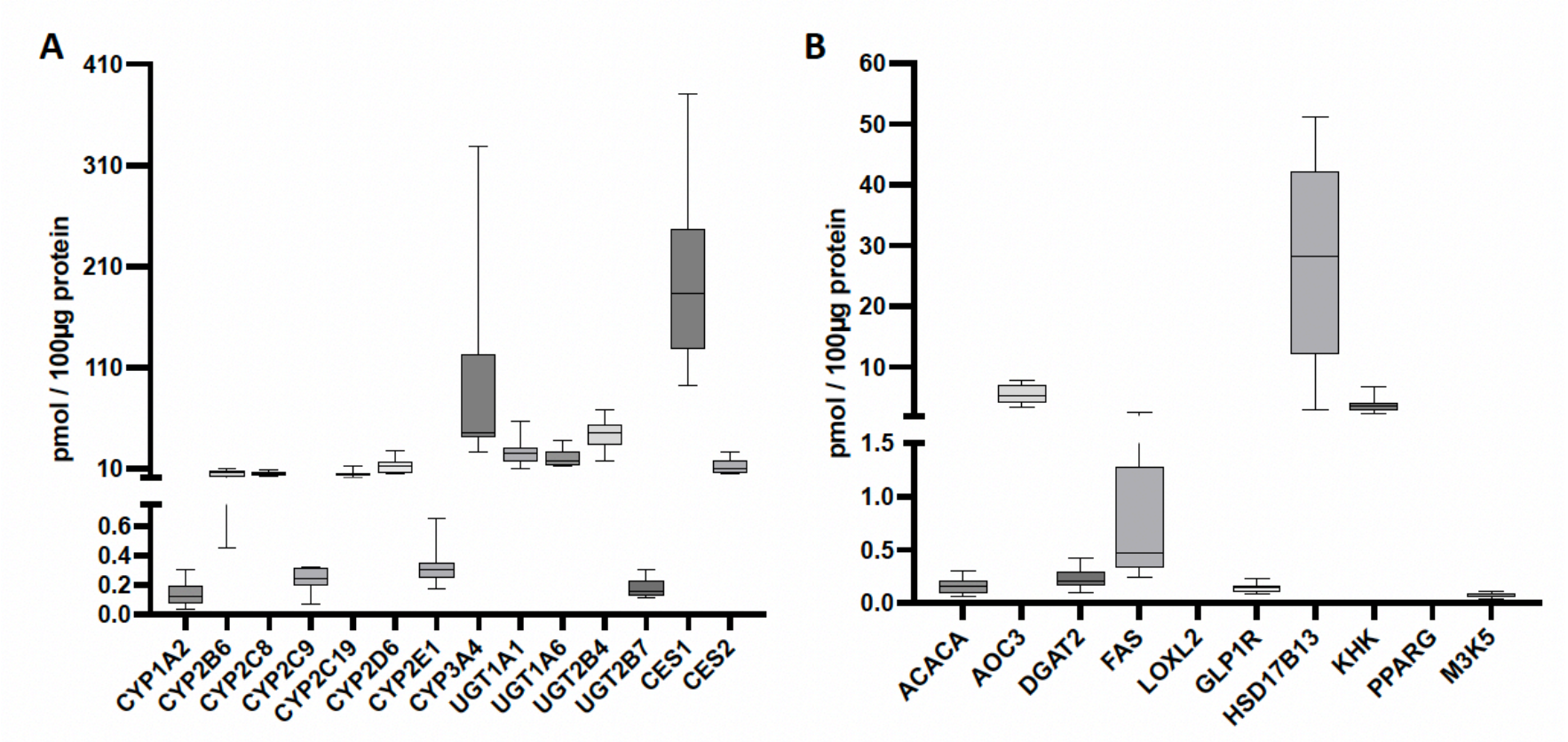

Figure 5.2 Absolute quantification of protein targets in liver tissue EVs.

Abundance of (A) drug metabolising enzymes and (B) drug target proteins associated with treatment of metabolic associated fatty liver disease in EVs isolated from liver tissue.

Drug Metabolising Enzymes

CYP1A2		LT-EV		TPR/Sensitivity
		D	ND	100%
L-HMG	D	11	0	TNR/Specificity
	ND	0	0	–

CYP2B6		LT-EV		TPR/Sensitivity
		D	ND	100%
L-HMG	D	11	0	TNR/Specificity
	ND	0	0	–

CYP2C8		LT-EV		TPR/Sensitivity
		D	ND	100%
L-HMG	D	11	0	TNR/Specificity
	ND	0	0	–

CYP2C9		LT-EV		TPR/Sensitivity
		D	ND	100%
L-HMG	D	11	0	TNR/Specificity
	ND	0	0	–

CYP2C19		LT-EV		TPR/Sensitivity
		D	ND	100%
L-HMG	D	11	0	TNR/Specificity
	ND	0	0	–

CYP2D6		LT-EV		TPR/Sensitivity
		D	ND	100%
L-HMG	D	11	0	TNR/Specificity
	ND	0	0	–

CYP2E1		LT-EV		TPR/Sensitivity
		D	ND	100%
L-HMG	D	11	0	TNR/Specificity
	ND	0	0	–

CYP3A4		LT-EV		TPR/Sensitivity
		D	ND	100%
L-HMG	D	11	0	TNR/Specificity
	ND	0	0	–

CYP3A5		LT-EV		TPR/Sensitivity
		D	ND	100%
L-HMG	D	2	0	TNR/Specificity
	ND	0	9	100%

UGT1A1		LT-EV		TPR/Sensitivity
		D	ND	100%
L-HMG	D	11	0	TNR/Specificity
	ND	0	0	–

UGT1A6		LT-EV		TPR/Sensitivity
		D	ND	100%
L-HMG	D	11	0	TNR/Specificity
	ND	0	0	–

UGT2B4		LT-EV		TPR/Sensitivity
		D	ND	100%
L-HMG	D	11	0	TNR/Specificity
	ND	0	0	–

UGT2B7		LT-EV		TPR/Sensitivity
		D	ND	100%
L-HMG	D	11	0	TNR/Specificity
	ND	0	0	–

CES1		LT-EV		TPR/Sensitivity
		D	ND	100%
L-HMG	D	11	0	TNR/Specificity
	ND	0	0	–

CES2		LT-EV		TPR/Sensitivity
		D	ND	100%
L-HMG	D	11	0	TNR/Specificity
	ND	0	0	–

MAFLD drug targets

ACACA		LT-EV		TPR/Sensitivity
		D	ND	100%
L-HMG	D	11	0	TNR/Specificity
	ND	0	0	–

ACACB		LT-EV		TPR/Sensitivity
		D	ND	100%
L-HMG	D	11	0	TNR/Specificity
	ND	0	0	–

AOC3		LT-EV		TPR/Sensitivity
		D	ND	100%
L-HMG	D	11	0	TNR/Specificity
	ND	0	0	–

CCR5		LT-EV		TPR/Sensitivity
		D	ND	100%
L-HMG	D	11	0	TNR/Specificity
	ND	0	0	–

DGAT2		LT-EV		TPR/Sensitivity
		D	ND	100%
L-HMG	D	11	0	TNR/Specificity
	ND	0	0	–

FASN		LT-EV		TPR/Sensitivity
		D	ND	100%
L-HMG	D	11	0	TNR/Specificity
	ND	0	0	–

GLP1R		LT-EV		TPR/Sensitivity
		D	ND	100%
L-HMG	D	11	0	TNR/Specificity
	ND	0	0	–

HSD17B13		LT-EV		TPR/Sensitivity
		D	ND	100%
L-HMG	D	11	0	TNR/Specificity
	ND	0	0	–

KHK		LT-EV		TPR/Sensitivity
		D	ND	100%
L-HMG	D	11	0	TNR/Specificity
	ND	0	0	–

LOXL2		LT-EV		TPR/Sensitivity
		D	ND	–
L-HMG	D	0	0	TNR/Specificity
	ND	0	0	–

LGALS3		LT-EV		TPR/Sensitivity
		D	ND	82%
L-HMG	D	9	2	TNR/Specificity
	ND	0	0	–

MAP3K5		LT-EV		TPR/Sensitivity
		D	ND	100%
L-HMG	D	11	0	TNR/Specificity
	ND	0	0	–

PPARA		LT-EV		TPR/Sensitivity
		D	ND	0%
L-HMG	D	0	10	TNR/Specificity
	ND	0	1	100%

PPARG		LT-EV		TPR/Sensitivity
		D	ND	–
L-HMG	D	0	0	TNR/Specificity
	ND	0	0	–

Figure 5.3 Confusion matrices for detection of protein targets in paired liver tissue (homogenate (L-HMG) and liver tissue EVs (LT-EV).

Concordance between DME protein abundance in liver tissue homogenate and EVs

The potential utility of EV derived markers to define between subject variability in DME abundance is dependent on the concordance between the absolute abundance of DME proteins in L-HMG and LT-EVs. Moderate to strong correlations were observed for 13 of the 14 DME proteins assessed. Pearson coefficient (r) values describing the association between the absolute protein abundance in L-HMG and LT-EV for these DMEs ranged from 0.595 to 0.962 (Table 5.6). Although CYP3A5 was quantified in L-HMG and LT-EVs, only 2 of the 11 subjects were CYP3A5 expressors and as such this target was excluded from the quantitative correlation analysis.

Table 5.6 Correlation of drug metabolising enzymes absolute abundance in liver homogenate and liver tissue EVs.
ns: not significant, p-value <0.05 (*), <0.01 (**), <0.001 (***), <0.0001 (****).

Target	Pearson r	Significance
CYP2B6	0.962	****
CYP3A4	0.912	****
CYP1A2	0.858	***
CYP2D6	0.790	**
CYP2C19	0.786	**
CYP2C8	0.760	**
CYP2C9	0.758	**
CES2	0.722	*
UGT2B4	0.713	*
UGT1A1	0.709	*
UGT1A6	0.671	*
CYP2E1	0.654	*
CES1	0.595	*
UGT2B7	0.229	ns

Nine of the 15 DMEs evaluated here (CYP 1A2, 2B6, 2C8, 2C9, 2C19, 2D6, 2E1 and 3A4, and UGT1A1) are considered liver enriched with only medium to low expression in extra-hepatic tissue (Table 5.1). DMEs evaluated here that exhibit high expression in extra-hepatic tissue were CES 1 and 2, both of which exhibit high expression in the intestine and lung, and UGTs 1A6, 2B4 and 2B7, each of which exhibit high extra-hepatic expression in the kidneys and either medium or high expression in the intestine. Weaker correlations between the absolute protein abundance in LT-

EV and L-HMG for proteins that exhibit high extra-hepatic expression, particularly UGT2B7 (r = 0.229), is attributed to the presence of these proteins in extra-hepatic EVs isolated from the liver tissue; noting that prior analyses have demonstrated that extra-hepatic EVs account for ~50% of EVs detected in this tissue (Useckaite et al., 2023).

Relationship between the correlation of protein abundances in liver tissue homogenate and EV and the extent of extra-hepatic protein expression.

While liver tissue represents an enriched source of liver derived EVs, this source still contains a significant pool of EVs originating from other tissues. PK studies have demonstrated accumulation of both endogenous and exogenous EVs in the liver (Tamasi et al., 2023, Zhang et al., 2020a), while our previous analysis of the hepatic EV proteome demonstrated that ~50% of EVs in the liver originate from distant organs including the brain and intestine (Useckaite et al., 2023). As EVs account for a minor proportion (<1 %) of total protein in liver tissue, the abundance of protein targets in L-HMG will be negligibly influenced by the presence of protein originating from extra-hepatic EVs. For protein targets that exhibit high extra-hepatic expression, the proportion of extra-hepatic EV derived protein relative to liver-specific EV protein in the LT-EV fraction (~50%) may be significant. As such, the observed abundance of protein targets with high extra-hepatic expression in LT-EV, but not L-HMG, will be impacted by the contribution of vesicles originating in other organs such as intestine, lung or kidneys, thereby weakening the correlation of the protein abundances between L-HMG and LT-EV. To address this phenomenon, we explored the relationship between the correlation of protein abundance in L-HMG and LT-EV and the extent of extra-hepatic expression.

The 22 protein targets detected in all LT-EV samples were classified into three groups based on tissue enrichment reported in the Human Protein Atlas. Group 1 contained tissue specific or enriched proteins with high hepatic expression, Group 2 contained proteins with enrichment in liver as well as 1-2 other tissues, and Group 3 contained proteins that are enriched in non-hepatic tissues or expressed ubiquitously. All Group 1 proteins were strongly positively correlated with Pearson r values ranging from 0.654 to 0.962. Four out of seven Group 2 proteins also exhibited moderate positive correlations with r values between 0.595 and 0.722, while all Group 3 proteins had weak or

no correlation with r values < 0.351 (Table 5.7, Figure 5.4). The association between hepatic expression grouping and correlation was assessed by one-way ANOVA with Tukey multiple comparison test which found significantly higher mean Pearson r in Group 1 compared to Groups 2 and 3 (p = 0.0135 and p = 0.0002, respectively).

Table 5.7 Impact of extra-hepatic protein expression on correlation of protein targets in liver homogenate with liver tissue EVs.
ns: not significant, p-value <0.05 (*), <0.01 (**), <0.001 (***), <0.0001 (****).

Protein Group	Target	Pearson r	Significance
Group 1	CYP2B6	0.962	****
	HSD17B13	0.914	****
	CYP3A4	0.912	****
	CYP1A2	0.858	***
	CYP2D6	0.790	**
	CYP2C19	0.786	**
	CYP2C8	0.760	**
	CYP2C9	0.758	**
	UGT1A1	0.709	*
	CYP2E1	0.654	*
Group 2	CES2	0.722	*
	UGT2B4	0.713	*
	UGT1A6	0.671	*
	CES1	0.595	*
	UGT2B7	0.229	ns
	DGAT2	-0.048	ns
	KHK	-0.259	ns
Group 3	ACACA	0.351	ns
	FASN	0.265	ns
	AOC3	0.084	ns
	MAP3K5	-0.134	ns
	GLP1R	-0.454	ns

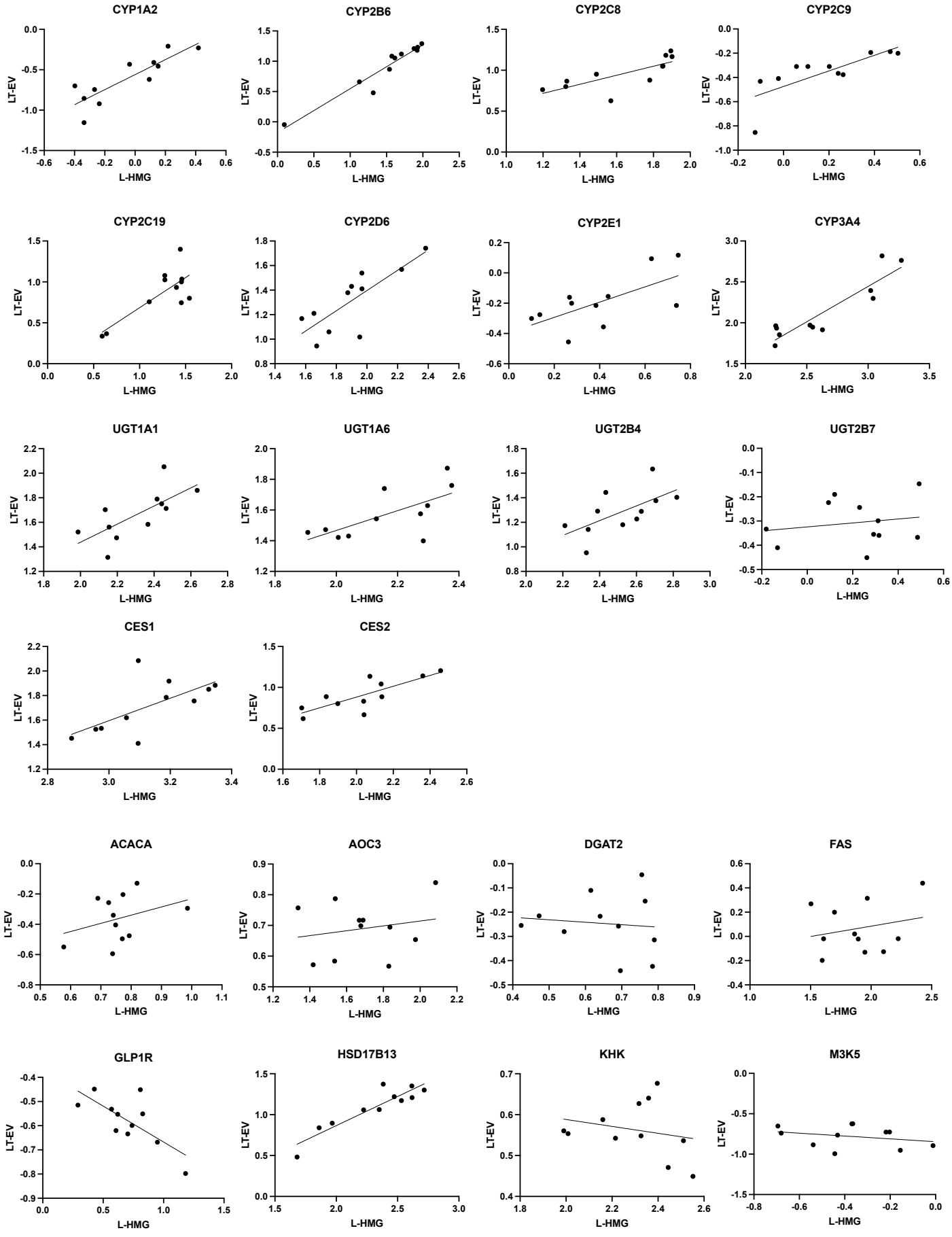

Figure 5.4 Correlation of protein expression (log units) in liver tissue EVs (LT-EV) with liver tissue homogenate (L-HMG).

Concordance of correlated protein pairs in liver tissue homogenate and EVs

To evaluate the extent to which EV derived proteins represented the overall profile of the tissue, correlation matrices were generated containing the protein targets that exhibited significant correlations between matched L-HMG and LT-EVs in the previous section (Figure 5.5A & B). In liver tissue, 84 % of proteins were positively correlated, at least to a weak extent ($r > 0.2$), of which 59 % were at least moderately correlated with an $r > 0.5$. A distinct pattern of expression in respective LT-EVs was observed with only 68 % of targets exhibiting positive correlations, of which 44 % had $r > 0.5$. Correlation (Pearson r) of protein target pairs in L-HMG was plotted against that in LT-EVs (Figure 5.5C, Table 5.8) and were predominantly located in the top right quadrant, indicating positive correlation in both L-HMG and LT-EV. Forty-four per cent of pairs were concordant in tissue and EVs, having either the same classification of strength and direction of correlation in tissue and EVs (e.g. strong, moderate or weak in both) or Pearson r differing by less than 20%. These points are shown in blue in Table 5.8 and Figure 5.5C and track closely along the line of identity.

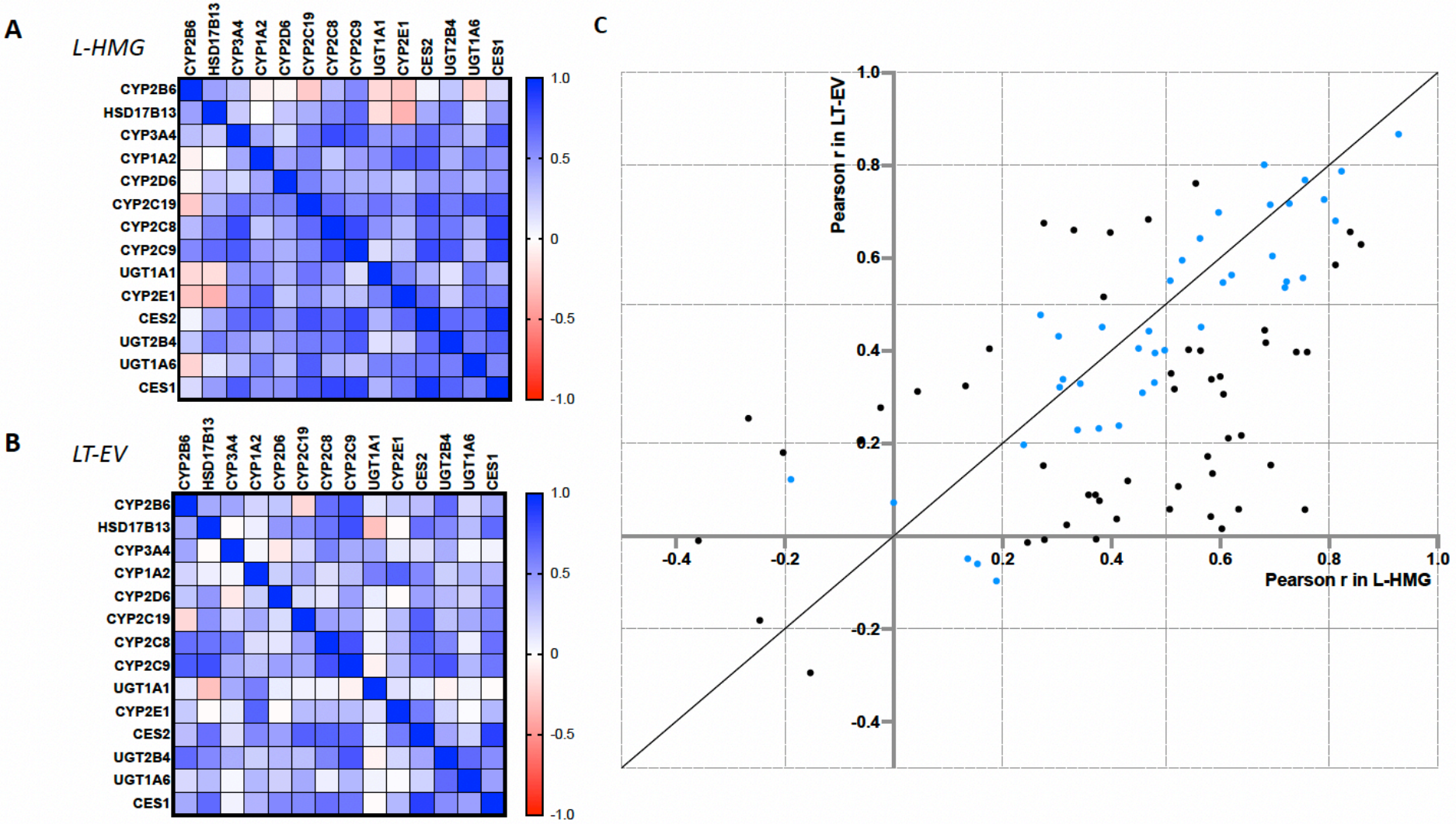

Figure 5.5 Concordance of co-expressed protein targets in paired EVs and tissue.

Correlation matrices for proteins targets in (A) liver homogenate (L-HMG) and (B) liver tissue EVs (LT-EV). (C) Concordance of protein target pairs plotted in L-HMG against LT-EV. Grid lines mark thresholds for the correlation classifications: no (-0.2 < r < 0.2), weak (-0.5 < r < -0.2; 0.2 < r < 0.5), moderate (-0.8 < r < -0.5; 0.5 < r < 0.8) and strong (-1.0 < r < -0.8; 0.8 < r < 1.0). Points labelled in blue exhibited concordance of protein correlation in tissue and EVs.

Table 5.8 Concordance of Pearson r between liver homogenate (L-HMG) and matched liver tissue EVs (LT-EV) for pairs of protein targets.
Blue font denotes concordance of protein correlation in tissue and EVs (r <20% different or matching classification).

Protein target pair	Pearson r L-HMG	Pearson r LT-EV	% difference	Classification
CES2-CES1	0.928	0.867	-7%	strong-strong
HSD17B13-CYPC9	0.681	0.801	18%	moderate-strong
CYP2C8-CYP2C9	0.823	0.787	-4%	strong-moderate
UGT2B4-CYP2C9	0.756	0.768	2%	moderate-moderate
CYP2B6-CYP2C9	0.555	0.761	37%	moderate-moderate
CES2-CYP2C19	0.791	0.726	-8%	moderate-moderate
CYP1A2-CYP2E1	0.727	0.717	-1%	moderate-moderate
CES2-CYP2C8	0.692	0.715	3%	moderate-moderate
UGT2B4-UGT1A6	0.597	0.698	17%	moderate-moderate
CES1-HSD17B13	0.468	0.683	46%	weak-moderate
CES2-CYP2C9	0.812	0.680	-16%	strong-moderate
UGT2B4-CYP2B6	0.276	0.675	144%	weak-moderate
CYP2B6-CYP2C8	0.331	0.660	99%	weak-moderate
CES1-CYP2C8	0.839	0.656	-22%	strong-moderate
CES2-HSD17B13	0.398	0.655	65%	weak-moderate
HSD17B13-CYPC8	0.563	0.642	14%	moderate-moderate
CES1-CYP2C9	0.859	0.629	-27%	strong-moderate
CES2-CYP2E1	0.696	0.604	-13%	moderate-moderate
CYP1A2-UGT1A1	0.530	0.595	12%	moderate-moderate
CYP3A4-CYP2C8	0.812	0.585	-28%	strong-moderate
UGT2B4-CYP2C8	0.621	0.563	-9%	moderate-moderate
CES1-CYP2C19	0.752	0.557	-26%	moderate-moderate
CES1-CYP2D6	0.508	0.551	8%	moderate-moderate
CES2-CYP1A2	0.722	0.549	-24%	moderate-moderate
UGT2B4-HSD17B13	0.605	0.547	-10%	moderate-moderate
UGT2B4-CES1	0.719	0.536	-25%	moderate-moderate
HSD17B13-CYPC19	0.386	0.516	33%	weak-moderate
HSD17B13-CYP2D6	0.270	0.477	76%	weak-weak
UGT1A6-CES1	0.565	0.451	-20%	moderate-weak
CYP2D6-CYP2C9	0.383	0.451	18%	weak-weak
CYP2C19-CYP2C8	0.682	0.444	-35%	moderate-weak
CES2-CYP2D6	0.469	0.442	-6%	moderate-moderate
CYP2B6-CYP3A4	0.303	0.431	42%	weak-weak
CES2-UGT2B4	0.684	0.417	-39%	moderate-weak
CYP2B6-HSD17B13	0.450	0.405	-10%	weak-weak
CES1-CYP2B6	0.176	0.404	130%	no-weak
CYP2C19-CYP2C9	0.542	0.402	-26%	moderate-weak
CYP3A4-UGT1A1	0.498	0.401	-19%	weak-weak
CYP1A2-CYP2C19	0.564	0.400	-29%	moderate-weak
UGT1A6-CYP2C19	0.740	0.397	-46%	moderate-weak
CYP3A4-CYP2C9	0.760	0.397	-48%	moderate-weak
UGT2B4-CYP3A4	0.480	0.395	-18%	weak-weak
CES1-CYP1A2	0.510	0.351	-31%	moderate-weak
CES1-CYP2E1	0.600	0.344	-43%	moderate-weak
UGT1A6-CYP2C9	0.311	0.338	9%	weak-weak
UGT1A6-CYP1A2	0.584	0.338	-42%	moderate-weak
UGT2B4-CYP2D6	0.479	0.331	-31%	weak-weak
CYP2C8-CYP2E1	0.343	0.329	-4%	weak-weak
UGT1A6-HSD17B13	0.132	0.324	145%	no-weak
CYP2C9-CYP2E1	0.305	0.321	5%	weak-weak

CYP2C19-CYP2E1	0.516	0.317	-39%	moderate-weak
CES2-CYP2B6	0.044	0.312	610%	no-weak
CYP1A2-CYP2C9	0.457	0.309	-32%	weak-weak
UGT2B4-CYP2C19	0.606	0.306	-49%	moderate-weak
CYP2B6-CYP2D6	-0.024	0.277	-1263%	no-weak
CYP2B6-CYP2E1	-0.267	0.254	-195%	weak(-)-weak(+)
CYP1A2-CYP2D6	0.414	0.238	-42%	weak-weak
UGT2B4-CYP1A2	0.377	0.232	-39%	weak-weak
UGT1A6-CYP2D6	0.338	0.229	-32%	weak-weak
CES2-UGT1A6	0.639	0.217	-66%	moderate-no
CYP3A4-CYP2C19	0.615	0.211	-66%	moderate-weak
CYP2B6-CYP1A2	-0.062	0.205	-433%	no-weak
UGT2B4-CYP2E1	0.239	0.197	-18%	weak-no
UGT1A6-CYP2B6	-0.203	0.180	-189%	weak-no
CYP2D6-CYP2C19	0.577	0.172	-70%	moderate-no
CES2-CYP3A4	0.693	0.153	-78%	moderate-no
CYP1A2-CYP2C8	0.275	0.152	-45%	weak-no
UGT1A1-CYP2E1	0.586	0.135	-77%	moderate-no
CYP2B6-UGT1A1	-0.189	0.122	-165%	no-no
CYP2D6-CYP2C8	0.430	0.119	-72%	weak-no
CYP3A4-CYP2E1	0.523	0.107	-80%	moderate-no
CES2-UGT1A1	0.358	0.089	-75%	weak-no
CYP2D6-UGT1A1	0.371	0.089	-76%	weak-no
UGT1A6-CYP2C8	0.378	0.076	-80%	weak-no
HSD17B13-CYP1A2	0.000	0.072	-181085%	no-no
CYP2C8-UGT1A1	0.507	0.058	-89%	moderate-no
CYP2C19-UGT1A1	0.634	0.058	-91%	moderate-no
CES1-CYP3A4	0.756	0.057	-92%	moderate-no
UGT1A6-UGT1A1	0.583	0.042	-93%	moderate-no
CYP3A4-CYP1A2	0.410	0.037	-91%	weak-no
UGT1A6-CYP3A4	0.318	0.024	-92%	weak-no
UGT1A6-CYP2E1	0.603	0.016	-97%	moderate-no
CES1-UGT1A1	0.372	-0.007	-102%	weak-no
CYP2D6-CYP2E1	0.277	-0.008	-103%	weak-no
HSD17B13-CYP2E1	-0.359	-0.010	-97%	weak-no
HSD17B13-CYP3A4	0.246	-0.014	-106%	weak-no
UGT2B4-UGT1A1	0.136	-0.049	-136%	no-no
CYP2C9-UGT1A1	0.154	-0.060	-139%	no-no
CYP3A4-CYP2D6	0.189	-0.097	-151%	no-no
CYP2B6-CYPC19	-0.246	-0.182	-26%	weak-no
HSD17B13-UGT1A1	-0.153	-0.295	93%	no-weak

Characterisation of EVs isolated from liver tissue

To ensure the robustness of the data, EVs isolated from the liver tissue were characterised in accordance with the MISEV guidelines (Welsh et al., 2024). In contrast to the method used here, previously reported protocols for the isolation of tissue EVs involve a mechanical approach to dissociating the tissue, such as mincing; however, this results in cell lysis and release of intracellular materials (Crescitelli et al., 2021). To minimise this type of contamination and facilitate the

assessment of EV-derived content, here a gentle method was employed to enzymatically dissociate the extracellular contents and release EVs trapped in the tissue, followed by a size exclusion chromatography based separation for further purification.

Sections of liver tissue were imaged by TEM to visualise the cellular architecture and presence of vesicles. The particles exhibited typical size, morphology and staining consistent with lipid bilayers and can be observed in the extracellular space between intact hepatic cells (Figure 5.6). LT-EV isolates (n=11) were assessed for yield and expression of characteristic protein markers. Particle count, reported here as the mean total yield (± SD) from a 500 µL concentrated pool of EVs isolated from 0.2 g of tissue, was 2.66 x 10^{12} (± 1.54 x 10^{12}) particles and mean size was 83.4 (± 17.0) nm (Figures 5.7A & B). Mean (± SD) total protein yield from paired L-HMG and LT-EV was 29.0 (± 5.8) mg and 1.6 (± 0.4) mg per 0.2 g tissue, respectively and the particle to protein ratio calculated for LT-EV was between 3.24 x 10^{11} and 1.88 x 10^{12} particles/µg protein (Figures 5.7C & D).

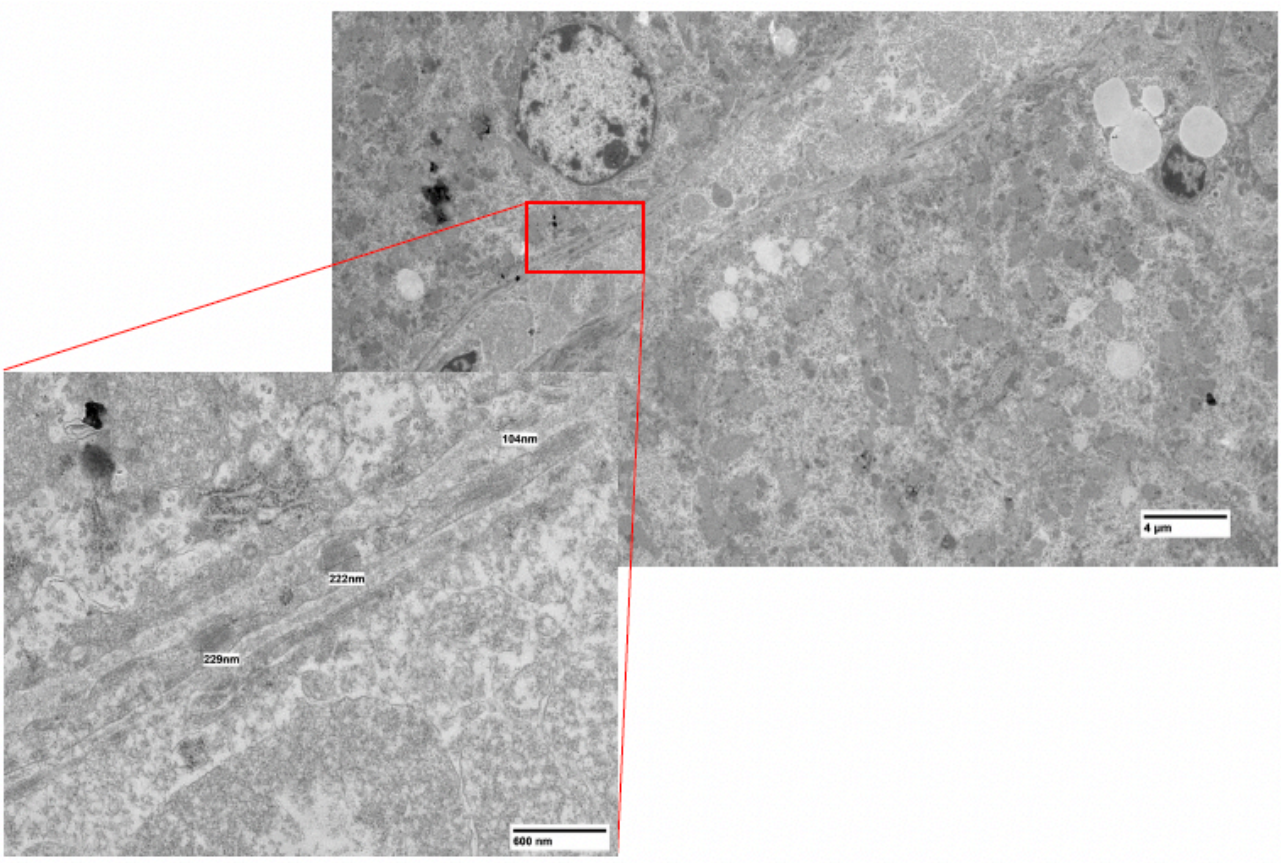

Figure 5.6 Transmission electron microscopy (TEM) image of liver tissue section.
EVs in extracellular space labelled by size. Magnification 1200 x and 9300 x.

The abundance of EV (CD9, CD81, TSG101, CANX), hepatocyte-specific (ASGR1) and co-isolated matrix (albumin) markers is reported per 100 µg of protein from L-HMG and LT-EV. Absolute quantification of EV markers was performed using our previously validated quantitative LC-MS/MS method (Newman et al., 2022c). EVs isolated from tissue were significantly enriched in the membrane markers, CD81 and CD9, the hepatocyte-specific surface marker ASGR1, as well as cytosolic protein TSG101 and endoplasmic reticulum marker CANX (Figure 5.7E-I). It is noted that CANX has been previously used to indicate the presence of intracellular organelle material arising from non-vesicular or non-endolysosomal pathways; however, there is still no universally accepted negative marker of EVs (Welsh et al., 2024). A population of vesicles expressing CANX are plausibly released by hepatic cells, as we have detected typically ER-derived proteins such as CYP450s in circulating EVs (Rodrigues et al., 2021). We also previously observed tissue-related differences in EV marker abundance, reporting higher expression of CANX in tissue EVs from liver compared to those from intestine (Useckaite et al., 2023). Albumin levels were measured as an indication of soluble protein co-isolating with EVs. Albumin was highly abundant in liver tissue but was significantly depleted in matched EV isolates (Figure 5.7J).

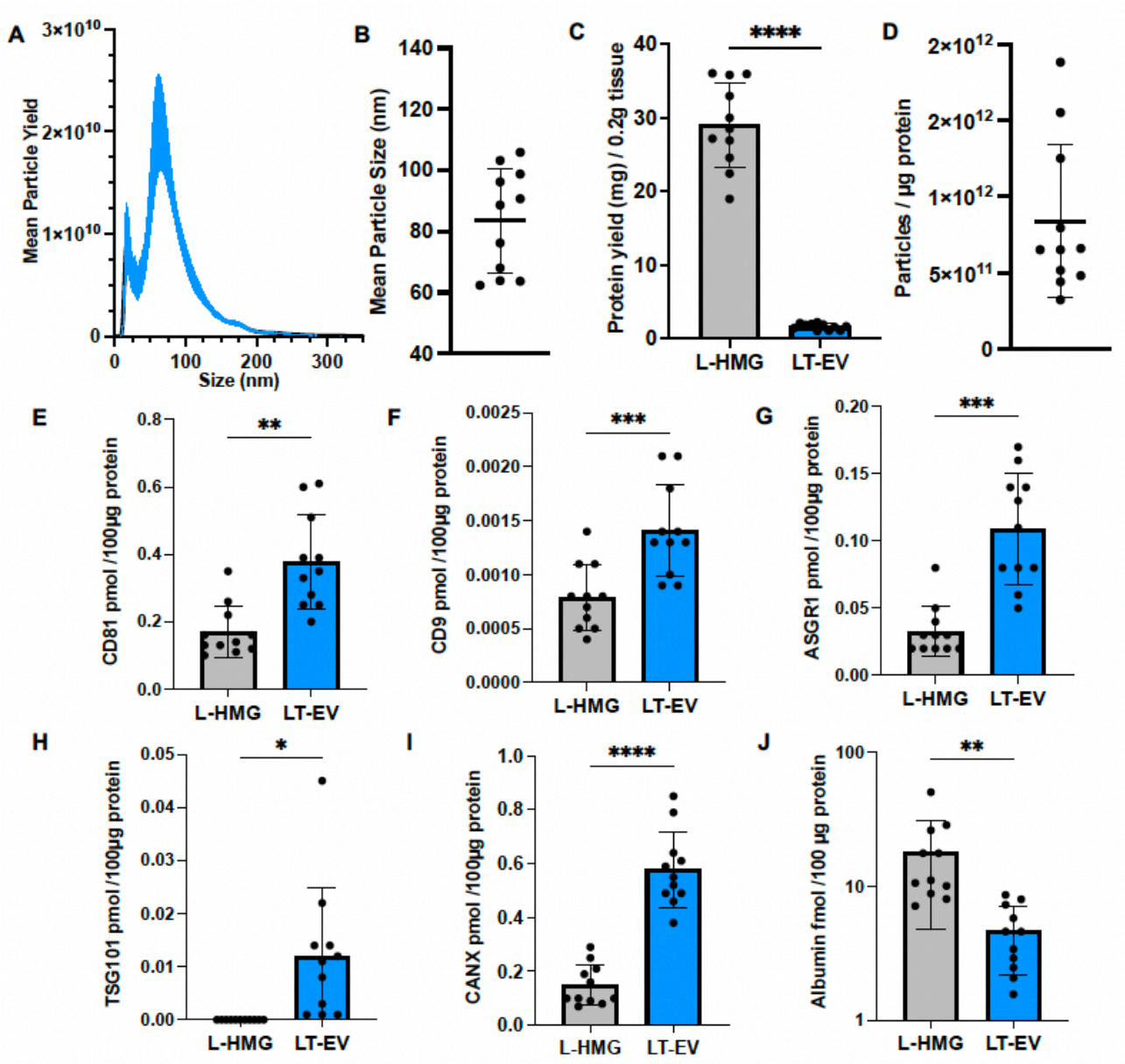

Figure 5.7 Characterisation of EVs isolated from liver tissue.

A) Size distribution (nm) of particles against mean particle yield in a 500 µL concentrated EV isolate from 0.2 g tissue. B) Mean particle size of EV isolates. C) Total protein yield D) Particle to protein ratio in EV isolates. (E-J) Concentration of EV and contaminant markers in liver tissue homogenate (L-HMG) and liver tissue EVs (LT-EV), analysed by liquid chromatography mass spectrometry. Data reported as mean ± SD and statistical testing by paired t-tests. ** p<0.01, *** p<0.001, **** p<0.0001.

Discussion

To the best of our knowledge, this study represents the first quantitative comparison of protein abundances in paired liver tissue and tissue derived EVs. In our prior work, the application of mass spectrometry for total proteome analysis revealed the capacity for liver derived EVs to broadly reflect the protein expression in the originating tissue (Useckaite et al., 2023). Here, we used targeted LC-MS/MS based proteomic assays to quantify the absolute abundance of 29 proteins involved in the interactions of drugs with the liver. These analyses were performed to establish the fundamental capacity of liver derived EVs to (i) define between subject variability in DME protein abundance, and (ii) track within subject changes in the abundance of MAFLD drug targets.

Addressing the primary objective of the current study, DMEs and MAFLD drug target proteins were readily detected in EVs from liver tissue. The majority of CYP and UGT enzymes exhibited robust correlation with tissue expression ($r > 0.6$). In contrast, several MAFLD drug targets lacked significant correlation. In line with the described impact of extra-hepatic expression of targets in this study, a notable exception was 17-beta hydroxysteroid dehydrogenase 13 (HSD17B13), for which a strong significant correlation was observed between EVs and tissue ($r = 0.914$). This liver-enriched enzyme associates with lipid droplets and plays a key role in lipid metabolism. Recently identified genetic variants linking loss-of-function to protection against disease progression have prompted the investigation of hepatic HSD17B13 downregulation as a novel therapeutic strategy for MAFLD (Lindén and Romeo, 2023).

We explored the capacity for EVs to represent the overall profile of the targets of interest based on the concordance of correlations in tissue and matched EVs. Whilst the expression profile in tissue may be more influenced by total protein abundance, the co-ordinated expression of proteins in the EVs may be affected both by differential sorting and the relative abundance of extra-hepatic EVs in the tissue. Indeed, we found less than half of the proteins with concordant expression in tissue had this relationship represented by the EVs.

EVs are released from all cells into the extracellular milieu and display functional activities in the local tissue environment, while a proportion will enter the bloodstream and act at distal sites

(Crewe and Scherer, 2022). Considering the role of EVs as intercellular messengers, the differential packaging of certain classes of proteins will impact recipient cell physiology both locally and systemically. While molecular cargo present in the cytosol or plasma membrane may be indiscriminately incorporated into vesicles during biogenesis, additionally there are various regulated sorting mechanisms that are generally not well understood (Mathivanan et al., 2021). Hepatic cells contribute to the total population of EVs in the blood under normal physiological conditions and several members of CYP and UGT families have been identified as cargo at both mRNA and protein level (Rodrigues et al., 2022, Rodrigues et al., 2021, Rowland et al., 2019). Moreover, the activity of these enzymes is retained and contributes to extrahepatic metabolism. In this regard, the enrichment of DMEs in liver derived EVs and close relationship with hepatic expression described here, have possible physiological significance. We examined a range of DME proteins responsible for metabolic clearance of xenobiotics, which is performed primarily in the liver. Other tissues that express DMEs at lower levels contribute less to systemic metabolic clearance and rather have a more profound effect on local tissue exposure. Since hepatic expression of CYPs and UGTs can be regulated by levels of their substrates and various other environmental triggers, the transfer of hepatic EVs containing these enzymes in representative abundance may mediate an appropriate modulation of biotransformation in extra-hepatic sites (Gerth et al., 2019, Kumar et al., 2017). Indeed, our previous studies showed that changes in CYP3A4 content of circulating EVs that were specifically enriched for hepatic origin using hepatocyte marker ASGR1, can be used to predict individual exposure to midazolam and other victim substrates in the context of both strong (rifampicin) and weaker (modafinil) inducers (Rodrigues et al., 2022, Rodrigues et al., 2021).

In contrast to the relationship between EV and tissue expression for DMEs, limited correlation was observed in the set of MAFLD drug target proteins. We selected proteins representing the various therapeutic approaches (e.g. targeting lipogenesis and insulin resistance, inflammation and fibrosis) for which investigational compounds have completed or testing is ongoing in phase 2/3 clinical trials (Dufour et al., 2022). Some of these have failed to meet efficacy endpoints, a persistent feature of the MAFLD therapeutic landscape, as a pharmacological treatment is yet to be approved for the condition. The paucity of non-invasive biomarkers to accurately measure efficacy of

treatments over the course of clinical development is recognised as a key challenge for compound prioritisation and managing the impact of disease heterogeneity within patient cohorts (Ratziu and Friedman, 2020). A substantial body of evidence suggests that molecular information found in EVs such as non-coding RNA, proteins and lipids have diagnostic and prognostic value for MAFLD and are being actively explored as biomarkers (Newman et al., 2022a). A limitation of this study was the use of liver tissue samples obtained from generally healthy individuals. The abundance profile of EV proteins likely differs in disease and selective export of proteins and other cargo via EVs has been observed from steatotic hepatocytes (Mleczko et al., 2022) and activated hepatic stellate cells (Li et al., 2020). We also previously found an increase in the fraction of miRNA-122 encapsulated in liver derived plasma EVs relative to total circulating levels in steatohepatitis patients compared to controls (Newman et al., 2022b). Further to understanding disease-related differences in protein packaging, accounting for the potential impact of drug treatment will be imperative to the application of EVs as markers of response.

Using TEM imaging, we identified intact cells and the presence of EVs in the extracellular space in the liver tissue samples. These EVs were recovered using a gentle tissue dissociation method to limit the risk of contamination with intracellular material. EV samples were also characterised in accordance with MISEV (Welsh et al., 2024), evaluating size profile and abundance of typical EV markers using a previously validated targeted assay (REF). SEC was used to further purify EVs from other components in the enzymatically treated tissue-conditioned media and we pooled SEC fractions containing EV markers. Though albumin concentration was significantly depleted relative to starting tissue, we cannot fully exclude the recovery of other soluble and non-EV proteins.

In summary, this study provides fundamental evidence for the relationship between protein abundance in liver tissue and liver derived EVs for proteins with key roles in normal liver function and metabolic disease. Our results shed light on the differential packaging of drug metabolising enzymes and drug targets for MAFLD, which may be linked to the function of hepatic EVs in normal physiological contexts. Future studies to elucidate the mechanisms of protein packaging in health and disease will help to inform appropriate selection of EV biomarkers for specific purposes. The

possibility to track both variability in drug exposure and the efficacy of pharmacologic interventions *in vivo* using a minimally invasive EV liquid biopsy promises to enhance not just the development of novel therapies for MAFLD, but precision medicine strategies more broadly.

CHAPTER 6
EXPLORING THE FEASIBILITY OF EV LIQUID BIOPSY FOR MAFLD DRUG TARGETS

Context in Thesis

This thesis has so far presented the development of methodology and results that underpin a framework for utilising circulating EVs in biomarker analysis. The focus has been on addressing methodological and fundamental biology challenges and opportunities associated with applying this framework to human biospecimens in the context of clinical trials for MAFLD. The preceding chapter showcased the capability to quantify proteins in liver tissue derived EVs (LT-EVs), which may serve as valuable pharmacodynamic or target engagement markers. This finding supports the potential to predict and monitor treatment response in patients based on the abundance of these proteins in circulating EVs. To this end, the primary aim of the following chapter was to evaluate the feasibility of quantifying MAFLD drug target proteins in circulating global EVs and liver enriched plasma EVs, employing targeted proteomic assays previously developed for LT-EV.

The successful implementation of EV biomarkers in clinical settings will require longitudinal assessments, which underscores the necessity for reproducible EV isolation methods. A key challenge in EV research for biomarker development, however, is reproducibility of results between studies due to inconsistency of isolation methods. Even when the same technology is employed, variability between batches and manufacturers or changes in access to identical products can hinder this consistency. Since a new generation SEC column was introduced from an alternative supplier, the work here also describes the reoptimisation of the SEC protocol. Data obtained is compared with previous findings from this thesis to evaluate the relative performance. The work underscores the challenges associated with the reliance on manufacturers when using commercially available tools for EV isolation. Application of the new protocol to a population of MAFLD patients and healthy controls revealed differences in the global and liver derived circulating EV populations that were not observed using the previous protocol in Chapter 4. The potential variations in EV subpopulations

and the extent and profile of contaminants isolated by different SEC columns highlight the difficulty of comparing results across studies without standardised EV isolation protocols.

Introduction

It was demonstrated in the results of the previous chapter that EVs derived from liver tissue harbour key protein cargo associated with drug metabolism and targets for drugs involved in investigational treatments for MAFLD. The robust correlations observed for liver-enriched drug metabolising enzymes between liver tissue EVs and paired total tissue, underpin the potential to define between-subject variability in drug exposure using EVs. Indeed, the capacity to predict exposure to medications metabolised by CYP enzymes has been previously demonstrated in previous work using ASGR1+ IP of plasma EVs to quantify protein abundance (Rodrigues et al., 2022, Rodrigues et al., 2021, Qiu et al., 2023). Metabolic drug interactions could be accurately characterised since the changes in CYP abundance in the presence of CYP inducing agents were commensurate to the known strength of the inducer. While factors affecting the pharmacokinetics of a drug can be elucidated using an EV liquid biopsy, this approach has not been demonstrated for characterising the pharmacodynamic profile.

Based on those studies (Rodrigues et al., 2022, Rodrigues et al., 2021, Qiu et al., 2023), as well as data reported in this thesis (Chapter 4, (Newman et al., 2022b)), approximately 10% of EVs isolated from plasma by SEC, on average, are captured by ASGR1 IP, but this can vary considerably between subjects reflecting differences in EV release from the liver. Given that only a minor proportion of circulating vesicles are of interest to the analysis, robust quantification is dependent on the high sensitivity of the LC-MS method and efficient recovery of the target EV subpopulations. While LC-MS has demonstrated sufficient sensitivity for quantifying liver derived protein cargo such as CYP and UGT enzymes at the concentrations found in ASGR1+ EVs in the blood (Rodrigues et al., 2021), the implementation of this workflow for quantifying an expanded repertoire of target proteins is dependent on the comprehensive optimisation of the LC-MS method used to detect surrogate peptides as well as the performance of the EV isolation method.

SEC is one of the most commonly used methods for isolating EVs from plasma and its popularity has increased significantly in recent years (Royo et al., 2020). Although still second in frequency to ultracentrifugation overall, SEC is the top choice for studies on EV diagnostics and characterisation (Williams et al., 2023), owing to its relatively efficient removal of contaminant proteins and gentle nature of the procedure that recovers vesicles intact and avoids the physical disruption or aggregation induced by high speed centrifugation (Monguió-Tortajada et al., 2019). The challenge of separating EVs from other components in plasma based on size exclusion is presented by the predominating abundance of non-vesicular particles with overlapping size ranges. In particular, very low density lipoproteins (VLDLs) and chylomicrons, with respective size ranges of 30-80 nm and 75-1200 nm, cannot be excluded using SEC. High density lipoproteins (HDLs, <20 nm) are typically removed and, while low density lipoproteins (LDLs) are also smaller than most EVs, at 20-30 nm, their far greater numbers tend to result in partial co-elution (Figure 6.1) (Liangsupree et al., 2021).

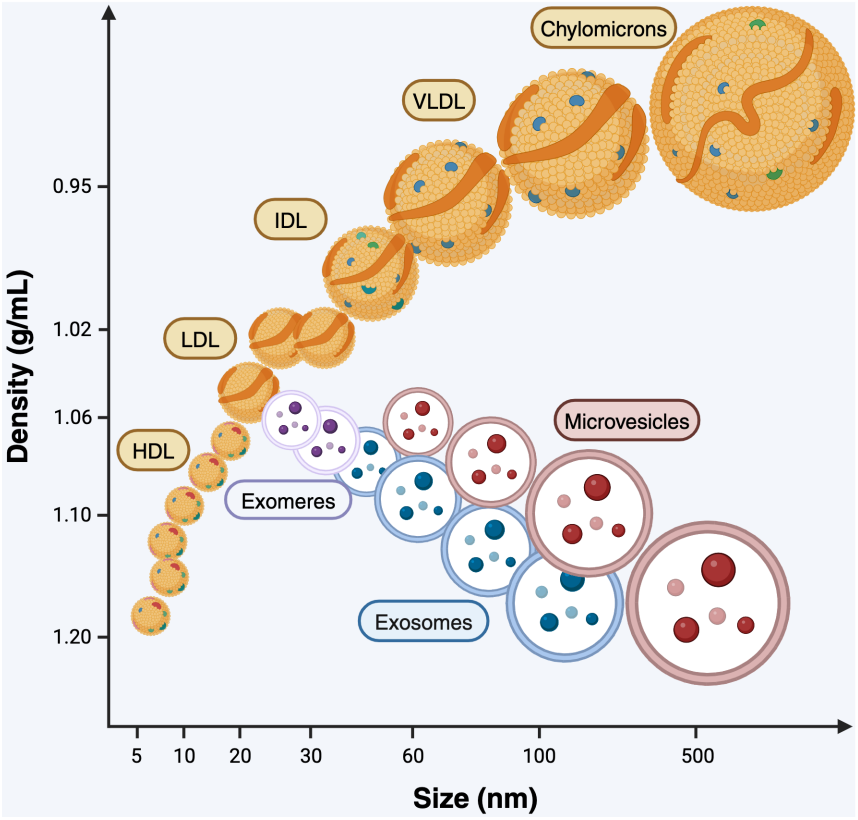

Figure 6.1 Overlapping density and size ranges of extracellular particle subtypes.

HDL: high density lipoprotein; LDL: low density lipoprotein; IDL: intermediate density lipoprotein; VLDL: very low density lipoprotein. Figure adapted from Liangsupree et al., 2021.

Moreover, the size based separation alone cannot distinguish EV subpopulations. Using the basic definition of EV subtype size ranges, SEC columns are designed to recover a diverse mixture enriched for exosomes (30-150 nm) and small microvesicles (<200 nm) as well as some exomeres, a class of extracellular particle with a lipid monolayer, typically <50 nm in size (Wang et al., 2023). The heterogeneity in size, among several other biophysical properties, influences the composition of molecular cargo likely to be found in the isolated populations, since the loading of cargo may be restricted in smaller vesicles or influenced by packaging mechanisms through different intracellular biogenesis pathways (Chevillet et al., 2014, Kaddour et al., 2021). Indeed when EVs are separated by floatation on iodixanol or sucrose gradients, certain molecules may be relatively enriched in EVs of higher or lower density (Kowal et al., 2016). Thus, in addition to the differing levels of contaminating non-EV particles, each isolation method may be inherently biased towards capturing populations of EVs with certain biophysical properties, impacting downstream analysis of molecular components.

There are many commercially available premade SEC columns as well as chromatography resins for in-house column preparation, which introduces significant diversity in the characteristics of the SEC materials and the opportunity to optimise protocols for intended applications. As reported in studies comparing the performance of different columns and resins, the dimensions of the column and properties of the stationary phase, including the pore size, bead size and extent of cross-linking, determines the exclusion limit and elution rate and impacts the recovery and resolution of EVs from contaminants (Contreras et al., 2023, Lane et al., 2019, Benayas et al., 2023). Further, EV recovery and reproducibility of separation may be impacted by adsorptive interactions of the column surface material with EVs or matrix effects introduced by the composition and viscosity of the plasma (Fekete et al., 2022, Monguió-Tortajada et al., 2019).

The work reported so far in this thesis, employed the iZon qEV Original (Legacy) SEC columns, principally with the 70 nm resin. Though in Chapter 2, the EV marker profile was also compared to the 35 nm resin and demonstrated that this lower exclusion limit enhanced recovery of typical EV proteins with the trade-off for less efficient removal of soluble protein. Unfortunately, with the discontinuation of the qEV columns, a different product had to be selected from an alternative

manufacturer (STEMCELL TECHNOLOGIES) for subsequent EV isolations. Considering the potential impact of the different column on the recovery of EVs containing the markers of interest, the collection of EV-containing fractions was reoptimised and the characteristics of EV isolates compared to that previously observed using qEV columns.

The previous results chapter of this thesis provided the methodology and evidence for the capacity to quantify potential markers of target engagement for MAFLD in EVs from liver tissue. With the envisioned next step of translating this to a liver specific EV liquid biopsy in clinical samples, the aim of this exploratory analysis was to evaluate the feasibility of quantifying the protein targets in plasma EVs using the newly optimised SEC method followed by ASGR1 immunoprecipitation to selectively isolate the circulating liver derived EV subpopulation. The sensitivity of the SEC protocol to differences in the circulating EV profile between MAFLD patients and controls is also evaluated.

Methods

Blood samples

Male and female patients (n=18) aged 18 years or over presenting to Flinders Medical Centre with a clinical diagnosis of MAFLD were enrolled into the study. Consistent with emerging consensus in the field that recognises the interplay of alcohol consumption with metabolic determinants, the study did not exclude patients based on alcohol consumption and two patients self-reported alcohol use above limits for 'significant' consumption. Patients under 18 years of age, with diagnosed viral disease, post-transplantation or with cognitive impairment were excluded from the study. The study protocol was approved by the Southern Adelaide Clinical Human Research Ethics Committee (SAHREC 30.22).

Males and females (n=16) aged between 18 and 65 years were recruited as control subjects matched to patients by age and sex. Participants were generally healthy at screening with a BMI between 18 and 29 kg/m^2, no history of liver disease and no recent (< 3 weeks) or current infections. Controls were enrolled in the study in accordance with the protocol approved by SAHREC (261.18). Written informed consent was obtained from all participants prior to enrolment.

Plasma Collection

Venous blood was collected using a 21-gauge needle into K_3EDTA plasma Vacuette (Greiner Bio-one, Frickenhausen, Germany) and processed within an hour of collection. Samples were centrifuged in two cycles of 15 minutes at 2500 g at room temperature and plasma was aliquoted and stored at -80^{o}C.

Isolation of Extracellular Vesicles

Size exclusion chromatography

Global EVs were isolated from plasma using 2mL size exclusion chromatography columns (STEMCELL Technologies). Columns were equilibrated to room temperature and flushed with 20 mL of 0.2 µm filtered phosphate buffered saline (PBS). The sample reservoir was loaded with 1 mL plasma and eluate was collected from the column in 0.5 mL volumes. As the sample passed through the top filter into the gel matrix, the reservoir was topped up with up to 2 mL PBS at a time, ensuring the filter did not run dry. The first 5 fractions (2.5 mL) were discarded and the following 6 fractions (3 mL) containing EVs were collected and pooled. Pooled EV isolates were concentrated using Amicon Ultra-4 centrifugal filters (Merck Millipore). Dilute EV fractions were added to the reservoir of pre-conditioned filter units and centrifuged for 30-45 min at 4000 g at 10^{o}C. Final volume of concentrated EV samples was 200 µL in PBS.

Liver Specific Immunoprecipitation

Plasma EVs were enriched for hepatocyte origin based on surface expression of ASGR1 using our previously reported protocol (Rodrigues et al., 2021, Rodrigues et al., 2022, Newman et al., 2022b). Dynabeads M280 streptavidin magnetic beads (1 mg) (Thermo Fisher Scientific) were pre-washed with PBS and conjugated to 5µg of biotinylated anti-ASGR1 antibody (Sapphire Bioscience, Cat# LS-C430149, 0.5 mg/mL) by incubation at room temperature for 30 minutes with gentle agitation. Antibody-conjugated beads were separated using a DynaMag-2 magnet (Thermo Fisher Scientific), washed with 0.1 % bovine serum albumin in PBS and resuspended in 100 µL of 0.2 µM filtered PBS. Half of the concentrated volume of EVs prepared by SEC was added to the beads and incubated for 24 hours at 4^{o}C on a rotating mixer. Beads with bound immunocomplex were separated from solution using the magnet, washed and resuspended in PBS.

Transmission Electron Microscopy

Samples were prepared adapting a previously published protocol, with some modification (Newman et al., 2021). Briefly, Ted-Pella B 300M carbon-coated grids (Ted-Pella, Redding, CA, USA) were cleaned and hydrophilized using plasma glow discharge for 45 s (Quorum GloQube plus glow discharge system, Quorum Technologies, UK) prior to use. Two µL of EV sample was diluted up to 10 µL of 0.2-µm-filtered PBS and was placed on carbon-coated grids for 4 min. Carbon grids were washed once (15 s) at room temperature (RT) with 0.2 µm filtered PBS and were contrasted with 2% uranyl acetate (2 min, RT), washed once, and examined by FEI TECNAI Spirit G2 TEM (Thermo Fisher Scientific, Waltham, MA, USA) operated at 100 kV. TEM images were acquired at 30,000 × and 68,000 ×.

Nanoparticle Tracking Analysis

Particle analysis was performed to determine abundance and size distribution of plasma EV samples, using a NanoSight Ns300 (Malvern Panalytical, UK, software v.3.4). EVs were diluted 1:1000 with 0.2 µM filtered PBS and analysed in five 60 second videos with a continuous flow, with syringe pump speed of 100. Camera level 13 was used for capture and detection threshold 5 was used for data analysis.

Targeted Proteomics

Targeted proteomics using LC-MRM-MS was performed as described in the primary methods section of this chapter with few modifications. Total protein from 100 µL each of global EVs and immunoprecipitated EVs were prepared for trypsin digest. SIL peptides were spiked into digested protein samples at final concentration of ALB at 2 nM, CD9 at 0.4 nM, CD81, CANX and TSG101 each at 0.4 nM and MAFLD drug targets each at 1 nM, except ASGR1 at 2.5 nM. Where indicated, 100 µL of supernatant from protein digests containing SIL peptides were lyophilised for 2 hr and reconstituted in 25 µL of 25 % acetonitrile in water. The MRM method described in Chapter 2 was used to measure EV markers and contaminants. MAFLD drug targets were assayed in a separate MRM method using the same gradient elution conditions described in the primary methods section of this chapter. Considering the expected lower abundance in plasma EVs, to increase sensitivity for the targets, one quantifier and one qualifier ion transition per peptide was included for a limited

selection of analytes that were quantifiable in liver tissue EVs (ACACA, ASGR1, AOC3, DGAT2, FASN, GLP1R, HSD17B13, KHK and MAP3K5).

Data Analysis

MassHunter Software (v.B.09.00) was used to calculate peak areas for endogenous analytes and ratios to spiked SIL peptides. Linearity of response was assessed by standard curves of SIL spiked into EV matrix. Lower limit of quantification was determined by evaluating peak areas in blanks and SIL in mobile phase over the course of the analysis and sample peaks with at least 5x signal to noise ratio were included for quantification. Control and patient sample groups were compared using unpaired t-tests.

Results

Reoptimisation of EV collection from size exclusion chromatography columns

While thus far the isolation of global EVs has been performed using iZon qEV columns, the unavailability of this product necessitated the introduction of an alternative column from a different supplier. The 0.5-2 mL capacity SEC columns from STEMCELL Technologies were obtained and subject to a robust characterisation of the EV population isolated for the purpose of quality control and determination of optimal EV fraction collection. EV isolation was optimised for 1 mL sample loading and, following discard of a 2 mL void volume, 9 x 500 µL fractions were individually collected and evaluated.

Particle analysis by NTA revealed the greatest number of particles in the size range of EVs (mean and mode size ranges between 101.8-132.7 nm and 73.6-121.6 nm, respectively) in fractions 3 to 7. In these fractions there was a combined particle count of 1.22×10^{11} particles and total protein content of 444.5 µg per mL of starting plasma (Figure 6.2A). The EV marker LCMS panel was used to confirm the presence of EVs and showed a clear elution of CD81-, CD9-, TSG101- positive vesicles in fractions 2-7. CANX was also abundant in these EV-containing fractions, supporting the possibility of a CANX-positive EV population (Figure 6.2B). The marker of soluble protein contamination, albumin, was not completely separated from EV fractions, but increased sharply in

fraction 9 (Figure 6.2C). Based on these data, the fractions 2-7 were pooled to maximise EV recovery and minimise albumin contamination from plasma. Liver enriched markers ASGR1 and CYP3A4 were quantified in pooled fractions 2-7 and subsequent 500 µL fractions 8-11 (Figure 6.2D). All ASGR1 was recovered in fraction 2-7 as well as > 54 % of CYP3A4 signal. CYP3A4 was also abundant in fraction 8, suggesting a possible later-eluting population of vesicles containing this protein but devoid of the classical EV markers.

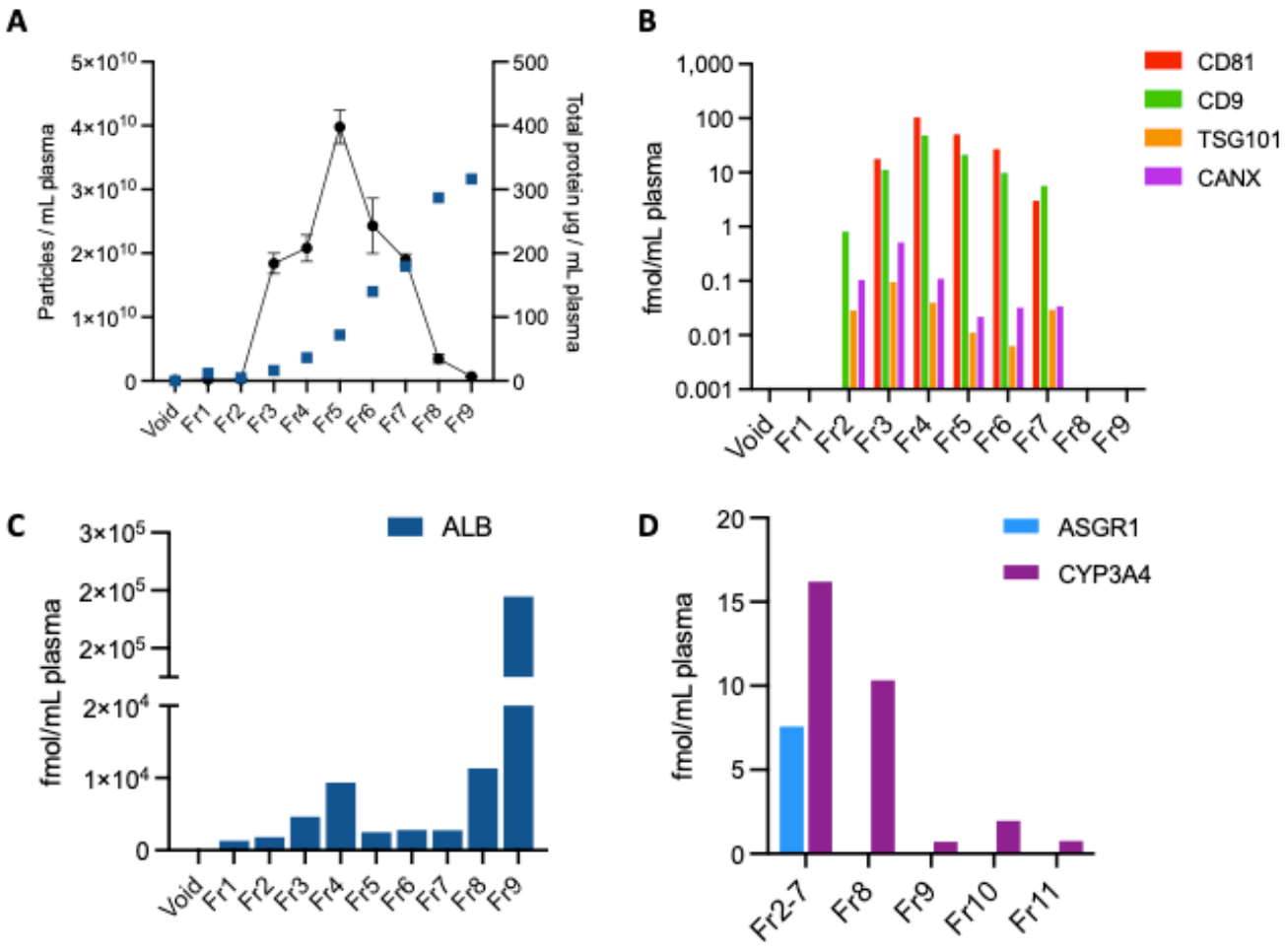

Figure 6.2 Reoptimising STEMCELL SEC columns.

(A) Particle count and total protein content, (B) concentration of EV markers, (C) concentration of albumin in 500 µL SEC fractions (Fr) following a pooled 2 mL void volume. (D) Concentration of liver enriched markers in pooled fractions 2-7 and subsequent 500µL non-EV fractions.

In a separate experiment, pooled plasma was isolated in triplicate from the same column to assess reproducibility of EV marker quantification in pooled Fr2-7. CD81, CD9 and TSG101 were highly abundant with respective mean concentrations of 247.9, 53.4 and 22.0 fmol / mL plasma, while CANX was bellow limit of quantification in these isolates. Significant levels of albumin was co-isolated in each replicate isolation, 530-6000 x greater abundance than the EV markers. Each of the quantified markers exhibited acceptable reproducibility between isolations (CV 1.8-11 %) (Table 6.1).

Table 6.1 Reproducibility of EV marker quantification in pooled fractions 2-7.
LOD – limit of detection

	Concentration (fmol/mL plasma)				
	ALB	**CD81**	**CD9**	**CANX**	**TSG101**
Isolation 1	123312	220.4	53.1	< LOD	22.2
Isolation 2	152418	242.8	58.1	< LOD	21.5
Isolation 3	119771	280.5	48.9	< LOD	22.4
Mean	131833	247.9	53.4	–	22.0
CV %	11.1%	10.0%	7.1%	–	1.8%

Comparative performance of STEMCELL SEC columns

The recovery of EVs using the newly optimised STEMCELL SEC protocol was compared to previous data obtained with qEV Legacy columns. It should be noted that a direct comparison of columns using matched plasma samples could not be done here, and rather explore representative differences in performance based on data from previous studies reported in this thesis. Particle analysis by NTA was used to examine the particle concentration in EV isolates and define the size distribution by mean and mode diameter and the 10^{th}, 50^{th} and 90^{th} percentiles (Figure 6.3). Median particle count per mL of starting plasma was 2.2×10^{11} for STEMCELL and 6.38×10^{10} for qEV70 Legacy and mean particle sizes were 128.6 nm and 102.6 nm, respectively. Despite the differences in concentration and size profile between the two SEC columns, with the new protocol isolating an apparently greater number of particles of a larger diameter, no statistically significant differences were recorded.

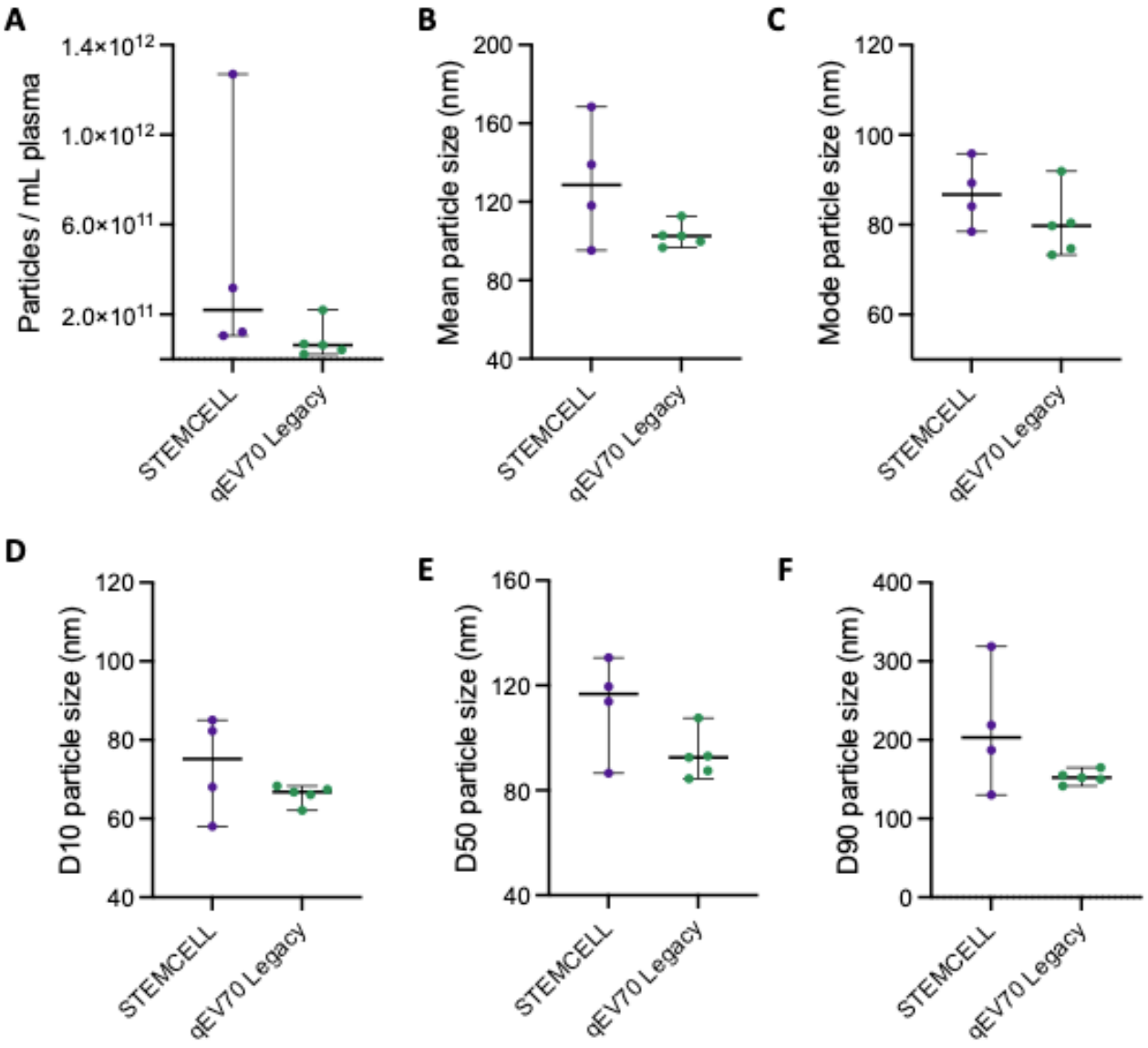

Figure 6.3 Size exclusion chromatography column comparison.

(A) Particle concentration and size distribution profile by (B) mean, (C) mode and (D-F) 10th, 50th and 90th percentiles compared by nanoparticle tracking analysis of EVs isolated by STEMCELL and qEV70 Legacy SEC columns.

The concentration of protein markers (CD81, CD9, TSG101, CANX, ALB and ASGR1) were compared between the SEC columns to explore the recovery of EVs and liver specific EVs and the extent of soluble protein contamination. Table 6.2 reports ranges observed across biological replicates. EV markers CD81, CD9 and TSG101 appeared to be enriched in STEMCELL isolates compared to previous observations from qEV columns. CD81 was notably up to 112 x greater in abundance. Recognising the limitation that the same plasma samples could not be compared

between columns, we have noted in the course of using both protocols that abundances for the generic EV markers from STEMCELL columns are consistently much greater than that in the qEV column isolates. CANX was detected in all the STEMCELL isolates and quantified in 75%, meanwhile, could be detected and quantified in only one from this set of qEV70 isolates. Albumin contamination varied more widely within replicate samples from STEMCELL columns and was also more abundant in these isolates compared to qEV70 Legacy. As with the qEV isolates, ASGR1 was quantifiable and represented the isolation of a hepatocyte derived population among global plasma EVs that may be extracted using the IP protocol following STEMCELL SEC.

Table 6.2 Comparison of concentration range for EV markers in isolates from STEMCELL and qEV70 Legacy SEC columns.

	Concentration range (fmol/mL plasma)	
Protein marker	**STEMCELL (n = 4)**	**qEV70 Legacy (n = 5)**
CD81	33.8 – 280.5	1.2 – 2.5
CD9	16.1 – 48.9	3.8 – 23.2
TSG101	0.03 – 21.5	1.0 – 1.5
CANX	< LOD – 0.14	< LOD – 4.0
ALB	3976 – 123312	1466 – 16715
ASGR1	2.3 – 7.6	1.5 – 2.5

The EV morphology and size profile was also assessed in TEM images of STEMCELL EVs and compared to the image of control group EVs isolated by qEV70 Legacy in Chapter 4. Particles of EV shape and size were markedly more abundant in the frame for STEMCELL isolates, however, there was some cloudiness obscuring part of the image (Figure 6.4). This could be due to co-isolated proteins and protein aggregates in the same which typically appear as granularity in the background of TEM. Far less of this background was observed in qEV70 Legacy image. Both of the images, though, showed the presence of small particles < 30 nm. Particles in this size range are well below the diffraction limit and not detectable by NTA. It is difficult to distinguish EVs from similarly sized lipoproteins by TEM, however, since the double membrane structure of EVs precludes a diameter less than 30 nm, these observed small particles are likely to be HDLs, LDLs, or possibly exomeres.

Despite STEMCELL columns retaining some non-EV material in resulting isolates, the EV marker protein profile suggested the protocol was suitable for use within the workflow described so far in this thesis, and arguably more effective for recovering global EVs expressing typical EV markers than qEV70 Legacy columns.

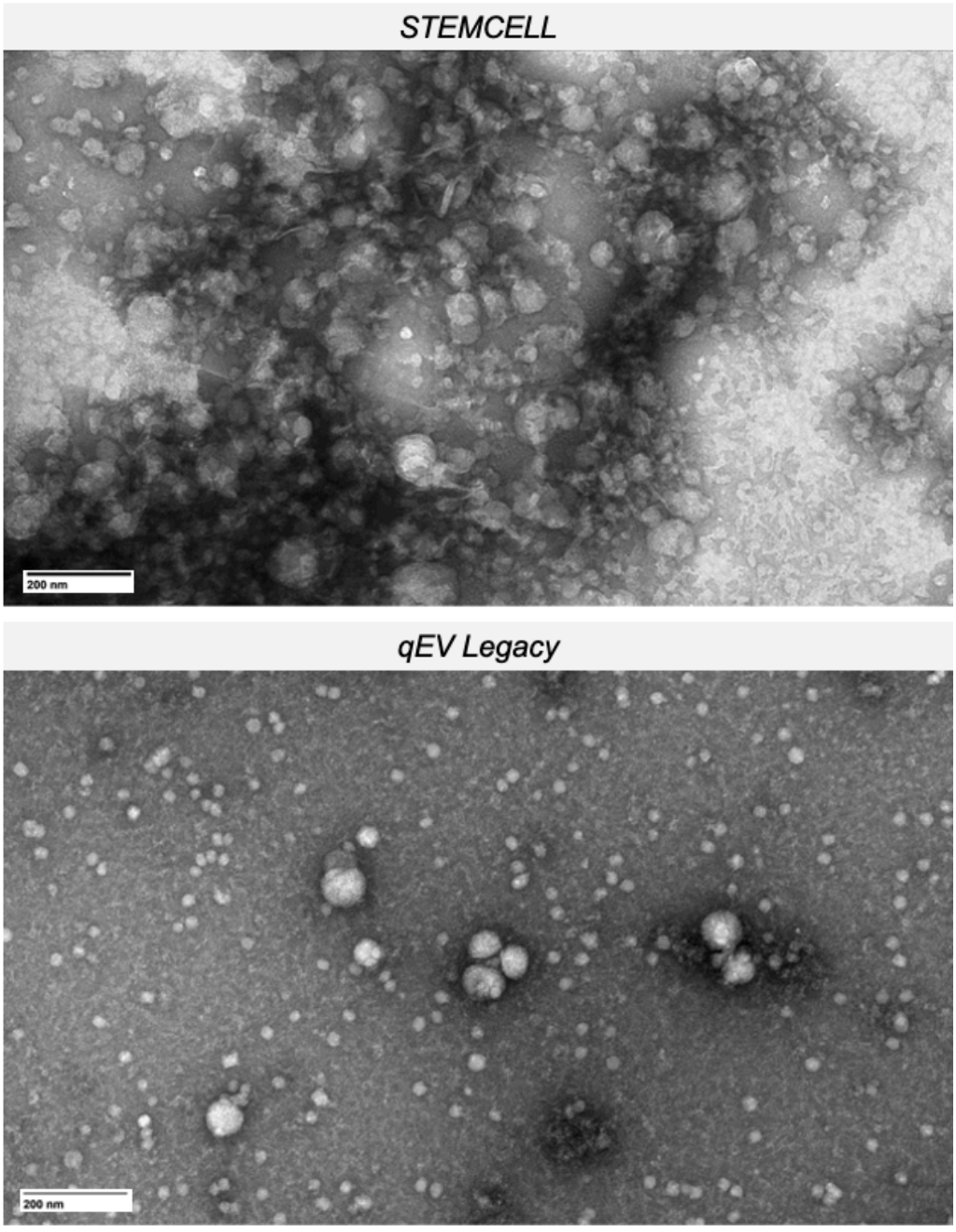

Figure 6.4 TEM images of plasma EVs from STEMCELL and qEV70 Legacy SEC columns. Images taken at 30,000 x magnification.

Understanding differences in plasma EV profile of MAFLD patients

MAFLD and control sample donor characteristics

Plasma samples were collected from patients with MAFLD and control subjects. The groups were matched for age, sex and ethnicity, while BMI was significantly higher in MAFLD patients (Table 6.3). Clinical characteristics related to MAFLD diagnoses were available for the disease population and are given in Table 6.4. Given the invasiveness of a liver biopsy, the procedure is not routinely performed for clinical diagnosis so recent biopsy results were not available for these patients. Local practice guidelines instead recommend the use of FibroScan and assessment by scoring systems such as Fibrosis-4 Index (FIB-4) and NAFLD Fibrosis Score (NFS). Based on defined cut-offs for FibroScan in MAFLD, number of patients with stage F0/1, F2, F3 and F4 were 2, 4, 4 and 8 patients, respectively. FIB-4 and NFS scoring systems detected significant fibrosis in 1 and 4 patients, respectively, and at least half of patients were classified indeterminant for each.

Table 6.3 Comparison of demographic characteristics of control and MAFLD groups. Data presented as mean ± SD and groups compared by unpaired t-tests.

Characteristics	Control (n=16)	MAFLD (n=18)	p-value
Age (years) mean ± SD	53.2 (11.3)	54.9 (14.2)	n.s.
Sex - % Female	62.5	50	n.s.
Ethnicity - % Caucasian	100	94.4	n.s.
BMI (kg/m2) mean ± SD	23.2 (2.8)	36.4 (5.9)	<0.001

Table 6.4 Clinical characteristics of MAFLD population. Data given as mean ± SD except where indicated.

Clinical characteristic	MAFLD (n = 18)
FibroScan (n)	
F0/1 (2-7 kPa)	2
F2 (7-10 kPa)	4
F3 (10-14 kPa)	4
F4 (>14 kPa)	8
FIB-4 (n)	
no signif. fibrosis (score < 1.3)	5
signif. fibrosis (score > 3.25)	1
Indeterminant	12
NFS (n)	
no signif. fibrosis (score < -1.455)	5
signif. fibrosis (score > 0.675)	4
indeterminant	9
Type 2 diabetes mellitus (n)	8
Hypertension (n)	7
Dyslipidemia (n)	6
Waist circumference (cm)	119.7 (11.7)
ALT (U/L)	62.9 (36)
AST (U/L)	45.3 (15.6)
GGT (IU/L)	104.6 (75.5)
Total bilirubin (mg/dL)	11.7 (5.7)
Triglycerides (mmol/L)	1.7 (0.5)
Cholesterol (mmol/L)	4.6 (1.2)
HDL (mmol/L)	1.2 (0.2)
LDL (mmol/L)	2.4 (1.2)
Albumin (g/L)	39.7 (3.8)
Glucose (mmol/L)	6.5 (1.8)
HbA1c (%)	6.0 (0.8)
Platelet count ($x10^9$/L)	225.5 (72.1)

Global EV concentration and size profile

The aim of this analysis was to evaluate the application of the STEMCELL SEC isolation protocol for understanding perturbations in the profile of plasma EVs in MAFLD. Significantly greater concentration of global EVs were observed in the MAFLD group compared to controls with 4.49 x 10^{10} and 7.38 x 10^{10} mean particles per mL of plasma, respectively. Though the plot of size distribution against particle count suggested more particles with diameter above 100 nm, there was no significant difference in mean size between the groups (Figure 6.5A-C). Like the TEM image of STEMCELL EVs described in the previous section, here there was significant background, with granularity possibly related to protein contamination, which appeared to impact control and MAFLD EV isolates equally (Figure 6.5 D & E). Particles of various sizes up to approximately 100 nm were observed in each of the images in panels D and E, potentially including some HDL and LDL particles < 30 nm. Consistent with observations of NTA, some larger particles were seen in the MAFLD group. Panel F in Fig. 6.5 shows a representative image of a particle more than 400 nm in diameter from a MAFLD isolate.

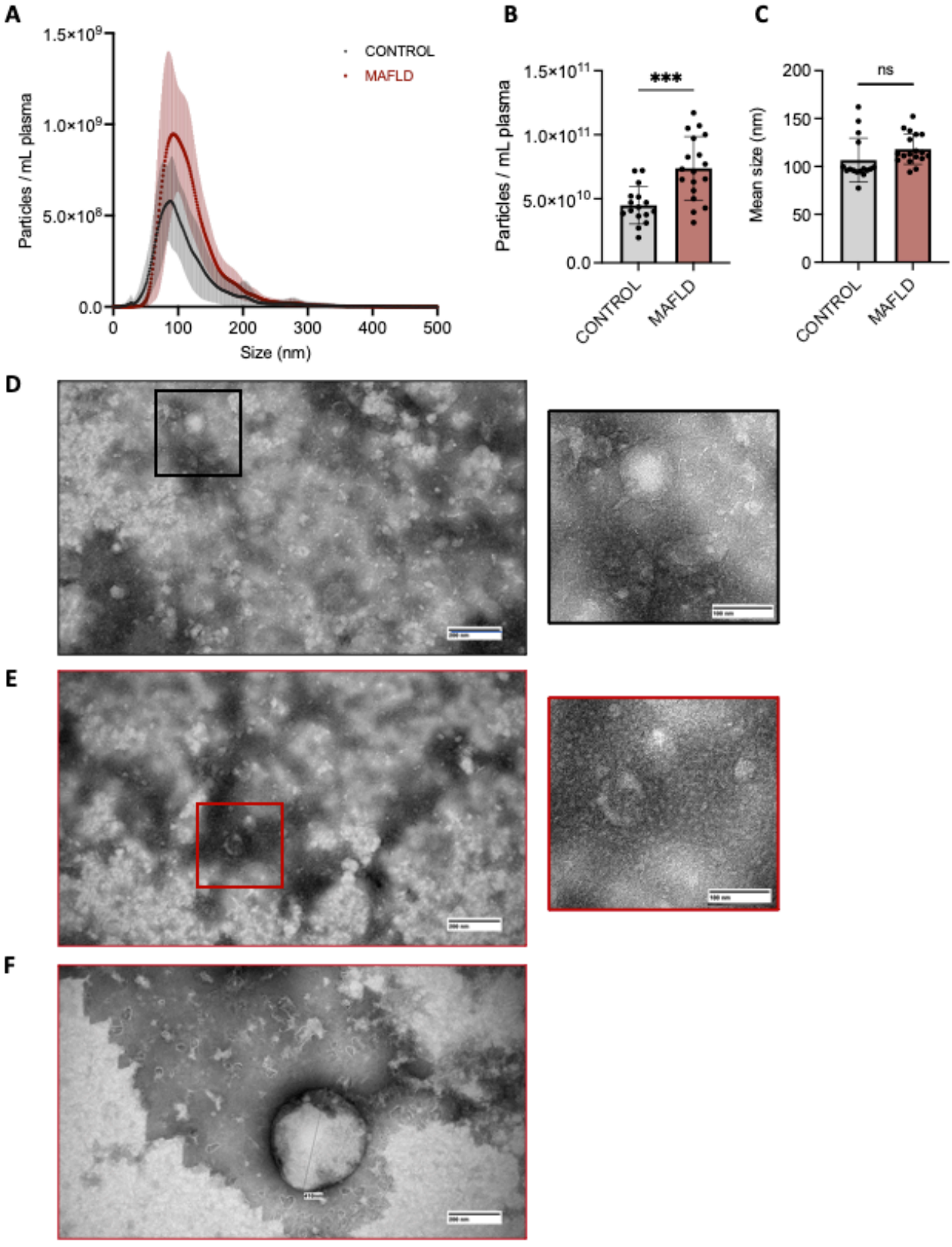

Figure 6.5 Global plasma EV concentration and size profile from control subjects (n=16) and MAFLD patients (n=18).

(A) Particle count by size distribution, B) Particle concentration presented as mean ± SD. C) Mean particle size (nm) presented as mean ± SD. TEM images at 30,000 x and 68,000 x magnification of (D) control EVs and (E-F) MAFLD EVs. ns not significant, *** $p < 0.001$.

Protein profile of global EVs and liver specific EVs in MAFLD

Next the protein profile was explored by targeted LCMS in global EVs and paired liver derived EVs enriched by anti-ASGR1 IP (Figure 6.6). In global EVs, CD81, TSG101 and CANX abundance did not differ significantly between MAFLD and controls, while CD9 abundance was more than 3-fold greater in MAFLD ($p = 0.0005$). While only 25 % of control samples had quantifiable levels of CANX, 56 % of MAFLD samples could be quantified. Strikingly, the difference in CD9 abundance was recapitulated in ASGR1+ EVs (2.6-fold greater in MAFLD vs control, $p = 0.004$). Meanwhile, CD81 and TSG101 were 2.7-fold ($p = 0.03$) and 3.9-fold ($p = 0.05$) higher, respectively, in ASGR1+ EVs from MAFLD patients, despite no difference in these markers in global EVs.

Given the systemic nature of MAFLD, changes in global EVs may be driven by EV release from other affected tissues, such as the adipose tissue or platelets and immune cells in the circulation. However, the selective analysis of EV markers in ASGR1+ EVs determined that greater numbers of liver derived vesicles positive for CD81, CD9 and TSG101 were present in the circulation of MAFLD patients compared to controls.

In controls samples, IP captured between 3.5 and 10.1 % of EV marker abundance in global EVs (Table 6.5). With the exception of TSG101, a similar proportion was captured from MAFLD samples. An apparently greater capture of CANX was observed but in the few quantifiable samples, did not reach statistical significance. Despite large variability between MAFLD biological replicates, TSG101 capture was on average 2.5-fold greater in MAFLD than controls ($p < 0.033$), suggesting that the liver is an important source of total TSG101 in MAFLD plasma.

Co-isolated albumin in global EVs was significantly greater in MAFLD compared to controls ($p = 0.05$) (Figure 6.6), while the IP method markedly improved purity to a similar extent in each group, only recovering up to 1.2 % (Table 6.5). It is possible that some albumin is in fact associated with EVs released from the liver, if not encapsulated, then adsorbed as part of the EV corona (Hallal et al., 2022).

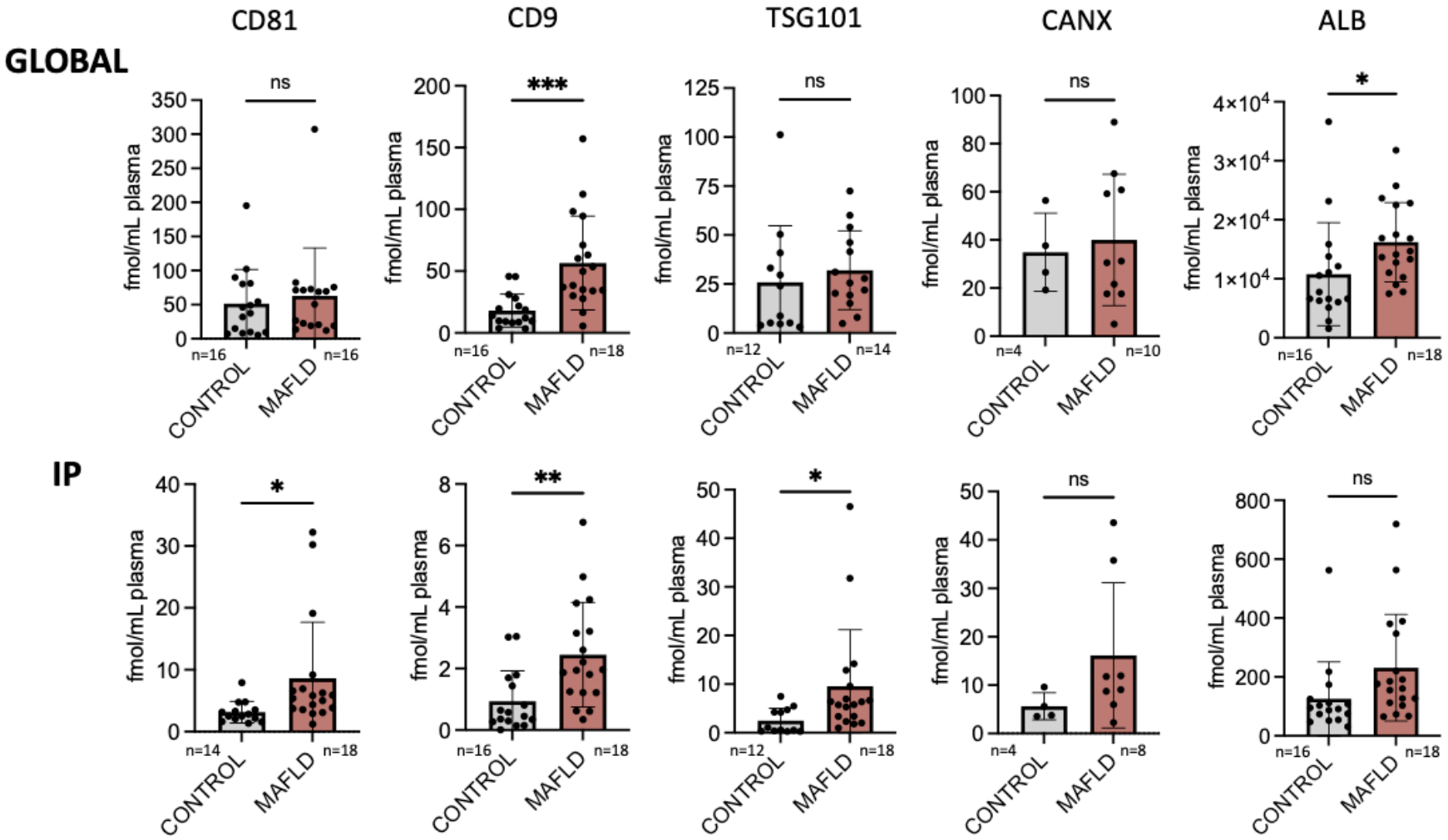

Figure 6.6 EV protein concentration profile in global (top panel) and paired IP (bottom panel) plasma EVs from control subjects and MAFLD patients.
N numbers for each analysis includes samples for which marker abundance was ≥ LLOQ. Data presented as mean ± SD and compared using unpaired t-tests. * $p < 0.05$, ** $p < 0.01$, *** $p < 0.001$, ns not significant.

Table 6.5 Percentage of global protein marker abundance captured in ASGR1+ EVs in control and MAFLD.
N = number of quantifiable samples included for analysis. Unpaired t-test * $p < 0.05$.

	Control		MAFLD	
Protein marker	**Mean (SD) %**	**n**	**Mean (SD) %**	**n**
CD81	10.1 (17.1)	14	13.0 (14.5)	16
CD9	3.5 (2.9)	16	4.2 (3.3)	18
TSG101*	8.7 (4.4)	12	21.6 (33.9)	14
CANX	16.1 (1.9)	4	29.1 (21.4)	8
ALB	1.2 (1.4)	16	1.2 (1.4)	18

Feasibility of detecting MAFLD drug targets in plasma EVs

MAFLD drug targets are associated with ASGR1+ EVs

Results given in the main part of this chapter demonstrated that the MAFLD drug target proteins could be quantified in EVs isolated from liver tissue. Of these, HSD17B13 exhibits high liver-specificity, while the other targets were enriched in liver as well as 1-2 other tissues or had significant extra-hepatic or ubiquitous expression. Given that almost half of the EVs present in liver tissue may arise from other sources (Useckaite et al., 2023), total liver tissue EVs were captured by anti-ASGR1 IP to confirm that the markers can be detected from the liver specific origin despite interference of extra-hepatic EVs in the tissue. It should be noted that the IP protocol designed for capture from plasma was not reoptimised for application to liver tissue EVs. As a markedly enriched source of ASGR1, the method was not expected to achieve total recovery of ASGR1+ EVs and on average 16.3 % of ASGR1 signal was captured from triplicate IP using biologically distinct pools of LT-EVs. Of the EV markers, CD81 and CANX were relatively enriched in the captured EVs (Figure 6.7A). MAFLD drug targets were highly abundant in the captured EVs, especially the highly liver-enriched marker HSD17B13 (Figure 6.7B). Aside from GLP1R, which was not detected in these samples, these data demonstrate that the markers of interest can be detected in association with ASGR1+ EVs in the tissue and supports the possibility to determine the abundance of liver derived EV proteins from the circulation by IP.

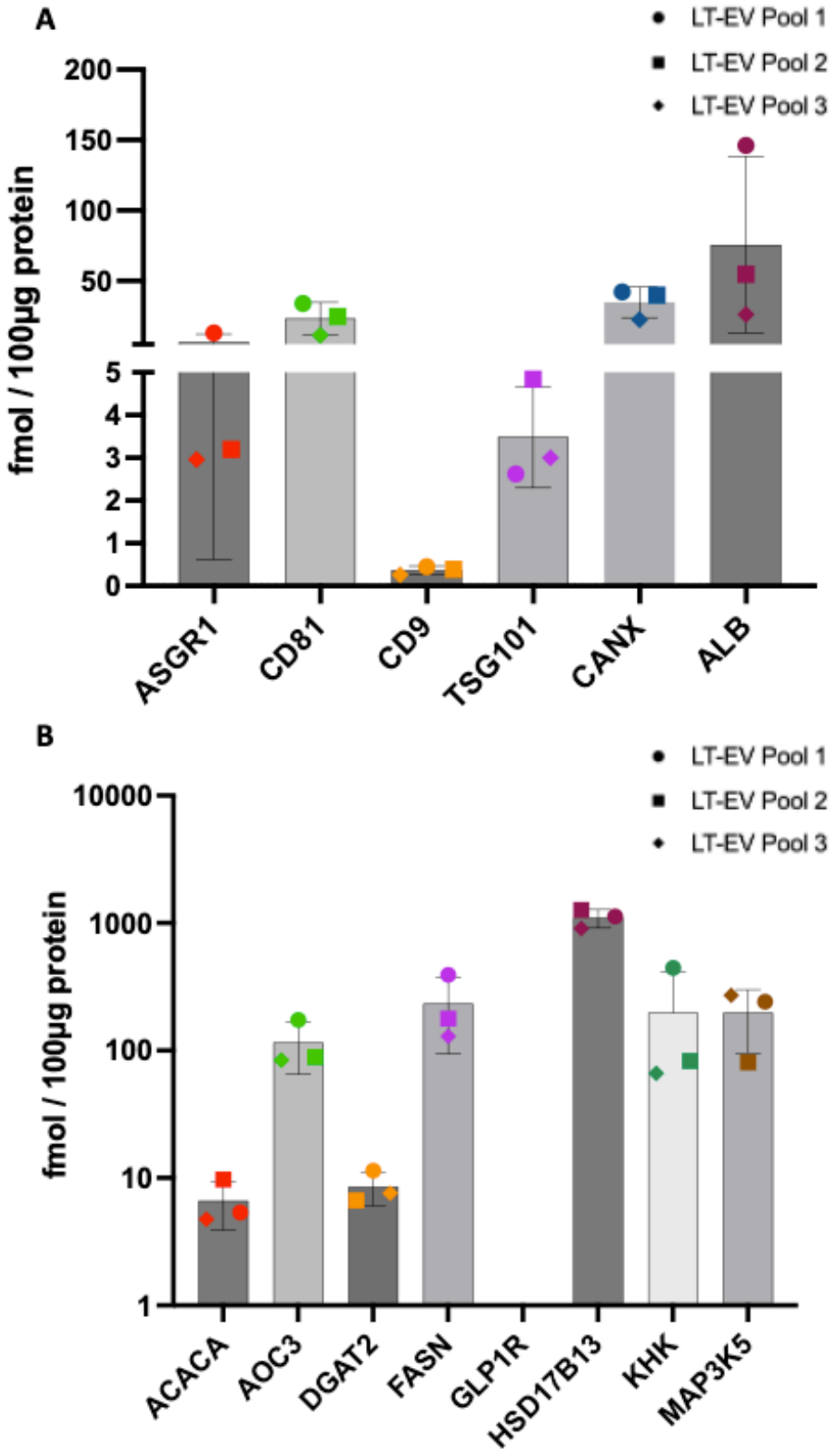

Figure 6.7 Quantification of EV markers (A) and MAFLD drug targets (B) captured in ASGR1+ EVs immunoprecipitated from liver tissue EVs.

Data presented as mean ± SD, n = 3 biological replicate pooled liver tissue EVs (LT-EVs).

Quantification of targets in global EVs from MAFLD and control plasma

Global plasma EVs isolated by STEMCELL SEC columns were analysed using the LC-MS method for the panel of MAFLD drug targets. The assay exhibited linearity of response for SIL peptides spiked in EV matrix with R^2 of standard curves between 0.988 and 0.999 (Figure 6.8). As described in methods, the assay initially developed in liver tissue EVs, was modified to increase sensitivity for expected lower abundance of the analytes in plasma, however, only four of the nine analytes could be quantified in global plasma EV samples (Figure 6.9). AOC3 and MAP3K5 could each be quantified in 69% of control samples and 94% and 100%, respectively of MAFLD samples. DGAT2 was quantified in 75% and 56% of controls and MAFLD samples, respectively, while FASN was quantified in only 25% of controls and 27% of MAFLD samples. Differences in abundance for quantified samples were not significant between control and MAFLD groups, based on unpaired t-tests.

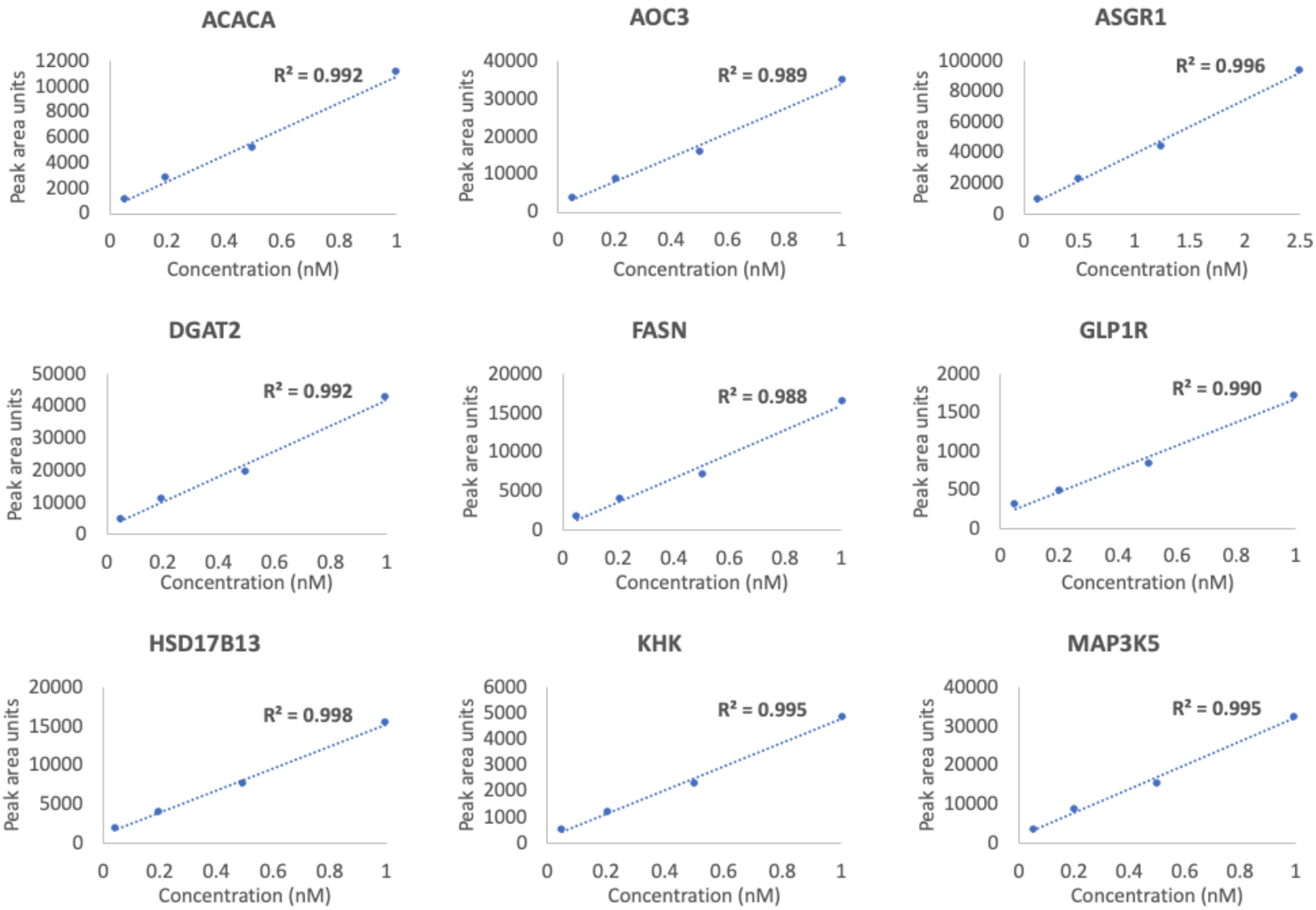

Figure 6.8 Standard curves of analytes in MAFLD drug targets panel.

Curves generated using stable isotope labelled peptides spiked in global plasma EV matrix.

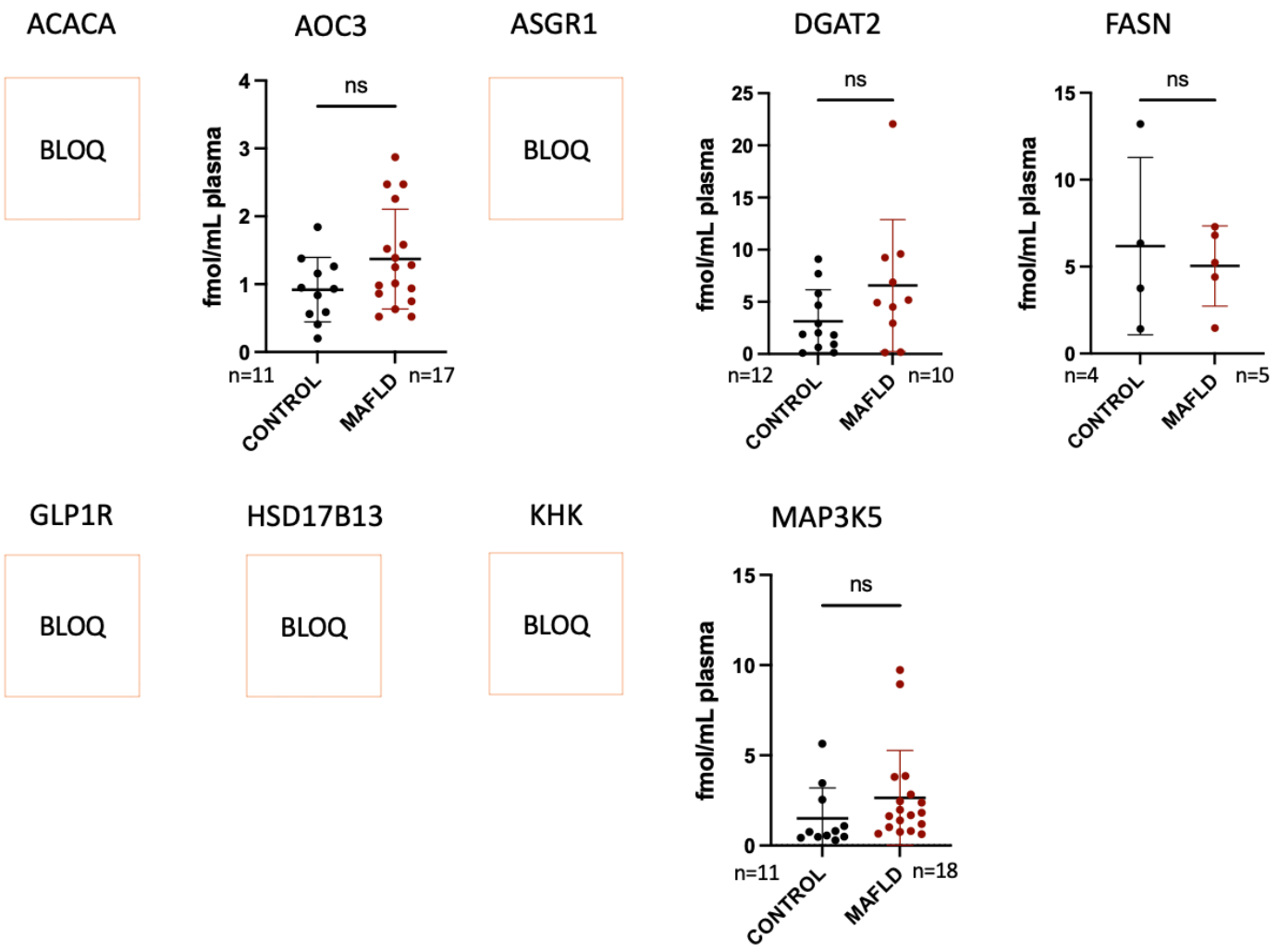

Figure 6.9 Concentration of MAFLD drug target proteins in global plasma EVs from control subjects and MAFLD patients.

N numbers for each target includes samples for which marker abundance was ≥ LLOQ. Data presented as mean ± SD and compared using unpaired t-tests. ns: not significant. BLOQ: below limit of quantification.

Lyophilisation of IP EV samples increases sensitivity for MAFLD drug targets

Plasma EV samples isolated from MAFLD and control subjects were purified further using ASGR1+ IP. In order to understand the impact of the matrix and possibility of boosting sensitivity in IP samples, global and IP EV samples were generated from a donor with known high circulating ASGR1+ EVs and digested protein from each was kept neat in buffer or lyophilised and reconstituted in mobile phase to 4-fold greater concentration. Neat and concentrated samples were analysed for EV markers and MAFLD drug targets. All but three (ACACA, GLP1R and MAP3K5) analytes could be quantified. The concentrating step increased the raw peak areas for endogenous analytes between 2.2- and 9.3 -fold in the IP samples, while in global samples the greatest fold change in peak area was only 2.3 and, for several analytes produced no change in signal (Table 6.6). Equal amounts of standard peptides spiked prior to lyophilisation and into neat samples resulted in SIL normalised peak area responses differing <17 %, suggesting the data was not impacted by losses during the concentrating process. Although samples were concentrated by a factor of four, the variability in observed peak area fold changes and the general lack thereof in global samples, may be explained by analyte-dependent differences in chemical noise caused by contaminants co-eluting around the analyte peak. IP samples are a much cleaner matrix compared to global samples, so particularly in the latter, also concentrating components of the matrix will to some degree maintain the ion suppression observed in neat samples. Overall the increase in signal achieved by the lyophilisation, especially in IP EVs, is a useful adaption to the workflow to improve assay sensitivity.

Table 6.6 Fold change (concentrated/neat) in peak area units of endogenous and SIL peptides for EV markers and MAFLD drug targets in IP and global EVs.
– endogenous analyte BLOQ

Assay	Analyte	Endogenous		SIL	
		IP	Global	IP	Global
EV markers	CD81	3.2	1.0	4.0	1.0
	CD9	2.3	2.1	2.8	2.1
	TSG101	2.5	1.5	2.8	1.5
	CANX	3.5	2.3	3.2	2.4
	ALB	3.3	1.9	3.3	2.0
MAFLD drug targets	ACACA	–	–	6.0	1.6
	AOC3	4.0	1.0	5.2	1.3
	ASGR1	6.4	1.1	5.8	1.3
	DGAT2	9.3	1.1	8.1	1.0
	FASN	5.4	1.4	5.9	1.2
	GLP1R	–	–	1.3	1.0
	HSD17B13	8.1	1.0	8.1	1.0
	KHK	3.2	1.5	3.2	1.4
	MAP3K5	–	–	1.6	0.8

Quantification of targets in IP EVs from MAFLD and control plasma

The capacity to quantify MAFLD drug target proteins in the concentrated IP EV samples was evaluated in the MAFLD and control cohorts (Figure 6.10). Like the global EVs, ACACA, GLP1R and HSD17B13 could not be quantified in these samples, despite the additional purification and concentration. While each were BLOQ in global samples, ASGR1 was quantifiable in 81 % of controls and 78 % of MAFLD IP samples, and KHK was quantifiable in just 2 of the controls. Respectively, AOC3, DGAT2 and MAP3K5 could be quantified in 63, 69 and 38 % of controls and 83, 44 and 72 % of MAFLD samples. FASN was quantified in 56 % of control and 67 % MAFLD samples, more than twice that found in global. There remained no significant differences in abundance of the targets between the MAFLD and control subjects.

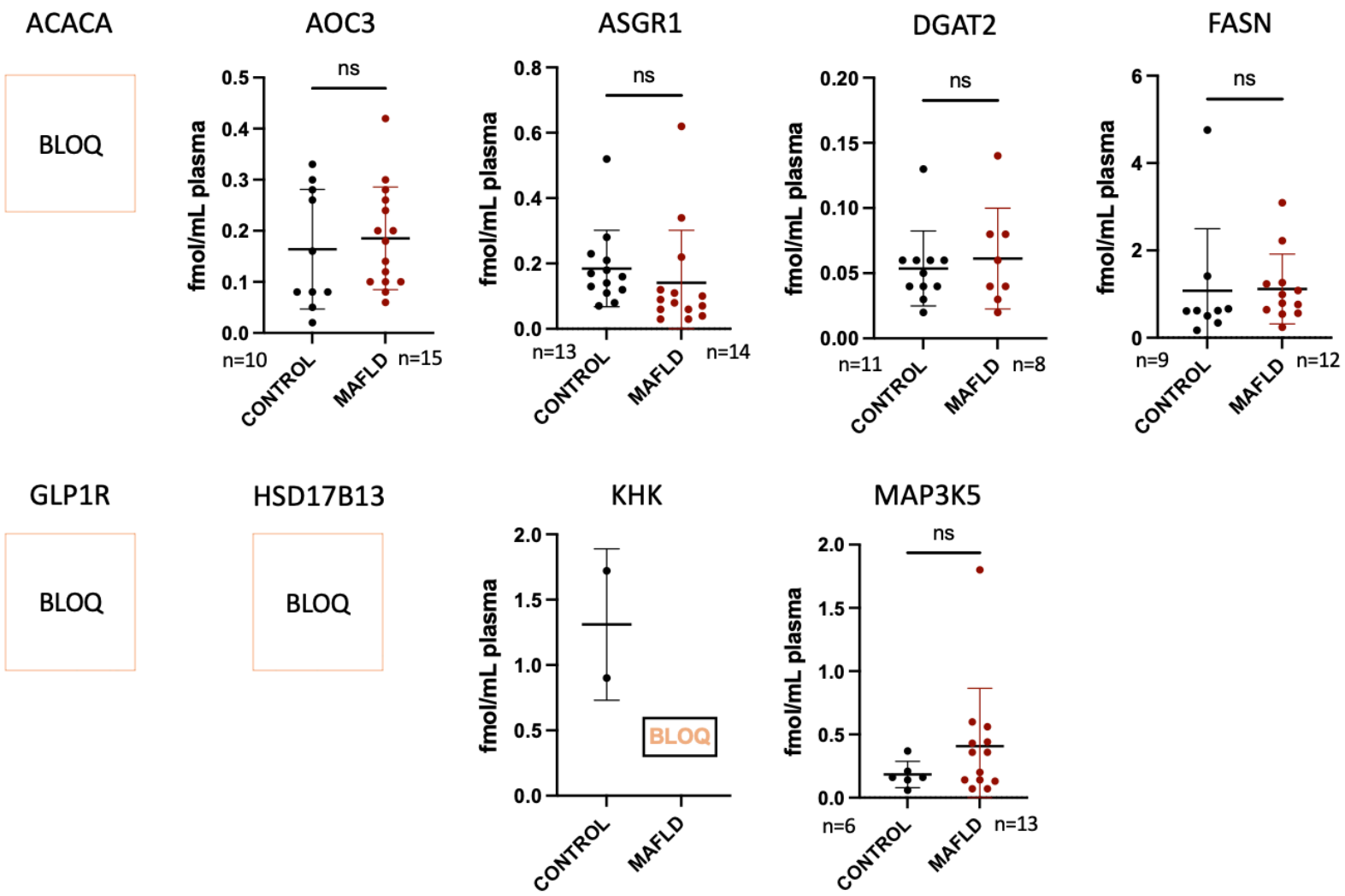

Figure 6.10 Concentration of MAFLD drug target proteins in ASGR1+ IP plasma EVs from control subjects and MAFLD patients.

N numbers for each target includes samples for which marker abundance was ≥ LLOQ. Data presented as mean ± SD and compared using unpaired t-tests. ns: not significant. BLOQ: below limit of quantification.

Discussion

The aim of this exploratory analysis was to assess the feasibility of quantifying MAFLD drug target proteins in liver derived plasma EVs using a new SEC protocol for the global EV isolation. Despite successfully quantifying targets in liver EVs recovered from tissue and in association with ASGR1, there was limited capacity to quantify these targets in the circulating EVs of the present samples. A persistent challenge for biomarker development in EV research is exemplified by the variations in performance of EV isolation methods used in this study. Even within the same technology, differences in the composition of the columns can influence the relative enrichment of EV populations, contaminant profile and repeatability. When using ready-made columns, there is an inherent reliance on the manufacturer for consistency within and between batches. Ongoing commercial development has ultimately lead to the discontinuation of existing SEC columns or the specific resin constituents, and release of new products with a trend towards lower exclusion limits of the resin (Kaddour et al., 2021). As qEV70 (Legacy) SEC columns became unavailable, an alternative column was introduced from a new supplier to isolate EVs from plasma.

Shifting to the new column revealed differences in EV marker abundance, with STEMCELL columns potentially proving more effective in preparing global isolates that express the typical EV markers. Importantly, STEMCELL does not report the exclusion limit of the resin used in their columns, while the exclusion limit of qEV was 70 nm. In comparisons with the 35 nm qEV column, previously reported in Chapter 2, greater abundance of EV markers and soluble protein contamination was observed with the lower exclusion limit. Taken together, these observations suggest a greater recovery of smaller sized EVs as well as a different contaminant profile using STEMCELL columns. While there were no significant differences in particle analysis, there is an inherent caveat to using NTA for accurate concentration and size determination. Particularly in polydisperse samples like EV isolates, the diffraction limit will impair detection of particles less than 50 nm (Bachurski et al., 2019).

Notably, particle concentration and the abundance of several EV markers were found to be greater in MAFLD patients compared to controls, which contrasts with an earlier study in this thesis

(Chapter 4). The possibility that the new SEC columns recover more EVs or enrich for different subpopulations may explain this discrepancy, emphasising the challenge of comparing results between studies without standard isolation methods.

The goal of quantifying changes in the protein targets in clinical samples to evaluate treatment response, requires the assay to have sufficient sensitivity and dynamic range to cover expected variability between subjects as well as changes in abundance within subjects. Plasma is a highly complex matrix from which to isolate EVs and detect low abundance proteins. The chromatographic resolution of target peaks may be compromised in the presence of significant matrix contamination and suppression of ion detection in the MS source is enhanced particularly when co-eluting contaminants are highly hydrophobic. Given the abundance of particles in the size range of LDLs observed by TEM and limitation of SEC to remove other lipoprotein species in the EV size range, these contaminants represent a significant barrier to the successful quantification of low abundance targets in plasma EVs. Improvements to the initial global EV isolation will thus be crucial to ensure the adequate recovery of target EV subpopulations containing markers of interest while minimising the impact of co-isolated matrix contaminants that may cause signal suppression in LCMS analyses.

Although the lack of paired blood and tissue samples from disease patients is a key limitation of this work, the presented findings highlight the need for additional optimisation of SEC global EV isolation to enhance the quantitative analysis of potential pharmacodynamic markers. Further studies using matched tissue will also allow for validation of the quantitative relationship between changes in tissue and circulating EVs. For the assessment of changes in EV biomarkers over time, ensuring consistency in EV recovery and purity will be a vital consideration for isolation methods in longitudinal study designs.

CHAPTER 7
MAJOR CONCLUSIONS AND FUTURE DIRECTIONS

Major Conclusions

Overall, this thesis addresses several limitations of current techniques for the collection and analysis of extracellular vesicles, which presently reinforce the barriers to the clinical translation of EV liquid biopsy. EVs are an attractive source of biomarkers to provide similar insights to solid organ biopsy through a much less invasive collection procedure. However, the key components of the fundamental workflow for EV analysis in clinical samples, including blood collection and processing, isolation of EVs from the biofluid, characterisation & reporting, and downstream analysis of molecular cargo, are each accompanied by unique challenges which ultimately play an important role in determining the quality of the sample and outcome of analysis. Characteristics of the sample donors introduce pre-analytical factors that influence the abundance and protein cargo of circulating EVs under basal physiological conditions and may include variation related to diurnal, prandial or sex differences. Since an understanding of basal variability is a fundamental consideration in the interpretation of disease-associated changes, EV characterisation and targeted LCMS proteomic analysis were used to define normal ranges for EV concentration and size distribution and the abundance of global EV and liver specific EV markers. Interestingly, ASGR1 abundance increased in samples collected in the afternoon, suggesting that the relative contribution of the liver to the circulating EV pool changed within the day and presenting an important consideration for study protocols that sample liver-derived EV biomarkers from the blood.

The initial isolation of global EVs from the biofluid was done predominantly using size exclusion chromatography, which is relatively effective at resolving EV sized particles from the smaller soluble proteins. Nonetheless, the complexity of biofluids poses a challenge to EV isolation, since sources such as plasma are replete with several classes of non-vesicular particles, especially soluble proteins and lipoprotein particles, at orders of magnitude greater abundance than and sharing many of the biophysical properties of EVs. As different isolation methods applied to biofluids will result in varied EV recovery and purity, recommendations for sample characterisation and quality

assessment include the enrichment of EV-associated proteins and depletion of contaminant protein markers. Here, the development and validation of a targeted LCMS method allowed a panel of markers to be quantified in EVs isolated from serum and plasma and from patients with MAFLD. The requisition of small volumes of starting material to achieve characterisation with capacity for multiplexed, high-throughput, absolute quantification provides an advantage for translation to clinical sample testing, given the often limited availability of sample to be used across multiple control experiments in addition to any primary analyses. Throughout this thesis, the development and application of MRM methods permitted the analysis of both markers of EVs or contaminants and EV-derived biomarkers of interest on the same platform using the same sample, offering the potential to integrate quality assessment or data normalisation.

While western blots were used as a benchmark in the development of the EV marker MRM method in Chapter 2, the MS-based technique was used thereafter for EV protein characterisation, supporting alignment of subsequent study design and reporting to best practice and MISEV recommendations. Data from all studies were also uploaded to EV-TRACK and obtained scores in or higher than the 95th percentile of all experiments on the same sample type (Van Deun et al., 2017) Recognising the broad utility to EV researchers for characterisation and reporting purposes, this work underpinned the invitation to provide recommendations for targeted mass spectrometry of EV proteins as a contributing author of the 2023 iteration of MISEV (Welsh et al., 2024).

The capacity for standard EV isolation methods to distinguish the vast heterogeneity of EV subpopulations in a biofluid is another key limitation affecting the specificity of EV derived biomarker analyses. Accordingly, the purity of isolation may be considered not only in the context of co-isolated matrix contaminants but also in the recovery of vesicles of particular origin containing the markers of interest. Advanced approaches to cell-type specific EV isolation thus provide the opportunity to enrich rare disease-associated cargo that may otherwise be obscured by a background of abundant impurities and irrelevant subpopulations of EVs. This thesis demonstrated a novel application of the two step protocol to enrich global circulating EVs for liver origin using immunoprecipitation against hepatocyte-specific surface protein ASGR1. The selective isolation of liver-specific EVs from patients with MAFLD at different stages of severity was shown to improve the analysis of miRNA with

diagnostic potential compared to total plasma RNA and global EVs. ASGR1+ EV miRNA expression increased with disease severity and accounted for a greater proportion of total plasma miRNA. These outcomes are in line with the reported changes in packaging and export of miRNA in EVs from hepatocytes in the disease state, justifying the additional purification steps for circulating RNA biomarker analysis.

While liver derived EVs in the blood are relatively rare, EVs isolated directly from liver tissue are an enriched population containing hepatic protein markers and can be used to investigate the profile in EVs relative to the tissue. A panel of markers involved in the interaction of drugs with the liver, including drug metabolising enzymes and molecular drug targets of investigational treatments for MAFLD, were developed for absolute quantification in liver tissue derived EVs (LT-EVs). Accounting for possible contribution from extra-hepatic EVs also present in the tissue, LT-EVs could report on tissue abundance of drug metabolising enzymes, supporting the capacity to define between subject variability in pharmacokinetic phenotype. This provides an additional layer of validation for previous work by our group that reported the use of circulating EVs to predict metabolic drug-drug interactions (DDIs) *in vivo*. Importantly, changes in DME abundance in liver-specific EVs represented the magnitude of DDIs perpetrated by weak-to-moderate and strong CYP inducers, which could obviate the need for probe substrate administration of traditional PK phenotyping methods in healthy volunteer trials. Further, patients with hepatic impairment due to conditions such as MAFLD may be more susceptible to toxicity associated with reduced DME abundance, so a minimally invasive EV liquid biopsy offers a tool to predict exposure and support precision dosing in these vulnerable populations. This thesis also aimed to expand the capability to track markers of a drug's pharmacodynamic (PD) profile *in vivo* within individuals. The finding that proteins involved in key disease pathways in MAFLD and identified as potential molecular targets for pharmacological treatment, can be quantified in liver tissue EVs, raises the possibility of tracking changes in response to treatment or to predict patients' susceptibility to particular targeted therapies.

Although the final analysis exploring the feasibility of applying EVs for this purpose found a limited capacity to quantify MAFLD drug targets in circulating global and liver enriched EVs, the variable performance of SEC-based global EV isolation from plasma was highlighted as a possible

aspect of the workflow that requires further optimisation. Achieving robust quantification of these potential PD markers in circulating EVs will require greater rigour of global EV isolation methods from plasma, ensuring sufficient recovery of target EV populations and minimising co-isolation of interfering matrix components. Reproducibility will be particularly important for any longitudinal assessments of EV biomarkers to monitor changes and response to treatment within subjects over the course of a clinical trial.

Limitations and Future Directions

Optimising SEC for lipoprotein removal

SEC was employed for global EV isolation in this work based on several characteristics which favour subsequent immunoprecipitation and clinical translation. Specifically, it does not apply physical forces that could alter surface composition and is a simple benchtop method requiring no sophisticated equipment while also being amenable to upscaling and automation with the use of liquid handling robots. Commercially, developments in SEC resins have led to a trend in decreased exclusion limit and the discontinuation of those with higher exclusion limits (Monguió-Tortajada et al., 2019). Although resulting in increased recovery of EVs in reduced size ranges, this is accompanied by greater lipoprotein co-isolation (Van Deun et al., 2020).

Since the membranes of both lipoproteins and EVs are rich in phospholipids and these lipids act as a significant source of ion suppression in mass spectrometry, the increase in signal for EV contained protein markers in SEC isolates with a lower exclusion limit may be counteracted by enhanced matrix effects (Wang et al., 2023). Hence, in addition to the impact of abundant lipoprotein co-isolation, using SEC columns that recover more vesicles in a smaller size range may not necessarily improve biomarker detection if these smaller sized vesicles are less concentrated with the cargo of interest. To this point, the characterisation of circulating EVs in Chapter 5 found that STEMCELL SEC columns successfully enriched EV marker proteins in greater abundance than previously observed with qEV columns and were sensitive to the differences in both global and liver-

specific EV profile between MAFLD and control subjects. However, there was limited ability to detect and quantify liver derived protein markers in the EVs.

Although combining SEC with immunoprecipitation markedly depletes matrix contaminants, it remains important for the initial global isolation from plasma to achieve sufficient purity and yield of target EV subpopulations. As lipoproteins can interact with EV surfaces, their abundant co-isolation contributes to the density of the EV coronal layer which may obscure target epitopes and reduce the efficacy of immunoprecipitation (Hallal et al., 2022). Further work is required to optimise the isolation of EV subpopulations containing rare targets and subsequent LCMS detection and quantification. This will include exploring the performance of alternative SEC resins for EV recovery and removal of lipoproteins. Size based separation may also be combined with ion exchange to exploit differences in charge between the particle types. EV membrane components confer a greater negative charge than lipoproteins and several recent studies have demonstrated an improvement in purity without compromising EV yield. For example, ion exchange absorption was performed to capture EVs following SEC elution which depleted lipoproteins and improved the analysis of plasma EV cancer-associated proteome (Wang et al., 2023). Alternatively, columns can be set up to perform dual mode chromatography, containing a layer of cation exchange resin beneath the SEC resin, to achieve bi-dimensional separation in a single step (Ter-Ovanesyan et al., 2023, Van Deun et al., 2020).

Multi-omics of liver-specific EVs

The analyses of EV cargo reported in this thesis was limited to targeted techniques, including LC-MRM-MS and RT-qPCR. *A priori* selection of targets was based on established EV markers, previously reported biomarkers and changes in molecular pathways related to the disease for the purpose of addressing shortcomings in EV characterisation and to demonstrate the value of tissue-specific isolation from the blood. Targeted analyses typically provide enhanced sensitivity and absolute quantification and are ideal for translational biomarkers to convey specific, actionable information. However, there are several other classes of EV molecular cargo that may be informative

and untargeted analytical techniques offer a means to comprehensively interrogate disease-associated changes and molecular signatures.

Extending from the methodological advancements described in this thesis, there is opportunity to explore the capacity for circulating liver-specific EVs to convey total transcriptomic, metabolomic and proteomic information, as well as the distribution of post-translational and epigenetic modifications. Multi-omic analyses can deepen the understanding of disease processes in an unbiased manner to reveal new candidates for targeted biomarker development or deconvolute disease heterogeneity and define sub-phenotypes for predicting treatment outcomes. Given MAFLD is a complex and heterogenous disease that is poorly recapitulated by animal models, focussing the collection of this information to hepatically released EVs could reduce the reliance on solid tissue biopsy for systems biology and biomarker discovery in human studies with low invasiveness and access to longitudinal sample collection.

For example, gene expression analyses using liver tissue have been used to define molecular subtypes of NAFLD based on key dysregulated biological pathways (Liu et al., 2022, Hoang et al., 2019). By linking the dominant disease processes and related histological and clinical features with the mode of action of targeted therapeutics, this information paves the way for precision medicine strategies. However, owing to a range of post transcriptional regulatory processes, gene expression does not tend to corelate strongly with protein abundance (Vogel and Marcotte, 2012), which may favour proteomic analysis for a more dynamic representation of the activity of cellular pathways. Moreover, the profile of differential miRNA expression can be explored in EVs and integrated with mRNA interaction analysis to reflect the changes in translational regulation in MAFLD (Kim et al., 2021). Future studies may incorporate multiple sets of liver specific omics data to interrogate the diversity of EV molecular cargo and identify the most informative species or combinations thereof. These studies would benefit from matched patient liver tissue and plasma ASGR1+ EVs to determine the coverage achieved by liver derived EVs, possibility for detection in a liquid biopsy and association with histological and clinical characteristics of the donors.

Clinical Translation

Owing to the ability of EVs to convey timely, dynamic molecular information about organ function, impact of disease processes and changes in response to interventions, it is highly appealing to translate an EV biomarker strategy to clinical settings, particularly to assist in the development and trials of pharmacological treatments for MAFLD. While the findings in this thesis serve to advance the framework for utilising circulating EVs for these applications and contribute to evidence for their diagnostic, prognostic and predictive value, a number of obstacles to clinical translation remain. As highlighted in the final exploratory analysis, the variable performance of global EV isolation methods impact the recovery of target EV populations and contaminant profiles. While the work described in this thesis strongly indicates the promising future directions of EV biomarker research, it is distinctly supportive of the capacity for the SEC technology to provide reliable data within studies. Currently, the results from one study may not be comparable to those of another, even when the same technology is used for isolation. As products are discontinued or manufacturers report only vague characterisation of their proprietary materials, it is difficult to ensure the continuity of the product and consistency of results. The potential for inconsistencies between batches or products is especially problematic for the application to longitudinal analysis of clinical samples. Future development of materials and protocols in-house will help to enhance the level of control over critical aspects of the workflow with the aim to assure quality and reproducibility of EV analysis over time.

Clinical trials of novel MAFLD drugs that target certain molecular drivers of disease tend to result in low efficacy when tested in unselected populations (Ratziu and Friedman, 2020). Thus patient enrolment based on predictive biomarkers that reflect disease phenotype and susceptibility to particular treatments may be crucial to improving trial success rates for MAFLD. For any precision medicine strategies employed in clinical trials, like biomarker-driven patient enrolment for targeted therapeutics, it may also be necessary to translate this for post-approval clinical use. Essentially, if a new drug is proven effective in a subset of patients identified based on a molecular signature, these patients could also be routinely identifiable in the clinic for the ongoing optimal use of the drug. Future translation of an EV liquid biopsy test will require validation of cost-effectiveness and, if not

developed for an approved *in vitro* diagnostic, require adaptation for use in existing diagnostic workflows. At present, the methods described in this thesis are labour-intensive and will benefit from further work to increase throughput and reduce hands-on time, ideally automating the isolation of plasma EVs and liver specific capture.

Finally, clinical translation of EV biomarkers will require the establishment of a widely accepted data normalisation strategy. This remaining question presents a challenge to the comparison of data and reproducibility across laboratories and studies and invokes caution in interpretation of changes associated with a condition. In the context of EVs, the role of normalisation is to account for variability in EV number associated with between- or within- individual or condition-associated differences in vesicle secretion or technical variability in EV recovery. In this regard, the selected characteristic, or set thereof, will be associated with EVs and inform on the number released from a tissue of interest or reflect the sample yield. Given the inherent heterogeneity of EVs in biofluids, the diversity of molecular cargo that offer potential biomarkers and the persisting limitations of standard tools to analyse EV samples, these requirements are not necessarily straightforward to address. For instance, counting vesicles by NTA or other light scattering techniques is impacted by the small size and low refractive index of the particles, meaning a significant population, ostensibly containing important diagnostic information, fall below the diffraction limit. Further confounding is caused by the inability to distinguish non-vesicular contaminants in the size range. Similarly, normalising protein biomarker abundance to total protein in EV isolates from biofluids introduces error in that a large proportion of this is contributed by co-isolated soluble protein. Some choose to normalise RNA biomarkers to total RNA, but this requires the use of highly sensitive equipment such as a Bioanalyser or a Qubit to be reliable (Crossland et al., 2016). Thus, in the absence of reliable normalisation to EV number and differentiation from contaminants, the measurement of protein and RNA in EVs throughout this thesis was determined in constant amounts of sample input, i.e. the volume of serum or plasma. Recognising the ease of analysing equivalent volumes of a liquid sample type and lack of consensus surrogates for EV number, the MISEV guidelines support this approach for analysing EVs from blood (Théry et al., 2018).

The abundance of classical EV marker proteins, including tetraspanins, are commonly used to demonstrate the enrichment of EVs in isolates and characterise samples. The development of the EV marker LCMS panel in this thesis, offers the possibility to use the markers to adjust the abundance of EV protein targets detected on the same platform in the same sample. However, their proposed use for normalisation is complicated by the assumption that a given marker will exhibit constant expression per vesicle, whereas, tetraspanin expression has been shown to be heterogeneously distributed across single EVs in a sample (Mizenko et al., 2021). EV subpopulations exhibit variable positivity for individual markers or clusters of markers and may be devoid of common tetraspanin proteins altogether (Kowal et al., 2016). The role of these marker proteins in normalisation will depend on the capacity to account for total sample heterogeneity. In the context of bulk EV analysis, like LCMS, an appropriate combination of marker proteins could provide reasonable coverage of the varied subpopulations present in an isolate to calculate an average estimate of EV number. As an example, the data generated in Chapter 5 was used to explore the correlation between EV marker abundance and particle count in liver tissue EV isolates. A sum of the abundances of CD9, CANX and ASGR1 was produced to represent small, large and hepatocyte-derived EVs, respectively. This was positively correlated with particle yield with moderate strength (Pearson r = 0.69), suggesting possible utility as a surrogate for EV number in the sample. The strength of the relationship using the sum of the markers exceeded that off any one marker alone (CD9 r = 0.45; CANX r = 0.40; ASGR1 r = 0.17). Despite this, applying this normaliser did not significantly improve the correlations of liver-enriched protein targets in LT-EVs with the paired tissue.

When assessing biomarkers carried by specific tissue derived subpopulations, it will be important to normalise to the release from the origin of interest rather than non-specific fluctuations in EV number. Particularly as MAFLD is a multisystem disease with widespread inflammation, higher global circulating EVs may arise from immune cells, adipocytes or other affected extra-hepatic tissues. In future studies, it would be valuable to analyse matched liver tissue, liver tissue-isolated EVs, and ASGR1+ immunocaptured EVs from the blood of the same patient at the time of biopsy. This approach would help to determine the relationship between variations in tissue specific EV

release and the abundance of circulating levels of target markers. By establishing the true abundance of the biomarker in the tissue and the amount secreted in EVs, this information may be used as a reference point to assess the impact of various normalisation strategies on the accuracy of liquid biopsy results.

REFERENCE LIST

ABBATE, V., MARCANTONI, M., GIULIANTE, F., VECCHIO, F. M., GATTO, I., MELE, C., SAVIANO, A., ARCIUOLO, D., GAETANI, E., FERRARI, M. C., GIARRETTA, I., ARDITO, F., RICCARDI, L., NICOLETTI, A., PONZIANI, F. R., GASBARRINI, A., POMPILI, M. & POLA, R. 2017. HepPar1-Positive Circulating Microparticles Are Increased in Subjects with Hepatocellular Carcinoma and Predict Early Recurrence after Liver Resection. *International Journal of Molecular Sciences,* 18**,** 1043.

ACHOUR, B., AL-MAJDOUB, Z. M., GRYBOS-GAJNIAK, A., LEA, K., KILFORD, P., ZHANG, M., KNIGHT, D., BARBER, J., SCHAGEMAN, J. & ROSTAMI-HODJEGAN, A. 2021. Liquid Biopsy Enables Quantification of the Abundance and Interindividual Variability of Hepatic Enzymes and Transporters. *Clinical Pharmacology & Therapeutics,* 109**,** 222-232.

ALMEIDA, P. H., MATIELO, C. E. L., CURVELO, L. A., ROCCO, R. A., FELGA, G., DELLA GUARDIA, B. & BOTEON, Y. L. 2021. Update on the management and treatment of viral hepatitis. *World J Gastroenterol,* 27**,** 3249-3261.

ANDO, Y. & JOU, J. H. 2021. Nonalcoholic Fatty Liver Disease and Recent Guideline Updates. *Clinical Liver Disease,* 17**,** 23-28.

ARBELAIZ, A., AZKARGORTA, M., KRAWCZYK, M., SANTOS-LASO, A., LAPITZ, A., PERUGORRIA, M. J., ERICE, O., GONZALEZ, E., JIMENEZ-AGÜERO, R., LACASTA, A., IBARRA, C., SANCHEZ-CAMPOS, A., JIMENO, J. P., LAMMERT, F., MILKIEWICZ, P., MARZIONI, M., MACIAS, R. I. R., MARIN, J. J. G., PATEL, T., GORES, G. J., MARTINEZ, I., ELORTZA, F., FALCON-PEREZ, J. M., BUJANDA, L. & BANALES, J. M. 2017. Serum extracellular vesicles contain protein biomarkers for primary sclerosing cholangitis and cholangiocarcinoma. *Hepatology,* 66**,** 1125-1143.

AZPARREN-ANGULO, M., ROYO, F., GONZALEZ, E., LIEBANA, M., BROTONS, B., BERGANZA, J., GOÑI-DE-CERIO, F., MANICARDI, N., ABAD-JORDÀ, L., GRACIA-SANCHO, J. & FALCON-PEREZ, J. M. 2021. Extracellular vesicles in hepatology: Physiological role, involvement in pathogenesis, and therapeutic opportunities. *Pharmacology & Therapeutics,* 218**,** 107683.

BACHURSKI, D., SCHULDNER, M., NGUYEN, P. H., MALZ, A., REINERS, K. S., GRENZI, P. C., BABATZ, F., SCHAUSS, A. C., HANSEN, H. P., HALLEK, M. & POGGE VON STRANDMANN, E. 2019. Extracellular vesicle measurements with nanoparticle tracking analysis - An accuracy and repeatability comparison between NanoSight NS300 and ZetaView. *J Extracell Vesicles,* 8**,** 1596016.

BALA, S., PETRASEK, J., MUNDKUR, S., CATALANO, D., LEVIN, I., WARD, J., ALAO, H., KODYS, K. & SZABO, G. 2012. Circulating microRNAs in exosomes indicate hepatocyte injury and inflammation in alcoholic, drug-induced, and inflammatory liver diseases. *Hepatology (Baltimore, Md.),* 56**,** 1946-1957.

BALAPHAS, A., MEYER, J., SADOUL, R., MOREL, P., GONELLE-GISPERT, C. & BÜHLER, L. H. 2019. Extracellular vesicles: Future diagnostic and therapeutic tools for liver disease and regeneration. *Liver International,* 39**,** 1801-1817.

BENAYAS, B., MORALES, J., EGEA, C., ARMISÉN, P. & YÁÑEZ-MÓ, M. 2023. Optimization of extracellular vesicle isolation and their separation from lipoproteins by size exclusion chromatography. *Journal of Extracellular Biology,* 2**,** e100.

BHATTACHARYYA, S. N., HABERMACHER, R., MARTINE, U., CLOSS, E. I. & FILIPOWICZ, W. 2006. Relief of microRNA-Mediated Translational Repression in Human Cells Subjected to Stress. *Cell,* 125**,** 1111-1124.

BÖING, A. N., VAN DER POL, E., GROOTEMAAT, A. E., COUMANS, F. A. W., STURK, A. & NIEUWLAND, R. 2014. Single-step isolation of extracellular vesicles by size-exclusion chromatography. *Journal of extracellular vesicles,* 3**,** 10.3402/jev.v3.23430.

BOTHA, J., PUGSLEY, H. R. & HANDBERG, A. 2021. Conventional, High-Resolution and Imaging Flow Cytometry: Benchmarking Performance in Characterisation of Extracellular Vesicles. *Biomedicines,* 9**,** 124.

BOWALGAHA, K., ELLIOT, D. J., MACKENZIE, P. I., KNIGHTS, K. M., SWEDMARK, S. & MINERS, J. O. 2005. S-Naproxen and desmethylnaproxen glucuronidation by human liver microsomes

and recombinant human UDP-glucuronosyltransferases (UGT): role of UGT2B7 in the elimination of naproxen. *Br J Clin Pharmacol,* 60**,** 423-33.
BRAHMER, A., NEUBERGER, E., ESCH-HEISSER, L., HALLER, N., JORGENSEN, M. M., BAEK, R., MÖBIUS, W., SIMON, P. & KRÄMER-ALBERS, E.-M. 2019. Platelets, endothelial cells and leukocytes contribute to the exercise-triggered release of extracellular vesicles into the circulation. *Journal of Extracellular Vesicles,* 8**,** 1615820.
BRENNAN, K., MARTIN, K., FITZGERALD, S. P., O'SULLIVAN, J., WU, Y., BLANCO, A., RICHARDSON, C. & MC GEE, M. M. 2020. A comparison of methods for the isolation and separation of extracellular vesicles from protein and lipid particles in human serum. *Scientific Reports,* 10**,** 1039.
BRUNO, S., CHIABOTTO, G. & CAMUSSI, G. 2020. Extracellular Vesicles: A Therapeutic Option for Liver Fibrosis. *International journal of molecular sciences,* 21**,** 4255.
BUKONG, T. N., MOMEN-HERAVI, F., KODYS, K., BALA, S. & SZABO, G. 2014. Exosomes from hepatitis C infected patients transmit HCV infection and contain replication competent viral RNA in complex with Ago2-miR122-HSP90. *PLoS pathogens,* 10**,** e1004424-e1004424.
BUSCHMANN, D., KIRCHNER, B., HERMANN, S., MÄRTE, M., WURMSER, C., BRANDES, F., KOTSCHOTE, S., BONIN, M., STEINLEIN, O. K., PFAFFL, M. W., SCHELLING, G. & REITHMAIR, M. 2018. Evaluation of serum extracellular vesicle isolation methods for profiling miRNAs by next-generation sequencing. *Journal of extracellular vesicles,* 7**,** 1481321-1481321.
BUZZETTI, E., PINZANI, M. & TSOCHATZIS, E. A. 2016. The multiple-hit pathogenesis of non-alcoholic fatty liver disease (NAFLD). *Metabolism,* 65**,** 1038-1048.
CAI, S., CHENG, X., PAN, X. & LI, J. 2017. Emerging role of exosomes in liver physiology and pathology. *Hepatology Research,* 47**,** 194-203.
CARPINTERO-FERNÁNDEZ, P., FAFIÁN-LABORA, J. & O'LOGHLEN, A. 2017. Technical Advances to Study Extracellular Vesicles. *Frontiers in molecular biosciences,* 4**,** 79-79.
CASTOLDI, M., KORDES, C., SAWITZA, I. & HÄUSSINGER, D. 2016. Isolation and characterization of vesicular and non-vesicular microRNAs circulating in sera of partially hepatectomized rats. *Scientific Reports,* 6**,** 31869.
CERMELLI, S., RUGGIERI, A., MARRERO, J. A., IOANNOU, G. N. & BERETTA, L. 2011. Circulating MicroRNAs in Patients with Chronic Hepatitis C and Non-Alcoholic Fatty Liver Disease. *PLOS ONE,* 6**,** e23937.
CHARRIER, A., CHEN, R., CHEN, L., KEMPER, S., HATTORI, T., TAKIGAWA, M. & BRIGSTOCK, D. R. 2014. Exosomes mediate intercellular transfer of pro-fibrogenic connective tissue growth factor (CCN2) between hepatic stellate cells, the principal fibrotic cells in the liver. *Surgery,* 156**,** 548-555.
CHEN, C., DENG, Y., HU, X., REN, H., ZHU, J., FU, S., XIE, J. & PENG, Y. 2018a. miR-128-3p regulates 3T3-L1 adipogenesis and lipolysis by targeting Pparg and Sertad2. *Journal of Physiology and Biochemistry,* 74**,** 381-393.
CHEN, L., CHARRIER, A., ZHOU, Y., CHEN, R., YU, B., AGARWAL, K., TSUKAMOTO, H., LEE, L. J., PAULAITIS, M. E. & BRIGSTOCK, D. R. 2014. Epigenetic regulation of connective tissue growth factor by MicroRNA-214 delivery in exosomes from mouse or human hepatic stellate cells. *Hepatology,* 59**,** 1118-1129.
CHEN, L., CHEN, R., KEMPER, S., CHARRIER, A. & BRIGSTOCK, D. R. 2015. Suppression of fibrogenic signaling in hepatic stellate cells by Twist1-dependent microRNA-214 expression: Role of exosomes in horizontal transfer of Twist1. *American journal of physiology. Gastrointestinal and liver physiology,* 309**,** G491-G499.
CHEN, L., CHEN, R., KEMPER, S., CONG, M., YOU, H. & BRIGSTOCK, D. R. 2018b. Therapeutic effects of serum extracellular vesicles in liver fibrosis. *Journal of Extracellular Vesicles,* 7**,** 1461505.
CHEN, L., CHEN, R., VELAZQUEZ, V. M. & BRIGSTOCK, D. R. 2016. Fibrogenic Signaling Is Suppressed in Hepatic Stellate Cells through Targeting of Connective Tissue Growth Factor (CCN2) by Cellular or Exosomal MicroRNA-199a-5p. *The American journal of pathology,* 186**,** 2921-2933.
CHEVILLET, J. R., KANG, Q., RUF, I. K., BRIGGS, H. A., VOJTECH, L. N., HUGHES, S. M., CHENG, H. H., ARROYO, J. D., MEREDITH, E. K., GALLICHOTTE, E. N., POGOSOVA-AGADJANYAN, E. L., MORRISSEY, C., STIREWALT, D. L., HLADIK, F., YU, E. Y.,

HIGANO, C. S. & TEWARI, M. 2014. Quantitative and stoichiometric analysis of the microRNA content of exosomes. *Proceedings of the National Academy of Sciences of the United States of America,* 111**,** 14888-14893.
CHIRIACÒ, M. S., BIANCO, M., NIGRO, A., PRIMICERI, E., FERRARA, F., ROMANO, A., QUATTRINI, A., FURLAN, R., ARIMA, V. & MARUCCIO, G. 2018. Lab-on-Chip for Exosomes and Microvesicles Detection and Characterization. *Sensors,* 18.
COLELLA, A. D., CHEGENII, N., TEA, M. N., GIBBINS, I. L., WILLIAMS, K. A. & CHATAWAY, T. K. 2012. Comparison of Stain-Free gels with traditional immunoblot loading control methodology. *Analytical Biochemistry,* 430**,** 108-110.
CONDE-VANCELLS, J., RODRIGUEZ-SUAREZ, E., EMBADE, N., GIL, D., MATTHIESEN, R., VALLE, M., ELORTZA, F., LU, S. C., MATO, J. M. & FALCON-PEREZ, J. M. 2008. Characterization and Comprehensive Proteome Profiling of Exosomes Secreted by Hepatocytes. *Journal of Proteome Research,* 7**,** 5157-5166.
CONTRERAS, H., ALARCÓN-ZAPATA, P., NOVA-LAMPERTI, E., ORMAZABAL, V., VARAS-GODOY, M., SALOMON, C. & ZUNIGA, F. A. 2023. Comparative study of size exclusion chromatography for isolation of small extracellular vesicle from cell-conditioned media, plasma, urine, and saliva. *Frontiers in Nanotechnology,* 5.
CRESCITELLI, R., LÄSSER, C. & LÖTVALL, J. 2021. Isolation and characterization of extracellular vesicle subpopulations from tissues. *Nature Protocols,* 16**,** 1548-1580.
CREWE, C. & SCHERER, P. E. 2022. Intercellular and interorgan crosstalk through adipocyte extracellular vesicles. *Rev Endocr Metab Disord,* 23**,** 61-69.
CROSSLAND, R. E., NORDEN, J., BIBBY, L. A., DAVIS, J. & DICKINSON, A. M. 2016. Evaluation of optimal extracellular vesicle small RNA isolation and qRT-PCR normalisation for serum and urine. *Journal of Immunological Methods,* 429**,** 39-49.
CUI, Y., XU, H.-F., LIU, M.-Y., XU, Y.-J., HE, J.-C., ZHOU, Y. & CANG, S.-D. 2019. Mechanism of exosomal microRNA-224 in development of hepatocellular carcinoma and its diagnostic and prognostic value. *World journal of gastroenterology,* 25**,** 1890-1898.
CUSI, K., CHANG, Z., HARRISON, S., LOMONACO, R., BRIL, F., ORSAK, B., ORTIZ-LOPEZ, C., HECHT, J., FELDSTEIN, A. E., WEBB, A., LOUDEN, C., GOROS, M. & TIO, F. 2014. Limited value of plasma cytokeratin-18 as a biomarker for NASH and fibrosis in patients with non-alcoholic fatty liver disease. *Journal of Hepatology,* 60**,** 167-174.
DANIELSON, K. M., ESTANISLAU, J., TIGGES, J., TOXAVIDIS, V., CAMACHO, V., FELTON, E. J., KHOORY, J., KREIMER, S., IVANOV, A. R., MANTEL, P. Y., JONES, J., AKUTHOTA, P., DAS, S. & GHIRAN, I. 2016. Diurnal Variations of Circulating Extracellular Vesicles Measured by Nano Flow Cytometry. *PLoS One,* 11**,** e0144678.
DASGUPTA, D., NAKAO, Y., MAUER, A. S., THOMPSON, J. M., SEHRAWAT, T. S., LIAO, C.-Y., KRISHNAN, A., LUCIEN, F., GUO, Q., LIU, M., XUE, F., FUKUSHIMA, M., KATSUMI, T., BANSAL, A., PANDEY, M. K., MAIERS, J. L., DEGRADO, T., IBRAHIM, S. H., REVZIN, A., PAVELKO, K. D., BARRY, M. A., KAUFMAN, R. J. & MALHI, H. 2020. IRE1A Stimulates Hepatocyte-Derived Extracellular Vesicles That Promote Inflammation in Mice With Steatohepatitis. *Gastroenterology,* 159**,** 1487-1503.e17.
DE JONG, O. G., VERHAAR, M. C., CHEN, Y., VADER, P., GREMMELS, H., POSTHUMA, G., SCHIFFELERS, R. M., GUCEK, M. & VAN BALKOM, B. W. M. 2012. Cellular stress conditions are reflected in the protein and RNA content of endothelial cell-derived exosomes. *Journal of Extracellular Vesicles,* 1**,** 18396.
DENG, L., JIANG, W., WANG, X., MERZ, A., HIET, M.-S., CHEN, Y., PAN, X., JIU, Y., YANG, Y., YU, B., HE, Y., TU, Z., NIU, J., BARTENSCHLAGER, R. & LONG, G. 2019. Syntenin regulates hepatitis C virus sensitivity to neutralizing antibody by promoting E2 secretion through exosomes. *Journal of Hepatology,* 71**,** 52-61.
DENHAM, J. & SPENCER, S. J. 2020. Emerging roles of extracellular vesicles in the intercellular communication for exercise-induced adaptations. *American Journal of Physiology-Endocrinology and Metabolism,* 319**,** E320-E329.
DEVHARE, P. B., SASAKI, R., SHRIVASTAVA, S., DI BISCEGLIE, A. M., RAY, R. & RAY, R. B. 2017. Exosome-Mediated Intercellular Communication between Hepatitis C Virus-Infected Hepatocytes and Hepatic Stellate Cells. *Journal of virology,* 91**,** e02225-16.

DONGIOVANNI, P., MERONI, M., LONGO, M., FARGION, S. & FRACANZANI, A. L. 2018. miRNA Signature in NAFLD: A Turning Point for a Non-Invasive Diagnosis. *International journal of molecular sciences,* 19**,** 3966.

DUFOUR, J.-F., ANSTEE, Q. M., BUGIANESI, E., HARRISON, S., LOOMBA, R., PARADIS, V., TILG, H., WONG, V. W.-S. & ZELBER-SAGI, S. 2022. Current therapies and new developments in NASH. *Gut,* 71**,** 2123.

EGUCHI, A., LAZARO, R. G., WANG, J., KIM, J., POVERO, D., WILLLIAMS, B., HO, S. B., STÄRKEL, P., SCHNABL, B., OHNO-MACHADO, L., TSUKAMOTO, H. & FELDSTEIN, A. E. 2017. Extracellular vesicles released by hepatocytes from gastric infusion model of alcoholic liver disease contain a MicroRNA barcode that can be detected in blood. *Hepatology,* 65**,** 475-490.

EGUCHI, A., YAN, R., PAN, S. Q., WU, R., KIM, J., CHEN, Y., ANSONG, C., SMITH, R. D., TEMPAKU, M., OHNO-MACHADO, L., TAKEI, Y., FELDSTEIN, A. E. & TSUKAMOTO, H. 2020. Comprehensive characterization of hepatocyte-derived extracellular vesicles identifies direct miRNA-based regulation of hepatic stellate cells and DAMP-based hepatic macrophage IL-1β and IL-17 upregulation in alcoholic hepatitis mice. *Journal of Molecular Medicine,* 98**,** 1021-1034.

ENDZELIŅŠ, E., BERGER, A., MELNE, V., BAJO-SANTOS, C., SOBOĻEVSKA, K., ĀBOLS, A., RODRIGUEZ, M., ŠANTARE, D., RUDŅICKIHA, A., LIETUVIETIS, V., LLORENTE, A. & LINĒ, A. 2017. Detection of circulating miRNAs: comparative analysis of extracellular vesicle-incorporated miRNAs and cell-free miRNAs in whole plasma of prostate cancer patients. *BMC Cancer,* 17**,** 730.

ESLAM, M., NEWSOME, P. N., SARIN, S. K., ANSTEE, Q. M., TARGHER, G., ROMERO-GOMEZ, M., ZELBER-SAGI, S., WAI-SUN WONG, V., DUFOUR, J.-F., SCHATTENBERG, J. M., KAWAGUCHI, T., ARRESE, M., VALENTI, L., SHIHA, G., TIRIBELLI, C., YKI-JÄRVINEN, H., FAN, J.-G., GRØNBÆK, H., YILMAZ, Y., CORTEZ-PINTO, H., OLIVEIRA, C. P., BEDOSSA, P., ADAMS, L. A., ZHENG, M.-H., FOUAD, Y., CHAN, W.-K., MENDEZ-SANCHEZ, N., AHN, S. H., CASTERA, L., BUGIANESI, E., RATZIU, V. & GEORGE, J. 2020a. A new definition for metabolic dysfunction-associated fatty liver disease: An international expert consensus statement. *Journal of Hepatology,* 73**,** 202-209.

ESLAM, M., SANYAL, A. J., GEORGE, J., SANYAL, A., NEUSCHWANDER-TETRI, B., TIRIBELLI, C., KLEINER, D. E., BRUNT, E., BUGIANESI, E., YKI-JÄRVINEN, H., GRØNBÆK, H., CORTEZ-PINTO, H., GEORGE, J., FAN, J., VALENTI, L., ABDELMALEK, M., ROMERO-GOMEZ, M., RINELLA, M., ARRESE, M., ESLAM, M., BEDOSSA, P., NEWSOME, P. N., ANSTEE, Q. M., JALAN, R., BATALLER, R., LOOMBA, R., SOOKOIAN, S., SARIN, S. K., HARRISON, S., KAWAGUCHI, T., WONG, V. W.-S., RATZIU, V., YILMAZ, Y. & YOUNOSSI, Z. 2020b. MAFLD: A Consensus-Driven Proposed Nomenclature for Metabolic Associated Fatty Liver Disease. *Gastroenterology,* 158**,** 1999-2014.e1.

FANG, T., LV, H., LV, G., LI, T., WANG, C., HAN, Q., YU, L., SU, B., GUO, L., HUANG, S., CAO, D., TANG, L., TANG, S., WU, M., YANG, W. & WANG, H. 2018. Tumor-derived exosomal miR-1247-3p induces cancer-associated fibroblast activation to foster lung metastasis of liver cancer. *Nature communications,* 9**,** 191-191.

FEKETE, S., KIZEKAI, L., SARISOZEN, Y. T., LAWRENCE, N., SHINER, S. & LAUBER, M. 2022. Investigating the secondary interactions of packing materials for size-exclusion chromatography of therapeutic proteins. *Journal of Chromatography A,* 1676**,** 463262.

FIANDACA, M. S., KAPOGIANNIS, D., MAPSTONE, M., BOXER, A., EITAN, E., SCHWARTZ, J. B., ABNER, E. L., PETERSEN, R. C., FEDEROFF, H. J., MILLER, B. L. & GOETZL, E. J. 2015. Identification of preclinical Alzheimer's disease by a profile of pathogenic proteins in neurally derived blood exosomes: A case-control study. *Alzheimers Dement,* 11**,** 600-7.e1.

GÁMEZ-VALERO, A., MONGUIÓ-TORTAJADA, M., CARRERAS-PLANELLA, L., FRANQUESA, M. L., BEYER, K. & BORRÀS, F. E. 2016. Size-Exclusion Chromatography-based isolation minimally alters Extracellular Vesicles' characteristics compared to precipitating agents. *Scientific Reports,* 6**,** 33641.

GARCIA-MARTINEZ, I., ALEN, R., RADA, P. & VALVERDE, A. M. 2020. Insights Into Extracellular Vesicles as Biomarker of NAFLD Pathogenesis. *Frontiers in Medicine,* 7.

GARCIA-MARTINEZ, I., SANTORO, N., CHEN, Y., HOQUE, R., OUYANG, X., CAPRIO, S., SHLOMCHIK, M. J., COFFMAN, R. L., CANDIA, A. & MEHAL, W. Z. 2016. Hepatocyte

mitochondrial DNA drives nonalcoholic steatohepatitis by activation of TLR9. *The Journal of clinical investigation,* 126**,** 859-864.
GERTH, K., KODIDELA, S., MAHON, M., HAQUE, S., VERMA, N. & KUMAR, S. 2019. Circulating Extracellular Vesicles Containing Xenobiotic Metabolizing CYP Enzymes and Their Potential Roles in Extrahepatic Cells Via Cell–Cell Interactions. *International Journal of Molecular Sciences,* 20.
GHO, Y. S. & LEE, C. 2017. Emergent properties of extracellular vesicles: a holistic approach to decode the complexity of intercellular communication networks. *Molecular BioSystems,* 13**,** 1291-1296.
GIUGLIANO, S., KRISS, M., GOLDEN-MASON, L., DOBRINSKIKH, E., STONE, A. E. L., SOTO-GUTIERREZ, A., MITCHELL, A., KHETANI, S. R., YAMANE, D., STODDARD, M., LI, H., SHAW, G. M., EDWARDS, M. G., LEMON, S. M., GALE, M., JR., SHAH, V. H. & ROSEN, H. R. 2015. Hepatitis C virus infection induces autocrine interferon signaling by human liver endothelial cells and release of exosomes, which inhibits viral replication. *Gastroenterology,* 148**,** 392-402.e13.
GJORGJIEVA, M., SOBOLEWSKI, C., DOLICKA, D., CORREIA DE SOUSA, M. & FOTI, M. 2019. miRNAs and NAFLD: from pathophysiology to therapy. *Gut,* 68**,** 2065.
GOETZL, E. J., KAPOGIANNIS, D., SCHWARTZ, J. B., LOBACH, I. V., GOETZL, L., ABNER, E. L., JICHA, G. A., KARYDAS, A. M., BOXER, A. & MILLER, B. L. 2016. Decreased synaptic proteins in neuronal exosomes of frontotemporal dementia and Alzheimer's disease. *FASEB journal : official publication of the Federation of American Societies for Experimental Biology,* 30**,** 4141-4148.
GOETZL, E. J., NOGUERAS-ORTIZ, C., MUSTAPIC, M., MULLINS, R. J., ABNER, E. L., SCHWARTZ, J. B. & KAPOGIANNIS, D. 2019. Deficient neurotrophic factors of CSPG4-type neural cell exosomes in Alzheimer disease. *FASEB journal : official publication of the Federation of American Societies for Experimental Biology,* 33**,** 231-238.
GOETZL, E. J., SCHWARTZ, J. B., MUSTAPIC, M., LOBACH, I. V., DANEMAN, R., ABNER, E. L. & JICHA, G. A. 2017. Altered cargo proteins of human plasma endothelial cell-derived exosomes in atherosclerotic cerebrovascular disease. *Faseb j,* 31**,** 3689-3694.
GOTANDA, K., HIROTA, T., SAITO, J., FUKAE, M., EGASHIRA, Y., IZUMI, N., DEGUCHI, M., KIMURA, M., MATSUKI, S., IRIE, S. & IEIRI, I. 2016. Circulating intestine-derived exosomal miR-328 in plasma, a possible biomarker for estimating BCRP function in the human intestines. *Scientific Reports,* 6**,** 32299.
GREENING, D. W. & SIMPSON, R. J. 2018. Understanding extracellular vesicle diversity – current status. *Expert Review of Proteomics***,** null-null.
GREENING, D. W., XU, R., GOPAL, S. K., RAI, A. & SIMPSON, R. J. 2017. Proteomic insights into extracellular vesicle biology – defining exosomes and shed microvesicles. *Expert Review of Proteomics,* 14**,** 69-95.
GUSTAFSON, C. M., SHEPHERD, A. J., MILLER, V. M. & JAYACHANDRAN, M. 2015. Age- and sex-specific differences in blood-borne microvesicles from apparently healthy humans. *Biology of Sex Differences,* 6**,** 10.
HALLAL, S., TŰZESI, Á., GRAU, G. E., BUCKLAND, M. E. & ALEXANDER, K. L. 2022. Understanding the extracellular vesicle surface for clinical molecular biology. *J Extracell Vesicles,* 11**,** e12260.
HARDY, T., OAKLEY, F., ANSTEE, Q. M. & DAY, C. P. 2016. Nonalcoholic Fatty Liver Disease: Pathogenesis and Disease Spectrum. *Annual Review of Pathology: Mechanisms of Disease,* 11**,** 451-496.
HE, M., QIN, H., POON, T. C. W., SZE, S.-C., DING, X., CO, N. N., NGAI, S.-M., CHAN, T.-F. & WONG, N. 2015. Hepatocellular carcinoma-derived exosomes promote motility of immortalized hepatocyte through transfer of oncogenic proteins and RNAs. *Carcinogenesis,* 36**,** 1008-1018.
HE, X., YU, J., XIONG, L., LIU, Y., FAN, L., LI, Y., CHEN, B., CHEN, J. & XU, X. 2019. Exosomes derived from liver cancer cells reprogram biological behaviors of LO2 cells by transferring Linc-ROR. *Gene,* 719**,** 144044.
HERNÁNDEZ, A., ARAB, J. P., REYES, D., LAPITZ, A., MOSHAGE, H., BAÑALES, J. M. & ARRESE, M. 2020. Extracellular Vesicles in NAFLD/ALD: From Pathobiology to Therapy. *Cells,* 9**,** 817.

HIRSOVA, P., IBRAHIM, S. H., KRISHNAN, A., VERMA, V. K., BRONK, S. F., WERNEBURG, N. W., CHARLTON, M. R., SHAH, V. H., MALHI, H. & GORES, G. J. 2016a. Lipid-Induced Signaling Causes Release of Inflammatory Extracellular Vesicles From Hepatocytes. *Gastroenterology,* 150**,** 956-967.

HIRSOVA, P., IBRAHIM, S. H., VERMA, V. K., MORTON, L. A., SHAH, V. H., LARUSSO, N. F., GORES, G. J. & MALHI, H. 2016b. Extracellular vesicles in liver pathobiology: Small particles with big impact. *Hepatology,* 64**,** 2219-2233.

HOANG, S. A., OSEINI, A., FEAVER, R. E., COLE, B. K., ASGHARPOUR, A., VINCENT, R., SIDDIQUI, M., LAWSON, M. J., DAY, N. C., TAYLOR, J. M., WAMHOFF, B. R., MIRSHAHI, F., CONTOS, M. J., IDOWU, M. & SANYAL, A. J. 2019. Gene Expression Predicts Histological Severity and Reveals Distinct Molecular Profiles of Nonalcoholic Fatty Liver Disease. *Scientific Reports,* 9**,** 12541.

HOFMANN, L., LUDWIG, S., SCHULER, P. J., HOFFMANN, T. K., BRUNNER, C. & THEODORAKI, M.-N. 2020. The Potential of CD16 on Plasma-Derived Exosomes as a Liquid Biomarker in Head and Neck Cancer. *International Journal of Molecular Sciences,* 21.

HUANG, C. Y., HUANG, X. P., ZHU, J. Y., CHEN, Z. G., LI, X. J., ZHANG, X. H., HUANG, S., HE, J. B., LIAN, F., ZHAO, Y. N. & WU, G. B. 2015. miR-128-3p suppresses hepatocellular carcinoma proliferation by regulating PIK3R1 and is correlated with the prognosis of HCC patients. *Oncol Rep,* 33**,** 2889-98.

IBRAHIM, S. H., GORES, G. J., HIRSOVA, P., KIRBY, M., MILES, L., JAESCHKE, A. & KOHLI, R. 2014. Mixed lineage kinase 3 deficient mice are protected against the high fat high carbohydrate diet-induced steatohepatitis. *Liver International,* 34**,** 427-437.

IBRAHIM, S. H., HIRSOVA, P. & GORES, G. J. 2018. Non-alcoholic steatohepatitis pathogenesis: sublethal hepatocyte injury as a driver of liver inflammation. *Gut,* 67**,** 963-972.

IBRAHIM, S. H., HIRSOVA, P., TOMITA, K., BRONK, S. F., WERNEBURG, N. W., HARRISON, S. A., GOODFELLOW, V. S., MALHI, H. & GORES, G. J. 2016. Mixed lineage kinase 3 mediates release of C-X-C motif ligand 10-bearing chemotactic extracellular vesicles from lipotoxic hepatocytes. *Hepatology (Baltimore, Md.),* 63**,** 731-744.

JAMALY, S., RAMBERG, C., OLSEN, R., LATYSHEVA, N., WEBSTER, P., SOVERSHAEV, T., BRÆKKAN, S. K. & HANSEN, J.-B. 2018. Impact of preanalytical conditions on plasma concentration and size distribution of extracellular vesicles using Nanoparticle Tracking Analysis. *Scientific Reports,* 8**,** 17216.

JAMWAL, R. & BARLOCK, B. J. 2020. Nonalcoholic Fatty Liver Disease (NAFLD) and Hepatic Cytochrome P450 (CYP) Enzymes. *Pharmaceuticals,* 13.

JAYACHANDRAN, M., LUGO, G., HEILING, H., MILLER, V. M., RULE, A. D. & LIESKE, J. C. 2015. Extracellular vesicles in urine of women with but not without kidney stones manifest patterns similar to men: a case control study. *Biology of sex differences,* 6**,** 2-2.

JEPPESEN, D. K., FENIX, A. M., FRANKLIN, J. L., HIGGINBOTHAM, J. N., ZHANG, Q., ZIMMERMAN, L. J., LIEBLER, D. C., PING, J., LIU, Q., EVANS, R., FISSELL, W. H., PATTON, J. G., ROME, L. H., BURNETTE, D. T. & COFFEY, R. J. 2019. Reassessment of Exosome Composition. *Cell,* 177**,** 428-445.e18.

JIANG, H., QIAN, Y., SHEN, Z., LIU, Y., HE, Y., GAO, R., SHEN, M., CHEN, S., FU, Q. & YANG, T. 2021. Circulating microRNA-135a-3p in serum extracellular vesicles as a potential biological marker of non-alcoholic fatty liver disease. *Mol Med Rep,* 24**,** 498.

JONAS, W. & SCHÜRMANN, A. 2020. Genetic and epigenetic factors determining NAFLD risk. *Molecular Metabolism***,** 101111.

JULICH-HAERTEL, H., URBAN, S. K., KRAWCZYK, M., WILLMS, A., JANKOWSKI, K., PATKOWSKI, W., KRUK, B., KRASNODĘBSKI, M., LIGOCKA, J., SCHWAB, R., RICHARDSEN, I., SCHAAF, S., KLEIN, A., GEHLERT, S., SÄNGER, H., CASPER, M., BANALES, J. M., SCHUPPAN, D., MILKIEWICZ, P., LAMMERT, F., KRAWCZYK, M., LUKACS-KORNEK, V. & KORNEK, M. 2017. Cancer-associated circulating large extracellular vesicles in cholangiocarcinoma and hepatocellular carcinoma. *Journal of Hepatology,* 67**,** 282-292.

KADDOUR, H., TRANQUILLE, M. & OKEOMA, C. M. 2021. The Past, the Present, and the Future of the Size Exclusion Chromatography in Extracellular Vesicles Separation. *Viruses* [Online], 13.

KAKAZU, E., MAUER, A. S., YIN, M. & MALHI, H. 2016. Hepatocytes release ceramide-enriched pro-inflammatory extracellular vesicles in an IRE1α-dependent manner. *Journal of lipid research,* 57**,** 233-245.

KAKIZAKI, M., YAMAMOTO, Y., YABUTA, S., KUROSAKI, N., KAGAWA, T. & KOTANI, A. 2019. The immunological function of extracellular vesicles in hepatitis B virus-infected hepatocytes. *PLOS ONE,* 13**,** e0205886.

KANWAR, S. S., DUNLAY, C. J., SIMEONE, D. M. & NAGRATH, S. 2014. Microfluidic device (ExoChip) for on-chip isolation, quantification and characterization of circulating exosomes. *Lab on a Chip,* 14**,** 1891-1900.

KARIMI, N., CVJETKOVIC, A., JANG, S. C., CRESCITELLI, R., HOSSEINPOUR FEIZI, M. A., NIEUWLAND, R., LÖTVALL, J. & LÄSSER, C. 2018. Detailed analysis of the plasma extracellular vesicle proteome after separation from lipoproteins. *Cellular and Molecular Life Sciences,* 75**,** 2873-2886.

KEINICKE, H., SUN, G., MENTZEL, C. M. J., FREDHOLM, M., JOHN, L. M., ANDERSEN, B., RAUN, K. & KJAERGAARD, M. 2020. FGF21 regulates hepatic metabolic pathways to improve steatosis and inflammation. *Endocrine connections,* 9**,** 755-768.

KIM, T. H., LEE, Y., LEE, Y.-S., GIM, J.-A., KO, E., YIM, S. Y., JUNG, Y. K., KANG, S., KIM, M. Y., KIM, H., KIM, B.-H., KIM, J. H., SEO, Y. S., YIM, H. J., YEON, J. E., UM, S. H. & BYUN, K. S. 2021. Circulating miRNA is a useful diagnostic biomarker for nonalcoholic steatohepatitis in nonalcoholic fatty liver disease. *Scientific Reports,* 11**,** 14639.

KOECK, E. S., IORDANSKAIA, T., SEVILLA, S., FERRANTE, S. C., HUBAL, M. J., FREISHTAT, R. J. & NADLER, E. P. 2014. Adipocyte exosomes induce transforming growth factor beta pathway dysregulation in hepatocytes: a novel paradigm for obesity-related liver disease. *Journal of Surgical Research,* 192**,** 268-275.

KOGURE, T., LIN, W.-L., YAN, I. K., BRACONI, C. & PATEL, T. 2011. Intercellular nanovesicle-mediated microRNA transfer: a mechanism of environmental modulation of hepatocellular cancer cell growth. *Hepatology (Baltimore, Md.),* 54**,** 1237-1248.

KOLIHA, N., WIENCEK, Y., HEIDER, U., JÜNGST, C., KLADT, N., KRAUTHÄUSER, S., JOHNSTON, I. C. D., BOSIO, A., SCHAUSS, A. & WILD, S. 2016. A novel multiplex bead-based platform highlights the diversity of extracellular vesicles. *Journal of Extracellular Vesicles,* 5**,** 29975.

KONOSHENKO, M. Y., LEKCHNOV, E. A., VLASSOV, A. V. & LAKTIONOV, P. P. 2018. Isolation of Extracellular Vesicles: General Methodologies and Latest Trends. *BioMed research international,* 2018**,** 8545347-8545347.

KORNEK, M., LYNCH, M., MEHTA, S. H., LAI, M., EXLEY, M., AFDHAL, N. H. & SCHUPPAN, D. 2012. Circulating microparticles as disease-specific biomarkers of severity of inflammation in patients with hepatitis C or nonalcoholic steatohepatitis. *Gastroenterology,* 143**,** 448-458.

KORNEK, M., POPOV, Y., LIBERMANN, T. A., AFDHAL, N. H. & SCHUPPAN, D. 2011. Human T cell microparticles circulate in blood of hepatitis patients and induce fibrolytic activation of hepatic stellate cells. *Hepatology (Baltimore, Md.),* 53**,** 230-242.

KOSTALLARI, E., HIRSOVA, P., PRASNICKA, A., VERMA, V. K., YAQOOB, U., WONGJARUPONG, N., ROBERTS, L. R. & SHAH, V. H. 2018. Hepatic stellate cell–derived platelet-derived growth factor receptor-alpha-enriched extracellular vesicles promote liver fibrosis in mice through SHP2. *Hepatology,* 68**,** 333-348.

KOWAL, J., ARRAS, G., COLOMBO, M., JOUVE, M., MORATH, J. P., PRIMDAL-BENGTSON, B., DINGLI, F., LOEW, D., TKACH, M. & THÉRY, C. 2016. Proteomic comparison defines novel markers to characterize heterogeneous populations of extracellular vesicle subtypes. *Proceedings of the National Academy of Sciences,* 113**,** E968-E977.

KRANENDONK, M. E. G., VISSEREN, F. L. J., VAN HERWAARDEN, J. A., NOLTE-'T HOEN, E. N. M., DE JAGER, W., WAUBEN, M. H. M. & KALKHOVEN, E. 2014. Effect of extracellular vesicles of human adipose tissue on insulin signaling in liver and muscle cells. *Obesity,* 22**,** 2216-2223.

KREIMER, S., BELOV, A. M., GHIRAN, I., MURTHY, S. K., FRANK, D. A. & IVANOV, A. R. 2015. Mass-Spectrometry-Based Molecular Characterization of Extracellular Vesicles: Lipidomics and Proteomics. *Journal of Proteome Research,* 14**,** 2367-2384.

KROH, E. M., PARKIN, R. K., MITCHELL, P. S. & TEWARI, M. 2010. Analysis of circulating microRNA biomarkers in plasma and serum using quantitative reverse transcription-PCR (qRT-PCR). *Methods (San Diego, Calif.),* 50**,** 298-301.

KUGERATSKI, F. G., HODGE, K., LILLA, S., MCANDREWS, K. M., ZHOU, X., HWANG, R. F., ZANIVAN, S. & KALLURI, R. 2021. Quantitative proteomics identifies the core proteome of exosomes with syntenin-1 as the highest abundant protein and a putative universal biomarker. *Nature Cell Biology,* 23**,** 631-641.

KUMAR, S., SINHA, N., GERTH, K. A., RAHMAN, M. A., YALLAPU, M. M. & MIDDE, N. M. 2017. Specific packaging and circulation of cytochromes P450, especially 2E1 isozyme, in human plasma exosomes and their implications in cellular communications. *Biochemical and Biophysical Research Communications,* 491**,** 675-680.

LANE, R. E., KORBIE, D., TRAU, M. & HILL, M. M. 2019. Optimizing Size Exclusion Chromatography for Extracellular Vesicle Enrichment and Proteomic Analysis from Clinically Relevant Samples. *PROTEOMICS,* 19**,** 1800156.

LARSSEN, P., WIK, L., CZARNEWSKI, P., ELDH, M., LÖF, L., RONQUIST, K. G., DUBOIS, L., FREYHULT, E., GALLANT, C. J., OELRICH, J., LARSSON, A., RONQUIST, G., VILLABLANCA, E. J., LANDEGREN, U., GABRIELSSON, S. & KAMALI-MOGHADDAM, M. 2017. Tracing Cellular Origin of Human Exosomes Using Multiplex Proximity Extension Assays*. *Molecular & Cellular Proteomics,* 16**,** 502-511.

LEE, Y.-T., TRAN, B. V., WANG, J. J., LIANG, I. Y., YOU, S., ZHU, Y., AGOPIAN, V. G., TSENG, H.-R. & YANG, J. D. 2021. The Role of Extracellular Vesicles in Disease Progression and Detection of Hepatocellular Carcinoma. *Cancers,* 13.

LI, J., LIU, H., MAUER, A. S., LUCIEN, F., RAITER, A., BANDLA, H., MOUNAJJED, T., YIN, Z., GLASER, K. J., YIN, M. & MALHI, H. 2019. Characterization of Cellular Sources and Circulating Levels of Extracellular Vesicles in a Dietary Murine Model of Nonalcoholic Steatohepatitis. *Hepatol Commun,* 3**,** 1235-1249.

LI, X., CHEN, R., KEMPER, S. & BRIGSTOCK, D. R. 2020. Dynamic Changes in Function and Proteomic Composition of Extracellular Vesicles from Hepatic Stellate Cells during Cellular Activation. *Cells,* 9**,** 290.

LI, X., LIU, R., HUANG, Z., GURLEY, E. C., WANG, X., WANG, J., HE, H., YANG, H., LAI, G., ZHANG, L., BAJAJ, J. S., WHITE, M., PANDAK, W. M., HYLEMON, P. B. & ZHOU, H. 2018. Cholangiocyte-derived exosomal long noncoding RNA H19 promotes cholestatic liver injury in mouse and humans. *Hepatology (Baltimore, Md.),* 68**,** 599-615.

LIANG, K., LIU, F., FAN, J., SUN, D., LIU, C., LYON, C. J., BERNARD, D. W., LI, Y., YOKOI, K., KATZ, M. H., KOAY, E. J., ZHAO, Z. & HU, Y. 2017. Nanoplasmonic Quantification of Tumor-derived Extracellular Vesicles in Plasma Microsamples for Diagnosis and Treatment Monitoring. *Nature biomedical engineering,* 1**,** 0021.

LIANGSUPREE, T., MULTIA, E. & RIEKKOLA, M.-L. 2021. Modern isolation and separation techniques for extracellular vesicles. *Journal of Chromatography A,* 1636**,** 461773.

LIEBLER, D. C. & ZIMMERMAN, L. J. 2013. Targeted quantitation of proteins by mass spectrometry. *Biochemistry,* 52**,** 3797-3806.

LINDÉN, D. & ROMEO, S. 2023. Therapeutic opportunities for the treatment of NASH with genetically validated targets. *Journal of Hepatology*.

LIU, X.-L., PAN, Q., ZHANG, R.-N., SHEN, F., YAN, S.-Y., SUN, C., XU, Z.-J., CHEN, Y.-W. & FAN, J.-G. 2016. Disease-specific miR-34a as diagnostic marker of non-alcoholic steatohepatitis in a Chinese population. *World journal of gastroenterology,* 22**,** 9844-9852.

LIU, X. L., PAN, Q., CAO, H. X., XIN, F. Z., ZHAO, Z. H., YANG, R. X., ZENG, J., ZHOU, H. & FAN, J. G. 2020. Lipotoxic Hepatocyte-Derived Exosomal MicroRNA 192-5p Activates Macrophages Through Rictor/Akt/Forkhead Box Transcription Factor O1 Signaling in Nonalcoholic Fatty Liver Disease. *Hepatology,* 72**,** 454-469.

LIU, Z., LI, Y. & YU, C. 2022. Identification of the Non-Alcoholic Fatty Liver Disease Molecular Subtypes Associated With Clinical and Immunological Features via Bioinformatics Methods. *Frontiers in Immunology,* 13.

LUBEL, J. S., ROBERTS, S. K., STRASSER, S. I., THOMPSON, A. J., PHILIP, J., GOODWIN, M., CLARKE, S., CRAWFORD, D. H. G., LEVY, M. T. & SHACKEL, N. 2021. Australian recommendations for the management of hepatocellular carcinoma: a consensus statement. *Medical Journal of Australia,* 214**,** 475-483.

LUCCHETTI, D., BATTAGLIA, A., RICCIARDI-TENORE, C., COLELLA, F., PERELLI, L., DE MARIA, R., SCAMBIA, G., SGAMBATO, A. & FATTOROSSI, A. 2020. Measuring Extracellular Vesicles by Conventional Flow Cytometry: Dream or Reality? *Int J Mol Sci,* 21.

MA, J., CAO, H., RODRIGUES, R. M., XU, M., REN, T., HE, Y., HWANG, S., FENG, D., REN, R., YANG, P., LIANGPUNSAKUL, S., SUN, J. & GAO, B. 2020. Chronic-plus-binge alcohol intake induces production of proinflammatory mtDNA-enriched extracellular vesicles and steatohepatitis via ASK1/p38MAPKα-dependent mechanisms. *JCI insight,* 5**,** e136496.

MAKAROVA, J., TURCHINOVICH, A., SHKURNIKOV, M. & TONEVITSKY, A. 2021. Extracellular miRNAs and Cell-Cell Communication: Problems and Prospects. *Trends Biochem Sci*.

MALHI, H. 2019. Emerging role of extracellular vesicles in liver diseases. *American Journal of Physiology-Gastrointestinal and Liver Physiology,* 317**,** G739-G749.

MALHI, H., SEHRAWAT, T. S., ARAB, J. P., LIU, M., AMROLLAHI, P., WAN, M., FAN, J., NAKAO, Y., POSE, E., NAVARRO-CORCUERA, A., DASGUPTA, D., LIAO, C.-Y., HE, L., MAUER, A. S., AVITABILE, E., VENTURA-COTS, M., BATALLER, R. A., SANYAL, A. J., CHALASANI, N. P., HEIMBACH, J. K., WATT, K. D., GORES, G. J., GINES, P., KAMATH, P. S., SIMONETTO, D. A., HU, T. Y. & SHAH, V. H. 2021. Circulating Extracellular Vesicles Carrying Sphingolipid Cargo for the Diagnosis and Dynamic Risk Profiling of Alcoholic Hepatitis. *Hepatology,* 73**,** 571-585.

MANN, J., REEVES, H. L. & FELDSTEIN, A. E. 2018. Liquid biopsy for liver diseases. *Gut,* 67**,** 2204.

MARABITA, F., DE CANDIA, P., TORRI, A., TEGNÉR, J., ABRIGNANI, S. & ROSSI, R. L. 2016. Normalization of circulating microRNA expression data obtained by quantitative real-time RT-PCR. *Briefings in bioinformatics,* 17**,** 204-212.

MARRERO, J. A., KULIK, L. M., SIRLIN, C. B., ZHU, A. X., FINN, R. S., ABECASSIS, M. M., ROBERTS, L. R. & HEIMBACH, J. K. 2018. Diagnosis, Staging, and Management of Hepatocellular Carcinoma: 2018 Practice Guidance by the American Association for the Study of Liver Diseases. *Hepatology,* 68**,** 723-750.

MASTORIDIS, S., BERTOLINO, G. M., WHITEHOUSE, G., DAZZI, F., SANCHEZ-FUEYO, A. & MARTINEZ-LLORDELLA, M. 2018. Multiparametric Analysis of Circulating Exosomes and Other Small Extracellular Vesicles by Advanced Imaging Flow Cytometry. *Frontiers in Immunology,* 9.

MATEESCU, B., KOWAL, E. J. K., VAN BALKOM, B. W. M., BARTEL, S., BHATTACHARYYA, S. N., BUZÁS, E. I., BUCK, A. H., DE CANDIA, P., CHOW, F. W. N., DAS, S., DRIEDONKS, T. A. P., FERNÁNDEZ-MESSINA, L., HADERK, F., HILL, A. F., JONES, J. C., VAN KEUREN-JENSEN, K. R., LAI, C. P., LÄSSER, C., DI LIEGRO, I., LUNAVAT, T. R., LORENOWICZ, M. J., MAAS, S. L. N., MÄGER, I., MITTELBRUNN, M., MOMMA, S., MUKHERJEE, K., NAWAZ, M., PEGTEL, D. M., PFAFFL, M. W., SCHIFFELERS, R. M., TAHARA, H., THÉRY, C., TOSAR, J. P., WAUBEN, M. H. M., WITWER, K. W. & NOLTE-'T HOEN, E. N. M. 2017. Obstacles and opportunities in the functional analysis of extracellular vesicle RNA – an ISEV position paper. *Journal of Extracellular Vesicles,* 6**,** 1286095.

MATHIEU, M., MARTIN-JAULAR, L., LAVIEU, G. & THÉRY, C. 2019. Specificities of secretion and uptake of exosomes and other extracellular vesicles for cell-to-cell communication. *Nature Cell Biology,* 21**,** 9-17.

MATHIVANAN, S., FONSEKA, P., NEDEVA, C. & ATUKORALA, I. 2021. *New Frontiers: Extracellular Vesicles*, Springer International Publishing.

MATSUMOTO, A., TAKAHASHI, Y., CHANG, H.-Y., WU, Y.-W., YAMAMOTO, A., ISHIHAMA, Y. & TAKAKURA, Y. 2020. Blood concentrations of small extracellular vesicles are determined by a balance between abundant secretion and rapid clearance. *Journal of Extracellular Vesicles,* 9**,** 1696517.

MIR, B. & GOETTSCH, C. 2020. Extracellular Vesicles as Delivery Vehicles of Specific Cellular Cargo. *Cells,* 9.

MITCHELL, M. I., BEN-DOV, I. Z., LIU, C., YE, K., CHOW, K., KRAMER, Y., GANGADHARAN, A., PARK, S., FITZGERALD, S., RAMNAUTH, A., PERLIN, D. S., DONATO, M., BHOY, E., MANOUCHEHRI DOULABI, E., POULOS, M., KAMALI-MOGHADDAM, M. & LOUDIG, O. 2021. Extracellular Vesicle Capture by AnTibody of CHoice and Enzymatic Release (EV-CATCHER): A customizable purification assay designed for small-RNA biomarker identification and evaluation of circulating small-EVs. *Journal of Extracellular Vesicles,* 10**,** e12110.

MIZENKO, R. R., BROSTOFF, T., ROJALIN, T., KOSTER, H. J., SWINDELL, H. S., LEISEROWITZ, G. S., WANG, A. & CARNEY, R. P. 2021. Tetraspanins are unevenly distributed across single extracellular vesicles and bias sensitivity to multiplexed cancer biomarkers. *Journal of Nanobiotechnology,* 19**,** 250.

MIZUTANI, K., TERAZAWA, R., KAMEYAMA, K., KATO, T., HORIE, K., TSUCHIYA, T., SEIKE, K., EHARA, H., FUJITA, Y., KAWAKAMI, K., ITO, M. & DEGUCHI, T. 2014. Isolation of prostate cancer-related exosomes. *Anticancer Res,* 34**,** 3419-23.

MLECZKO, J. E., ROYO, F., SAMUELSON, I., CLOS-GARCIA, M., WILLIAMS, C., CABRERA, D., AZPARREN-ANGULO, M., GONZALEZ, E., GARCIA-VALLICROSA, C., CAROBBIO, S., RODRIGUEZ-CUENCA, S., AZKARGORTA, M., VAN LIEMPD, S., ELORTZA, F., VIDAL-PUIG, A., MORA, S. & FALCON-PEREZ, J. M. 2022. Extracellular vesicles released by steatotic hepatocytes alter adipocyte metabolism. *Journal of Extracellular Biology,* 1**,** e32.

MOMEN-HERAVI, F., BALA, S., KODYS, K. & SZABO, G. 2015. Exosomes derived from alcohol-treated hepatocytes horizontally transfer liver specific miRNA-122 and sensitize monocytes to LPS. *Scientific Reports,* 5**,** 9991.

MONGUIÓ-TORTAJADA, M., GÁLVEZ-MONTÓN, C., BAYES-GENIS, A., ROURA, S. & BORRÀS, F. E. 2019. Extracellular vesicle isolation methods: rising impact of size-exclusion chromatography. *Cellular and Molecular Life Sciences,* 76**,** 2369-2382.

MOON, A. M., SINGAL, A. G. & TAPPER, E. B. 2020. Contemporary Epidemiology of Chronic Liver Disease and Cirrhosis. *Clinical Gastroenterology and Hepatology,* 18**,** 2650-2666.

MØRK, M., NIELSEN, M. H., BÆK, R., JØRGENSEN, M. M., PEDERSEN, S. & KRISTENSEN, S. R. 2018. Postprandial Increase in Blood Plasma Levels of Tissue Factor-Bearing (and Other) Microvesicles Measured by Flow Cytometry: Fact or Artifact? *TH open : companion journal to thrombosis and haemostasis,* 2**,** e147-e157.

MØRK, M., PEDERSEN, S., BOTHA, J., LUND, S. M. & KRISTENSEN, S. R. 2016. Preanalytical, analytical, and biological variation of blood plasma submicron particle levels measured with nanoparticle tracking analysis and tunable resistive pulse sensing. *Scand J Clin Lab Invest,* 76**,** 349-60.

MUKHERJEE, K., GHOSHAL, B., GHOSH, S., CHAKRABARTY, Y., SHWETHA, S., DAS, S. & BHATTACHARYYA, S. N. 2016. Reversible HuR-microRNA binding controls extracellular export of miR-122 and augments stress response. *EMBO reports,* 17**,** 1184-1203.

MUSTAPIC, M., EITAN, E., WERNER, J. K., BERKOWITZ, S. T., LAZAROPOULOS, M. P., TRAN, J., GOETZL, E. J. & KAPOGIANNIS, D. 2017. Plasma Extracellular Vesicles Enriched for Neuronal Origin: A Potential Window into Brain Pathologic Processes. *Frontiers in Neuroscience,* 11.

NAKAO, Y., AMROLLAHI, P., PARTHASARATHY, G., MAUER, A. S., SEHRAWAT, T. S., VANDERBOOM, P., NAIR, K. S., NAKAO, K., ALLEN, A. M., HU, T. Y. & MALHI, H. 2021. Circulating extracellular vesicles are a biomarker for NAFLD resolution and response to weight loss surgery. *Nanomedicine: Nanotechnology, Biology and Medicine***,** 102430.

NEWMAN, L. A., FAHMY, A., SORICH, M. J., BEST, O. G., ROWLAND, A. & USECKAITE, Z. 2021. Importance of between and within Subject Variability in Extracellular Vesicle Abundance and Cargo when Performing Biomarker Analyses. *Cells,* 10**,** 485.

NEWMAN, L. A., MULLER, K. & ROWLAND, A. 2022a. Circulating cell-specific extracellular vesicles as biomarkers for the diagnosis and monitoring of chronic liver diseases. *Cellular and Molecular Life Sciences,* 79**,** 232.

NEWMAN, L. A., SORICH, M. J. & ROWLAND, A. 2020. Role of Extracellular Vesicles in the Pathophysiology, Diagnosis and Tracking of Non-Alcoholic Fatty Liver Disease. *Journal of Clinical Medicine,* 9**,** 2032.

NEWMAN, L. A., USECKAITE, Z., JOHNSON, J., SORICH, M. J., HOPKINS, A. M. & ROWLAND, A. 2022b. Selective Isolation of Liver-Derived Extracellular Vesicles Redefines Performance of miRNA Biomarkers for Non-Alcoholic Fatty Liver Disease. *Biomedicines,* 10**,** 195.

NEWMAN, L. A., USECKAITE, Z. & ROWLAND, A. 2022c. Addressing MISEV guidance using targeted LC-MS/MS: A method for the detection and quantification of extracellular vesicle-enriched and contaminant protein markers from blood. *Journal of Extracellular Biology,* 1**,** e56.

NEWMAN, L. A., USECKAITE, Z., WU, T., SORICH, M. J. & ROWLAND, A. 2023. Analysis of Extracellular Vesicle and Contaminant Markers in Blood Derivatives Using Multiple Reaction

Monitoring. *In:* GREENING, D. W. & SIMPSON, R. J. (eds.) *Serum/Plasma Proteomics: Methods and Protocols.* New York, NY: Springer US.
NGUYEN, A., WANG, T. & TURKO, I. V. 2021. Quantitative proteomic analysis for evaluating affinity isolation of extracellular vesicles. *Journal of Proteomics,* 249**,** 104359.
NIK MOHAMED KAMAL, N. N. S. B. & SHAHIDAN, W. N. S. 2020. Non-Exosomal and Exosomal Circulatory MicroRNAs: Which Are More Valid as Biomarkers? *Frontiers in Pharmacology,* 10.
NOETEL, A., ELFIMOVA, N., ALTMÜLLER, J., BECKER, C., BECKER, D., LAHR, W., NÜRNBERG, P., WASMUTH, H., TEUFEL, A., BÜTTNER, R., DIENES, H. P. & ODENTHAL, M. 2013. Next generation sequencing of the Ago2 interacting transcriptome identified chemokine family members as novel targets of neuronal microRNAs in hepatic stellate cells. *Journal of Hepatology,* 58**,** 335-341.
NOJIMA, H., FREEMAN, C. M., SCHUSTER, R. M., JAPTOK, L., KLEUSER, B., EDWARDS, M. J., GULBINS, E. & LENTSCH, A. B. 2016. Hepatocyte exosomes mediate liver repair and regeneration via sphingosine-1-phosphate. *Journal of hepatology,* 64**,** 60-68.
NOREN HOOTEN, N., MCFARLAND, M. H., FREEMAN, D. W., MODE, N. A., EZIKE, N., ZONDERMAN, A. B. & EVANS, M. K. 2019. Association of Extracellular Vesicle Protein Cargo with Race and Clinical Markers of Mortality. *Scientific Reports,* 9**,** 17582.
OGGERO, S., AUSTIN-WILLIAMS, S. & NORLING, L. V. 2019. The Contrasting Role of Extracellular Vesicles in Vascular Inflammation and Tissue Repair. *Frontiers in Pharmacology,* 10.
PALVIAINEN, M., SARASWAT, M., VARGA, Z., KITKA, D., NEUVONEN, M., PUHKA, M., JOENVÄÄRÄ, S., RENKONEN, R., NIEUWLAND, R., TAKATALO, M. & SILJANDER, P. R. M. 2020. Extracellular vesicles from human plasma and serum are carriers of extravesicular cargo—Implications for biomarker discovery. *PLOS ONE,* 15**,** e0236439.
PAN, J., ZHOU, C., ZHAO, X., HE, J., TIAN, H., SHEN, W., HAN, Y., CHEN, J., FANG, S., MENG, X., JIN, X. & GONG, Z. 2018. A two-miRNA signature (miR-33a-5p and miR-128-3p) in whole blood as potential biomarker for early diagnosis of lung cancer. *Scientific Reports,* 8**,** 16699.
PANAGOPOULOU, M. S., WARK, A. W., BIRCH, D. J. S. & GREGORY, C. D. 2020. Phenotypic analysis of extracellular vesicles: a review on the applications of fluorescence. *Journal of Extracellular Vesicles,* 9**,** 1710020.
PARK, J., GO, E.-B., OH, J. S., LEE, J. K. & LEE, S.-Y. 2021. Multiple-Cycle Polymeric Extracellular Vesicle Precipitation and Its Evaluation by Targeted Mass Spectrometry. *International Journal of Molecular Sciences,* 22.
PERUMPAIL, B. J., KHAN, M. A., YOO, E. R., CHOLANKERIL, G., KIM, D. & AHMED, A. 2017. Clinical epidemiology and disease burden of nonalcoholic fatty liver disease. *World journal of gastroenterology,* 23**,** 8263-8276.
PETTA, S., VANNI, E., BUGIANESI, E., DI MARCO, V., CAMMA, C., CABIBI, D., MEZZABOTTA, L. & CRAXI, A. 2015. The combination of liver stiffness measurement and NAFLD fibrosis score improves the noninvasive diagnostic accuracy for severe liver fibrosis in patients with nonalcoholic fatty liver disease. *Liver Int,* 35**,** 1566-73.
PIROLA, C. J., FERNÁNDEZ GIANOTTI, T., CASTAÑO, G. O., MALLARDI, P., SAN MARTINO, J., MORA GONZALEZ LOPEZ LEDESMA, M., FLICHMAN, D., MIRSHAHI, F., SANYAL, A. J. & SOOKOIAN, S. 2015. Circulating microRNA signature in non-alcoholic fatty liver disease: from serum non-coding RNAs to liver histology and disease pathogenesis. *Gut,* 64**,** 800-812.
POEL, D., BUFFART, T. E., OOSTERLING-JANSEN, J., VERHEUL, H. M. W. & VOORTMAN, J. 2018. Evaluation of several methodological challenges in circulating miRNA qPCR studies in patients with head and neck cancer. *Experimental & Molecular Medicine,* 50**,** e454-e454.
POVERO, D., EGUCHI, A., LI, H., JOHNSON, C. D., PAPOUCHADO, B. G., WREE, A., MESSER, K. & FELDSTEIN, A. E. 2014. Circulating extracellular vesicles with specific proteome and liver microRNAs are potential biomarkers for liver injury in experimental fatty liver disease. *PloS one,* 9**,** e113651-e113651.
POVERO, D., EGUCHI, A., NIESMAN, I. R., ANDRONIKOU, N., DE MOLLERAT DU JEU, X., MULYA, A., BERK, M., LAZIC, M., THAPALIYA, S., PAROLA, M., PATEL, H. H. & FELDSTEIN, A. E. 2013. Lipid-induced toxicity stimulates hepatocytes to release angiogenic microparticles that require Vanin-1 for uptake by endothelial cells. *Science signaling,* 6**,** ra88-ra88.

POVERO, D., PANERA, N., EGUCHI, A., JOHNSON, C. D., PAPOUCHADO, B. G., DE ARAUJO HORCEL, L., PINATEL, E. M., ALISI, A., NOBILI, V. & FELDSTEIN, A. E. 2015. Lipid-induced hepatocyte-derived extracellular vesicles regulate hepatic stellate cell via microRNAs targeting PPAR-γ. *Cellular and molecular gastroenterology and hepatology,* 1**,** 646-663.e4.

POVERO, D., YAMASHITA, H., REN, W., SUBRAMANIAN, M. G., MYERS, R. P., EGUCHI, A., SIMONETTO, D. A., GOODMAN, Z. D., HARRISON, S. A., SANYAL, A. J., BOSCH, J. & FELDSTEIN, A. E. 2020. Characterization and Proteome of Circulating Extracellular Vesicles as Potential Biomarkers for NASH. *Hepatology Communications,* 4**,** 1263-1278.

PRASUN, P., GINEVIC, I. & OISHI, K. 2021. Mitochondrial dysfunction in nonalcoholic fatty liver disease and alcohol related liver disease. *Translational gastroenterology and hepatology,* 6**,** 4-4.

QIU, R., FONSECA, K., BERGMAN, A., LIN, J., TESS, D., NEWMAN, L., FAHMY, A., USECKAITE, Z., ROWLAND, A., VOURVAHIS, M. & RODRIGUES, D. 2023. Study of the ketohexokinase inhibitor PF-06835919 as a clinical cytochrome P450 3A inducer: Integrated use of oral midazolam and liquid biopsy. *Clin Transl Sci*.

QU, Z., WU, J., WU, J., JI, A., QIANG, G., JIANG, Y., JIANG, C. & DING, Y. 2017. Exosomal miR-665 as a novel minimally invasive biomarker for hepatocellular carcinoma diagnosis and prognosis. *Oncotarget,* 8**,** 80666-80678.

RATZIU, V. & FRIEDMAN, S. L. 2020. Why do so many NASH trials fail? *Gastroenterology*.

REGA-KAUN, G., RITZEL, D., KAUN, C., EBENBAUER, B., THALER, B., PRAGER, M., DEMYANETS, S., WOJTA, J. & HOHENSINNER, P. J. 2019. Changes of Circulating Extracellular Vesicles from the Liver after Roux-en-Y Bariatric Surgery. *International Journal of Molecular Sciences,* 20**,** 2153.

RODRIGUES, A. D., VAN DYK, M., SORICH, M. J., FAHMY, A., USECKAITE, Z., NEWMAN, L. A., KAPETAS, A. J., MOUNZER, R., WOOD, L. S., JOHNSON, J. G. & ROWLAND, A. 2021. Exploring the Use of Serum-Derived Small Extracellular Vesicles as Liquid Biopsy to Study the Induction of Hepatic Cytochromes P450 and Organic Anion Transporting Polypeptides. *Clin Pharmacol Ther*.

RODRIGUES, A. D., WOOD, L. S., VOURVAHIS, M. & ROWLAND, A. 2022. Leveraging Human Plasma-Derived Small Extracellular Vesicles as Liquid Biopsy to Study the Induction of Cytochrome P450 3A4 by Modafinil. *Clinical Pharmacology & Therapeutics,* 111**,** 425-434.

RODRIGUES, D. & ROWLAND, A. 2019. From Endogenous Compounds as Biomarkers to Plasma-Derived Nanovesicles as Liquid Biopsy; Has the Golden Age of Translational Pharmacokinetics-Absorption, Distribution, Metabolism, Excretion-Drug–Drug Interaction Science Finally Arrived? *Clinical Pharmacology & Therapeutics,* 105**,** 1407-1420.

ROJALIN, T., PHONG, B., KOSTER, H. J. & CARNEY, R. P. 2019. Nanoplasmonic Approaches for Sensitive Detection and Molecular Characterization of Extracellular Vesicles. *Frontiers in chemistry,* 7**,** 279-279.

ROSA-FERNANDES, L., ROCHA, V. B., CARREGARI, V. C., URBANI, A. & PALMISANO, G. 2017. A Perspective on Extracellular Vesicles Proteomics. *Frontiers in chemistry,* 5**,** 102-102.

ROWLAND, A., MINERS, J. O. & MACKENZIE, P. I. 2013. The UDP-glucuronosyltransferases: Their role in drug metabolism and detoxification. *The International Journal of Biochemistry & Cell Biology,* 45**,** 1121-1132.

ROWLAND, A., RUANGLERTBOON, W., VAN DYK, M., WIJAYAKUMARA, D., WOOD, L. S., MEECH, R., MACKENZIE, P. I., RODRIGUES, A. D., MARSHALL, J.-C. & SORICH, M. J. 2019. Plasma extracellular nanovesicle (exosome)-derived biomarkers for drug metabolism pathways: a novel approach to characterize variability in drug exposure. *British Journal of Clinical Pharmacology,* 85**,** 216-226.

ROWLAND, A., VAN DYK, M., HOPKINS, A., MOUNZER, R., POLASEK, T., ROSTAMI, A. & MJ, S. 2018. Physiologically Based Pharmacokinetic Modeling to Identify Physiological and Molecular Characteristics Driving Variability in Drug Exposure. *Clin Pharmacol Ther.,* 104**,** 1219-1228.

ROYO, F., MORENO, L., MLECZKO, J., PALOMO, L., GONZALEZ, E., CABRERA, D., COGOLLUDO, A., VIZCAINO, F. P., VAN-LIEMPD, S. & FALCON-PEREZ, J. M. 2017. Hepatocyte-secreted extracellular vesicles modify blood metabolome and endothelial function by an arginase-dependent mechanism. *Scientific Reports,* 7.

ROYO, F., THÉRY, C., FALCÓN-PÉREZ, J. M., NIEUWLAND, R. & WITWER, K. W. 2020. Methods for Separation and Characterization of Extracellular Vesicles: Results of a Worldwide Survey Performed by the ISEV Rigor and Standardization Subcommittee. *Cells,* 9.

SCHROEDER, J. C., PUNTIGAM, L., HOFMANN, L., JESKE, S. S., BECCARD, I. J., DOESCHER, J., LABAN, S., HOFFMANN, T. K., BRUNNER, C., THEODORAKI, M. N. & SCHULER, P. J. 2020. Circulating Exosomes Inhibit B Cell Proliferation and Activity. *Cancers (Basel),* 12.

SEHRAWAT, T. S., ARAB, J. P., LIU, M., AMROLLAHI, P., WAN, M., FAN, J., NAKAO, Y., POSE, E., NAVARRO-CORCUERA, A., DASGUPTA, D., LIAO, C.-Y., HE, L., MAUER, A. S., AVITABILE, E., VENTURA-COTS, M., BATALLER, R. A., SANYAL, A. J., CHALASANI, N. P., HEIMBACH, J. K., WATT, K. D., GORES, G. J., GINES, P., KAMATH, P. S., SIMONETTO, D. A., HU, T. Y., SHAH, V. H. & MALHI, H. 2021. Circulating Extracellular Vesicles Carrying Sphingolipid Cargo for the Diagnosis and Dynamic Risk Profiling of Alcoholic Hepatitis. *Hepatology,* 73**,** 571-585.

SENNEPIN, A. D., CHARPENTIER, S., NORMAND, T., SARRÉ, C., LEGRAND, A. & MOLLET, L. M. 2009. Multiple reprobing of Western blots after inactivation of peroxidase activity by its substrate, hydrogen peroxide. *Analytical Biochemistry,* 393**,** 129-131.

SHAH, R., PATEL, T. & FREEDMAN, J. E. 2018. Circulating Extracellular Vesicles in Human Disease. *New England Journal of Medicine,* 379**,** 958-966.

SHAO, H., IM, H., CASTRO, C. M., BREAKEFIELD, X., WEISSLEDER, R. & LEE, H. 2018. New Technologies for Analysis of Extracellular Vesicles. *Chemical reviews,* 118**,** 1917-1950.

SHARMA, P. & ARORA, A. 2020. Clinical presentation of alcoholic liver disease and non-alcoholic fatty liver disease: spectrum and diagnosis. *Translational gastroenterology and hepatology,* 5**,** 19-19.

SHARMA, P., LUDWIG, S., MULLER, L., HONG, C. S., KIRKWOOD, J. M., FERRONE, S. & WHITESIDE, T. L. 2018. Immunoaffinity-based isolation of melanoma cell-derived exosomes from plasma of patients with melanoma. *Journal of extracellular vesicles,* 7**,** 1435138-1435138.

SHI, M., JIANG, Y., YANG, L., YAN, S., WANG, Y. G. & LU, X. J. 2018. Decreased levels of serum exosomal miR-638 predict poor prognosis in hepatocellular carcinoma. *J Cell Biochem,* 119**,** 4711-4716.

SHI, M., LIU, C., COOK, T. J., BULLOCK, K. M., ZHAO, Y., GINGHINA, C., LI, Y., ARO, P., DATOR, R., HE, C., HIPP, M. J., ZABETIAN, C. P., PESKIND, E. R., HU, S.-C., QUINN, J. F., GALASKO, D. R., BANKS, W. A. & ZHANG, J. 2014. Plasma exosomal α-synuclein is likely CNS-derived and increased in Parkinson's disease. *Acta neuropathologica,* 128**,** 639-650.

SIDHOM, K., OBI, P. O. & SALEEM, A. 2020. A Review of Exosomal Isolation Methods: Is Size Exclusion Chromatography the Best Option? *International Journal of Molecular Sciences,* 21.

SIMON, T. G., ROELSTRAETE, B., KHALILI, H., HAGSTRÖM, H. & LUDVIGSSON, J. F. 2020. Mortality in biopsy-confirmed nonalcoholic fatty liver disease: results from a nationwide cohort. *Gut***,** gutjnl-2020-322786.

SORICH, M. J., MUTLIB, F., VAN DYK, M., HOPKINS, A. M., POLASEK, T. M., MARSHALL, J. C., RODRIGUES, A. D. & ROWLAND, A. 2019. Use of Physiologically Based Pharmacokinetic Modeling to Identify Physiological and Molecular Characteristics Driving Variability in Axitinib Exposure: A Fresh Approach to Precision Dosing in Oncology. *Journal of Clinical Pharmacology,* 59**,** 872-879.

SRINIVAS, A. N., SURESH, D., SANTHEKADUR, P. K., SUVARNA, D. & KUMAR, D. P. 2020. Extracellular Vesicles as Inflammatory Drivers in NAFLD. *Front Immunol,* 11**,** 627424.

SUGIMACHI, K., MATSUMURA, T., HIRATA, H., UCHI, R., UEDA, M., UEO, H., SHINDEN, Y., IGUCHI, T., EGUCHI, H., SHIRABE, K., OCHIYA, T., MAEHARA, Y. & MIMORI, K. 2015. Identification of a bona fide microRNA biomarker in serum exosomes that predicts hepatocellular carcinoma recurrence after liver transplantation. *Br J Cancer,* 112**,** 532-8.

SUMIDA, Y., NAKAJIMA, A. & ITOH, Y. 2014. Limitations of liver biopsy and non-invasive diagnostic tests for the diagnosis of nonalcoholic fatty liver disease/nonalcoholic steatohepatitis. *World journal of gastroenterology,* 20**,** 475-485.

SUN, N., LEE, Y.-T., ZHANG, R. Y., KAO, R., TENG, P.-C., YANG, Y., YANG, P., WANG, J. J., SMALLEY, M., CHEN, P.-J., KIM, M., CHOU, S.-J., BAO, L., WANG, J., ZHANG, X., QI, D., PALOMIQUE, J., NISSEN, N., HAN, S.-H. B., SADEGHI, S., FINN, R. S., SAAB, S., BUSUTTIL, R. W., MARKOVIC, D., ELASHOFF, D., YU, H.-H., LI, H., HEANEY, A. P.,

POSADAS, E., YOU, S., YANG, J. D., PEI, R., AGOPIAN, V. G., TSENG, H.-R. & ZHU, Y. 2020. Purification of HCC-specific extracellular vesicles on nanosubstrates for early HCC detection by digital scoring. *Nature Communications,* 11**,** 4489.

SUNG, S., KIM, J. & JUNG, Y. 2018. Liver-Derived Exosomes and Their Implications in Liver Pathobiology. *International journal of molecular sciences,* 19**,** 3715.

SUZUKI, A. & DIEHL, A. M. 2017. Nonalcoholic Steatohepatitis. *Annual Review of Medicine,* 68**,** 85-98.

SWEN, J. J., VAN DER WOUDEN, C. H., MANSON, L. E. N., ABDULLAH-KOOLMEES, H., BLAGEC, K., BLAGUS, T., BÖHRINGER, S., CAMBON-THOMSEN, A., CECCHIN, E., CHEUNG, K.-C., DENEER, V. H. M., DUPUI, M., INGELMAN-SUNDBERG, M., JONSSON, S., JOEFIELD-ROKA, C., JUST, K. S., KARLSSON, M. O., KONTA, L., KOOPMANN, R., KRIEK, M., LEHR, T., MITROPOULOU, C., RIAL-SEBBAG, E., ROLLINSON, V., RONCATO, R., SAMWALD, M., SCHAEFFELER, E., SKOKOU, M., SCHWAB, M., STEINBERGER, D., STINGL, J. C., TREMMEL, R., TURNER, R. M., VAN RHENEN, M. H., DÁVILA FAJARDO, C. L., DOLŽAN, V., PATRINOS, G. P., PIRMOHAMED, M., SUNDER-PLASSMANN, G., TOFFOLI, G., GUCHELAAR, H.-J., BUUNK, A., GOOSSENS, H., BAAS, G., ALGERA, M., SCHUIL-VLASSAK, E., AMBAGTS, T., DE HOOG-SCHOUTEN, L., MUSAAFIR, S., BOSCH, R., TJONG, C., STEEMAN, S., VAN DER PLAS, M., BALDEW, G., DEN HOLLANDER, I., DE WAAL, Z., HEIJN, A., NELEMANS, L., KOUWEN-LUBBERS, K., VAN LEEUWEN, M., HOOGENBOOM, S., VAN DOREMALEN, J., TON, C., BEETSTRA, B., MEIJS, V., DIKKEN, J., DUBERO, D., SLAGER, M., HOUBEN, T., KANIS, T., OVERMARS, W., NIJENHUIS, M., STEFFENS, M., BERGS, I., KARAMPERIS, K., SIAMOGLOU, S., IVANTSIK, O., SAMIOU, G.-C., KORDOU, Z., TSERMPINI, E., FERENTINOS, P., KARAIVAZOGLOU, A., RIGAS, G., GERASIMOU, H., VOUKELATOU, G., GEORGILA, E., TSERMPINI, E. E., MENDRINOU, E., CHALIKIOPOULOU, K., KOLLIOPOULOU, A., MITROPOULOS, K., STRATOPOULOS, A., LIOPETAS, I., TSIKRIKA, A., BARBA, E., EMMANOUIL, G., STAMOPOULOU, T., STATHOULIAS, A., GIANNOPOULOS, P., KANELLAKIS, F., et al. 2023. A 12-gene pharmacogenetic panel to prevent adverse drug reactions: an open-label, multicentre, controlled, cluster-randomised crossover implementation study. *The Lancet,* 401**,** 347-356.

SZABO, G. & MOMEN-HERAVI, F. 2017. Extracellular vesicles in liver disease and potential as biomarkers and therapeutic targets. *Nature Reviews Gastroenterology &Amp; Hepatology,* 14**,** 455.

TAMASI, V., NÉMETH, K. & CSALA, M. 2023. Role of Extracellular Vesicles in Liver Diseases. *Life,* 13**,** 1117.

TAN, D. S., THOMAS, G. V., GARRETT, M. D., BANERJI, U., DE BONO, J. S., KAYE, S. B. & WORKMAN, P. 2009. Biomarker-driven early clinical trials in oncology: a paradigm shift in drug development. *Cancer J,* 15**,** 406-20.

TANG, J., LI, Y., LIU, K., ZHU, Q., YANG, W. H., XIONG, L. K. & GUO, D. L. 2018. Exosomal miR-9-3p suppresses HBGF-5 expression and is a functional biomarker in hepatocellular carcinoma. *Minerva Med,* 109**,** 15-23.

TER-OVANESYAN, D., GILBOA, T., BUDNIK, B., NIKITINA, A., WHITEMAN, S., LAZAROVITS, R., TRIEU, W., KALISH, D., CHURCH, G. M. & WALT, D. R. 2023. Improved isolation of extracellular vesicles by removal of both free proteins and lipoproteins. *eLife,* 12**,** e86394.

TETTA, C., BRUNO, S., FONSATO, V., DEREGIBUS, M. C. & CAMUSSI, G. 2011. The role of microvesicles in tissue repair. *Organogenesis,* 7**,** 105-115.

THÉRY, C., WITWER, K. W., AIKAWA, E., ALCARAZ, M. J., ANDERSON, J. D., ANDRIANTSITOHAINA, R., ANTONIOU, A., ARAB, T., ARCHER, F., ATKIN-SMITH, G. K., AYRE, D. C., BACH, J.-M., BACHURSKI, D., BAHARVAND, H., BALAJ, L., BALDACCHINO, S., BAUER, N. N., BAXTER, A. A., BEBAWY, M., BECKHAM, C., BEDINA ZAVEC, A., BENMOUSSA, A., BERARDI, A. C., BERGESE, P., BIELSKA, E., BLENKIRON, C., BOBIS-WOZOWICZ, S., BOILARD, E., BOIREAU, W., BONGIOVANNI, A., BORRÀS, F. E., BOSCH, S., BOULANGER, C. M., BREAKEFIELD, X., BREGLIO, A. M., BRENNAN, M. Á., BRIGSTOCK, D. R., BRISSON, A., BROEKMAN, M. L. D., BROMBERG, J. F., BRYL-GÓRECKA, P., BUCH, S., BUCK, A. H., BURGER, D., BUSATTO, S., BUSCHMANN, D., BUSSOLATI, B., BUZÁS, E. I., BYRD, J. B., CAMUSSI, G., CARTER, D. R. F., CARUSO, S., CHAMLEY, L. W., CHANG, Y.-T., CHEN, C., CHEN, S., CHENG, L., CHIN, A. R.,

CLAYTON, A., CLERICI, S. P., COCKS, A., COCUCCI, E., COFFEY, R. J., CORDEIRO-DA-SILVA, A., COUCH, Y., COUMANS, F. A. W., COYLE, B., CRESCITELLI, R., CRIADO, M. F., D'SOUZA-SCHOREY, C., DAS, S., DATTA CHAUDHURI, A., DE CANDIA, P., DE SANTANA, E. F., DE WEVER, O., DEL PORTILLO, H. A., DEMARET, T., DEVILLE, S., DEVITT, A., DHONDT, B., DI VIZIO, D., DIETERICH, L. C., DOLO, V., DOMINGUEZ RUBIO, A. P., DOMINICI, M., DOURADO, M. R., DRIEDONKS, T. A. P., DUARTE, F. V., DUNCAN, H. M., EICHENBERGER, R. M., EKSTRÖM, K., EL ANDALOUSSI, S., ELIE-CAILLE, C., ERDBRÜGGER, U., FALCÓN-PÉREZ, J. M., FATIMA, F., FISH, J. E., FLORES-BELLVER, M., FÖRSÖNITS, A., FRELET-BARRAND, A., et al. 2018. Minimal information for studies of extracellular vesicles 2018 (MISEV2018): a position statement of the International Society for Extracellular Vesicles and update of the MISEV2014 guidelines. *Journal of Extracellular Vesicles,* 7**,** 1535750.

THOMOU, T., MORI, M. A., DREYFUSS, J. M., KONISHI, M., SAKAGUCHI, M., WOLFRUM, C., RAO, T. N., WINNAY, J. N., GARCIA-MARTIN, R., GRINSPOON, S. K., GORDEN, P. & KAHN, C. R. 2017. Adipose-derived circulating miRNAs regulate gene expression in other tissues. *Nature,* 542**,** 450-455.

TIAN, Y., GONG, M., HU, Y., LIU, H., ZHANG, W., ZHANG, M., HU, X., AUBERT, D., ZHU, S., WU, L. & YAN, X. 2019. Quality and efficiency assessment of six extracellular vesicle isolation methods by nano-flow cytometry. *Journal of extracellular vesicles,* 9**,** 1697028-1697028.

UHLÉN, M., FAGERBERG, L., HALLSTRÖM, B. M., LINDSKOG, C., OKSVOLD, P., MARDINOGLU, A., SIVERTSSON, Å., KAMPF, C., SJÖSTEDT, E., ASPLUND, A., OLSSON, I., EDLUND, K., LUNDBERG, E., NAVANI, S., SZIGYARTO, C. A., ODEBERG, J., DJUREINOVIC, D., TAKANEN, J. O., HOBER, S., ALM, T., EDQVIST, P. H., BERLING, H., TEGEL, H., MULDER, J., ROCKBERG, J., NILSSON, P., SCHWENK, J. M., HAMSTEN, M., VON FEILITZEN, K., FORSBERG, M., PERSSON, L., JOHANSSON, F., ZWAHLEN, M., VON HEIJNE, G., NIELSEN, J. & PONTÉN, F. 2015. Proteomics. Tissue-based map of the human proteome. *Science,* 347**,** 1260419.

UNALP-ARIDA, A. & RUHL, C. E. 2017. Liver fibrosis scores predict liver disease mortality in the United States population. *Hepatology,* 66**,** 84-95.

USECKAITE, Z., MUKHOPADHYA, A., MORAN, B. & O'DRISCOLL, L. 2020. Extracellular vesicles report on the MET status of their cells of origin regardless of the method used for their isolation. *Scientific Reports,* 10**,** 19020.

USECKAITE, Z., NEWMAN, L. A., HOPKINS, A. M., KLEBE, S., COLELLA, A. D., CHEGENI, N., WILLIAMS, R., SORICH, M. J., RODRIGUES, A. D., CHATAWAY, T. K. & ROWLAND, A. 2023. Proteomic profiling of paired human liver homogenate and tissue derived extracellular vesicles. *PROTEOMICS,* n/a**,** 2300025.

USECKAITE, Z., RODRIGUES, A. D., HOPKINS, A. M., NEWMAN, L. A., JOHNSON, J. G., SORICH, M. J. & ROWLAND, A. 2021. Role of extracellular vesicle derived biomarkers in drug metabolism and disposition. *Drug Metabolism and Disposition***,** DMD-MR-2021-000411.

VALLABHAJOSYULA, P., KORUTLA, L., HABERTHEUER, A., YU, M., ROSTAMI, S., YUAN, C. X., REDDY, S., LIU, C., KORUTLA, V., KOEBERLEIN, B., TROFE-CLARK, J., RICKELS, M. R. & NAJI, A. 2017. Tissue-specific exosome biomarkers for noninvasively monitoring immunologic rejection of transplanted tissue. *J Clin Invest,* 127**,** 1375-1391.

VAN DEUN, J., JO, A., LI, H., LIN, H.-Y., WEISSLEDER, R., IM, H. & LEE, H. 2020. Integrated Dual-Mode Chromatography to Enrich Extracellular Vesicles from Plasma. *Advanced Biosystems,* 4**,** 1900310.

VAN DEUN, J., MESTDAGH, P., AGOSTINIS, P., AKAY, Ö., ANAND, S., ANCKAERT, J., MARTINEZ, Z. A., BAETENS, T., BEGHEIN, E., BERTIER, L., BERX, G., BOERE, J., BOUKOURIS, S., BREMER, M., BUSCHMANN, D., BYRD, J. B., CASERT, C., CHENG, L., CMOCH, A., DAVELOOSE, D., DE SMEDT, E., DEMIRSOY, S., DEPOORTER, V., DHONDT, B., DRIEDONKS, T. A. P., DUDEK, A., ELSHARAWY, A., FLORIS, I., FOERS, A. D., GÄRTNER, K., GARG, A. D., GEEURICKX, E., GETTEMANS, J., GHAZAVI, F., GIEBEL, B., KORMELINK, T. G., HANCOCK, G., HELSMOORTEL, H., HILL, A. F., HYENNE, V., KALRA, H., KIM, D., KOWAL, J., KRAEMER, S., LEIDINGER, P., LEONELLI, C., LIANG, Y., LIPPENS, L., LIU, S., LO CICERO, A., MARTIN, S., MATHIVANAN, S., MATHIYALAGAN, P., MATUSEK, T., MILANI, G., MONGUIÓ-TORTAJADA, M., MUS, L. M., MUTH, D. C., NÉMETH, A., NOLTE-'T HOEN, E. N. M., O'DRISCOLL, L., PALMULLI, R., PFAFFL, M. W.,

PRIMDAL-BENGTSON, B., ROMANO, E., ROUSSEAU, Q., SAHOO, S., SAMPAIO, N., SAMUEL, M., SCICLUNA, B., SOEN, B., STEELS, A., SWINNEN, J. V., TAKATALO, M., THAMINY, S., THÉRY, C., TULKENS, J., VAN AUDENHOVE, I., VAN DER GREIN, S., VAN GOETHEM, A., VAN HERWIJNEN, M. J., VAN NIEL, G., VAN ROY, N., VAN VLIET, A. R., VANDAMME, N., VANHAUWAERT, S., VERGAUWEN, G., VERWEIJ, F., WALLAERT, A., WAUBEN, M., WITWER, K. W., ZONNEVELD, M. I., DE WEVER, O., VANDESOMPELE, J., HENDRIX, A. & CONSORTIUM, E.-T. 2017. EV-TRACK: transparent reporting and centralizing knowledge in extracellular vesicle research. *Nature Methods,* 14**,** 228-232.

VAN EIJNDHOVEN, M. A., ZIJLSTRA, J. M., GROENEWEGEN, N. J., DREES, E. E., VAN NIELE, S., BAGLIO, S. R., KOPPERS-LALIC, D., VAN DER VOORN, H., LIBREGTS, S. F., WAUBEN, M. H., DE MENEZES, R. X., VAN WEERING, J. R., NIEUWLAND, R., VISSER, L., VAN DEN BERG, A., DE JONG, D. & PEGTEL, D. M. 2016. Plasma vesicle miRNAs for therapy response monitoring in Hodgkin lymphoma patients. *JCI insight* [Online], 1. [Accessed 2016/11//].

VANDERBOOM, P. M., DASARI, S., RUEGSEGGER, G. N., PATAKY, M. W., LUCIEN, F., HEPPELMANN, C. J., LANZA, I. R. & NAIR, K. S. 2021. A size-exclusion-based approach for purifying extracellular vesicles from human plasma. *Cell Rep Methods,* 1.

VEERMAN, R. E., TEEUWEN, L., CZARNEWSKI, P., GÜCLÜLER AKPINAR, G., SANDBERG, A., CAO, X., PERNEMALM, M., ORRE, L. M., GABRIELSSON, S. & ELDH, M. 2021. Molecular evaluation of five different isolation methods for extracellular vesicles reveals different clinical applicability and subcellular origin. *Journal of Extracellular Vesicles,* 10**,** e12128.

VERMA, V. K., LI, H., WANG, R., HIRSOVA, P., MUSHREF, M., LIU, Y., CAO, S., CONTRERAS, P. C., MALHI, H., KAMATH, P. S., GORES, G. J. & SHAH, V. H. 2016. Alcohol stimulates macrophage activation through caspase-dependent hepatocyte derived release of CD40L containing extracellular vesicles. *Journal of Hepatology,* 64**,** 651-660.

VOGEL, C. & MARCOTTE, E. M. 2012. Insights into the regulation of protein abundance from proteomic and transcriptomic analyses. *Nat Rev Genet,* 13**,** 227-32.

WAGSCHAL, A., NAJAFI-SHOUSHTARI, S. H., WANG, L., GOEDEKE, L., SINHA, S., DELEMOS, A. S., BLACK, J. C., RAMÍREZ, C. M., LI, Y., TEWHEY, R., HATOUM, I., SHAH, N., LU, Y., KRISTO, F., PSYCHOGIOS, N., VRBANAC, V., LU, Y.-C., HLA, T., DE CABO, R., TSANG, J. S., SCHADT, E., SABETI, P. C., KATHIRESAN, S., COHEN, D. E., WHETSTINE, J., CHUNG, R. T., FERNÁNDEZ-HERNANDO, C., KAPLAN, L. M., BERNARDS, A., GERSZTEN, R. E. & NÄÄR, A. M. 2015. Genome-wide identification of microRNAs regulating cholesterol and triglyceride homeostasis. *Nature medicine,* 21**,** 1290-1297.

WANG, G., ZHAO, W., WANG, H., QIU, G., JIANG, Z., WEI, G. & LI, X. 2019. Exosomal MiR-744 Inhibits Proliferation and Sorafenib Chemoresistance in Hepatocellular Carcinoma by Targeting PAX2. *Medical science monitor : international medical journal of experimental and clinical research,* 25**,** 7209-7217.

WANG, R., DING, Q., YAQOOB, U., DE ASSUNCAO, T. M., VERMA, V. K., HIRSOVA, P., CAO, S., MUKHOPADHYAY, D., HUEBERT, R. C. & SHAH, V. H. 2015. Exosome Adherence and Internalization by Hepatic Stellate Cells Triggers Sphingosine 1-Phosphate-dependent Migration. *The Journal of biological chemistry,* 290**,** 30684-30696.

WANG, T., ANDERSON, K. W. & TURKO, I. V. 2017. Assessment of Extracellular Vesicles Purity Using Proteomic Standards. *Analytical chemistry,* 89**,** 11070-11075.

WANG, Y., ZHANG, Y., LI, Z., WEI, S., CHI, X., YAN, X., LV, H., ZHAO, L. & ZHAO, L. 2023. Combination of size-exclusion chromatography and ion exchange adsorption for improving the proteomic analysis of plasma-derived extracellular vesicles. *PROTEOMICS,* 23**,** 2200364.

WEBBER, J. & CLAYTON, A. 2013. How pure are your vesicles? *Journal of extracellular vesicles,* 2**,** 10.3402/jev.v2i0.19861.

WELSH, J. A., GOEBERDHAN, D. C. I., O'DRISCOLL, L., BUZAS, I., BLENKIRON, C., BUSSOLATI, B., CAI, H., DI VIZIO, D., P., D. T. A., ERDBRÜGGER, U., FALCON-PEREZ, J. M., FU, Q.-L., F., H. A., LENASSI, M., LIM, S. K., MAHONEY, M. G., MOHANTY, S., MÖLLER, A., NIEUWLAND, R. & WITWER, K. W. 2024. Minimal information for studies of extracellular vesicles (MISEV2023): from basic to advanced approaches. *Journal of Extracellular Vesicles,* e12404.

WELSH, J. A., VAN DER POL, E., ARKESTEIJN, G. J. A., BREMER, M., BRISSON, A., COUMANS, F., DIGNAT-GEORGE, F., DUGGAN, E., GHIRAN, I., GIEBEL, B., GÖRGENS, A., HENDRIX, A., LACROIX, R., LANNIGAN, J., LIBREGTS, S. F. W. M., LOZANO-ANDRÉS, E., MORALES-KASTRESANA, A., ROBERT, S., DE ROND, L., TERTEL, T., TIGGES, J., DE WEVER, O., YAN, X., NIEUWLAND, R., WAUBEN, M. H. M., NOLAN, J. P. & JONES, J. C. 2020. MIFlowCyt-EV: a framework for standardized reporting of extracellular vesicle flow cytometry experiments. *Journal of extracellular vesicles,* 9**,** 1713526-1713526.

WILLIAMS, S., JALAL, A. R., LEWIS, M. P. & DAVIES, O. G. 2023. A survey to evaluate parameters governing the selection and application of extracellular vesicle isolation methods. *J Tissue Eng,* 14**,** 20417314231155114.

WITEK, R. P., YANG, L., LIU, R., JUNG, Y., OMENETTI, A., SYN, W. K., CHOI, S. S., CHEONG, Y., FEARING, C. M., AGBOOLA, K. M., CHEN, W. & DIEHL, A. M. 2009. Liver Cell–Derived Microparticles Activate Hedgehog Signaling and Alter Gene Expression in Hepatic Endothelial Cells. *Gastroenterology,* 136**,** 320-330.e2.

WITWER, K. W., BUZÁS, E. I., BEMIS, L. T., BORA, A., LÄSSER, C., LÖTVALL, J., NOLTE-'T HOEN, E. N., PIPER, M. G., SIVARAMAN, S., SKOG, J., THÉRY, C., WAUBEN, M. H. & HOCHBERG, F. 2013. Standardization of sample collection, isolation and analysis methods in extracellular vesicle research. *Journal of extracellular vesicles,* 2**,** 10.3402/jev.v2i0.20360.

WITWER, K. W., GOBERDHAN, D. C. I., O'DRISCOLL, L., THÉRY, C., WELSH, J. A., BLENKIRON, C., BUZÁS, E. I., DI VIZIO, D., ERDBRÜGGER, U., FALCÓN-PÉREZ, J. M., FU, Q.-L., HILL, A. F., LENASSI, M., LÖTVALL, J., NIEUWLAND, R., OCHIYA, T., ROME, S., SAHOO, S. & ZHENG, L. 2021. Updating MISEV: Evolving the minimal requirements for studies of extracellular vesicles. *Journal of Extracellular Vesicles,* 10**,** e12182.

WONG, M. C. S., HUANG, J. L. W., GEORGE, J., HUANG, J., LEUNG, C., ESLAM, M., CHAN, H. L. Y. & NG, S. C. 2019. The changing epidemiology of liver diseases in the Asia–Pacific region. *Nature Reviews Gastroenterology & Hepatology,* 16**,** 57-73.

WONG, V. W.-S., ADAMS, L. A., DE LÉDINGHEN, V., WONG, G. L.-H. & SOOKOIAN, S. 2018. Noninvasive biomarkers in NAFLD and NASH — current progress and future promise. *Nature Reviews Gastroenterology & Hepatology,* 15**,** 461-478.

XIN, S., ZHAN, Q., CHEN, X., XU, J. & YU, Y. 2020. Efficacy of serum miRNA test as a non-invasive method to diagnose nonalcoholic steatohepatitis: a systematic review and meta-analysis. *BMC Gastroenterology,* 20**,** 186.

XUE, X., WANG, X., ZHAO, Y., HU, R. & QIN, L. 2018. Exosomal miR-93 promotes proliferation and invasion in hepatocellular carcinoma by directly inhibiting TIMP2/TP53INP1/CDKN1A. *Biochemical and Biophysical Research Communications,* 502**,** 515-521.

YOUNOSSI, Z., TACKE, F., ARRESE, M., CHANDER SHARMA, B., MOSTAFA, I., BUGIANESI, E., WAI-SUN WONG, V., YILMAZ, Y., GEORGE, J., FAN, J. & VOS, M. B. 2019. Global Perspectives on Nonalcoholic Fatty Liver Disease and Nonalcoholic Steatohepatitis. *Hepatology,* 69**,** 2672-2682.

ZAMOR, P. J., DELEMOS, A. S. & RUSSO, M. W. 2017. Viral hepatitis and hepatocellular carcinoma: etiology and management. *Journal of gastrointestinal oncology,* 8**,** 229-242.

ZAROVNI, N., CORRADO, A., GUAZZI, P., ZOCCO, D., LARI, E., RADANO, G., MUHHINA, J., FONDELLI, C., GAVRILOVA, J. & CHIESI, A. 2015. Integrated isolation and quantitative analysis of exosome shuttled proteins and nucleic acids using immunocapture approaches. *Methods,* 87**,** 46-58.

ZHANG, G., HUANG, X., XIU, H., SUN, Y., CHEN, J., CHENG, G., SONG, Z., PENG, Y., SHEN, Y., WANG, J. & CAI, Z. 2020a. Extracellular vesicles: Natural liver-accumulating drug delivery vehicles for the treatment of liver diseases. *J Extracell Vesicles,* 10**,** e12030.

ZHANG, L., PAROT, J., HACKLEY, V. A. & TURKO, I. V. 2020b. Quantitative Proteomic Analysis of Biogenesis-Based Classification for Extracellular Vesicles. *Proteomes,* 8.

ZHANG, X., JI, X., WANG, Q. & LI, J. Z. 2018. New insight into inter-organ crosstalk contributing to the pathogenesis of non-alcoholic fatty liver disease (NAFLD). *Protein & cell,* 9**,** 164-177.

ZHANG, Y.-J., HU, Y., LI, J., CHI, Y.-J., JIANG, W.-W., ZHANG, F. & LIU, Y.-L. 2017. Roles of microRNAs in immunopathogenesis of non-alcoholic fatty liver disease revealed by integrated analysis of microRNA and mRNA expression profiles. *Hepatobiliary & Pancreatic Diseases International,* 16**,** 65-79.

APPENDICES

Appendix 1

Article published in Cellular and Molecular Life Sciences, 2021.

Cellular and Molecular Life Sciences (2022) 79:232
https://doi.org/10.1007/s00018-022-04256-8

UNSOLICITED REVIEW

Circulating cell-specific extracellular vesicles as biomarkers for the diagnosis and monitoring of chronic liver diseases

Lauren A. Newman[1] · Kate Muller[2] · Andrew Rowland[1]

Received: 30 January 2022 / Revised: 2 March 2022 / Accepted: 17 March 2022 / Published online: 10 April 2022

Abstract

Chronic liver diseases represent a burgeoning health problem affecting billions of people worldwide. The insufficient performance of current minimally invasive tools is recognised as a significant barrier to the clinical management of these conditions. Extracellular vesicles (EVs) have emerged as a rich source of circulating biomarkers closely linked to pathological processes in originating tissues. Here, we summarise the contribution of EVs to normal liver function and to chronic liver pathologies; and explore the use of circulating EV biomarkers, with a particular focus on techniques to isolate and analyse cell- or tissue-specific EVs. Such approaches present a novel strategy to inform disease status and monitor changes in response to treatment in a minimally invasive manner. Emerging technologies that support the selective isolation and analysis of circulating EVs derived only from hepatic cells, have driven recent advancements in EV-based biomarker platforms for chronic liver diseases and show promise to bring these techniques to clinical settings.

Keywords Chronic liver disease · Non-alcoholic fatty liver disease · Metabolic-associated fatty liver disease · Extracellular vesicles · Minimally invasive biomarkers · Tissue-specific biomarkers

Introduction

Chronic liver diseases represent a significant global health burden that is set to grow in the coming decades [1, 2]. Alcohol-related liver disease and non-alcoholic fatty liver disease (NAFLD) are two of the most common aetiologies and are precipitated, respectively, by excessive alcohol consumption and the combination of high calorie diet and sedentary lifestyle [3, 4]. The growing prevalence of NAFLD, in particular, parallels that of obesity, type 2 diabetes and other features of metabolic syndrome [5]. The pathology of each of these disorders, as well as chronic infection with hepatitis B (HBV) or hepatitis C (HCV) viruses, manifest inflammatory and pro-fibrogenic processes in the liver that may progress to cirrhosis and hepatocellular carcinoma (HCC). Accordingly, chronic liver disease is a leading cause of mortality in many parts of the world [6, 7].

By way of example, independent of other factors, the average all-cause mortality among NAFLD patients is 11.7% higher compared to individuals without the disease (hazard ratio (HR) 1.93 [1.86–2.00]). The impact of NAFLD on mortality increases with increasing disease severity and ranges from 8.3% (HR 1.71 [1.64–1.79]) for simple steatosis up to 18.4% (HR 2.44 [2.22–2.69]) for non-alcoholic steatohepatitis (NASH) with fibrosis [8]. Adding to the challenge, the capacity to treat NAFLD diminishes with increasing disease severity. Targeted weight loss slows progression in mild disease, but is less effective in moderate to severe disease [9]. Importantly, while there have been considerable breakthroughs in the prevention and treatment of viral hepatitis in recent years [10], no medicine is currently approved for NAFLD and progress has been slow with costly failures in late phase trials due to an inability to easily monitor treatment response.

Despite significant shortcomings in accuracy and practicality, liver biopsy remains the gold standard diagnostic tool to assess the presence and stage of various liver diseases. This technique is currently the most reliable way to determine the pattern and severity of inflammation and fibrosis

✉ Andrew Rowland
andrew.rowland@flinders.edu.au

[1] Department of Clinical Pharmacology, College of Medicine and Public Health, Flinders University, Adelaide, SA, Australia

[2] Department of Gastroenterology and Hepatology, College of Medicine and Public Health, Flinders Medical Centre, Adelaide, SA, Australia

[11]. For patients with NAFLD, a diagnosis of the more severe form steatohepatitis (NASH) can only be made by histological identification of cardinal features, such as hepatocellular ballooning and lobular inflammation [5]. Since liver biopsy is a highly invasive technique, it comes with the risk of severe complications and cannot be regularly repeated to track changes in the liver over time [3]. Moreover, the technique is associated with considerable interobserver and sampling variability, produces only a limited representation of total liver tissue and, consequently, often underestimates disease severity [12]. These issues limit its widespread and repeated use and give rise to the urgent need for non-invasive biomarkers, to aid diagnosis and monitoring of patients with chronic liver disease. Currently, various scoring systems may be applied to non-invasively stratify patient risk, such as FIB-4 index, Maddrey Discriminant Function (MDF) and Model for End-stage Liver Disease (MELD), which rely on blood biochemistry. Non-invasive diagnoses may employ imaging studies (e.g. magnetic resonance imaging and ultrasound) [13, 14] and liver stiffness may be assessed via transient elastography (e.g. FibroScan) to estimate the degree of fibrosis [15].

In 2019, the American Association for the Study of Liver Diseases identified the insufficient performance of these current non-invasive tools to diagnose early disease and track progression as the critical barrier to treating chronic liver diseases [16]. The limitation being these approaches lack specificity and sensitivity, particularly for mild and early disease. To meet this demand, considerable research effort has focussed on the development of blood-based biomarkers that can reflect early pathological processes, disease progression and response to treatment [11]. In recent times, circulating extracellular vesicles (EVs) have emerged as a potential source of such biomarkers. These nanosized particles contain a distinct molecular signature of protein, RNA and lipid moieties, that is both indicative of their cell type of origin, and also the homeostatic or pathological stimuli that induced their release [17]. EVs are shown to play a role in immune modulation and autoimmune disease, tissue repair, neurodegenerative disease, cardiovascular disease and the development and proliferation of tumours [18]. A breadth of work now evidences the crucial biological activities of EVs in multiple facets of chronic liver pathophysiology, including the cell injury, inflammation and fibrosis shared across diverse aetiologies [5]. Technological developments in high-throughput multi-omics approaches promise to unveil the intricacies of EV molecular cargo and streamline the clinical application of highly sensitive, disease-specific biomarkers [19].

The purpose of this review is to summarise the key works that establish how EVs contribute to normal liver physiology and processes central to the development and progression of chronic liver diseases. The current state and future direction of circulating EV biomarker analyses will also be explored, with a particular focus on techniques to selectively isolate and analyse cell- or tissue-specific EVs for the detection and tracking of chronic liver diseases.

Extracellular vesicles

EVs are a heterogenous population of small, non-replicating, membrane-encapsulated particles, released by virtually all cell types. Alongside soluble factors and signalling molecules, they have emerged as a fundamental constituent of the cellular secretome [20]. Regular release under basal conditions contributes to the maintenance of homeostasis, while changes to the magnitude and composition of EVs communicate responses to stressful or pathological stimuli between neighbouring and distant cells. Signalling is mediated by receptor-ligand interactions on the EV and cell surfaces, which may directly trigger intracellular pathways or result in the fusion or internalisation of vesicles and their associated cargo [21]. The importance of the role of EVs in intercellular communication is underscored by its evolutionary conservation [11]. Signalling or regulatory molecules transferred in this way are stable and protected from degradation, may be transported through the systemic circulation to distant organs and can easily be taken up by target cells. Notably, the expression of specific surface proteins, such as integrins, promote homing of EVs to target recipient cells [22].

EV subtypes

As the field of EV research has matured, so too has the complexity of defining distinct EV subpopulations. Vesicles secreted not only by different cell types, but also from the same cell, possess inherent heterogeneity in physical and biochemical properties [19]. Conventionally, EV subtypes are characterised based on their mode of biogenesis. Exosomes, typically 50–150 nm in diameter, are produced via the endosomal pathway. Inward protrusions of the early endosomal membrane create intraluminal vesicles (ILVs) which leads to the formation of multivesicular bodies (MVB). MVB trafficking and fusion to the plasma membrane results in the extracellular release of ILVs, thereby giving rise to exosomes. The production of exosomes may be dependent or independent of the endosomal sorting complex required for transport (ESCRT) machinery. ESCRT-0, -I, -II, and -III protein complexes associate sequentially to facilitate membrane fission and loading of EV cargo [22]. ESCRT-independent exosome release occurs via the production of ceramide and sphingolipid membrane rafts and the activity of neutral sphingomyelinase 2 [23]. Alternatively, microvesicles (MVs), 100–1000 nm in size, shed directly

from the plasma membrane. Specific membrane domains are enriched with proteins that permit curvature and budding via higher order oligomerisation and rearrangement of actin-cytoskeletal networks. ESCRT proteins and ceramides are also implicated in MV formation, in addition to ADP-ribosylation factor 6 (ARF6) which participates in cargo selection [22]. MV formation is highly dependent on calcium influx and amenable to activation by cell stress [24, 25].

Given the challenge of identifying the exact intracellular origin of EVs isolated from the extracellular milieu, other characteristics such as size, density and expression of specific surface markers are employed to distinguish EV subpopulations. Though, a recent report of comprehensive EV proteomic characterisation revealed significant heterogeneity in marker expression within subtypes, particularly amongst small EVs with or without endosomal origin [26]. Importantly, most of the commonly used isolation techniques produce a mixture of vesicle populations of varying purity and enrichment. Accordingly, current guidance imparted by the Minimal Information for the Study of Extracellular Vesicles (MISEV) [27], states that isolates should be described generically as "extracellular vesicles", but may be classified as small EVs (< 200 nm) or medium/large EVs (> 200 nm), by specific molecular components (e.g. ASGR1 + EV) or by cell of origin (hepatocyte-derived EV). It should be noted that for the purpose of biomarker discovery, rigorous separation of EV subtypes may only be necessary to the degree to which sufficient sensitivity and specificity can be achieved.

EV composition and cargo

EVs contain biologically functional cargo, comprised of proteins (including metabolically active enzymes), lipids, metabolites and nucleic acids, such as messenger RNA, microRNA, long non-coding RNA and DNA [28] (Fig. 1). EV-enriched proteins are largely derived from their pathways of biogenesis. Tetraspanins (CD63, CD81 and CD9) and human leukocyte antigen class 1 (HLA-I) are transmembrane proteins commonly found in EV membranes, while tumour susceptibility gene 101 (TSG101), ALG-2 interacting protein (ALIX) and syntenin are cytosolic proteins involved in EV formation that are ultimately exported in vesicles [27]. In addition to general markers of EVs, cell type-specific proteins expressed on cell membranes may be integrated into the membrane of secreted EVs [29]. The identification of cell-type specific surface proteins on EVs has been exploited for immunoaffinity-based isolation of cell- or tissue-specific EVs from the global circulating

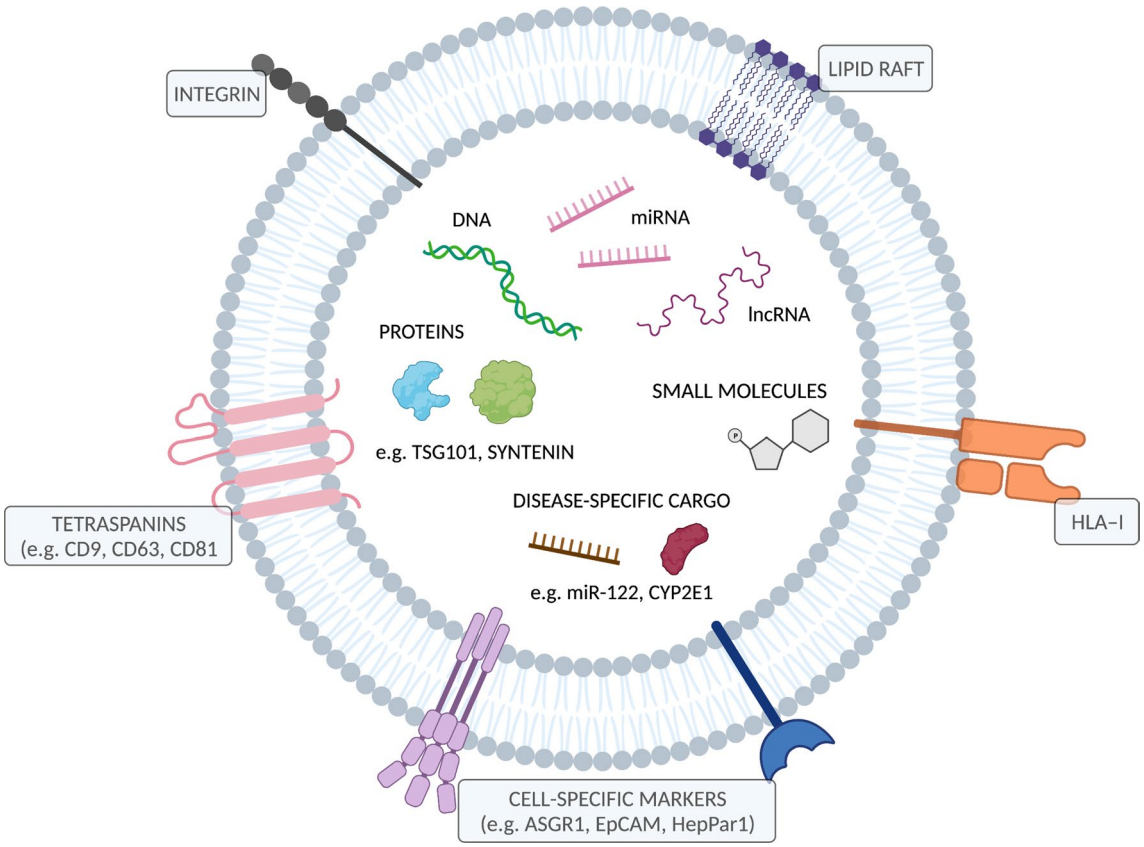

Fig. 1 Structure and cargo of an extracellular vesicle. Figure was created using BioRender.com

pool. This has vast potential to improve the sensitivity and specificity of low abundance and ubiquitously expressed disease biomarkers against the background noise resulting from constitutive systemic EV release.

Current evidence for the selective packaging of EV molecular cargo is supported by high variability and discordance in protein and RNA levels between EVs and their parental cell [7, 22]. While the exact mechanisms for regulated sorting of cargo remain unclear, the roles of various RNA-binding proteins, Rab GTPases, and post-translational modifications, such as ubiquitination and phosphorylation, have been reported [24, 30]. The abundance and composition of EVs may be altered in response to ER stress [31] or phenotypic activation. Li, et. al. [7] demonstrated that, compared to quiescent hepatic stellate cells, EV were released at 4.5-fold greater rate upon transdifferentiation to a myofibroblastic phenotype, and contained more abundant proteomic information associated with extracellular matrix production and metabolic activity.

EVs as minimally invasive biomarkers

EVs are considered attractive biomarkers for a host of reasons. Vesicles are abundant and highly stable in biofluids, exhibiting longer half-lives than other circulating components, such as free proteins or RNA complexes [20]. Durable lipid bilayer membranes protect molecular cargo from degradation, thereby providing a sort of "biomarker reservoir" [32]. Since this diverse cargo is dynamic in nature, directly related to the phenotype of parent cells, it may be used to understand function at the organ, tissue or cellular level and track changes in real time. In line with this application, and in contrast to traditional tissue biopsy, sampling of EVs is easily performed through access to peripheral blood and is repeatable with minimal patient risk. As will be explored throughout this review, the pertinence of EVs as a biomarker source is underpinned by the biological activity of these entities across elements of chronic liver disease. These mechanistic links may be the key to establishing a disease-specific molecular signature from affected tissues. Notably, changes in EVs have been demonstrated at earlier stages than overt tissue damage or other clinical and histological signs [33]. However, as total blood EV is comprised of vesicles released from multiple tissues into the circulation, the development of biomarker strategies is increasingly geared towards selective analysis based on tissue-specific markers [34].

EV-based therapeutics

In addition to their role as a key diagnostic and monitoring tool for the treatment of liver diseases, the application of EVs as a therapeutic intervention for multiple forms of liver disease has emerged. The properties of EV membranes make them ideal vehicles for therapeutic cargo, including miRNA, small interfering RNA (siRNA), chemotherapy agents or other drugs, which may act to promote tissue regeneration, reduce or reverse inflammation and fibrosis, or target cancer cells in the liver. Promising results have been demonstrated regarding the use of mesenchymal stem cell-derived EVs in various pre-clinical models. However, the requirements to initiate human trials are very different between a biomarker and an intervention. EV-based therapeutics face several challenges related to the cost and scale of manufacturing pure EVs that adhere to regulatory and quality control standards for use in humans. Meanwhile, much of the recent research regarding the role of EVs as biomarkers has come from human data. Beyond pre-clinical studies identifying EV cargo that reflect molecular changes in liver diseases, a key focus of the present review is the detection of circulating EVs in human patients. Thus, the application of EVs as therapeutics will not be extensively reviewed here but may be found in references [22, 35, 36].

EVs in normal liver physiology

The liver is the largest internal organ in the body, functionally and anatomically complex and responsible for a diverse set of metabolic, synthetic, digestive, detoxifying, storage and regulatory roles. Approximately, 80% of total liver volume is comprised of hepatocytes, which are responsible for the central physiological processes, while a further 6.5% accounts for non-parenchymal cells that function in support of hepatocytes and maintenance of the hepatic microenvironment [20, 37]. These cells include liver sinusoidal endothelial cells (LSECs), hepatic stellate cells (HSCs), cholangiocytes and the population of liver-resident macrophages, known as Kupffer cells. The organised lobular architecture of the liver facilitates cooperation and inter-regulatory functions of diverse cell types through anatomical proximity [38]. Effective cell-to-cell communication is also achieved by the network of EV interactions, as each cell is both a donor and recipient of EVs from the same and other hepatic cell types (Fig. 2). The bi-directional transfer of molecular information is imperative to homeostatic control in the liver as well as the broader inter-organ communicative landscape.

Hepatic cell-derived EVs

The function of EVs derived from different hepatic cell types is summarised in Table 1. Multiple enzymes involved in the metabolism of carbohydrates, lipids, endogenous compounds and xenobiotics are among key molecular cargo identified in hepatocyte-derived EVs [39]. Hepatic

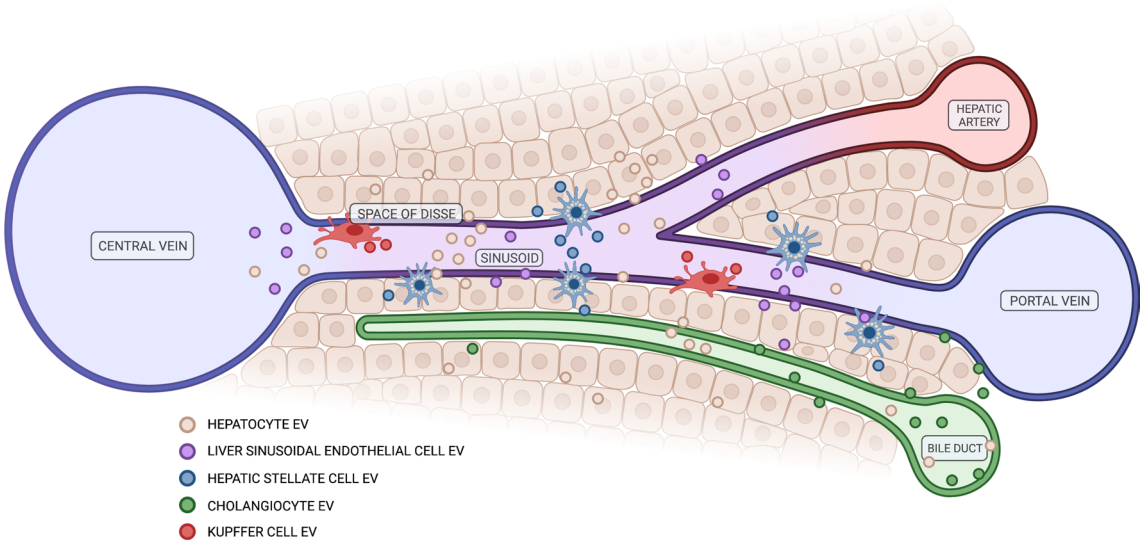

Fig. 2 Extracellular vesicle release by various hepatic cells in normal liver function. Figure was created using BioRender.com

metabolic activity may be transferred to or induced in extra-hepatic niches. For example, hepatocyte-derived EVs carrying arginase-1 were found to regulate endothelial cell function and alter serum metabolites associated with oxidative stress in the systemic vasculature [40]. In the liver, hepatocyte-EVs have also been shown to promote the proliferation of cholangiocytes and other hepatocytes in paracrine and autocrine fashions, respectively [37, 41]. Hepatocyte-derived EVs have demonstrated the remarkable capacity to mediate regeneration of functional liver mass. Nojima, et. al. [42] EV-mediated transfer of sphingosine-1-phosphate (S1P), sphingosine kinase 2 (SK2) and ceramidase between hepatocytes promoted liver regeneration in mice following 70% hepatectomy. HSC are the key fibrogenic cells in the liver, and exchange of EVs between them is crucial in balancing extracellular matrix (ECM) production and degradation. LSEC-derived EVs contribute to modulation of this balance. The EVs normally maintain HSC quiescence, but when stimulated, EVs containing upregulated sphingosine kinase 1 (SK1) are released to activate HSC [43]. Quiescent HSC (qHSC) release EVs containing miRNAs (miR-214 and -199-5p) and the transcription factor, Twist-1 [44, 45]. This cargo suppresses connective tissue growth factor (CTGF) to maintain quiescence in other qHSC or downregulate profibrotic genes, including α-smooth muscle actin (αSMA) and collagen, in activated HSC (aHSC) [7, 21]. Conversely, aHSC-derived EVs promote ECM production by transferring CTGF [46]. Lastly, EVs from cholangiocytes participate

Table 1 Hepatic cell EVs function and cargo

Originating cell	Example cargo	Recipient cells	Functions	References
Hepatocytes	DMET proteins and mRNA	Hepatocytes, extrahepatic cells	Transfer metabolic activity	Conde-Vancells et al. [39], Kumar et al. [51], Rowland et al. [52], Rodriguez et al. [53]
	Arginase-1	Endothelial cells	Regulate endothelial cells in systemic vasculature	Royo et al. [40]
	S1P, SK2, ceramidase	Hepatocytes	Promote proliferation and liver regeneration	Nojima et al. [42]
Liver sinusoidal endothelial cells	SK1	HSC	Modulate quiescent/active phenotype	Wang et al. [43]
Hepatic stellate cells	miR-214, miR-199-5p, Twist-1, CTGF	HSC	Modulate quiescent/active phenotype	Charrier et al. [46], Chen et al. [21], Chen et al. [45], Chen et al. [44] and Li et al. 2020
Cholangiocytes	lncRNA H19	Hepatocytes	Regulate bile acid homeostasis	Li et al. [47]
	Hedgehog ligands	LSEC	Promote wound-healing response	Witek et al. [48]

in bile acid homeostasis through the transfer of long non-coding RNA H19 to hepatocytes [47], and in wound-healing responses by delivering hedgehog ligands to promote angiogenesis, growth and differentiation in recipient LSECs [48].

Metabolism

Hepatic metabolism plays a critical role in regulating the abundance of endogenous chemicals, such as bile acids, fatty acids, steroid hormones and bilirubin. Similarly, it serves as a major clearance mechanism for xenobiotics including drugs, dietary chemicals and environmental toxins. Specifically, metabolic clearance is the major route of elimination for more than 80% of pharmaceutical drugs [49, 50]. Notably, the mRNA transcripts and active proteins of drug metabolising enzymes and transporters (DMET), cytochrome P450 (CYPs), UDP-glucuronosyltransferase (UGTs), glutathione S-transferase and organic anion transporting polypeptides (OATPs) have been detected in EVs derived from hepatocytes and in the blood. CYP protein and mRNA is enriched in circulating EVs relative to total plasma, which suggests selective packaging [51–53]. The transfer of DMET in circulating EVs has physiological significance with respect to protection of extra-hepatic cells from systemic toxicants or increasing metabolic activity in tissues with lower basal DMET expression, such as the lungs or brain [54]. Clinically, this notion has potential applications as liquid biopsy to indicate chronic alcohol, nicotine or illicit drug use, liver disease, or to assess metabolic drug–drug interactions (DDIs) and inter-individual variability in drug exposure. For example, CYP2E1 is induced by chronic use of alcohol or paracetamol overdose. This is reflected in greater release of hepatocyte EVs that transfer the capacity for CYP2E1-mediated metabolism, resulting in oxidative stress and acute injury in hepatic and non-hepatic cells [51]. A recent review described how disease-associated alterations in CYP protein expression and activity may impact drug exposure in patients with NAFLD [55]. The capacity to monitor changing pharmacokinetic profile is paramount for the development of novel therapeutics for NAFLD and in optimal dosing of existing treatments for common comorbidities.

Assessing variability in metabolic clearance within or between individuals, resulting from variable hepatic DMET expression or activity, DDIs, presence of liver disease or other factors, is an appealing avenue for EV-based DMET profiling. Work by our group showed that EV-derived CYP3A4 was highly concordant with apparent oral clearance of its probe substrate midazolam in healthy subjects pre- and post-dosing of the inducer, rifampicin [52]. Since then, Achour, et. al. [49] evaluated hepatic elimination based on circulating EV mRNA of clinically important DMET, reporting sound correlations with protein expression in liver tissue. Interestingly, this study normalised the data to a panel of 13 liver-specific RNA markers (e.g. apolipoprotein A2 and fibrinogen-beta) as part of a novel shedding factor to account for variability in liver EV release into the bloodstream. Instead, we recently applied our novel two-step anti-ASGR1 immunocapture technique to selectively isolate hepatocyte-derived EVs from global EVs and successfully tracked the induction of CYPs 3A4, 3A5 and 2D6 and OATPs 1B1 and 1B3 during pregnancy and following rifampicin administration [53]. Together these reports position EV liquid biopsy as a viable strategy for individual DMET phenotyping to aid precision dosing or classification of clinical trial participants at enrolment.

EVs in liver pathobiology

Chronic liver diseases result from prolonged injurious stimuli that exceed the regenerative capacity of the liver. Over time, unresolved inflammatory and fibrogenic activation from disorders such as ALD, NAFLD, HBV and HCV infection can ultimately lead to fibrosis, cirrhosis and HCC [20]. EVs have emerged as potent pathogenic drivers in several of these processes and a breadth of pre-clinical data establishes the key molecular information carried in EVs that mediate liver cell cross-talk in different chronic liver diseases. In several instances, these EV cargoes have been analysed in the circulation of animal models or human patients and demonstrate the capacity for circulating EVs derived from specific cellular sources to reflect pathological events in affected organs. For each chronic liver disease, Table 2 lists the cell-specific EVs and their cargoes, with recipient cells and resulting function (if defined), divided into studies that examined EVs in circulation and in vitro studies of EV cargo yet to be translated to circulating EVs.

Non-alcoholic fatty liver disease

NAFLD is the most common chronic liver disease, currently estimated to affect more than 25% of the global population [56]. The condition may be considered a hepatic manifestation of the metabolic syndrome as it is often implicated with other features, such as insulin resistance (IR), obesity and type 2 diabetes mellitus [5]. In line with this, recent expert consensus supports the updated nomenclature of metabolic associated fatty liver disease (MAFLD), to reflect advancing knowledge of disease phenotype, heterogeneity in drivers and coexisting conditions and diagnostic criteria that is based on inclusion rather than exclusion (particularly around alcohol use) [57, 58].

The condition presents as a spectrum of clinical disease with some patients exhibiting simple steatosis (NAFL) while

Table 2 EV cargo from specific cellular origins, effect on recipient cells and detection in circulation in chronic liver diseases

Condition	Originating cell (or source)	Cargo	Recipient cells	Function	Additional information	References
NAFLD	*Cargo detected in circulating EVs*					
	Hepatocytes	miR-122, -192, -128-3p	N/A	N/A	Increased in plasma of NAFLD patients	Newman et al. [68]
	Hepatocytes	mtDNA	N/A	TLR9 activation → inflammation	Increased in plasma of NASH patients	Garcia-Martinez et al. [70]
	Hepatocytes	ASGR1, CYP2E1	N/A	N/A	Increased in plasma of mice over-expressing IRE1α	Dasgupta et al. [31]
	Adipocytes	miR-99b	Hepatocytes	Suppress FGF-21 → promotes steatosis	Demonstrated transfer of cargo via circulation in mice with genetically altered miRNA processing in adipocytes	Thomou et al. [72]
	Hepatocytes Macrophages Neutrophils Platelets	ASGR1, CYP2E1 Galectin 3 Ly-6G/6C CD61	N/A	N/A	Increased in NAFLD mouse model	Li et al. [33]
	Hepatocytes	ASGR1, SLC27A5	N/A	N/A	Increased in NASH patient serum	Povero et al. [3]
	NK T-cells Macrophages	Valpha24/Vbeta11 CD14	N/A	Inflammation	Increased in NAFLD patient serum	Kornek et al. [85]
	Hepatocytes	ASGR2, CYP2E1	N/A	N/A	Decreased in patients with NAFLD resolution	Nakao et al. [109]
	Hepatocytes	ASGR1, HepPar1	N/A	N/A	Decreased in patients with bariatric surgery	Rega-Kaun et al. [131]
	Cargo not yet analysed in circulating EVs					
	Lipotoxic hepatocytes	TRAIL	Hepatocytes, macrophages	Hepatocyte death, macrophage activation & pro-inflammatory cytokine (IL-1β, IL-6)	Upregulated, in vitro	Hirsova et al. [62]
	Lipotoxic hepatocytes	CXCL10	Macrophages	Macrophage chemotaxis	Upregulated, in vitro	Ibrahim et al. [63, 64]
	Lipotoxic hepatocytes	C16:0 ceramide, SK1	Macrophages	Macrophage chemotaxis	Upregulated, in vitro	Kakazu et al., [65], Dasgupta et al. [31]
	Lipotoxic hepatocytes	miR-128-3p	HSC	Suppress PPARγ → profibrotic gene expression	Upregulated, in vitro	Povero et al. [66]
	Lipotoxic hepatocytes	VNN1	LSEC	Promote pathologic angiogenesis	Upregulated, in vitro	Povero et al. [67]
	Adipocytes	MCP-1, IL-6, MIF	Hepatocytes	Promote insulin resistance	Adipose tissue explant EVs applied to hepatocytes in vitro	Kranendonk et al., [71]

Table 2 (continued)

Condition	Originating cell (or source)	Cargo	Recipient cells	Function	Additional information	References
	Adipocytes	miRNA profile	Hepatocytes, HSC	Target TGF-β pathway → inhibits fibrolytic enzymes e.g. MMP-7	Adipose tissue EVs applied to hepatocytes in vitro	Koeck et al., [18]
ALD	*Cargo detected in circulating EVs*					
	Hepatocytes	mtDNA	Macrophages	TLR9 activation → pro-inflammatory cytokine release (IL-1β, IL-17)	Increased in murine AH model	Eguchi et al. [75]
	Hepatocytes	mtDNA	Neutrophils	Neutrophilia, macrophage recruitment to liver	Increased in murine chronic-plus-binge ethanol feeding model	Ma et al., [76]
	Hepatocytes	CD40 ligand	Macrophages	Phenotypic activation → Upregulated pro-inflammatory cytokine (IL-1β, IL-6, TNF-α)	Increased in human AH patients	Verma et al., [77]
	Hepatocytes	miR-122	Monocytes	Suppress haem oxygenase 1 → sensitise to pro-inflammatory stimuli	Increased in human acute alcohol use and mice binge and chronic alcohol consumption	Momen-Heravi et al., [78]
	Serum EV	miR -122, -155	N/A	N/A	Increased in EV-fraction of circulation in mice	Bala et al., [79]
	Serum/plasma EV	let-7f, miR -29a, -340	N/A	Target genes involved in inflammation and cancer development	Increased in mice with AH	Eguchi et al., [17]
	Hepatocytes	ASGR2, CYP2E1 Sphingolipids	N/A	Promote inflammation and cell death in AH	Increased in AH patient serum	Sehrawat et al., [13]
Viral Hepatitis	*Cargo detected in circulating EVs*					
	HCV-infected hepatocytes	Replication competent HCV-RNA	Hepatocytes	Viral transmission	Identified in human HCV patients	Bukong et al., [83]
	HCV-infected hepatocytes	miR-19a	HSC	TGF-β pathway activation → profibrotic gene expression	Upregulated in human HCV patients	Devhare et al., [84]
	CD8 + and CD4 + T cell	CD147	HSC	Induce MMP enzymes → promote ECM degradation in HCV-related fibrosis	Increased in active HCV patients	Kornek et al., [85]
	Cargo not yet analysed in circulating EVs					
	HBV-infected hepatocytes	HBV RNA and protein	Peripheral blood monocytes	Induce PDL-1 expression	Identified in vitro	Kakizaki et al., [81]
	HCV-infected hepatocytes	HCV protein E2	N/A	Mimic viral particles → hinders neutralising antibody response	Identified in vitro	Deng et al., [82]

Table 2 (continued)

Condition	Originating cell (or source)	Cargo	Recipient cells	Function	Additional information	References
	LSEC	IFN-stimulated genes	Hepatocytes, LSEC	Promote antiviral response	Identified in vitro	Giugliano et al., [38]
HCC	*Cargo detected in circulating EVs*					
	Malignant hepatocytes	miR-93 miR-224 miR-665	Hepatocytes	Promote HCC proliferation	Each upregulated in human HCC patients	Xue et al., [89], Cui et al., [90], Qu et al., [91]
	Malignant hepatocytes	miR-9-3p miR-638 miR-718 miR-744	Hepatocytes	Inhibit HCC proliferation	Each downregulated in HCC patients	Tang et al., [92], Shi et al., [93], Sugimachi et al., [94], Wang et al., [95]
	Malignant hepatocytes	miR-1247-3p	Fibroblasts	Phenotypic switch to cancer-associated fibroblasts in lung metastasis, increased pro-inflammatory cytokine (IL-6 and IL-8) secretion	Increased in HCC patients with lung metastasis	Fang et al., [99]
	Tumour (HCC/ICC/PSC) EV in serum	Proteomic signature	N/A	N/A	Differential expression between pathologies and healthy controls	Arbelaiz et al. [100]
	Tumour (HCC) EV in serum	Annexin V, EpCAM, ASGR1, CD133	N/A	N/A	Panel of markers distinguishes HCC from cholangiocarcinoma	Julich-Hartel et al., [125]
	Tumour (HCC) EV in plasma	HepPar1	N/A	N/A	Increased with HCC recurrence	Abbate et al. [126]
	Tumour (HCC) EV in plasma	ASGR1, EpCAM, CD147, 10 mRNA transcripts	N/A	N/A	Differential expression between HCC, other primary malignancies and non-cancer	Sun et al. [32]
	Cargo not yet analysed in circulating EVs					
	Malignant hepatocytes	miRNA profile	Hepatocytes	Modulate TAK1 pathway → promote cancer growth	Identified in vitro	Kogure et al. [96]
	Malignant hepatocytes	linc-ROR	Healthy hepatocytes	Inhibit apoptosis and enhance proliferation	Upregulated in vitro	He et al. [97]
	Malignant hepatocytes	MET proto-oncogene, caveolins, S100 family members	Healthy hepatocytes	Mobilisation, tumour invasion	Identified in vitro	He et al. [98]
Fibrosis	*Cargo detected in circulating EVs*					
	Activated HSC	PDGFRα	HSC	Promote migration	Upregulated in human liver fibrosis patients	Kostallari et al. [30]

Table 2 (continued)

Condition	Originating cell (or source)	Cargo	Recipient cells	Function	Additional information	References
	LSEC	SK1, S1P mRNA and protein	HSC	Promote AKT phosphorylation and migration	Upregulated in human AH patients and mice with experimental liver fibrosis	Wang et al. [43]
	Hepatocytes, activated HSC	Hedgehog ligands	HSC, endothelial progenitor cells	Promote proliferation and angiogenesis	Upregulated in rats undergoing bile duct ligation	Witek et al. [48]
	Serum EV	miR -34c, -151-3p, -483-5p, -532-5p and -687	Hepatocytes, activated HSC	Decrease hepatocyte death, hepatic fibrosis and inflammation	Downregulated in human liver fibrosis patient and mice with experimental liver fibrosis	Chen et al. [1]
	Cargo not yet analysed in circulating EVs					
	Activated HSC	Proteomic profile associated with ECM production and metabolic activity	HSC	Activate HSC, promote fibrogenesis	Identified in vitro	Li et al. [7]

a fraction (~ 30%) will develop non-alcoholic steatohepatitis (NASH) [59]. NAFLD is the product of multiple dysregulated signalling pathways in the liver that involves abnormal lipid metabolism leading to lipotoxicity and inflammation [31]. While several risk factors relating to diet and lifestyle are linked to the incidence of NAFLD, genetic predispositions have also been noted, as recently reviewed by Jonas, et. al. [60]. Further, the contribution of gut dysbiosis, liver-adipose cross-talk and increased cardiovascular disease-related mortality, underscores the systemic nature of this condition [61]. Current diagnostic tools remain inadequate for the early detection, risk stratification and monitoring of NAFL and NASH, presenting a significant hindrance to the clinical management of patients and development of effective pharmaceutical interventions [16].

Numerous reports to date demonstrate changes in EVs released by hepatocytes under lipotoxic stress and their contributions to cellular and inter-organ cross-talk to promote inflammation and fibrosis in the liver. These were described in detail in a previous review [5]. Key molecular cargo of lipotoxic hepatocyte-derived EVs include the death receptor ligand, TRAIL, which triggers hepatocyte death and macrophage activation with increased pro-inflammatory cytokine expression (interleukin [IL]-1β and IL-6) [62]. The macrophage chemoattractant C-X-C motif ligand 10 (CXCL10) was also detected in EVs induced by steatosis-related JNK activation in the liver [63, 64]. Further, lipotoxic EV release was found to be dependent on ceramide pathways, activated by the ER stress sensor inositol-requiring enzyme-1α (IRE1α). IRE1α-stimulated EVs contained C16:0 ceramide and SK1 which promoted macrophage chemotaxis in vitro [65] and macrophage recruitment and hepatic inflammation in mice [31]. The authors also showed that mice over-expressing IRE1α had significantly elevated circulating EVs and their hepatocellular origin was identified by electron microscopy (EM) with immunogold labelling of ASGR1 and CYP2E1. Lipotoxic hepatocyte-derived EVs also modulate HSC phenotype in NAFLD. Specifically, EVs containing miR-128-3p suppressed peroxisome proliferator-activated receptor-γ (PPARγ) in HSC, resulting in upregulated profibrotic gene expression [66]. The effect was dependent on EV internalisation by HSC, mediated by Vanin-1 (VNN1) on the surface of vesicles. Increased VNN1 expression on lipotoxic EVs was previously implicated with EV internalisation by LSEC resulting in pathologic angiogenesis [67]. Increased expression of miR-128-3p was also identified in our recent work, alongside miR-122 and -192, in NAFL and NASH patient plasma EVs. This was only observed in circulating EVs derived specifically from hepatocytes (expressing ASGR1) [68]. Mitochondrial dysfunction and oxidative stress are common pathogenic events in fatty liver diseases related to both aetiologies, non-alcoholic and alcoholic (discussed in the following section)

[69]. Mitochondrial DNA (mtDNA) has been identified as important EV cargo that promotes inflammation via TLR9 activation, thereby contributing to the transition from simple steatosis to steatohepatitis. Garcia-Martinez, et. al. [70] found greater levels of mtDNA in plasma microvesicles of mice and patients with NASH, with concomitant increase in hepatocyte-specific marker, Arg-1, and demonstrated the capacity for these particles to activate TLR9.

EVs from visceral adipose tissue actively contribute to NAFLD pathogenesis by exacerbating systemic IR, inflammation and hepatic fibrosis [71]. Differentially expressed miRNAs in adipocyte-EVs from lean and obese individuals target the TGF-β pathway in hepatocytes and HSC, resulting in the inhibition of fibrolytic enzymes such as matrix metalloproteinase (MMP)-7 [18]. Another study emphasised the important contribution of adipocyte-EV to circulating miRNA levels and their capacity to modulate gene expression in the liver [72]. The authors showed that fibroblast growth factor (FGF)-21 is a liver protein target of adipocyte-EV derived miR-99b. FGF-21 is implicated in many metabolic pathways and its suppression contributes to hepatic steatosis [73]. In all, the current evidence positions EVs as key players in the pathogenesis and progression of NAFLD and supports the investigation of biomarkers within EV derived from adipocytes and hepatic cell populations.

Alcoholic liver disease

Alcoholic liver disease (ALD) follows a similar clinical course to that of NAFLD. Hepatic steatosis and alcoholic hepatitis (AH) may resolve with alcohol abstinence, but progressive disease can lead to cirrhosis and liver failure [74]. Liver biopsy is not usually necessary for ALD diagnosis as a history of significant alcohol consumption along with clinical, radiologic and biochemical findings are often sufficient. However, diagnosis may be complicated in alcoholic patients with unreliable history or co-existing risk factors for other conditions such as NAFLD; in such cases the threshold for "significant" alcohol intake may be reduced. The lack of accurate non-invasive biomarkers limits the dynamic assessment of inflammatory activity and degree of fibrosis in ALD, as well as the risk of developing cirrhosis. Considering that ALD accounts for 50% of cirrhosis-related deaths [13], biomarker discovery is an area of intense research focus to improve the management of ALD and development of pharmacological strategies to halt or reverse the disease.

EV-mediated macrophage activation is increasingly recognised as a key feature of the inflammatory process in AH and parallels hepatic injury and fibrosis. A mouse model of AH had significantly increased EV levels in circulation and vesicles isolated from primary hepatocytes were found to be enriched in mtDNA [75]. These EV activated TLR9 resulting in upregulated pro-inflammatory cytokine, IL-1β and IL-17 production in liver macrophages and promoted fibrogenic activation of HSC. Another study similarly found that hepatocyte-derived mtDNA-enriched vesicles released in response to chronic and binge ethanol feeding in mice contributed to macrophage and neutrophil infiltration in the liver [76]. Verma, et. al. [77] treated hepatocytes with ethanol in vitro, and showed greater release of EVs expressing CD40-ligand. These stimulated macrophage-to-M1 phenotypic switching, characterised by upregulated pro-inflammatory cytokine expression (TNFα, IL-1β and IL-6). Increased CD40L-expressing EVs were also detected in the serum of patients with AH. Similarly, Momen-Heravi, et. al. [78] demonstrated that EV containing miR-122 is transferred from ethanol-treated hepatocytes to monocytes, resulting in suppression of haem oxygenase 1 (HO-1) and subsequent sensitisation to pro-inflammatory stimuli, such as lipopolysaccharide. In addition, mice and humans subjected to acute alcohol binge, and mice also to chronic consumption, had more EVs in circulation. The levels of miR-122 and -155 in the EVs changed over time post-binge, suggesting variable packaging in response to alcohol. This notion is supported by earlier data comparing specific miRNA expression in circulating vesicle or protein fractions across models of liver injury with different aetiologies [79]. The authors showed that in models of inflammatory (i.e. NAFLD) or alcohol-induced disease, miR-122 and -155 was mostly EV-associated, while predominantly protein-associated in DILI. This distinctive distribution of miRNA in chronic liver disease in contrast to the acute condition, DILI, supports the investigation of biomarkers localised in EVs in the circulation to improve performance and disease-specificity. EV miRNA profile was also explored in mice with AH induced by continuous intragastric ethanol infusion. Three miRNAs in blood EVs, including let-7f-5p, miR-29a-3p and miR-340-5p, discriminated AH mice from controls, as well as from obese mice and those with NASH or cholestatic injury [17]. Various sphingolipids have also been implicated with inflammation and cell death in AH. Serum EVs from AH patients were recently shown to be significantly enriched in six sphingolipid species compared to healthy controls, heavy drinkers, NASH patients and alcoholic cirrhosis patients. The cargo was positively correlated with disease severity and predicted 90-day survival [13].

Viral hepatitis

Viral infections represent a significant cause of chronic liver diseases and are the most common aetiology for HCC [6]. In addition to certain viral factors, the carcinogenic nature of HBV and HCV are linked to chronic inflammation, fibrosis and changes in signalling pathways implicated in

hepatocyte survival and tumour surveillance and suppression [80]. While viral infections can be diagnosed by serological techniques and monitored with respect to viral load and immune status [11], a better understanding of the role of EVs in pathogenesis and disease progression may facilitate non-invasive assessment of liver damage and identify early markers of increased HCC risk.

EVs are potent modulators of immune function. Hepatocytes infected with replicating HBV release EVs that induce programmed death ligand-1 (PDL-1) in recipient monocytes, possibly suppressing host antiviral activity [81]. Another study showed that HCV-infected hepatocytes secrete EVs coated with the HCV protein E2. These EV mimic viral particles thereby hindering the neutralising antibody response [82]. Conversely, LSEC-derived EVs stimulated by interferon (IFN)-I and -III, contribute to the antiviral response [38]. Interestingly, EVs were found to participate in viral spread during HCV infection. Using a rigorous multi-step approach to remove free virus contamination, Bukong, et. al. [83] isolated EVs from infected patient sera and Huh7.5 cell culture supernatant. The EVs contained replication competent HCV-RNA in complex with argonaute-2, heat shock protein 90 and miR-122, which mediated new infection in hepatocytes. Hepatocyte-derived EV also activates HSC to promote fibrosis in HCV. TGF-β pathway activation was found to be triggered by EV-derived miR-19a in vitro and increased levels of the miRNA were detected in serum EV from chronic HCV patients compared to healthy controls and patients with non-HCV-related liver disease of similar fibrosis grade [84]. A previous study, however, found elevated circulating CD8 + and CD4 + T cell-derived EVs in patients with active HCV, that promoted ECM degradation by induction of MMP enzymes in HSC [85]. In summation, these reports provide avenues for development of novel biomarkers or therapeutic tools for chronic viral hepatitis.

Hepatocellular carcinoma

Hepatocellular carcinoma accounts for more than 80% of primary liver malignancies and a third of global cancer-related deaths [86]. Chronic liver diseases, especially with cirrhosis, are major risk factors for HCC. Prognosis is poor, exhibiting only 20% 5-year overall survival, often due to late stage diagnoses [86]. Ultrasound has acceptable sensitivity and specificity for HCC screening, but its capacity to detect early lesions is limited [32]. Serum alpha-fetoprotein (AFP) is a biomarker of widely variable performance that may be elevated in late stages, but only in a subset of patients [11]. Accordingly, a combination of ultrasound and AFP assessment is recommended for surveillance by the Australian practice guidelines [87]. The use of ultrasound is also endorsed by the American Association for the Study of Liver Diseases (AASLD), with or without AFP [88]. EVs are one of three liquid biopsy approaches in oncology, among circulating tumour DNA and tumour cells [32]. Since EVs carrying tumour-derived information are present in circulation earlier and persist through to advanced disease, they present the opportunity to initiate curative interventions.

The dysregulation of multiple signalling pathways and complex network of interactions between malignant and non-malignant cells in the tumour microenvironment are critical to tumour progression. EVs are known to play a role in regulating cell proliferation, migration, angiogenesis, metastasis, epithelial-to-mesenchymal transition (EMT), and immune escape. Specific HCC-EV miRNA cargo, for example, has been linked to enhanced HCC proliferation (including miR-93, -224 and -665) [89–91], while other cargo was found to have an inhibitory effect (miR-9-3p, -638, -718 and -744) [92–95]. Kogure et al. [96] reported that selectively packaged miRNA and protein in HCC-derived EVs modulate the TGF-β activated kinase 1 (TAK1) pathway in other hepatic cells to promote cancer growth. More recently, HCC-derived EVs were found to inhibit apoptosis and enhance proliferation of hepatocytes via transfer of long intergenic non-coding RNA regulator of reprogramming (linc-ROR) [97].

EVs also promote the invasion of HCC tumours through normal liver tissue, as metastatic HCC-derived EV mobilise healthy hepatocytes via transfer of oncogenic cargo, such as mesenchymal-epithelial transition (MET) proto-oncogene, caveolins and S100 family members [98]. EV from metastatic HCC also contain miR-1247-3p which facilitates the conversion of normal fibroblasts to cancer-associated fibroblasts (CAFs) in lung metastases and increased pro-inflammatory cytokine (IL-6 and IL-8) secretion [99]. In HCC patients, lung metastasis was positively correlated with serum levels of EV-derived miR-1247-3p. EV protein cargo in serum was also shown to aid differential diagnosis of intrahepatic cholangiocarcinoma, HCC and primary sclerosing cholangitis, which is challenging with current non-invasive tools [100]. These studies support the role of tumour-derived EV cargo in encouraging a tumour-favourable environment for progression and metastasis through communication with cancerous and non-cancerous cells, and advance the notion that promising biomarker candidates linked to oncogenic processes may be detected in circulating EVs.

Fibrosis

Liver fibrosis is a significant cause of morbidity and strong independent risk factor for mortality in chronic liver diseases, especially NAFLD [101]. While effective treatment of the precipitating condition may reverse fibrosis in some

patients, specific antifibrotic treatment options are scarce [1] and patients may advance to cirrhosis and liver failure, often necessitating liver transplantation [43]. HSC activation is the principal event at the cellular level leading to ECM deposition and, under persistent profibrogenic conditions, can produce fibrous scar and severely compromise liver function [1, 7]. Fibrosis is a typical progression common among multiple chronic liver diseases and can be characterised by a number of molecular pathways not specifically altered by a particular condition. These may be monitored via EV-derived markers as described below; thus, in conjunction with disease-specific markers that identify the precipitating condition, fibrosis markers may be helpful in tracking the severity of this complication.

EVs from HSCs of both quiescent and myofibroblast phenotypes form a complex interplay of pro- and anti-fibrotic EV signalling in the injured liver. One study determined that HSCs treated with PDGF-BB in vitro released EVs enriched with PDGF receptor-alpha (PDGFRα) via a mechanism of selective packaging [30]. The EVs promoted migration in recipient HSC and liver fibrosis in healthy mice, while inhibiting EV export of PDGFRα ameliorated fibrosis in carbon tetrachloride (CCL_4)-treated mice. Patients with liver fibrosis also had increased levels of PDGFRα in serum EV. HSC phenotype is further modulated by LSEC-derived EV. Wang et al. [43] showed that the EV specifically transfer SK1 and S1P cargo, which upregulate AKT phosphorylation and migration. Expression of each at RNA and protein level was detectable in EVs from mice with experimental liver fibrosis and human patients with alcoholic fibrosis.

The Hedgehog (Hh) pathway is critical to the wound-healing response and tissue remodelling in chronic liver injury. Hh ligands released in EVs from damaged hepatocytes and aHSC, promote proliferation and angiogenesis in recipient HSC and endothelial progenitor cells, respectively; and have been detected at increased levels in the plasma and bile of rats with fibrosis induced by bile duct ligation [48]. Further, discordant miRNA and protein cargo in EVs from qHSC and aHSC, either stimulate or inhibit fibrosis depending on the phenotype of originating and recipient cells. Serum EVs from healthy individuals contain "anti-fibrotic" miRNA which decreased CTGF, αSMA and collagen gene expression when applied to aHSC in vitro and reduced hepatic fibrosis and inflammation in CCL_4-treated mice [1]. Meanwhile, a proteomic comparison of qHSC- and aHSC-derived EV revealed greater protein content in the latter, associated with profibrotic, inflammatory and chemotactic functions [7]. Accordingly, the presence of distinct pro- and anti-fibrotic EV populations in the liver presents the intriguing possibility to track fibrogenic activity and develop novel anti-fibrotic therapies.

Analysis of circulating tissue-specific EV biomarkers

The studies described thus far indicate the potential for biomarkers with mechanistic links to chronic liver pathology to be released in EVs and detected in the circulation (Fig. 3). However, the EVs harbouring these molecules of interest account for a relatively small proportion of the complex circulating mixture of vesicles, which are also derived from multiple other cells and organs. In plasma, platelets are a major source of EVs (originating up to 90%), followed by other haematopoietic or endothelial cell types [102, 103]. While the reported proportion of hepatocyte-derived EVs in circulation varies widely [3, 33], this may be as small as a fraction of a percent. Since conventional methods separate vesicles from other blood components based on physical properties, producing bulk isolates of heterogenous composition, the background noise from non-hepatic EVs may preclude the sensitive detection of disease-related changes. This is likely to be particularly apparent in the diagnosis of early-stage patients [104]. Evidently, the inability to efficiently isolate relevant subpopulations of EVs containing candidate biomarkers represents a major barrier to their clinical translation. Immunoaffinity capture fits within a broader framework of EV sample collection and analysis for blood-based biomarker contexts. The methodology can be summarised in a generic workflow (Fig. 4) that incorporates best practice (as reviewed by Useckaite, et. al. [105]) and recommendations for characterisation and reporting [27, 106]. While the review of common isolation methods is beyond the present scope and described in detail elsewhere [102, 107], the following section will discuss the application of immunoaffinity-based capture methods to detect cell- or tissue-specific EVs and analyse their cargo in the context of chronic liver diseases. Supplemented by emerging technologies, we envision this to serve as a foundation for the implementation of informed and actionable biomarker strategies with broader relevance to any condition or application. Studies described in this section are also listed in Table 2 under *Cargo detected in circulating EVs* for the particular disease.

Technologies to assess tissue-specific EVs

Given the biogenesis pathway and cell of origin influence surface protein expression on EVs, the isolation of particular subpopulations can be achieved by immunoaffinity capture (IAC) [108]. IAC is based on the interactions of EV surface molecules with antibodies, most commonly against tetraspanins, that are covalently linked to a fixed

phase, such as magnetic or non-magnetic beads, plastic or silica plates, porous monolithic microtips or microfluidic devices [102]. Compared to conventional isolation methods, the use of antibodies permits the extraction of highly pure and specific EVs, lending itself to customisation against EV markers of interest [107, 108]. For instance, ASGR and CYP2E1 are known membrane-localised EV constituents with high specificity for EVs of hepatocyte origin, and have been applied for the selective analysis of hepatocyte-derived biomarkers for liver disease in vivo [109]. However, targeting specific EV populations inherently reduces yield. Efficient recovery by IAC depends on the availability of antibodies with sufficient specificity and stability. The high cost of antibodies also limits scaling of capture protocols to large sample volumes [107]. Though some techniques can be performed directly from biofluids, IAC is usually preceded by global EV enrichment. Variability between different global isolation methods with respect to subtype enrichment and cargo [110], underscores the importance of confirming compatibility of a chosen method with downstream analyses. Despite present limitations, emerging immunoaffinity-based technologies show promise to improve clinical biomarker analyses in a robust, timely and cost-effective manner.

Immunobead- or plate-based capture

The most common approach to selectively isolate EV subtypes involves incubation of EVs with antibodies conjugated to magnetic beads or on plates [111]. EVs positive for cell- or disease-specific surface markers can then be selectively removed from the mixture by magnetic forces or immobilisation on the plate surface. This may also be used to improve the purity of samples, pre-enriched by precipitation or ultracentrifugation, by targeting tetraspanins [107]. The method is compatible with downstream analyses, including polymerase chain reaction (PCR), for direct quantification of molecular cargo [111], however, tight covalent bonds make the elution of bead- or plate-bound EVs challenging. Use of low pH buffers can release intact EVs but may interfere with subsequent investigations of functional activity [108]. Nonetheless, for diagnostic purposes, pull-down of specific EV samples presents the opportunity to comprehensively interrogate cargo across multi-omics platforms and identify disease-specific molecular signatures. Immunoprecipitation of cell-specific EVs from biofluids has been applied in biomarker discovery by a select number of groups, in the context of neuronal pathology [112–115], cerebrovascular disease [116], transplant rejection [117], melanoma [118] and prostate cancer [119]. These reports consistently support the notion that EVs preferentially enriched for tissue origin are most informative of disease and thus enhance sensitivity and specificity of biomarker analyses. We recently isolated hepatocyte-derived EVs by anti-ASGR1 immunoprecipitation for the study of DMET induction by rifampicin and in pregnancy [53] and to compare the performance of miRNA biomarkers for NAFLD in unfractionated plasma, global circulating EVs and liver-specific EVs [68]. Only in applying the selective isolation technique, was a strong significant trend observed in biomarker expression with disease severity in NAFLD patients; thereby providing the first evidence for the utility of tissue-specific EV isolation techniques to improve diagnostic performance in chronic liver disease.

Flow cytometry

Flow cytometry is a powerful technique that can be applied to the enumeration and sizing of EVs from biofluids and phenotyping of specific subpopulations [120]. Particles in suspension are passed through a laser beam and measured based on light scatter and fluorescent emission. Conventional flow cytometers were designed for measuring single cells, thus the limit of detection is substantially larger than the typical EV size distribution (between 200 and 500 nm depending on the instrument) [121]. Although modern developments in high-resolution flow cytometry have seen increased sensitivity towards lower limits (~ 100 nm), this still misses a significant portion of smaller EVs, as revealed by complementary techniques, such as nanoparticle tracking analysis (NTA) [122]. Alternatively, larger complexes can be formed using immunobeads to detect the smaller range of EVs. This is useful for detecting EV subtypes based on surface composition but provides no direct insight into vesicle size [121]. Multiplexed flow cytometry approaches allow the high-throughput analysis of multiple markers of interest [110, 123]; however, like other immunolabelling approaches (e.g. Fluorescent NTA and immunogold-label EM), cargo detection is restricted to surface expression.

In chronic liver disease, such as NAFLD, flow cytometry approaches uphold the potential for cell-specific circulating EVs to diagnose and track progression. In a diet-induced mouse model of NASH, Li et al. [33] followed changes in circulating EVs derived from hepatocytes (ASGR1 +, CYP2E1 +), macrophages (Galectin 3 +), neutrophils (Ly-6G/6C +) and platelets (CD61 +). Hepatocyte-specific EV levels were significantly elevated over the course of feeding, occurring prior to histological evidence of inflammation and correlated with NAFLD activity score and features of NASH, including lobular inflammation and ballooning. Similarly, macrophage- and neutrophil-derived EVs were

increased and strongly associated with hepatic inflammation and fibrosis.

Povero et al. [3] also investigated changes in circulating hepatocyte-derived EVs, bearing ASGR1 and bile acyl-coenzyme A synthetase (SLC27A5), in human NASH patients with and without cirrhosis. SLC27A5 is a key enzyme in fatty acid uptake and synthesis. While greater expression is observed in steatotic hepatocytes, down-regulation has been associated with progression to cirrhosis due to loss of fat and functional parenchyma. In serum, SLC27A5 + EVs increased up to fourfold in NASH compared to healthy controls then decreased slightly in cirrhotic NASH. Meanwhile, ASGR1 + EV levels increased with disease severity, at almost twofold in pre-cirrhotic NASH and threefold in cirrhotic patients, compared to healthy controls. Liver-specific EV numbers exhibited strong correlations with features of NASH, including fibrosis stage, as well as various clinically relevant scores, such as FibroTest, Enhanced Liver Fibrosis (ELF) test and NAFLD Fibrosis Score (NFS). In addition, hepatocyte-derived EVs could predict clinically significant portal hypertension (hepatic venous pressure gradient [HVPG] ≥ 10 mmHg) in cirrhotic NASH patients with sensitivity of 92% and specificity of 75% (area under the receiver operating characteristic curve [AUROC] = 0.79), identifying the cut-off as ≥ 668 EVs/µl serum. Proteomic profiling also revealed several differentially expressed proteins that could distinguish advanced NASH from healthy controls (AUROC = 0.77) and pre-cirrhotic from cirrhotic NASH (AUROC = 0.80). Considering this analysis was performed on global circulating EVs and in late-stage NAFLD cohorts, the potential benefit of selectively analysing hepatocyte-derived EV protein cargo may be explored in simple steatosis or early NASH development.

It is noted that the above studies by and employed nanoscale flow cytometry with detection thresholds set to count EVs in the range of 110–1000 nm [33] and 200–1000 nm [3], respectively. Although limited to the larger EV range, earlier reports utilising conventional flow cytometers have also shown compelling results in support of tissue-specific EV biomarkers for chronic liver disease. Specifically, the profiling of immune cell-derived EVs discriminated patients with NAFL, NASH and HCV infection and healthy controls, and paralleled the extent of hepatic inflammation. Chronic HCV patients had greater circulating CD4 + and CD8 + T cell-derived EVs, while NAFLD patients had more EVs from invariant natural killer T cells and CD14 + macrophages. AUROC values ranged from 0.652 to 0.999 for various cohort pairs [124]. Later work demonstrated that the combination of surface markers, Annexin V, EpCAM, ASGR1 and CD133, could be used to identify tumour-associated EVs in circulation and distinguish between liver cancers (HCC and cholangiocarcinoma) and tumour-free cirrhosis [125]. Similarly, EVs expressing hepatocyte paraffin 1 (HepPar1) were found in great abundance in the circulation of patients with HCC, compared to virtually undetectable levels in tumour-free cirrhosis and healthy controls, and were proposed as an early marker of recurrence [126].

Microfluidic devices

Recent innovations in microfluidic hardware have driven the development of compact chip-like devices for the detection and isolation of EVs from biofluids. Microfluidic devices sort particles through a network of microchannels of varying diameter, ranging from tens to hundreds of microns

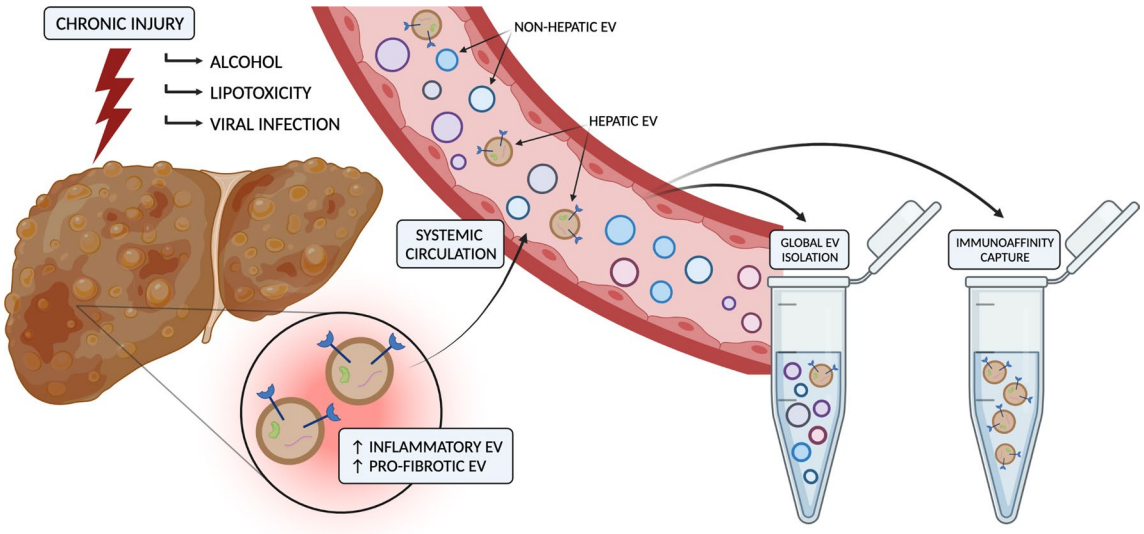

Fig. 3 Extracellular vesicle liquid biopsy for chronic liver diseases. Figure was created using BioRender.com

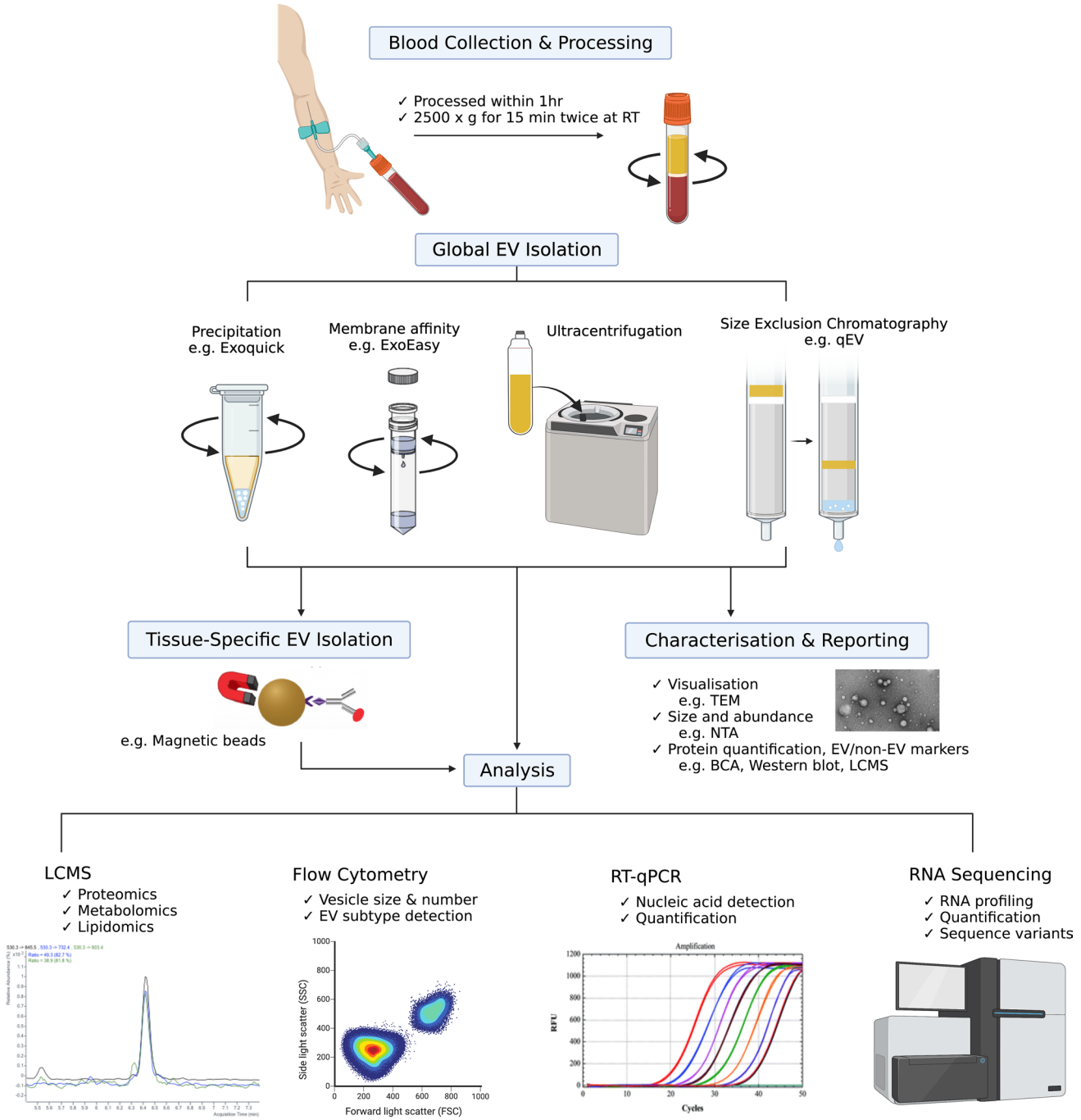

Fig. 4 Generic workflow for the sample collection and analysis of extracellular vesicle-derived biomarkers. Figure was created using BioRender.com

[102, 121]. Vesicle isolation is achieved either by actively applying electric, magnetic or acoustic forces, or in a passive manner, depending on immunoaffinity interactions and size exclusion [127]. In IA-based devices, antibody-functionalised surfaces immobilise target EVs flowing through the chip, to separate highly specific, pure vesicle subtypes. For example, the ExoChip device contains anti-CD63 to selectively capture exosomal small EV and has been applied for biomarker discovery in pancreatic cancer patients [128]. Progress in the design of these devices continue to improve sensitivity, reduce non-specific interactions and enhance capture efficiency by increasing surface area and mixing [127].

Key advantages of IA microfluidic chips include rapid processing time and low sample volume, requiring as little as ten microliters of plasma but taking up to a few hundred microliters [86]. It is noted that reducing sample input may be detrimental to downstream analyses, whereby biomarker yield in smaller volumes is insufficient for diagnostic purposes [102]. Despite their current complexity and cost, the development of integrated on-chip analysis of EV cargo positions microfluidic devices as promising novel tools for point of care testing (POCT) [129]. Captured EVs may be lysed by chemical (e.g. Triton X-100) or physical (e.g. electrical) means, and intraluminal nucleic acid amplified and analysed on-chip by quantitative PCR. Protein cargo may be detected by ELISA or released for off-chip proteomics [121, 127].

Recently, Sun et al. [32] designed an EV purification system, called EV Click Chips, to isolate HCC-derived EVs directly from 500 µl of plasma, via surface expression of ASGR1, EpCAM and CD147. Expression of 10 HCC-specific mRNA transcripts, analysed by digital droplet PCR in the captured EVs, gave exceptional diagnostic performance across several cohorts. Specifically, HCC was distinguished from all non-cancer (AUROC = 0.87) and from other primary malignancies (AUROC = 0.95) and early HCC detection could be achieved amongst at-risk cirrhosis patients of viral hepatitis, ALD or NASH aetiology (AUROC = 0.93), outperforming serum AFP (AUROC = 0.69). While the application of microfluidic devices is mainly at the proof-of-concept stage [111], longitudinal follow-up and validation in larger cohorts may soon see this novel non-invasive tool implemented in clinical settings for early diagnosis and patient monitoring.

Nano-plasmonic enhanced scattering assay.

Nano-plasmonic enhanced scattering assay (nPES) is a novel IAC technology that can isolate and quantify target EVs using capture and detection antibodies [104]. The assay, initially developed for tumour-derived EV from pancreatic cancer patients [130], was shown to considerably reduce cost, sample volume and analysis time and improved sensitivity compared to ELISA [104]. Similar to microfluidic devices, nPES is attractive for POCT given the assay consumes as little as 1–5 µl and can be performed directly from biofluids [13].

One research group recently developed a novel nPES assay to quantify hepatocyte-specific EVs as biomarkers for AH diagnosis [13] and for NAFLD resolution in obese patients undergoing weight loss surgery [109]. EV capture was achieved through ASGR2 or CYP2E1 and confirmed by CD63 positivity; and the capacity for circulating hepatocyte-specific EV levels to differentiate patients from controls was demonstrated in each cohort. Interestingly, hepatocyte-EVs correlated with steatosis and inflammation in NAFLD. The findings by Nakao and co-workers are in line with an earlier study that showed a 68% reduction in circulating hepatocyte-EVs (ASGR1 + , HepPar1 +) after bariatric surgery; however, the use of flow cytometry limited vesicle detection to those within 200–900 nm diameter [131].

Finally, lipidomic analysis revealed differential sphingolipid cargo in global EVs that was integrated in multivariable logistic regression models with MELD score and log global EV count to predict 90-day mortality in AH (AUC = 0.91) [13]; and with body mass index and small EV (110,000×*g* UC pellet) count to identify NAFLD (AUC = 0.80) [109]. Given the shortfalls of global EV analysis, further development and validation of nPES and other technologies to selectively analyse molecular signatures in cell-specific EVs may advance clinical translation of predictive models such as these.

Concluding remarks

EVs mediate a vast array of complex biological functions, related to the maintenance of liver homeostasis as well as the initiation and progression of liver diseases. A multiplicity of reports underpins the mechanistic link between EV-mediated cellular crosstalk and pathogenic processes that translate to differential expression in EV-based biomarkers across human patients and healthy subjects. The stability and accessibility of EV in peripheral blood are among attractive characteristics that compel their application as minimally invasive biomarkers. In the field of chronic liver disease, such tools for diagnosis and tracking of disease status and response to therapeutic intervention is in critical demand. The advancement of platforms designed to specifically isolate and analyse EVs, derived from cells or tissues relevant to the condition of interest, may greatly enhance the sensitivity and reproducibility of circulating EV biomarker analyses. It is our overarching view that clinical use will be supported by the development of these technologies and a holistic approach to evaluating disease-specific EV signatures of composite molecular species.

Acknowledgements We acknowledge funding from the National Health and Medical Research Council of Australia [Grant ID 1158210]. Figures were created using BioRender.com.

Author contributions LAN and AR designed and planned the work; LAN conducted the research; LAN and AR drafted the paper: LAN, KM and AR reviewed and edited the paper. AR is the guarantor of the article submission. All the authors have read and approved the final version of the manuscript.

Funding Open Access funding enabled and organized by CAUL and its Member Institutions. Andrew Rowland is supported by a Beat Cancer Mid-Career Fellowship from Cancer Council SA.

Data availability Enquiries about data availability should be directed to the authors.

Declarations

Conflict of interests All the authors declare no conflict of interest.

References

1. Chen L, Chen R, Kemper S, Cong M, You H, Brigstock DR (2018) Therapeutic effects of serum extracellular vesicles in liver fibrosis. J Extracell Vesic 7(1):1461505. https://doi.org/10.1080/20013078.2018.1461505
2. Moon AM, Singal AG, Tapper EB (2020) Contemporary epidemiology of chronic liver disease and cirrhosis. Clin Gastroenterol Hepatol 18(12):2650–2666. https://doi.org/10.1016/j.cgh.2019.07.060
3. Povero D, Yamashita H, Ren W, Subramanian MG, Myers RP, Eguchi A, Simonetto DA, Goodman ZD, Harrison SA, Sanyal AJ, Bosch J, Feldstein AE (2020) Characterization and proteome of circulating extracellular vesicles as potential biomarkers for NASH. Hepatol Commun 4(9):1263–1278. https://doi.org/10.1002/hep4.1556
4. Hernández A, Arab JP, Reyes D, Lapitz A, Moshage H, Bañales JM, Arrese M (2020) Extracellular vesicles in NAFLD/ALD: from pathobiology to therapy. Cells 9(4):817. https://doi.org/10.3390/cells9040817
5. Newman LA, Sorich MJ, Rowland A (2020) Role of extracellular vesicles in the pathophysiology, diagnosis and tracking of non-alcoholic fatty liver disease. J Clin Med 9(7):2032
6. Wong MCS, Huang JLW, George J, Huang J, Leung C, Eslam M, Chan HLY, Ng SC (2019) The changing epidemiology of liver diseases in the Asia-Pacific region. Nat Rev Gastroenterol Hepatol 16(1):57–73. https://doi.org/10.1038/s41575-018-0055-0
7. Li X, Chen R, Kemper S, Brigstock DR (2020) dynamic changes in function and proteomic composition of extracellular vesicles from hepatic stellate cells during cellular activation. Cells 9(2):290
8. Simon TG, Roelstraete B, Khalili H, Hagström H, Ludvigsson JF (2020) Mortality in biopsy-confirmed nonalcoholic fatty liver disease: results from a nationwide cohort. Gut. https://doi.org/10.1136/gutjnl-2020-322786
9. Ando Y, Jou JH (2021) Nonalcoholic fatty liver disease and recent guideline updates. Clin Liver Dis 17(1):23–28. https://doi.org/10.1002/cld.1045
10. Almeida PH, Matielo CEL, Curvelo LA, Rocco RA, Felga G, Della Guardia B, Boteon YL (2021) Update on the management and treatment of viral hepatitis. World J Gastroenterol 27(23):3249–3261. https://doi.org/10.3748/wjg.v27.i23.3249
11. Mann J, Reeves HL, Feldstein AE (2018) Liquid biopsy for liver diseases. Gut 67(12):2204. https://doi.org/10.1136/gutjnl-2017-315846
12. Sumida Y, Nakajima A, Itoh Y (2014) Limitations of liver biopsy and non-invasive diagnostic tests for the diagnosis of nonalcoholic fatty liver disease/nonalcoholic steatohepatitis. World J Gastroenterol 20(2):475–485. https://doi.org/10.3748/wjg.v20.i2.475
13. Sehrawat TS, Arab JP, Liu M, Amrollahi P, Wan M, Fan J, Nakao Y, Pose E, Navarro-Corcuera A, Dasgupta D, Liao C-Y, He L, Mauer AS, Avitabile E, Ventura-Cots M, Bataller RA, Sanyal AJ, Chalasani NP, Heimbach JK, Watt KD, Gores GJ, Gines P, Kamath PS, Simonetto DA, Hu TY, Shah VH, Malhi H (2021) circulating extracellular vesicles carrying sphingolipid cargo for the diagnosis and dynamic risk profiling of alcoholic hepatitis. Hepatology 73(2):571–585. https://doi.org/10.1002/hep.31256
14. Wong VW-S, Adams LA, de Lédinghen V, Wong GL-H, Sookoian S (2018) Noninvasive biomarkers in NAFLD and NASH—current progress and future promise. Nat Rev Gastroenterol Hepatol 15(8):461–478. https://doi.org/10.1038/s41575-018-0014-9
15. Petta S, Vanni E, Bugianesi E, Di Marco V, Camma C, Cabibi D, Mezzabotta L, Craxi A (2015) The combination of liver stiffness measurement and NAFLD fibrosis score improves the noninvasive diagnostic accuracy for severe liver fibrosis in patients with nonalcoholic fatty liver disease. Liver Int 35(5):1566–1573. https://doi.org/10.1111/liv.12584
16. Younossi Z, Tacke F, Arrese M, Chander Sharma B, Mostafa I, Bugianesi E, Wai-Sun Wong V, Yilmaz Y, George J, Fan J, Vos MB (2019) Global perspectives on nonalcoholic fatty liver disease and nonalcoholic steatohepatitis. Hepatology 69(6):2672–2682. https://doi.org/10.1002/hep.30251
17. Eguchi A, Lazaro RG, Wang J, Kim J, Povero D, Willliams B, Ho SB, Stärkel P, Schnabl B, Ohno-Machado L, Tsukamoto H, Feldstein AE (2017) Extracellular vesicles released by hepatocytes from gastric infusion model of alcoholic liver disease contain a MicroRNA barcode that can be detected in blood. Hepatology 65(2):475–490. https://doi.org/10.1002/hep.28838
18. Koeck ES, Iordanskaia T, Sevilla S, Ferrante SC, Hubal MJ, Freishtat RJ, Nadler EP (2014) Adipocyte exosomes induce transforming growth factor beta pathway dysregulation in hepatocytes: a novel paradigm for obesity-related liver disease. J Surg Res 192(2):268–275. https://doi.org/10.1016/j.jss.2014.06.050
19. Gho YS, Lee C (2017) Emergent properties of extracellular vesicles: a holistic approach to decode the complexity of intercellular communication networks. Mol BioSyst 13(7):1291–1296. https://doi.org/10.1039/C7MB00146K
20. Sung S, Kim J, Jung Y (2018) Liver-derived exosomes and their implications in liver pathobiology. Int J Mol Sci 19(12):3715. https://doi.org/10.3390/ijms19123715
21. Chen L, Charrier A, Zhou Y, Chen R, Yu B, Agarwal K, Tsukamoto H, Lee LJ, Paulaitis ME, Brigstock DR (2014) Epigenetic regulation of connective tissue growth factor by MicroRNA-214 delivery in exosomes from mouse or human hepatic stellate cells. Hepatology 59(3):1118–1129. https://doi.org/10.1002/hep.26768
22. Malhi H (2019) Emerging role of extracellular vesicles in liver diseases. Am J Physiol Gastrointest Liver Physiol 317(5):G739–G749. https://doi.org/10.1152/ajpgi.00183.2019
23. Mathieu M, Martin-Jaular L, Lavieu G, Théry C (2019) Specificities of secretion and uptake of exosomes and other extracellular vesicles for cell-to-cell communication. Nat Cell Biol 21(1):9–17. https://doi.org/10.1038/s41556-018-0250-9

24. Greening DW, Simpson RJ (2018) Understanding extracellular vesicle diversity—current status. Expert Rev Proteom. https://doi.org/10.1080/14789450.2018.1537788
25. Tetta C, Bruno S, Fonsato V, Deregibus MC, Camussi G (2011) The role of microvesicles in tissue repair. Organogenesis 7(2):105–115. https://doi.org/10.4161/org.7.2.15782
26. Kowal J, Arras G, Colombo M, Jouve M, Morath JP, Primdal-Bengtson B, Dingli F, Loew D, Tkach M, Théry C (2016) Proteomic comparison defines novel markers to characterize heterogeneous populations of extracellular vesicle subtypes. Proc Natl Acad Sci 113(8):E968–E977. https://doi.org/10.1073/pnas.1521230113
27. Théry C, Witwer KW, Aikawa E, Alcaraz MJ, Anderson JD, Andriantsitohaina R, Antoniou A, Arab T, Archer F, Atkin-Smith GK, Ayre DC, Bach J-M, Bachurski D, Baharvand H, Balaj L, Baldacchino S, Bauer NN, Baxter AA, Bebawy M, Beckham C, Bedina Zavec A, Benmoussa A, Berardi AC, Bergese P, Bielska E, Blenkiron C, Bobis-Wozowicz S, Boilard E, Boireau W, Bongiovanni A, Borràs FE, Bosch S, Boulanger CM, Breakefield X, Breglio AM, Brennan MÁ, Brigstock DR, Brisson A, Broekman MLD, Bromberg JF, Bryl-Górecka P, Buch S, Buck AH, Burger D, Busatto S, Buschmann D, Bussolati B, Buzás EI, Byrd JB, Camussi G, Carter DRF, Caruso S, Chamley LW, Chang Y-T, Chen C, Chen S, Cheng L, Chin AR, Clayton A, Clerici SP, Cocks A, Cocucci E, Coffey RJ, Cordeiro-da-Silva A, Couch Y, Coumans FAW, Coyle B, Crescitelli R, Criado MF, D'Souza-Schorey C, Das S, Datta Chaudhuri A, de Candia P, De Santana EF, De Wever O, del Portillo HA, Demaret T, Deville S, Devitt A, Dhondt B, Di Vizio D, Dieterich LC, Dolo V, Dominguez Rubio AP, Dominici M, Dourado MR, Driedonks TAP, Duarte FV, Duncan HM, Eichenberger RM, Ekström K, El Andaloussi S, Elie-Caille C, Erdbrügger U, Falcón-Pérez JM, Fatima F, Fish JE, Flores-Bellver M, Försönits A, Frelet-Barrand A, Fricke F, Fuhrmann G, Gabrielsson S, Gámez-Valero A, Gardiner C, Gärtner K, Gaudin R, Gho YS, Giebel B, Gilbert C, Gimona M, Giusti I, Goberdhan DCI, Görgens A, Gorski SM, Greening DW, Gross JC, Gualerzi A, Gupta GN, Gustafson D, Handberg A, Haraszti RA, Harrison P, Hegyesi H, Hendrix A, Hill AF, Hochberg FH, Hoffmann KF, Holder B, Holthofer H, Hosseinkhani B, Hu G, Huang Y, Huber V, Hunt S, Ibrahim AG-E, Ikezu T, Inal JM, Isin M, Ivanova A, Jackson HK, Jacobsen S, Jay SM, Jayachandran M, Jenster G, Jiang L, Johnson SM, Jones JC, Jong A, Jovanovic-Talisman T, Jung S, Kalluri R, Kano S-I, Kaur S, Kawamura Y, Keller ET, Khamari D, Khomyakova E, Khvorova A, Kierulf P, Kim KP, Kislinger T, Klingeborn M, Klinke DJ, Kornek M, Kosanović MM, Kovács ÁF, Krämer-Albers E-M, Krasemann S, Krause M, Kurochkin IV, Kusuma GD, Kuypers S, Laitinen S, Langevin SM, Languino LR, Lannigan J, Lässer C, Laurent LC, Lavieu G, Lázaro-Ibáñez E, Le Lay S, Lee M-S, Lee YXF, Lemos DS, Lenassi M, Leszczynska A, Li ITS, Liao K, Libregts SF, Ligeti E, Lim R, Lim SK, Linē A, Linnemannstöns K, Llorente A, Lombard CA, Lorenowicz MJ, Lörincz ÁM, Lötvall J, Lovett J, Lowry MC, Loyer X, Lu Q, Lukomska B, Lunavat TR, Maas SLN, Malhi H, Marcilla A, Mariani J, Mariscal J, Martens-Uzunova ES, Martin-Jaular L, Martinez MC, Martins VR, Mathieu M, Mathivanan S, Maugeri M, McGinnis LK, McVey MJ, Meckes DG, Meehan KL, Mertens I, Minciacchi VR, Möller A, Møller Jørgensen M, Morales-Kastresana A, Morhayim J, Mullier F, Muraca M, Musante L, Mussack V, Muth DC, Myburgh KH, Najrana T, Nawaz M, Nazarenko I, Nejsum P, Neri C, Neri T, Nieuwland R, Nimrichter L, Nolan JP, Nolte-'t Hoen ENM, Noren Hooten N, O'Driscoll L, O'Grady T, O'Loghlen A, Ochiya T, Olivier M, Ortiz A, Ortiz LA, Osteikoetxea X, Østergaard O, Ostrowski M, Park J, Pegtel DM, Peinado H, Perut F, Pfaffl MW, Phinney DG, Pieters BCH, Pink RC, Pisetsky DS, Pogge von Strandmann E, Polakovicova I, Poon IKH, Powell BH, Prada I, Pulliam L, Quesenberry P, Radeghieri A, Raffai RL, Raimondo S, Rak J, Ramirez MI, Raposo G, Rayyan MS, Regev-Rudzki N, Ricklefs FL, Robbins PD, Roberts DD, Rodrigues SC, Rohde E, Rome S, Rouschop KMA, Rughetti A, Russell AE, Saá P, Sahoo S, Salas-Huenuleo E, Sánchez C, Saugstad JA, Saul MJ, Schiffelers RM, Schneider R, Schøyen TH, Scott A, Shahaj E, Sharma S, Shatnyeva O, Shekari F, Shelke GV, Shetty AK, Shiba K, Siljander PRM, Silva AM, Skowronek A, Snyder OL, Soares RP, Sódar BW, Soekmadji C, Sotillo J, Stahl PD, Stoorvogel W, Stott SL, Strasser EF, Swift S, Tahara H, Tewari M, Timms K, Tiwari S, Tixeira R, Tkach M, Toh WS, Tomasini R, Torrecilhas AC, Tosar JP, Toxavidis V, Urbanelli L, Vader P, van Balkom BWM, van der Grein SG, Van Deun J, van Herwijnen MJC, Van Keuren-Jensen K, van Niel G, van Royen ME, van Wijnen AJ, Vasconcelos MH, Vechetti IJ, Veit TD, Vella LJ, Velot É, Verweij FJ, Vestad B, Viñas JL, Visnovitz T, Vukman KV, Wahlgren J, Watson DC, Wauben MHM, Weaver A, Webber JP, Weber V, Wehman AM, Weiss, DJ Welsh, JA Wendt, S, Wheelock AM, Wiener Z, Witte, L Wolfram, J, Xagorari A, Xander, P Xu, J Yan, X Yáñez-Mó, M Yin, H Yuana, Y, Zappulli V, Zarubova J, Žėkas V, Zhang J-y, Zhao Z, Zheng L, Zheutlin AR, Zickler AM, Zimmermann P, Zivkovic AM, Zocco D, Zuba-Surma EK (2018) Minimal information for studies of extracellular vesicles 2018 (MISEV2018): a position statement of the International Society for Extracellular Vesicles and update of the MISEV2014 guidelines. J Extracell Vesicles **7**(1):5750. https://doi.org/10.1080/20013078.2018.1535750
28. Jeppesen DK, Fenix AM, Franklin JL, Higginbotham JN, Zhang Q, Zimmerman LJ, Liebler DC, Ping J, Liu Q, Evans R, Fissell WH, Patton JG, Rome LH, Burnette DT, Coffey RJ (2019) Reassessment of exosome composition. Cell 177(2):428-445.e18. https://doi.org/10.1016/j.cell.2019.02.029
29. Larssen P, Wik L, Czarnewski P, Eldh M, Löf L, Ronquist KG, Dubois L, Freyhult E, Gallant CJ, Oelrich J, Larsson A, Ronquist G, Villablanca EJ, Landegren U, Gabrielsson S, Kamali-Moghaddam M (2017) tracing cellular origin of human exosomes using multiplex proximity extension assays*. Mol Cell Proteomics 16(3):502–511. https://doi.org/10.1074/mcp.M116.064725
30. Kostallari E, Hirsova P, Prasnicka A, Verma VK, Yaqoob U, Wongjarupong N, Roberts LR, Shah VH (2018) Hepatic stellate cell–derived platelet-derived growth factor receptor-alpha-enriched extracellular vesicles promote liver fibrosis in mice through SHP2. Hepatology 68(1):333–348. https://doi.org/10.1002/hep.29803
31. Dasgupta D, Nakao Y, Mauer AS, Thompson JM, Sehrawat TS, Liao C-Y, Krishnan A, Lucien F, Guo Q, Liu M, Xue F, Fukushima M, Katsumi T, Bansal A, Pandey MK, Maiers JL, DeGrado T, Ibrahim SH, Revzin A, Pavelko KD, Barry MA, Kaufman RJ, Malhi H (2020) IRE1A stimulates hepatocyte-derived extracellular vesicles that promote inflammation in mice with steatohepatitis. Gastroenterology 159(4):1487-1503.e17. https://doi.org/10.1053/j.gastro.2020.06.031
32. Sun N, Lee Y-T, Zhang RY, Kao R, Teng P-C, Yang Y, Yang P, Wang JJ, Smalley M, Chen P-J, Kim M, Chou S-J, Bao L, Wang J, Zhang X, Qi D, Palomique J, Nissen N, Han S-HB, Sadeghi S, Finn RS, Saab S, Busuttil RW, Markovic D, Elashoff D, Yu H-H, Li H, Heaney AP, Posadas E, You S, Yang JD, Pei R, Agopian VG, Tseng H-R, Zhu Y (2020) Purification of HCC-specific extracellular vesicles on nanosubstrates for early HCC detection by digital scoring. Nat Commun 11(1):4489. https://doi.org/10.1038/s41467-020-18311-0
33. Li J, Liu H, Mauer AS, Lucien F, Raiter A, Bandla H, Mounajjed T, Yin Z, Glaser KJ, Yin M, Malhi H (2019) Characterization of cellular sources and circulating levels of extracellular vesicles in a dietary murine model of nonalcoholic steatohepatitis. Hepatol Commun 3(9):1235–1249. https://doi.org/10.1002/hep4.1404

34. Shah R, Patel T, Freedman JE (2018) circulating extracellular vesicles in human disease. N Engl J Med 379(10):958–966. https://doi.org/10.1056/NEJMra1704286
35. Bruno S, Chiabotto G, Camussi G (2020) extracellular vesicles: a therapeutic option for liver fibrosis. Int J Mol Sci 21(12):4255. https://doi.org/10.3390/ijms21124255
36. Szabo G (2017) Momen-Heravi F (2017) Extracellular vesicles in liver disease and potential as biomarkers and therapeutic targets. Nat Rev Gastroenterol Hepatol 14:455. https://doi.org/10.1038/nrgastro.2017.71
37. Azparren-Angulo M, Royo F, Gonzalez E, Liebana M, Brotons B, Berganza J, Goñi-de-Cerio F, Manicardi N, Abad-Jordà L, Gracia-Sancho J, Falcon-Perez JM (2021) Extracellular vesicles in hepatology: physiological role, involvement in pathogenesis, and therapeutic opportunities. Pharmacol Ther 218:107683. https://doi.org/10.1016/j.pharmthera.2020.107683
38. Giugliano S, Kriss M, Golden-Mason L, Dobrinskikh E, Stone AEL, Soto-Gutierrez A, Mitchell A, Khetani SR, Yamane D, Stoddard M, Li H, Shaw GM, Edwards MG, Lemon SM, Gale M Jr, Shah VH, Rosen HR (2015) Hepatitis C virus infection induces autocrine interferon signaling by human liver endothelial cells and release of exosomes, which inhibits viral replication. Gastroenterology 148(2):392-402.e13. https://doi.org/10.1053/j.gastro.2014.10.040
39. Conde-Vancells J, Rodriguez-Suarez E, Embade N, Gil D, Matthiesen R, Valle M, Elortza F, Lu SC, Mato JM, Falcon-Perez JM (2008) Characterization and comprehensive proteome profiling of exosomes secreted by hepatocytes. J Proteome Res 7(12):5157–5166. https://doi.org/10.1021/pr8004887
40. Royo F, Moreno L, Mleczko J, Palomo L, Gonzalez E, Cabrera D, Cogolludo A, Vizcaino FP, Van-Liempd S, Falcon-Perez JM (2017) Hepatocyte-secreted extracellular vesicles modify blood metabolome and endothelial function by an arginase-dependent mechanism. Sci Rep 7:1. https://doi.org/10.1038/srep42798
41. Cai S, Cheng X, Pan X, Li J (2017) Emerging role of exosomes in liver physiology and pathology. Hepatol Res 47(2):194–203. https://doi.org/10.1111/hepr.12794
42. Nojima H, Freeman CM, Schuster RM, Japtok L, Kleuser B, Edwards MJ, Gulbins E, Lentsch AB (2016) Hepatocyte exosomes mediate liver repair and regeneration via sphingosine-1-phosphate. J Hepatol 64(1):60–68. https://doi.org/10.1016/j.jhep.2015.07.030
43. Wang R, Ding Q, Yaqoob U, de Assuncao TM, Verma VK, Hirsova P, Cao S, Mukhopadhyay D, Huebert RC, Shah VH (2015) Exosome adherence and internalization by hepatic stellate cells triggers sphingosine 1-phosphate-dependent migration. J Biol Chem 290(52):30684–30696. https://doi.org/10.1074/jbc.M115.671735
44. Chen L, Chen R, Velazquez VM, Brigstock DR (2016) Fibrogenic signaling is suppressed in hepatic stellate cells through targeting of connective tissue growth factor (CCN2) by cellular or exosomal MicroRNA-199a-5p. Am J Pathol 186(11):2921–2933. https://doi.org/10.1016/j.ajpath.2016.07.011
45. Chen, L., Chen, R., Kemper, S., Charrier, A., and Brigstock, D.R., *Suppression of fibrogenic signaling in hepatic stellate cells by Twist1-dependent microRNA-214 expression: Role of exosomes in horizontal transfer of Twist1.* American journal of physiology. Gastrointestinal and liver physiology, 2015. **309**(6): G491-G499. https://doi.org/10.1152/ajpgi.00140.2015
46. Charrier A, Chen R, Chen L, Kemper S, Hattori T, Takigawa M, Brigstock DR (2014) Exosomes mediate intercellular transfer of pro-fibrogenic connective tissue growth factor (CCN2) between hepatic stellate cells, the principal fibrotic cells in the liver. Surgery 156(3):548–555. https://doi.org/10.1016/j.surg.2014.04.014
47. Li X, Liu R, Huang Z, Gurley EC, Wang X, Wang J, He H, Yang H, Lai G, Zhang L, Bajaj JS, White M, Pandak WM, Hylemon PB, Zhou H (2018) Cholangiocyte-derived exosomal long noncoding RNA H19 promotes cholestatic liver injury in mouse and humans. Hepatology 68(2):599–615. https://doi.org/10.1002/hep.29838
48. Witek RP, Yang L, Liu R, Jung Y, Omenetti A, Syn WK, Choi SS, Cheong Y, Fearing CM, Agboola KM, Chen W, Diehl AM (2009) Liver cell-derived microparticles activate hedgehog signaling and alter gene expression in hepatic endothelial cells. Gastroenterology 136(1):320-330.e2. https://doi.org/10.1053/j.gastro.2008.09.066
49. Achour B, Al-Majdoub ZM, Grybos-Gajniak A, Lea K, Kilford P, Zhang M, Knight D, Barber J, Schageman J, Rostami-Hodjegan A (2021) Liquid biopsy enables quantification of the abundance and interindividual variability of hepatic enzymes and transporters. Clin Pharmacol Ther 109(1):222–232. https://doi.org/10.1002/cpt.2102
50. Rodrigues A, Rowland A (2019) From endogenous compounds as biomarkers to plasma-derived nanovesicles as liquid biopsy; has the golden age of translational PK-ADME-DDI science finally arrived? Clin Pharmacol Ther 105(6):1407–1420
51. Kumar S, Sinha N, Gerth KA, Rahman MA, Yallapu MM, Midde NM (2017) Specific packaging and circulation of cytochromes P450, especially 2E1 isozyme, in human plasma exosomes and their implications in cellular communications. Biochem Biophys Res Commun 491(3):675–680. https://doi.org/10.1016/j.bbrc.2017.07.145
52. Rowland A, Ruanglertboon W, van Dyk M, Wijayakumara D, Wood LS, Meech R, Mackenzie PI, Rodrigues AD, Marshall J-C, Sorich MJ (2019) Plasma extracellular nanovesicle (exosome)-derived biomarkers for drug metabolism pathways: a novel approach to characterize variability in drug exposure. Br J Clin Pharmacol 85(1):216–226. https://doi.org/10.1111/bcp.13793
53. Rodrigues AD, van Dyk M, Sorich MJ, Fahmy A, Useckaite Z, Newman LA, Kapetas AJ, Mounzer R, Wood LS, Johnson JG, Rowland A (2021) Exploring the use of serum-derived small extracellular vesicles as liquid biopsy to study the induction of hepatic cytochromes P450 and organic anion transporting polypeptides. Clin Pharmacol Ther. https://doi.org/10.1002/cpt.2244
54. Gerth K, Kodidela S, Mahon M, Haque S, Verma N, Kumar S (2019) Circulating extracellular vesicles containing xenobiotic metabolizing CYP enzymes and their potential roles in extrahepatic cells via cell–cell interactions. Int J Mol Sci 20(24):1. https://doi.org/10.3390/ijms20246178
55. Jamwal R, Barlock BJ (2020) Nonalcoholic fatty liver disease (NAFLD) and hepatic cytochrome P450 (CYP) enzymes. Pharmaceuticals 13(9). https://doi.org/10.3390/ph13090222
56. Srinivas AN, Suresh D, Santhekadur PK, Suvarna D, Kumar DP (2020) Extracellular vesicles as inflammatory drivers in NAFLD. Front Immunol 11:627424. https://doi.org/10.3389/fimmu.2020.627424
57. Eslam M, Sanyal AJ, George J, Sanyal A, Neuschwander-Tetri B, Tiribelli C, Kleiner DE, Brunt E, Bugianesi E, Yki-Järvinen H, Grønbæk H, Cortez-Pinto H, George J, Fan J, Valenti L, Abdelmalek M, Romero-Gomez M, Rinella M, Arrese M, Eslam M, Bedossa P, Newsome PN, Anstee QM, Jalan R, Bataller R, Loomba R, Sookoian S, Sarin SK, Harrison S, Kawaguchi T, Wong VW-S, Ratziu V, Yilmaz Y, Younossi Z (2020) MAFLD: a consensus-driven proposed nomenclature for metabolic associated fatty liver disease. Gastroenterology 158(7):1999-2014.e1. https://doi.org/10.1053/j.gastro.2019.11.312
58. Eslam M, Newsome PN, Sarin SK, Anstee QM, Targher G, Romero-Gomez M, Zelber-Sagi S, Wai-Sun Wong V, Dufour J-F, Schattenberg JM, Kawaguchi T, Arrese M, Valenti L, Shiha G, Tiribelli C, Yki-Järvinen H, Fan J-G, Grønbæk H, Yilmaz Y, Cortez-Pinto H, Oliveira CP, Bedossa P, Adams LA, Zheng

M-H, Fouad Y, Chan W-K, Mendez-Sanchez N, Ahn SH, Castera L, Bugianesi E, Ratziu V, George J (2020) A new definition for metabolic dysfunction-associated fatty liver disease: an international expert consensus statement. J Hepatol 73(1):202–209. https://doi.org/10.1016/j.jhep.2020.03.039
59. Suzuki A, Diehl AM (2017) Nonalcoholic steatohepatitis. Annu Rev Med 68(1):85–98. https://doi.org/10.1146/annurev-med-051215-031109
60. Jonas W, Schürmann A (2020) Genetic and epigenetic factors determining NAFLD risk. Mol Metab 101111. https://doi.org/10.1016/j.molmet.2020.101111
61. Zhang X, Ji X, Wang Q, Li JZ (2018) New insight into inter-organ crosstalk contributing to the pathogenesis of non-alcoholic fatty liver disease (NAFLD). Protein Cell 9(2):164–177. https://doi.org/10.1007/s13238-017-0436-0
62. Hirsova P, Ibrahim SH, Krishnan A, Verma VK, Bronk SF, Werneburg NW, Charlton MR, Shah VH, Malhi H, Gores GJ (2016) Lipid-induced signaling causes release of inflammatory extracellular vesicles from hepatocytes. Gastroenterology 150(4):956–967. https://doi.org/10.1053/j.gastro.2015.12.037
63. Ibrahim SH, Gores GJ, Hirsova P, Kirby M, Miles L, Jaeschke A, Kohli R (2014) Mixed lineage kinase 3 deficient mice are protected against the high fat high carbohydrate diet-induced steatohepatitis. Liver Int 34(3):427–437. https://doi.org/10.1111/liv.12353
64. Ibrahim SH, Hirsova P, Tomita K, Bronk SF, Werneburg NW, Harrison SA, Goodfellow VS, Malhi H, Gores GJ (2016) Mixed lineage kinase 3 mediates release of C-X-C motif ligand 10-bearing chemotactic extracellular vesicles from lipotoxic hepatocytes. Hepatology 63(3):731–744. https://doi.org/10.1002/hep.28252
65. Kakazu E, Mauer AS, Yin M, Malhi H (2016) Hepatocytes release ceramide-enriched pro-inflammatory extracellular vesicles in an IRE1α-dependent manner. J Lipid Res 57(2):233–245. https://doi.org/10.1194/jlr.M063412
66. Povero D, Panera N, Eguchi A, Johnson CD, Papouchado BG, de Araujo Horcel L, Pinatel EM, Alisi A, Nobili V, Feldstein AE (2015) Lipid-induced hepatocyte-derived extracellular vesicles regulate hepatic stellate cell via microRNAs targeting PPAR-γ. Cell Mol Gastroenterol Hepatol 1(6):646-663.e4. https://doi.org/10.1016/j.jcmgh.2015.07.007
67. Povero D, Eguchi A, Niesman IR, Andronikou N, de Mollerat du Jeu, X., Mulya, A., Berk, M., Lazic, M., Thapaliya, S., Parola, M., Patel, H.H., Feldstein, A.E. (2013) Lipid-induced toxicity stimulates hepatocytes to release angiogenic microparticles that require Vanin-1 for uptake by endothelial cells. Sci Signal 6(296):88. https://doi.org/10.1126/scisignal.2004512
68. Newman LA, Useckaite Z, Johnson J, Sorich MJ, Hopkins AM, Rowland A (2022) Selective isolation of liver-derived extracellular vesicles redefines performance of miRNA biomarkers for non-alcoholic fatty liver disease. Biomedicines 10(1):195
69. Prasun P, Ginevic I, Oishi K (2021) Mitochondrial dysfunction in nonalcoholic fatty liver disease and alcohol related liver disease. Transl Gastroenterol Hepatol 6:4–4. https://doi.org/10.21037/tgh-20-125
70. Garcia-Martinez I, Santoro N, Chen Y, Hoque R, Ouyang X, Caprio S, Shlomchik MJ, Coffman RL, Candia A, Mehal WZ (2016) Hepatocyte mitochondrial DNA drives nonalcoholic steatohepatitis by activation of TLR9. J Clin Investig 126(3):859–864. https://doi.org/10.1172/JCI83885
71. Kranendonk ME, Visseren FL, van Herwaarden JA, Nolte-'t Hoen EN, de Jager W, Wauben MH, Kalkhoven E (2014) Effect of extracellular vesicles of human adipose tissue on insulin signaling in liver and muscle cells. Obesity (Silver Spring) 22(10):2216–2223. https://doi.org/10.1002/oby.20847
72. Thomou T, Mori MA, Dreyfuss JM, Konishi M, Sakaguchi M, Wolfrum C, Rao TN, Winnay JN, Garcia-Martin R, Grinspoon SK, Gorden P, Kahn CR (2017) Adipose-derived circulating miRNAs regulate gene expression in other tissues. Nature 542(7642):450–455. https://doi.org/10.1038/nature21365
73. Keinicke H, Sun G, Mentzel CMJ, Fredholm M, John LM, Andersen B, Raun K, Kjaergaard M (2020) FGF21 regulates hepatic metabolic pathways to improve steatosis and inflammation. Endocr Connect 9(8):755–768. https://doi.org/10.1530/EC-20-0152
74. Sharma P, Arora A (2020) Clinical presentation of alcoholic liver disease and non-alcoholic fatty liver disease: spectrum and diagnosis. Transl Gastroenterol Hepatol 5:19–19. https://doi.org/10.21037/tgh.2019.10.02
75. Eguchi A, Yan R, Pan SQ, Wu R, Kim J, Chen Y, Ansong C, Smith RD, Tempaku M, Ohno-Machado L, Takei Y, Feldstein AE, Tsukamoto H (2020) Comprehensive characterization of hepatocyte-derived extracellular vesicles identifies direct miRNA-based regulation of hepatic stellate cells and DAMP-based hepatic macrophage IL-1β and IL-17 upregulation in alcoholic hepatitis mice. J Mol Med 98(7):1021–1034. https://doi.org/10.1007/s00109-020-01926-7
76. Ma J, Cao H, Rodrigues RM, Xu M, Ren T, He Y, Hwang S, Feng D, Ren R, Yang P, Liangpunsakul S, Sun J, Gao B (2020) Chronic-plus-binge alcohol intake induces production of pro-inflammatory mtDNA-enriched extracellular vesicles and steatohepatitis via ASK1/p38MAPKα-dependent mechanisms. JCI Insight 5(14):e136496. https://doi.org/10.1172/jci.insight.136496
77. Verma VK, Li H, Wang R, Hirsova P, Mushref M, Liu Y, Cao S, Contreras PC, Malhi H, Kamath PS, Gores GJ, Shah VH (2016) Alcohol stimulates macrophage activation through caspase-dependent hepatocyte derived release of CD40L containing extracellular vesicles. J Hepatol 64(3):651–660. https://doi.org/10.1016/j.jhep.2015.11.020
78. Momen-Heravi F, Bala S, Kodys K, Szabo G (2015) Exosomes derived from alcohol-treated hepatocytes horizontally transfer liver specific miRNA-122 and sensitize monocytes to LPS. Sci Rep 5(1):9991. https://doi.org/10.1038/srep09991
79. Bala S, Petrasek J, Mundkur S, Catalano D, Levin I, Ward J, Alao H, Kodys K, Szabo G (2012) Circulating microRNAs in exosomes indicate hepatocyte injury and inflammation in alcoholic, drug-induced, and inflammatory liver diseases. Hepatology 56(5):1946–1957. https://doi.org/10.1002/hep.25873
80. Zamor PJ, deLemos AS, Russo MW (2017) Viral hepatitis and hepatocellular carcinoma: etiology and management. J Gastrointest Oncol 8(2):229–242. https://doi.org/10.21037/jgo.2017.03.14
81. Kakizaki M, Yamamoto Y, Yabuta S, Kurosaki N, Kagawa T, Kotani A (2019) The immunological function of extracellular vesicles in hepatitis B virus-infected hepatocytes. PLoS ONE 13(12):e0205886. https://doi.org/10.1371/journal.pone.0205886
82. Deng L, Jiang W, Wang X, Merz A, Hiet M-S, Chen Y, Pan X, Jiu Y, Yang Y, Yu B, He Y, Tu Z, Niu J, Bartenschlager R, Long G (2019) Syntenin regulates hepatitis C virus sensitivity to neutralizing antibody by promoting E2 secretion through exosomes. J Hepatol 71(1):52–61. https://doi.org/10.1016/j.jhep.2019.03.006
83. Bukong TN, Momen-Heravi F, Kodys K, Bala S, Szabo G (2014) Exosomes from hepatitis C infected patients transmit HCV infection and contain replication competent viral RNA in complex with Ago2-miR122-HSP90. PLoS Pathog 10(10):e1004424–e1004424. https://doi.org/10.1371/journal.ppat.1004424
84. Devhare PB, Sasaki R, Shrivastava S, Di Bisceglie AM, Ray R, Ray RB (2017) Exosome-mediated intercellular communication between Hepatitis C virus-infected hepatocytes and hepatic stellate cells. J Virol 91(6):e02225-e2316. https://doi.org/10.1128/JVI.02225-16
85. Kornek M, Popov Y, Libermann TA, Afdhal NH, Schuppan D (2011) Human T cell microparticles circulate in blood of

hepatitis patients and induce fibrolytic activation of hepatic stellate cells. Hepatology (Baltimore, Md.) 53(1):230–242. https://doi.org/10.1002/hep.23999
86. Lee YT, Tran BV, Wang JJ, Liang IY, You S, Zhu Y, Agopian VG, Tseng HR, Yang JD (2021) The role of extracellular vesicles in disease progression and detection of hepatocellular carcinoma. Cancers 13(12). https://doi.org/10.3390/cancers13123076
87. Lubel JS, Roberts SK, Strasser SI, Thompson AJ, Philip J, Goodwin M, Clarke S, Crawford DHG, Levy MT, Shackel N (2021) Australian recommendations for the management of hepatocellular carcinoma: a consensus statement. Med J Aust 214(10):475–483. https://doi.org/10.5694/mja2.50885
88. Marrero JA, Kulik LM, Sirlin CB, Zhu AX, Finn RS, Abecassis MM, Roberts LR, Heimbach JK (2018) Diagnosis, staging, and management of hepatocellular carcinoma: 2018 practice guidance by the American association for the study of liver diseases. Hepatology 68(2):723–750. https://doi.org/10.1002/hep.29913
89. Xue X, Wang X, Zhao Y, Hu R, Qin L (2018) Exosomal miR-93 promotes proliferation and invasion in hepatocellular carcinoma by directly inhibiting TIMP2/TP53INP1/CDKN1A. Biochem Biophys Res Commun 502(4):515–521. https://doi.org/10.1016/j.bbrc.2018.05.208
90. Cui Y, Xu H-F, Liu M-Y, Xu Y-J, He J-C, Zhou Y, Cang S-D (2019) Mechanism of exosomal microRNA-224 in development of hepatocellular carcinoma and its diagnostic and prognostic value. World J Gastroenterol 25(15):1890–1898. https://doi.org/10.3748/wjg.v25.i15.1890
91. Qu Z, Wu J, Wu J, Ji A, Qiang G, Jiang Y, Jiang C, Ding Y (2017) Exosomal miR-665 as a novel minimally invasive biomarker for hepatocellular carcinoma diagnosis and prognosis. Oncotarget 8(46):80666–80678. https://doi.org/10.18632/oncotarget.20881
92. Tang J, Li Y, Liu K, Zhu Q, Yang WH, Xiong LK, Guo DL (2018) Exosomal miR-9–3p suppresses HBGF-5 expression and is a functional biomarker in hepatocellular carcinoma. Minerva Med 109(1):15–23. https://doi.org/10.23736/s0026-4806.17.05167-9
93. Shi M, Jiang Y, Yang L, Yan S, Wang YG, Lu XJ (2018) Decreased levels of serum exosomal miR-638 predict poor prognosis in hepatocellular carcinoma. J Cell Biochem 119(6):4711–4716. https://doi.org/10.1002/jcb.26650
94. Sugimachi K, Matsumura T, Hirata H, Uchi R, Ueda M, Ueo H, Shinden Y, Iguchi T, Eguchi H, Shirabe K, Ochiya T, Maehara Y, Mimori K (2015) Identification of a bona fide microRNA biomarker in serum exosomes that predicts hepatocellular carcinoma recurrence after liver transplantation. Br J Cancer 112(3):532–538. https://doi.org/10.1038/bjc.2014.621
95. Wang G, Zhao W, Wang H, Qiu G, Jiang Z, Wei G, Li X (2019) Exosomal MiR-744 inhibits proliferation and sorafenib chemoresistance in hepatocellular carcinoma by targeting PAX2. Med Sci Monit 25:7209–7217. https://doi.org/10.12659/MSM.919219
96. Kogure T, Lin W-L, Yan IK, Braconi C, Patel T (2011) Intercellular nanovesicle-mediated microRNA transfer: a mechanism of environmental modulation of hepatocellular cancer cell growth. Hepatology 54(4):1237–1248. https://doi.org/10.1002/hep.24504
97. He X, Yu J, Xiong L, Liu Y, Fan L, Li Y, Chen B, Chen J, Xu X (2019) Exosomes derived from liver cancer cells reprogram biological behaviors of LO2 cells by transferring Linc-ROR. Gene 719:144044. https://doi.org/10.1016/j.gene.2019.144044
98. He M, Qin H, Poon TCW, Sze S-C, Ding X, Co NN, Ngai S-M, Chan T-F, Wong N (2015) Hepatocellular carcinoma-derived exosomes promote motility of immortalized hepatocyte through transfer of oncogenic proteins and RNAs. Carcinogenesis 36(9):1008–1018. https://doi.org/10.1093/carcin/bgv081
99. Fang T, Lv H, Lv G, Li T, Wang C, Han Q, Yu L, Su B, Guo L, Huang S, Cao D, Tang L, Tang S, Wu M, Yang W, Wang H (2018) Tumor-derived exosomal miR-1247-3p induces cancer-associated fibroblast activation to foster lung metastasis of liver cancer. Nat Commun 9(1):191–191. https://doi.org/10.1038/s41467-017-02583-0
100. Arbelaiz A, Azkargorta M, Krawczyk M, Santos-Laso A, Lapitz A, Perugorria MJ, Erice O, Gonzalez E, Jimenez-Agüero R, Lacasta A, Ibarra C, Sanchez-Campos A, Jimeno JP, Lammert F, Milkiewicz P, Marzioni M, Macias RIR, Marin JJG, Patel T, Gores GJ, Martinez I, Elortza F, Falcon-Perez JM, Bujanda L, Banales JM (2017) Serum extracellular vesicles contain protein biomarkers for primary sclerosing cholangitis and cholangiocarcinoma. Hepatology 66(4):1125–1143. https://doi.org/10.1002/hep.29291
101. Unalp-Arida A, Ruhl CE (2017) Liver fibrosis scores predict liver disease mortality in the United States population. Hepatology 66(1):84–95. https://doi.org/10.1002/hep.29113
102. Konoshenko MY, Lekchnov EA, Vlassov AV, Laktionov PP (2018) Isolation of extracellular vesicles: general methodologies and latest trends. Biomed Res Int 2018:8545347–8545347. https://doi.org/10.1155/2018/8545347
103. Balaphas A, Meyer J, Sadoul R, Morel P, Gonelle-Gispert C, Bühler LH (2019) Extracellular vesicles: future diagnostic and therapeutic tools for liver disease and regeneration. Liver Int 39(10):1801–1817. https://doi.org/10.1111/liv.14189
104. Rojalin T, Phong B, Koster HJ, Carney RP (2019) Nanoplasmonic approaches for sensitive detection and molecular characterization of extracellular vesicles. Front Chem 7:279–279. https://doi.org/10.3389/fchem.2019.00279
105. Useckaite Z, Rodrigues AD, Hopkins AM, Newman LA, Johnson JG, Sorich MJ, Rowland A (2021) Role of extracellular vesicle derived biomarkers in drug metabolism and disposition. Drug Metab Dispos. https://doi.org/10.1124/dmd.121.000411
106. Newman LA, Fahmy A, Sorich MJ, Best OG, Rowland A, Useckaite Z (2021) Importance of between and within subject variability in extracellular vesicle abundance and cargo when performing biomarker analyses. Cells 10(3):485
107. Sidhom K, Obi PO, Saleem A (2020) A review of exosomal isolation methods: is size exclusion chromatography the best option? Int J Mol Sci 21(18):1. https://doi.org/10.3390/ijms21186466
108. Mitchell MI, Ben-Dov IZ, Liu C, Ye K, Chow K, Kramer Y, Gangadharan A, Park S, Fitzgerald S, Ramnauth A, Perlin DS, Donato M, Bhoy E, Manouchehri Doulabi E, Poulos M, Kamali-Moghaddam M, Loudig O (2021) Extracellular Vesicle Capture by AnTibody of CHoice and Enzymatic Release (EV-CATCHER): a customizable purification assay designed for small-RNA biomarker identification and evaluation of circulating small-EVs. J Extracell Vesicles 10(8):e12110. https://doi.org/10.1002/jev2.12110
109. Nakao Y, Amrollahi P, Parthasarathy G, Mauer AS, Sehrawat TS, Vanderboom P, Nair KS, Nakao K, Allen AM, Hu TY, Malhi H (2021) Circulating extracellular vesicles are a biomarker for NAFLD resolution and response to weight loss surgery. Nanomed Nanotechnol Biol Med 1:102430. https://doi.org/10.1016/j.nano.2021.102430
110. Mastoridis S, Bertolino GM, Whitehouse G, Dazzi F, Sanchez-Fueyo A, Martinez-Llordella M (2018) Multiparametric analysis of circulating exosomes and other small extracellular vesicles by advanced imaging flow cytometry. Front Immunol 9(1583):1. https://doi.org/10.3389/fimmu.2018.01583
111. Zarovni N, Corrado A, Guazzi P, Zocco D, Lari E, Radano G, Muhhina J, Fondelli C, Gavrilova J, Chiesi A (2015) Integrated isolation and quantitative analysis of exosome shuttled proteins and nucleic acids using immunocapture approaches. Methods 87:46–58. https://doi.org/10.1016/j.ymeth.2015.05.028

112. Mustapic M, Eitan E, Werner JK, Berkowitz ST, Lazaropoulos MP, Tran J, Goetzl EJ, Kapogiannis D (2017) Plasma extracellular vesicles enriched for neuronal origin: a potential window into brain pathologic processes. Front Neurosci 11(278):1. https://doi.org/10.3389/fnins.2017.00278
113. Shi M, Liu C, Cook TJ, Bullock KM, Zhao Y, Ginghina C, Li Y, Aro P, Dator R, He C, Hipp MJ, Zabetian CP, Peskind ER, Hu S-C, Quinn JF, Galasko DR, Banks WA, Zhang J (2014) Plasma exosomal α-synuclein is likely CNS-derived and increased in Parkinson's disease. Acta Neuropathol 128(5):639–650. https://doi.org/10.1007/s00401-014-1314-y
114. Fiandaca MS, Kapogiannis D, Mapstone M, Boxer A, Eitan E, Schwartz JB, Abner EL, Petersen RC, Federoff HJ, Miller BL, Goetzl EJ (2015) Identification of preclinical Alzheimer's disease by a profile of pathogenic proteins in neurally derived blood exosomes: a case-control study. Alzheimers Dement 11(6):600–7.e1. https://doi.org/10.1016/j.jalz.2014.06.008
115. Goetzl EJ, Kapogiannis D, Schwartz JB, Lobach IV, Goetzl L, Abner EL, Jicha GA, Karydas AM, Boxer A, Miller BL (2016) Decreased synaptic proteins in neuronal exosomes of frontotemporal dementia and Alzheimer's disease. FASEB J 30(12):4141–4148. https://doi.org/10.1096/fj.201600816R
116. Goetzl EJ, Schwartz JB, Mustapic M, Lobach IV, Daneman R, Abner EL, Jicha GA (2017) Altered cargo proteins of human plasma endothelial cell-derived exosomes in atherosclerotic cerebrovascular disease. Faseb j 31(8):3689–3694. https://doi.org/10.1096/fj.201700149
117. Vallabhajosyula P, Korutla L, Habertheuer A, Yu M, Rostami S, Yuan CX, Reddy S, Liu C, Korutla V, Koeberlein B, Trofe-Clark J, Rickels MR, Naji A (2017) Tissue-specific exosome biomarkers for noninvasively monitoring immunologic rejection of transplanted tissue. J Clin Invest 127(4):1375–1391. https://doi.org/10.1172/jci87993
118. Sharma P, Ludwig S, Muller L, Hong CS, Kirkwood JM, Ferrone S, Whiteside TL (2018) Immunoaffinity-based isolation of melanoma cell-derived exosomes from plasma of patients with melanoma. J Extracell Vesicles 7(1):1435138–1435138. https://doi.org/10.1080/20013078.2018.1435138
119. Mizutani K, Terazawa R, Kameyama K, Kato T, Horie K, Tsuchiya T, Seike K, Ehara H, Fujita Y, Kawakami K, Ito M, Deguchi T (2014) Isolation of prostate cancer-related exosomes. Anticancer Res 34(7):3419–3423
120. Welsh JA, Van Der Pol E, Arkesteijn GJA, Bremer M, Brisson A, Coumans F, Dignat-George F, Duggan E, Ghiran I, Giebel B, Görgens A, Hendrix A, Lacroix R, Lannigan J, Libregts SFWM, Lozano-Andrés E, Morales-Kastresana A, Robert S, De Rond L, Tertel T, Tigges J, De Wever O, Yan X, Nieuwland R, Wauben MHM, Nolan JP, Jones JC (2020) MIFlowCyt-EV: a framework for standardized reporting of extracellular vesicle flow cytometry experiments. J Extracell Vesicles 9(1):1713526–1713526. https://doi.org/10.1080/20013078.2020.1713526
121. Panagopoulou MS, Wark AW, Birch DJS, Gregory CD (2020) Phenotypic analysis of extracellular vesicles: a review on the applications of fluorescence. J Extracell Vesicles 9(1):1710020. https://doi.org/10.1080/20013078.2019.1710020
122. Botha J, Pugsley HR, Handberg A (2021) Conventional, high-resolution and imaging flow cytometry: benchmarking performance in characterisation of extracellular vesicles. Biomedicines 9(2):124. https://doi.org/10.3390/biomedicines9020124
123. Koliha N, Wiencek Y, Heider U, Jüngst C, Kladt N, Krauthäuser S, Johnston ICD, Bosio A, Schauss A, Wild S (2016) A novel multiplex bead-based platform highlights the diversity of extracellular vesicles. J Extracell Vesicles 5(1):29975. https://doi.org/10.3402/jev.v5.29975
124. Kornek M, Lynch M, Mehta SH, Lai M, Exley M, Afdhal NH, Schuppan D (2012) Circulating microparticles as disease-specific biomarkers of severity of inflammation in patients with hepatitis C or nonalcoholic steatohepatitis. Gastroenterology 143(2):448–458. https://doi.org/10.1053/j.gastro.2012.04.031
125. Julich-Haertel H, Urban SK, Krawczyk M, Willms A, Jankowski K, Patkowski W, Kruk B, Krasnodębski M, Ligocka J, Schwab R, Richardsen I, Schaaf S, Klein A, Gehlert S, Sänger H, Casper M, Banales JM, Schuppan D, Milkiewicz P, Lammert F, Krawczyk M, Lukacs-Kornek V, Kornek M (2017) Cancer-associated circulating large extracellular vesicles in cholangiocarcinoma and hepatocellular carcinoma. J Hepatol 67(2):282–292. https://doi.org/10.1016/j.jhep.2017.02.024
126. Abbate V, Marcantoni M, Giuliante F, Vecchio FM, Gatto I, Mele C, Saviano A, Arciuolo D, Gaetani E, Ferrari MC, Giarretta I, Ardito F, Riccardi L, Nicoletti A, Ponziani FR, Gasbarrini A, Pompili M, Pola R (2017) HepPar1-positive circulating microparticles are increased in subjects with hepatocellular carcinoma and predict early recurrence after liver resection. Int J Mol Sci 18(5):1043
127. Chiriacò MS, Bianco M, Nigro A, Primiceri E, Ferrara F, Romano A, Quattrini A, Furlan R, Arima V, Maruccio G (2018) Lab-on-chip for exosomes and microvesicles detection and characterization. Sensors 18(10):1. https://doi.org/10.3390/s18103175
128. Kanwar SS, Dunlay CJ, Simeone DM, Nagrath S (2014) Microfluidic device (ExoChip) for on-chip isolation, quantification and characterization of circulating exosomes. Lab Chip 14(11):1891–1900. https://doi.org/10.1039/C4LC00136B
129. Shao H, Im H, Castro CM, Breakefield X, Weissleder R, Lee H (2018) New technologies for analysis of extracellular vesicles. Chem Rev 118(4):1917–1950. https://doi.org/10.1021/acs.chemrev.7b00534
130. Liang K, Liu F, Fan J, Sun D, Liu C, Lyon CJ, Bernard DW, Li Y, Yokoi K, Katz MH, Koay EJ, Zhao Z, Hu Y (2017) Nanoplasmonic quantification of tumor-derived extracellular vesicles in plasma microsamples for diagnosis and treatment monitoring. Nat Biomed Eng 1:0021. https://doi.org/10.1038/s41551-016-0021
131. Rega-Kaun G, Ritzel D, Kaun C, Ebenbauer B, Thaler B, Prager M, Demyanets S, Wojta J, Hohensinner PJ (2019) Changes of circulating extracellular vesicles from the liver after Roux-en-Y bariatric surgery. Int J Mol Sci 20(9):2153

Appendix 2

Article published in Journal of Extracellular Biology, 2022.

Received: 13 May 2022 | Revised: 3 August 2022 | Accepted: 14 August 2022

DOI: 10.1002/jex2.56

RESEARCH ARTICLE

Addressing MISEV guidance using targeted LC-MS/MS: A method for the detection and quantification of extracellular vesicle-enriched and contaminant protein markers from blood

Lauren A. Newman | **Zivile Useckaite** | **Andrew Rowland**

College of Medicine and Public Health, Flinders University, Adelaide, South Australia

Correspondence
Andrew Rowland, College of Medicine and Public Health, Flinders University, Adelaide, South Australia.
Email: andrew.rowland@flinders.edu.au

Funding information
National Health and Medical Research Council, Grant/Award Number: 1158210

Abstract

Extracellular vesicles (EVs) are membrane-bound nanosized particles released by cells into bodily fluids containing an array of molecular cargo. Several characteristics, including stability and accessibility in biofluids such as blood and urine, make EVs and associated cargo attractive biomarkers and therapeutic tools. To promote robust characterisation of EV isolates, the minimal requirements for the study of extracellular vesicles (MISEV) guidelines recommend the analysis of proteins in EV samples, including positive EV-associated markers and negative contaminant markers based on commonly co-isolated components of the starting material. Western blot is conventionally used to address the guidelines; however, this approach is limited in terms of quantitation and throughput and requires larger volumes than typically available for patient samples. The increasing application of EVs as liquid biopsy in clinical contexts requires a high-throughput multiplexed approach for analysis of protein markers from small volumes of starting material. Here, we document the development and validation of a targeted liquid chromatography tandem mass spectrometry (LC-MS/MS) assay for the quantification of markers associated with EVs and non-vesicle contaminants from human blood samples. The assay was highly sensitive, requiring only a fraction of the sample consumed for immunoblots, fully quantitative and high throughput. Application of the assay to EVs isolated by size exclusion chromatography (SEC) and precipitation revealed differences in yield, purity and recovery of subpopulations.

KEYWORDS
extracellular vesicles, liquid chromatography tandem mass spectrometry, plasma, protein markers, sample characterization, serum

1 | INTRODUCTION

In recent years, the field of extracellular vesicle (EV) research has exploded with publications documenting their biological properties, functionality, and potential diagnostic, prognostic and therapeutic applications in human disease (Shao et al., 2018; Théry et al., 2018; Van Deun et al., 2017). The term EV describes a heterogenous population of membrane-bound vesicles; including small EVs, such as exosomes (50–150 nm), that arise from endosomal pathways within the cell, and EVs of various sizes up to 1000 nm in diameter, shed directly from the plasma membrane (microvesicles) (Kowal et al., 2016; Newman et al., 2020). Whilst originally perceived simply as a pathway for cellular garbage disposal, EVs are increasingly recognised for their roles in local and

systemic intercellular communication, diverse physiological processes and disease progression (Newman et al., 2020; Shao et al., 2018). These functions are facilitated via the transfer of biologically active cargo, including nucleic acids, proteins and lipids, into recipient cells resulting in phenotypic and functional changes (Greening et al., 2017; Newman et al., 2020).

The stability conferred through encapsulation within the vesicle membrane and accessibility in biological fluids such as blood and urine, makes EV cargo attractive as biomarkers and therapeutic tools (Hirsova et al., 2016). However, their clinical application is hindered by several challenges, particularly with respect to the competing imperatives of recovery and purity of isolated preparations (Newman et al., 2020; Van Deun et al., 2017; Webber & Clayton, 2013). To promote the standardisation of EV methodologies and reporting, the International Society for Extracellular Vesicles (ISEV) has provided guidelines that set out the minimal requirements for the study of extracellular vesicles (MISEV) (Théry et al., 2018). Researchers must provide robust evidence to claim the presence of EVs in isolates and assign physiological properties or functions to them. In addition, the EV-TRACK knowledgebase provides a platform for the detailed recording of experimental procedures through a checklist of 115 parameters, from which studies are assigned an EV-METRIC reflecting the capacity for the experiments to be properly interpreted and reproduced (Van Deun et al., 2017).

A key component of the EV-METRIC is analysing samples for the presence of accepted EV markers and absence or depletion of markers not associated with EVs (Van Deun et al., 2017) (±EV markers). EV enriched proteins are derived from the plasma membrane or cytosol and reflect the process of biogenesis and sorting of cargo (Shao et al., 2018). MISEV (2018) defines two categories of proteins to be analysed in all preparations, in order to robustly claim the presence of EVs (Van Deun et al., 2017). Markers frequently identified from Category 1 (transmembrane or GPI-anchored proteins) include tetraspanins (CD9, CD81, CD63) and major histocompatibility complex class 1 (MHC1) (Kowal et al., 2016; Shao et al., 2018; Théry et al., 2018). Category 2 comprises proteins that are incorporated from the cytosol into EVs, largely due to lipid- or membrane protein-binding capacity. Examples of these are tumour susceptibility gene 101 (TSG101), heat shock 70 kDa proteins and flotillins -1 & -2 (Van Deun et al., 2017). A third category of commonly co-isolated contaminants is also given for assessing purity. These are selected with respect to EV source; for example, apolipoproteins or albumin in blood-derived EV isolates (Théry et al., 2018). Further, proteins expressed in intracellular compartments other than plasma membrane or endosome, such as endoplasmic reticulum (ER) or nucleus, may be used as markers of large EVs, cellular components or apoptotic blebs (Shao et al., 2018). Common examples include calnexin, endoplasmin (GP96), or histones (Kowal et al., 2016; Théry et al., 2018; Webber & Clayton, 2013), and comprise Category 4, which must be addressed by researchers claiming the specific isolation of small EVs (Théry et al., 2018).

Currently, western blotting is the most common approach used to address reporting requirements relating to analysis of ±EV markers (Théry et al., 2018). While western blotting is an established method for protein detection, the approach has many inherent limitations that impact applicability to certain sample types. By way of example, as an antibody-based (immunoblotting) method, western blotting is semi-quantitative and can reliably detect only one analyte per sample. This may not be an issue when working with EVs isolated from cell culture media as sample volumes are plentiful, allowing for multiple parallel analyses, and there is a greater ratio of vesicles to particulate contamination (Kreimer et al., 2015; Van Deun et al., 2017). This does, however, become a key limitation in the context of addressing reporting requirements when working with biospecimens from clinical trials or patient cohorts, as the resulting EV sample volume is often insufficient to accommodate multiple western blot analyses as control experiments. Additionally, the biospecimen sample matrix is typically more complex and variable between samples, which can impact the quality of western blot analysis. Importantly, western blots can also be limited by the performance of antibodies, as non-specific binding can increase background and reduce confidence in analyte detection (Liebler & Zimmerman, 2013). As EVs become an increasingly important "liquid biopsy" platform and their application to clinical biospecimens gains increasing attention, there is a need for a robust, higher throughput, multiplexed approach to address ±EV marker reporting requirements, ideally utilising the same platform that is applied to biomarkers of interest. Particularly when working with biospecimens, different EV isolation methods are known to enrich specific EV sub-populations and differ in terms of EV recovery and the extent and composition of vesicular and non-vesicular contamination. Accordingly, it is important to consider the compatibility of isolation strategy with the analytical platform.

In recent years liquid chromatography mass spectrometry (LC-MS/MS) analyses have facilitated expansive proteomic profiling of EVs (Rosa-Fernandes et al., 2017; Shao et al., 2018). LC-MS/MS has been applied in both untargeted and targeted workflows, to qualitatively screen for the presence of proteins and to quantify the abundance of specific proteins, respectively. Targeted LC-MS/MS based protein quantification typically involves the enzymatic digestion of proteins into peptides, separation by reverse phase liquid chromatography, and quantification of specific fragmentation patterns associated with the peptide of interest using a triple quadrupole (QQQ) mass spectrometer (Kreimer et al., 2015; Rosa-Fernandes et al., 2017). This approach, referred to as multiple reaction monitoring (MRM), is highly sensitive, reproducible, and depending on instrument configuration can simultaneously analyse up to 20 proteins in a single sample. Additionally, targeted LC-MS/MS analysis enables absolute analyte quantification in a complex matrix when the magnitude of the response for the endogenous analyte is normalised using a stable isotope labelled (SIL) peptide and compared to an external calibrator spiked into a comparable matrix at a known concentration (Greening et al., 2017; Kreimer et al., 2015).

Few studies have previously employed targeted LC-MS/MS assays to assess purity of EVs from blood (Park et al., 2021; Wang et al., 2017), and have been useful in the development of novel isolation strategies (Nguyen et al., 2021) or to gain insight to

membrane origin of circulating vesicles (Zhang et al., 2020). Of these studies, only that by Park et al. (2021) was performed on clinically relevant volumes of sample (100 μl plasma, while others used up to 200 ml). However, the proteins included in this panel covered cytosolic EV-enriched proteins and non-EV contaminants while transmembrane (MISEV category 1) proteins were notably absent. Thus, the present manuscript describes the development and validation of a novel MRM-based panel specifically designed to address MISEV guidelines. This approach is sensitive, fully quantitative and high throughput. Establishing the presence of EV markers and depletion of contaminants is a critical component of sample characterisation, likely to be expanded upon in new iterations of MISEV (Witwer et al., 2021). Since the 2018 guidelines recognised the challenge of performing several characterisation experiments when sample volume is limited, we validate the application of this platform in small starting volumes. Hence, the method described here may be generalised to other EV-based research applications, of different cell-types or (patho)physiological condition, but we anticipate its particular value for the analysis of clinical biospecimens.

2 | METHODS

2.1 | Blood samples

Venous blood from healthy volunteers was collected into Z Serum Sep Clot Activator tubes or K_3EDTA plasma vacuettes (Greiner Bio-one, Frickenhausen, Germany) and centrifuged twice at 2500 g for 15 min at 10°C. Serum or plasma was extracted and stored at −20°C until analysis. The study was approved by the Southern Adelaide Clinical Human Research Ethics Committee (SAHREC; number 261.18). Serum and plasma samples from patients with non-alcoholic fatty liver disease (NAFLD) were purchased from Discovery Life Sciences (Hunstville, AL, USA).

2.2 | EV isolation

2.2.1 | qEV size exclusion chromatography

qEV Original (Legacy) 35 and 70 nm size exclusion chromatography (SEC) columns (iZon Science, Christchurch, NZ) were used to isolate EVs from serum or plasma. Prior to EV isolation, columns were equilibrated to room temperature (RT) and washed with 10 ml of 0.2 μm filtered phosphate-buffered saline (PBS). Serum (500 μl) was loaded into the sample reservoir and allowed to completely pass into the column before PBS was added (no more than 2 ml at any time) to begin elution. The first six fractions (3 ml) eluted from the column was discarded and vesicles were collected as pooled fractions 7–11 (2.5 ml) into 5 ml Protein LoBind tubes (Eppendorf). Pooled vesicle fractions were mixed gently by inversion and concentrated to 100 μl using Amicon Ultra-4 centrifuge filters (30 kDa, Millipore-Sigma) pre-conditioned with PBS. Concentrated vesicle isolates were stored at −80°C until analysis.

2.2.2 | ExoQuick precipitation

Serum was centrifuged for 15 min at 3000 × *g* at 10°C to remove debris. Spun serum (500 μl) was combined with ExoQuick™ precipitation solution (126 μl) and mixed eight to 10 times by gentle inversion. Samples were incubated for 30 min on ice then centrifuged for 30 min at 1500 g at 4°C to pellet EVs and again for 5 min in the same conditions, each time aspirating all supernatant. The pellets were resuspended in 100 μl of filtered PBS/RIPA buffer and stored at −80°C until analysis.

2.3 | Nanoparticle tracking analysis

Nanoparticle tracking analysis (NTA) was performed to quantify particle concentration and size distribution in EV samples using a NanoSight NS300 (Malvern Analytical, UK). Samples were diluted between 1:500 and 1:20000 in freshly 0.2 μm filtered PBS. Five 60-s videos were captured at camera level 14 with a continuous sample flow (flow rate 100). Videos were analysed at detection threshold five using NTA 3.0 software.

2.4 | Transmission electron microscopy

Samples were prepared based on a previously published protocol (Newman et al., 2021). Briefly, Ted-Pella B 300 M carbon-coated grids (Ted-Pella, Redding, CA, USA) were cleaned and hydrophilized using plasma glow discharge for 15 seconds

(Gatan SOLARUS Advanced Plasma Cleaning System, Gatan, Inc., Pleasanton, CA, USA) prior to use. Five microlitres of sample in 0.2 μm-filtered PBS was placed on carbon-coated grids for 5 min. Carbon grids were washed once (15 s) at RT with 0.2 μm filtered PBS and were contrasted with 2% uranyl acetate (3 min, RT), washed once, and examined by FEI TECNAI Spirit G2 TEM (Thermo Fisher Scientific, Waltham, MA, USA) operated at 100 kV. TEM images were acquired at magnifications of 49,000× and 68,000× (Figure S1).

2.5 | Human liver microsome preparation

Pooled human liver microsomes (HLMs) were prepared by differential centrifugation as described by Bowalgaha et al. (2005). Briefly, liver portions (<1 cm thickness) were suspended in phosphate buffer (0.1 M, pH 7.4) containing potassium chloride (KCl; 1.15% w/v) and minced using scissors. The minced liver tissue was homogenized, initially with a Janke and Kunkle Ultra Turax at a speed of 24000 rpm, and then with a Potter-Elvehem homogenizer (driven by a power drill) at a speed of 1480 rpm. The homogenized tissue was centrifuged at 3000 g for 10 min at 4°C, and again at 10,000 g for 10 min at 4°C. The supernatant layer was collected and centrifuged at 105,000 g for 1 h at 4°C. The resulting pellet was re-suspended in phosphate buffer (0.1 M, pH 7.4) containing KCl (1.15% w/v) and then centrifuged at 105,000 g for 1 h at 4°C. The final microsomal pellet was suspended in phosphate buffer (0.1 M, pH 7.4) containing glycerol (20% v/v), aliquoted into 400 μl samples, and stored at –80°C until use. Equal protein amounts of microsomes from five human livers (H7, female 44 years old [y/o]; H10, female 67 y/o; H12, male 66y/o; H29, male 45y/o; and H40, female 54y/o) were used for the purpose of this study. Approval for the use of human liver tissue in xenobiotic metabolism studies was obtained from both the Clinical Investigation Committee of Flinders Medical Centre and from the donors' next of kin. All livers were obtained within 60 min of death and were immediately sliced and frozen in liquid nitrogen. Once frozen, livers were stored at -80°C until use.

2.6 | Protein isolation from EVs for immunoblots

EVs isolated by qEV were lysed by mixing an equal volume (6 μl) of EV sample in PBS with ice-cold RIPA (Radioimmunoprecipitation assay) lysis buffer (Thermo Fisher Scientific, IL, USA). ExoQuick isolated EVs (pellet) was lysed in 100 μl of the above RIPA lysis buffer. All samples were incubated on ice for 25 min, centrifuged at 10,000 g for 10 min at 4°C. Soluble protein was measured by micro BCA assay (Thermo Fisher Scientific, IL, USA), according to manufacturer's instructions. Briefly, working reagent (WR) was prepared using MA:MB:MC at 25:24:1 ratio. Lysed samples were diluted up to 300 μl in 0.2 μm-filtered PBS. In a 96-well plate, equal volume of WR and either sample or bovine serum albumin (BSA) standard were mixed and assayed in duplicate. Absorbance of samples at 562 nm were compared to that of BSA standard curve (0–200 μg/ml) to determine protein concentration, using a SuperMax plate reader (Molecular Devices, CA, USA).

2.7 | Protein isolation from HLM and serum for immunoblots

HLM and serum protein was isolated by mixing equal volumes of HLM and ice-cold RIPA buffer, incubated on ice for 25 min, centrifuged at 10,000 g for 10 min at 4°C. Soluble protein was measured, as above, by micro BCA assay (Thermo Fisher Scientific, IL, USA).

2.8 | Immunoblotting

EV, HLM, and serum protein (35 μg), isolated as described above, was used for immunoblotting as we previously described (Useckaite et al., 2020), except that 5% BSA/TBS containing 0.1% Tween 20 (TBST) was used. Protein lysates (EV, HLM, and serum) were resolved on gradient SDS gels (Bio-Rad Laboratories, CA, USA) and the proteins where then transferred to Immun-Blot LF polyvinylidene difluoride (PVDF) membrane, 0.45 lm (Bio-Rad Laboratories, CA, USA), using a Turbo Blot transfer unit (Bio-Rad Laboratories, CA, USA). Stain-free imaging of the gel was performed using a ChemiDoc MP imager (Bio-Rad Laboratories, CA, USA) with a 1-min stain activation time as previously described (Colella et al., 2012). Total protein images were obtained at pre-blocking of PVDF (Figure S2). PVDF membranes were blocked with 5% (w/v) BSA in TBST and incubated overnight at 4°C with primary antibodies.

Primary antibodies (in 5%BSA/TBST) from Abcam (Abcam, Cambridge, MA, USA) were anti-human CD9 (Cat.#:ab92959; 1/1000); anti-human CD63 (Cat.#:ab68418; 1/1000); anti-human CD81 (Cat.#:ab109201; 1/1000); and anti-human Calnexin (Cat.#:ab2791; 1/1000). Primary antibody for anti-human TSG101 was from Invitrogen (Thermo Fishes Scientific, IL, USA; Cat.#:PA5-31260; 1/1000). Secondaries from Cell Signalling Cell Signalling Technology, MA, USA) were anti-mouse IgG, HRP-linked

(Cat.#:7076; 1/1000) or anti-rabbit IgG, HRP-linked (Cat.#:7-74; 1/1000). HLM-lysate was included in all gels as a positive control. Serum lysate was added as a positive control for Albumin.

SuperSignal West Femto Chemiluminescent Substrate Kit (Thermo Fisher Scientific, IL, USA) was used for detection, imaging was performed using an automated ChemiDoc Touch Imaging System (Bio-Rad Laboratories, CA, USA) and densitometric analysis was performed using ImageJ tool (https://imagej.nih.gov/ij/index.html).

2.9 | Peptide digestion

EVs isolated by SEC columns and by ExoQuick precipitation, 50 and 10 μl, respectively, were diluted up to 100 μl in PBS; containing between 70 and 20 μg of SEC EV protein and 1132–1683 μg of ExoQuick EV protein. EVs were lysed by vortexing for 10 min using a MixMate sample mixer (Eppendorf) followed by three freeze-thaw cycles. Lysed samples were mixed with 50 μl of ammonium bicarbonate (pH 7.8) and incubated with dithiothreitol (12.5 mM) for 90 min at 60°C. Samples were cooled to RT prior to addition of iodoacetamide (23.5 mM) and incubation for 60 min at 37°C. Trypsin Gold was then added to protein samples in a ratio of 1:40 and incubated for 17 h at 37°C. Samples were mixed with 20 μl of formic acid (10% v/v) in order to terminate digestions, then centrifuged at 16,000 g for 10 min at 4°C. Resulting supernatant (100 μl) was spiked with a SIL peptide cocktail (final [nM]: ALB: 10; CD81: 0.4; CD9: 0.1; CANX, TSG101: 0.2). SIL peptides were obtained from Vivitide (MA, USA), all of isotopic purity >99%. Digested samples containing SIL peptides were run immediately and stored in the autosampler at 15°C over the course of the run. A 5 μl aliquot of digested protein was injected for analysis by LC-MS/MS (Table S1). HLM and serum, diluted 1:100 in PBS, were digested in the same conditions and run as positive controls.

2.10 | Chromatography

Chromatographic separation of analytes was performed on an Agilent Advance Bio Peptide Map column (100 mm × 2.1 mm, 2.7 μm) using an Agilent 1290 Infinity II liquid chromatography system. The temperature of the sample and column compartments was maintained at 15°C and 30°C, respectively. A panel of analytes comprising the EV makers CD81, CD9, and TSG101, and contaminants calnexin (CANX) and albumin (ALB), were separated by gradient elution with a flow rate of 0.2 ml/min. The mobile phase consisted of 0.1% formic acid in water (mobile phase A) and 0.1% formic acid in acetonitrile (mobile phase B) held in a proportion of 97% A and 3% B for the first 3 min. The proportion of mobile phase B was then increased linearly to 30% over 30 min then increased to 50% in 5 min and held for 1 min before returning to 3% over a further 5 min. Lastly, mobile phase B was held at 3% to re-equilibrate the column for 5 min.

2.11 | Mass spectrometry

Column eluant was monitored by mass spectrometry using an Agilent 6495B QQQ mass spectrometer operating in positive electron spray (ESI+) mode. Target proteins were included in the panel in accordance with MISEV reporting guidelines. Proteotypic peptides for each protein marker were screened in EV samples and/or positive controls (HLM) and confirmed using Skyline software. Peptides contained between seven and 22 amino acids for uniqueness and mass range of QQQ instrument. Peptides had no methionine or cysteine residues. Sites of mutagenesis or post-translational modifications were avoided. For one peptide per protein, one quantifier and two qualifier ion transitions were included for optimisation of the MRM method based on signal intensity (Table 1). Three types of each analyte were detected; synthetic isotope labelled (SIL), endogenous and synthetic light peptide; as the latter was spiked into samples to supplement endogenous levels where required for assay validation. Skyline software was used to verify transitions and to select the optimal collision energy for each transition from seven predicted voltages. MassHunter Optimiser Software was used to optimise source parameters: capillary voltage, nebuliser pressure and nozzle voltage; and cell accelerator voltage was optimised manually between 3 and 8 V. Identities of endogenous peptides were confirmed by comparing retention time and quantifier/qualifier transition ratios to respective SIL peptide standards.

2.12 | Assay validation and calibration

Calibration standards ($n = 8$) were prepared to span the concentration ranges associated with qEV70 EV isolates, and to ensure a robust minimal concentration to exclude contamination (CANX and ALB) from human serum. In this range, assay linearity was determined for each analyte according to linear regression analysis. Assay sensitivity was determined for the panel. The limit of detection (LOD) was defined as a signal to noise ratio of 3:1 and the lower limit of quantification (LLOQ) as 5× the LOD.

TABLE 1 Analyte sequences and transitions used for multiple reaction monitoring

Analyte	Type	Sequence	Retention time (min)	Precursor Ion	Product Ions			Collision energy (eV)
ALB	SIL	H2N-LVNEVTEFA**K**ˆ-OH	20.7	579.3	603.3 (y5+)	702.4 (y6+)	**945.5 (y8+)**	18.8
	Light	H2N-LVNEVTEFAK-OH	20.7	575.3	595.3 (y5+)	694.4 (y6+)	**937.5 (y8+)**	18.8
CD81	SIL	H2N-QFYDQALQQAVVDDDANNA**K**ˆ-OH	23.9	754.4	870.4 (y8+)	**969.4 (y9+)**	1068.5 (y10+)	17.3
	Light	H2N-QFYDQALQQAVVDDDANNAK-OH	23.9	751.7	862.4 (y8+)	**961.4 (y9+)**	1060.5 (y10+)	17.3
CD9	SIL	H2N-DVLETFTV**K**ˆ-OH	24.3	530.3	603.4 (y5+)	732.4 (y6+)	**846.5 (y7+)**	22.3
	Light	H2N-DVLETFTVK-OH	24.3	526.3	595.4 (y5+)	724.4 (y6+)	**837.5 (y7+)**	22.3
CANX	SIL	H2N-IVDDWANDGWGL**K**ˆ-OH	27.2	748.9	797.4 (y7+)	**868.4 (y8+)**	1054.5 (y9+)	24.1
	Light	H2N-IVDDWANDGWGLK-OH	27.2	744.9	789.4 (y7+)	**860.4 (y8+)**	1046.5 (y9+)	24.1
TSG101	SIL	H2N-GVIDLDVFL**K**ˆ-OH	32.5	563.8	742.5 (y6+)	**857.5 (y7+)**	970.6 (y8+)	18.4
	Light	H2N-GVIDLDVFLK-OH	32.5	559.8	734.4 (y6+)	**849.5 (y7+)**	962.6 (y8+)	18.4

Note: SIL (ˆ): Stable isotope labelled peptide; bold and underlined letter = heavy labelled amino acid. Bold values indicate product ions used as quantifier transitions.

Precision was assessed on the basis of intra- and inter-day variability in the slope produced by calibration curves run in triplicate on three separate days. Variability was recorded as percent relative standard deviation (% RSD) of triplicate injections (within run) and of average slope across different days (between runs). Repeatability was assessed by five consecutive injections of a mid QC sample and variability recorded as % RSD. Accuracy was determined based on the recovery of SIL peptide spiked into quality control (QC) samples at low (ALB: 6; CD81: 0.6; CD9: 0.06; CANX, TSG101: 0.12 [nM]), mid (ALB: 10; CD81: 1; CD9: 0.1; CANX, TSG101: 0.2 [nM]) and high (ALB: 18; CD81: 1.8; CD9: 0.18; CANX, TSG101: 0.36 [nM]) concentrations within the calibration curve. Carryover was assessed in two consecutive blank injections following the highest calibration standard.

The stability of analytes was evaluated in duplicate EV samples. Samples were kept at −20°C, 4°C, or 15°C and analysed at baseline and after 6, 24, and 48 h. Concentration was determined at each time point and changes from baseline of less than 20% were accepted as stable.

Matrix effects were assessed based on absolute and relative recovery of SIL peptides spiked in EV matrix or mobile phase. Calibrators 1 and 6 and a middle QC sample were prepared and analysed in each matrix and used to generate curves. Matrix effects were reported as % difference in slope and precision in each matrix was based on triplicate injections of each QC.

The reproducibility of the protocol was assessed based on the reproducibility of detecting analytes and of quantifying analytes. EVs were isolated in triplicate from the serum of three donors by each of the three isolation methods as described above, and peptide digests were performed in duplicate, as also previously described. Reproducible detection across replicate isolations was defined by samples with average normalised response > LOD and reproducible detection in peptide digests was defined by equivalent response (both duplicates are < or > LOD) in each pair.

Additional analyses were performed to demonstrate the generalizability of the assay. Specifically, these analyses demonstrate the capacity to detect EV markers in plasma from healthy controls and serum and plasma from subjects with NAFLD. These analyses were performed using EVs isolated by two distinct isolation approaches.

2.13 | Statistical analysis

Statistical analyses were performed using GraphPad Prism software version 9 (San Diego, CA, USA). Comparisons of group means were assessed by repeated measures one-way ANOVA with Tukey test for multiple comparisons. Linear regression analysis was performed using Microsoft Excel version 16.

2.14 | EV-TRACK

We have submitted all relevant data of our experiments to the EV-TRACK knowledgebase (EV-TRACK ID: EV220163) (Van Deun et al., 2017).

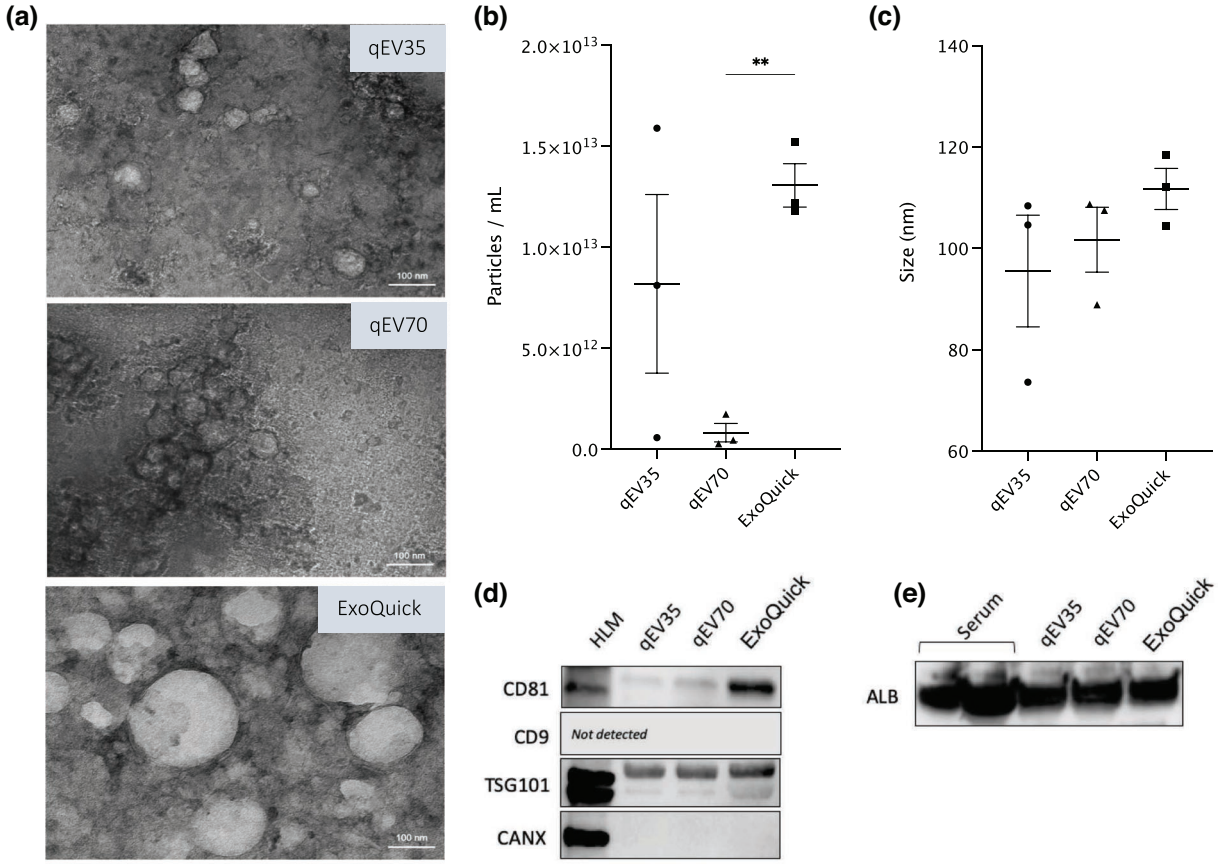

FIGURE 1 Characterisation of extracellular vesicles isolated by SEC and precipitation. (a) Transmission electron microscopy images. Direct magnification ×30,000. Scale bar = 100 nm. (b) Concentration and (c) Mean size of particles measured by nanoparticle tracking analysis. Data shown as mean ± standard deviation; $^{**}p < 0.01$; ($n = 3$), One-way ANOVA and Tukey test for multiple comparisons. (d) Representative images of key proteins considered to be markers of EVs (CD81, CD9, and TSG101), according to MISEV 2018 guidelines, in EVs isolated by qEV35, qEV70, and ExoQuick against HLM (non-EV control). Endoplasmic reticulum protein, CANX, was included as a marker of cellular structures considered to be enriched in cells relative to EVs (i.e., non-EV component, negative EV marker). (e) Representative image showing albumin contamination in EV samples isolated by qEV35, qEV70, and ExoQuick. Thirty-five micrograms of lysed EV or serum protein loaded per lane. Two lanes of albumin represent 35 μg of protein that leaked to the neighbouring well due to pipetting error

3 | RESULTS

3.1 | Characterisation of EVs

EVs were isolated from human serum ($n = 3$) by each of three commercially available methods; qEV70 and qEV35 SEC columns, and ExoQuick precipitation. TEM images revealed characteristic morphology and structurally intact vesicles isolated by each method, however, high background from non-vesicular contamination was prevalent in the ExoQuick image (Figure 1a). The mean particle concentration varied between methods, with significantly more particles isolated by ExoQuick compared to qEV70 (Figure 1b). Mean particle size measured by NTA was consistent across the three isolation methods (Figure 1c), although TEM images demonstrated the presence of a sub-population of larger vesicles in the ExoQuick isolate.

Irrespective of EV isolation method, common EV markers CD81 and TSG101 were detected by immunoblots in all EV samples (Figure 1d and Figure S2–S4), although differences in apparent abundance were observed (Figure S6). TSG101 abundance was comparable between EVs isolated by each of the SEC columns, while a greater amount was detected in ExoQuick samples. Similarly, samples isolated by SEC columns displayed low levels of CD81, with the highest signal detected in ExoQuick-isolated samples. Two bands were observed for TSG101 protein, in line with other publications using the same antibody (Hofmann et al., 2020; Schroeder et al., 2020). CD9 expression was not detected in any of the samples. The ER protein, CANX, was included in the analysis as a marker of non-EV cellular structures (EV negative marker). CANX expression was below the LOD of the immunoblot method. While this method cannot provide a quantitative assessment, the lack of CANX detection suggests minimal contamination with cellular debris.

TABLE 2 Mass spectrometer instrument settings

Parameter	Setting			
Time segment (min)	0–22	22–26	26–30	30–48
Delta EMV (V)	300	300	300	300
Capillary voltage (V)	3000	2500	3000	3000
Nebulizer pressure (psi)	30	25	30	30
Nozzle voltage (V)	1000	500	500	500
Cell accelerator voltage	5	3	5	4

Since EVs were isolated from human serum, an additional immunoblot was run to compare albumin contamination across EV samples resulting from different methods of EV isolation (Figure 1e and S5). Lysed serum protein was analysed as a positive control. Similar size bands were observed at approximately 70 kDa across all EV samples, irrespective of isolation method. Importantly, blots were loaded with equivalent amount protein (35 μg) for each sample type, so they do not reflect the analyte abundance in equal volumes of starting material. Specifically, the volumes of serum corresponding to amount of loaded protein for EV samples isolated by qEV35, qEV70 and ExoQuick are 103, 115, and 1.9 μl, respectively (Table S1). This consideration of co-isolated contaminants per serum volume highlights the vastly greater levels of albumin recovered in ExoQuick isolates compared to SEC. Indeed, SEC has been reported to isolate a greater ratio of vesicle to serum proteins, compared to precipitation reagents or conventional techniques such as ultracentrifugation, and can reproducibly isolate vesicles containing characteristic EV markers (Monguió-Tortajada et al., 2019; Vanderboom et al., 2021). As qEV35 enriches for vesicles 35–350 nm in diameter while qEV70 enriches those 70–1000 nm, the former is prone to greater co-isolation of lipoproteins from the blood. For these reasons, development of the peptide assay was primarily performed using vesicles isolated by qEV70.

3.2 | MRM method development

Target proteins were selected to address the category reporting requirements outlined in the MISEV guidelines for EVs derived from blood products (serum or plasma) (Théry et al., 2018). The final protein panel comprised CD81 (Category 1[a]), CD9 (Category 1[b]) and TSG101 (Category 2a) as positive vesicle markers, albumin (ALB; Category 3) to represent matrix-associated contamination in EV isolates from the blood, and calnexin (CANX; Category 4) as a marker of cellular debris or large vesicles. Selected tryptic peptides corresponding to each target protein were detected in vesicles isolates and/or positive controls (HLM) and one precursor ion with three product ion transitions of greatest intensities were included for optimisation (Table 1). Instrument settings were optimised as described in materials and methods and values for optimised parameters are given in Table 2. Chromatograms of SIL peptides spiked into digested EVs (qEV70) is shown in Figure S7. Retention times were highly reproducible for each analyte measured in calibration standards with RSD between 0.04% and 0.07 %.

3.3 | Assay validation

3.3.1 | Linearity and sensitivity

Calibration curves were generated for each analyte in the panel to encompass the concentration range typically observed for normal human serum (calibrators 1–6) and at points two and four times beyond that, as may be observed with increased levels of circulating EVs in various disease states (calibrators 7 and 8) (Nguyen et al., 2021; Povero et al., 2020; Sehrawat et al., 2021). The required range varied considerably between positive and negative EV markers: Albumin was validated between 2.0 and 80 pmol/ml while this range was 100-fold less for CD9 (Table 3). Linearity of response was assessed by linear regression analysis and produced coefficient of determination (r^2) values for each analyte ranging between 0.9966 and 0.9999 (Figure 2). The sensitivity of the assay was determined with respect to LOD and LLOQ, calculated as described in materials and methods. For most of the analytes, the validated calibration range extended towards the lower end of the assay's sensitivity. Details of these characteristics are summarised in Table 3.

TABLE 3 Details of calibration and quantification for analytes in the EV marker panel

Analyte	Calibration range (pmol/ml)	Calibration curve coefficient of determination (r^2)	Limit of detection (LOD) (pmol/ml)	Lower limit of quantification (LLOQ) (pmol/ml)
ALB	2.0–80	0.9999	0.004	0.020
CD81	0.2–8.0	0.9985	0.050	0.230
CD9	0.02–0.8	0.9982	0.005	0.025
CANX	0.04–1.6	0.9984	0.007	0.035
TSG101	0.04–1.6	0.9966	0.006	0.031

TABLE 4 Assay precision

	Variability (% RSD)	
Analyte	Intra-day	Inter-day
ALB	0.4	0.4
CD81	5.6	7.6
CD9	3.0	6.2
CANX	4.5	3.9
TSG101	13	4.6

Note: Relative standard deviation (% RSD) of slopes of triplicate calibration curves run within day and on three different days.

TABLE 5 Assay accuracy

	QC Concentration (pmol/ml)								
Analyte	Low			Mid			High		
	Nominal	Measured	% True	Nominal	Measured	% True	Nominal	Measured	% True
ALB	6.0	6.75	112	10	10.9	107	18	20.2	110
CD81	0.6	0.550	92	1.0	0.972	97	1.8	1.72	96
CD9	0.06	0.063	105	0.1	0.094	94	0.18	0.187	104
CANX	0.12	0.112	93	0.2	0.232	116	0.36	0.340	94
TSG101	0.12	0.120	100	0.2	0.212	106	0.36	0.392	109

3.3.2 | Assay precision, repeatability and accuracy

Assay precision was assessed based on intra- and inter-day variability in the slope of calibration curves run in triplicate on three separate days. The %RSD ranged from 0.4% to 13% for within-run variability in analyte response, and between runs, variability ranged from 0.4% to 8% (Table 4). Instrument repeatability was also determined in five consecutive injections of the same sample and gave % RSD < 9 % for all analytes. Relative accuracy (within matrix) of the assay was determined by measurement of low, mid and high QC samples. These QC points were selected within the concentration range typically observed for normal human serum (calibrators 1–6); nominal concentrations are given in Table 5. For all analytes, accuracy ranged from 92% to 112% at low, 97%–116 % at mid, and 94%–110 % at high QC concentration (Table 5).

3.3.3 | Carryover

Carryover was assessed in two consecutive "blank" injections of mobile phase following injection of the highest calibration standard. Blank injections involved a full LC injection cycle. Albumin response was detectable in both injections (injection 1 = 4× LOD; injection 2 = LOD) but did not reach the LLOQ. For all other analytes, peak area response was less than LOD in both first and second injections.

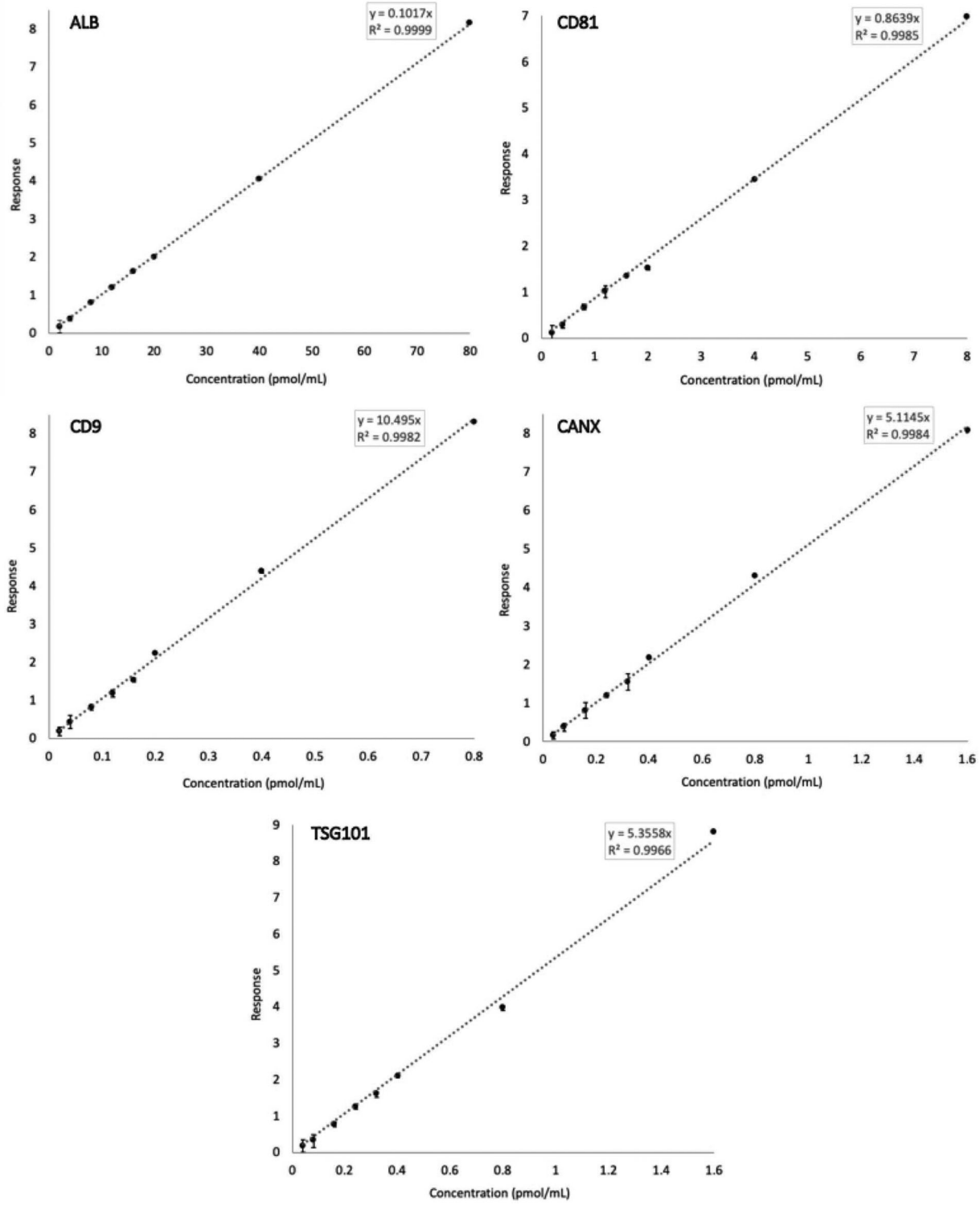

FIGURE 2 Calibration curves for the five analytes in the EV Marker Panel, produced by linear regression analysis. Error bars represent % relative standard deviation (% RSD) ($n = 3$)

3.3.4 | Short-term stability

Analytes were tested for short term stability with storage at −20°C, 4°C, or 15°C. Concentration was determined at baseline and monitored in duplicate samples at 6, 24, and 48 h. To calculate concentration, peak area response for endogenous analytes (or light peptide supplemented where required) was normalised to known concentrations of respective SIL peptide spiked in at

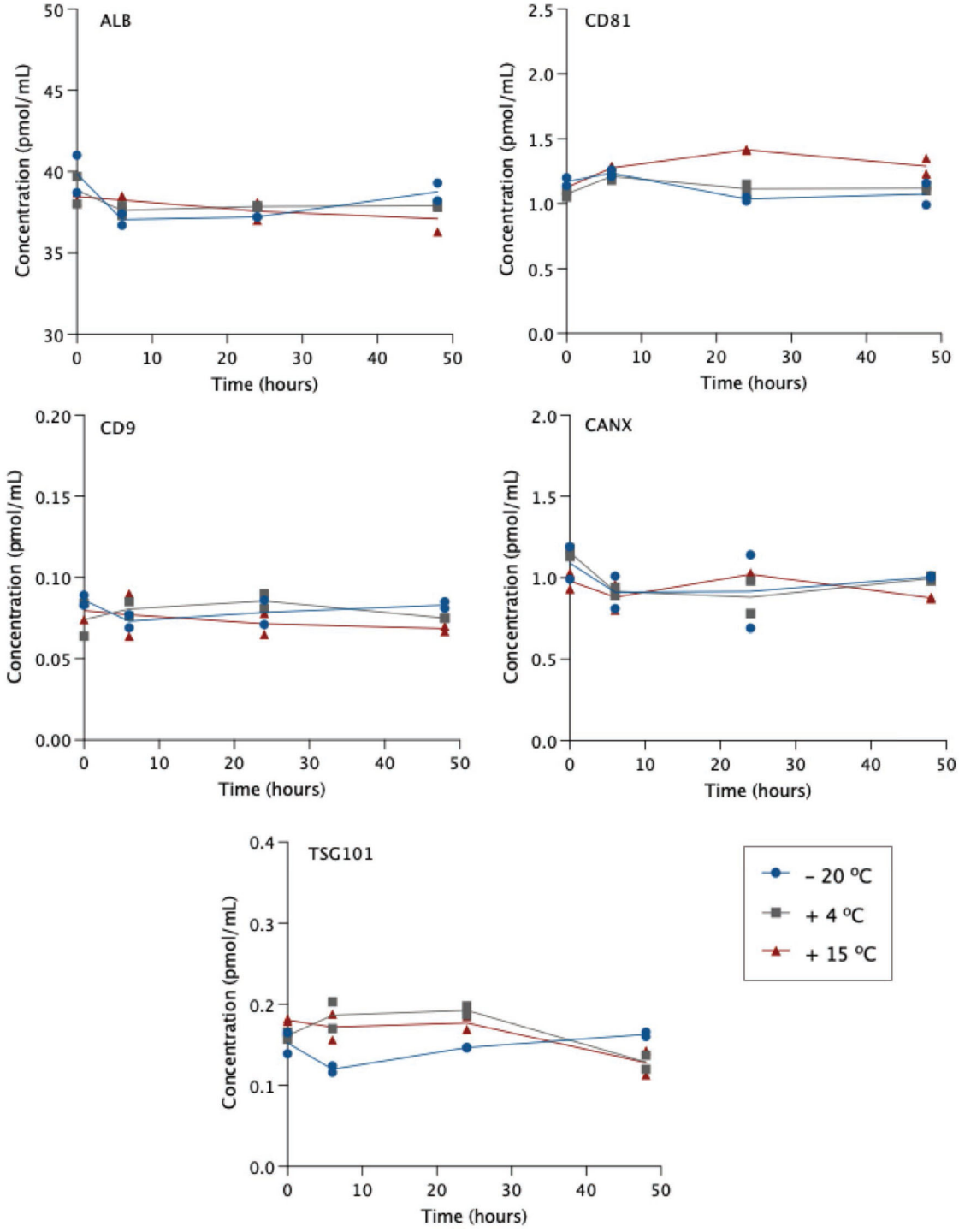

FIGURE 3 Short-term stability of peptide concentration at different storage temperature

baseline. Concentration of all analytes was generally stable across each time point compared to baseline measures (Figure 3). ALB concentration varied less than 7% in all cases and variability between duplicates remained low over time (<4% RSD). Indeed, there were no notable trends in %RSD as most measures varied no more than 19% between duplicates; except for CANX, for which variability increased up to the 24 h mark, especially in samples kept at −20°C (up to 34%). CANX concentration was otherwise stable over time, with most variability ± 17% from baseline. CD81 concentration was stable in samples stored at −20°C and 4°C with <13% change from baseline. In 15°C samples, a slight decrease in SIL peptide response led to overestimated concentration by 26% at 24 h. Since SIL was spiked in at baseline and monitored concurrently with the light analyte, different rates of degradation will affect calculations of analyte concentration. When light and SIL peptide responses were assessed individually, there were also

TABLE 6 Relative recovery of SIL peptides in EV matrices compared to qEV70

	qEV35				
	Relative recovery (%)		Precision (%RSD)		
Analyte	r^2	% of curve in qEV70	Lower	Mid	Upper
ALB	0.9999	107	16	6.9	10
CD81	0.9955	91	18	13	7.1
CD9	0.9994	147	18	3.6	9.1
CANX	0.9993	128	3.3	8.6	2.3
TSG101	0.9909	164	14	3.5	2.2
Analyte	ExoQuick				
	Relative recovery (%)		Precision (%RSD)		
	r^2	% of curve in qEV70	Lower	Mid	Upper
ALB	0.9973	40	7.4	6.2	2.5
CD81	0.9770	22	27	15	14
CD9	0.9980	133	9.1	6.1	2.9
CANX	0.9998	127	2.3	4.3	0.9
TSG101	0.9974	171	10	3.6	1.7

slight reductions in ALB and CD9 for samples kept at 15°C, but since signal was reduced in each light and SIL to a similar extent, no effect was observed in concentration. Lastly, TSG101 concentration was particularly stable over time in samples kept at −20°C and in 4°C and 15°C samples for 24 h. In the latter two, however, levels had decreased by 20% and 29%, respectively by 48 h. Overall, these data indicate that peptide concentration is stable during storage at −20°C and can also remain in the autosampler over the typical course of assay runs without significantly affecting results.

3.3.5 | Matrix effects

It is widely established that EV isolation methods are not equivalent in terms of both vesicle recovery and purity. The presence of non-vesicular contaminants can impact downstream analyses including detection and quantification of EV cargo by LC-MS/MS Thus, the effect of different EV matrices was assessed based on absolute and relative recovery of SIL peptides spiked into EV matrix or mobile phase. Relative recovery was determined in qEV35 and ExoQuick matrix using qEV70 as a comparator. Standard curves were generated using calibrators 1 and 6 and a middle QC. R^2 values exceeded 0.99 for all analytes; with the exception of CD81 in ExoQuick, which gave $r^2 = 0.977$ (Table 6). The ExoQuick CD81 curve was affected by imprecision at the lower calibration points. Precision is reported as %RSD of triplicate injections at each concentration level. The results were comparable with that observed in qEV70 matrix, though greater variability in CD81 quantification was observed in ExoQuick samples at the lower calibration point (27%RSD). Only 22% of the CD81 response was recovered in ExoQuick matrix compared to qEV70, these data indicate that this analyte is impacted in ExoQuick matrix such that limits of detection and quantification occur at higher concentrations. Similarly, ALB response in ExoQuick was 40% of that in qEV70. The response for the remaining analytes were greater in alternate matrices compared to qEV70, most notably TSG101 was 164% and 171% in qEV35 and ExoQuick, respectively. Hence, this analyte, along with CD9 and CANX, may be detected and quantified at lower concentrations in qEV35 and ExoQuick EVs.

To determine absolute recovery, the slope of the SIL peptide standard curves in each EV matrix were compared to that in mobile phase. Across each analyte, recovery in qEV70 matrix was observed at 38%–69% of mobile phase, with TSG101 most impacted (Table 7). On average, qEV35 matrix exhibited the least impact on analytes (absolute recovery 52%–88%). In ExoQuick matrix, albumin and CD81 peptide signals were significantly suppressed with recovery of just 22% and 13%, respectively.

The generalisability of the assay is demonstrated by analyses in serum and plasma from healthy donors and subjects with NAFLD. Analysis of markers in EVs isolated from plasma of NAFLD patients ($n = 4$) and healthy controls ($n = 5$) by qEV70 demonstrated a comparable capacity (relative to healthy serum) to detect positive EV markers and albumin. However, calnexin was only detected in 20% of healthy plasma EV samples. In EVs isolated by ExoQuick from NAFLD patient serum, markers were consistently detected across samples (Table S2).

TABLE 7 Absolute recovery of SIL peptides in EV matrices

	Recovery (% of curve in mobile phase)		
Analyte	**qEV70**	**qEV35**	**ExoQuick**
ALB	55	59	22
CD81	58	52	13
CD9	57	84	76
CANX	69	88	87
TSG101	38	54	57

TABLE 8 Reproducibility of analyte detection in EVs isolated by SEC or precipitation

	Isolations > LOD (%) ($n = 9$)			Equivalent duplicate digests (%) ($n = 9$)		
Analyte	**qEV70**	**qEV35**	**ExoQuick**	**qEV70**	**qEV35**	**ExoQuick**
ALB	100	100	100	100	100	100
CD81	78	100	100	67	100	100
CD9	100	100	100	100	100	100
CANX	100	100	78	100	100	100
TSG101	89	100	100	89	89	100

TABLE 9 Reproducibility of analyte quantification in EVs isolated by SEC or precipitation

	Concentration (pmol/ml)			Isolation variability (% RSD)			Digest variability (% RSD)		
Analyte	**qEV70**	**qEV35**	**ExoQuick**	**qEV70**	**qEV35**	**ExoQuick**	**qEV70**	**qEV35**	**ExoQuick**
ALB	34	122	27984	36	30	6.5	2.5	8.1	3.4
CD81	0.25	0.38	8.54	19	37	20	3.8	6.4	20
CD9	0.04	0.16	0.24	18	22	13	20	9.2	6.9
CANX	<LLOQ	0.19	0.54	–	17	5.3	–	14	3.1
TSG101	<LLOQ	<LLOQ	1.55	–	–	14	–	–	6.9

3.3.6 | Reproducibility of analyte detection and quantification

The reproducibility of the protocol was evaluated using the SEC and precipitation-based EV isolation methods. EVs were isolated from human serum ($n = 3$) in triplicate using each of the three methods and duplicate peptide digests were analysed on the panel (i.e., 18 per isolation method). Concentration of analytes was determined based on normalised response (endogenous/SIL) in isolates from equivalent volumes of starting material using the three methods of isolation. Reproducibility was assessed based on analyte detection and analyte quantification, using LOD and LLOQ adjusted to reflect the observed effects of alternate EV matrices on relative recovery, as described above.

Given the primary function of the EV Marker Panel is to demonstrate the presence or absence of positive and negative markers in accordance with the MISEV guidelines, we first sought to determine the reproducibility of analyte detection in replicate samples. Reproducibility of isolation was based on average normalised response > LOD across triplicate isolations, and reproducibility of peptide digests was defined by equivalent response (both duplicates are < or > LOD) in each pair (Table 8). Albumin and CD9 was detected in 100% of isolations and digests from all isolation methods. CD81 was also detectable in 100% of isolations and digests from qEV35 and ExoQuick EVs. However, from two of the donors, CD81 was not detected in qEV70 EVs in one isolation each, which reduced isolation reproducibility to 78% overall for this analyte. Further, some discrepancy between duplicate digests was observed, which may be attributed to the low abundance of CD81 in these samples. CANX and TSG101 were also detected reproducibly across isolations and digests in each isolation method. To expand the applications of the assay beyond the binary determination of analyte detection, to those such as quantifying marker abundance for use as a normalisation strategy, the assay must demonstrate reproducibility of quantification. To this end, variability in concentration was determined in triplicate isolations and duplicate digests and presented as %RSD (Table 9). The variability of digests was less than 20% for all analytes above LLOQ in each isolation method. Cases in which replicate values were < LLOQ were considered reproducible,

since the effect of noise precludes the calculation of accurate %RSD. TSG101, for example, could not be quantified in EVs from either SEC method. Meanwhile, this analyte was reproducibly quantifiable in ExoQuick isolates, exhibiting 14% and 6.9% RSD in isolations and digests, respectively. Similarly, CANX was < LLOQ in qEV70 but could be reproducibly quantified in qEV35 and ExoQuick EVs. Since CANX is relatively enriched in cells compared to EVs, HLM were analysed as a positive control. Normalised to injected protein, CANX signal in EVs compared to HLM was 3.5% and 0.65% in qEV35 and ExoQuick, respectively. Positive EV marker CD9 could be reproducibly quantified across qEV70 and ExoQuick EVs (13% and 18% RSD, respectively). CD81 quantification was also reproducible in ExoQuick isolates but more variable in qEV35 at 37%, which was driven by the lack of quantifiable levels of the analyte in two of the triplicate isolations from one donor. Albumin concentration was 823-fold and 3.6-fold higher in ExoQuick and qEV35 isolates, respectively, compared to qEV70, and each exceeded the upper limit of quantification validated for the assay in qEV70 matrix. Relative to an equivalent volume of serum, the amount of albumin in samples isolated by each method was 0.7%, 0.003%, and 0.001%, respectively. Despite significant depletion, albumin remains highly abundant in EV isolates compared to positive EV markers. Albumin quantification was reproducible across isolations in ExoQuick samples, while using SEC, variability was up to 36%. This suggests that while SEC columns, particularly qEV70, are more effective at removing albumin, the samples may be inconsistently affected by free protein contamination. Figure 4 shows the distribution of measured concentrations of analytes across all technical replicates with each isolation method with reference to limits of detection and quantification. Notably, ExoQuick samples are enriched for both CD81 and TSG101 in comparison to SEC samples, while the differences in CD9 are much less pronounced (Figure 4). While qEV70 samples have higher purity (less albumin and calnexin), tetraspanins are more abundant in qEV35 EVs. Differences in marker abundance may be attributed to the columns enriching for vesicles of different size range. Further, recovery of vesicles (particularly CD81- and/or CD9- positive vesicles) is possibly compromised by decreasing contamination.

4 | DISCUSSION

Here we describe the development and validation of a targeted LC/MS-MS peptide assay for the quantification of markers associated with EVs and non-vesicle contaminants. A total of five EV ± markers were included in the panel in accordance with the MISEV guidelines (Théry et al., 2018). As stated, samples should be characterised based on the presence of established transmembrane (CD9, CD81) or cytosolic (TSG101) proteins that incorporate in EVs due to roles in biogenesis and trafficking, and the absence or depletion of matrix-associated contaminants (e.g., serum protein, ALB) and non-endosomal intracellular compartment proteins (e.g., ER protein, CANX). The described workflow of in-solution peptide digest coupled with multiplexed panel format provides a high-throughput quantitative platform for the analysis of clinical samples, requiring only a fraction of that used for immunoblotting. In this regard, LC-MS/MS represents a valuable approach to streamline the acquisition of data for addressing reporting criteria, while reducing reagent costs, labour, and consumption of human biospecimens, which are often scarce in volume and irreplaceable.

Assay validation and calibration was primarily performed in EVs isolated by qEV70. Numerous studies (Brennan et al., 2020; Gámez-Valero et al., 2016; Veerman et al., 2021) compare the characteristics and molecular composition of EV isolates produced by various available methods, and increasingly, SEC is selected as the method of choice (Liangsupree et al., 2021; Monguió-Tortajada et al., 2019; Sidhom et al., 2020). Nonetheless, no single isolation method is considered suitable for all applications and downstream analyses. In the context of proteomic analyses, SEC has been favoured for the relative purity and detection of EV-associated proteins that can be achieved with marked reproducibility (Monguió-Tortajada et al., 2019; Vanderboom et al., 2021; Veerman et al., 2021). By comparison, methods that rely on precipitating agents, including ExoQuick, facilitate high recovery but may interfere with vesicle surface composition and co-isolate large amounts of soluble proteins that mask less abundant EV proteins (Gámez-Valero et al., 2016; Veerman et al., 2021). Similarly, conventional techniques such as ultracentrifugation suffer poor reproducibility and significant contamination with protein aggregates (Vanderboom et al., 2021).

The concentration range over which the assay was validated comprised eight calibrators to cover concentrations observed in healthy donor serum and beyond to increased levels that may be observed in various disease contexts (Nguyen et al., 2021; Povero et al., 2020; Sehrawat et al., 2021). For all analytes, calibration curves were linear (all $r^2 > 0.99$) and the assay exhibited good precision and accuracy. Notably, the concentration range validated for albumin was 100-fold greater than that for CD9 (Table 3). This aligns with previous findings that highly abundant serum proteins remain at concentrations in SEC isolates many orders of magnitude above that of EV markers (Nguyen et al., 2021; Vanderboom et al., 2021). Blood is a complex matrix from which to extract EVs, given their numbers are predominated by soluble proteins and various types of lipoproteins with similar physical properties. Irrespective, LC-MS/MS boasts exceptional sensitivity and the present assay exhibited detection limits in the picomolar range. The value of this sensitivity was realised in the context of sample consumption; where for SEC methods, the volume of serum used in immunoblotting was ~100 μl on average, while only 12.5 μl in equivalent serum volume was injected for LC-MS/MS analysis (Table S1, Figure S8). Importantly, the latter approach permitted multiplexed analysis without compromising reliability of detection or requiring additional sample.

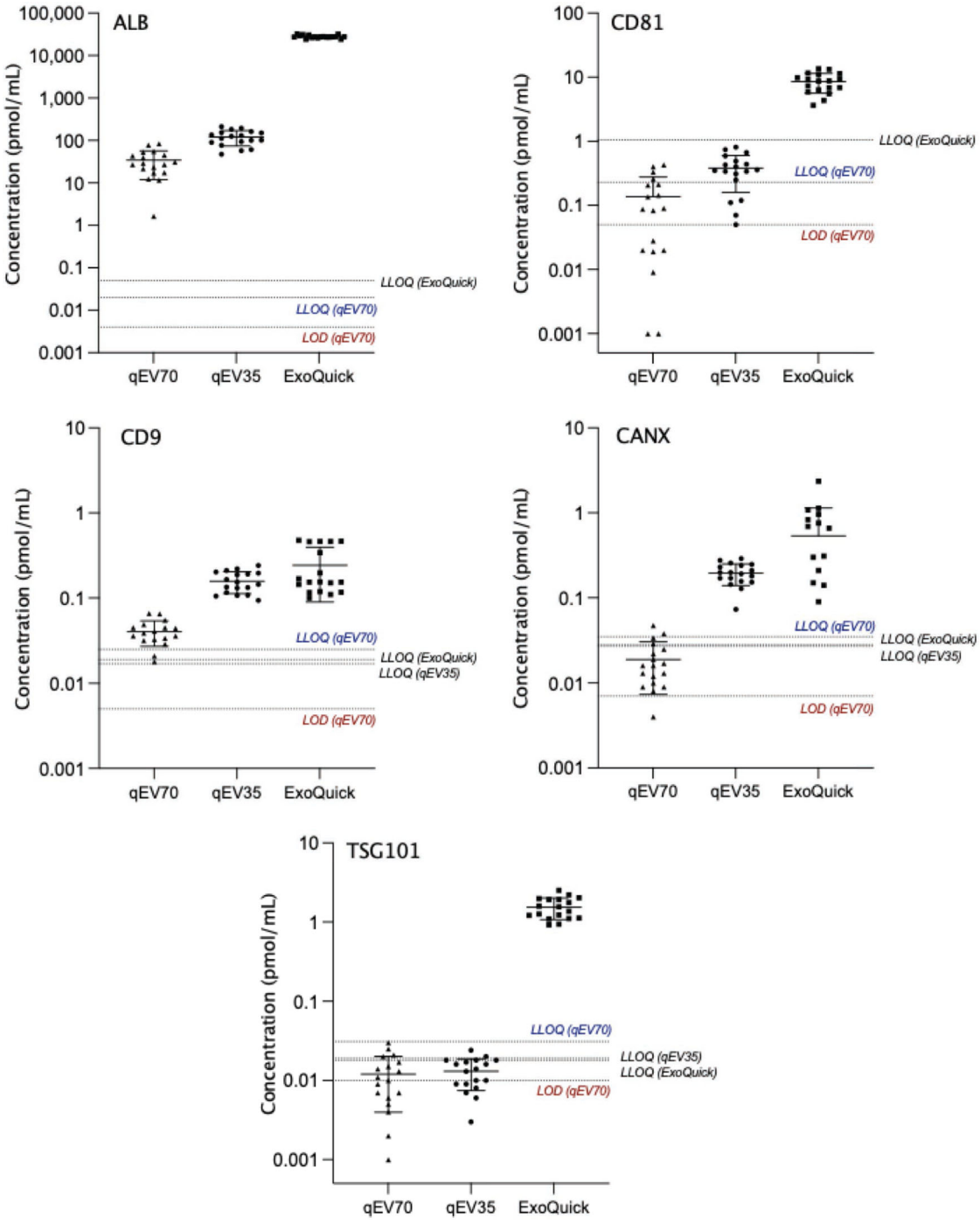

FIGURE 4 Mean (±SD) concentration of analytes measured in duplicate peptide digests from triplicate EV isolations using different methods ($n = 3$). Lower limit of quantification (LLOQ) and limit of detection (LOD) are indicated for qEV70 and LLOQ is given for analytes in alternate matrices where matrix effects (relative recovery differs >20%) were observed

For immunoblotting, each biological repeat sample was run on a gel once, transferred onto PVDF membrane and re-probed for CD9, CD81, TSG101, and CANX. The ability to re-probe the membrane following peroxidase deactivation has been previously demonstrated (Sennepin et al., 2009) and offers a time and sample-saving solution for multiple detections by western blot. However, in our case, this approach introduced several challenges. EV markers, CD9 and CD81 have a similar molecular weight (MW), with predicted bands at 25 kDa. As PVDF membranes were first probed and imaged for CD81, followed by the stripping, re-blocking and re-probing procedure for CD9, it was not possible to confidently assess both. In this case, stripping of the membrane was not successful and CD81 bands were still visible at MW of 25 kDa. Under ideal conditions, enough sample is available to run a gel for one or two markers at different MW. When working with clinical samples of limited sample volume,

there is often only enough sample for one immunoblot, presenting a challenge to the fulfilment of MISEV criteria (Théry et al., 2018). In this study, lysed EV samples were run only once using a set volume of starting material, thereby accentuating the limitations of immunoblotting that are overcome by our LC-MS/MS approach. With respect to quantitation, immunoblotting can successfully determine the presence and relative abundance of analytes between sample types or groups. Densitometric analysis was performed here but was affected by high background in some positive control (HLM) lanes (Figure S6A & D), resulting in an overestimation of protein yield and skewed representation of the data from these lanes. In contrast, the LC-MS/MS assay could be validated for the absolute quantification of analytes using stable isotope-labelled peptides spiked into samples at known concentrations.

The degree and composition of contamination are key determinants of signal intensity and reproducibility in LC-MS/MS analysis. Peptides derived from non-vesicular material may co-elute with target EV markers and suppress ionisation; and those exhibiting similar mass to charge ratios may interfere with particular MRM transitions (Liebler & Zimmerman, 2013). The presence of different vesicle populations or contaminants, isolated by different methods, introduces different sources of interference (i.e., lipid or peptide composition) and therefore greater variability in marker detection and quantification. These matrix effects were evident in that the absolute recovery of several analytes was reduced in EV matrix irrespective of isolation method (Table 7).

The reproducibility of the assay was considered within two distinct frameworks defined by the potential applications. Primarily, the EV Marker Panel can be used to demonstrate the presence and absence of EV (±) markers in line with the characterisation and reporting criteria (Théry et al., 2018). Hence, reproducibility was assessed based on analyte response around the defined LOD. As the detection of analytes was highly reproducible across replicate isolations and digests using all methods (Table 8), we demonstrate that the EV Marker Panel is fit-for-purpose. Importantly, this can be achieved using only a fraction of the sample that would otherwise be required for conventional methods, such as immunoassays.

In addition to addressing reporting requirements, quantification of EV markers may serve other functions, such as normalisation of EV-associated biomarker abundance, although such application would require assessment of quantitative reproducibility. While target analyte response is expected to be more variable in samples with greater levels of contamination, here, we found that in ExoQuick samples—which invariably contain large amounts of co-precipitated serum proteins—EV marker quantification was highly reproducible both in terms of replicate isolations and digests. Of the positive EV markers, CD9 quantification was most consistent across tested isolation methods and may be suitable for the purpose of normalising circulating biomarkers. The choice of isolation method is a key consideration for the analysis of both the biomarker and normaliser; but as seen in ExoQuick samples, certain levels of contamination may not be detrimental, providing acceptable reproducibility of isolation and quantification is achieved (Kreimer et al., 2015). The potential for human error is higher with SEC isolation due to greater hands-on time. A recent study also found more variability in proteomic profiles using methods that require more time and careful collection of EV-containing fractions (e.g., qEV70 and OptiPrep density gradient), in comparison to quicker and easier methods (including ExoQuick and ExoEasy) (Veerman et al., 2021). Even so, automation of SEC can mitigate user influence and improve reproducibility (Monguió-Tortajada et al., 2019). Given the major source of protein in most EV preparations are contaminants, and vesicle recovery and purity differ markedly across isolation strategies (Théry et al., 2018; Useckaite et al., 2021), the decision to normalise LC-MS/MS analyses to volume rather than total protein content is to avoid normalising to an artefact. For clinical samples, patient groups may have more vesicles and EV protein, so the analysis of less sample compared to controls could diminish the ability to detect important differences. When applied to EVs isolated by SEC or precipitation methods, the assay demonstrated the differences in recovery and purity of EVs from equivalent starting material. As ExoQuick is a high recovery, low purity method, high abundance of EV-positive markers and albumin contamination were observed. Meanwhile, SEC methods show intermediate vesicle recovery and purity, with most substantial albumin depletion achieved by qEV70. Previous studies have also reported very low abundance or non-detection of TSG101 in SEC EVs from blood (Brennan et al., 2020; Buschmann et al., 2018; Veerman et al., 2021). The heterogenous presence and relative abundance of tetraspanins and other biogenesis pathway-related proteins in EVs is influenced by originating cell types (Koliha et al., 2016; Kugeratski et al., 2021). EVs isolated from the circulation generally comprise a large majority of haematopoietic cell-derived vesicles, especially platelet EVs (Koliha et al., 2016; Kugeratski et al., 2021; Matsumoto et al., 2020; Palviainen et al., 2020). Notably, platelet-derived EVs have been shown to be devoid of CD81 (Koliha et al., 2016), which may account for the levels of this marker observed in lower recovery isolation methods such as SEC.

Though endogenous CD81 was more abundant in ExoQuick, assay sensitivity was reduced in this matrix. The success of other EV applications such as untargeted profiling studies is dependent on pure sample preparations, since peptides derived from abundant serum proteins will be sampled more frequently than scarcer EV peptides in the MS (Liebler & Zimmerman, 2013). With minimal non-EV interference, profiling may reveal subtype-specific or tissue-specific vesicle markers (Karimi et al., 2018). Ultimately, these techniques performed in pure samples should continue to generate insights into EV biogenesis, functions, and diagnostic or prognostic value, and promote the development of novel affinity tools for the selective isolation of subpopulations to improve the utility of liquid biopsy (Newman et al., 2022; Rodrigues et al., 2021).

To summarise, we have developed and validated a targeted LC-MS/MS method for the detection and quantification of a panel of positive and negative EV markers in EVs from blood. The described workflow may be applied for the fulfillment of standard characterisation and reporting criteria, described by the MISEV guidelines, or to quantify changes in EV proteins

as a biomarker normalisation strategy. We illustrate how our approach overcomes several challenges faced with the use of immunoblotting when working with limited volume of clinical samples, particularly in regard to sensitivity, throughput and quantitation.

ACKNOWLEDGMENTS

The authors acknowledge the instruments and scientific and technical assistance of Microscopy Australia at Adelaide Microscopy, The University of Adelaide, a facility that is funded by the University, and State and Federal Governments. The authors would also like to acknowledge the instruments and technical assistance at Australian Wine Research Institute, Urrbrae South Australia. Immunoblot imaging was performed at Flinders Proteomics Facility (FPF), Flinders Medical Centre (FMC), Bedford Park, South Australia. This research was funded by the National Health and Medical Research Council of Australia [Grant ID 1158210]. A.R is supported by Beat Cancer Fellowships from Cancer Council SA.

CONFLICT OF INTEREST

All authors declare no conflicts of interest.

PATIENT CONSENT

Human blood samples were obtained from healthy volunteers following confirmation of informed consent.

ORCID

Lauren A. Newman https://orcid.org/0000-0003-3303-1666

REFERENCES

Bowalgaha, K., Elliot, D. J., Mackenzie, P. I., Knights, K. M., Swedmark, S., & Miners, J. O. (2005). S-Naproxen and desmethylnaproxen glucuronidation by human liver microsomes and recombinant human UDP-glucuronosyltransferases (UGT): Role of UGT2B7 in the elimination of naproxen. *British Journal of Clinical Pharmacology*, *60*, 423–433. https://doi.org/10.1111/j.1365-2125.2005.02446.x

Brennan, K., Martin, K., Fitzgerald, S. P., O'Sullivan, J., Wu, Y., Blanco, A., Richardson, C., & Mc Gee, M. M. (2020). A comparison of methods for the isolation and separation of extracellular vesicles from protein and lipid particles in human serum. *Scientific Reports*, *10*, 1039. https://doi.org/10.1038/s41598-020-57497-7

Buschmann, D., Kirchner, B., Hermann, S., Märte, M., Wurmser, C., Brandes, F., Kotschote, S., Bonin, M., Steinlein, O. K., Pfaffl, M. W., Schelling, G., & Reithmair, M. (2018). Evaluation of serum extracellular vesicle isolation methods for profiling miRNAs by next-generation sequencing. *Journal of Extracellular Vesicles*, *7*, 1481321–1481321. https://doi.org/10.1080/20013078.2018.1481321

Colella, A. D., Chegenii, N., Tea, M. N., Gibbins, I. L., Williams, K. A., & Chataway, T. K. (2012). Comparison of Stain-Free gels with traditional immunoblot loading control methodology. *Analytical Biochemistry*, *430*, 108–110. https://doi.org/10.1016/j.ab.2012.08.015

Gámez-Valero, A., Monguió-Tortajada, M., Carreras-Planella, L., Franquesa, M. L., Beyer, K., & Borràs, F. E. (2016). Size-exclusion chromatography-based isolation minimally alters extracellular vesicles' characteristics compared to precipitating agents. *Scientific Reports*, *6*, 33641. https://doi.org/10.1038/srep33641

Greening, D. W., Xu, R., Gopal, S. K., Rai, A., & Simpson, R. J. (2017). Proteomic insights into extracellular vesicle biology—Defining exosomes and shed microvesicles. *Expert Review of Proteomics*, *14*, 69–95. https://doi.org/10.1080/14789450.2017.1260450

Hirsova, P., Ibrahim, S. H., Verma, V. K., Morton, L. A., Shah, V. H., Larusso, N. F., Gores, G. J., & Malhi, H. (2016). Extracellular vesicles in liver pathobiology: Small particles with big impact. *Hepatology*, *64*, 2219–2233. https://doi.org/10.1002/hep.28814

Hofmann, L., Ludwig, S., Schuler, P. J., Hoffmann, T. K., Brunner, C., & Theodoraki, M-N. (2020). The potential of CD16 on plasma-derived exosomes as a liquid biomarker in head and neck cancer. *International Journal of Molecular Sciences*, *21*, 3739. https://doi.org/10.3390/ijms21113739

Karimi, N., Cvjetkovic, A., Jang, S. C., Crescitelli, R., Hosseinpour Feizi, M. A., Nieuwland, R., Lötvall, J., & Lässer, C. (2018). Detailed analysis of the plasma extracellular vesicle proteome after separation from lipoproteins. *Cellular and Molecular Life Sciences*, *75*, 2873–2886. https://doi.org/10.1007/s00018-018-2773-4

Koliha, N., Wiencek, Y., Heider, U., JÃ¼Ngst, C., Kladt, N., Krauthäuser, S., Johnston, I. C. D., Bosio, A., Schauss, A., & Wild, S. (2016). A novel multiplex bead-based platform highlights the diversity of extracellular vesicles. *Journal of Extracellular Vesicles*, *5*, 29975. https://doi.org/10.3402/jev.v5.29975

Kowal, J., Arras, G., Colombo, M., Jouve, M., Morath, J. P., Primdal-Bengtson, B., Dingli, F., Loew, D., Tkach, M., & Théry, C. (2016). Proteomic comparison defines novel markers to characterize heterogeneous populations of extracellular vesicle subtypes. *Proceedings of the National Academy of Sciences*, *113*, E968–E977. https://doi.org/10.1073/pnas.1521230113

Kreimer, S., Belov, A. M., Ghiran, I., Murthy, S. K., Frank, D. A., & Ivanov, A. R. (2015). Mass-spectrometry-based molecular characterization of extracellular vesicles: Lipidomics and proteomics. *Journal of Proteome Research*, *14*, 2367–2384. https://doi.org/10.1021/pr501279t

Kugeratski, F. G., Hodge, K., Lilla, S., Mcandrews, K. M., Zhou, X., Hwang, R. F., Zanivan, S., & Kalluri, R. (2021). Quantitative proteomics identifies the core proteome of exosomes with syntenin-1 as the highest abundant protein and a putative universal biomarker. *Nature Cell Biology*, *23*, 631–641. https://doi.org/10.1038/s41556-021-00693-y

Liangsupree, T., Multia, E., & Riekkola, M-L. (2021). Modern isolation and separation techniques for extracellular vesicles. *Journal of Chromatography A*, *1636*, 461773. https://doi.org/10.1016/j.chroma.2020.461773

Liebler, D. C., & Zimmerman, L. J. (2013). Targeted quantitation of proteins by mass spectrometry. *Biochemistry*, *52*, 3797–3806. https://doi.org/10.1021/bi400110b

Matsumoto, A., Takahashi, Y., Chang, H. Y., Wu, Y. W., Yamamoto, A., Ishihama, Y., & Takakura, Y. (2020). Blood concentrations of small extracellular vesicles are determined by a balance between abundant secretion and rapid clearance. *Journal of Extracellular Vesicles*, *9*, 1696517. https://doi.org/10.1080/20013078.2019.1696517

Monguió-Tortajada, M., Gálvez-Montón, C., Bayes-Genis, A., Roura, S., & Borràs, F. E. (2019). Extracellular vesicle isolation methods: Rising impact of size-exclusion chromatography. *Cellular and Molecular Life Sciences*, *76*, 2369–2382. https://doi.org/10.1007/s00018-019-03071-y

Newman, L. A., Fahmy, A., Sorich, M. J., Best, O. G., Rowland, A., & Useckaite, Z. (2021). Importance of between and within subject variability in extracellular vesicle abundance and cargo when performing biomarker analyses. *Cells*, *10*, 485.

Newman, L. A., Sorich, M. J., & Rowland, A. (2020). Role of extracellular vesicles in the pathophysiology, diagnosis and tracking of non-alcoholic fatty liver disease. *Journal of Clinical Medicine*, *9*, 2032.

Newman, L. A., Useckaite, Z., Johnson, J., Sorich, M. J., Hopkins, A. M., & Rowland, A. (2022). Selective isolation of liver-derived extracellular vesicles redefines performance of miRNA biomarkers for non-alcoholic fatty liver disease. *Biomedicines*, *10*, 195.

Nguyen, A., Wang, T., & Turko, I. V. (2021). Quantitative proteomic analysis for evaluating affinity isolation of extracellular vesicles. *Journal of Proteomics*, *249*, 104359. https://doi.org/10.1016/j.jprot.2021.104359

Palviainen, M., Saraswat, M., Varga, Z., Kitka, D., Neuvonen, M., Puhka, M., Joenväärä, S., Renkonen, R., Nieuwland, R., Takatalo, M., & Siljander, P. R. M. (2020). Extracellular vesicles from human plasma and serum are carriers of extravesicular cargo—Implications for biomarker discovery. *PLoS One*, *15*, e0236439. https://doi.org/10.1371/journal.pone.0236439

Park, J., Go, E-B., Oh, J. S., Lee, J. K., & Lee, S-Y. (2021). Multiple-cycle polymeric extracellular vesicle precipitation and its evaluation by targeted mass spectrometry. *International Journal of Molecular Sciences*, *22*, 4311. https://doi.org/10.3390/ijms22094311

Povero, D., Yamashita, H., Ren, W., Subramanian, M. G., Myers, R. P., Eguchi, A., Simonetto, D. A., Goodman, Z. D., Harrison, S. A., Sanyal, A. J., Bosch, J., & Feldstein, A. E. (2020). Characterization and proteome of circulating extracellular vesicles as potential biomarkers for NASH. *Hepatology Communications*, *4*, 1263–1278. https://doi.org/10.1002/hep4.1556

Rodrigues, A. D., van Dyk, M., Sorich, M. J., Fahmy, A., Useckaite, Z., Newman, L. A., Kapetas, A. J., Mounzer, R., Wood, L. S., Johnson, J. G., & Rowland, A. (2021). Exploring the use of serum-derived small extracellular vesicles as liquid biopsy to study the induction of hepatic cytochromes P450 and organic anion transporting polypeptides. *Clinical Pharmacology & Therapeutics*, *110*, 248–258. https://doi.org/10.1002/cpt.2244

Rosa-Fernandes, L., Rocha, V. B., Carregari, V. C., Urbani, A., & Palmisano, G. (2017). A perspective on extracellular vesicles proteomics. *Frontiers in Chemistry*, *5*, 102–102. https://doi.org/10.3389/fchem.2017.00102

Schroeder, J. C., Puntigam, L., Hofmann, L., Jeske, S. S., Beccard, I. J., Doescher, J., Laban, S., Hoffmann, T. K., Brunner, C., Theodoraki, M-N., & Schuler, P. J. (2020). Circulating exosomes inhibit B cell proliferation and activity. *Cancers (Basel)*, *12*, 2110. https://doi.org/10.3390/cancers12082110

Sehrawat, T. S., Arab, J. P., Liu, M., Amrollahi, P., Wan, M., Fan, J., Nakao, Y., Pose, E., Navarro-Corcuera, A., Dasgupta, D., Liao, C. Y., He, L., Mauer, A. S., Avitabile, E., Ventura-Cots, M., Bataller, R. A., Sanyal, A. J., Chalasani, N. P., Heimbach, J. K., …, Malhi, H. (2021). Circulating extracellular vesicles carrying sphingolipid cargo for the diagnosis and dynamic risk profiling of alcoholic hepatitis. *Hepatology*, *73*, 571–585. https://doi.org/10.1002/hep.31256

Sennepin, A. D., Charpentier, S., Normand, T., Sarré, C., Legrand, A., & Mollet, L. M. (2009). Multiple reprobing of Western blots after inactivation of peroxidase activity by its substrate, hydrogen peroxide. *Analytical Biochemistry*, *393*, 129–131. https://doi.org/10.1016/j.ab.2009.06.004

Shao, H., Im, H., Castro, C. M., Breakefield, X., Weissleder, R., & Lee, H. (2018). New technologies for analysis of extracellular vesicles. *Chemical Reviews*, *118*, 1917–1950. https://doi.org/10.1021/acs.chemrev.7b00534

Sidhom, K., Obi, P. O., & Saleem, A. (2020). A review of exosomal isolation methods: Is size exclusion chromatography the best option? *International Journal of Molecular Sciences*, *21*, 6466. https://doi.org/10.3390/ijms21186466

Théry, C., Witwer, K. W., Aikawa, E., Alcaraz, M. J., Anderson, J. D., Andriantsitohaina, R., Antoniou, A., Arab, T., Archer, F., Atkin-Smith, G. K., Ayre, D. C., Bach, J-M., Bachurski, D., Baharvand, H., Balaj, L., Baldacchino, S., Bauer, N. N., Baxter, A. A., Bebawy, M., …, Zuba-Surma, E. K. (2018). Minimal information for studies of extracellular vesicles 2018 (MISEV2018): A position statement of the International Society for Extracellular Vesicles and update of the MISEV2014 guidelines. *Journal of Extracellular Vesicles*, *7*, 1535750. https://doi.org/10.1080/20013078.2018.1535750

Useckaite, Z., Mukhopadhya, A., Moran, B., & O'Driscoll, L. (2020). Extracellular vesicles report on the MET status of their cells of origin regardless of the method used for their isolation. *Scientific Reports*, *10*, 19020. https://doi.org/10.1038/s41598-020-75817-9

Useckaite, Z., Rodrigues, A. D., Hopkins, A. M., Newman, L. A., Johnson, J., Sorich, M. J., & Rowland, A. (2021). Role of extracellular vesicle derived biomarkers in drug metabolism and disposition. *Drug Metabolism and Disposition*, *49*, 961–971. https://doi.org/10.1124/dmd.121.000411

Vanderboom, P. M., Dasari, S., Ruegsegger, G. N., Pataky, M. W., Lucien, F., Heppelmann, C. J., Lanza, I. R., & Nair, K. S. (2021). A size-exclusion-based approach for purifying extracellular vesicles from human plasma. *Cell Reports Methods*, *1*, 100055. https://doi.org/10.1016/j.crmeth.2021.100055

Van Deun, J., Mestdagh, P., Agostinis, P., Akay, Ö., Anand, S., Anckaert, J., Martinez, Z. A., Baetens, T., Beghein, E., Bertier, L., Berx, G., Boere, J., Boukouris, S., Bremer, M., Buschmann, D., Byrd, J. B., Casert, C., Cheng, L., Cmoch, A., …, Hendrix, A. (2017). EV-TRACK: Transparent reporting and centralizing knowledge in extracellular vesicle research. *Nature Methods*, *14*, 228–232. https://doi.org/10.1038/nmeth.4185

Veerman, R. E., Teeuwen, L., Czarnewski, P., Güclüler Akpinar, G., Sandberg, A., Cao, X., Pernemalm, M., Orre, L. M., Gabrielsson, S., & Eldh, M. (2021). Molecular evaluation of five different isolation methods for extracellular vesicles reveals different clinical applicability and subcellular origin. *Journal of Extracellular Vesicles*, *10*, e12128. https://doi.org/10.1002/jev2.12128

Wang, T., Anderson, K. W., & Turko, I. V. (2017). Assessment of extracellular vesicles purity using proteomic standards. *Analytical Chemistry*, *89*, 11070–11075. https://doi.org/10.1021/acs.analchem.7b03119

Webber, J., & Clayton, A. (2013). How pure are your vesicles? *Journal of Extracellular Vesicles*, *2*, 19861. https://doi.org/10.3402/jev.v2i0.19861

Witwer, K. W., Goberdhan, D. C., O'driscoll, L., Théry, C., Welsh, J. A., Blenkiron, C., Buzás, E. I., Di Vizio, D., Erdbrügger, U., Falcón-Pérez, J. M., Fu, Q. L., Hill, A. F., Lenassi, M., Lötvall, J., Nieuwland, R., Ochiya, T., Rome, S., Sahoo, S., & Zheng, L. (2021). Updating MISEV: Evolving the minimal requirements for studies of extracellular vesicles. *Journal of Extracellular Vesicles*, *10*, e12182. https://doi.org/10.1002/jev2.12182

Zhang, L., Parot, J., Hackley, V. A., & Turko, I. V. (2020). Quantitative proteomic analysis of biogenesis-based classification for extracellular vesicles. *Proteomes*, *8*, 33. https://doi.org/10.3390/proteomes8040033

SUPPORTING INFORMATION

Additional supporting information can be found online in the Supporting Information section at the end of this article.

How to cite this article: Newman, L. A., Useckaite, Z., & Rowland, A. (2022). Addressing MISEV guidance using targeted LC-MS/MS: A method for the detection and quantification of extracellular vesicle-enriched and contaminant protein markers from blood. *Journal of Extracellular Biology*, *1,* e56. https://doi.org/10.1002/jex2.56

Appendix 3

Article published in Cells, 2021.

cells

MDPI

Article

Importance of between and within Subject Variability in Extracellular Vesicle Abundance and Cargo when Performing Biomarker Analyses

Lauren A. Newman, Alia Fahmy, Michael J. Sorich, Oliver G. Best, Andrew Rowland and Zivile Useckaite *

College of Medicine and Public Health, Flinders University, Adelaide, SA 5042, Australia; lauren.newman@flinders.edu.au (L.A.N.); alia.fahmy@flinders.edu.au (A.F.); michael.sorich@flinders.edu.au (M.J.S.); giles.best@flinders.edu.au (O.G.B.); andrew.rowland@flinders.edu.au (A.R.)

* Correspondence: zivile.useckaite@flinders.edu.au, Tel.: +61-8-8204-7546

Abstract: Small extracellular vesicles (sEV) have emerged as a potential rich source of biomarkers in human blood and present the intriguing potential for a 'liquid biopsy' to track disease and the effectiveness of interventions. Recently, we have further demonstrated the potential for EV derived biomarkers to account for variability in drug exposure. This study sought to evaluate the variability in abundance and cargo of global and liver-specific circulating sEV, within (diurnal) and between individuals in a cohort of healthy subjects (n = 10). We present normal ranges for EV concentration and size and expression of generic EV protein markers and the liver-specific asialoglycoprotein receptor 1 (ASGR1) in samples collected in the morning and afternoon. EV abundance and cargo was generally not affected by fasting, except CD9 which exhibited a statistically significant increase (p = 0.018). Diurnal variability was observed in the expression of CD81 and ASGR1, which significantly decreased (p = 0.011) and increased (p = 0.009), respectively. These results have potential implications for study sampling protocols and normalisation of biomarker data when considering the expression of sEV derived cargo as a biomarker strategy. Specifically, the novel finding that liver-specific EVs exhibit diurnal variability in healthy subjects should have broad implications in the study of drug metabolism and development of minimally invasive biomarkers for liver disease.

Keywords: extracellular vesicles; diurnal variability; biomarkers; liquid biopsy; liver specific

Citation: Newman, L.A.; Fahmy, A.; Sorich, M.J.; Best, O.G.; Rowland, A.; Useckaite, Z. Importance of between and within Subject Variability in Extracellular Vesicle Abundance and Cargo when Performing Biomarker Analyses. *Cells* **2021**, *10*, 485. https://doi.org/10.3390/cells10030485

Academic Editor: Alexander E. Kalyuzhny

Received: 15 February 2021
Accepted: 21 February 2021
Published: 24 February 2021

1. Introduction

Small extracellular vesicles (sEVs), in particular exosomes, have emerged as a rich source of circulating biomarkers with applications including tracking variability in disease, intervention efficacy, and drug exposure [1–3]. sEVs are heterogeneous membrane encapsulated particles of less than 150 nm in diameter that are secreted into the blood and other biofluids by virtually all cell types [4]. The sEV class comprises multiple specific EV types including exosomes (classical and non-classical), arrestin-domain-containing protein 1-mediated microvesicles (ARMM), small apoptotic EV, and small autophagic EV; however, multiple larger EV classes also exist [5]. These vesicles contain a complement of nucleic acid (microRNA (miRNA), mRNA, and non-coding RNA), protein, and small molecule cargo that are derived from their cell of origin [6]. For the purpose of this study, we refer to this heterogenous population of isolated vesicles as EVs.

Some EV cargo is explicitly packaged through defined pathways that are specific to a particular EV type while other cargo is indiscriminately incorporated as a by-product from the cellular milieu [6]. Accordingly, the composition of EV cargo depends on EV type and the cell of origin. Differences in cargo between EV types have been extensively studied and several markers have been proposed to discriminate sEV based on their type

(e.g., CD9, CD63, CD81, TSG101, and Calnexin). EVs derived from the same cell have been shown to vary in molecular composition [7]; yet, the degree of normal variability in the abundance of circulating sEV and their cargo remains poorly defined [8]. In order to robustly define thresholds of accuracy, precision and sensitivity for an EV derived biomarker, it is essential to understand the normal degree of variability in circulating EV and to understand patterns (e.g., circadian) associated with EV abundance.

Of growing interest is the understanding of how EV derived from a specific cellular or subcellular location may be applied to gain even greater understanding of organ function. There are a number of studies that have defined protocols for the isolation of tissue- and organelle- specific EVs based on selective surface proteins [9–12]. By way of example, liver-derived EVs can be selectively captured via the hepatocyte-specific surface protein asialoglycoprotein receptor 1 (ASGR1), and may be of great value to the study of drug metabolism [2] or liver diseases [4]. In order to robustly define abnormal expression, these applications require an understanding of the normal range of expression between individuals, typical variability in expression within an individual, and the contribution of different tissues to the global EV pool in circulation. This study sought to evaluate the variability in circulating global and liver specific sEV abundance and cargo, and to define patterns of variability, within (diurnal) and between individuals, that have the potential to confound sEV derived biomarker analyses. The experimental design for the study is summarised in Figure 1.

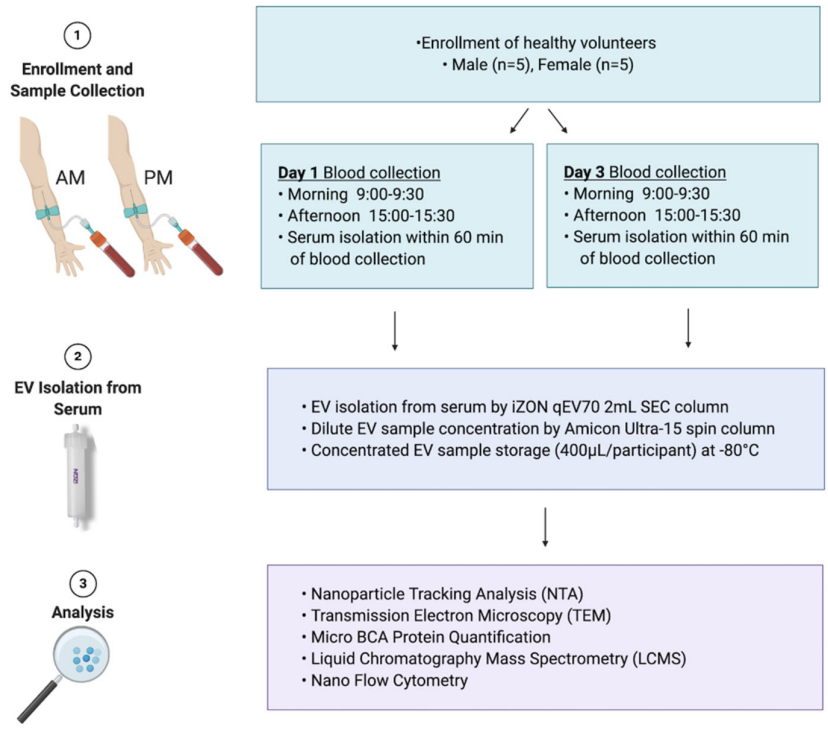

Figure 1. Study design. A cohort of healthy males and females aged 18 to 65 years were recruited (n = 10) for extracellular vesicle variability study (EVV). Blood was collected in the morning (AM) and the afternoon (PM) on day 1 and day 3 of the study. Participants were fed on day 1 and fasted on day 3 for morning blood collection. Serum was isolated from whole blood and used for extracellular vesicles (EV) isolation. EVs were isolated using qEV70 2 mL SEC column, concentrated to the volume of 400 µL in phosphate buffered saline (PBS) and used for downstream analyses. These included nanoparticle tracking analysis (NTA) to determine EV concentration/yield, transmission electron microscopy (TEM) for EV size estimations and morphology assessment, microBCA protein quantification, liquid chromatography mass spectrometry (LCMS) for EV protein

quantification, and nano flow cytometry for EV surface marker characterisation (EV-TRACK ID: EV210044).

2. Materials and Methods

2.1. Study Cohort

EVV is a single-centre, open-label, single-sequence biomarker study involving a cohort of healthy males and females aged 18 to 65 years. Characteristics of the study cohort are detailed in Table 1. The study protocol was approved by the Southern Adelaide Clinical Human Research Ethics Committee (SAHREC 261.18), and written informed consent was obtained from each participant prior to study enrolment. The study was conducted according to the principles stated in the Declaration of Helsinki, and was compliant with CPMP/ICH/135/95 GCP standards.

Table 1. Characteristics of EVV Study Cohort.

Characteristic	Healthy Females (n = 5)	Healthy Males (n = 5)
Age (years) Mean (Range)	28 (22–35)	30 (23–38)
Height (cm) Mean (± SD)	166.8 (5.7)	184.2 (8.0)
Weight (kg) Mean (± SD)	55.4 (3.8)	86.4 (5.4)
BMI (kg/m^2) Mean (± SD)	20.0 (2.4)	25.5 (1.2)

2.2. Collection of Blood/Serum

Morning samples were collected between 9:00 and 9:30 am, while afternoon samples were collected between 3:00 and 3:30 pm. Participants presented fed for blood collection on day 1 and after an overnight fast on day 3. The participants were free to consume their regular meals of choice for the duration of the study when not required to be fasted. Eight millilitres of whole blood was collected into Z Serum Sep Clot Activator tubes (Greiner Bio-One, Frickenhausen, Germany) using a 21-gauge Vacuette Safety Blood Collection sealed vacuum device (Greiner Bio-One, Frickenhausen, Germany). To ensure sample quality the device was primed by collecting a 5 mL 'discard' tube immediately prior to sample collection. Serum was isolated from whole blood within 60 min of sample collection by two cycles of centrifugation at 2500× g for 15 min at 4 °C.

2.3. Extracellular Vesicle Isolation

Global EVs were isolated from serum by size exclusion chromatography (SEC) performed using 2 mL qEV70 columns (Izon Science, Christchurch, New Zealand). SEC methods have been shown to effectively separate EVs from lipoproteins and other contaminants in serum, and is attractive for clinical biomarker applications due to its scalability and efficiency [13–15]. The use of 2 mL columns ensured all downstream analyses came from the same isolation. Prior to EV isolation, SEC columns were conditioned by washing with 10 mL of freshly 0.2 μm filtered phosphate-buffered saline (PBS). Thawed serum (2 mL) was added to the sample reservoir and EVs were eluted in PBS, which was added to the sample reservoir as the last of the serum entered the column. For the duration of the EV isolation, the volume of PBS in the reservoir was kept below 2 mL. The initial six fractions of flow-through were discarded, EVs were collected in the pooled fractions 7 to 11 using Protein LoBind tubes (Eppendorf, South Pacific, Australia). Resulting pooled EV fractions were mixed by gentle inversion 8 to 10 times and concentrated using pre-conditioned 30 kDa Amicon Ultra-4 centrifuge filters (Millipore-Sigma, Bedford, MA, USA) to a final volume of 400 μL in PBS. EV samples were aliquoted to avoid freeze–thaw and stored at −80 °C until analysed or processed further.

2.4. Human Liver Microsome Preparation

Pooled human liver microsomes (HLMs) were prepared by mixing equal protein amounts of microsomes from five human livers (H7, 44-year-old woman; H10, 67-year-

old woman; H12, 66-year-old man; H29, 45-year-old man; and H40, 54-year-old woman) obtained from the human liver "bank" of the Department of Clinical Pharmacology (Flinders University, Adelaide, SA, Australia). Approval for the use of human liver tissue in xenobiotic metabolism studies was obtained from both the Clinical Investigation Committee of Flinders Medical Centre and from the donors' next of kin. HLMs were prepared by differential centrifugation, as described by Bowalgaha et. al. [16].

2.5. Nanoparticle Tracking Analysis

Nanoparticle tracking analysis (NTA) was performed to determine global particle abundance and size distribution using the NanoSight NS300 (Malvern Panalytical, Malvern, United Kingdom, Software Version 3.4). Samples were diluted between 1:1000 and 1:5000 using freshly 0.2 μm filtered PBS; five 60-s videos were captured and analysed under constant flow conditions (flow rate 50) using NTA 3.4 software.

2.6. Transmission Electron Microscopy (TEM)

Samples were prepared adapting a previously published protocol, with some modification [17]. Briefly, Ted-Pella B 300M carbon-coated grids (Ted-Pella, Redding, CA, USA) were cleaned and hydrophilized using plasma glow discharge for 15 s (Gatan SOLARUS Advanced Plasma Cleaning System, Gatan, Inc., Pleasanton, CA, USA) prior to use. Five μL of sample in 0.2-μm-filtered PBS was placed on carbon-coated grids for 5 min. Carbon grids were washed once (15 s) at room temperature (RT) with 0.2 μm filtered PBS and were contrasted with 2% uranyl acetate (3 min, RT), washed once, and examined by FEI TECNAI Spirit G2 TEM (Thermo Fisher Scientific, Waltham, MA, USA) operated at 100 kV. TEM images were acquired at 30,000× and 68,000× (Figure S1).

2.7. Micro BCA Protein Quantification

A micro bicinchoninic acid (BCA) reagent kit (ThermoFisher Scientific, Waltham, MA, USA), with a bovine serum albumin (BSA) standard curve (0–200 μg/mL), was used to determine total protein in samples, as per the manufacturer's recommendations. EVs were lysed by addition of RIPA buffer 1:1 and incubation on ice for 25 min, followed by centrifugation at 10,000× *g* for 10 min at 4 °C. Working reagent (WR) was prepared using MA:MB:MC at a 25:24:1 ratio, respectively. EV containing samples were diluted between 1:20–1:100 in 0.2-μm-filtered PBS; 150 μL of the WR was mixed with either 150 μL of the BSA standard or 150 μL of sample in duplicate using a 96-well plate. The plate was covered and incubated at 37 °C for 2 h. Absorbance was measured at 562 nm using a SpectraMax plate reader (Molecular Devices, San Jose, CA, USA).

2.8. Trypsin Digest

EV protein was prepared for LCMS analysis by trypsin digestion. EVs (50 μL) diluted up to 100 μL in PBS were vortexed for 10 min using a MixMate (Eppendorf, South Pacific, Australia) and subject to three freeze–thaw cycles to cause lysis. Dithiothreitol (12.5 mM) and 50 μL of ammonium bicarbonate (pH 7.8) were added to samples and incubated for 90 min at 60 °C. Samples were cooled to room temperature, then incubated with iodoacetamide (23.5 mM) for 60 min at 37 °C. The samples were then incubated for 18 h at 37 °C with Trypsin Gold (Madison, WI, USA) at a Trypsin to protein ratio of 1:40. Trypsin digestion was terminated by addition of 20 μL formic acid and centrifuged at 16,000× *g* for 10 min at 4 °C. Supernatant (100 μL) was extracted and stable isotope labelled (SIL) peptide standards (New England Peptide, Gardner, MA, USA) were added at 2.5 nM concentration. A 5 μL aliquot was injected for analysis by LC-MS/MS. Serum (diluted 1:10,000) and HLM were digested in the same conditions and run as positive controls.

2.9. Liquid Chromatography Mass Spectrometry (LCMS)

Chromatographic separation of analytes was performed on an Agilent Advance Bio Peptide Map column (100 mm × 2.1 mm, 2.7 μm) using an Agilent 1290 Infinity II liquid chromatography system (Agilent, Santa Clara, CA, USA). The temperature of the sample and column compartments was maintained at 4 and 30 °C, respectively. A panel of analytes comprising the EV makers CD9, CD63, CD81, and contaminants calnexin V and albumin, were separated by gradient elution with a flow rate of 0.2 mL/min. The mobile phase consisted of 0.1% formic acid in water (mobile phase A) and in acetonitrile (mobile phase B) held in a proportion of 90% A and 10% B for the first 2 min. The proportion of mobile phase B was then increased linearly to 60% over 13 min before returning to 10% over the next 4 min and held for a further minute to re-equilibrate. Total run time was 20 min. EV marker TSG101 was run independently using isocratic elution at a flow rate of 0.2 mL/min. Mobile phase A was held at 80% and total run time was 6 min. The liver-specific EV protein marker ASGR1, also run independently, was separated by gradient elution at 0.2 mL/min. Mobile phase B was increased linearly from 10% to 40% over 8 min then returned to 10% over 1.4 min. The column was re-equilibrated with a total run time of 10 min. Column eluant was monitored by mass spectrometry using an Agilent 6495B Triple Quadrupole mass spectrometer operating in positive electron spray (ESI^+) mode. Multiple reaction monitoring (MRM) was performed with one quantifier and one qualifier ion transition for each peptide. Identities of endogenous peptides were confirmed by comparing retention time and quantifier/qualifier transition ratios to respective SIL peptide standards. Analyte peptide sequences are given in Supplementary Table 1.

2.10. Nano Flow Cytometry (nFC)

Flow cytometry analysis was performed on the Beckman Coulter CytoFLEX S Flow Cytometer (Beckman Coulter, Brea, CA, USA) as previously described [18]. Briefly, for daily calibration of the flow cytometer, Megamix FSC & SSC Plus, BioCytex fluorescent beads (BioCytex, Marseille, France) were used in sizes of 100, 160, 200, 240, 300, 500, and 900 nm. The gating strategy is described in Figure S2. The VSSC and SSC threshold was set as the trigger channel below the 0.1-μm bead population. A rectangular gate was set on the VSSC-H log × BSSC-H log cytogram containing the 100 nm and 240 nm bead populations and defined as '100 nm–240 nm Megamix gate' followed by a "stable time gate" set on the time histogram, in order to identify the microparticle region. To avoid swarm effects each was serially diluted from 1:2 to 1:500 and measured with a flow rate of 10 μL/min prior to antibody labelling. EVs were labelled with 0.05 μL of anti-CD63-AlexaFluor488 (Invitrogen/Thermo Fisher Scientific, Waltham, MA, USA, Cat.MA5-18149) or anti-CD9-BV405, (R&D Systems, Minneapolis, MN, USA, Cat.FAB1880V), anti-CD81-Alexa700 (Biolegend, San Diego, CA, USA, Cat.349518), anti ASGR1-BV421 (BD Biosciences, San Jose, CA, USA, Cat.74269) in 100 μL PBS for 30 min on ice in the dark. To avoid false positive event measurement, all antibodies used were run in PBS alone to ensure the absence of antibody aggregates and non-specific binding to the particles in PBS. To avoid carry-over effects between each sample measurement, a washing step was performed with filtered PBS for 1 min at an increased flow rate of 60 μL/min. EV lysis was performed by incubating PBS-diluted EVs in 0.05% Triton™ X-100 for 30 min at room temperature.

Based on recommendations in the MIFlowCyt-EV guidelines [19], buffer only (PBS) control, buffer with antibodies, unstained controls (EVs in PBS), and stained EVs were run under the same settings (Figure S2).

2.11. Statistical Analysis

Statistical analysis was performed using GraphPad Prism software (San Diego, CA, USA, version 9.0). The D'Agostino-Pearson omnibus K2 test was used to assess normality and log transformation was applied to NTA and mass spectrometry data. All variables

passed normality and lognormality tests, so parametric tests were applied, except in the case of total protein concentration, to which Wilcoxon test was used instead. Data was presented as mean ± 95% confidence interval and range. Statistical comparisons were performed between different time points (AM and PM, fed and fast) using paired t-tests and between independent groups (sex) using one-way ANOVA. Statistical significance was set at 0.05.

2.12. EV-TRACK

We have submitted all relevant data of our experiments to the EV-TRACK knowledgebase (EV-TRACK ID: EV210044) [20].

3. Results

3.1. Purity Assessment of EV Isolations from Serum

In order to assess the purity of EV isolations, a few samples were selected at random and imaged by TEM to evaluate the background, composition, and EV structure. Representative images from TEM analysis (Figure 2, Figure S1) indicated that EV populations obtained by qEV70 SEC columns had limited non-vesicular contamination and the majority of EVs were 40–140 nm in size. EVs were round and appeared structurally intact.

Adhering to EV TRACK transparent reporting platform recommendation, assessment of non-EV-enriched proteins was performed in all EV samples to evaluate EV sample purity and potential non-vesicular contamination [20]. Calnexin V and albumin levels were measured by LC-MS. Total protein matched serum and HLM samples were used as positive controls for albumin and Calnexin V, respectively. The abundance of negative markers in EV samples is presented as a mean percentage of expression ± SD relative to HLM and serum for the respective markers. Compared to HLM, minimal expression of Calnexin V was detected in EV samples (0.52 ± 0.40%). Similarly, albumin expression in EVs was minimal compared to the serum control (0.95 ± 0.32%).

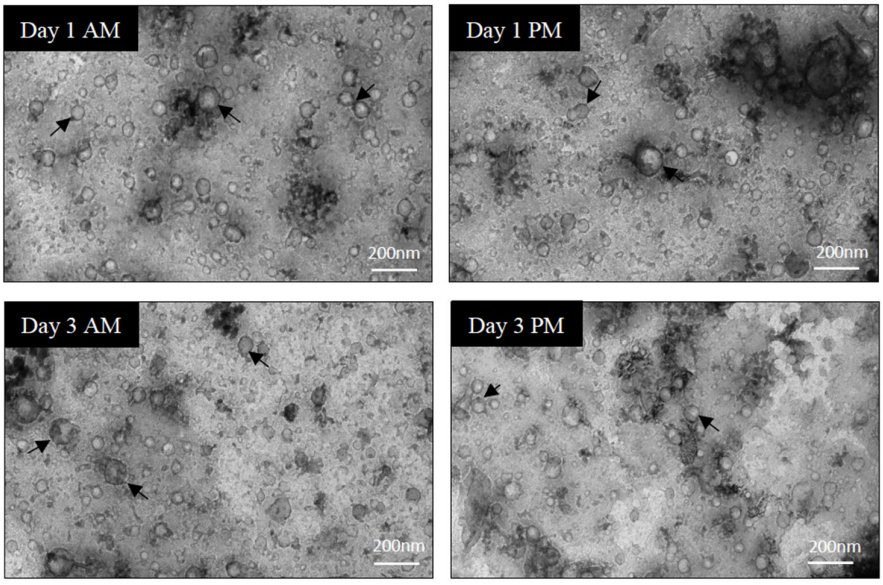

Figure 2. Sample quality assessment and characterisation of EVs using transmission electron microscopy (TEM). Direct mag: 30,000×, no sharpening, normal contrast. Scale bar = 200 nm.

3.2. Normal Variability

Normal variability between individuals was assessed with respect to EV characteristics and the abundance of EV-associated protein markers on study day 1. Nanoparticle

tracking analysis (NTA) was employed to determine size and concentration of particles in EV isolates (Figure 3A, B). The mean (± range) was 2.82×10^{11} (3.02×10^{10}–1.26×10^{12}) and 2.40×10^{11} (4.37×10^{10}–1.02×10^{12}) particles/mL for AM and PM samples, respectively (Table 2). Mode size of particles was 83.0 (64.9–99.3) nm in the morning and 84.7 (76.0–92.9) nm in the afternoon. Total protein in lysed EV samples was determined by microBCA assay and varied widely between participants in the morning and afternoon (Figure 3C). Mean (± range) concentration in respective AM and PM samples was 2773 (26.4–2799.0) µg/mL and 1318 (27.9–1345.9) µg/mL (Table 2). Quantification of EV protein, particle concentration, and size in the present study was consistent with previously reported ranges for EVs isolated by qEV from human serum [14].

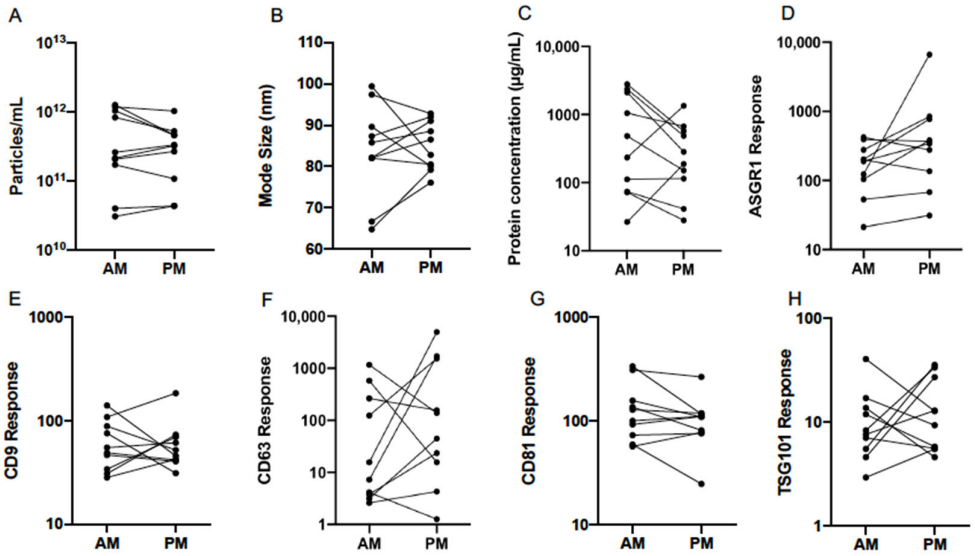

Figure 3. Variability of serum EV particle abundance (**A**), size (**B**), total protein concentration (**C**), and expression of EV-associated protein markers (**D**–**H**), quantified by nanoparticle tracking analysis (NTA), microBCA assay, and liquid chromatography mass spectrometry (LCMS) in the morning (AM) and afternoon (PM) of study day 1 in healthy volunteers (n = 10). ASGR1: asialoglycoprotein receptor 1; CD: cluster of differentiation; TSG101: tumour suppressor gene 101.

Table 2. Geometric mean, 95% confidence interval (CI), minimum and maximum of particle count, mode size, total protein concentration, and EV-associated protein marker abundance quantified in EVs isolated in the morning and afternoon on study day 1 from serum of healthy volunteers (n = 10).

	Particle Count (Particles/mL)		**Mode Size (nm)**	
	AM	PM	AM	PM
Mean	2.82×10^{11}	2.40×10^{11}	83.0	84.7
95% CI Lower	1.07×10^{11}	1.12×10^{11}	75.2	80.5
95% CI Upper	7.24×10^{11}	5.13×10^{11}	91.8	89.1
Minimum	3.02×10^{10}	4.37×10^{10}	64.9	76.0
Maximum	1.26×10^{12}	1.02×10^{12}	99.3	92.9
	Protein Concentration (µg/mL)		**ASGR1 Response**	
	AM	PM	AM	PM
Mean	347.5	219.8	147.9	331.9
95% CI Lower	104.2	90.8	76.6	115.9
95% CI Upper	1161.5	533.3	286.4	952.8
Minimum	26.4	27.9	21.2	31.2
Maximum	2799.0	1345.9	421.7	6622.2
	CD9 Response		**CD63 Response**	

	AM	PM	AM	PM
Mean	57.2	55.9	28.2	86.9
95% CI Lower	38.6	39.8	5.2	12.5
95% CI Upper	84.5	79.6	153.5	605.3
Minimum	28.2	31.0	2.6	1.3
Maximum	140.0	183.7	1158.8	4954.5
	CD81 Response		**TSG101 Response**	
	AM	PM	AM	PM
Mean	120.0	94.2	9.11	11.6
95% CI Lower	77.1	61.7	−0.73	6.6
95% CI Upper	187.1	143.9	15.5	20.4
Minimum	56.6	24.6	2.9	4.6
Maximum	334.2	264.9	40.9	35.8

Markers were selected based on the Minimal Information for Studies of Extracellular Vesicles (MISEV) guidelines for confirming the presence of EV-enriched proteins and include those derived from the plasma membrane, endosomal pathway, and cytosol [21]. The panel was comprised of tetraspanins CD9, CD63 and CD81, and the cytosolic protein tumour susceptibility gene 101 (TSG101), as well as the hepatocyte-specific surface protein asialoglycoprotein receptor 1 (ASGR1), which is known to be expressed on EVs derived from this cell type [4,22]. The expression of protein markers was quantified by LCMS and assessed for variability between subjects in AM and PM EVs (Figure 3D–H). Generic EV markers (tetraspanins and TSG101) showed relatively low variation between subjects, except for CD63 which was significantly more variable in both the morning and afternoon. The relative response values ranged from 2.6 to 1158.8 in AM samples and 1.3 to 4954.5 in PM samples (Table 2). The liver-specific EV protein ASGR1 exhibited similarly high variability, but only in the afternoon, as the range of values exceeded 16 times that of the morning EV samples. In the context of biomarker applications, understanding these differences in marker expression within and between individuals may aid the optimisation of sampling protocols.

3.3. Effect of Fasting

Quantification by NTA of serum EVs collected from participants in fed and fasted states, revealed respective mean (± 95% CI) particle concentrations of 2.82×10^{11} (1.07×10^{11}–7.24×10^{11}) and 2.09×10^{11} (6.61×10^{10}–6.46×10^{11}) particles/mL. No significant differences were detected by paired statistical tests (Table 3, Figure 4A,B). The mode particle size was slightly higher after fasting at 92.0 (80.4–105.4) nm compared to 83.0 (75.2–91.8) nm from fed individuals, but this difference did not reach statistical significance (p = 0.093).

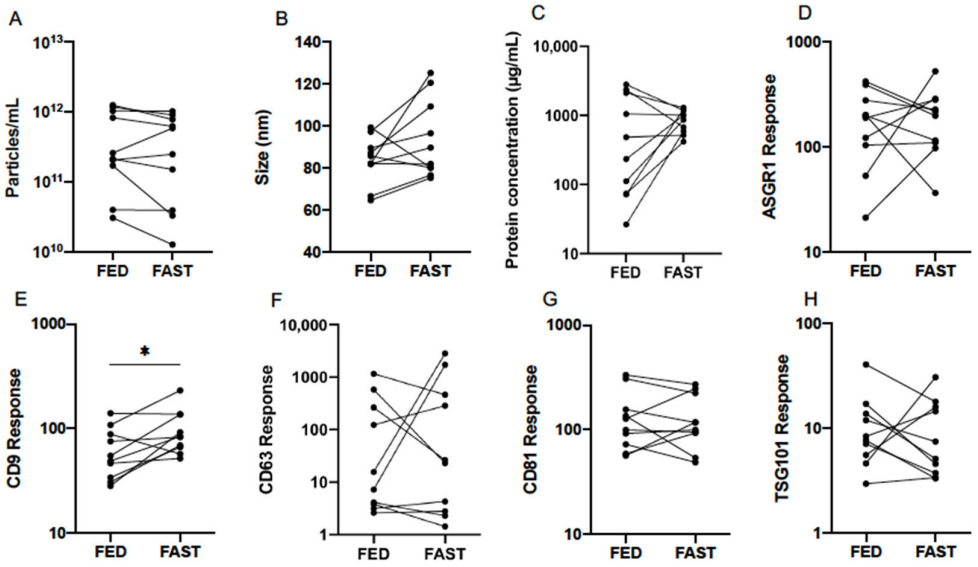

Figure 4. Effect of fed and fasted state on serum EV particle abundance (**A**), size (**B**), total protein concentration (**C**), and expression of EV-associated protein markers (**D**-**H**), quantified by nanoparticle tracking analysis (NTA), microBCA assay, and liquid chromatography mass spectrometry (LCMS) from healthy volunteers (n = 10). Statistical analysis performed using paired t-tests. * $p \leq 0.05$.

Total protein concentration and the abundance of EV protein markers in fed and fasted states were also compared (Table 3, Figure 4C–H). Mean protein concentration (± 95% CI) in respective fed and fasted states was 345.7 (104.2–1161.5) µg/mL and 822.2 (619.4–1094.0) µg/mL. While the difference between groups was not significant, the inter-individual variability was notably greater in fed samples (Figure 4C). Assuming constant stoichiometry, it follows that a lack of difference in particle concentration should be accompanied by no change in EV protein marker abundance. This was true of all markers except for CD9, which exhibited a statistically significant increase in fasted individuals (p = 0.018). Similarly to observations of variability in CD63 abundance throughout the day (Figure 3F), a wide range was exhibited in fed and fasted states (Table 3, Figure 4F).

Table 3. Geometric mean and 95% confidence interval (CI) of particle count, mode size, total protein concentration, and EV-associated protein marker abundance quantified in EVs isolated from serum of healthy volunteers (n = 10) in fed state and after an overnight fast. Statistical analysis performed using paired t-tests. ns: not significant; * $p \leq 0.05$.

	Particle Count (Particles/mL)				**Mode Size (nm)**			
	Fed	Fast	Difference	*p*	Fed	Fast	Difference	*p*
Mean	2.82×10^{11}	2.09×10^{11}			83.0	92.0		
95% CI Lower	1.07×10^{11}	6.61×10^{10}	ns	0.193	75.2	80.4	ns	0.093
95% CI Upper	7.24×10^{11}	6.46×10^{11}			91.8	105.4		
	Protein Concentration (µg/mL)				**ASGR1 Response**			
	Fed	Fast	Difference	*p*	Fed	Fast	Difference	*p*
Mean	347.5	822.2			147.9	168.7		
95% CI Lower	104.2	619.4	ns	0.1602	76.6	99.1	ns	0.732
95% CI Upper	1161.5	1094.0			286.4	287.7		
	CD9 Response				**CD63 Response**			
	Fed	Fast	Difference	*p*	Fed	Fast	Difference	*p*
Mean	57.2	90.6			28.2	41.5		
95% CI Lower	38.6	65.0	*	0.018	5.2	5.3	ns	0.680
95% CI Upper	84.5	126.2			153.5	322.9		

	CD81 Response				TSG101 Response			
	Fed	Fast	Difference	*p*	Fed	Fast	Difference	*p*
Mean	120.0	117.2			9.1	7.9		
95% CI Lower	77.1	76.6	ns	0.886	5.4	4.4	ns	0.668
95% CI Upper	187.1	179.5			15.5	14.1		

3.4. Diurnal Variability

In order to establish potential patterns of EV variability in healthy subjects, the analysis of EVs collected on study days 1 and 3 were pooled and compared between morning and afternoon. EV abundance and size as measured by NTA was consistent between the two time points (Figure 5A,B). Mean (± 95% CI) particle count in respective AM and PM samples was 2.29×10^{11} (1.23×10^{11}–4.79×10^{11}) and 2.40×10^{11} (1.41×10^{11}–3.89×10^{11}) particles/mL (Table 4). Mode size of particles was 87.1 (81.3–95.5) nm in AM and 83.2 (77.6–87.1) nm in PM samples.

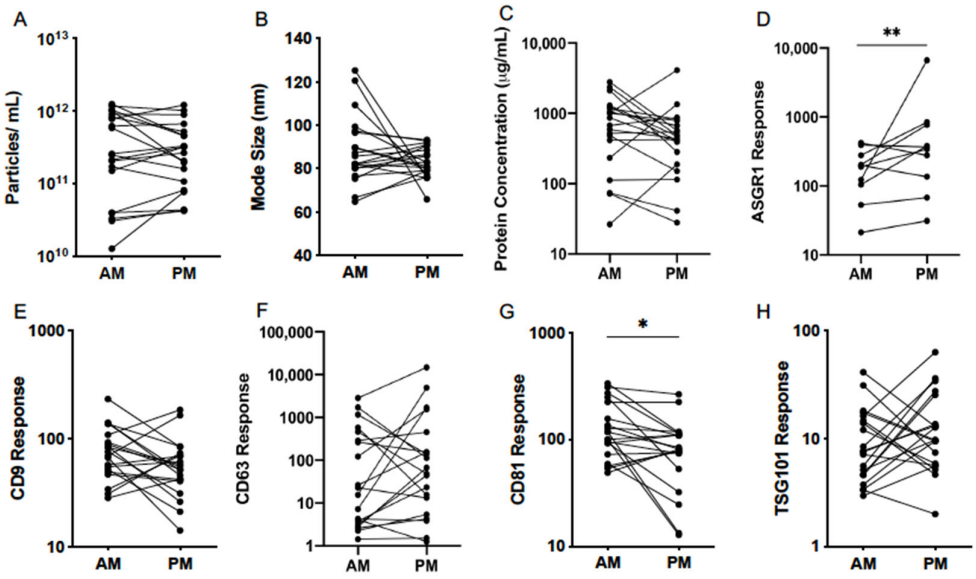

Figure 5. Diurnal variability of serum EV particle abundance (**A**), size (**B**), total protein concentration (**C**) and expression of EV-associated protein markers (**D**-**H**), quantified by nanoparticle tracking analysis (NTA), microBCA assay and liquid chromatography mass spectrometry (LCMS) in the morning (AM) and afternoon (PM) on study days 1 and 3 in healthy volunteers (n = 20). Statistical analysis performed using paired t-tests. * $p \leq 0.05$, ** $p \leq 0.01$.

Analysis of EV protein and abundance of generic markers revealed no difference in total protein concentration or response for CD9, CD63, and TSG101 at different times of the day (Table 4, Figure 5C,E,F,H). Interestingly, however, CD81 was significantly lower in the afternoon compared to the morning (p = 0.011) (Figure 5G). With no concomitant change in particle number, this result may suggest a lower CD81 abundance per vesicle or a decrease in the proportion of $CD81^+$ EVs. Additionally, a significant increase in ASGR1 response was observed from AM to PM samples (p = 0.009), suggesting that the proportional contribution of the liver to the circulating global EV pool was greater in the afternoon (Figure 5D).

Table 4. Pooled analysis of EVs collected from serum of healthy volunteers on study days 1 and 3 (n = 20) for comparison of morning and afternoon. Data presented as geometric mean and 95% confidence interval (CI) of particle count, mode size, total protein concentration, and EV-associated protein marker abundance. Statistical analysis performed using paired t-tests. ns: not significant, * $p \leq 0.05$, ** $p \leq 0.01$.

	Particle Count (Particles/mL)				**Mode Size (nm)**			
	AM	PM	Difference	*p*	AM	PM	Difference	*p*
Mean	2.29×10^{11}	2.40×10^{11}			87.1	83.2		
95% CI Lower	1.23×10^{11}	1.41×10^{11}	ns	0.863	81.3	77.6	ns	0.240
95% CI Upper	4.79×10^{11}	3.89×10^{11}			95.5	87.1		
	Protein Concentration (μg/mL)				**ASGR1 Response**			
	AM	PM	Difference	*p*	AM	PM	Difference	*p*
Mean	537.0	380.2			147.9	331.1		
95% CI Lower	295.1	223.9	ns	0.123	97.7	169.8	**	0.009
95% CI Upper	955	660.7			223.9	645.7		
	CD9 Response				**CD63 Response**			
	AM	PM	Difference	*p*	AM	PM	Difference	*p*
Mean	72.4	52.5			33.8	67.6		
95% CI Lower	56.2	38.9	ns	0.075	10.2	19.5	ns	0.239
95% CI Upper	93.3	70.8			114.8	234.4		
	CD81 Response				**TSG101 Response**			
	AM	PM	Difference	*p*	AM	PM	Difference	*p*
Mean	117.5	72.4			8.5	11.0		
95% CI Lower	49.0	12.9	*	0.011	5.9	7.6	ns	0.293
95% CI Upper	331.1	263.0			12.0	16.2		

3.5. Effect of Sex

The impact of sex was next explored as a potential source of variability in serum EV abundance and composition. Pooled analysis was performed for EVs collected on study days 1 and 3 in the morning and afternoon and compared between female (n = 10) and male (n = 10) healthy subjects. In this cohort, EV concentration in AM samples as determined by NTA was more than 10 times greater in males compared to females ($p < 0.0001$) (Figure 6A). Mean (± 95% CI) particle count in female and male cohorts was 7.41×10^{10} (3.47×10^{10}–1.58×10^{11}) and 7.76×10^{11} (5.62×10^{11}–1.10×10^{12}) particles/mL (Table 5). This difference was less substantial in PM samples, at 1.10×10^{11} (6.03×10^{10}–1.95×10^{11}) particles/mL in females and 5.01×10^{11} (3.24×10^{11}–7.94×10^{11}) particles/mL in males, but retained statistical significance (p = 0.0002). Meanwhile, mode size of particles did not vary with sex in either the morning or afternoon (Table 5, Figure 6B). In AM EVs, mean (± 95% CI) protein concentration was 330.4 (154.5–706.3) μg/mL in females and 865.0 (335.0–2238.7) μg/mL in males. This significantly higher mean concentration in male subjects (p = 0.037) did not persist into the afternoon (Table 5, Figure 6C).

The mean abundance of EV protein markers quantified by LC-MS showed no variations according to sex (Figure 6D–H, Table 5). Interestingly, the previously described diurnal pattern of ASGR1 response was exhibited in female and male subjects alike and no significant differences were observed between the two cohorts (Figure 6D). CD63 response also showed the same degree of variability between subjects as observed for the combined cohort, indicating that this finding was not singly influenced by either sex (Figure 6F).

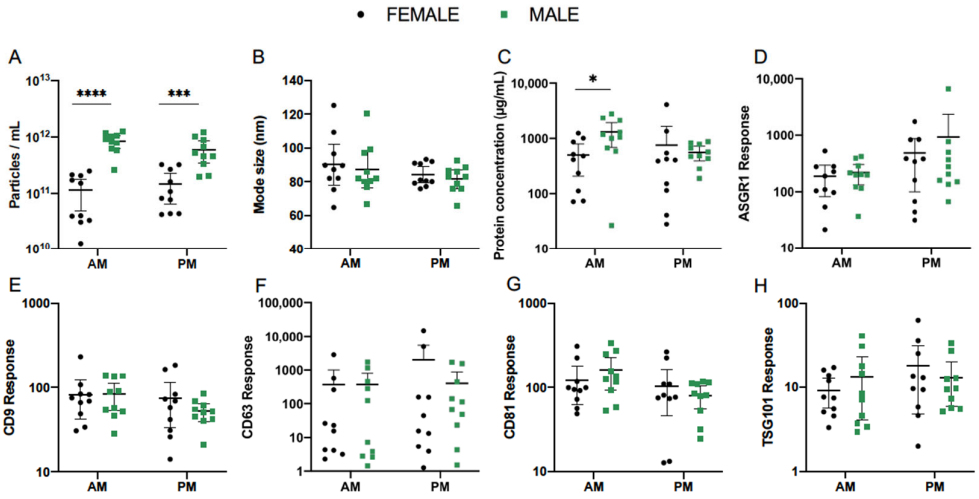

Figure 6. Effect of sex on serum EV particle abundance (**A**), size (**B**), total protein concentration (**C**), and expression of EV-associated protein markers (**D**–**H**), quantified by nanoparticle tracking analysis (NTA), microBCA assay, and liquid chromatography mass spectrometry (LCMS). Pooled analysis of EVs collected from serum of healthy female (n = 10) and male (n = 10) volunteers on study days 1 and 3. Statistical analysis performed using one-way ANOVA. * $p \leq 0.05$, *** $p \leq 0.001$, **** $p \leq 0.0001$.

Table 5. Pooled analysis of EVs collected from serum of healthy female (n = 10) and male (n = 10) volunteers on study days 1 and 3 in the morning and afternoon. Data presented as geometric mean and 95% confidence interval (CI) of particle count, mode size, total protein concentration, and EV-associated protein marker abundance. Statistical analysis performed using one-way ANOVA. ns: not significant, * $p \leq 0.05$, *** $p \leq 0.001$, **** $p \leq 0.0001$.

	Particle Count (Particles/mL)							
	AM				PM			
	Female	Male	Difference	p	Female	Male	Difference	p
Mean	7.41×10^{10}	7.76×10^{11}	****	<0.0001	1.10×10^{11}	5.01×10^{11}	***	0.0002
95% CI Lower	3.47×10^{10}	5.62×10^{11}			6.03×10^{10}	3.24×10^{11}		
95% CI Upper	1.58×10^{11}	1.10×10^{12}			1.95×10^{11}	7.94×10^{11}		
	Mode Size (nm)							
	AM				PM			
	Female	Male	Difference	p	Female	Male	Difference	p
Mean	88.8	86.0	ns	0.610	83.9	81.3	ns	0.622
95% CI Lower	77.8	76.5			79.2	75.8		
95% CI Upper	101.4	96.8			88.8	87.2		
	Protein Concentration (µg/mL)							
	AM				PM			
	Female	Male	Difference	p	Female	Male	Difference	p
Mean	330.4	865.0	*	0.037	289.1	509.3	ns	0.822
95% CI Lower	154.5	335.0			97.5	358.1		
95% CI Upper	706.3	2238.7			855.1	722.8		
	ASGR1 Response							
	AM				PM			

	Female	Male	Difference	*p*	Female	Male	Difference	*p*
Mean	136.5	183.2			248.9	321.4		
95% CI Lower	70.2	110.4	ns	0.801	94.6	129.1	ns	0.844
95% CI Upper	265.5	304.1			654.6	799.8		
	CD9 Response							
	AM				PM			
	Female	Male	Difference	*p*	Female	Male	Difference	*p*
Mean	70.6	73.5			56.8	49.3		
95% CI Lower	46.7	49.8	ns	0.987	32.1	37.8	ns	0.837
95% CI Upper	106.9	108.4			100.7	64.4		
	CD63 Response							
	AM				PM			
	Female	Male	Difference	*p*	Female	Male	Difference	*p*
Mean	29.6	39.5			57.9	78.9		
95% CI Lower	5.1	5.3	ns	0.964	6.5	15.2	ns	0.959
95% CI Upper	171.0	293.1			515.2	408.3		
	CD81 Response							
	AM				PM			
	Female	Male	Difference	*p*	Female	Male	Difference	*p*
Mean	103.50	135.8			73.0	71.9		
95% CI Lower	69.2	87.5	ns	0.641	35.4	48.4	ns	0.999
95% CI Upper	155.2	210.9			150.3	107.2		
	TSG101 Response							
	AM				PM			
	Female	Male	Difference	*p*	Female	Male	Difference	*p*
Mean	8.0	9.0			11.7	10.5		
95% CI Lower	5.3	4.6	ns	0.945	5.7	6.6	ns	0.944
95% CI Upper	12.1	17.6			24.2	16.7		

3.6. Single EV Analysis by Nano Flow Cytometry

In addition to EV sample analysis by LC-MS, the presence of EV markers CD9, CD63, CD81, and ASGR1 was confirmed by nano flow cytometry (Figures S3–S6). A Cytoflex S instrument was used to analyse surface EV protein markers on intact, individual EVs, providing an additional insight into the EVV study using an alternative platform.

Normal ranges of EVs positive for CD9, CD63, CD81, and ASGR1 and quantification by mean fluorescence intensity (MFI) was assessed for normal variability between the individuals and diurnal variability on day 1 (Figure S3). No significant differences were observed for tetraspanin EV protein markers or for the liver-specific EV protein ASGR1, however, ASGR1 levels were noticeably the most variable between individuals in both the AM and the PM, being more pronounced in the PM samples (Figure S4A, S4E). MFI values ranged from 241.4 to 582.0 in AM samples and 235.1 to 884.0 in PM samples. Importantly, the range of observed PM sample values was 1.6 times greater than that of morning EV samples (Figure S4E). Difference in MFI from AM to PM for $CD9^+$, $CD63^+$, and $CD81^+$ EVs

was 3.5-, 1.5-, and 1.2-fold, respectively. Single EV analysis revealed a greater inter-individual variability in fed samples for ASGR1, CD63 and CD81 (Figure S4), and CD9 and CD81 levels were significantly different ($p = 0.049$ and $p = 0.002$, respectively) between fed and fasted samples.

Differences in diurnal variability were observed for ASGR1 and CD81 (Figure S5). ASGR1 was noticeably the most variable between individuals in both the morning and afternoon and the difference was more pronounced in the afternoon (Figure S5A, S5E). MFI values ranged from 201.4 to 582.0 in AM samples and from 235.1 to 884.0 in PM samples. MFI values for ASGR1 were higher in PM samples ($p = 0.002$). Importantly, the range of observed PM sample values was 1.7 times greater that of morning EV samples. The difference in MFI between CD81 positive EVs in AM and PM samples was 1.1-fold with MFI range between 6.4 and 137.0 in the AM samples and between 9.3 and 155.8 in the PM samples ($p = 0.036$).

Differences in MFI values of CD81 positive EV populations were observed between males and females in both morning ($p = 0.038$) and afternoon samples ($p = 0.028$) (Figure S6D, S6E). Interestingly, inter-individual variability was greater in females than males in the AM and PM samples with MFI values ranging between 16.4–137.0 in female AM and 6.4–97.5 in male AM samples. Similarly, MFI values in the range between 31.6–155.8 was observed in female PM samples and between 9.3–96.0 in the male PM samples.

4. Discussion

Here, we report for the first time a diurnal pattern of expression for the liver-specific EV marker ASGR1 in healthy human serum. We observed greater abundance and wider variability between subjects in samples collected in the afternoon, indicating that the contribution of the liver to the global pool of circulating EVs changes throughout the day. Importantly, this pattern was consistent in males and females. Notably, in contrast to the observed diurnal variability in expression of ASGR1$^+$ EVs, no difference in expression was observed between fed and fasted states. This observation indicates that the diurnal variability in expression of ASGR1$^+$ EVs is not a post-prandial phenomenon. Data presented here indicate that accounting for diurnal variability in EV expression may be particularly important for the analysis of liver-specific biomarkers. Liver-specific EV markers are of relevance to the use of EVs in the study of drug metabolism [2,23] and non-alcoholic fatty liver disease (NAFLD) [4]. While not addressed specifically in the current study, these data also raise the possibility that diurnal variability may cofound the analysis of EV markers originating from other tissues and have broader implications for the design of sampling protocols for other tissue-specific markers that may vary in a similar manner.

The potential for circulating EVs and their molecular cargo to be applied as minimally invasive biomarkers is increasingly recognised for the diagnosis of a variety of conditions or tracking individual responses to pharmacological interventions [24]. However, a comprehensive understanding of how these circulating markers fluctuate in normal physiology is currently lacking. Thus, the present study involved the analysis of EVs isolated from the serum of healthy subjects collected at multiple time points. We reported ranges, reflective of the normal variability between individuals, for particle size and concentration of EV isolates, total EV protein concentration and the abundance of EV-associated protein markers. In establishing normal ranges for the characteristics and composition of EVs, investigators may better define the thresholds for disease-associated changes, thereby strengthening the foundations for diagnostic or prognostic applications.

As EVs and their molecular cargo are involved in numerous functions vital for homeostasis, their biogenesis and composition are readily altered by different cellular and extracellular stimuli, including changes in nutrient availability [25]. Circulating biomarkers may fluctuate in response to feeding or alternatively, their quantification may be confounded by natural variation in unrelated blood parameters, especially triglyceride and lipoprotein levels [26]. To explore the effect of prandial state on the characteristics of EVs and abundance of associated protein markers in healthy individuals, serum EVs were

compared with and without an overnight fast and it was found that particle number and size was not altered by fasting. These data contrast with prior reports of circulating EVs post-prandially. Mørk et. al. [27] found that food intake resulted in a 61% increase in particle count and a significantly greater median size. However, that study and later work by Jamaly et. al. [26], reported strong correlations between particle count and plasma triglyceride concentrations after feeding, suggesting the similarly sized lipoprotein particles interfered with measurements. Blood serum EVs are unavoidably co-isolated with a range of non-vesicular materials such as protein aggregates and lipoproteins [28,29]. Neither of the aforementioned studies investigated EV purity. The latter of which isolated vesicles by ultracentrifugation, which is known to be more susceptible to lipoprotein contamination [18], rather than size exclusion chromatography (qEV).

It is important to note that NTA lacks the capacity to distinguish vesicles from other particles of comparable size, such as contaminating protein aggregates or lipoproteins [26]. Our assessments of EV purity by TEM and non-EV protein controls indicated highly pure vesicle preparations. Thus, effective removal of lipoproteins from both fed and fasted EV samples may account for differences seen in previous reports and mitigate the need for fasting in biomarker testing.

For the most part, the abundance of EV-associated protein markers, reported here, agrees with a recent study [30] that employed a flow cytometry approach with specific detection of EV protein markers, including the tetraspanins (CD9, CD63, and CD81). While a significant increase in CD9 abundance was observed here, Mørk et. al. [30] found no changes between prandial states. It should be noted, however, that flow cytometry methods are limited to vesicles > 100 nm in diameter, while LCMS permits analysis of all digested vesicular proteins in the samples [31].

The effect of circadian rhythm is well appreciated across numerous physiological systems and presents in circulation as oscillations in haematological parameters, blood and immune cell activation, and expression of surface markers [28]. This study sought to ascertain whether the characteristics of EVs and expression of associated markers exhibit diurnal variability. Particle size and concentration of EV isolates collected in the morning and afternoon did not vary, while the abundance of CD81 decreased and ASGR1 increased significantly.

While there is very limited commentary on the presence of diurnal variation in EV particle number and size over the course of a day, one study utilising nFC, reported an upward trend in EV size as well as a wider range in evening samples compared to the morning [31]. As previously mentioned, these disparate conclusions may be attributed to the capacity for NTA to quantify particles in a size range below that of flow cytometry. Taken together, the results presented here do not support fluctuations in the number or size of EVs diurnally, but point to potential changes in their molecular composition. Accordingly, attention should be given to the time of day at which EVs are sampled to reduce the effects of intra- and inter-individual variability on the sensitivity of biomarker analyses.

Lastly, the participants' sex was explored as a potential covariate associated with variability in EVs from healthy subjects. NTA analysis revealed that EV samples taken in the morning from males had more than 10 times greater particle concentration than those from females. This difference persisted, albeit at to a lesser extent, in the afternoon. Notably, the stark difference in particle concentration between sexes was not accompanied by greater levels of generic EV markers in male subjects. Sex differences have been observed in prior studies using flow cytometry, whereby plasma-derived phosphatidylserine and other microvesicle markers [32], and urinary $CD63^+$ EV levels were each higher in women [33]. Recently, however, an NTA analysis of plasma EVs isolated by precipitation found no difference in particle count between males and females [34]. The pool of circulating EVs is contributed to by numerous cell types, but is largely made up of those released by platelets [8]. Though currently unclear, particle number in male subjects in our study may have been influenced by undefined factors, such as diet, physical activity, and immune

activation that prompted the release of particular EV subpopulations bearing cell-type specific markers [28,35,36]. While interesting as an observation, in the absence of controlling for other sources of variability, the data presented here demonstrating differences between sexes in particle abundance should be interpreted with caution as other factors such as exercise may have confounded the results in this small cohort.

Flow cytometry is an appealing tool that lends itself to the analysis of individual protein markers on the surface of intact EVs [18]. Based on our results, it is evident that the data obtained by flow cytometry is not directly comparable to that from LCMS and has some limitations. A large proportion of EVs cannot be included in the quantification due to their size and the limit of detection of the flow cytometer. Conventional flow cytometers are capable of detecting EVs of 100 nm in diameter or greater, thus excluding all smaller EVs [37]. In this study, EVs between 100 and 900 nm were analysed. While observed diurnal variations were not consistent between study participants, every participant showed some level of diurnal variation. This phenomenon was previously shown, however, and studies involving a larger number of participants are required to fully appreciate diurnal changes [31].

Moreover, further detailing the daily time course of changes in EVs and their cargo may facilitate the tracking of therapeutic interventions. Such objectives would be serviced by longitudinal studies, testing in more frequent intervals of the circadian clock, and repeating measures across multiple days. Assessment of normal variability in healthy subjects might also be extended to include the effects of race and other demographic or clinical features.

5. Conclusions

Circulating EVs have immeasurable potential to be utilised as biomarkers. The value of this diagnostic and prognostic tool with respect to sensitivity and specificity, however, requires a fundamental understanding of the differences that naturally exist in the healthy population. The findings of this study should, therefore, inform EV sampling and may be of particular importance in the context of liver-specific EV-derived biomarkers.

Supplementary Materials: The following are available online at www.mdpi.com/2073-4409/10/3/485/s1, Figure S1: Unedited images for TEM analyses, Figure S2: Gating strategy for flow cytometry analysis, Figure S3: Flow cytometry analysis establishing normal ranges of variability on marker abundance, Figure S4: Flow cytometry analysis investigating the impact of fasting on EV marker abundance, Figure S5: Flow cytometry analysis investigating diurnal impact on EV marker abundances, Figure S6: Flow cytometry analysis investigating impact of sex on EV marker abundance. Supplementary Table S1: Analyte peptide sequences.

Author Contributions: "Conceptualization, L.A.N, A.R, M.J.S, and Z.U.; methodology, L.A.N., A.F., O.G.B., and Z.U.; software, L.A.N. and Z.U.; validation, L.A.N., A.F., and Z.U.; formal analysis, L.A.N. and Z.U.; investigation, L.A.N., A.R., A.F., and Z.U; resources, A.R.; data curation, L.A.N. and Z.U.; writing—original draft preparation, L.A.N., A.R., and Z.U.; writing—review and editing, L.A.N., A.R., and Z.U.; supervision, Z.U.; project administration, Z.U.; funding acquisition, A.R. All authors have read and agreed to the published version of the manuscript.

Funding: This work was supported by a grant from the National Health and Medical Research Council of Australia [Grant ID 1158210]. Andrew Rowland and Michael Sorich are supported by Beat Cancer Fellowships from Cancer Council SA. Zivile Useckaite is supported by a Fellowship from Pfizer Worldwide Research and Development.

Institutional Review Board Statement: The study was conducted according to the guidelines of the Declaration of Helsinki, and approved by the Institutional Ethics Committee (SAHREC 261.18) of Southern Adelaide Human Clinical Research Ethics Committee (protocol code HREC/18/SAC/310; 14 Nov 2018).

Informed Consent Statement: Informed consent was obtained from all subjects involved in the study.

Data Availability Statement: All data are included in the paper or attached as Supplementary Material.

Acknowledgments: The authors acknowledge the instruments and scientific and technical assistance of Microscopy Australia at Adelaide Microscopy, The University of Adelaide, a facility that is funded by the University, and State and Federal Governments. The authors would also like to acknowledge the instruments and technical assistance at Australian Wine Research Institute, Urrbrae South Australia. Nano Flow Cytometry experiments were performed at Flow Flinders Medical Centre (FMC), Bedford Park, South Australia. Figure 1 was created with BioRender.com.

Conflicts of Interest: The authors declare no conflict of interest.

References

1. Shah, R.; Patel, T.; Freedman, J.E. Circulating Extracellular Vesicles in Human Disease. *N. Engl. J. Med.* **2018**, *379*, 958–966, doi:10.1056/nejmra1704286.
2. Rowland, A.; Ruanglertboon, W.; Van Dyk, M.; Wijayakumara, D.; Wood, L.S.; Meech, R.; MacKenzie, P.I.; Rodrigues, A.D.; Marshall, J.; Sorich, M.J. Plasma extracellular nanovesicle (exosome)-derived biomarkers for drug metabolism pathways: A novel approach to characterize variability in drug exposure. *Br. J. Clin. Pharmacol.* **2019**, *85*, 216–226, doi:10.1111/bcp.13793.
3. Rodrigues, D.; Rowland, A. From Endogenous Compounds as Biomarkers to Plasma-Derived Nanovesicles as Liquid Biopsy; Has the Golden Age of Translational Pharmacokinetics-Absorption, Distribution, Metabolism, Excretion-Drug–Drug Interaction Science Finally Arrived? *Clin. Pharmacol. Ther.* **2019**, *105*, 1407–1420, doi:10.1002/cpt.1328.
4. Newman, L.A.; Sorich, M.J.; Rowland, A. Role of Extracellular Vesicles in the Pathophysiology, Diagnosis and Tracking of Non-Alcoholic Fatty Liver Disease. *J. Clin. Med.* **2020**, *9*, 2032, doi:10.3390/jcm9072032.
5. Jeppesen, D.K.; Fenix, A.M.; Franklin, J.L.; Higginbotham, J.N.; Zhang, Q.; Zimmerman, L.J.; Liebler, D.C.; Ping, J.; Liu, Q.; Evans, R.; et al. Reassessment of Exosome Composition. *Cell* **2019**, *177*, 428–445.e18, doi:10.1016/j.cell.2019.02.029.
6. Mir, B.; Goettsch, C. Extracellular Vesicles as Delivery Vehicles of Specific Cellular Cargo. *Cells* **2020**, *9*, 1601, doi:10.3390/cells9071601.
7. Kowal, J.; Arras, G.; Colombo, M.; Jouve, M.; Morath, J.P.; Primdal-Bengtson, B.; Dingli, F.; Loew, D.; Tkach, M.; Théry, C. Proteomic comparison defines novel markers to characterize heterogeneous populations of extracellular vesicle subtypes. *Proc. Natl. Acad. Sci. USA* **2016**, *113*, E968–E977, doi:10.1073/pnas.1521230113.
8. Oggero, S.; Austin-Williams, S.; Norling, L.V. The Contrasting Role of Extracellular Vesicles in Vascular Inflammation and Tissue Repair. *Front. Pharmacol.* **2019**, *10*, 1479, doi:10.3389/fphar.2019.01479.
9. Goetzl, E.J.; Schwartz, J.B.; Mustapic, M.; Lobach, I.V.; Daneman, R.; Abner, E.L.; Jicha, G.A. Altered cargo proteins of human plasma endothelial cell–derived exosomes in atherosclerotic cerebrovascular disease. *FASEB J.* **2017**, *31*, 3689–3694, doi:10.1096/fj.201700149.
10. Gotanda, K.; Hirota, T.; Saito, J.; Fukae, M.; Egashira, Y.; Izumi, N.; Deguchi, M.; Kimura, M.; Matsuki, S.; Irie, S.; et al. Circulating intestine-derived exosomal miR-328 in plasma, a possible biomarker for estimating BCRP function in the human intestines. *Sci. Rep.* **2016**, *6*, 32299, doi:10.1038/srep32299.
11. Goetzl, E.J.; Nogueras-Ortiz, C.; Mustapic, M.; Mullins, R.J.; Abner, E.L.; Schwartz, J.B.; Kapogiannis, D. Deficient neurotrophic factors of CSPG4-type neural cell exosomes in Alzheimer disease. *FASEB J.* **2019**, *33*, 231–238, doi:10.1096/fj.201801001.
12. Mustapic, M.; Eitan, E.; Werner, J.K.J.; Berkowitz, S.T.; Lazaropoulos, M.P.; Tran, J.; Goetzl, E.J.; Kapogiannis, D. Plasma Extracellular Vesicles Enriched for Neuronal Origin: A Potential Window into Brain Pathologic Processes. *Front. Neurosci.* **2017**, *11*, 278, doi:10.3389/fnins.2017.00278.
13. Monguió-Tortajada, M.; Gálvez-Montón, C.; Bayes-Genis, A.; Roura, S.; Borràs, F.E. Extracellular vesicle isolation methods: Rising impact of size-exclusion chromatography. *Cell. Mol. Life Sci.* **2019**, *76*, 2369–2382, doi:10.1007/s00018-019-03071-y.
14. Buschmann, D.; Kirchner, B.; Hermann, S.; Märte, M.; Wurmser, C.; Brandes, F.; Kotschote, S.; Bonin, M.; Steinlein, O.K.; Pfaffl, M.W.; et al. Evaluation of serum extracellular vesicle isolation methods for profiling miRNAs by next-generation sequencing. *J. Extracell. Vesicles* **2018**, *7*, 1481321, doi:10.1080/20013078.2018.1481321.
15. Böing, A.N.; Van Der Pol, E.; Grootemaat, A.E.; Coumans, F.A.W.; Sturk, A.; Nieuwland, R. Single-step isolation of extracellular vesicles by size-exclusion chromatography. *J. Extracell. Vesicles* **2014**, *3*, 10 3402 3 23430 10 3402 3 23430, doi:10.3402/jev.v3.23430.
16. Bowalgaha, K.; Elliot, D.J.; MacKenzie, P.I.; Knights, K.M.; Swedmark, S.; Miners, J.O. S-Naproxen and desmethylnaproxen glucuronidation by human liver microsomes and recombinant human UDP-glucuronosyltransferases (UGT): Role of UGT2B7 in the elimination of naproxen. *Br. J. Clin. Pharmacol.* **2005**, *60*, 423–433, doi:10.1111/j.1365-2125.2005.02446.x.
17. Useckaite, Z.; Mukhopadhya, A.; Moran, B.; O'Driscoll, L. Extracellular vesicles report on the MET status of their cells of origin regardless of the method used for their isolation. *Sci. Rep.* **2020**, *10*, 1–11, doi:10.1038/s41598-020-75817-9.
18. Brennan, K.; Martin, K.; Fitzgerald, S.P.; O'Sullivan, J.; Wu, Y.; Blanco, A.; Richardson, C.; Mc Gee, M.M. A comparison of methods for the isolation and separation of extracellular vesicles from protein and lipid particles in human serum. *Sci. Rep.* **2020**, *10*, 1–13, doi:10.1038/s41598-020-57497-7.

19. Welsh, J.A.; Van Der Pol, E.; Arkesteijn, G.J.; Bremer, M.; Brisson, A.; Coumans, F.; Dignat-George, F.; Duggan, E.; Ghiran, I.; Giebel, B.; et al. MIFlowCyt-EV: A framework for standardized reporting of extracellular vesicle flow cytometry experiments. *J. Extracell. Vesicles* **2020**, *9*, 1713526, doi:10.1080/20013078.2020.1713526.
20. Van Deun, J.; EV-TRACK Consortium; Mestdagh, P.; Agostinis, P.; Akay, Özden; Anand, S.; Anckaert, J.; Martinez, Z.A.; Baetens, T.; Beghein, E.; et al. EV-TRACK: Transparent reporting and centralizing knowledge in extracellular vesicle research. *Nat. Methods* **2017**, *14*, 228–232, doi:10.1038/nmeth.4185.
21. Théry, C.; Witwer, K.W.; Aikawa, E.; Alcaraz, M.J.; Anderson, J.D.; Andriantsitohaina, R.; Antoniou, A.; Arab, T.; Archer, F.; Atkin-Smith, G.K.; et al. Minimal information for studies of extracellular vesicles 2018 (MISEV2018): A position statement of the International Society for Extracellular Vesicles and update of the MISEV2014 guidelines. *J. Extracell. Vesicles* **2018**, *7*, 1535750, doi:10.1080/20013078.2018.1535750.
22. Povero, D.; Yamashita, H.; Ren, W.; Subramanian, M.G.; Myers, R.P.; Eguchi, A.; Simonetto, D.A.; Goodman, Z.D.; Harrison, S.A.; Sanyal, A.J.; et al. Characterization and Proteome of Circulating Extracellular Vesicles as Potential Biomarkers for NASH. *Hepatol. Commun.* **2020**, *4*, 1263–1278, doi:10.1002/hep4.1556.
23. Achour, B.; Al-Majdoub, Z.M.; Grybos-Gajniak, A.; Lea, K.; Kilford, P.; Zhang, M.; Knight, D.; Barber, J.; Schageman, J.; Rostami-Hodjegan, A. Liquid Biopsy Enables Quantification of the Abundance and Interindividual Variability of Hepatic Enzymes and Transporters. *Clin. Pharmacol. Ther.* **2021**, *109*, 222–232, doi:10.1002/cpt.2102.
24. Greening, D.W.; Simpson, R.J. Understanding extracellular vesicle diversity–current status. *Expert Rev. Proteom.* **2018**, *15*, 887–910, doi:10.1080/14789450.2018.1537788.
25. De Jong, O.G.; Verhaar, M.C.; Chen, Y.; Vader, P.; Gremmels, H.; Posthuma, G.; Schiffelers, R.M.; Gucek, M.; Van Balkom, B.W. Cellular stress conditions are reflected in the protein and RNA content of endothelial cell-derived exosomes. *J. Extracell. Vesicles* **2012**, *1*, 18396 10 3402 1 0 18396, doi:10.3402/jev.v1i0.18396.
26. Jamaly, S.; Ramberg, C.; Olsen, R.; Latysheva, N.; Webster, P.; Sovershaev, T.; Brækkan, S.K.; Hansen, J.-B. Impact of preanalytical conditions on plasma concentration and size distribution of extracellular vesicles using Nanoparticle Tracking Analysis. *Sci. Rep.* **2018**, *8*, 1–11, doi:10.1038/s41598-018-35401-8.
27. Mørk, M.; Pedersen, S.; Botha, J.; Lund, S.M.; Kristensen, S.R. Preanalytical, analytical, and biological variation of blood plasma submicron particle levels measured with nanoparticle tracking analysis and tunable resistive pulse sensing. *Scand. J. Clin. Lab. Investig.* **2016**, *76*, 349–360, doi:10.1080/00365513.2016.1178801.
28. Witwer, K.W.; Buzás, E.I.; Bemis, L.T.; Bora, A.; Lässer, C.; Lötvall, J.; Nolte-'t Hoen, E.N.; Piper, M.G.; Sivaraman, S.; Skog, J.; et al. Standardization of sample collection, isolation and analysis methods in extracellular vesicle research. *J. Extracell. Vesicles* **2013**, *2*, doi:10.3402/jev.v2i0.20360.
29. Tian, Y.; Gong, M.; Hu, Y.; Liu, H.; Zhang, W.; Zhang, M.; Hu, X.; Aubert, D.; Zhu, S.; Wu, L.; et al. Quality and efficiency assessment of six extracellular vesicle isolation methods by nano-flow cytometry. *J. Extracell. Vesicles* **2020**, *9*, 1697028, doi:10.1080/20013078.2019.1697028.
30. Mørk, M.; Nielsen, M.H.; Bæk, R.; Jørgensen, M.M.; Pedersen, S.; Kristensen, S.R. Postprandial Increase in Blood Plasma Levels of Tissue Factor–Bearing (and Other) Microvesicles Measured by Flow Cytometry: Fact or Artifact? *TH Open* **2018**, *2*, e147–e157, doi:10.1055/s-0038-1642021.
31. Danielson, K.M.; Estanislau, J.; Tigges, J.; Toxavidis, V.; Camacho, V.; Felton, E.J.; Khoory, J.; Kreimer, S.; Ivanov, A.R.; Mantel, P.-Y.; et al. Diurnal Variations of Circulating Extracellular Vesicles Measured by Nano Flow Cytometry. *PLoS ONE* **2016**, *11*, e0144678, doi:10.1371/journal.pone.0144678.
32. Gustafson, C.M.; Shepherd, A.J.; Miller, V.M.; Jayachandran, M. Age- and sex-specific differences in blood-borne microvesicles from apparently healthy humans. *Biol. Sex Differ.* **2015**, *6*, 1–10, doi:10.1186/s13293-015-0028-8.
33. Jayachandran, M.; Lugo, G.; Heiling, H.; Miller, V.M.; Rule, A.D.; Lieske, J.C. Extracellular vesicles in urine of women with but not without kidney stones manifest patterns similar to men: A case control study. *Biol. Sex Differ.* **2015**, *6*, 2, doi:10.1186/s13293-015-0021-2.
34. Hooten, N.N.; McFarland, M.H.; Freeman, D.W.; Mode, N.A.; Ezike, N.; Zonderman, A.B.; Evans, M.K. Association of Extracellular Vesicle Protein Cargo with Race and Clinical Markers of Mortality. *Sci. Rep.* **2019**, *9*, 1–11, doi:10.1038/s41598-019-53640-1.
35. Denham, J.; Spencer, S.J. Emerging roles of extracellular vesicles in the intercellular communication for exercise-induced adaptations. *Am. J. Physiol. Metab.* **2020**, *319*, E320–E329, doi:10.1152/ajpendo.00215.2020.
36. Brahmer, A.; Neuberger, E.; Esch-Heisser, L.; Haller, N.; Jorgensen, M.M.; Baek, R.; Möbius, W.; Simon, P.; Krämer-Albers, E.-M. Platelets, endothelial cells and leukocytes contribute to the exercise-triggered release of extracellular vesicles into the circulation. *J. Extracell. Vesicles* **2019**, *8*, 1615820, doi:10.1080/20013078.2019.1615820.
37. Lucchetti, D.; Battaglia, A.; Ricciardi-Tenore, C.; Colella, F.; Perelli, L.; De Maria, R.; Scambia, G.; Sgambato, A.; Fattorossi, A. Measuring Extracellular Vesicles by Conventional Flow Cytometry: Dream or Reality? *Int. J. Mol. Sci.* **2020**, *21*, 6257, doi:10.3390/ijms21176257.

Appendix 4

Article published in Biomedicines, 2022.

biomedicines

MDPI

Article

Selective Isolation of Liver-Derived Extracellular Vesicles Redefines Performance of miRNA Biomarkers for Non-Alcoholic Fatty Liver Disease

Lauren A. Newman [1], Zivile Useckaite [1], Jillian Johnson [2], Michael J. Sorich [1], Ashley M. Hopkins [1] and Andrew Rowland [1,*]

[1] College of Medicine and Public Health, Flinders University, Adelaide, SA 5042, Australia; lauren.newman@flinders.edu.au (L.A.N.); zivile.useckaite@flinders.edu.au (Z.U.); michael.sorich@flinders.edu.au (M.J.S.); ashley.hopkins@flinders.edu.au (A.M.H.)

[2] Early Clinical Development, Pfizer Global Research and Development, Groton, CT 06340, USA; jillian.johnson@pfizer.com

* Correspondence: andrew.rowland@flinders.edu.au; Tel.: +61-882-047-546

Abstract: Non-alcoholic fatty liver disease (NAFLD) is the most common chronic liver disease. Definitive diagnosis of the progressive form, non-alcoholic steatohepatitis (NASH), requires liver biopsy, which is highly invasive and unsuited to early disease or tracking changes. Inadequate performance of current minimally invasive tools is a critical barrier to managing NAFLD burden. Altered circulating miRNA profiles show potential for minimally invasive tracking of NAFLD. The selective isolation of the circulating extracellular vesicle subset that originates from hepatocytes presents an important opportunity for improving the performance of miRNA biomarkers of liver disease. The expressions of miR-122, -192, and -128-3p were quantified in total cell-free RNA, global EVs, and liver-specific EVs from control, NAFL, and NASH subjects. In ASGR1+ EVs, each miR biomarker trended positively with disease severity and expression was significantly higher in NASH subjects compared with controls. The c-statistic defining the performance of ASGR1+ EV derived miRNAs was invariably >0.78. This trend was not observed in the alternative sources. This study demonstrates the capacity for liver-specific isolation to transform the performance of EV-derived miRNA biomarkers for NAFLD, robustly distinguishing patients with NAFL and NASH.

Keywords: microRNA biomarkers; extracellular vesicles; liver-specific isolation; non-alcoholic fatty liver disease; non-alcoholic steatohepatitis

Citation: Newman, L.A.; Useckaite, Z.; Johnson, J.; Sorich, M.J.; Hopkins, A.M.; Rowland, A. Selective Isolation of Liver-Derived Extracellular Vesicles Redefines Performance of miRNA Biomarkers for Non-Alcoholic Fatty Liver Disease. *Biomedicines* **2022**, *10*, 195. https://doi.org/10.3390/biomedicines10010195

Academic Editors: François R. Jornayvaz and Karim Gariani

Received: 15 October 2021
Accepted: 12 January 2022
Published: 17 January 2022

1. Introduction

Non-alcoholic fatty liver disease (NAFLD) is the most common chronic liver disease, affecting up to a third of the global population [1]. The disease manifests on a spectrum of severity, with most individuals presenting with benign hepatic fat accumulation (non-alcoholic fatty liver; NAFL) and approximately 30% exhibiting a more severe form known as non-alcoholic steatohepatitis (NASH) [2]. While insulin resistance, obesity, and other features of the metabolic syndrome are commonly associated with NAFLD, the aetiology of the disease remains largely unknown, particularly with respect to its progression to NASH [3,4]. Treatment guidelines consistently identify early detection and intervention as key to improving the clinical outcomes and to reducing the burden of NAFLD [5,6]. NAFLD is an independent mortality risk factor, with all-cause mortality on average, 11.7% higher in individuals with NAFLD compared with those without. The impact on mortality among individuals with NAFLD is proportional to disease severity and ranges from 8.3% for NAFL up to 18.4% for NASH and fibrosis [7].

NAFLD is diagnosed in individuals that exhibit fatty changes in more than 5% of hepatocytes where other causes of steatosis have been excluded [8,9]. Liver biopsy is the gold

standard for NAFLD staging and the only approach to reliably defining fibrosis [10]. The key limitation is that liver biopsy is an invasive procedure that carries a substantial risk of complication, including bleeding and infection. This precludes biopsy in low-risk patients and limits utility in high-risk patients, as the procedure can only be performed once every two years. Additionally, given the sporadic infiltration of NAFLD and the limited tissue sample achieved with a needle biopsy, there is a substantial risk of inaccurate diagnosis that underestimates disease stage [9]. Given these limitations, a range of minimally invasive approaches to diagnose and stage NAFLD have been proposed. These approaches are typically based on factors such as serum biomarkers, body composition, comorbid diseases, and abdominal imaging [8–10]. Different combinations of these factors produce the fatty liver index, hepatic steatosis index, and liver fat scores, which are used as screening tools for NAFLD. While strong predictive performance has been reported for some indices, there is insufficient robustness to facilitate translation to routine clinical care, particularly for mild and early disease [11]. Indeed, in 2019, the American Association for the Study of Liver Diseases identified the inadequate performance of these tools as a critical barrier to the effective treatment of patients with NAFLD [6].

MicroRNAs (miRNA) are small non-coding RNA that have been shown to reflect disease-associated changes across numerous pathological conditions [12]. Altered expression of miRNAs that mediate pathways involved in lipid metabolism, inflammatory activation, and the development of fibrosis have been observed in tissue from individuals with NAFLD. The abundance of these miRNAs in blood has been postulated as potential biomarkers used to diagnosis and track NAFLD [13,14]. This approach potentially confers several advantages over liver biopsy. In addition to mitigating the risks of tissue biopsy, circulating miRNA analysis facilitates longitudinal evaluation of disease and potentially a more robust overview of disease stage. The stability of cell-free (cf) miRNA in blood is attributable to protection by RNA binding proteins, such as argonaute 2 (Ago2), high-density lipoproteins (HDL), or encapsulation within extracellular vesicles (EVs) [15].

EVs are small membrane-bound particles released by virtually all cell types into various biological fluids including blood, urine, and cerebrospinal fluid [16,17]. EVs carry an array of nucleic acid (including miRNA), protein, and lipid cargo derived from the parent cell [17,18]. It has been proposed that isolating EVs from biological fluids may improve the fidelity of miRNA biomarker analyses as the EV fraction provides a source of miRNA that is selectively packaged in a more disease-specific manner [19]. Additionally, circulating EVs express cell surface markers from the originating tissue. Thus, in contrast with circulating miRNA bound to Ago2 and HDL, it is theoretically possible to selectively isolate EV miRNA that originates from a specific tissue. It has been proposed [20] that analysis of EVs selectively isolated from an afflicted organ provide the most informative description of biomarker expression, as this fraction is less affected by 'noise' associated with non-specific fluctuations in global EV and, in the case of miRNA, total circulating expression.

To date, studies of cell-free miRNA in NAFLD have focussed broadly on expression in whole plasma and serum. When simplified to a dichotomous analysis of healthy versus NAFLD, moderate diagnostic performance in terms of discriminating these two groups has been reported for a number of miRNAs both as individual markers and panels [13,21]. Despite intriguing preliminary results, the consistency of results from miRNA profiling studies remains insufficient to be applied in practice [15]. Furthermore, this dichotomous grouping of healthy versus disease limits meaningful interpretation of an individual's NAFLD risk, which differs substantially with disease severity. For the current study, three representative miRNAs were selected based on their reported liver specificity (miR-122), associations with steatosis and fibrosis (miR-122, -192, and -128-3p) and association with inflammation (miR-192). This study sought to identify trends in the expressions of these three miRNAs; to determine whether the sequential refinement of the source from which biomarkers are quantified; and to improve their predictive power with respect to differentiating NAFL, NASH, and control subjects.

2. Materials and Methods

2.1. Study Population and Blood Samples

Clinically annotated K_2EDTA plasma from NAFLD patients (NAFL n = 8; biopsy-proven NASH n = 6) and healthy donors (n = 14) matched for age and sex were purchased from Discovery Life Sciences (Hunstville, AL, USA). The inclusion criteria included a clinical diagnosis of NAFL or NASH by a physician, and the exclusion criterion was the presence of a viral disease. The samples were aliquoted for EV isolation and total RNA analysis according to the study workflow depicted in Figure 1 and stored at −80 °C. All analyses were performed on all the patients, unless otherwise indicated. The demographic data describing each of the three study populations are presented in Table 1. All relevant data have been submitted to the EV-TRACK knowledgebase (ID EV210168) [22].

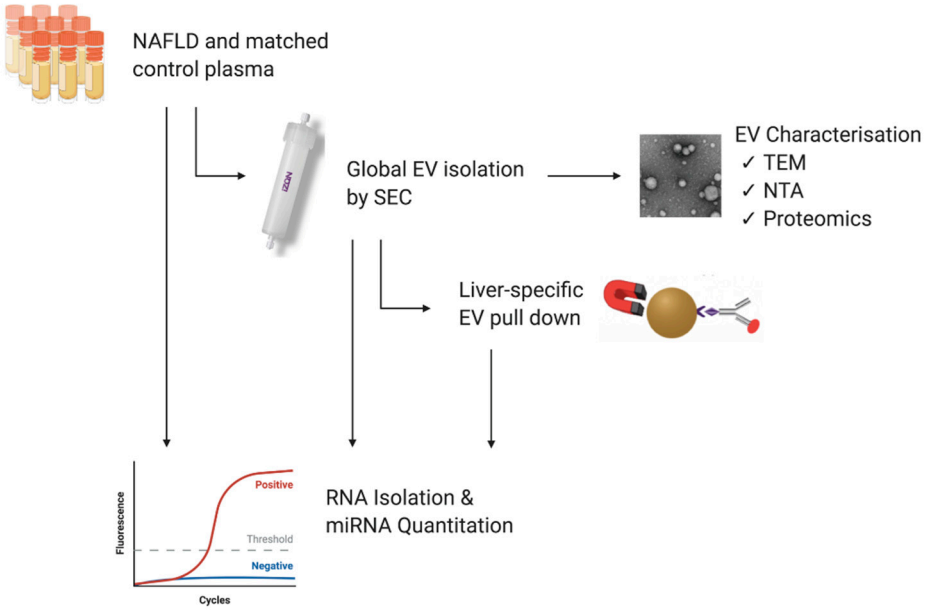

Figure 1. Study workflow. Plasma samples from patients with non-alcoholic fatty liver disease and matched healthy controls were purchased from Discovery Life Sciences (DLS). Samples were aliquoted for miRNA quantitation directly from plasma and from EVs following their isolation by qEV size exclusion chromatography (SEC) and immunoprecipitation (IP). EVs isolated by qEV were characterised by transmission electron microscopy (TEM), nanoparticle tracking analysis (NTA), and protein expression. Figure was created using BioRender.com [https://app.biorender.com/; accessed 17 January 2022].

Table 1. Demographic information for control, non-alcoholic fatty liver (NAFL) and non-alcoholic steatohepatitis (NASH) study populations.

Characteristic		Control (n = 14)	NAFL (n = 8)	NASH (n = 6)
Age	Mean (±SD) years	46.5 (15.7)	48.7 (17.7)	53.2 (15.4)
Sex	Female (%)	42.9	57.1	50.0
Race	Caucasian (%)	78.6	57.1	83.3
	Other (%)	21.4	14.3	16.7
	Unknown (%)	0	28.6	0

2.2. Isolation of Extracellular Vesicles

2.2.1. Size Exclusion Chromatography

Global EVs were isolated using qEV2 70 nm size exclusion chromatography (SEC) columns (iZon Science, Christchurch, New Zealand). Prior to performing the isolations, the columns were equilibrated to room temperature and washed with 10 mL of 0.2 µm

filtered phosphate-buffered saline (PBS). Plasma (1700 µL) was diluted up to 2 mL with PBS, loaded into the sample reservoir, and allowed to completely pass into the column, before eluting with PBS. The first six fractions eluted from the column were discarded, and vesicles were collected as a pool of fractions 7 to 11 (10 mL). Pooled vesicle fractions were concentrated to 400 µL using Amicon Ultra-15 centrifuge 30 kDa filters (Millipore-Sigma, Bedford, MA, USA) pre-conditioned with PBS and stored at −80 °C until analysis.

2.2.2. Liver-Specific EV Immunoprecipitation

EVs specifically derived from the liver were separated from global EV isolates following a previously published protocol [23]. Briefly, 1.5 mg of Dynabeads M280 streptavidin magnetic beads (Cat#11205D, Thermo Fisher Scientific, Waltham, MA, USA) were pre-washed with PBS and incubated with 15 µg of biotinylated anti-asialoglycoprotein receptor 1 (ASGR1) polyclonal antibody (Cat#LS-C685544, 0.5 mg/mL, Sapphire Bioscience, Redfern, NSW, Australia) for 30 min at RT with gentle agitation. Antibody-conjugated beads were separated using a DynaMag-2 magnet (Thermo Fisher Scientific, Waltham, MA, USA), washed with 0.1% bovine serum albumin in PBS, and resuspended in PBS. Concentrated qEV70 vesicles (150 µL) were added to antibody-coated beads and incubated for 24 h at 4 °C on a rotating mixer. ASGR1+ EVs bound to the antibody-bead complexes were separated on the magnet, washed, and resuspended in PBS.

2.3. Transmission Electron Microscopy

Samples were prepared based on a previously published protocol [17]. Briefly, 5 µL of the EV sample in filtered PBS was placed on carbon-coated grids for 4 min (Ted-Pella B 300M, Mason Technology, Dublin, Ireland). Grids were washed for 15 s with 0.2 µm filtered PBS at room temperature and were contrasted with 2% uranyl acetate (3 min at room temperature), washed once, and examined by FEI TECNAI Spirit G2 TEM (Thermo Fisher Scientific, Waltham, MA, USA).

2.4. Nanoparticle Tracking Analysis

Nanoparticle tracking analysis (NTA) was performed to quantify particle concentration and size distribution in EV samples using a NanoSight NS300 (Malvern Analytical, Malvern, UK). Samples were diluted between 1:500 and 1:2000 in PBS. Ten 60-s videos were captured at camera level 14 with continuous sample flow (flow rate 100), and the videos were analysed at a detection threshold of 5 using NTA 3.4 software.

2.5. Total Protein Concentration

EVs were lysed by the addition of a RIPA buffer at a ratio of 1:1, incubated on ice for 25 min and centrifuged at 10,000× *g* for 10 min at 4 °C. Total protein concentration was determined using Pierce MicroBCA Protein Assay following manufacturer's instructions (Thermo Fisher Scientific, Waltham, MA, USA).

2.6. Peptide Digestion

EVs (50 µL) were diluted up to 100 µL in PBS, vortexed for 10 min using a MixMate sample mixer (Eppendorf South Pacific, North Ryde, NSW, Australia), and then lysed by freezing and thawing for three times. Lysed EVs were combined with 50 µL of ammonium bicarbonate (pH 7.8) and incubated with dithiothreitol (DTT; 12.5 mM) for 90 min at 60 °C. Samples were cooled to room temperature prior to the addition of iodoacetamide (IAA; 23.5 mM) and incubation for 60 min at 37 °C. Trypsin Gold was then added to the EV protein samples in a ratio of 1:40 and incubated for 18 h at 37 °C. Digests were terminated by the addition of 20 µL of formic acid (10% *v*/*v*), then centrifuged at 16,000× *g* for 10 min at 4 °C. A 100 µL aliquot of the resulting supernatant was combined with SIL peptide standards (25–2500 pM cocktail; Vivitide, Gardner, MA, USA) and a 5 µL aliquot was injected for analysis by LC–MS/MS.

2.7. LC–MS Peptide Analysis

Chromatographic separation of peptide analytes was performed on an Agilent Advance Bio Peptide Map column (100 × 2.1 mm, 2.7 µm) using an Agilent 1290 Infinity II liquid chromatography system. The temperatures of the column and sample compartment were maintained at 30 and 4 °C, respectively. Separation was achieved by gradient elution with a flow rate of 0.2 mL/min. The mobile phase consisted of 0.1% formic acid in water (mobile phase A) and 0.1% formic acid in acetonitrile (mobile phase B). The proportion of mobile phase B was held at 10% for 2 min and then increased to 60% over 13 min, before returning to 10% for 1 min. The column was re-equilibrated for 30 s, and the total run time was 16.5 min. Column eluant was monitored by mass spectrometry using an Agilent 6495B Triple Quadrupole mass spectrometer operating in positive electron spray (ESI +) mode. Multiple reaction monitoring (MRM) was performed with one quantifier and one qualifier ion transition for each peptide. The identities of the endogenous peptides were confirmed by comparing retention time and quantifier/qualifier transition ratios to respective SIL peptide standards and relative abundance determined by quantifier ion peak area.

2.8. RNA Isolation

Total RNA was isolated from plasma and EV samples using TRIzol LS™ Reagent (Thermo Fisher Scientific, Waltham, MA, USA) as per manufacturer's instructions with some modifications. Briefly, 750 µL TRIzol LS was added to 200 µL of plasma and 100 µL of EVs (diluted up to 200 µL in RNase-free water). Samples were spiked with 2.5 femtomoles of cel-miR-54 mirVana mimic (MC10279, Thermo Fisher Scientific, Waltham, MA, USA) to normalise for technical variability in RNA extraction and RT-qPCR efficiency. This exogenous control was employed in the absence of established endogenous genes for normalisation of plasma or EV-derived miRNA RT-qPCR data [24,25]. Isopropyl RNA precipitation was facilitated by addition of 40 µg of RNase-free glycogen (Thermo Fisher Scientific, Waltham, MA, USA), and the RNA pellet was washed with ice cold 80% ethanol. RNA was resuspended in 30 µL of RNase-free water.

2.9. RT-qPCR

Equal volumes of RNA (5 µL) were reverse transcribed using the TaqMan microRNA Reverse Transcription Kit (Thermo Fisher Scientific, Waltham, MA, USA). Since the concentration of circulating cfRNA is usually below the limit of quantification for photometric or colorimetric techniques, equivalent mass could not be reliably determined. Thus, RNA input was based on a fixed volume rather than RNA mass (ng), as in previous studies [12,26,27]. Instead, alterations in miRNA levels in equivalent volumes of plasma or EV isolates were detected relative to the exogenous spike in. TaqMan Small RNA Assays (Thermo Fisher Scientific, Waltham, MA, USA) were used to carry out qPCR assays with primers specific to the miRNA of interest (hsa-miR-122 (002245), hsa-miR-192 (00491), miR-128a (002216), and cel-miR-54 (001361)) in a Rotor-Gene 3000 (Corbett Research, Sydney, NSW, Australia). Samples were assayed in duplicate and the same cycle threshold set across all runs.

2.10. Statistical Analysis

Cycle threshold (Ct) values derived from RT-PCR were used to calculate relative quantities (RQ) according to the following formula:

$$\text{RQ} = 2^{-(\text{mean biomarker Ct} - \text{mean spike–in Ct})}$$

Statistical analysis was performed using GraphPad Prism software version 9.0 (San Diego, CA, USA). The data are presented as mean ± SD unless specified. Statistical comparisons between the NAFL, NASH, and control groups were performed using the Kruskal–Wallis test and Dunn's test for multiple comparisons. Statistical significance was set at 0.05. A receiver operating characteristic (ROC) analysis was used to assess

the diagnostic capacity of miRNA biomarkers between pairs of groups. Ordinal logistic regression was performed using R version 1.4 (Boston, MA, USA) to determine diagnostic value across the three groups.

3. Results

3.1. Isolation and Characterization of Circulating EVs from NAFLD and Control Subjects

The concentration and size of global EV particles isolated from NAFL, NASH, and control subjects was determined by NTA. An apparent higher mean EV concentration (±SD) of 4.17 × 10^{11} (±1.76 × 10^{11}) particles/mL was observed in control subjects compared with NAFL (2.34 × 10^{11} (±9.03 × 10^{10}) particles/mL) and NASH (2.73 × 10^{11} (±1.01 × 10^{11}) particles/mL) subjects (Figure 2a, Table 2). However, given the marked within group heterogeneity, no statistically significant differences in EV concentration were detected between groups. Mean particle size, given in Table 2, also did not vary between control, NAFL, and NASH groups.

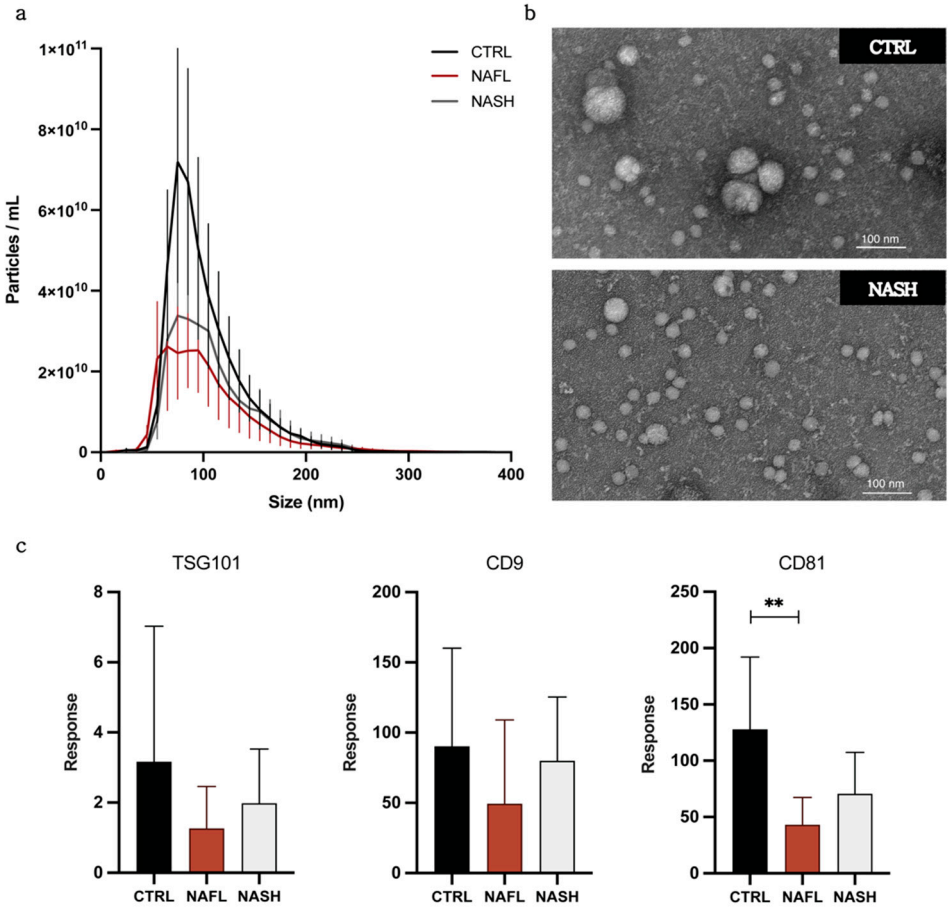

Figure 2. Characterisation of global circulating EV isolated from control, NAFL, and NASH subjects. (**a**) Particle concentration and size distribution by nanoparticle tracking analysis (NTA) (n = 5). Error bars denote SEM. (**b**) Representative TEM images of NASH patient and control global EVs. (**c**) Relative abundance of EV protein markers determined by mass spectrometry. Error bars denote SD. ** $p \leq 0.01$.

Table 2. Mean concentration and size of particles in qEV isolates from control, NAFL, and NASH subjects determined by nanoparticle tracking analysis.

Group (n = 5)	Concentration (Particles/mL)	Mean Size (nm)
Control	$4.17 \times 10^{11} \pm 1.76 \times 10^{11}$	102.9 ± 2.7
NAFL	$2.34 \times 10^{11} \pm 9.03 \times 10^{10}$	113.3 ± 10.4
NASH	$2.73 \times 10^{11} \pm 1.01 \times 10^{11}$	110.1 ± 8.6

Global EVs were also analysed by TEM to assess sample composition and morphology. TEM images of EVs from NASH and control subjects isolated by qEV revealed characteristic EV morphology, size, and removal of non-vesicular contaminants (Figures 2b and S1). While the EVs were predominantly of similar size between NASH and control subjects, the presence of a few larger EVs was noted in the control sample.

Established positive and negative EV protein markers were probed by targeted LC-MS peptide analysis [17]. Positive markers, as described by the Minimal Information for Studies of Extracellular Vesicles (MISEV) [28], include tetraspanins, CD81 (Class 1a), CD9 (Class 1b), and tumour susceptibility gene 101 (TSG101; Class 2a) and were detected in EV isolates from control, NAFL, and NASH subjects (Figure 2c). Only CD81 showed a significantly lower abundance in NAFL compared with control samples; however, total protein concentration did not differ between groups (Figure S2). Samples were also analysed for negative markers of matrix contamination and cellular debris; albumin (Class 3b) and Calnexin V (Class 4c). Minimal expression was observed for both negative markers; the mean abundance of albumin and calnexin in EV preparations was 0.21% and 0.94% of abundance in respective positive controls (plasma for albumin and human liver microsomes for calnexin).

Taken together, these data indicate that qEV size exclusion chromatography permits the isolation of pure EVs with characteristic molecular and physical properties from the circulation of patients with NAFLD and healthy controls. Characterisation of liver-specific EV isolates was performed with respect to particle concentration and ASGR1 abundance and is reported as Supplementary Data. Data are reported in accordance with MISEV guidance. EV-TRACK study identifier is EV210168.

3.2. Expression of Total Cell-Free, Global EV, and Liver-Specific EV miRNA Biomarkers

Expression of miRNA was quantified in total cfRNA, global EVs, and liver-specific EVs isolated by anti-asialoglycoprotein receptor 1 (ASGR1) immunoprecipitation. Relative quantities (RQ) for miR-122, -192, and -128-3p were calculated after normalisation to an exogenous spike-in (cel-miR-54) and compared between control, NAFL, and NASH subjects (Figure 3). The expressions of all three miRNA biomarkers were significantly greater in ASGR1+ EVs from NASH subjects compared with controls (p = 0.012 (miR-122), p = 0.013 (miR-192), and p = 0.032 (miR-128-3p)). Interestingly, this trend was not observed when miRNA was analysed from total cell-free or global EV sources. In global EVs, only miR-128-3p exhibited altered expression with significantly lower RQ in NAFL (p = 0.009) and NASH (p = 0.019) subjects compared with controls. The apparent alterations in expression were consistent irrespective of using total cell-free or global EV as the source of RNA (Figure 3c), indicating that the isolation of global EVs did not confer an appreciable benefit towards the capacity for miR-128-3p expression to distinguish the groups. Conversely, RQ for miR-122 and -192 did not vary between disease or control subjects in total cfRNA or global EV analysis. Overall, these data suggest that the selective analysis of miRNA biomarkers from liver-specific EVs has the potential to elucidate a useful trend in expression corresponding with disease stage, particularly for biomarkers with high tissue specificity such as the liver-specific miR-122 and, to a lesser extent, miR-192 and -128-3p.

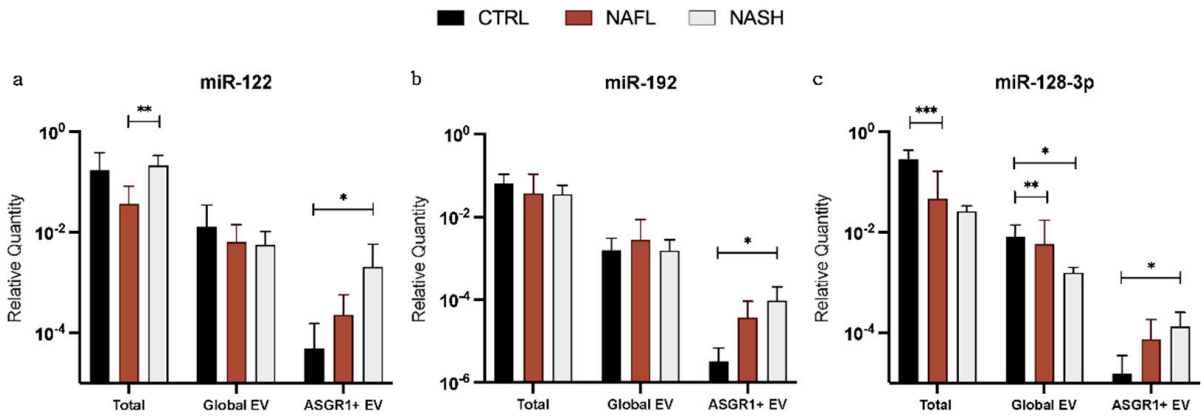

Figure 3. Differential expression of miRNA biomarkers in NAFLD. Relative quantities of miR-122 (**a**), miR-192 (**b**), and miR-128-3p (**c**) normalised to cel-miR-54 in total circulating RNA, global EVs, and asialoglycoprotein receptor 1 (ASGR1) positive EVs isolated from patients with NAFL and NASH and from controls. Statistical analysis performed by the Kruskal-Wallis test with Dunn's for multiple comparisons. * $p \leq 0.05$, ** $p \leq 0.01$, *** $p \leq 0.001$. Error bars represent standard deviation.

3.3. The Proportion of Circulating miRNA Contained in EVs Changes with NAFLD

To further explore the distribution of miRNA biomarkers amongst circulating fractions, RQs were used to calculate the expression of miRNA biomarkers in global EVs as a percentage of total cfRNA and in ASGR1+ EVs as a percentage of global EVs (Table 3). It has been observed that RNA isolation from unfractionated samples results in substantially higher yield compared with EVs due to the contribution of other circulating miRNA complexes. To ensure sufficient sensitivity, the equivalent starting volume for EV RNA isolation was 2.5× that for total cfRNA and reported proportions were normalised accordingly. The results demonstrated that, in control samples, mean (±SD) percentage expression in global EVs/total RNA was no greater than 5.6% (±10.0%), suggesting that only a minor proportion of total cell-free RNA is found in EVs. Likewise, in control subjects, the mean percentage expression in ASGR1+/global EVs was similarly low. Interestingly however, there was a positive trend in proportional expression of all miRNA biomarkers with NAFLD. In NASH, 27.1% of vesicular miR-122 signal came from ASGR1+ EVs compared to just 2.4% in control subjects ($p = 0.035$) (Table 3, Figure 4a). Significantly greater ASGR1+/global EV expression was also observed for miR-128-3p between NASH and control subjects ($p = 0.022$) (Figure 4c), while a similar difference in miR-192 fell short of statistical significance ($p = 0.067$) (Figure 4b). While only a small fraction of each miRNA is released in EVs expressing ASGR1—so a larger fraction may be derived from cells other than hepatocytes—these data suggest that, in NAFLD, the contribution of the liver to circulating EV-derived miRNA increases.

Table 3. Expression of miRNA biomarkers in global EVs as a percentage of total circulating RNA and in asialoglycoprotein receptor 1 positive (ASGR1+) EVs as a percentage of global EVs from control, NAFL, and NASH subjects.

Expression (%)		miR-122		miR-192		miR-128-3p	
		Mean	SD	Mean	SD	Mean	SD
Global EV/Total	Control	5.6	10.0	5.1	14.5	2.3	3.7
	NAFL	23.3	27.3	8.7	6.7	17.0	26.2
	NASH	5.1	10.6	3.0	3.4	2.6	1.0
ASGR1+ EV/Global EV	Control	2.4	6.6	0.5	0.8	0.6	1.4
	NAFL	9.9	20.7	10.4	17.0	13.3	20.2
	NASH	27.1	37.2	8.8	9.8	10.5	10.1

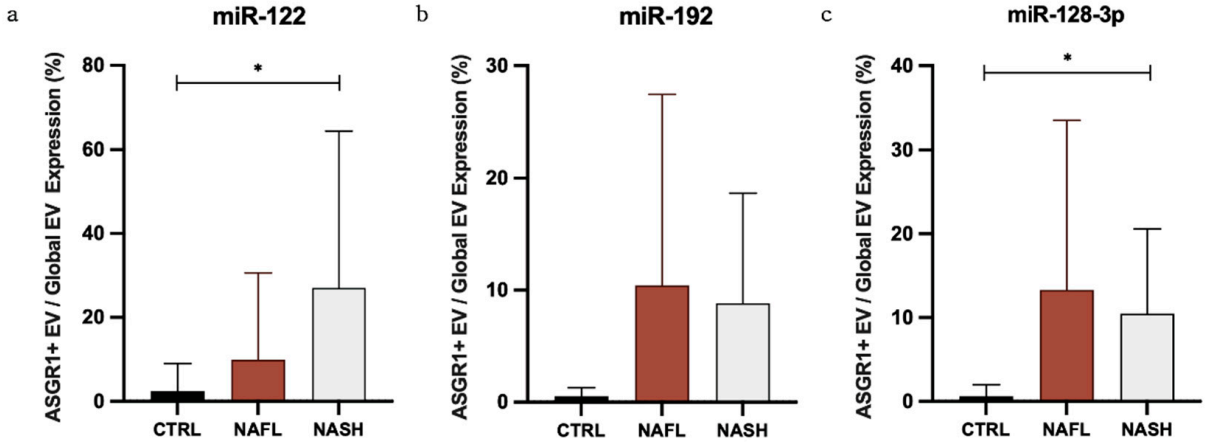

Figure 4. Relative expression of miRNA in liver-specific EVs. Expressions of miR-122 (**a**), miR-192 (**b**), and miR-128-3p (**c**) in asialoglycoprotein receptor 1 positive (ASGR1+) EVs as a percentage of global EVs in NAFL and NASH patients compared with controls. Statistical analysis performed by the Kruskal–Wallis test with Dunn's for multiple comparisons. * $p \leq 0.05$. Error bars represent standard deviation.

3.4. Association between miRNA Expression and Disease Severity

Ordinal logistic regression was performed to evaluate associations between miRNA abundance and the probability of a subject being healthy (control), NAFL, or NASH. Significant associations between miRNA expression and group status were observed for all three miRNAs in liver-specific EVs (Figure 5). The C-statistic for miR-122 was 0.80 with an odds ratio (OR) of 0.60 ($p = 0.004$), indicating that, for every 1 unit decrease in ΔCt, the subject was 40% more likely to be NASH than NAFL or NAFL than control. Similarly, the C-statistics for miR-192 and miR-128-3p were 0.84 and 0.78, with ORs of 0.51 ($p = 0.005$) and 0.65 ($p = 0.016$), respectively. The expressions of miR-122 and miR-192 in total cfRNA and global EVs demonstrated no significant association with group status. Robust predictive performance was observed for total cfRNA and global EV derived miR-128-3p, with C-statistics of 0.78 ($p = 0.007$) and 0.83 ($p = 0.009$), respectively. Of the miRNA sources, only liver-specific EVs demonstrated a consistent trend amongst all miRNAs across increasing disease state.

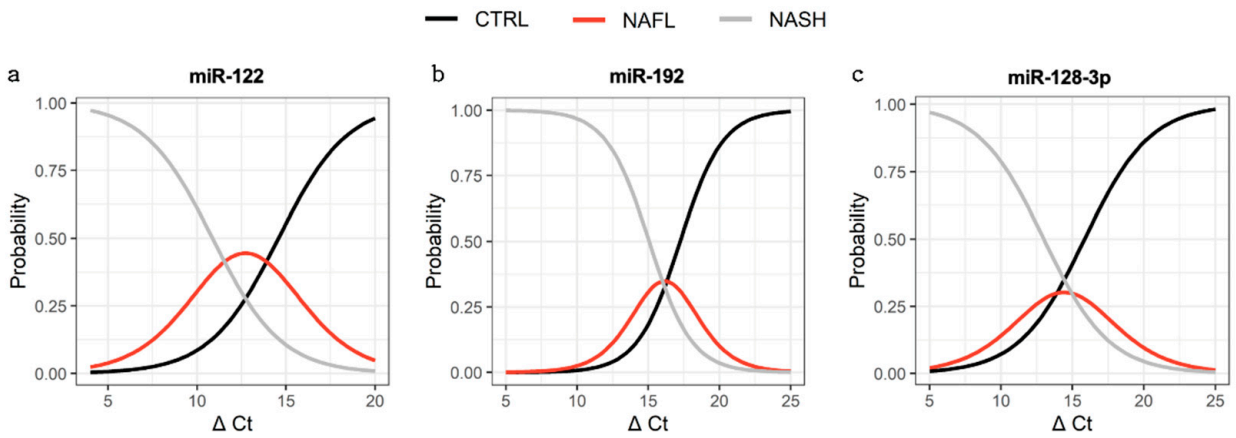

Figure 5. Ordinal logistic regression models. Ordinal regression applied to distinguish control, NAFL and NASH subjects using ASGR1+ EV-derived miR-122 (**a**), miR-192 (**b**), and miR-128-3p (**c**).

3.5. Capacity to Distinguish Subjects with Disease from Control

A receiver operator characteristic (ROC) analysis was undertaken to establish the performance of each miRNA marker in the current analysis in a manner consistent with prior studies, as summarised in our recent review [13] (Table 4). The abundance of total plasma RNA derived miR-192 and miR-128-3p, but not miR-122, robustly distinguished individuals with NAFLD from controls (AUC $\geq$ 0.714). Comparatively poor performance was observed for global EV-derived miRNAs, with only miR-128-3p (AUC = 0.888) distinguishing these groups. As per the ordinal logistic regression analysis, liver-specific EV-derived miRNAs demonstrated the strongest performance with respect to distinguishing individuals with NAFLD from controls. AUC values for liver-specific EV derived miRNAs were invariably >0.8. An extended ROC analysis defining the performance of miRNA marker with respect to distinguishing individual paired groups (i.e., control vs. NAFL, control vs. NASH, and NAFL vs. NASH) is reported in Supplementary Materials (Table S2, Figure S4).

Table 4. Area under the receiver operator characteristic curve for miRNA biomarkers isolated from total cell-free RNA, global EVs, and ASGR1+ EVs.

Source	All NAFLD—CTRL					
	miR-122		miR-192		miR-128-3p	
	AUC	*p*	AUC	*p*	AUC	*p*
Total RNA	0.607	0.335	0.714	0.054 *	0.924	0.0001 *
Global EV	0.505	0.963	0.582	0.462	0.888	0.001 *
ASGR1+ EV	0.830	0.004*	0.895	0.003 *	0.803	0.014 *

* denotes significant *p*-values ($\leq$0.05).

4. Discussion

This study provides the first direct evidence supporting transformative improvement in the predictive performance of existing NAFLD miRNA biomarkers achieved by isolating liver-specific EVs. Specifically, it is demonstrated that following anti-ASGR1 immunoprecipitation, the expression of liver-specific EV-derived miR-122, -192, and -128-3p is significantly associated with disease severity. In all cases, there was a significant trend of greater miRNA expression in subjects with NASH compared with NAFL, and NAFL compared with control subjects (Figure 3). Notably, this trend was not observed with either total cell-free or global EV-derived RNA. Rather, an analysis from these two sources of RNA revealed a significant decrease in miR-128-3p expression with disease, while miR-122 and -192 were not altered in comparison with the controls. In all cases, liver-specific (ASGR1+) EV-derived miRNA biomarkers demonstrated strong capacity to predict subject status

as the control, NAFL, or NASH (Figure 5) with c-statistics > 0.78. This performance was not observed with either total cfRNA or global EV-derived miRNAs. While the improved predictive performance associated with liver-specific isolation provides additional support for these markers reflecting a hepatic manifestation, the possibility that these markers may also be associated with more systemic comorbidities cannot currently be excluded.

Indeed, each of the miRNAs investigated here is abundant in liver tissue, especially miR-122, which accounts for about 70% of all miRNA expression in the liver [29]. However, miR-122 is also found in cardiac and skeletal muscles; miR-192 is abundant in the kidneys, intestine, and adipose tissue [30]; and miR-128-3p is expressed in numerous tissues types, including in the CNS [31] and adipose tissue [32]. miR-128-3p also acts as a tumour suppressor miR and is reported to be dysregulated in several cancers, including lung [33], colorectal [34], and hepatocellular [35,36] cancer. Fundamentally, circulating miRNAs lack tissue specificity; their presence and stability in biological fluids results from release by multiple cell types and localisation within EV, lipoprotein, and Ago protein complexes [37]. The mechanisms of miRNA export from cells are known to be differentially affected by disease states; accordingly, perturbation in the relative expression of circulating miRNAs in vesicular or non-vesicular compartments are anticipated [12,15]. Consistent with this phenomenon, it was observed that the fraction of total circulating miR-122 (which accounts for 70% of hepatic miRNA) contained within liver-specific EVs increased with disease stage. This observation further supports the hypothesis proposed by several recent studies that optimising the circulating miRNA source is a key step in translating miRNA biomarker analysis [12,15,19,38].

Jiang et al. [39] recently reported that, compared with total serum-derived miRNA, differences in EV-derived miRNAs, including miR-122 (ROC = 0.79), more effectively discriminated subjects with NAFLD from healthy controls. In contrast with Jiang, et al. [39], in the current study isolation of global EVs did not improve the predictive performance of miRNA biomarkers with respect to identifying individuals with NAFLD. It is plausible that differences in performance gains achieved by global EV isolation relate to differences in the composition of the NAFLD cohort (i.e., the proportion of individuals with NAFL versus NASH or the proportion of individuals with non-hepatic co-morbidities). While this study did not reproduce the improvement in predictive performance achieved by isolating global EVs, we did demonstrate that further refinement of the miRNA source by tissue-specific EV isolation markedly improved performance. This outcome is consistent with analyses demonstrating improved signal to noise for minimally invasive protein biomarkers in plasma for neuronal pathology [40–43] and cerebrovascular disease [44] with tissue-specific isolation. As per the current study, selectively enriching the biomarker source was consistently found to increase sensitivity and specificity of analyses. One study further showed that the expression of miR-382 in intestine-specific EVs, but not global EVs, could predict the functional activity of human breast cancer resistance proteins [45]. Furthermore, we recently applied the liver-specific EV isolation method used here to describe the induction of hepatic drug metabolising enzymes and transporters resulting from metabolic drug interactions and pregnancy [23]. Collectively, these reports highlight the emerging potential to leverage tissue-specific EVs as minimally invasive liquid biopsy platform.

The use of anti-ASGR1 immunoprecipitation facilitated the analysis of EV encapsulated miRNA biomarkers released only by hepatocytes. Given the reported high abundance of miR-122 in hepatocytes, a high proportional expression of miR-122 in ASGR1+ EV relative to global EV-derived miRNA was anticipated. However, in EVs isolated from control subjects, the fraction of EV-derived miR-122 recovered from ASGR1+ EVs was strikingly low (2.4% of global EV derived miR-122 and 0.13% of total circulating miR-122). This low expression of miRNA in ASGR1+ EVs likely reflects the low fraction of circulating EVs that are derived from hepatocytes. The substantial expression of miR-122 from non-hepatic sources emphasises the potential for trivial changes in non-hepatocyte-derived miRNAs to markedly impact NAFLD biomarker analysis in the absence of liver-specific EV isolation. Interestingly, the fraction of global EV and cfRNA-derived miR-122, -192, and -128-3p

recovered in ASGR1+ EVs was markedly higher in NAFL and NASH subjects compared with controls, despite the circulating EV count remaining unchanged. This marked increase in ASGR1+ EV-derived miRNA expression is consistent with the reported roles of these miRNAs in the inflammatory processes and remodelling associated with NAFLD and supports the biological rationale for their use as biomarkers for this disease. It is worth noting that, while the expression of miR-122 and -128-3p was significantly increased in NAFL and NASH compared with control subjects (Figure 4), the proportion of these miRNAs in ASGR1+ EV still accounted for <30% of global EV expression and <2.5% of total cfRNA expression for each miRNA.

It is conceivable that a population of miRNA-containing hepatic EVs does not express ASGR1 on their surface and hence are not captured by the immunoprecipitation method applied in the current analysis. Alternatively, various extra-hepatic tissues expressing these miRNAs may contribute more profoundly to their abundance in circulating global EVs. NAFLD is notably the hepatic manifestation of a broader multi-system disease associated with systemic inflammation and metabolic disturbances in several organs. It is likely that perturbations in other organs may contribute to the observed differences in global EV cargo derived from subjects with NAFL and NASH. This explanation further emphasises the potential benefits of selectively isolating liver-specific EVs for biomarker analyses. The data presented in a recent study by Povero et al. [46] indicated that EVs expressing ASGR1 comprise approximately 20% of the circulating global pool and that the number of hepatocyte-derived EVs increases with severity of NASH. However, in the limited sample size analysed here, no differences in global EV abundance were observed between groups. In this context, it is not clear if the increased proportional expression of miRNA with disease was due to greater number of ASGR1+ EVs or increased packaging and export of miRNA biomarkers into vesicles.

The observed increase in ASGR1+ EV miRNA expression is consistent with a large body of work describing the dysregulated miRNA profile in NAFLD liver and selective export into EVs. miRNAs have emerged as major players in the pathogenesis and progression of NAFLD, with altered hepatic expression of miR-122, -192, and -128-3p disrupting several facets of hepatic lipid metabolism, insulin sensitivity, and cholesterol-lipoprotein trafficking [29,35,47]. Prior studies have also emphasised the pathogenic consequences of vesicular miRNAs from hepatocytes in response to lipotoxic injury in NAFLD [13]. EV-derived miR-192 was recently reported to induce pro-inflammatory polarisation of liver macrophages [30] and EV miR-128-3p internalised by hepatic stellate cells led to marked fibrogenic activation [48]. Decreased cellular miR-122 abundance has been observed in conjunction with increased abundance in circulating EVs. This observation has been attributed to accelerated miR-122 export via the exosomal pathways resulting from metabolic and ER stress in hepatocytes [49,50]. Indeed, multiple reports [51–53] support the notion that miR-122 increases specifically in the circulating vesicle fraction in NAFLD, while other liver pathologies (e.g., drug-induced liver damage) are better characterised by changes in the protein-associated fraction [12,53]. Further studies are required to elucidate the intracellular source of miRNAs that are packaged into EVs and the specific mechanisms of export during NAFLD and normal physiology. Nonetheless, the present findings are promising with respect to increasing specificity by targeting analyses to liver-derived miRNA expression.

It is acknowledged that additional clinical data regarding the patient cohort would have been useful and that the inability to access these data is a limitation of the current study. Specifically, NAFL and NASH are hepatic manifestations of metabolic syndrome and are closely associated with multiple comorbidities including type 2 diabetes and obesity, which if unaccounted for, may confound biomarker screening. By way of example, while the miRNA markers evaluated here have previously been associated with NAFL and NASH [13], the current study is unable to definitively exclude that these markers are specific to the hepatic manifestations of the syndrome and not alternative comorbidities observed in this patient population. Additionally, it is acknowledged that, while the purity of ASGR1+ EVs in control EV preparations (Figure S3 and Table S1) was extensively

characterised, limitations regarding sample volume precluded comparable analyses in the NAFL and NASH samples. Future studies confirming the observations reported here will benefit from more extensive clinical data and the capacity to undertake additional characterisation of post immunoprecipitation samples.

To date, studies of cell-free miRNA biomarkers have dichotomised subjects to discriminate controls from subjects with either NAFL or NASH or simply pooled as NAFLD. As summarised in our recent review [13], ROC analysis has identified strong predictive performance of several miRNA markers quantified from total cell-free RNA [13]. Up to 7-fold increases in circulating miR-122 and -192 has been previously reported in NAFLD patients [54,55]; however, such significant dysregulation in total cfRNA was not observed in comparison to controls in this cohort. For a number of group pairings, however, ROC analysis produced similarly strong discrimination of cohorts, as seen previously [13]. However, in order to investigate the capacity for miRNA biomarkers from different sources (ASGR1+ EV, global EV, and total cfRNA), to predict an individual's disease status across control, NAFL, and NASH groups simultaneously, ordinal logistic regression was applied. With this more robust approach that incorporated the biological link of increased biomarker expression in a directional manner, ASGR1+ EVs consistently exhibited excellent diagnostic accuracy. For miR-122 and -192, statistically significant associations were achieved only by the analysis of liver-specific EV miRNA.

5. Conclusions

The findings presented here represent the first direct evidence supporting the hypothesis that tissue-specific isolation enhances predictive performance of EV-derived miRNA biomarkers. This study further provides the necessary foundational evidence demonstrating that liver-derived EVs represent a promising solution to current shortcomings with regard to the clinical management of NAFLD. Specifically, this study determined that refining the source from which circulating miR biomarkers are analysed enhanced their capacity to distinguish NAFLD patients from controls. While total cfRNA has long dominated the focus of this field, the belief that markers obtained from a particular blood compartment may better represent disease-associated changes has emerged with the promise of improved biomarker specificity and reproducibility. Here, we show that the selective isolation of liver-specific EVs by anti-ASGR1 immunoprecipitation has the potential to elucidate useful trends in miR expression, which may be applied to track NAFLD patients across the spectrum of clinical disease. This approach not only facilitates the use of biomarkers with ubiquitous expression in unrelated tissues, which may otherwise limit their utility, but also opens the possibility of discovering other highly disease-specific biomarkers, such as EV-derived proteins, from just the affected organ. Such tools can facilitate early diagnosis, identification of patients at greatest risk of progression, serial sampling, and longitudinal monitoring. Thus, the development of liver-EV biomarkers will improve patient management universally, with profound impacts on clinical practice, utilisation of healthcare resources, and advancement of therapeutics.

Supplementary Materials: The following are available online at https://www.mdpi.com/article/10.3390/biomedicines10010195/s1, Figure S1: Unedited TEM images, Figure S2: Total protein concentration in global EVs, Table S1: Particle concentration in global EV isolates, ASGR1 immunocapture, and non-captured samples, Figure S3: ASGR1 abundance in global EVs and anti-ASGR1 immunoprecipitation captured and non-captured portions, Table S2: Area under the receiver operator characteristic curve analysis, Figure S4: Receiver operator characteristic curve analysis.

Author Contributions: L.A.N., J.J. and A.R. designed the research. L.A.N. and Z.U. performed the research. L.A.N., Z.U., A.M.H. and A.R. analyzed the data. L.A.N. and A.R. wrote the manuscript. M.J.S., J.J. and A.R. revised the manuscript. A.R. supervised the work. A.R. acquired funding. All authors have read and agreed to the published version of the manuscript.

Funding: This research was funded by the National Health and Medical Research Council of Australia (grant ID 1158210). A.R and M.J.S were supported by Beat Cancer Fellowships from Cancer Council SA. Z.U. was supported by a Fellowship from Pfizer Worldwide Research and Development.

Institutional Review Board Statement: Not applicable as clinical samples were purchased from a biobank (Discovery Life Sciences, Huntsville, AL, USA).

Informed Consent Statement: Not applicable as clinical samples were purchased from a biobank (Discovery Life Sciences, Huntsville, AL, USA).

Data Availability Statement: The data that support the findings of this study are available from the corresponding author upon reasonable request.

Acknowledgments: The authors acknowledge the instruments, and scientific and technical assistance of Microscopy Australia at Adelaide Microscopy, The University of Adelaide, a facility that is funded by the university and by state and federal governments. The authors also acknowledge the instruments and technical assistance at Australian Wine Research Institute, Urrbrae, South Australia.

Conflicts of Interest: J.J. is an employee and stock holder of Pfizer Inc. A.R. and M.J.S. report grant funding from Pfizer Inc. All authors declare no conflicts of interest. The funders had no role in the design of the study; in the collection, analyses, or interpretation of data; in the writing of the manuscript; or in the decision to publish the results.

References

1. Garcia-Martinez, I.; Alen, R.; Rada, P.; Valverde, A.M. Insights into extracellular vesicles as biomarker of NAFLD pathogenesis. *Front. Med.* **2020**, *7*, 395. [CrossRef]
2. Suzuki, A.; Diehl, A.M. Nonalcoholic steatohepatitis. *Annu. Rev. Med.* **2017**, *68*, 85–98. [CrossRef] [PubMed]
3. Buzzetti, E.; Pinzani, M.; Tsochatzis, E.A. The multiple-hit pathogenesis of non-alcoholic fatty liver disease (NAFLD). *Metabolism* **2016**, *65*, 1038–1048. [CrossRef] [PubMed]
4. Ibrahim, S.H.; Hirsova, P.; Gores, G.J. Non-alcoholic steatohepatitis pathogenesis: Sublethal hepatocyte injury as a driver of liver inflammation. *Gut* **2018**, *67*, 963–972. [CrossRef] [PubMed]
5. Ando, Y.; Jou, J.H. Nonalcoholic fatty liver disease and recent guideline updates. *Clin. Liver Dis.* **2021**, *17*, 23–28. [CrossRef] [PubMed]
6. Younossi, Z.; Tacke, F.; Arrese, M.; Sharma, B.C.; Mostafa, I.; Bugianesi, E.; Wong, V.W.-S.; Yilmaz, Y.; George, J.; Fan, J.; et al. Global perspectives on nonalcoholic fatty liver disease and nonalcoholic steatohepatitis. *Hepatology* **2019**, *69*, 2672–2682. [CrossRef]
7. Simon, T.G.; Roelstraete, B.; Khalili, H.; Hagström, H.; Ludvigsson, J.F. Mortality in biopsy-confirmed nonalcoholic fatty liver disease: Results from a nationwide cohort. *Gut* **2020**, *70*, 1375–1382. [CrossRef]
8. Perumpail, B.J.; Khan, M.A.; Yoo, E.R.; Cholankeril, G.; Kim, D.; Ahmed, A. Clinical epidemiology and disease burden of nonalcoholic fatty liver disease. *World J. Gastroenterol.* **2017**, *23*, 8263–8276. [CrossRef]
9. Sumida, Y.; Nakajima, A.; Itoh, Y. Limitations of liver biopsy and non-invasive diagnostic tests for the diagnosis of nonalcoholic fatty liver disease/nonalcoholic steatohepatitis. *World J. Gastroenterol.* **2014**, *20*, 475–485. [CrossRef]
10. Hardy, T.; Oakley, F.; Anstee, Q.M.; Day, C.P. Nonalcoholic Fatty Liver Disease: Pathogenesis and Disease Spectrum. *Annu. Rev. Pathol. Mech. Dis.* **2016**, *11*, 451–496. [CrossRef]
11. Cusi, K.; Chang, Z.; Harrison, S.; Lomonaco, R.; Bril, F.; Orsak, B.; Ortiz-Lopez, C.; Hecht, J.; Feldstein, A.E.; Webb, A.; et al. Limited value of plasma cytokeratin-18 as a biomarker for NASH and fibrosis in patients with non-alcoholic fatty liver disease. *J. Hepatol.* **2014**, *60*, 167–174. [CrossRef] [PubMed]
12. Castoldi, M.; Kordes, C.; Sawitza, I.; Häussinger, D. Isolation and characterization of vesicular and non-vesicular microRNAs circulating in sera of partially hepatectomized rats. *Sci. Rep.* **2016**, *6*, 31869. [CrossRef] [PubMed]
13. Newman, L.A.; Sorich, M.J.; Rowland, A. Role of Extracellular Vesicles in the Pathophysiology, Diagnosis and Tracking of Non-Alcoholic Fatty Liver Disease. *J. Clin. Med.* **2020**, *9*, 2032. [CrossRef]
14. Dongiovanni, P.; Meroni, M.; Longo, M.; Fargion, S.; Fracanzani, A.L. miRNA Signature in NAFLD: A Turning Point for a Non-Invasive Diagnosis. *Int. J. Mol. Sci.* **2018**, *19*, 3966. [CrossRef]
15. Endzeliņš, E.; Berger, A.; Melne, V.; Bajo-Santos, C.; Soboļevska, K.; Ābols, A.; Rodriguez, M.; Šantare, D.; Rudņickiha, A.; Lietuvietis, V.; et al. Detection of circulating miRNAs: Comparative analysis of extracellular vesicle-incorporated miRNAs and cell-free miRNAs in whole plasma of prostate cancer patients. *BMC Cancer* **2017**, *17*, 730. [CrossRef]
16. Carpintero-Fernández, P.; Fafián-Labora, J.; O'Loghlen, A. Technical advances to study extracellular vesicles. *Front. Mol. Biosci.* **2017**, *4*, 00079. [CrossRef]
17. Newman, L.; Fahmy, A.; Sorich, M.; Best, O.; Rowland, A.; Useckaite, Z. Importance of between and within subject variability in extracellular vesicle abundance and cargo when performing biomarker analyses. *Cells* **2021**, *10*, 485. [CrossRef] [PubMed]

18. Rodrigues, D.; Rowland, A. From Endogenous Compounds as Biomarkers to Plasma-Derived Nanovesicles as Liquid Biopsy; Has the Golden Age of Translational Pharmacokinetics-Absorption, Distribution, Metabolism, Excretion-Drug–Drug Interaction Science Finally Arrived? *Clin. Pharmacol. Ther.* **2019**, *105*, 1407–1420. [CrossRef]
19. Kamal, N.N.S.B.N.M.; Shahidan, W.N.S. Non-exosomal and exosomal circulatory micrornas: Which are more valid as biomarkers? *Front. Pharmacol.* **2020**, *10*, 1500. [CrossRef]
20. Shah, R.; Patel, T.; Freedman, J.E. Circulating extracellular vesicles in human disease. *NEJM* **2018**, *379*, 958–966. [CrossRef]
21. Xin, S.; Zhan, Q.; Chen, X.; Xu, J.; Yu, Y. Efficacy of serum miRNA test as a non-invasive method to diagnose nonalcoholic steatohepatitis: A systematic review and meta-analysis. *BMC Gastroenterol.* **2020**, *20*, 186. [CrossRef]
22. Van Deun, J.; Mestdagh, P.; Agostinis, P.; Akay, Ö.; Anand, S.; Anckaert, J.; Martinez, Z.A.; Baetens, T.; Beghein, E.; Bertier, L.; et al. EV-TRACK: Transparent reporting and centralizing knowledge in extracellular vesicle research. *Nat. Methods* **2017**, *14*, 228–232. [PubMed]
23. Rodrigues, A.D.; van Dyk, M.; Sorich, M.J.; Fahmy, A.; Useckaite, Z.; Newman, L.A.; Kapetas, A.J.; Mounzer, R.; Wood, L.S.; Johnson, J.G.; et al. Exploring the use of serum-derived small extracellular vesicles as liquid biopsy to study the induction of hepatic cytochromes P450 and organic anion transporting polypeptides. *Clin. Pharmacol. Ther.* **2021**, *110*, 248–258. [CrossRef]
24. Kroh, E.M.; Parkin, R.K.; Mitchell, P.; Tewari, M. Analysis of circulating microRNA biomarkers in plasma and serum using quantitative reverse transcription-PCR (qRT-PCR). *Methods* **2010**, *50*, 298–301. [CrossRef] [PubMed]
25. Poel, D.; Buffart, T.E.; Oosterling-Jansen, J.; Verheul, H.M.W.; Voortman, J. Evaluation of several methodological challenges in circulating miRNA qPCR studies in patients with head and neck cancer. *Exp. Mol. Med.* **2018**, *50*, e454. [CrossRef]
26. Mateescu, B.; Kowal, E.J.K.; Van Balkom, B.W.M.; Bartel, S.; Bhattacharyya, S.N.; Buzás, E.I.; Buck, A.H.; de Candia, P.; Chow, F.W.; Das, S.; et al. Obstacles and opportunities in the functional analysis of extracellular vesicle RNA—An ISEV position paper. *J. Extracell. Vesicles* **2017**, *6*, 1286095. [CrossRef] [PubMed]
27. Marabita, F.; De Candia, P.; Torri, A.; Tegnér, J.; Abrignani, S.; Rossi, R.L. Normalization of circulating microRNA expression data obtained by quantitative real-time RT-PCR. *Briefings Bioinform.* **2016**, *17*, 204–212. [CrossRef]
28. Théry, C.; Witwer, K.W.; Aikawa, E.; Alcaraz, M.J.; Anderson, J.D.; Andriantsitohaina, R.; Antoniou, A.; Arab, T.; Archer, F.; Atkin-Smith, G.K.; et al. Minimal information for studies of extracellular vesicles 2018 (MISEV2018): A position statement of the International Society for Extracellular Vesicles and update of the MISEV2014 guidelines. *J. Extracell. Vesicles* **2018**, *7*, 1535750. [CrossRef]
29. Gjorgjieva, M.; Sobolewski, C.; Dolicka, D.; De Sousa, M.; Foti, M. miRNAs and NAFLD: From pathophysiology to therapy. *Gut* **2019**, *68*, 2065–2079. [CrossRef] [PubMed]
30. Liu, X.-L.; Pan, Q.; Cao, H.-X.; Xin, F.-Z.; Zhao, Z.-H.; Yang, R.-X.; Zeng, J.; Zhou, H.; Fan, J.-G. Lipotoxic hepatocyte-derived exosomal MicroRNA 192-5p activates macrophages through Rictor/Akt/Forkhead box transcription factor O1 signaling in nonalcoholic fatty liver disease. *Hepatology* **2020**, *72*, 454–469. [CrossRef]
31. Noetel, A.; Elfimova, N.; Altmüller, J.; Becker, C.; Becker, D.; Lahr, W.; Nürnberg, P.; Wasmuth, H.; Teufel, A.; Büttner, R.; et al. Next generation sequencing of the Ago2 interacting transcriptome identified chemokine family members as novel targets of neuronal microRNAs in hepatic stellate cells. *J. Hepatol.* **2013**, *58*, 335–341. [CrossRef]
32. Chen, C.; Deng, Y.; Hu, X.; Ren, H.; Zhu, J.; Fu, S.; Xie, J.; Peng, Y. miR-128-3p regulates 3T3-L1 adipogenesis and lipolysis by targeting Pparg and Sertad2. *J. Physiol. Biochem.* **2018**, *74*, 381–393. [CrossRef]
33. Pan, J.; Zhou, C.; Zhao, X.; He, J.; Tian, H.; Shen, W.; Han, Y.; Chen, J.; Fang, S.; Meng, X.; et al. A two-miRNA signature (miR-33a-5p and miR-128-3p) in whole blood as potential biomarker for early diagnosis of lung cancer. *Sci. Rep.* **2018**, *8*, 16699. [CrossRef]
34. Liu, T.; Zhang, X.; Du, L.; Wang, Y.; Liu, X.; Tian, H.; Wang, L.; Li, P.; Zhao, Y.; Duan, W.; et al. Exosome-transmitted miR-128-3p increase chemosensitivity of oxaliplatin-resistant colorectal cancer. *Mol. Cancer* **2019**, *18*, 43. [CrossRef] [PubMed]
35. Zhang, Y.-J.; Hu, Y.; Li, J.; Chi, Y.-J.; Jiang, W.-W.; Zhang, F.; Liu, Y.-L. Roles of microRNAs in immunopathogenesis of non-alcoholic fatty liver disease revealed by integrated analysis of microRNA and mRNA expression profiles. *Hepatobiliary Pancreat. Dis. Int.* **2017**, *16*, 65–79. [CrossRef]
36. Huang, C.-Y.; Huang, X.-P.; Zhu, J.-Y.; Chen, Z.-G.; Li, X.-J.; Zhang, X.-H.; Huang, S.; He, J.-B.; Lian, F.; Zhao, Y.-N.; et al. miR-128-3p suppresses hepatocellular carcinoma proliferation by regulating PIK3R1 and is correlated with the prognosis of HCC patients. *Oncol. Rep.* **2015**, *33*, 2889–2898. [CrossRef] [PubMed]
37. Makarova, J.; Turchinovich, A.; Shkurnikov, M.; Tonevitsky, A. Extracellular miRNAs and Cell–Cell Communication: Problems and prospects. *Trends Biochem. Sci.* **2021**, *46*, 640–651. [CrossRef]
38. Van Eijndhoven, M.A.J.; Zijlstra, J.M.; Groenewegen, N.J.; Drees, E.E.E.; Van Niele, S.; Baglio, S.R.; Koppers-Lalic, D.; Van Der Voorn, H.; Libregts, S.F.; Wauben, M.H.; et al. Plasma vesicle miRNAs for therapy response monitoring in Hodgkin lymphoma patients. *JCI Insight* **2016**, *1*, e89631. [CrossRef]
39. Jiang, H.; Qian, Y.; Shen, Z.; Liu, Y.; He, Y.; Gao, R.; Shen, M.; Chen, S.; Fu, Q.; Yang, T. Circulating microRNA-135a-3p in serum extracellular vesicles as a potential biological marker of non-alcoholic fatty liver disease. *Mol. Med. Rep.* **2021**, *24*, 12137. [CrossRef]
40. Mustapic, M.; Eitan, E.; Werner, J.K.; Berkowitz, S.T.; Lazaropoulos, M.P.; Tran, J.; Goetzl, E.J.; Kapogiannis, D. Plasma Extracellular Vesicles Enriched for Neuronal Origin: A Potential Window into Brain Pathologic Processes. *Front. Neurosci.* **2017**, *11*, 278. [CrossRef]

41. Fiandaca, M.S.; Kapogiannis, D.; Mapstone, M.; Boxer, A.; Eitan, E.; Schwartz, J.B.; Abner, E.L.; Petersen, R.C.; Federoff, H.J.; Miller, B.L.; et al. Identification of preclinical Alzheimer's disease by a profile of pathogenic proteins in neurally derived blood exosomes: A case-control study. *Alzheimers Dement.* **2015**, *11*, 600–607. [CrossRef] [PubMed]
42. Shi, M.; Liu, C.; Cook, T.J.; Bullock, K.M.; Zhao, Y.; Ginghina, C.; Li, Y.; Aro, P.; Dator, R.; He, C.; et al. Plasma exosomal α-synuclein is likely CNS-derived and increased in Parkinson's disease. *Acta Neuropathol.* **2014**, *128*, 639–650. [CrossRef] [PubMed]
43. Goetzl, E.J.; Kapogiannis, D.; Schwartz, J.B.; Lobach, I.V.; Goetzl, L.; Abner, E.L.; Jicha, G.A.; Karydas, A.M.; Boxer, A.; Miller, B.L. Decreased synaptic proteins in neuronal exosomes of frontotemporal dementia and Alzheimer's disease. *FASEB J.* **2016**, *30*, 4141–4148. [CrossRef]
44. Goetzl, E.J.; Schwartz, J.B.; Mustapic, M.; Lobach, I.V.; Daneman, R.; Abner, E.L.; Jicha, G.A. Altered cargo proteins of human plasma endothelial cell–derived exosomes in atherosclerotic cerebrovascular disease. *FASEB J.* **2017**, *31*, 3689–3694. [CrossRef]
45. Gotanda, K.; Hirota, T.; Saito, J.; Fukae, M.; Egashira, Y.; Izumi, N.; Deguchi, M.; Kimura, M.; Matsuki, S.; Irie, S.; et al. Circulating intestine-derived exosomal miR-328 in plasma, a possible biomarker for estimating BCRP function in the human intestines. *Sci. Rep.* **2016**, *6*, 32299. [CrossRef] [PubMed]
46. Povero, D.; Yamashita, H.; Ren, W.; Subramanian, M.G.; Myers, R.P.; Eguchi, A.; Simonetto, D.A.; Goodman, Z.D.; Harrison, S.A.; Sanyal, A.J.; et al. Characterization and proteome of circulating extracellular vesicles as potential biomarkers for NASH. *Hepatol. Commun.* **2020**, *4*, 1263–1278. [CrossRef] [PubMed]
47. Wagschal, A.; Najafi-Shoushtari, S.H.; Wang, L.; Goedeke, L.; Sinha, S.; Delemos, A.S.; Black, J.C.; Ramírez, C.; Li, Y.; Tewhey, R.; et al. Genome-wide identification of microRNAs regulating cholesterol and triglyceride homeostasis. *Nat. Med.* **2015**, *21*, 1290–1297. [CrossRef] [PubMed]
48. Povero, D.; Panera, N.; Eguchi, A.; Johnson, C.D.; Papouchado, B.G.; de Araujo Horcel, L.; Pinatel, E.M.; Alisi, A.; Nobili, V.; Feldstein, A.E. Lipid-induced hepatocyte-derived extracellular vesicles regulate hepatic stellate cells via MicroRNA Targeting Peroxisome Proliferator-Activated Receptor-γ. *Cell. Mol. Gastroenterol. Hepatol.* **2015**, *1*, 646–663. [CrossRef] [PubMed]
49. Mukherjee, K.; Ghoshal, B.; Ghosh, S.; Chakrabarty, Y.; Shwetha, S.; Das, S.; Bhattacharyya, S.N. Reversible HuR-micro RNA binding controls extracellular export of miR-122 and augments stress response. *EMBO Rep.* **2016**, *17*, 1184–1203. [CrossRef]
50. Bhattacharyya, S.N.; Habermacher, R.; Martine, U.; Closs, E.; Filipowicz, W. Relief of microRNA-Mediated translational repression in human cells subjected to stress. *Cell* **2006**, *125*, 1111–1124. [CrossRef]
51. Povero, D.; Eguchi, A.; Li, H.; Johnson, C.D.; Papouchado, B.G.; Wree, A.; Messer, K.; Feldstein, A.E. Circulating extracellular vesicles with specific proteome and liver micrornas are potential biomarkers for liver injury in experimental fatty liver disease. *PLoS ONE* **2014**, *9*, e113651. [CrossRef]
52. Pirola, C.J.; Fernandez Gianotti, T.; Castano, G.O.; Mallardi, P.; San Martino, J.; Mora Gonzalez Lopez Ledesma, M.; Flichman, D.; Mirshahi, F.; Sanyal, A.J.; Sookoian, S. Circulating microRNA signature in non-alcoholic fatty liver disease: From serum non-coding RNAs to liver histology and disease pathogenesis. *Gut* **2015**, *64*, 800–812. [CrossRef] [PubMed]
53. Bala, S.; Petrasek, J.; Mundkur, S.; Catalano, D.; Levin, I.; Ward, J.; Alao, H.; Kodys, K.; Szabo, G. Circulating microRNAs in exosomes indicate hepatocyte injury and inflammation in alcoholic, drug-induced, and inflammatory liver diseases. *Hepatology* **2012**, *56*, 1946–1957. [CrossRef] [PubMed]
54. Cermelli, S.; Ruggieri, A.; Marrero, J.A.; Ioannou, G.N.; Beretta, L. Circulating MicroRNAs in patients with chronic hepatitis C and non-alcoholic fatty liver disease. *PLoS ONE* **2011**, *6*, e23937. [CrossRef]
55. Liu, X.-L.; Pan, Q.; Zhang, R.-N.; Shen, F.; Yan, S.-Y.; Sun, C.; Xu, Z.-J.; Chen, Y.-W.; Fan, J.-G. Disease-specific miR-34a as diagnostic marker of non-alcoholic steatohepatitis in a Chinese population. *World J. Gastroenterol.* **2016**, *22*, 9844–9852. [CrossRef] [PubMed]

Appendix 5

Book chapter published in Methods in Molecular Biology, 2023.

Chapter 20

Analysis of Extracellular Vesicle and Contaminant Markers in Blood Derivatives Using Multiple Reaction Monitoring

Lauren A. Newman, Zivile Useckaite, Ting Wu, Michael J. Sorich, and Andrew Rowland

Abstract

Extracellular vesicles (EVs) are naturally occurring membranous particles that can be isolated from blood and other biofluids. EVs have drawn considerable attention for their potential as a minimally invasive biomarker source for a range of conditions, based on tissue-specific expression of proteins and other molecular information. To promote robust characterization of EV isolates, the International Society for Extracellular Vesicles (ISEV) has established consensus minimal requirements for the study of extracellular vesicles (MISEV) reporting guidelines. A core element of MISEV guidance is the recommendation for the analysis of protein markers in samples, including positive EV-associated markers and negative contaminant markers based on commonly co-isolated components of the sample matrix. Furthermore, there is growing interest in circulating EVs enriched for tissue-specific origin, and in this context, the degree of nontarget EV "contamination" (e.g., EVs derived from blood cells) may inform assessment of sample purity. The increasing application of EVs as a liquid biopsy for clinical applications requires a high-throughput multiplexed approach that enables analysis of protein markers from small volumes of starting material, ideally utilizing the same platform for measuring biomarkers of interest. To this end, targeted liquid chromatography mass spectrometry using multiple reaction monitoring (LC-MRM-MS) is a key platform for the quantitative assessment of target proteins within EV samples. Here we describe a protocol for the isolation of EVs from blood and parallel analytical methods targeting general EV markers and blood cell-derived EV markers, along with guidance of best practice for sample collection and processing.

Key words Extracellular vesicles, Protein markers, Liquid chromatography tandem mass spectrometry, Multiple reaction monitoring, EV characterization, Serum, Plasma

1 Introduction

Extracellular vesicles (EVs) are nanosized membrane-bound particles released by cells and can be found in a variety of biological fluids, including blood. Different populations of EVs exist, as defined by their mode of biogenesis within a cell. However, most

David W. Greening and Richard J. Simpson (eds.), *Serum/Plasma Proteomics: Methods and Protocols*, Methods in Molecular Biology, vol. 2628, https://doi.org/10.1007/978-1-0716-2978-9_20,

isolation methods recover a heterogenous population of vesicles, including exosomes (50–150 nm diameter originating from the endosomal pathway) and microvesicles (up to 1000 nm and shed directly from the plasma membrane) [1]. EVs containing assorted profiles of proteins, lipids, or nucleic acids represent a promising new source of biomarkers, such as for several types of cancer [2], immunological disorders [3, 4], neuronal pathologies [5–7], and liver disease [8, 9], and can be assessed in patients in a minimally invasive manner. However, the full potential for clinical translation of EV biomarkers may only be realized in the context of clearly defined and reproducible protocols for EV sample collection and analyses. To this end, recommendations for experimental design and reporting described in the minimal requirements for the study of extracellular vesicles (MISEV) [10] provide a framework to improve rigor and reproducibility in EV research. A variety of techniques are available for the isolation of EVs from biofluids, such as those employing resin- or polymer-based precipitation, size exclusion chromatography (SEC), membrane affinity chromatography, ultracentrifugation, density separation, and immunoaffinity capture [11]. Each differs in terms of vesicle recovery and purity and, since no one method is preferred for all applications, the choice must be considered on the basis of compatibility with downstream analyses. In line with MISEV recommendations, a key assessment of EV recovery and overall sample purity can be achieved by characterizing the abundance of protein markers expected in EV samples and those considered contaminants. Positive EV markers include plasma membrane or cytosolic proteins that are incorporated in EVs during biogenesis and release from cells. Negative EV markers comprise matrix-associated contaminants co-isolated with EVs and tend to be highly abundant in the starting material. Further, proteins expressed in intracellular compartments not involved in EV biogenesis, such as nucleus or endoplasmic reticulum, can be included to denote cellular debris and other non-vesicle particles. These criteria are reflected in the protocol described below, in that protein markers selected to address the recommendations for protein characterization include cluster of differentiation (CD) 81 and CD9, tumor susceptibility gene (TSG)101, albumin (ALB), and calnexin (CANX).

Beyond general EV markers, specific protein expression may be assessed to determine the likely origin of vesicles. Cell surface markers of the originating cell are incorporated into the membrane of released EVs, thereby potentially enabling tracking of tissue origin. Using most techniques to isolate EVs from blood will result in a "global" population of vesicles with diverse cellular or tissue origins. A large proportion of these EVs will be derived from platelets, erythrocytes, other blood cells such as leukocytes, and blood-adjacent endothelial cells [12, 13]. When seeking to track

protein or RNA expression changes in a specific tissue (e.g., liver, brain, gut, skeletal muscle), isolating the subset of circulating EVs originating from a specific tissue of interest (e.g., using immunoprecipitation (IP) against tissue-specific cell surface markers) may substantially improve the performance of EV biomarkers [8, 14, 15]. In this regard, blood cell-derived EVs may suitably be considered contaminating vesicles in tissue-specific EV samples isolated by IP. Accordingly, the protocol below also describes an analytical method to detect platelet- and erythrocyte- derived proteins (CD41 and CD233, respectively). The two analytical methods may be used individually or in combination to address specific research questions. In particular, with respect to purity, contamination markers may be considered in two categories:

1. Matrix-associated contamination, such as the highly abundant albumin protein co-isolated from serum or plasma.
2. Vesicle contamination, i.e., EVs not derived from an organ or tissue of interest.

As such, the blood cell-derived EV marker method may be applied to determine the degree of "contaminating" blood cell-derived vesicles and the efficacy of their removal from a tissue-enriched preparation.

Liquid chromatography tandem mass spectrometry (LC-MS/MS) using multiple reaction monitoring (MRM) is considered the gold standard for quantitative analysis of target proteins in complex samples. The technique involves the detection of proteotypic peptides as surrogates for the proteins of interest, by a mass spectrometer based on specific fragmentation patterns, known as transitions [16]. Absolute quantification may also be achieved in this way by adding heavy-labeled standard peptides corresponding to the endogenous analytes and comparing response to a calibration curve. As a highly sensitive, quantitative, and high-throughput technique, targeted LC-MRM-MS is an ideal platform to characterize EVs based on several proteins in a small amount of sample. This is particularly advantageous when limited volumes of patient blood are available to perform analyses of both MISEV recommended controls and biomarkers of interest [17].

Here we describe a step-by-step protocol for the setup of two LC-MRM-MS-based methods for the analysis of EV proteins in isolates derived from blood serum or plasma. We provide best practice guidance for blood collection and processing and EV isolation, such that the methods may be optimally applied for the characterization of EVs isolated from clinical samples.

2 Materials

2.1 Blood Serum/Plasma Collection

1. VACUETTE® Z Serum Sep Clot Activator tubes (Greiner Bio-One).
2. VACUETTE® K3E K_3EDTA tubes (Greiner Bio-One).
3. Blood Collection Set + Luer Adapter; 21-gauge needle (Greiner Bio-One).
4. Tourniquet.
5. Skin cleansing swabs.
6. Refrigerated centrifuge (<10 °C).
7. Protein LoBind tubes, 2 mL (Eppendorf).

2.2 Isolation of Extracellular Vesicles

1. Protein LoBind tubes, 5 mL (Eppendorf).
2. 10 mL conical bottom centrifuge tubes.
3. VacuCap® 60 Vacuum Filtration Devices—0.2 μm, 60 mm (Pall Corporation).
4. Elution buffer: 1 × phosphate-buffered saline (PBS, Ca/Mg free, pH 7.4, Gibco), 0.2 μm-filtered.
5. qEV Original Size Exclusion Columns (35 or 70 nm, Izon Science). Columns should be cleaned according to the manufacturer's instructions and stored in 20% ethanol at 4–8 °C after use.
6. Amicon Ultra-4 Centrifugal Filter Unit (30 kDa) concentrating device (Merck Millipore).
7. Refrigerated centrifuge (<10 °C) equipped with swing-out rotor.
8. ExoQuick™ Exosome Precipitation Solution (System Biosciences).

2.3 Isolation of Platelets and Red Blood Cells (RBCs) from Whole Blood

1. 50 mL centrifuge tubes.
2. 10 mL centrifuge tubes.
3. Lymphoprep™ density gradient medium: density of 1.077 g/mL (STEMCELL Technologies).
4. Disposable plastic transfer pipettes.
5. Heraeus Multifuge 3 S-R, fitted with swing-out 4 place rotor (centrifuge must have option to remove braking for separation of layers).

2.4 EV Protein Quantification, Extraction, and Digestion

1. EZQ™ Protein Quantitation Kit (Invitrogen).
2. Rinse buffer: 10% (v/v) methanol, 7% (v/v) acetic acid in high-performance liquid chromatography-grade water.

3. Gel DOC™ EZ Imaging System (purple UV sample tray) with Image Lab™ Software (Bio-Rad).
4. Benchtop centrifuge.
5. Plastic staining tray.
6. Benchtop vortex.
7. Ammonium bicarbonate solution (pH 7.72): dissolve weighed ammonium bicarbonate in Milli-Q water to a final concentration of 50 mM and adjust pH if necessary. Can be stored for several months.
8. Dithiothreitol (DTT) solution: dissolve 3.1 mg DTT in 100 µL Milli-Q water to a final concentration of 200 mM. Prepare fresh prior to use.
9. Iodoacetamide (IAA) solution: dissolve 7.4 mg iodoacetamide in 100 µL Milli-Q water to a final concentration of 400 mM. Prepare fresh immediately prior to use and protect from light.
10. Trypsin gold, mass spectrometry grade (Promega): reconstitute 100 µg of trypsin in 100 µL 50 mM acetic acid to a final concentration of 1 µg/µL. Aliquot reconstituted trypsin into Protein LoBind tubes. Repeated freeze-thaw cycles ($\leq$5) reduce enzymatic activity and should be avoided.
11. 10% (v/v) formic acid in Milli-Q water. Can be stored for several months.
12. Eppendorf MixMate with 1.5/2.0 mL tube rack.
13. Amber glass vials (2.0 mL, Agilent).
14. 250 µL pulled point conical glass inserts (Agilent).

2.5 Targeted Peptide Analysis by LC-MRM-MS

1. Custom stable isotope labeled (SIL) synthetic peptides, isotopic purity >99% (Vivitide). Reconstitute peptides in 25–50% acetonitrile in water with 0.1% (v/v) formic acid. Aliquot into Protein LoBind tubes, vacuum dry, and store at −80 °C.
2. Vacuum centrifuge.
3. AdvanceBio Peptide Mapping C18 column (2.1 × 100 mm, 2.7 µm, Agilent) fitted with an AdvanceBio Peptide Map Guard column (2.1 × 5 mm, 2.7 µm, Agilent).
4. Agilent 1290 Infinity II ultrahigh-performance liquid chromatography (UPLC) instrument.
5. Agilent 6495 triple quadruple (QQQ) mass spectrometer.
6. Solvent A: 0.1% (v/v) formic acid in Milli-Q water. Solvent B: 0.1% (v/v) formic acid in acetonitrile, all LC-MS grade.

3 Methods

3.1 Collection and Storage of Blood Serum/Plasma

Pre-analytical factors have a major impact on the recovery and purity of EV preparations. The MISEV2018 guidelines [10] contain generic best practice guidance for EV studies, while we recently distilled elements of this guidance pertaining to the analysis of EV-derived biomarkers in blood more specifically [11]. Importantly, differences in EV markers may be attributed to the collection of blood samples from donors at different times of the day or based on prandial state [14]. For the detection of low abundance EV proteins in the blood, various donor-related factors that influence EV recovery should be considered.

The method was developed and comprehensively validated in serum-derived EVs and was confirmed to reliably detect EV markers in plasma-derived samples as well [17]. Differences in EV abundance between serum and plasma may be observed due to platelet activation and vesiculation during in vitro clot formation in serum tubes post-collection. Artifactual EV release can be reduced with careful collection and handling procedures, for example, using a large diameter (21-gauge) needle and transporting tubes upright and with minimal agitation.

1. Collect whole blood by venepuncture using a using a 21-gauge Vacuette Safety Blood Collection sealed vacuum device into Z Serum Sep Clot Activator and EDTA tubes (*see* **Note 1**).
2. Discard 5 mL of blood before sample collection.
3. Mix tubes by inversion six to eight times. For serum, store vertically at room temp for 30 min to allow clotting (*see* **Note 2**). Process EDTA tubes immediately.
4. Separate blood serum or plasma (EDTA) in a refrigerated centrifuge (10 °C) at 2500 g for 15 min. Repeat centrifugation once more for 15 min (*see* **Note 3**).
5. Carefully extract supernatant, leaving 0.5–1 cm to prevent contamination with buffy coat or clot.
6. Aliquot appropriate volume required for EV isolation into 2 mL Protein LoBind tubes and store at −80 °C. Avoid freeze-thaw cycles.

3.2 Isolation of Extracellular Vesicles

EV isolation from blood plasma or serum can be achieved using a variety of strategies. Importantly, the choice of isolation method is based on the competing imperatives of vesicle recovery and degree of purity. We have found the use of size exclusion chromatography, in particular qEV70 which enriches samples for vesicles 70–1000 nm in diameter, to be favorable for our purposes. EV markers and other biomarkers of interest can be detected reproducibly in these samples, while co-isolation of matrix-associated

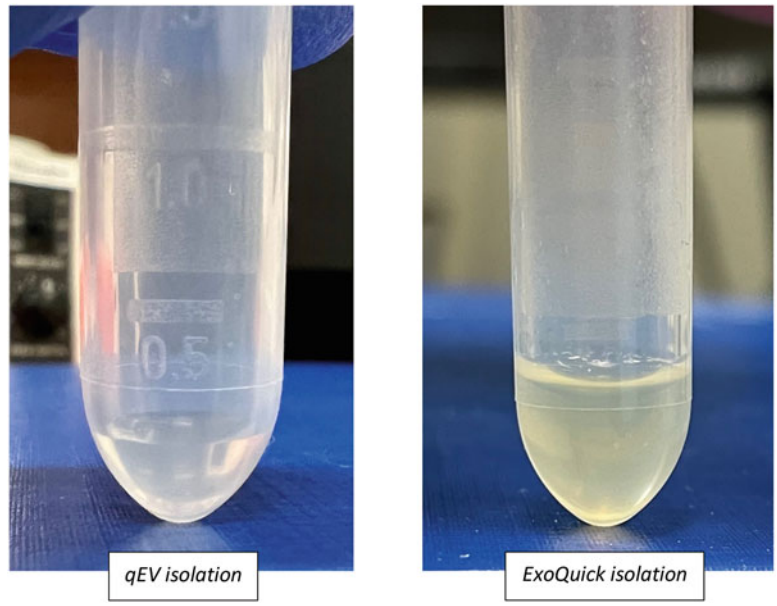

Fig. 1 Images of samples containing extracellular vesicles isolated by qEV size exclusion chromatography (left) or ExoQuick precipitation (right)

contaminants, especially albumin, is minimized. The EV marker analytical method has been validated on samples isolated using three commercial products—qEV70, qEV35, and ExoQuick—without modification to manufacturer instructions [17]. While there is no optimal EV isolation method and the choice may vary according to the scientific question and compatibility with downstream applications, it is important to note that interfering compounds in lower purity EV preparations may affect the detection of low abundance peptides. In the case of high recovery, low purity methods such as ExoQuick, dilute samples using distilled water prior to protein digestion. However, it should also be noted that dilution of samples is likely to compromise detection of low abundance proteins and proteins that are only expressed in specific subpopulations (e.g., liver-derived EVs). In Fig. 1, the low purity of ExoQuick isolations is apparent by the yellowy color, indicating high levels of soluble protein contamination, especially albumin. In contrast, qEV isolates are clear and free of particulate matter.

SEC methods result in high elution volumes and several EV-containing eluate fractions must be pooled and concentrated. Amicon filters can be used in accordance with manufacturer instructions to concentrate samples such that 100 μL of EVs represent 500 μL of starting material (plasma/serum). Fresh samples are preferable for peptide analysis, but if this is not practical, plasma/serum and isolated EVs can be stored at −80 °C (*see* **Note 4**).

3.3 Isolation of Platelet and Red Blood Cells from Whole Blood

The analytical method for blood cell-derived markers (CD41 and CD233) was developed using positive controls that were generated by isolating platelets and RBCs from whole blood. Identities of endogenous peptides in blood-derived EVs were then verified against positive controls based on relative ion abundance and retention time.

1. Collect 10 mL of blood by venepuncture into EDTA plasma vacutainer and immediately transfer to 50 mL tube using a transfer pipette.
2. Carefully overlay 10 mL of blood on 10 mL of Lymphoprep in a 50 mL tube (*see* **Note 5**).
3. Carefully transfer tube to centrifuge and spin at 750 g at 20 °C with no brake applied.
4. Following centrifugation, observe separation of whole blood in distinct layers of platelet-rich plasma, buffy coat, Lymphoprep, and RBCs (*see* Fig. 2).
5. Using a transfer pipette, sequentially remove plasma and buffy coat layers each into separate 10 mL tubes.
6. Discard Lymphoprep layer.
7. Collect RBCs into 2 mL Eppendorf Protein LoBind tube using a transfer pipette.
8. Fill the tube containing buffy coat layer to the rim with PBS and centrifuge at 500 g for 5 min at 4 °C, with braking applied.
9. Discard supernatant and resuspend pellet in 10 mL of PBS.

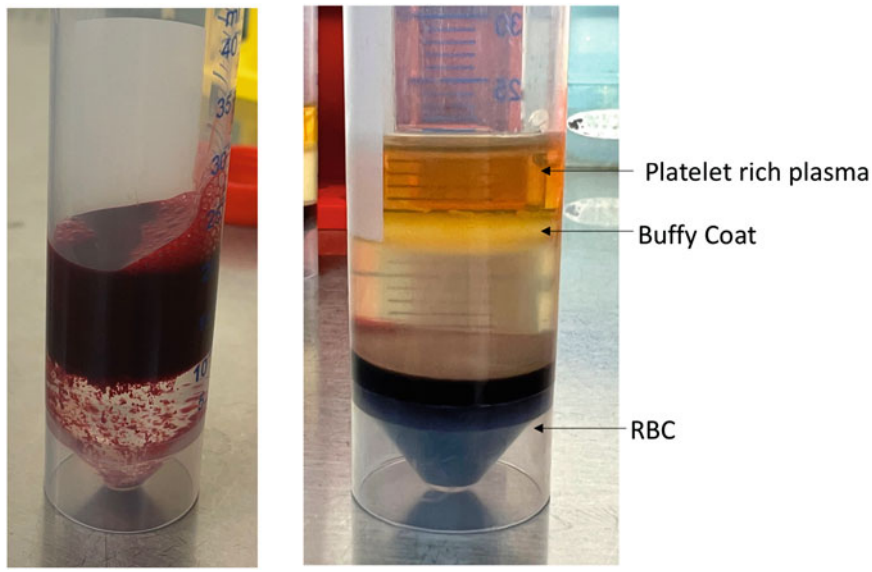

Fig. 2 Layering of whole blood over Lymphoprep and separation into distinct layers—platelet-rich plasma, buffy coat, and red blood cells (RBCs)

10. Repeat centrifugation (500 g for 5 min, 4 °C) and then discard supernatant and resuspend buffy coat pellet in 150 µL of PBS.
11. Centrifuge plasma at 2000 g for 5 min at 10 °C with braking applied. Observe platelet sedimentation as a white pellet at the bottom of the tube.
12. Remove supernatant (plasma) and resuspend in 100 µL of PBS (*see* **Note 6**).
13. Digest 200 µg of protein from platelet and RBC layers as positive controls for the detection of blood cell-derived markers.

3.4 Protein Digestion

1. Aliquot 100 µL of EV samples (~1 µg/µL) into 2 mL Eppendorf Protein LoBind tubes (*see* **Notes 7** and **8**). If required, dilute a suitable volume of sample up to 100 µL. Use distilled water to decrease the formation of salt adducts in mass spectrometer.
2. To lyse EVs, perform three freeze-thaw cycles by placing samples in a –80 °C freezer for at least 5 min followed by 37 °C water bath for at least 1 min, checking that samples are fully frozen/thawed before removing.
3. Vortex samples at 1400 rpm for 10 min at room temp using an Eppendorf MixMate.
4. To reduce disulfide bonds, add 10 µL of DTT (200 mM) and 50 µL ammonium bicarbonate (pH 7.72) and incubate samples on a heat block at 60 °C for 90 min.
5. Perform this step in the dark. Allow samples to cool to room temp (~10 min), then add 10 µL IAA (400 mM), and incubate in a shaking water bath at 37 °C for 60 min to alkylate free cysteine residues.
6. Add trypsin to samples in a ratio of 1:40 (w/w, enzyme to protein), and vortex briefly (5 s) at maximum speed using a benchtop vortex.
7. Incubate samples in a shaking water bath at 37 °C overnight (~17 h).
8. Add 20 µL formic acid (10% v/v) to samples and vortex briefly (5 s) at maximum speed using a benchtop vortex.
9. Incubate at 4 °C for 10 min, then transfer samples to refrigerated centrifuge, and spin at 16,000 g for 10 min at 4 °C.
10. Carefully remove 100 µL of clear supernatant from each tube and transfer to glass autosampler vials fitted with 250 µL pulled-point glass inserts (*see* **Note 9**). The digested protein samples can be analyzed by LC-MRM-MS immediately or stored at −20 °C.

3.5 SIL Peptides

1. Order custom SIL peptides for quantitative LC-MRM-MS assays (*see* **Note 10**).
2. Resuspend each SIL peptide in 25–50% acetonitrile with 0.1% formic acid in water and aliquot master stocks into 2 mL Protein LoBind tubes.
3. Use a vacuum centrifuge to dry aliquots and store at −80 °C (*see* **Note 11**).
4. Prepare a standard cocktail containing all SIL peptides at 10 × desired final concentration upon spiking of EV samples (*see* **Note 12**).
5. Spike the SIL cocktail into digested EV protein samples (*see* **Note 13**).

3.6 Analytical Method

The analytical method described here was set up and optimized on an Agilent 6495 QQQ mass spectrometer. Therefore, it is ideally reproduced and performed on a QQQ mass spectrometer; however, it could be applied on other instruments providing specific setup and optimization is performed.

Two analytical methods are described here. The general EV marker assay is designed to characterize EV samples based on positive (CD81, CD9, TSG101) and negative (ALB and CANX) marker proteins, for the purpose of assessing vesicle recovery and purity or for normalizing measurements of protein biomarkers against generic vesicle markers. The blood cell-derived marker assay includes peptides for specific platelet- and erythrocyte-derived proteins (CD41 and CD233, respectively) and may be useful for assessing vesicle contamination in global EVs and post tissue-specific EV enrichment.

General EV Marker Assay

1. Keep samples in the autosampler maintained at 4 °C. Set injection volume to 5 μL for analysis.
2. With a flow rate of 0.2 mL/min and column compartment maintained at 30 °C, set up chromatography gradient according to Table 1.
3. Divide acquisition into time segments according to Table 2 and set stop time to 48 min.
4. With the instrument in MRM mode, set up the acquisition of transitions for light (endogenous) and heavy (SIL) peptides according to Table 3 (*see* **Notes 14** and **15**).
5. Define source parameters according to Table 4 (*see* **Note 16**).
6. For each analyte, determine the limit of detection (LOD) based on 3:1 signal-to-noise ratio and lower limit of quantification (LLOQ) based on 5× LOD (*see* **Note 17**).

Table 1
Gradient setup for general EV marker analytical method chromatography

Time (min)	Mobile phase A (%)	Mobile phase B (%)
0	97	3
3	97	3
33	70	30
38	50	50
43	50	50
44	97	3

Mobile phase A consists of 0.1% formic acid in water. Mobile phase B consists of 0.1% formic acid in 25% acetonitrile in water

Table 2
Setup of acquisition time segments for general EV marker analytical method

Segment	Start time (min)	Ion mode	Delta EMV
T1	0	ESI+	300
T2	22	ESI+	300
T3	26	ESI+	300
T4	30	ESI+	300

7. Prepare a standard curve using SIL peptides spiked in EV matrix and analyze alongside samples for quantification.

Blood Cell-Derived Marker Assay

1. Keep samples in the autosampler maintained at 4 °C. Set injection volume to 5 μL for analysis.
2. With a flow rate of 0.2 mL/min and column compartment maintained at 30 °C, set up chromatography gradient according to Table 5.
3. Divide acquisition into time segments according to Table 6 and set stop time to 18 min.
4. With the instrument in MRM mode, set up the acquisition of transitions for light (endogenous) peptides according to Table 7 (*see* **Notes 14** and **15**).
5. Define source parameters according to Table 8 (*see* **Note 16**).
6. Determine the limit of detection (LOD) for each peptide based on 3:1 signal-to-noise ratio (*see* **Note 17**).

Table 3
Setup of transitions for general EV marker analytical method

Compound group	Compound name	Precursor ion	Product ion	RT (min)	Fragmentor	CE	CAV	Polarity	Dwell time (ms)
ALB	ALB_light_quant	575.3111	937.4625	21.0	380	18.8	5	Positive	50
	ALB_light_qual1	575.3111	694.3770	21.0	380	18.8	5	Positive	50
	ALB_light_qual2	575.3111	595.3086	21.0	380	18.8	5	Positive	50
	ALB_heavy_quant	579.3182	945.4767	21.0	380	18.8	5	Positive	50
	ALB_heavy_qual1	579.3182	702.3912	21.0	380	18.8	5	Positive	50
	ALB_heavy_qual2	579.3182	603.3228	21.0	380	18.8	5	Positive	50
CD81	CD81_light_quant	751.6855	961.4221	24.2	380	17.3	3	Positive	100
	CD81_light_qual1	751.6855	862.3537	24.2	380	17.3	3	Positive	100
	CD81_light_qual2	751.6855	1060.4905	24.2	380	17.3	3	Positive	50
	CD81_heavy_quant	754.3569	969.4363	24.2	380	17.3	3	Positive	100
	CD81_heavy_qual1	754.3569	870.3679	24.2	380	17.3	3	Positive	100
	CD81_heavy_qual2	754.3569	1068.5047	24.2	380	17.3	3	Positive	50
CD9	CD9_light_quant	526.2871	837.4716	24.7	380	22.3	3	Positive	100
	CD9_light_qual1	526.2871	724.3876	24.7	380	22.3	3	Positive	100
	CD9_light_qual2	526.2871	595.3450	24.7	380	22.3	3	Positive	50
	CD9_heavy_quant	530.2942	846.4858	24.7	380	22.3	3	Positive	100
	CD9_heavy_qual1	530.2942	732.4018	24.7	380	22.3	3	Positive	100
	CD9_heavy_qual2	530.2942	603.3592	24.7	380	22.3	3	Positive	50
CANX	CANX_light_quant	744.8595	860.4261	27.5	380	24.1	5	Positive	100
	CANX_light_qual1	744.8595	789.3890	27.5	380	24.1	5	Positive	100
	CANX_light_qual2	744.8595	1046.5054	27.5	380	24.1	5	Positive	50
	CANX_heavy_quant	748.8666	868.4403	27.5	380	24.1	5	Positive	100
	CANX_heavy_qual1	748.8666	797.4032	27.5	380	24.1	5	Positive	100
	CANX_heavy_qual2	748.8666	1054.5196	27.5	380	24.1	5	Positive	50
TSG101	TSG101_light_quant	559.8264	849.4716	32.9	380	18.4	4	Positive	100
	TSG101_light_qual1	559.8264	962.5557	32.9	380	18.4	4	Positive	100
	TSG101_light_qual2	559.8264	734.4447	32.9	380	18.4	4	Positive	50
	TSG101_heavy_quant	563.8335	857.4858	32.9	380	18.4	4	Positive	100
	TSG101_heavy_qual1	563.8335	970.5699	32.9	380	18.4	4	Positive	100
	TSG101_heavy_qual2	563.8335	742.4589	32.9	380	18.4	4	Positive	50

RT retention time, *CE* collision energy, *CAV* cell accelerator voltage

Table 4
Mass spectrometer source configuration (operating in positive mode) by time segment for general EV marker analytical method

	Time segment			
Parameter	**1**	**2**	**3**	**4**
Gas temp (°C)	200	200	200	200
Gas flow (L/min)	14	14	14	14
Nebulizer (psi)	30	25	30	30
Sheath gas temp (°C)	250	250	250	250
Sheath gas flow (L/min)	11	11	11	11
Capillary voltage (V)	3000	2500	3000	3000
Nozzle voltage (V)	1000	500	500	500
Ion funnel high-pressure RF	200	200	200	200
Ion funnel low-pressure RF	100	100	100	100

Table 5
Gradient setup for blood cell marker analytical method chromatography

Time (min)	Mobile phase A (%)	Mobile phase B (%)
0	97	3
12	70	30
14	50	50
17	97	3

Mobile phase A consists of 0.1% formic acid in water. Mobile phase B consists of 0.1% formic acid in 25% acetonitrile in water

Table 6
Setup of acquisition time segments for blood cell marker analytical method

Segment	Start time (min)	Ion mode	Delta EMV	Divert
T1	0	ESI+	0	Waste
T2	2	ESI+	300	MS
T3	10.5	ESI+	300	MS

Table 7
Setup of transitions for blood cell marker analytical method

Compound group	Compound name	Precursor ion	Product ion	RT (min)	Fragmentor	CE	CAV	Polarity	Dwell time (ms)
CD41	VAIV_light_quant	441.2820	499.2987	8.1	380	14.7	5	Positive	100
	VAIV_light_qual1	441.2820	598.3671	8.1	380	14.7	5	Positive	100
	VAIV_light_qual2	441.2820	400.2303	8.1	380	8.7	5	Positive	100
	IVLL_light_quant	512.3317	811.5036	11.5	380	16.9	5	Positive	100
	IVLL_light_qual1	512.3317	585.3355	11.5	380	13.9	5	Positive	100
	IVLL_light_qual2	512.3317	698.4196	11.5	380	16.9	5	Positive	100
CD233	LSVP_light_quant	431.7371	563.2824	9.2	380	14.4	5	Positive	100
	LSVP_light_qual1	431.7371	282.1448	9.2	380	11.4	5	Positive	100
	ADFL_light_quant	745.9037	787.4825	13.5	380	24.1	5	Positive	100
	ADFL_light_qual1	745.9037	334.1397	13.5	380	27.1	5	Positive	100
	ADFL_light_qual2	745.9037	1044.5837	13.5	380	24.1	5	Positive	100

RT retention time, *CE* collision energy, *CAV* cell accelerator voltage

Table 8
Mass spectrometer source configuration (operating in positive mode) by time segment for blood cell marker analytical method

	Time segment		
Parameter	**1**	**2**	**3**
Gas temp (°C)		200	200
Gas flow (L/min)		14	14
Nebulizer (psi)		40	40
Sheath gas temp (°C)		250	250
Sheath gas flow (L/min)		11	11
Capillary voltage (V)		3500	3500
Nozzle voltage (V)		0	0
Ion funnel high-pressure RF		90	90
Ion funnel low-pressure RF		60	60

Note: T1 is diverted to waste

4 Notes

1. To minimize the risk of sample hemolysis, warm up the venepuncture site to increase blood flow, avoid prolonged use of tourniquet, allow disinfectant to dry completely before venepuncture, and use 20–22-gauge needle.
2. Allow serum to clot for a minimum of 30 min. Blood taken from patients receiving anticoagulant therapy may take longer to clot. Do not exceed 2 h for clotting.
3. Separated plasma/serum does not need to be transferred to a new tube prior to second centrifugation. Subjecting tubes to two distinct spins facilitates the depletion of platelets and thereby ex vivo platelet-derived EV generation.
4. In our hands, EV markers have been detected in plasma and serum isolates stored at −80 °C for up to 3 years.
5. Take care not to cause mixing of Lymphoprep and whole blood. However, you may observe red blood cells sinking toward the bottom of the tube. Always keep Lymphoprep at room temp.
6. Although the supernatant is plasma with platelets depleted, for matched analysis of EVs from platelet-free plasma, an additional tube(s) of blood should be collected at the beginning to recover EVs as per standard blood collection and EV isolation protocol.

7. Since EV protein targets tend to be of such low abundance, we recommend the use of low protein-binding tubes (e.g., Eppendorf Protein LoBind tubes) for all EV protein work.
8. Total protein content can be measured in EVs using the EZQ Protein Quantitation kit. We have observed greater sensitivity compared to micro BCA (bicinchoninic acid) protein assay, which tends to overestimate protein concentration due to high background.
9. After centrifugation, EV peptide digests may contain precipitates that don't fully pellet and make drawing up clear supernatant challenging. If precipitates remain, we recommend placing tubes on ice for 10 min and then repeat centrifugation.
10. SIL peptides used for quantitative analysis of EV markers—light and heavy sequences—are given in Table 9. While blood cell markers can be verified using blood cell positive controls, candidate SIL peptides given in Table 10 may be included for quantification.
11. Resuspend in 25% acetonitrile with 0.1% formic acid in water for use and sonicate tubes for at least 20 min to minimize loss on tube walls.
12. For any required dilutions, use 25% acetonitrile with 0.1% formic acid in water.
13. If digested EV protein samples are to be stored, SIL peptides should be spiked in prior to account for any degradation over the storage time.

Table 9
Peptide sequences used in general EV marker analytical method. Bold and underline indicates isotope-labeled amino acids

Analyte	Type	Sequence
ALB	Light	H2N-LVNEVTEFAK-OH
	SIL	H2N-LVNEVTEFA**K**-OH
CD81	Light	H2N-QFYDQALQQAVVDDDANNAK-OH
	SIL	H2N-QFYDQALQQAVVDDDANNA**K**-OH
CD9	Light	H2N-DVLETFTVK-OH
	SIL	H2N-DVLETFTV**K**-OH
CANX	Light	H2N-IVDDWANDGWGLK-OH
	SIL	H2N-IVDDWANDGWGL**K**-OH
TSG101	Light	H2N-GVIDLDVFLK-OH
	SIL	H2N-GVIDLDVFL**K**-OH

Table 10
Peptide sequences used in blood cell marker analytical method. Bold and underline indicates isotope-labeled amino acids

Analyte	Type	Sequence
CD41	Light	H2N-VAIVVGAPR-OH
	Candidate SIL	H2N-VAIVVGAP**R**-OH
	Light	H2N-IVLLDVPVR-OH
	Candidate SIL	H2N-IVLLDVPV**R**-OH
CD233	Light	H2N-LSVPDGFK-OH
	Candidate SIL	H2N-LSVPDGF**K**-OH
	Light	H2N-ADFLEQPVLGFVR-OH
	Candidate SIL	H2N-ADFLEQPVLGFV**R**-OH

Table 11
Sensitivity of analytical methods

General EV markers	Analyte	LOD (pmol/mL)	LLOQ (pmol/mL)
	ALB	0.004	0.020
	CD81	0.046	0.228
	CD9	0.005	0.025
	CANX	0.007	0.035
	TSG101	0.006	0.031
Blood cell markers	Analyte	LOD (peak area response)	
	CD41_VAIV	6.33	
	CD41_IVLL	11.1	
	CD233_LSVP	9.92	
	CD233_ADFL	1.10	

Limit of detection (LOD) and lower limit of quantification (LLOQ) (pmol/mL) determined for General EV Markers, and LOD (peak area response) determined for blood cell markers

14. Retention times of analytes (given in Tables 3 and 7) are reflective of retention on an AdvanceBio Peptide Mapping column (2.1 mm × 100 mm × 2.7 μm) with a column guard attached.
15. Collision energy was optimized using the open-source software Skyline, and cell accelerator voltage was optimized manually between values of 3 and 8.
16. Key parameters for source optimization include nebulizer pressure, nozzle voltage, and capillary voltage (performed using MassHunter Optimizer software).
17. Assay sensitivity with our instrument and configuration is given in Table 11. For general EV markers, concentration at LOD and LLOQ could be determined using SIL peptides. For blood cell markers, peak area response at LOD is given.

References

1. Newman LA, Muller K, Rowland A (2022) Circulating cell-specific extracellular vesicles as biomarkers for the diagnosis and monitoring of chronic liver diseases. Cell Mol Life Sci 79(5): 232. https://doi.org/10.1007/s00018-022-04256-8
2. Hoshino A, Kim HS, Bojmar L, Gyan KE, Cioffi M, Hernandez J, Zambirinis CP, Rodrigues G, Molina H, Heissel S, Mark MT, Steiner L, Benito-Martin A, Lucotti S, Di Giannatale A, Offer K, Nakajima M, Williams C, Nogués L, Pelissier Vatter FA, Hashimoto A, Davies AE, Freitas D, Kenific CM, Ararso Y, Buehring W, Lauritzen P, Ogitani Y, Sugiura K, Takahashi N, Alečković M, Bailey KA, Jolissant JS, Wang H, Harris A, Schaeffer LM, García-Santos G, Posner Z, Balachandran VP, Khakoo Y, Raju GP, Scherz A, Sagi I, Scherz-Shouval R, Yarden Y, Oren M, Malladi M, Petriccione M, De Braganca KC, Donzelli M, Fischer C, Vitolano S, Wright GP, Ganshaw L, Marrano M, Ahmed A, DeStefano J, Danzer E, Roehrl MHA, Lacayo NJ, Vincent TC, Weiser MR, Brady MS, Meyers PA, Wexler LH, Ambati SR, Chou AJ, Slotkin EK, Modak S, Roberts SS, Basu EM, Diolaiti D, Krantz BA, Cardoso F, Simpson AL, Berger M, Rudin CM, Simeone DM, Jain M, Ghajar CM, Batra SK, Stanger BZ, Bui J, Brown KA, Rajasekhar VK, Healey JH, de Sousa M, Kramer K, Sheth S, Baisch J, Pascual V, Heaton TE, La Quaglia MP, Pisapia DJ, Schwartz R, Zhang H, Liu Y, Shukla A, Blavier L, DeClerck YA, LaBarge M, Bissell MJ, Caffrey TC, Grandgenett PM, Hollingsworth MA, Bromberg J, Costa-Silva B, Peinado H, Kang Y, Garcia BA, O'Reilly EM, Kelsen D, Trippett TM, Jones DR, Matei IR, Jarnagin WR, Lyden D (2020) Extracellular vesicle and particle biomarkers define multiple human cancers. Cell 182(4):1044–1061. e1018. https://doi.org/10.1016/j.cell.2020.07.009
3. Carrière J, Barnich N, Nguyen HTT (2016) Exosomes: from functions in host-pathogen interactions and immunity to diagnostic and therapeutic opportunities. In: Nilius B, de Tombe P, Gudermann T, Jahn R, Lill R, Petersen OH (eds) Reviews of physiology, biochemistry and pharmacology, vol 172. Springer International Publishing, Cham, pp 39–75. https://doi.org/10.1007/112_2016_7
4. Vallabhajosyula P, Korutla L, Habertheuer A, Yu M, Rostami S, Yuan CX, Reddy S, Liu C, Korutla V, Koeberlein B, Trofe-Clark J, Rickels MR, Naji A (2017) Tissue-specific exosome biomarkers for noninvasively monitoring immunologic rejection of transplanted tissue. J Clin Invest 127(4):1375–1391. https://doi.org/10.1172/jci87993
5. Anastasi F, Masciandaro SM, Carratore RD, Dell'Anno MT, Signore G, Falleni A, McDonnell LA, Bongioanni P (2021) Proteomics profiling of neuron-derived small extracellular vesicles from human plasma: enabling single-subject analysis. Int J Mol Sci 22(6):2951. https://doi.org/10.3390/ijms22062951
6. Goetzl EJ, Boxer A, Schwartz JB, Abner EL, Petersen RC, Miller BL, Kapogiannis D (2015) Altered lysosomal proteins in neural-derived plasma exosomes in preclinical Alzheimer disease. Neurology 85(1):40–47. https://doi.org/10.1212/WNL.0000000000001702
7. Mustapic M, Eitan E, Werner JK, Berkowitz ST, Lazaropoulos MP, Tran J, Goetzl EJ, Kapogiannis D (2017) Plasma extracellular vesicles enriched for neuronal origin: a potential window into brain pathologic processes. Front Neurosci 11:278. https://doi.org/10.3389/fnins.2017.00278
8. Newman LA, Useckaite Z, Johnson J, Sorich MJ, Hopkins AM, Rowland A (2022) Selective isolation of liver-derived extracellular vesicles redefines performance of miRNA biomarkers for non-alcoholic fatty liver disease. Biomedicine 10(1):195
9. Povero D, Yamashita H, Ren W, Subramanian MG, Myers RP, Eguchi A, Simonetto DA, Goodman ZD, Harrison SA, Sanyal AJ, Bosch J, Feldstein AE (2020) Characterization and proteome of circulating extracellular vesicles as potential biomarkers for NASH. Hepatol Commun 4(9):1263–1278. https://doi.org/10.1002/hep4.1556
10. Théry C, Witwer KW, Aikawa E, Alcaraz MJ, Anderson JD, Andriantsitohaina R, Antoniou A, Arab T, Archer F, Atkin-Smith GK, Ayre DC, Bach J-M, Bachurski D, Baharvand H, Balaj L, Baldacchino S, Bauer NN, Baxter AA, Bebawy M, Beckham C, Bedina Zavec A, Benmoussa A, Berardi AC, Bergese P, Bielska E, Blenkiron C, Bobis-Wozowicz S, Boilard E, Boireau W, Bongiovanni A, Borràs FE, Bosch S, Boulanger CM, Breakefield X, Breglio AM, Brennan MÁ, Brigstock DR, Brisson A, Broekman MLD, Bromberg JF, Bryl-Górecka P, Buch S, Buck AH, Burger D, Busatto S, Buschmann D, Bussolati B, Buzás EI, Byrd JB, Camussi G, Carter DRF, Caruso S, Chamley LW, Chang Y-T, Chen C, Chen S, Cheng L, Chin AR, Clayton A, Clerici SP, Cocks A, Cocucci E,

Coffey RJ, Cordeiro-da-Silva A, Couch Y, Coumans FAW, Coyle B, Crescitelli R, Criado MF, D'Souza-Schorey C, Das S, Datta Chaudhuri A, de Candia P, De Santana EF, De Wever O, del Portillo HA, Demaret T, Deville S, Devitt A, Dhondt B, Di Vizio D, Dieterich LC, Dolo V, Dominguez Rubio AP, Dominici M, Dourado MR, Driedonks TAP, Duarte FV, Duncan HM, Eichenberger RM, Ekström K, El Andaloussi S, Elie-Caille C, Erdbrügger U, Falcón-Pérez JM, Fatima F, Fish JE, Flores-Bellver M, Försönits A, Frelet-Barrand A, Fricke F, Fuhrmann G, Gabrielsson S, Gámez-Valero A, Gardiner C, Gärtner K, Gaudin R, Gho YS, Giebel B, Gilbert C, Gimona M, Giusti I, Goberdhan DCI, Görgens A, Gorski SM, Greening DW, Gross JC, Gualerzi A, Gupta GN, Gustafson D, Handberg A, Haraszti RA, Harrison P, Hegyesi H, Hendrix A, Hill AF, Hochberg FH, Hoffmann KF, Holder B, Holthofer H, Hosseinkhani B, Hu G, Huang Y, Huber V, Hunt S, Ibrahim AG-E, Ikezu T, Inal JM, Isin M, Ivanova A, Jackson HK, Jacobsen S, Jay SM, Jayachandran M, Jenster G, Jiang L, Johnson SM, Jones JC, Jong A, Jovanovic-Talisman T, Jung S, Kalluri R, S-i K, Kaur S, Kawamura Y, Keller ET, Khamari D, Khomyakova E, Khvorova A, Kierulf P, Kim KP, Kislinger T, Klingeborn M, Klinke DJ, Kornek M, Kosanović MM, Kovács ÁF, Krämer-Albers E-M, Krasemann S, Krause M, Kurochkin IV, Kusuma GD, Kuypers S, Laitinen S, Langevin SM, Languino LR, Lannigan J, Lässer C, Laurent LC, Lavieu G, Lázaro-Ibáñez E, Le Lay S, Lee M-S, Lee YXF, Lemos DS, Lenassi M, Leszczynska A, Li ITS, Liao K, Libregts SF, Ligeti E, Lim R, Lim SK, Linē A, Linnemannstöns K, Llorente A, Lombard CA, Lorenowicz MJ, Lörincz ÁM, Lötvall J, Lovett J, Lowry MC, Loyer X, Lu Q, Lukomska B, Lunavat TR, Maas SLN, Malhi H, Marcilla A, Mariani J, Mariscal J, Martens-Uzunova ES, Martin-Jaular L, Martinez MC, Martins VR, Mathieu M, Mathivanan S, Maugeri M, McGinnis LK, McVey MJ, Meckes DG, Meehan KL, Mertens I, Minciacchi VR, Möller A, Møller Jørgensen M, Morales-Kastresana A, Morhayim J, Mullier F, Muraca M, Musante L, Mussack V, Muth DC, Myburgh KH, Najrana T, Nawaz M, Nazarenko I, Nejsum P, Neri C, Neri T, Nieuwland R, Nimrichter L, Nolan JP, Nolte-'t Hoen ENM, Noren Hooten N, O'Driscoll L, O'Grady T, O'Loghlen A, Ochiya T, Olivier M, Ortiz A, Ortiz LA, Osteikoetxea X, Østergaard O, Ostrowski M, Park J, Pegtel DM, Peinado H, Perut F, Pfaffl MW, Phinney DG, Pieters BCH, Pink RC, Pisetsky DS, Pogge von Strandmann E, Polakovicova I, Poon IKH, Powell BH, Prada I, Pulliam L, Quesenberry P, Radeghieri A, Raffai RL, Raimondo S, Rak J, Ramirez MI, Raposo G, Rayyan MS, Regev-Rudzki N, Ricklefs FL, Robbins PD, Roberts DD, Rodrigues SC, Rohde E, Rome S, Rouschop KMA, Rughetti A, Russell AE, Saá P, Sahoo S, Salas-Huenuleo E, Sánchez C, Saugstad JA, Saul MJ, Schiffelers RM, Schneider R, Schøyen TH, Scott A, Shahaj E, Sharma S, Shatnyeva O, Shekari F, Shelke GV, Shetty AK, Shiba K, Siljander PRM, Silva AM, Skowronek A, Snyder OL, Soares RP, Sódar BW, Soekmadji C, Sotillo J, Stahl PD, Stoorvogel W, Stott SL, Strasser EF, Swift S, Tahara H, Tewari M, Timms K, Tiwari S, Tixeira R, Tkach M, Toh WS, Tomasini R, Torrecilhas AC, Tosar JP, Toxavidis V, Urbanelli L, Vader P, van Balkom BWM, van der Grein SG, Van Deun J, van Herwijnen MJC, Van Keuren-Jensen K, van Niel G, van Royen ME, van Wijnen AJ, Vasconcelos MH, Vechetti IJ, Veit TD, Vella LJ, Velot É, Verweij FJ, Vestad B, Viñas JL, Visnovitz T, Vukman KV, Wahlgren J, Watson DC, Wauben MHM, Weaver A, Webber JP, Weber V, Wehman AM, Weiss DJ, Welsh JA, Wendt S, Wheelock AM, Wiener Z, Witte L, Wolfram J, Xagorari A, Xander P, Xu J, Yan X, Yáñez-Mó M, Yin H, Yuana Y, Zappulli V, Zarubova J, Žėkas V, J-y Z, Zhao Z, Zheng L, Zheutlin AR, Zickler AM, Zimmermann P, Zivkovic AM, Zocco D, Zuba-Surma EK (2018) Minimal information for studies of extracellular vesicles 2018 (MISEV2018): a position statement of the International Society for Extracellular Vesicles and update of the MISEV2014 guidelines. J Extracell Vesicles 7(1):1535750. https://doi.org/10.1080/20013078.2018.1535750

11. Useckaite Z, Rodrigues AD, Hopkins AM, Newman LA, Johnson JG, Sorich MJ, Rowland A (2021) Role of extracellular vesicle derived biomarkers in drug metabolism and disposition. Drug Metab Dispos 49(11):961–971. DMD-MR-2021-000411. https://doi.org/10.1124/dmd.121.000411

12. Gustafson CM, Shepherd AJ, Miller VM, Jayachandran M (2015) Age- and sex-specific differences in blood-borne microvesicles from apparently healthy humans. Biol Sex Differ 6(1):10. https://doi.org/10.1186/s13293-015-0028-8

13. Konoshenko MY, Lekchnov EA, Vlassov AV, Laktionov PP (2018) Isolation of extracellular vesicles: general methodologies and latest trends. Biomed Res Int 2018:8545347–

8545347. https://doi.org/10.1155/2018/8545347

14. Newman LA, Fahmy A, Sorich MJ, Best OG, Rowland A, Useckaite Z (2021) Importance of between and within subject variability in extracellular vesicle abundance and cargo when performing biomarker analyses. Cell 10(3):485
15. Li Y, He X, Li Q, Lai H, Zhang H, Hu Z, Li Y, Huang S (2020) EV-origin: enumerating the tissue-cellular origin of circulating extracellular vesicles using exLR profile. Comput Struct Biotechnol J 18:2851–2859. https://doi.org/10.1016/j.csbj.2020.10.002
16. Liebler DC, Zimmerman LJ (2013) Targeted quantitation of proteins by mass spectrometry. Biochemistry 52(22):3797–3806. https://doi.org/10.1021/bi400110b
17. Newman LA, Useckaite Z, Rowland A (2022) Addressing MISEV guidance using targeted LC-MS/MS: A method for the detection and quantification of extracellular vesicle-enriched and contaminant protein markers from blood. Journal of Extracellular Biology 1(9):e56. https://doi.org/10.1002/jex2.56